

**Some pages of this thesis may have been removed for copyright restrictions.**

If you have discovered material in AURA which is unlawful e.g. breaches copyright, (either yours or that of a third party) or any other law, including but not limited to those relating to patent, trademark, confidentiality, data protection, obscenity, defamation, libel, then please read our [Takedown Policy](#) and [contact the service](#) immediately

# **CORROSION INHIBITORS FOR THE REHABILITATION OF REINFORCED CONCRETE**

**DANIEL JAMES ANSTICE**

Doctor of Philosophy

**ASTON UNIVERSITY**

March 2000

This copy of the thesis has been supplied on condition that anyone who consults it is understood to recognise that its copyright rests with its author and that no quotation from the thesis and no information derived from it may be published without proper acknowledgement.



## **ASTON UNIVERSITY**

### **CORROSION INHIBITORS FOR THE REHABILITATION OF REINFORCED CONCRETE**

**Daniel James ANSTICE**

**Doctor of Philosophy 2000**

#### **THESIS SUMMARY**

Four corrosion inhibitors namely sodium nitrite, sodium monofluorophosphate, ethanolamine and an alkanolamine-based mixture were studied by immersing mild steel bars for 42 days in model electrolytes of varied pH and chloride concentration which were intended to simulate the pore solution phase present within carbonated and/or chloride-contaminated concrete. Site trials were carried out on sodium monofluorophosphate and the alkanolamine-based inhibitor to study their depth of penetration into concrete. The influence of various carbonating atmospheres on the pore solution chemistry and microstructure of hydrated cement paste was investigated. Physical realkalisation of carbonated cement paste and a calcium nitrite-based corrosion rehabilitation system for chloride-contaminated cement paste were investigated by monitoring ionic transport within the pore solution phase of laboratory specimens.

The main findings were as follows:

- Sodium nitrite, sodium monofluorophosphate, ethanolamine and the alkanolamine-based mixture all behaved as passivating anodic inhibitors of steel corrosion in air-saturated aqueous solutions of varied pH and chloride concentration.
- Sodium monofluorophosphate failed to penetrate significantly into partially carbonated site concrete when applied as recommended by the supplier. Phosphate and fluoride penetrated 5mm into partially carbonated site concrete treated with sodium monofluorophosphate.
- The ethanolamine component of the alkanolamine-based inhibitor was found to have penetrated significant depths into partially carbonated site concrete.
- Carbonating hydrated cement paste over saturated solutions of sodium nitrite resulted in significant concentrations of nitrite in the pore solution of the carbonated paste. Saturated solutions of sodium chloride, ammonium nitrate, magnesium nitrate and sodium dichromate were investigated and identified as alternatives for controlling the relative humidity of the carbonating environment.
- Hardened carbonated cement paste can be physically realkalised to a limited extent due to the diffusion of hydroxyl ions under saturated conditions. A substantial proportion of the hydroxyl ions that diffused into the carbonated cement paste however, became bound into the cement matrix. Hydroxyl ion concentrations remained below 5mmol/l within the pore solution of the realkalised cement paste.
- Nitrite ions penetrated significant distances by diffusion within the pore solution of saturated uncarbonated hydrated cement paste.

**KEY WORDS:** Nitrite, Monofluorophosphate, Ethanolamine, Carbonation, Realkalisation

This thesis is dedicated to my parents

Bryn John Anstice and Angela Diane Anstice

## ACKNOWLEDGEMENTS

I would like to express my sincere gratitude to Professor C.L. Page under whose supervision this research was conducted and whose knowledge, expertise, guidance and support are greatly appreciated.

I would like to thank the Engineering and Physical Sciences Research Council and Aston Materials Services Ltd for providing funding and financial support for this research. I would also like to thank British Energy for providing two reinforced concrete columns at a Power Station in North East England to be treated with corrosion inhibitors.

I would like to thank the staff in the Civil Engineering Department at Aston University, in particular Mr C.J. Thompson, Dr M.M. Page, Dr V.T. Ngala, Mr P. Green and Mr W. Curtis for their assistance in carrying out this research. I would especially like to thank Dr L.Y. Li for his help in developing the computer programs used in this investigation.

I would like to thank my colleagues S. Gregory, L. Jordan, P. Purnell, G. Chadbourn, G. Abdelaziz, M.B. Ismail, G. Sergi, G. Seneviratne, A. Crowcombe and R. Neale for their help, discussions, motivation and humour during the course of this research.

I would like to take this opportunity to thank my grandparents for all their encouragement, love and moral support throughout my studies. I would like to thank my fiancée Louise for the support, love and patience she affords me on a daily basis. I would also like to send a special thanks to my brother who has always been an inspiration and a tower of strength in my life. Last, but by no means least, I would especially like to express my sincere appreciation to my parents whose unconditional financial and emotional support has formed the foundations from which I gain my strength in all things I do.

## GLOSSARY OF ABBREVIATIONS

OPC	-	Ordinary Portland Cement
GGBS	-	Ground Granulated Blast Furnace Slag
PFA	-	Pulverised Fuel Ash
C <sub>3</sub> S	-	Tricalcium Silicate (3CaO.SiO <sub>2</sub> )
C <sub>2</sub> S	-	Dicalcium Silicate (2CaO.SiO <sub>2</sub> )
C <sub>3</sub> A	-	Tricalcium Aluminate (3CaO.Al <sub>2</sub> O <sub>3</sub> )
C <sub>4</sub> AF	-	Tetracalcium Alumino-ferrite (4CaO.Al <sub>2</sub> O <sub>3</sub> .Fe <sub>2</sub> O <sub>3</sub> )
C-S-H	-	Calcium Silicate Hydrate
Na <sub>2</sub> O	-	Sodium Oxide
K <sub>2</sub> O	-	Potassium Oxide
Fe <sup>2+</sup>	-	Ferrous Ion
CO <sub>2</sub>	-	Carbon Dioxide
H <sub>2</sub> O	-	Water
H <sub>2</sub> CO <sub>3</sub>	-	Carbonic Acid
Ca(OH) <sub>2</sub>	-	Calcium Hydroxide
CaCO <sub>3</sub>	-	Calcium Carbonate
OH <sup>-</sup>	-	Hydroxyl Ion
NO <sub>2</sub> <sup>-</sup>	-	Nitrite Ion
Cl <sup>-</sup>	-	Chloride Ion
[NO <sub>2</sub> <sup>-</sup> ]/[Cl <sup>-</sup> ]	-	Nitrite to Chloride Ion Ratio
Na <sub>2</sub> PO <sub>3</sub> F	-	Sodium Monofluorophosphate
MFP	-	Sodium Monofluorophosphate (Proprietary Corrosion Inhibitor)
w/c	-	Water to Cement Ratio
NaCl	-	Sodium Chloride
HNO <sub>3</sub>	-	Nitric Acid
BaCl <sub>2</sub> .2H <sub>2</sub> O	-	Hydrated Barium Chloride



SEM	-	Scanning Electron Microscopy
XRD	-	X-ray diffraction
DTA	-	Differential Thermal Analysis
TGA	-	Thermo-Gravimetric Analysis
MIP	-	Mercury Intrusion Porosimetry
NaNO <sub>2</sub>	-	Sodium Nitrite
NH <sub>2</sub> CH <sub>2</sub> CH <sub>2</sub> OH	-	Ethanolamine
PO <sub>3</sub> F <sup>2-</sup>	-	Monofluorophosphate Ion
PO <sub>4</sub> <sup>3-</sup>	-	Phosphate Ion
[PO <sub>3</sub> F <sup>2-</sup> ]/[Cl <sup>-</sup> ]	-	Monofluorophosphate to Chloride Ion Ratio
NH <sub>4</sub> NO <sub>3</sub>	-	Ammonium Nitrate
Mg(NO <sub>3</sub> ) <sub>2</sub> .6H <sub>2</sub> O	-	Magnesium Nitrate
Na <sub>2</sub> Cr <sub>2</sub> O <sub>7</sub> .2H <sub>2</sub> O	-	Sodium Dichromate
CaCl <sub>2</sub>	-	Calcium Chloride
NO <sub>3</sub> <sup>-</sup>	-	Nitrate Ion
SO <sub>4</sub> <sup>2-</sup>	-	Sulphate Ion
CO <sub>3</sub> <sup>2-</sup>	-	Carbonate Ion
HCO <sub>3</sub> <sup>-</sup>	-	Bicarbonate Ion
Na <sup>+</sup>	-	Sodium Ion
K <sup>+</sup>	-	Potassium Ion
Mg <sup>2+</sup>	-	Magnesium Ion
Ca <sup>2+</sup>	-	Calcium Ion
Na <sub>2</sub> O <sub>eq</sub>	-	Sodium Oxide Equivalent
NaOH	-	Sodium Hydroxide
Ca(NO <sub>2</sub> ) <sub>2</sub>	-	Calcium Nitrite

## **LIST OF CONTENTS**

	<b>Page No.</b>
<b>TITLE PAGE</b>	<b>1</b>
<b>THESIS SUMMARY</b>	<b>2</b>
<b>DEDICATION</b>	<b>3</b>
<b>ACKNOWLEDGEMENTS</b>	<b>4</b>
<b>GLOSSARY OF ABBREVIATIONS</b>	<b>5</b>
<b>LIST OF CONTENTS</b>	<b>7</b>
<b>LIST OF TABLES</b>	<b>16</b>
<b>LIST OF FIGURES</b>	<b>18</b>
<b>CHAPTER ONE      INTRODUCTION</b>	<b>37</b>
1.1    HISTORICAL NOTE	37
1.2    FIELD OF STUDY	40
1.3    OBJECTIVES OF STUDY	44
1.4    OUTLINE OF THESIS	46
<b>CHAPTER TWO      LITERATURE REVIEW</b>	<b>48</b>
2.1    INTRODUCTION	48
2.2    MICROSTRUCTURE OF HYDRATED CEMENT PASTE	48
2.2.1    Introduction	48
2.2.2    Solid Phases	49
2.2.3    Pore Structure	49
2.2.4    Pore Solution Phase of Hydrated Cement Paste	53
2.3    THE CORROSION OF STEEL IN CONCRETE	54

2.3.1	Introduction	54
2.3.2	Steel in Concrete	54
2.3.3	Mechanisms of Corrosion of Steel in Concrete	55
2.3.4	Cathodically Restrained Dissolution	56
2.3.5	Carbonation	57
	2.3.5.1 <i>Mechanisms of Carbonation</i>	57
	2.3.5.2 <i>Mineralogical Formations</i>	57
	2.3.5.3 <i>Rate of Carbonation through Concrete</i>	58
	2.3.5.4 <i>Factors Influencing Carbonation</i>	58
	2.3.5.5 <i>Effects of Carbonation on Pore Structure</i>	60
2.3.6	Chloride Attack	61
	2.3.6.1 <i>Mechanism of Chloride Attack</i>	61
	2.3.6.2 <i>Critical Chloride to Hydroxyl Ion Ratio</i>	62
	2.3.6.3 <i>Transport of Chloride Ions through Concrete</i>	63
2.4	CORROSION INHIBITORS FOR USE WITH REINFORCED CONCRETE STRUCTURES	63
2.4.1	Introduction	63
2.4.2	Types of Corrosion Inhibitor	64
2.4.3	Corrosion Inhibitors as Preventative Measures	65
2.4.4	Corrosion Inhibitors for Rehabilitative Purposes	67
	2.4.4.1 <i>Nitrite Ions</i>	67
	2.4.4.2 <i>Sodium Monofluorophosphate</i>	69

2.4.4.3	<i>Organic Inhibitors</i>	72
2.4.4.4	<i>Physical Realkalisation</i>	74
2.4.4.5	<i>Electrochemical Realkalisation</i>	75
2.4.4.6	<i>Other Inhibitors</i>	77
<b>CHAPTER THREE MATERIALS AND EXPERIMENTAL TECHNIQUES</b>		84
3.1	<b>INTRODUCTION</b>	84
3.2	<b>MATERIALS</b>	84
3.2.1	Ordinary Portland Cement	84
3.2.2	Water	84
3.2.3	Steel	84
3.2.4	Counter Electrodes	84
3.2.5	Corrosion Inhibitors	85
3.2.6	Sodium Chloride	85
3.2.7	Potassium Nitrate	85
3.2.8	Carbon Dioxide Absorber	85
3.2.9	Pyroclean	85
3.2.10	Saturated Salt Solutions	86
3.2.11	Carbon Dioxide	86
3.3	<b>EXPERIMENTAL TECHNIQUES</b>	86
3.3.1	Manufacture of Cement Paste Specimens	86
3.3.2	Determination of Bulk Density	87
3.3.3	Pore Solution Expression	87



3.3.4	pH Meter	88
3.3.5	Corrosion Potential Measurements	88
3.3.6	Linear Polarisation	88
3.3.7	Gravimetric Measurements	89
3.3.8	Photography	90
3.3.9	Water and Acid Extraction	90
3.3.10	Ion Chromatography	90
3.3.11	Carbonation Depth	91
3.3.12	Hydroxyl Ions	91
3.3.13	Bicarbonate and Carbonate Ions	92
3.3.14	Evaporable Water Content	92
3.3.15	Water Desorption	93
3.3.16	X-ray Diffraction Analysis	94
3.3.17	Differential Thermal Analysis / Thermo-Gravimetric Analysis	95
3.3.18	Mercury Intrusion Porosimetry	96
3.3.19	Relative Humidity and Temperature	97
<b>CHAPTER FOUR</b>	<b>MECHANISMS OF INHIBITOR ACTION IN MODEL ELECTROLYTE SYSTEMS</b>	<b>105</b>
4.1	INTRODUCTION	105
4.2	EXPERIMENTAL PROCEDURES	106
4.2.1	Preparation of Model Electrolytes	106
4.2.2	Preparation of Mild Steel Bars	107

4.2.3	Gel Bridge Construction	108
4.2.4	Cell Assembly	108
4.2.5	Final Set-Up	108
4.2.6	pH Measurements	109
4.2.7	Electrochemical Monitoring	109
4.2.8	Gravimetric Measurements	109
4.2.9	Theoretical Weight Loss Determinations	109
4.2.10	Photography	110
4.3	DISCUSSION OF RESULTS	110
4.3.1	pH Determinations	110
4.3.2	Electrochemical Monitoring	110
	4.3.2.1 <i>Sodium Nitrite</i>	110
	4.3.2.2 <i>Sodium Monofluorophosphate</i>	113
	4.3.2.3 <i>Alkanolamine-based Inhibitor</i>	116
	4.3.2.4 <i>Ethanolamine</i>	118
	4.3.2.5 <i>Comparison of Inhibitor Efficiencies</i>	120
4.3.3	Weight Loss Determinations	121
4.3.4	Photographic Observations	123
4.4	CONCLUSIONS	124
<b>CHAPTER FIVE</b>	<b>SITE TRIALS TO DETERMINE THE DEPTH OF PENETRATION AND DISTRIBUTION OF INHIBITORS AND/OR THEIR DECOMPOSITION PRODUCTS</b>	<b>185</b>
5.1	INTRODUCTION	185

5.2	EXPERIMENTAL PROCEDURES	186
5.2.1	Pre-inhibitor Application Investigations	186
5.2.2	Application of Sodium Monofluorophosphate	187
5.2.3	Application of the Alkanolamine-based Inhibitor	187
5.2.4	Determination of Penetration Profiles	187
5.3	DISCUSSION OF RESULTS	188
5.3.1	Sodium Monofluorophosphate	188
5.3.2	Alkanolamine-based Inhibitor	189
5.4	CONCLUSIONS	189
<b>CHAPTER SIX</b>	<b>EFFECT OF CARBONATING ATMOSPHERE ON HYDRATED CEMENT PASTE</b>	<b>195</b>
6.1	INTRODUCTION	195
6.2	EXPERIMENTAL PROCEDURES	196
6.2.1	Preparation of Hydrated Cement Paste Specimens	196
6.2.2	Carbonation of Cement Paste Discs	196
6.2.3	Evaporable Water Determinations	197
6.2.4	Pore Solution Analysis	197
6.2.5	Porosity Determinations	198
6.2.6	Solid Phase Determinations	198
6.3	DISCUSSION OF RESULTS	198
6.3.1	Pore Solution Composition	198
6.3.2	Porosity and Pore Size Distribution	201

6.3.3	Solid Phases	201
6.4	CONCLUSIONS	203
<b>CHAPTER SEVEN</b>	<b>PHYSICAL REALKALISATION OF CARBONATED CEMENT PASTE</b>	228
7.1	INTRODUCTION	228
7.2	EXPERIMENTAL PROCEDURES	229
7.2.1	Preparation of Cement Paste Specimens	229
7.2.1.1	<i>Preparation of Uncarbonated Cement Paste Specimens</i>	229
7.2.1.2	<i>Preparation of Carbonated Cement Paste Specimens</i>	229
7.2.1.3	<i>Preparation of Repair Cement Paste</i>	230
7.2.2	Final Set-Up	231
7.2.3	Pore Solution Analysis	232
7.3	MATHEMATICAL MODELLING	232
7.3.1	Governing Equations	232
7.3.1.1	<i>Flux</i>	232
7.3.1.2	<i>Differential Equation of Diffusion</i>	233
7.3.1.3	<i>Ionic Binding</i>	233
7.3.1.4	<i>Mass Conservation</i>	234
7.3.1.5	<i>Ionic Concentration Profile</i>	235
7.3.2	Assumptions	235
7.3.3	Computer Simulation	235
7.4	DISCUSSION OF RESULTS	236
7.4.1	Experimental Results	236

7.4.2	Mathematical Modelling	238
7.5	CONCLUSIONS	240
<b>CHAPTER EIGHT</b>	<b>CALCIUM NITRITE-BASED CORROSION REHABILITATION SYSTEM</b>	<b>253</b>
8.1	INTRODUCTION	253
8.2	EXPERIMENTAL PROCEDURES	254
8.2.1	Preparation of Hydrated Cement Paste	254
	8.2.1.1 <i>Preparation of Chloride-Contaminated Cement Paste Specimens</i>	254
	8.2.1.2 <i>Preparation of Repair Cement Paste Specimens</i>	255
8.2.2	Final Set-Up	255
8.2.3	Pore Solution Analysis	255
8.3	MATHEMATICAL MODELLING	256
8.3.1	Introduction	256
8.3.2	Governing Equations	256
	8.3.2.1 <i>Mass Conservation</i>	256
	8.3.2.2 <i>Flux</i>	257
	8.3.2.3 <i>Ionic Concentration Profile</i>	257
8.3.3	Assumptions	258
8.3.4	Computer Simulation	259
8.4	DISCUSSION OF RESULTS	260
8.4.1	Experimental Results	260
8.4.2	Mathematical Modelling	260



8.5	CONCLUSIONS	262
<b>CHAPTER NINE</b>	<b>GENERAL CONCLUSIONS AND RECOMMENDATIONS FOR FURTHER WORK</b>	<b>285</b>
9.1	GENERAL CONCLUSIONS	285
9.2	RECOMMENDATIONS FOR FURTHER WORK	288
	<b>LIST OF REFERENCES</b>	<b>290</b>
	<b>APPENDICES</b>	<b>306</b>
	Appendix A: Potential Phase Composition Calculations	307
	Appendix B: Calculation of Free Ionic Concentrations	308
	Appendix C: Calculation of Hydroxyl Ion Concentrations and pH by Acid Titration	309
	Appendix D: Calculation of Bicarbonate and Carbonate Concentrations within the Pore Solutions	310
	Appendix E: Calculation of Evaporable Water Content	312
	Appendix F: Calculation of Capillary and Total Porosity	313
	Appendix G: Computer Program to Simulate Physical Realkalisation of Carbonated Cement Paste	314
	Appendix H: Computer Program to Simulate a Calcium Nitrite-based Corrosion Rehabilitation System	318

## LIST OF TABLES

Table	Page No.
2.1 A selection of carbonation depth equations	79
2.2 A summary of chloride threshold values	80
3.1 Chemical analysis of Ordinary Portland Cement	98
3.2 Potential Phase Compositions of Ordinary Portland Cement	98
3.3 Chemical Composition of Mild Steel Bars	98
4.1 Results of pH determinations on the model electrolytes	126
6.1 Relative Humidity of Air over Saturated Salt Solutions	205
6.2 Concentration of anions (mmol/l) in the pore solution of hydrated cement paste after carbonation in various atmospheres	205
6.3 Concentration of cations (mmol/l) in the pore solution of hydrated cement paste after carbonation in various atmospheres	205
6.4 Free anionic concentrations (mmol / g of cement) $\times 10^3$	206
6.5 Free cationic concentrations (mmol / g of cement) $\times 10^3$	206
6.6 Water desorption results for hydrated cement paste after carbonation in various atmospheres	207
6.7 Mercury intrusion porosimetry results for hydrated cement paste after carbonation in various atmospheres	207
6.8 XRD results for hydrated cement paste after carbonation in various atmospheres	208
6.9 TG mass loss results for hydrated cement paste after carbonation in various atmospheres	208
7.1 Experimentally determined initial hydroxyl ion concentrations	242
7.2 Experimentally determined pore solution hydroxyl ion profiles for set-ups 1 to 6	242

7.3	Experimentally determined pore solution hydroxyl ion profiles for set-ups 7 to 12	243
7.4	Assumed hydroxyl ion diffusion coefficients that gave best-fit data	243
7.5	Assumed constants for use in Langmuir adsorption isotherm that gave best-fit data	243
8.1	Experimentally determined initial anionic pore solution concentrations	263
8.2	Experimentally determined initial cationic pore solution concentrations	263
8.3	Experimentally determined nitrite ion profiles	264
8.4	Experimentally determined hydroxyl ion profiles	264
8.5	Experimentally determined chloride ion profiles	265
8.6	Experimentally determined sulphate ion profiles	265
8.7	Experimentally determined nitrate ion profiles	266
8.8	Experimentally determined sodium ion profiles	266
8.9	Experimentally determined potassium ion profiles	267
8.10	Experimentally determined calcium ion profiles	267
8.11	Assumed initial pore solution concentrations for modelling	268
8.12	Assumed diffusion coefficients that gave best-fit data	268
8.13	Numerically determined depth to which critical $[\text{NO}_2^-]/[\text{Cl}^-]$ ratio is achieved	268



## LIST OF FIGURES

Figure	Page No.
2.1 Principal hydration reactions of Portland cement materials	81
2.2 Pore size classification for cement pastes	81
2.3 Schematic representation of Feldman Sereda pore structural model	82
2.4 Hydroxyl ion concentrations of cement pastes of water/cement ratio 0.5 cured for 28 days unless otherwise stated	82
2.5 Simplified Equilibrium Potential-pH diagram for iron in water	83
2.6 Mechanism of pitting corrosion of iron in aqueous solutions containing chloride	83
3.1 Pore solution expression device	99
3.2 Schematic representation of pore solution expression device	99
3.3 EC & G FieldCorr Portable Corrosion Analyser	100
3.4 35mm camera mounted on a copy stand	100
3.5 JVC video camera with digital image capture facility	101
3.6 Profile grinding of a cylindrical core	101
3.7 Dionex DX-500 ion chromatography system	102
3.8 Philips X-ray diffractometer	102
3.9 Geometric arrangement of X-ray diffractometer	103
3.10 PL Thermal Sciences STA 1500	103
3.11 Micromeritics Pore Sizer 9310	104
3.12 Vaisala HM 34 Humidity and Temperature Meter	104
4.1 Mild steel bar ready for immersion in model electrolyte	127

4.2	Titanium mesh counter electrode	127
4.3	Schematic diagram of the cell assembly	128
4.4	Photograph showing experimental set-up for the immersion tests	128
4.5	Schematic plan of experimental set-up for the immersion tests	129
4.6	Icorr versus time for mild steel bars immersed for 42 days in air-saturated aqueous solutions of de-ionised water with various additions of sodium nitrite	130
4.7	Ecorr versus time for mild steel bars immersed for 42 days in air-saturated aqueous solutions of de-ionised water with various additions of sodium nitrite	130
4.8	Icorr versus time for mild steel bars immersed for 42 days in air-saturated aqueous solutions of de-ionised water with 0.01M sodium chloride and various additions of sodium nitrite	131
4.9	Ecorr versus time for mild steel bars immersed for 42 days in air-saturated aqueous solutions of de-ionised water with 0.01M sodium chloride and various additions of sodium nitrite	131
4.10	Icorr versus time for mild steel bars immersed for 42 days in air-saturated aqueous solutions of de-ionised water with 0.1M sodium chloride and various additions of sodium nitrite	132
4.11	Ecorr versus time for mild steel bars immersed for 42 days in air-saturated aqueous solutions of de-ionised water with 0.1M sodium chloride and various additions of sodium nitrite	132
4.12	Icorr versus time for mild steel bars immersed for 42 days in air-saturated aqueous solutions of 0.1M sodium hydroxide with various additions of sodium nitrite	133
4.13	Ecorr versus time for mild steel bars immersed for 42 days in air-saturated aqueous solutions of 0.1M sodium hydroxide with various additions of sodium nitrite	133

4.14	Icorr versus time for mild steel bars immersed for 42 days in air-saturated aqueous solutions of 0.1M sodium hydroxide with 0.1M sodium chloride and various additions of sodium nitrite	134
4.15	Ecorr versus time for mild steel bars immersed for 42 days in air-saturated aqueous solutions of 0.1M sodium hydroxide with 0.1M sodium chloride and various additions of sodium nitrite	134
4.16	Icorr versus time for mild steel bars immersed for 42 days in air-saturated aqueous solutions of 0.1M sodium hydroxide with 1.0M sodium chloride and various additions of sodium nitrite	135
4.17	Ecorr versus time for mild steel bars immersed for 42 days in air-saturated aqueous solutions of 0.1M sodium hydroxide with 1.0M sodium chloride and various additions of sodium nitrite	135
4.18	Ecorr versus Icorr for mild steel bars immersed for 42 days in air-saturated aqueous solutions of de-ionised water with varying amounts sodium chloride and sodium nitrite	136
4.19	Ecorr versus Icorr for mild steel bars immersed for 42 days in air-saturated aqueous solutions of 0.1M sodium hydroxide with varying amounts sodium chloride and sodium nitrite	136
4.20	Icorr versus time for mild steel bars immersed for 42 days in air-saturated aqueous solutions of de-ionised water with various additions of sodium monofluorophosphate	137
4.21	Ecorr versus time for mild steel bars immersed for 42 days in air-saturated aqueous solutions of de-ionised water with various additions of sodium monofluorophosphate	137
4.22	Icorr versus time for mild steel bars immersed for 42 days in air-saturated aqueous solutions of de-ionised water with 0.01M sodium chloride and various additions of sodium monofluorophosphate	138
4.23	Ecorr versus time for mild steel bars immersed for 42 days in air-saturated aqueous solutions of de-ionised water with 0.01M sodium chloride and various additions of sodium monofluorophosphate	138



4.24	Icorr versus time for mild steel bars immersed for 42 days in air-saturated aqueous solutions of de-ionised water with 0.1M sodium chloride and various additions of sodium monofluorophosphate	139
4.25	Ecorr versus time for mild steel bars immersed for 42 days in air-saturated aqueous solutions of de-ionised water with 0.1M sodium chloride and various additions of sodium monofluorophosphate	139
4.26	Icorr versus time for mild steel bars immersed for 42 days in air-saturated aqueous solutions of 0.1M sodium hydroxide with various additions of sodium monofluorophosphate	140
4.27	Ecorr versus time for mild steel bars immersed for 42 days in air-saturated aqueous solutions of 0.1M sodium hydroxide with various additions of sodium monofluorophosphate	140
4.28	Icorr versus time for mild steel bars immersed for 42 days in air-saturated aqueous solutions of 0.1M sodium hydroxide with 0.1M sodium chloride and various additions of sodium monofluorophosphate	141
4.29	Ecorr versus time for mild steel bars immersed for 42 days in air-saturated aqueous solutions of 0.1M sodium hydroxide with 0.1M sodium chloride and various additions of sodium monofluorophosphate	141
4.30	Icorr versus time for mild steel bars immersed for 42 days in air-saturated aqueous solutions of 0.1M sodium hydroxide with 1.0M sodium chloride and various additions of sodium monofluorophosphate	142
4.31	Ecorr versus time for mild steel bars immersed for 42 days in air-saturated aqueous solutions of 0.1M sodium hydroxide with 1.0M sodium chloride and various additions of sodium monofluorophosphate	142
4.32	Ecorr versus Icorr for mild steel bars immersed for 42 days in air-saturated aqueous solutions of de-ionised water with varying amounts sodium chloride and sodium monofluorophosphate	143
4.33	Ecorr versus Icorr for mild steel bars immersed for 42 days in air-saturated aqueous solutions of 0.1M sodium hydroxide with varying amounts sodium chloride and sodium monofluorophosphate	143

4.34	Icorr versus time for mild steel bars immersed for 42 days in air-saturated aqueous solutions of de-ionised water with various additions of an alkanolamine-based inhibitor	144
4.35	Ecorr versus time for mild steel bars immersed for 42 days in air-saturated aqueous solutions of de-ionised water with various additions of an alkanolamine-based inhibitor	144
4.36	Icorr versus time for mild steel bars immersed for 42 days in air-saturated aqueous solutions of de-ionised water with 0.01M sodium chloride and various additions of an alkanolamine-based inhibitor	145
4.37	Ecorr versus time for mild steel bars immersed for 42 days in air-saturated aqueous solutions of de-ionised water with 0.01M sodium chloride and various additions of an alkanolamine-based inhibitor	145
4.38	Icorr versus time for mild steel bars immersed for 42 days in air-saturated aqueous solutions of de-ionised water with 0.1M sodium chloride and various additions of an alkanolamine-based inhibitor	146
4.39	Ecorr versus time for mild steel bars immersed for 42 days in air-saturated aqueous solutions of de-ionised water with 0.1M sodium chloride and various additions of an alkanolamine-based inhibitor	146
4.40	Icorr versus time for mild steel bars immersed for 42 days in air-saturated aqueous solutions of 0.1M sodium hydroxide with various additions of an alkanolamine-based inhibitor	147
4.41	Ecorr versus time for mild steel bars immersed for 42 days in air-saturated aqueous solutions of 0.1M sodium hydroxide with various additions of an alkanolamine-based inhibitor	147
4.42	Icorr versus time for mild steel bars immersed for 42 days in air-saturated aqueous solutions of 0.1M sodium hydroxide with 0.1M sodium chloride and various additions of an alkanolamine-based inhibitor	148
4.43	Ecorr versus time for mild steel bars immersed for 42 days in air-saturated aqueous solutions of 0.1M sodium hydroxide with 0.1M sodium chloride and various additions of an alkanolamine-based inhibitor	148



4.44	Icorr versus time for mild steel bars immersed for 42 days in air-saturated aqueous solutions of 0.1M sodium hydroxide with 1.0M sodium chloride and various additions of an alkanolamine-based inhibitor	149
4.45	Ecorr versus time for mild steel bars immersed for 42 days in air-saturated aqueous solutions of 0.1M sodium hydroxide with 1.0M sodium chloride and various additions of an alkanolamine-based inhibitor	149
4.46	Ecorr versus Icorr for mild steel bars immersed for 42 days in air-saturated aqueous solutions of de-ionised water with varying amounts sodium chloride and an alkanolamine-based inhibitor	150
4.47	Ecorr versus Icorr for mild steel bars immersed for 42 days in air-saturated aqueous solutions of 0.1M sodium hydroxide with varying amounts sodium chloride and an alkanolamine-based inhibitor	150
4.48	Icorr versus time for mild steel bars immersed for 42 days in air-saturated aqueous solutions of de-ionised water with various additions of ethanolamine	151
4.49	Ecorr versus time for mild steel bars immersed for 42 days in air-saturated aqueous solutions of de-ionised water with various additions of ethanolamine	151
4.50	Icorr versus time for mild steel bars immersed for 42 days in air-saturated aqueous solutions of de-ionised water with 0.01M sodium chloride and various additions of ethanolamine	152
4.51	Ecorr versus time for mild steel bars immersed for 42 days in air-saturated aqueous solutions of de-ionised water with 0.01M sodium chloride and various additions of ethanolamine	152
4.52	Icorr versus time for mild steel bars immersed for 42 days in air-saturated aqueous solutions of de-ionised water with 0.1M sodium chloride and various additions of ethanolamine	153
4.53	Ecorr versus time for mild steel bars immersed for 42 days in air-saturated aqueous solutions of de-ionised water with 0.1M sodium chloride and various additions of ethanolamine	153
4.54	Icorr versus time for mild steel bars immersed for 42 days in air-saturated aqueous solutions of 0.1M sodium hydroxide with various additions of ethanolamine	154

4.55	Ecorr versus time for mild steel bars immersed for 42 days in air-saturated aqueous solutions of 0.1M sodium hydroxide with various additions of ethanolamine	154
4.56	Icorr versus time for mild steel bars immersed for 42 days in air-saturated aqueous solutions of 0.1M sodium hydroxide with 0.1M sodium chloride and various additions of ethanolamine	155
4.57	Ecorr versus time for mild steel bars immersed for 42 days in air-saturated aqueous solutions of 0.1M sodium hydroxide with 0.1M sodium chloride and various additions of ethanolamine	155
4.58	Icorr versus time for mild steel bars immersed for 42 days in air-saturated aqueous solutions of 0.1M sodium hydroxide with 1.0M sodium chloride and various additions of ethanolamine	156
4.59	Ecorr versus time for mild steel bars immersed for 42 days in air-saturated aqueous solutions of 0.1M sodium hydroxide with 1.0M sodium chloride and various additions of ethanolamine	156
4.60	Ecorr versus Icorr for mild steel bars immersed for 42 days in air-saturated aqueous solutions of de-ionised water with varying amounts sodium chloride and ethanolamine	157
4.61	Ecorr versus Icorr for mild steel bars immersed for 42 days in air-saturated aqueous solutions of 0.1M sodium hydroxide with varying amounts sodium chloride and ethanolamine	157
4.62	Comparison of corrosion rates, after 42 days, for mild steel bars immersed in air-saturated aqueous solutions of de-ionised water with various additions of inhibitors	158
4.63	Comparison of corrosion rates, after 42 days, for mild steel bars immersed in air-saturated aqueous solutions of 0.01M sodium chloride and various additions of inhibitors	158
4.64	Comparison of corrosion rates, after 42 days, for mild steel bars immersed in air-saturated aqueous solutions of 0.1M sodium chloride and various additions of inhibitors	159



4.65	Comparison of corrosion rates, after 42 days, for mild steel bars immersed in air-saturated aqueous solutions of 0.1M sodium hydroxide and various additions of inhibitors	159
4.66	Comparison of corrosion rates, after 42 days, for mild steel bars immersed in air-saturated aqueous solutions of 0.1M sodium hydroxide with 0.1M sodium chloride and various additions of inhibitors	160
4.67	Comparison of corrosion rates, after 42 days, for mild steel bars immersed in air-saturated aqueous solutions of 0.1M sodium hydroxide with 1.0M sodium chloride and various additions of inhibitors	160
4.68	Weight loss (experimental and theoretical) versus inhibitor concentration for mild steel bars immersed for 42 days in solutions of de-ionised water with various additions of sodium nitrite	161
4.69	Weight loss (experimental and theoretical) versus inhibitor concentration for mild steel bars immersed for 42 days in solutions of 0.01M sodium chloride and various additions of sodium nitrite	161
4.70	Weight loss (experimental and theoretical) versus inhibitor concentration for mild steel bars immersed for 42 days in solutions of 0.1M sodium chloride and various additions of sodium nitrite	162
4.71	Weight loss (experimental and theoretical) versus inhibitor concentration for mild steel bars immersed for 42 days in solutions of 0.1M sodium hydroxide with various additions of sodium nitrite	162
4.72	Weight loss (experimental and theoretical) versus inhibitor concentration for mild steel bars immersed for 42 days in solutions of 0.1M sodium hydroxide with 0.1M sodium chloride and various additions of sodium nitrite	163
4.73	Weight loss (experimental and theoretical) versus inhibitor concentration for mild steel bars immersed for 42 days in solutions of 0.1M sodium hydroxide with 1.0M sodium chloride and various additions of sodium nitrite	163
4.74	Weight loss (experimental and theoretical) versus inhibitor concentration for mild steel bars immersed for 42 days in solutions of de-ionised water with various additions of sodium monofluorophosphate	164



4.75	Weight loss (experimental and theoretical) versus inhibitor concentration for mild steel bars immersed for 42 days in solutions of 0.01M sodium chloride and various additions of sodium monofluorophosphate	164
4.76	Weight loss (experimental and theoretical) versus inhibitor concentration for mild steel bars immersed for 42 days in solutions of 0.1M sodium chloride and various additions of sodium monofluorophosphate	165
4.77	Weight loss (experimental and theoretical) versus inhibitor concentration for mild steel bars immersed for 42 days in solutions of 0.1M sodium hydroxide with various additions of sodium monofluorophosphate	165
4.78	Weight loss (experimental and theoretical) versus inhibitor concentration for mild steel bars immersed for 42 days in solutions of 0.1M sodium hydroxide with 0.1M sodium chloride and various additions of sodium monofluorophosphate	166
4.79	Weight loss (experimental and theoretical) versus inhibitor concentration for mild steel bars immersed for 42 days in solutions of 0.1M sodium hydroxide with 1.0M sodium chloride and various additions of sodium monofluorophosphate	166
4.80	Weight loss (experimental and theoretical) versus inhibitor concentration for mild steel bars immersed for 42 days in solutions of de-ionised water with various additions of an alkanolamine-based inhibitor	167
4.81	Weight loss (experimental and theoretical) versus inhibitor concentration for mild steel bars immersed for 42 days in solutions of 0.01M sodium chloride and various additions of an alkanolamine-based inhibitor	167
4.82	Weight loss (experimental and theoretical) versus inhibitor concentration for mild steel bars immersed for 42 days in solutions of 0.1M sodium chloride and various additions of an alkanolamine-based inhibitor	168
4.83	Weight loss (experimental and theoretical) versus inhibitor concentration for mild steel bars immersed for 42 days in solutions of 0.1M sodium hydroxide with various additions of an alkanolamine-based inhibitor	168
4.84	Weight loss (experimental and theoretical) versus inhibitor concentration for mild steel bars immersed for 42 days in solutions of 0.1M sodium hydroxide with 0.1M sodium chloride and various additions of an alkanolamine-based inhibitor	169

4.85	Weight loss (experimental and theoretical) versus inhibitor concentration for mild steel bars immersed for 42 days in solutions of 0.1M sodium hydroxide with 1.0M sodium chloride and various additions of an alkanolamine-based inhibitor	169
4.86	Weight loss (experimental and theoretical) versus inhibitor concentration for mild steel bars immersed for 42 days in solutions of de-ionised water with various additions of ethanolamine	170
4.87	Weight loss (experimental and theoretical) versus inhibitor concentration for mild steel bars immersed for 42 days in solutions of 0.01M sodium chloride and various additions of ethanolamine	170
4.88	Weight loss (experimental and theoretical) versus inhibitor concentration for mild steel bars immersed for 42 days in solutions of 0.1M sodium chloride and various additions of ethanolamine	171
4.89	Weight loss (experimental and theoretical) versus inhibitor concentration for mild steel bars immersed for 42 days in solutions of 0.1M sodium hydroxide with various additions of ethanolamine	171
4.90	Weight loss (experimental and theoretical) versus inhibitor concentration for mild steel bars immersed for 42 days in solutions of 0.1M sodium hydroxide with 0.1M sodium chloride and various additions of ethanolamine	172
4.91	Weight loss (experimental and theoretical) versus inhibitor concentration for mild steel bars immersed for 42 days in solutions of 0.1M sodium hydroxide with 1.0M sodium chloride and various additions of ethanolamine	172
4.92	Comparison of experimentally-determined weight loss measurements for mild steel bars immersed for 42 days in solutions of de-ionised water with various additions of inhibitors	173
4.93	Comparison of experimentally-determined weight loss measurements for mild steel bars immersed for 42 days in solutions of 0.01M sodium chloride with various additions of inhibitors	173
4.94	Comparison of experimentally-determined weight loss measurements for mild steel bars immersed for 42 days in solutions of 0.1M sodium chloride with various additions of inhibitors	174



4.95	Comparison of experimentally-determined weight loss measurements for mild steel bars immersed for 42 days in solutions of 0.1M sodium hydroxide with various additions of inhibitors	174
4.96	Comparison of experimentally-determined weight loss measurements for mild steel bars immersed for 42 days in solutions of 0.1M sodium hydroxide with 0.1M sodium chloride and various additions of inhibitors	175
4.97	Comparison of experimentally-determined weight loss measurements for mild steel bars immersed for 42 days in solutions of 0.1M sodium hydroxide with 1.0M sodium chloride and various additions of inhibitors	175
4.98	Bar, after removal of corrosion products, following immersion in de-ionised water	176
4.99	Bar, after removal of corrosion products, following immersion in 0.01M sodium chloride	176
4.100	Bar, after removal of corrosion products, following immersion in 0.1M sodium chloride	177
4.101	Typical pit on bar, after removal of corrosion products, following immersion in 0.1M sodium hydroxide with 1.0M sodium chloride	177
4.102	Bar, after removal of corrosion products, following immersion in 0.1M sodium hydroxide with 0.1M sodium chloride and 0.01M sodium nitrite	178
4.103	Bar, after removal of corrosion products, following immersion in 0.1M sodium hydroxide with 0.1M sodium chloride and 0.1M sodium nitrite	178
4.104	Bar, after removal of corrosion products, following immersion in 0.1M sodium hydroxide with 1.0M sodium chloride and 0.01M sodium nitrite	179
4.105	Bar, after removal of corrosion products, following immersion in 0.1M sodium hydroxide with 1.0M sodium chloride and 0.1M sodium nitrite	179
4.106	Bar, after removal of corrosion products, following immersion in 0.01M sodium chloride with 0.1M sodium monofluorophosphate	180

4.107	Bar, after removal of corrosion products, following immersion in 0.1M sodium chloride with 1.0M sodium monofluorophosphate	180
4.108	Bar, after removal of corrosion products, following immersion in 0.1M sodium hydroxide with 0.1M sodium chloride and 0.1M sodium monofluorophosphate	181
4.109	Bar, after removal of corrosion products, following immersion in 0.1M sodium hydroxide with 1.0M sodium chloride and 0.1M sodium monofluorophosphate	181
4.110	Bar, after removal of corrosion products, following immersion in 0.01M sodium chloride with 0.01M alkanolamine-based inhibitor	182
4.111	Bar, after removal of corrosion products, following immersion in 0.1M sodium chloride with 0.01M alkanolamine-based inhibitor	182
4.112	Bar, after removal of corrosion products, following immersion in 0.1M sodium chloride with 0.1M alkanolamine-based inhibitor	183
4.113	Bar, after removal of corrosion products, following immersion in 0.1M sodium chloride with 1.0M alkanolamine-based inhibitor	183
4.114	Bar, after removal of corrosion products, following immersion in 0.1M sodium hydroxide with 1.0M sodium chloride and 0.01M alkanolamine-based inhibitor	184
4.115	Bar, after removal of corrosion products, following immersion in 0.1M sodium chloride with 1.0M ethanolamine	184
5.1	Photograph of structure	191
5.2	Typical section of core showing depth of carbonation	191
5.3	Penetration profile for chloride in site concrete (water extraction method)	192
5.4	Penetration profile for phosphate in site concrete treated with sodium monofluorophosphate corrosion inhibitor (water extraction)	192
5.5	Penetration profile for fluoride in site concrete treated with sodium monofluorophosphate corrosion inhibitor (water extraction method)	193
5.6	Penetration profile for ethanolamine in site concrete treated with an alkanolamine-based corrosion inhibitor (water extraction method)	193



5.7	Penetration profile for ethanolamine in site concrete treated with an alkanolamine-based corrosion inhibitor (acid extraction method)	194
5.8	Penetration profile for phosphate in site concrete treated with an alkanolamine-based inhibitor (acid extraction method)	194
6.1	Experimental set-up used for the carbonation of cement pastes	209
6.2	Water desorption results for hydrated cement paste carbonated over saturated solutions of sodium chloride with various carbon dioxide concentrations	209
6.3	Water desorption results for hydrated cement paste carbonated over saturated solutions of sodium nitrite with various carbon dioxide concentrations	210
6.4	Water desorption results for hydrated cement paste carbonated over saturated solutions of ammonium nitrate with various carbon dioxide concentrations	210
6.5	Water desorption results for hydrated cement paste carbonated over saturated solutions of magnesium nitrate with various carbon dioxide concentrations	211
6.6	Water desorption results for hydrated cement paste carbonated over saturated solutions of sodium dichromate with various carbon dioxide concentrations	211
6.7	Pore size distribution curves for hydrated cement pastes carbonated over saturated solutions of sodium chloride with various carbon dioxide concentrations	212
6.8	Pore size distribution curves for hydrated cement pastes carbonated over saturated solutions of sodium nitrite with various carbon dioxide concentrations	212
6.9	Pore size distribution curves for hydrated cement pastes carbonated over saturated solutions of ammonium nitrate with various carbon dioxide concentrations	213
6.10	Pore size distribution curves hydrated cement pastes carbonated over saturated solutions of magnesium nitrate with various carbon dioxide concentrations	213

6.11	Pore size distribution curves for hydrated cement pastes carbonated over saturated solutions of sodium dichromate with various carbon dioxide concentrations	214
6.12	XRD traces of hydrated cement paste carbonated over saturated solutions of sodium chloride with various concentrations of carbon dioxide	215
6.13	XRD traces of hydrated cement paste carbonated over saturated solutions of sodium nitrite with various concentrations of carbon dioxide	216
6.14	XRD traces of hydrated cement paste carbonated over saturated solutions of ammonium nitrate with various concentrations of carbon dioxide	217
6.15	XRD traces of hydrated cement paste carbonated over saturated solutions of magnesium nitrate with various concentrations of carbon dioxide	218
6.16	XRD traces of hydrated cement paste carbonated over saturated solutions of sodium dichromate with various concentrations of carbon dioxide	219
6.17	DTA/TG trace for hydrated cement paste carbonated over a saturated solution of sodium chloride with 100% carbon dioxide	220
6.18	DTA/TG trace for hydrated cement paste carbonated over a saturated solution of sodium chloride with 5% carbon dioxide	220
6.19	DTA/TG trace for hydrated cement paste carbonated over a saturated solution of sodium chloride with 0.03% carbon dioxide	220
6.20	DTA/TG trace for hydrated cement paste carbonated over a saturated solution of sodium nitrite with 100% carbon dioxide	221
6.21	DTA/TG trace for hydrated cement paste carbonated over a saturated solution of sodium nitrite with 5% carbon dioxide	221
6.22	DTA/TG trace for hydrated cement paste carbonated over a saturated solution of sodium nitrite with 0.03% carbon dioxide	221
6.23	DTA/TG trace for hydrated cement paste carbonated over a saturated solution of ammonium nitrate with 100% carbon dioxide	222
6.24	DTA/TG trace for hydrated cement paste carbonated over a saturated solution of ammonium nitrate with 5% carbon dioxide	222



6.25	DTA/TG trace for hydrated cement paste carbonated over a saturated solution of ammonium nitrate with 0.03% carbon dioxide	222
6.26	DTA/TG trace for hydrated cement paste carbonated over a saturated solution of magnesium nitrate with 100% carbon dioxide	223
6.27	DTA/TG trace for hydrated cement paste carbonated over a saturated solution of magnesium nitrate with 5% carbon dioxide	223
6.28	DTA/TG trace for hydrated cement paste carbonated over a saturated solution of magnesium nitrate with 0.03% carbon dioxide	223
6.29	DTA/TG trace for hydrated cement paste carbonated over a saturated solution of sodium dichromate with 100% carbon dioxide	224
6.30	DTA/TG trace for hydrated cement paste carbonated over a saturated solution of sodium dichromate with 5% carbon dioxide	224
6.31	DTA/TG trace for hydrated cement paste carbonated over a saturated solution of sodium dichromate with 0.03% carbon dioxide	224
6.32	TG mass loss results for hydrated cement paste carbonated over saturated solutions of sodium chloride with various carbon dioxide concentrations	225
6.33	TG mass loss results for hydrated cement paste carbonated over saturated solutions of sodium nitrite with various carbon dioxide concentrations	225
6.34	TG mass loss for hydrated cement paste carbonated over saturated solutions of ammonium nitrate with various carbon dioxide concentrations	226
6.35	TG mass loss results for hydrated cement paste carbonated over saturated solutions of magnesium nitrate with various carbon dioxide concentrations	226
6.36	TG mass loss results for hydrated cement paste carbonated over saturated solutions of sodium dichromate with various carbon dioxide concentrations	227
7.1	Set-up number 1	244
7.2	Set-up number 2	244

7.3	Set-up number 3	244
7.4	Set-up number 4	244
7.5	Set-up number 5	245
7.6	Set-up number 6	245
7.7	Set-up number 7	245
7.8	Set-up number 8	245
7.9	Set-up number 9	246
7.10	Set-up number 10	246
7.11	Set-up number 11	246
7.12	Set-up number 12	246
7.13	Comparison of experimental and numerical results for set-up 1	247
7.14	Comparison of experimental and numerical results for set-up 2	247
7.15	Comparison of experimental and numerical results for set-up 3	248
7.16	Comparison of experimental and numerical results for set-up 4	248
7.17	Comparison of experimental and numerical results for set-up 5	249
7.18	Comparison of experimental and numerical results for set-up 6	249
7.19	Comparison of experimental and numerical results for set-up 7	250
7.20	Comparison of experimental and numerical results for set-up 8	250
7.21	Comparison of experimental and numerical results for set-up 9	251
7.22	Comparison of experimental and numerical results for set-up 10	251
7.23	Comparison of experimental and numerical results for set-up 11	252
7.24	Comparison of experimental and numerical results for set-up 12	252



8.1	Set-up A	269
8.2	Set-up B	269
8.3	Set-up C	269
8.4	Set-up D	270
8.5	Set-up E	270
8.6	Set-up F	270
8.7	Comparison of numerical and experimental nitrite ion profiles for set-up A	271
8.8	Comparison of numerical and experimental nitrite ion profiles for set-up B	271
8.9	Comparison of numerical and experimental nitrite ion profiles for set-up C	272
8.10	Comparison of numerical and experimental nitrite ion profiles for set-up D	272
8.11	Comparison of numerical and experimental nitrite ion profiles for set-up E	273
8.12	Comparison of numerical and experimental nitrite ion profiles for set-up F	273
8.13	Comparison of numerical and experimental hydroxyl ion profiles for set-up A	274
8.14	Comparison of numerical and experimental hydroxyl ion profiles for set-up B	274
8.15	Comparison of numerical and experimental hydroxyl ion profiles for set-up C	275
8.16	Comparison of numerical and experimental hydroxyl ion profiles for set-up D	275

8.17	Comparison of numerical and experimental hydroxyl ion profiles for set-up E	276
8.18	Comparison of numerical and experimental hydroxyl ion profiles for set-up F	276
8.19	Comparison of numerical and experimental chloride ion profiles for set-up A	277
8.20	Comparison of numerical and experimental chloride ion profiles for set-up B	277
8.21	Comparison of numerical and experimental chloride ion profiles for set-up C	278
8.22	Comparison of numerical and experimental chloride ion profiles for set-up D	278
8.23	Comparison of numerical and experimental chloride ion profiles for set-up E	279
8.24	Comparison of numerical and experimental chloride ion profiles for set-up F	279
8.25	Comparison of experimentally determined sulphate ion profiles for set-ups A, B and C	280
8.26	Comparison of experimentally determined sulphate ion profiles for set-ups D, E and F	280
8.27	Comparison of experimentally determined nitrate ion profiles for set-ups A, B and C	281
8.28	Comparison of experimentally determined nitrate ion profiles for set-ups D, E and F	281
8.29	Comparison of experimentally determined sodium ion profiles for set-ups A, B and C	282
8.30	Comparison of experimentally determined sodium ion profiles for set-ups D, E and F	282
8.31	Comparison of experimentally determined potassium ion profiles for set-ups A, B and C	283

8.32	Comparison of experimentally determined potassium ion profiles for set-ups D, E and F	283
8.33	Comparison of experimentally determined calcium ion profiles for set-ups A, B and C	284
8.34	Comparison of experimentally determined calcium ion profiles for set-ups D, E and F	284

## **CHAPTER ONE**

### **INTRODUCTION**

#### **1.1 HISTORICAL NOTE**

Concrete is derived from the Latin word 'concretus' meaning compounded. Concrete is a composite material made from mixing cement (usually a Portland cement or a blended cement which includes a combination of cementitious materials) plus fine aggregate (sand or gravel) plus coarse aggregate (crushed rocks or stone) plus water, all in given proportions, which are hydraulically bound together by the cement, i.e. the cement sets and hardens by virtue of a chemical reaction with the water. The earliest known example of concrete was a floor discovered in Yitah El in southern Galilee, Israel, dating around 7000 BC (British Cement Association, 1999). It consists of lime, made from burning limestone, which when mixed with water and stone set to form an early concrete.

The Romans employed lime as the first binding material to be used extensively in the ancient world for construction, having been produced by burning chalk or limestone with an appropriate fuel like charcoal, originally in the open and later in small, crude vertical kilns (Bensted, 1997). The lime along with water was added to sand and crushed stone or brick and broken tiles (Neville, 1995). Some of the Roman structures in which masonry was bonded by mortar, such as the Coliseum in Rome and the Pont du Gard near Nimes, have survived to this day, with the cementitious material still hard and firm. In the ruins of Pompeii, the mortar is often less weathered than the rather soft stone (Neville, 1987). The first technical specification for lime was written by Vitruvius, a famous Roman engineer and architect, in his work 'De Architectura', in the time of the emperor Augustus (63 BC - 14 AD).



Lime, even nearly 2000 years ago, was mixed with other ingredients such as natural pozzolana. This term was used to describe a powdered volcanic rock containing silica and alumina and it was named after the Pozzouli area of southern Italy where it had first been utilised. The term also covers materials such as santorin earth from Santorini, a Greek island and trass from southern Germany. The purpose of using these additives was to produce a better binding hydraulic lime.

The Romans brought an improved knowledge of lime production to Britain, however, hydraulic limes were not specifically used in Britain for many centuries after the decline of the Roman Empire. An advancement of knowledge was made in 1756 when John Smeaton, upon being commissioned to build a new lighthouse on Eddystone Rock off the Cornish coast, investigated in depth what would be the best building materials to use for the severe conditions involved. The conclusion of his investigations was that the best mortar was produced when pozzolana was mixed with lime that contained a high amount of clayey matter. By recognising the role of the clay, hitherto considered undesirable, Smeaton was the first to understand the chemical properties of hydraulic lime and his construction proved to be very successful.

In England in 1796, 'Roman Cement' was developed by James Parker. It was made by the calcination of argillaceous (clay-containing) limestone. This was the forerunner of Portland Cement. Roman cement was closely followed around 1800 by the production of what were termed 'natural cements', in France and the United States, from natural rocks.

Portland cement first appeared in 1824 when Joseph Aspdin, who described himself as a bricklayer from Leeds in his patent application, was granted the patent for producing Portland cement which was used for concrete to construct the Thames Tunnel the same year. This cement was produced by heating a mixture of finely-divided clay and hard limestone in a furnace until carbon dioxide had been driven off; this temperature was



much lower than that necessary for partial fusion required to cause clinkering. Aspdin named his product Portland cement because its colour resembled that of Portland stone, which had been quarried for centuries at Portland in Dorset. Construction altered rapidly when Portland cement appeared and concrete became the most widely used construction material. The prototype of modern cement was made in 1845 by Isaac Johnson, who burnt a mixture of clay and chalk until clinkering, so that the reactions necessary for the formation of strongly cementitious compounds took place (Neville, 1995).

Since the mid-19<sup>th</sup> century Portland cements, made by fusing limestone and clay to form a clinker and grinding the product with small quantities of gypsum (a retarder of early hydration), have been used for the vast bulk of concrete production worldwide. Concrete is, however, relatively weak in tension and this necessitates the inclusion of mild steel bars within the concrete in order to withstand the tensile stresses that are imposed on a structure. The use of metals in Portland cement concrete occurred soon after Aspdin obtained his patent for Portland cement. Brunel employed metal reinforcement in 1832 for a tunnel under the Thames River (Draffin, 1976). Aspdin's son, William, reinforced the concrete of a boundary wall at Portland Hall in 1850 (Idorn and Thaulow, 1983).

Patents for reinforced concrete were taken out in England as early as 1788, but there is no evidence that they were ever put into practice, and the concrete was not made with Portland cement (Kromer, 1993). A Newcastle builder called William Wilkinson patented the idea of reinforced concrete in 1854 for a concrete beam. However, Monier, a Parisian gardener is generally credited with the 'invention of reinforced concrete' via his patent in 1867 (Sigalov and Strongin, 1962). The principal American patent for reinforced concrete was granted to Thaddeus Hyatt in 1878 (Hime, 1994). This pioneer inventor was the first to outline principles by stating specifically that the steel must be able to resist sufficient tensile stress to balance the compressive stress to the concrete.

Frenchman Francois Hennebique is widely regarded as the most influential pioneer of reinforced concrete and, after being granted his first patent in 1892, he built the first reinforced concrete frame building in Britain at Weaver's Mill, Swansea. At the beginning of this century his patented 'Beton Arme' system was a huge commercial success and dominated the world market. Hennebique attracted to his fold many bright students and those engineers who graduated through his 'school' were sent to various parts of the world to act as his agents, designing and supervising reinforced concrete construction. The agent in Britain was L.G. Mouchel, founder of one of the country's largest firms of consultants (McBeth, 1998).

Reinforced concrete itself is, in the main, very durable, versatile and economic and this along with its exceptional load bearing capacity has led to its present reputation as a very successful composite construction material.

## **1.2 FIELD OF STUDY**

In recent years, the durability of reinforced concrete structures has been a subject under constant investigation. There are several forms of degradation of reinforced concrete and they can be classed into three main categories, physical degradation, chemical degradation and corrosion of the steel. Physical forms of degradation include freeze-thaw attack, abrasion, effects of high temperatures and differences in thermal expansion of the aggregate and of the hardened cement paste. Chemical forms of degradation of reinforced concrete include alkali-aggregate reaction, sulphate attack (including the recently discovered thaumasite form of sulphate attack), acid attack and delayed ettringite formation. Corrosion of steel in concrete represents the most common and serious form of degradation of reinforced concrete structures and the economic loss and damage caused by the corrosion of steel in concrete makes it arguably the largest single infrastructure problem facing industrialised countries.



When steel is embedded in dense concrete of good quality it is surrounded by a hydrated cement matrix with a pore electrolyte phase that has a pH value in the range of 13-14 (Page, 1999a). In this highly alkaline environment the steel will form and maintain an invisibly thin passive ferric oxide film on its surface. This film acts as a barrier to metal dissolution and chemical attack and therefore protects the steel from corroding at an appreciable rate in good quality concrete. However, in the early 1970's, it became obvious to engineers throughout the world that many reinforced concrete structures were deteriorating due to the corrosion of embedded steel, and thus would not last as long as was intended in their design.

Metallic corrosion is an electrochemical process, as was shown by U.R. Evans and co-workers in a series of pioneering researches initiated in the 1920's (Page, 1998). Corrosion occurs when a metal reacts with chemical species in the environment, e.g. oxygen and water, to form a compound. The depassivation of steel embedded in concrete is attributed mainly to three processes, i.e. cathodically restrained dissolution, carbonation and chloride attack. Cathodically restrained dissolution occurs in fully submerged structures where a lack of oxygen is apparent. This type of corrosion is associated with very low corrosion rates and is therefore not a major concern. However, carbonation and chloride attack are associated with much higher corrosion rates and are therefore the cause of great concern to those who own, use and operate structures. Carbonation leads to neutralisation of the pore solution phase of the concrete and in this type of environment the passive film on the steel cannot be maintained, thus allowing corrosion to proceed on the unprotected steel. Chloride attack occurs due to chloride ions that may be present in concrete either as constituents of the original mix materials or as external contaminants such as seawater and de-icing salts. Chloride ions attack the steel at defects in the passive film and this type of attack leads to localised rapid loss of cross section.

One American estimate is that \$150 billion worth of damage on their interstate highway bridges is attributed to corrosion. In a Transportation Research Record Report on the costs of de-icing (Transportation Research Record, 1991) the annual cost of bridge deck repairs was estimated to be between \$50 - \$200 million, with substructures and other components requiring \$100 million a year and a further \$50 to \$150 million a year on multi-storey car parks. In the United Kingdom, the Highways Agency estimated corrosion damage to total £616.5 million on motorway and trunk road bridges in England and Wales alone (Wallbank, 1989). These bridges represent only 10% of the total bridge inventory (Broomfield, 1997). The statistics for Europe, the Asian Pacific countries and Australia are similar. In the Middle East, reinforced concrete structures have had very short lifespans due to the severe environmental conditions of a warm climate and saline ground waters (Rasheeduzzafar et al., 1992).

It is not just the financial burden due to the corrosion of reinforcing steel that is a problem. Corrosion of steel in concrete is an expansive process that can lead to cracking and spalling of the concrete cover which, alone, can cause damage and even loss of life to the public. Chloride attack on post-tensioned tendons can lead to rapid loss of cross section and can therefore cause a catastrophic failure that, can also have fatal consequences.

During the 1960s, attempts were made to quantify the problem and from the 1970s the concrete repair industry has come up with various solutions for the control of corrosion of steel in concrete. These techniques can be classed into two main groups, i.e. electrochemical and non-electrochemical techniques. Electrochemical techniques include cathodic protection, cathodic prevention, electrochemical chloride extraction and electrochemical realkalisation. Non-electrochemical techniques include concrete modification, patch repair, protective coatings, silane and siloxane treatment, fusion bonded epoxy coated rebar, galvanised reinforcement, stainless steel reinforcement and



corrosion inhibitors. Some of these techniques are preventative measures whilst others are involved in the rehabilitation of structures.

The traditional approach for the rehabilitation of reinforced concrete is known as patch repair which involves removing the contaminated concrete, cleaning the exposed steel and replacing the concrete with a repair mortar. However, this approach, even if carried out efficiently, can be time consuming, disruptive and expensive. In addition, chlorides which have been left in the surrounding concrete could develop what is known as incipient anode activation (Vassie, 1984) which can lead to further corrosion in areas previously corrosion free. Incompatibility of the repair material with the original concrete can result in shrinkage which, in turn, can then lead to further chloride penetration (Keer, Chadwick and Thompson, 1990). Other methods that have become popular within the concrete repair industry involve stopping the corrosion via electrochemical methods such as cathodic protection and electrochemical chloride extraction. These methods can be expensive and they also require monitoring for the remaining service life of a structure.

Since the 1970s, corrosion inhibitors have been used as admixtures for new structures as a preventative measure. In terms of reinforced concrete, corrosion inhibitors are chemicals that cause changes at the steel/concrete interface which result in a reduction of the overall corrosion rate. One such inhibitor, calcium nitrite, has been tested extensively as a corrosion inhibiting admixture and has been applied to over 300 parking, marine and highway structures in the USA (Berke and Weil, 1994). More recently, researchers and producers of corrosion inhibitors have been investigating the possibility of applying these substances to stop corrosion on existing structures. There are now several commercially available proprietary repair systems that involve the inhibitors being applied as coatings on the concrete surface, applied into drilled holes in the concrete cover or incorporated into concrete overlays. The advantages of using corrosion inhibitors for the rehabilitation of reinforced concrete include reduced costs,

reduced pollution and reduced inconvenience to the owners and users of structures that may occur when other techniques are employed.

### **1.3 OBJECTIVES OF STUDY**

The purpose of this study is to answer questions regarding phenomena that are intrinsically linked to the application of corrosion inhibitors as a rehabilitation technique for reinforced concrete structures that are suffering from reinforcement corrosion.

Corrosion inhibitors can be generally classed into three categories i.e. anodic, cathodic and mixed. Their mechanisms of action vary widely and so do their inhibitive inefficiencies when used at different concentrations in contact with steel surfaces of variable initial conditions. This is significant because inhibitors, although they are claimed to penetrate the concrete easily and thus protect all the steel, may not only fail to provide adequate protection to the steel unless their concentrations are maintained at appropriate levels, but they may also stimulate intense pitting corrosion under adverse circumstances or cause enhanced susceptibility to other forms of concrete degradation such as alkali-silica reaction. Many questions involving corrosion inhibitors are unanswered by the existing literature. There is also a shortage of publications obtained from independent research in this field. The present study has therefore been carried out with the following objectives:

- (1) To present a critical appreciation of existing knowledge in the field of corrosion inhibitors for the rehabilitation of reinforced concrete and to evaluate the efficiency of some of the more promising inhibitor systems.
- (2) To establish whether the inhibitors investigated behave as anodic, cathodic or mixed inhibitors in air-saturated neutral and alkaline aqueous solutions with varying additions of chloride ions.



- (3) To gain an insight into the concentrations of inhibitors required for the inhibition of corrosion of steel in air-saturated neutral and alkaline aqueous solutions with varying additions of chloride ions. This may establish whether pitting is stimulated if inhibitor concentrations are not sufficient to inhibit corrosion fully.
- (4) To determine, by means of medium term site trials, how far two inhibitors and/or their decomposition products penetrate into concrete when surface applied. This may provide an indication of the sort of concentration profile one may expect to obtain under similar conditions.
- (5) To quantify the influence of the carbonating atmosphere on the pore solution chemistry and the microstructure of hydrated cement paste. This may clarify whether the accelerated carbonation regimes, required to produce carbonated cement paste for laboratory investigations over reasonable timescales, may affect the corrosion-related properties of concretes.
- (6) To carry out laboratory investigations into physical realkalisation of carbonated hydrated cement paste. This type of repair system involves the provision of an alkaline cement-based mortar layer over the entire surface of a carbonated structure.
- (7) To present a mathematical model to simulate the transport behaviour of hydroxyl ions in a saturated porous medium. This model will then be applied to predict the transport of hydroxyl ions associated with physical realkalisation of carbonated hydrated cement paste and the numerical results compared with those obtained experimentally.
- (8) To carry out laboratory investigations into a calcium nitrite-based corrosion rehabilitation system for chloride-contaminated hydrated cement paste. This system involves the provision of a nitrite-containing mortar layer over the entire surface of a chloride contaminated structure.
- (9) To present a mathematical model to simulate the transport behaviour of several ions in a saturated porous medium. This model will then be applied to predict the transport of ions associated with the calcium nitrite-based corrosion



inhibition system for chloride-contaminated hydrated cement paste and the numerical results compared with those obtained experimentally.

#### **1.4 OUTLINE OF THESIS**

This thesis is divided into nine chapters. This introduction is Chapter One.

Chapter Two comprises the literature review. This chapter gives a critical appreciation of the existing knowledge in the field.

Chapter Three describes the main materials used and the experimental techniques that were employed in this investigation.

Chapter Four investigates four corrosion inhibitors by studying the mechanisms of inhibitor action in model electrolyte systems.

Chapter Five assesses the depth of penetration and the distribution of two surface-applied corrosion inhibitors and/or their decomposition products by carrying out medium term site trials.

Chapter Six investigates the influence of various carbonating atmospheres on the pore solution chemistry and microstructure of hydrated cement paste.

Chapter Seven investigates the physical realkalisation repair system for carbonated cement paste. Laboratory experiments are carried out to monitor the transport of hydroxyl ions and a mathematical model is then developed to simulate the process. The numerical results obtained from the model are then compared with the results obtained experimentally.

Chapter Eight investigates a calcium nitrite-based corrosion inhibition system for chloride-contaminated hydrated cement paste. Laboratory experiments are carried out to monitor the transport of several ions and a mathematical model is then developed to simulate the process. The numerical results obtained from the model are then compared with the results obtained experimentally.

Chapter Nine summarises the general conclusions of the present study and outlines recommendations for further work.

## **CHAPTER TWO**

### **LITERATURE REVIEW**

#### **2.1 INTRODUCTION**

This literature review comprises four sections. Following this introduction, there is a section on the microstructure of hydrated cement paste which is included as the investigations presented in Chapters Four to Eight all deal with the aqueous pore solution phase present within hydrated cement paste and, in particular, Chapter Six investigates the influence of various carbonating atmospheres on both the pore solution chemistry and microstructure of hydrated cement paste. The reviews on the corrosion of steel in concrete and corrosion inhibitors for use with reinforced concrete structures are of obvious relevance to the investigations presented in Chapters Four to Eight.

#### **2.2 MICROSTRUCTURE OF HYDRATED CEMENT PASTE**

##### **2.2.1 Introduction**

The main compounds of Ordinary Portland Cement (OPC) are tricalcium silicate ( $C_3S$ ), dicalcium silicate ( $C_2S$ ), tricalcium aluminate ( $C_3A$ ) and tetracalcium alumino-ferrite ( $C_4AF$ ). When water is added to these compounds they gradually undergo a complex sequence of exothermic reactions which result in the formation of a hydrated cement paste that consists of solid phases (cement hydrates) and porosity. The principal hydration reactions of Portland cement are depicted by Double (1983) as shown in Fig. 2.1. The microstructure of hydrated cement paste is very important as it has a major influence on engineering properties such as strength, permeability, diffusivity, shrinkage, creep and hence durability of reinforced concrete (Powers, 1958; Sereda, Feldman and Ramachandran, 1980; Nyame and Illston, 1981; Parrott, 1987a).



Therefore, from an engineering point of view, it is very important that the microstructure of hydrated cement paste can be characterised.

### **2.2.2 Solid Phases**

When water is added to cement the calcium silicates react at different rates but form similar products which are known as calcium silicate hydrate gel (C-S-H gel) and crystals of calcium hydroxide. C-S-H gel is a rigid network of colloidal particles of poorly defined crystalline structure and constitutes the main binding material in hydrated cement paste, whilst calcium hydroxide is in the form of larger hexagonal crystals. In a fully hydrated cement paste C-S-H gel and calcium hydroxide occupy about 60% and 20% of the volume respectively. Other products produced by the remaining compounds are calcium aluminate trisulphate hydrate (ettringite) and calcium monosulphate hydrate, tricalcium aluminate hydrates, anhydrite clinker residue and other minor constituents (Diamond, 1976).

### **2.2.3 Pore Structure**

The overall porosity of hardened cement paste decreases as the water to cement ratio is reduced and the degree of hydration is increased. The deterioration of reinforced concrete structures occurs as a direct result of the diffusion and penetration of deleterious species into the hydrated cement matrix, which takes place within the pore fluid that travels through the pore structure.

Various authors have produced models to assist in understanding the role of the cement paste structure on concrete properties, as follows:-

The Powers-Brownyard model (Powers and Brownyard, 1948) assumes that hardened cement paste consists of three components namely unreacted cement, hydration products (comprising C-S-H gel and calcium hydroxide crystals) and capillary pores. The water present within hardened cement paste was categorised as evaporable water (present

within both the capillary pores and the gel pores) and non-evaporable water. The hydration products are considered to contain a fixed amount of non-evaporable water and gel porosity of 28% independent of the water/cement ratio and degree of hydration. This conclusion was based on water vapour sorption isotherms on severely dried pastes and this has been strongly criticised by Feldman (1969). The volume of hydration products occupy more volume than that of the cement from which they are formed and thus the capillary porosity was regarded as the remains of the initial volume occupied by water. Therefore, with increased hydration there is an associated decrease in capillary porosity and an increase in gel porosity. The Powers-Brownyard model explains why complete hydration does not occur if the water to cement ratio is below a certain value and it concludes that a given volume of cement can only react if an additional 120% of free space, by volume, is available. Brunauer (1962) and Brunauer and Greenberg (1962) considered the gel particles of the Powers-Brownyard model to consist of two or three layers of C-S-H gel which could be rolled into fibres.

Powers model (Powers, 1958) of the pore structure of hydrated cement paste is a slightly modified version of the Powers-Brownyard model. The gel pores are visualised as the spaces between gel particles within the matrix and vapour sorption isotherms indicated that the gel pores have a diameter of about 2nm (Powers, 1958). However, the Powers model is thought to be somewhat oversimplified since cement pastes contain a continuous distribution of pores classified by their behaviour in water (Young, 1988), as shown in Fig. 2.2. Water in the gel pores is adsorbed and becomes involved in structural bonding, whereas in the larger pores the water present acts as bulk water.

Feldman and Sereda (1970) proposed a model (see Fig. 2.3) which was based on studies of sorption properties, porosities and relationships between water content and physical properties. They considered the C-S-H gel structure to be an irregular array of single layers which may come together randomly to create interlayer spaces. The layers are considered to be bonded together through solid to solid contacts, whose strength is



thought to lie between the weak Van der Waals forces and the strong ionic or covalent bonds. They considered that much of the gel water of the Powers-Brownyard model enters the interlayer spaces and becomes part of the structure, and contributes to the rigidity of the system. They reported that most of this water cannot be removed from the system on drying until relative humidities of less than 10% are achieved (Feldman and Sereda, 1970).

Diamoni et al. (1977) modified the Feldman-Sereda model based on adsorption studies on hydrated tricalcium silicate paste after the removal of calcium hydroxide. Adsorption measurements were carried out which indicated that there were two kinds of pore in existence; a wider inter-gel-particle pore (diameter 3.2-200nm) which can be seen even in the inner C-S-H gel by scanning electron microscopy (SEM) and a smaller intra-gel pore (1.2-3.2nm) existing within the gel particles which cannot be observed by SEM. They also reported that pores of both types tended to have narrow entrances.

Wittmann (1976 and 1980) proposed a model, which describes the hardened cement paste as a gel consisting of separate particles that have no internal structure together with crystalline constituents. Emphasis is placed upon water molecules absorbed on or lying between the gel particles. Below 50% relative humidity, the particles were considered to be in contact but at higher relative humidities water molecules appeared to keep the gel particles apart. This model was used in the development of a theory for dimensional changes.

Richardson (1999) investigated the structure of C-S-H gel and found that inner product C-S-H, i.e. those products which lie within the original boundaries of the clinker particles (Taplin, 1959) present in Portland cement grains with diameters larger than 5 $\mu$ m, has a fine scale and homogeneous morphology with pores under 10nm in diameter. He also reported that the hydrated remains of particles of Portland cement with diameters less than 5 $\mu$ m, contain a less dense product with substantial porosity



surrounded by a zone of relatively dense C-S-H. He also reported that C-S-H has good bonding properties with respect to other products of hydration.

Various techniques have been developed and used to investigate the pore structure of hydrated cement paste. Mercury intrusion porosimetry (MIP) is a widely used technique for determining the total porosity, characteristic pore size and pore size distribution of hydrated cement paste. This method is based on the fact that a liquid that does not wet a porous solid will enter its pores only under pressure. Various authors have used MIP to investigate the pore structure of hydrated cement paste (Winslow and Diamond, 1970; Dullien, 1979; Marsh and Day, 1985; Marsh, Day and Bonner, 1985; Li and Roy 1986; Day and Marsh, 1988; Moukwa and Aitcin, 1988; Feldman and Beaudoin 1991; Garboczi and Bentz, 1991; Konecny and Naqvi 1993).

Capillary condensation methods are frequently used to study the characteristics of small pores in hardened cement paste and there are well developed techniques for measurement and analysis (Dullien, 1979; Gregg and Sing, 1982). Parrott (1981), Parrott, Hansen and Berger (1980), Litvan (1976) and Patel et al. (1985) used adsorption methods to investigate the pore structure of hydrated cement paste. Ngala (1995), McCarter (1993) and Parrott (1992) used water adsorption and desorption of cement paste and concrete in order to investigate the porosity of cover concrete.

Scanning electron microscopy can be used to give information about the pore structure of hydrated cement paste (Parrott et al., 1984; Bentz, 1994) by examining polished specimens impregnated with epoxy. Scanning electron microscopy is also frequently used to observe and characterise the cement paste/aggregate interface (Larbi, 1991). Back scattered electron images on polished cement paste sections can be used to investigate porosity, calcium hydroxide and other hydration products (Scrivener and Pratt, 1987; Scrivener, 1989).

A microhardness technique has been used by Larbi (1991) to examine the cement paste/aggregate transition zone. The microhardness technique is useful for indicating the compactness of cement paste. Page, Yu and Bertolini (1994) and Bertolini, Yu and Page (1996) used this technique to investigate the potential side effects of electrochemical chloride removal close to the cathode. Low temperature calorimetry has been used to study coarse porosity (Sellevold and Bager, 1981; Bager and Sellevold, 1986).

#### **2.2.4 Pore Solution Phase of Hydrated Cement Paste**

The aqueous solution phase contained within the capillary pores of the hydrated cement matrix has a major influence on the corrosion behaviour of reinforced concrete. Pore solutions can vary considerably in composition when considering different types of cement.

The pore solution of Portland cement pastes or concretes, cured at normal temperatures, is of a highly alkaline nature mainly consisting of sodium and potassium hydroxide and having a pH in the range of 13-14 (Nixon and Page, 1987). Other ions are present in low concentrations such as sulphate and calcium. This alkaline nature is established during the initial few days of curing and in good quality well cured dense concrete the composition of the pore solution changes very little with time. A direct relationship between the equivalent  $\text{Na}_2\text{O}$  content of the cement ( $\%\text{Na}_2\text{O} + 0.659\%\text{K}_2\text{O}$ ) and the pH of the pore solution, in terms of the hydroxyl ion content, has been established, as shown in Fig. 2.4 (Nixon and Page, 1987). The pH of the pore solution within Ordinary Portland Cement concrete rarely drops below 12.5 due to the buffering effect of calcium hydroxide.

In order to express small quantities of pore solution from within concrete very high pressures are required. A method was originally devised by Longuet, Burglen and Zelwer (1973) and this was refined by Barneyback and Diamond (1981). The resulting pore solutions can then be analysed by several methods such as acid titration and ion



chromatography. Doubts have been raised about the reliability of the method refined by Barneyback and Diamond (1981), however, research by Duchesne and Berube (1994) and Constantier and Diamond (1997) have concluded that the effects of different pressures on the pore solution composition results obtained are generally small. In addition, the data obtained via this method acceptably agrees with data obtained by equilibrating the pore solution with external solutions of known composition (Sergi, 1986; Nixon and Page, 1987).

## **2.3 THE CORROSION OF STEEL IN CONCRETE**

### **2.3.1 Introduction**

Corrosion of steel in concrete is the most common and expensive form of degradation of reinforced concrete. This section will discuss steel in concrete before describing the mechanisms and main causes of corrosion of steel in concrete.

### **2.3.2 Steel in Concrete**

When steel is surrounded by a hydrated cement matrix with a pore solution phase that has a pH of 13-14 a 'passive layer' is formed. The Pourbaix diagram, shown in Figure 2.5, indicates the passive behaviour of iron under such highly alkaline conditions. This passive layer is very important in terms of the durability of reinforced concrete as it restricts the corrosion rate to very low values. Thus, the steel embedded in an environment of this kind is said to be in a state of passivity.

A true passive layer is a very dense, thin layer of oxide that leads to a very slow rate of corrosion. However, the actual composition of the passive layer on steel in concrete is not yet fully known. Leek and Poole (1990) reported that the passivation of steel in concrete is due to a two component system consisting of a calcium hydroxide layer and a thin pH stabilised iron oxide/hydroxide film on the surface of the metal. Other authors (Nagayama and Cohen, 1962; O'Grady, 1980) have suggested a wide range of



compositions for the passive film on iron including a monolayer of solid solution  $\text{Fe}_2\text{O}_3$  and  $\text{Fe}_3\text{O}_4$ , and a three layer film of  $\text{Fe}_2\text{O}_3$  and a proton deficient  $\text{Fe}_3\text{O}_4$  with a defect structure, and a polymeric layer of amorphous  $\text{Fe}_2\text{O}_3$ . Hancock and Mayne (1958) reported the passive film on iron in a sodium hydroxide solution to be composed of a cubic form of ferric oxide ( $\gamma\text{-Fe}_2\text{O}_3$ ). However, it is known that the passive layer on steel in concrete is in a state of dynamic equilibrium, i.e. it is constantly undergoing breakdown and repair, and it is for this reason that if the passive layer can be maintained, then it is a far better form of protection to the steel than any artificial coating.

### **2.3.3 Mechanisms of Corrosion of Steel in Concrete**

Corrosion is the process of a refined metal reverting back to its natural state by an oxidation reaction with the non-metallic environment (e.g. oxygen and water). It is an electrochemical process that occurs on steel reinforcement when the passivating environment which normally exists in good quality dense concrete is not maintained, i.e. when depassivation occurs.

When corrosion occurs, the steel surface becomes the site of anodic and cathodic reactions which couple together to form a corrosion cell. At anodic sites, iron atoms undergo oxidation to form  $\text{Fe}^{2+}$  ions which pass into solution (see equation 2.1).



At cathodic sites, the excess free electrons left in the metal are consumed, in order to preserve electrical neutrality, converting oxygen and water to  $\text{OH}^-$  ions in a process of reduction (see equation 2.2)



The anodic and cathodic reactions (equations 2.1 and 2.2) are only the first steps in the process of creating rust. The process of creating rust can be expressed in several ways; such as where ferrous hydroxide is created (equation 2.3) which then becomes ferric hydroxide (equation 2.4) which, in turn, becomes hydrated ferric oxide (equation 2.5), better known as rust: -



Hydrated ferric oxide has a volume between two and ten times that of the steel which it replaces and this generates expansive forces that can lead to cracking and spalling of the concrete cover as well as a reduction in the bond at the steel/concrete interface. The loss of mechanical strength of steel due to corrosion is also a significant problem, especially in the tendons of pre-stressed or post-tensioned structures.

As mentioned earlier, corrosion will occur only when depassivation is achieved. Page (1999b) states that the three main causes of depassivation are deoxygenation, carbonation and chloride contamination.

#### **2.3.4 Cathodically Restrained Dissolution**

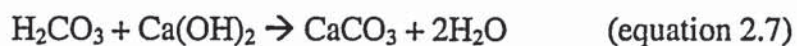
Deoxygenation leads to cathodically restrained dissolution which is normally only observed when the rate of diffusion of oxygen through the concrete cover to the steel becomes insufficient to balance the small anodic leakage current required to maintain the passive film on the steel in dynamic equilibrium. Cathodically restrained dissolution occurs only in buried or submerged structures and is associated with low overall rates of corrosion.



### 2.3.5 Carbonation

#### 2.3.5.1 Mechanisms of Carbonation

Carbonation is the result of the interaction of carbon dioxide in the atmosphere with alkaline hydroxides in the concrete. Carbon dioxide dissolves in water to form carbonic acid (equation 2.6) which, in turn, reacts with calcium hydroxide (present within the pore solution phase of concrete) to precipitate calcium carbonate (equation 2.7).



There is a lot more calcium hydroxide in the concrete than can be dissolved in the pore solution and this acts as a buffer which maintains the pH at about 12.5. However, when all reserves of calcium hydroxide have reacted with the carbonic acid, the pH of the pore solution phase will be lowered to below pH 8, at which the passive film cannot be maintained. Therefore, the steel will corrode if the moisture content within the pores of the concrete is sufficiently high. If corrosion is present in carbonated reinforced concrete then it is usually of a general rather than pitting nature, i.e. on a "microcell" level with apparently continuous corrosion observed along the reinforcing steel.

#### 2.3.5.2 Mineralogical Formations

There are three mineralogical forms of calcium carbonate, i.e. calcite, aragonite and vaterite. Brooks, Clark and Thurston (1951) point out that calcite and aragonite occur in nature as well defined minerals with calcite being the more stable. It appears that the major mineralogical form of calcium carbonate in carbonated concrete is calcite. Kondo, Daimon and Akiba (1969) and Asano et al. (1962) reported that the carbonation of hydrated  $\text{C}_3\text{S}$  produces calcite whereas unhydrated  $\text{C}_3\text{S}$  produces vaterite. Sauman (1971) reports that for C-S-H gel, on carbonation, vaterite is formed first but this is then



gradually converted to the more stable calcite. Cole and Kroone (1960) reported that vaterite is formed first before being transformed into aragonite which in turn is transformed into poorly crystallised calcite.

#### 2.3.5.3 Rate of Carbonation through Concrete

Carbonation proceeds through concrete as a front, i.e. there is a fairly sharp change in pH at the carbonation front. The carbonation process is controlled by diffusion and is governed by Fick's law. The carbonation depth can be approximated using equation 2.8 (Tuutti, 1982; Vaysburd, Sabnis, and Emmons, 1993).

$$d = k t^n \quad \text{(equation 2.8)}$$

where:       $n$  is usually taken as 0.5 (Parrott, 1987b)  
               $d$  = the penetration depth  
               $t$  = the time taken for the penetration to be achieved  
               $k$  = the proportionality constant.

A large number of factors affect the magnitude of the proportionality constant ( $k$ ) in equation 2.8 such as the quality of the concrete cover, w/c ratio, compaction, air carbon dioxide concentration, cement content, type and quality, climate and curing environment. Various equations to determine the depth of carbonation have been proposed to account for some of these factors as shown in Table 2.1 (Parrott, 1987b).

#### 2.3.5.4 Factors Influencing Carbonation

The depth of the cover concrete is very important in terms of the factors that influence corrosion due to carbonation. Wallbank (1989) found that in a survey of 200 randomly selected highway bridges over 90% had carbonation depths of 5mm or less. Skjolsvold (1986) showed that, for OPC concrete, an increase in the water to cement ratio results in an increase in the rate of carbonation. Grube and Lawrence (1984) point out that the

hydrated cement matrix is the most permeable phase in concrete and therefore carbonation increases with increasing cement content; however, a low cement content within the concrete will encourage carbonation due to the lack of the buffering capacity that is attributed to calcium hydroxide reserves. The carbon dioxide content of the exposure environment can affect the rate of carbonation. Carbonation can occur even at the concentrations which are present in air (0.03% by volume in air), however, the rate of carbonation increases with an increase in the concentration of carbon dioxide.

The relative humidity is a very important factor that influences carbonation. Tuutti (1982), Parrott (1987b and 1990) and Thomas and Matthews (1992) reported that the optimum relative humidity for carbonation to occur lies between 60% and 70%. In concrete that has a relative humidity below this range the carbon dioxide readily penetrates but the amount of water present within the pores may be insufficient to allow the carbonation reactions to occur. Arber and Vivian (1961) point out that the moisture content of concrete at high relative humidities inhibits the ingress of carbon dioxide.

Wet/dry cycling on the concrete surface will accelerate carbonation by allowing carbon dioxide gas in during the dry cycle and then supplying the water to dissolve it in the wet cycle. Wood (1990) suggested that the worst conditions for inducing carbonation are cyclic wetting and drying with a relative humidity between 60 and 90%.

The effect of the temperature of exposure on the rate of carbonation has received contradicting reviews in the literature. Rahman and Glassner (1989) observed that an increase in temperature significantly enhanced the carbonation process in OPC concrete whilst Thomas and Matthews (1992) showed that an insignificant increase in the rate of carbonation was observed with increase in temperature. High rates of carbonation in countries of the Middle East have been attributed to higher air temperatures by Fookes, Pollock and Kay (1981) and Bijen (1985).



Dhir (1989) and Loo et al. (1994) reported that increasing the water curing period decreases the rate of carbonation. Dhir (1989) and Loo et al. (1994) also reported that beyond 14 days of water curing the decrease in the rate of carbonation became more gradual. Poor compaction results in greater porosities and thus leads to more rapid carbon dioxide ingress.

#### 2.3.5.5 Effects of Carbonation on Pore Structure

Phihajavaara (1968) and Bier, Kropp and Hilsdorf (1987 and 1989) have reported that the porosity of the exposed surface is reduced as a result of carbonation due to the fact that the volume of the calcium carbonate formed exceeds that of the parent hydrates. Bier, Kropp and Hilsdorf (1987 and 1989) observed that the pore volume of OPC hardened cement paste was decreased whilst OPC/GGBS showed little or no reduction. They also observed that carbonation increased the capillary porosity of OPC/GGBS paste. Page and Ngala (1995) reported that in cement pastes, although total porosities were reduced, the proportion of coarse capillary pores was increased, this effect being considerably more pronounced for blended cement pastes than for OPC pastes. Malami and Kaloidas (1994) reported that the total specific pore volume of carbonated cement pastes were less than those obtained for uncarbonated cement pastes.

As a result of the reduction in total porosity of carbonated concrete the mechanical properties of concrete, such as compressive and flexural strengths, are enhanced (Meyer, 1968; Vaysburd, Sabnis and Emmons, 1993). The modulus of elasticity and surface hardness are increased by carbonation (Sereda, 1968). Hilsdorf, Kropp and Gunter (1984) reports that permeability is reduced due to carbonation. However, chloride penetration (Sergi, 1986) and chloride diffusion (Ahmed, 1990; Page and Ngala, 1995) have been found to be accelerated, for a given porosity, as a result of carbonation. Page and Ngala (1995) conclude that the electrostatic surface interactions, which are believed to dominate chloride diffusion in non-carbonated cement pastes, are not significant in the corresponding carbonated materials. Thus, carbonation increases the risk of pitting



corrosion. Dhir (1993) reported that carbonation also accelerates the process of sulphate attack.

### **2.3.6 Chloride Attack**

#### **2.3.6.1 Mechanisms of Chloride Attack**

Chloride ions can come from several sources. Chlorides can be cast into the concrete or they can diffuse in from the outside. Chlorides cast into the concrete can be due to admixtures such as calcium chloride (used as an accelerator until the mid-1970s), use of sea water in the initial concrete mix and contaminated aggregates (such as inadequately washed sea-dredged aggregates). Chlorides can diffuse into the concrete due to sea salt spray and direct sea water wetting, de-icing salts and, in some structures, due to holding salt, brine, aquaria, etc. Buenfeld (1986) reported that chloride can be present in concrete in several states, i.e. strongly bound by  $C_3A$  hydrates and  $C_4AF$  hydrates mainly in the form of calcium chloroaluminate, loosely bound by calcium silicate hydrates and as free ions in the pore solution phase.

As described earlier, the steel present in good quality concrete possesses a passive film that is constantly undergoing breakdown and repair. However, at breakdown locations a tiny rupture will form on the steel surface and  $FeOH^+$  and  $H^+$  ions are formed which, in turn, attract negative ions. Therefore, both hydroxyl and chloride ions are attracted to the rupture (Fig. 2.6). In order to initiate corrosion there needs to be a sufficient ratio of free chloride to hydroxyl ions known as a 'threshold ratio'. If this threshold ratio is not exceeded then the excess supply of hydroxyl ions will neutralise the acidity produced at the breakdown and the film will be repaired. However, if this threshold is exceeded, the acid rich environment at the base of the tiny breakdown will become more acidic causing corrosion to initiate which, in turn, causes the tiny rupture on the steel surface to develop into a continually growing pit thus resulting in localised loss of cross-section of the reinforcement. Hence, when corrosion is present due to chlorides it tends to be of a

pitting nature, i.e. on a macrocell level. The pH of the pore solution will not significantly drop with this type of attack.

#### **2.3.6.2 Critical Chloride to Hydroxyl Ion Ratio**

There have been several attempts to find a critical free chloride to hydroxyl ion ratio for corrosion of steel in concrete that can be applied to all types of concrete and exposure environments. However, it is a subject upon which engineers are yet to agree. Hausmann (1967) reported that the critical chloride to hydroxyl ion ratio is 0.6 over a pH range of 11.6 – 12.4. Lambert, Page and Vassie (1991) found that the critical ratio to initiate corrosion varied enormously. However, it has been argued by Glass and Buenfeld (1997) that this approach is not strictly correct, as hydroxyl ions are not the only inhibitive substance in concrete. Page and Treadaway (1982) point out that the chloride to hydroxyl ion ratio does not take into account the buffering properties of the cement matrix. Browne (1982) and Glass and Buenfeld (1997) suggest that chloride threshold levels be best defined by relating the risk of corrosion to the total chloride content by weight of cement. Glass and Buenfeld (1997) also give a summary of chloride threshold levels (Table 2.2).

There are several reasons why engineers cannot agree on a standard threshold chloride to hydroxyl ion ratio. The pH of the pore solution of concrete will vary with the type of cement and the water to cement ratio. The relationship between pH and hydroxyl ion concentration is logarithmic and therefore a tiny change in pH represents a massive change in hydroxyl ion concentration. Other factors such as the ability of certain cements to bind chlorides chemically (due to the aluminates in the concrete) and physically adsorb chlorides (on to the pore walls) are important as this removes them temporarily, or permanently, from the corrosion reaction. In very dry concrete corrosion may not occur even at high chloride concentrations due to the lack of water. Sealed or submerged concrete may stop water and/or oxygen from reaching the steel and thus stop corrosion from being initiated, even where high concentrations of chloride are present.



The initial surface condition and composition of the steel are also important when trying to establish the critical chloride to hydroxyl ion concentration.

#### **2.3.6.3 Transport of Chloride Ions through Concrete**

Transport of chloride ions in concrete is a rather complicated process that involves diffusion, adsorption and convection, accompanied by physical and chemical binding. In constantly wet environments, chloride penetration into concrete is predominantly diffusion controlled and concentration against depth profiles may be estimated, assuming Fick's second law of diffusion to be applicable, using equation 2.9 (Crank, 1975).

$$C = C_0 [1 - \text{erf} (x / 2(Dt)^{1/2})] \quad (\text{equation 2.9})$$

where:  $x$  = distance from exposed surface (m)

$C$  = chloride ion concentration at distance  $x$  ( $\text{kg}/\text{m}^3$ )

$C_0$  = chloride ion concentration at the exposed surface ( $\text{kg}/\text{m}^3$ )

$\text{erf}$  = error function

$D$  = diffusion coefficient ( $\text{m}^2/\text{s}$ )

$t$  = duration of exposure (s)

Diffusion occurs due to ionic concentration gradients. Sufficient moisture is required for diffusion to occur and the rate of diffusion is also affected by temperature (RILEM Report 12, 1995).

### **2.4 CORROSION INHIBITORS FOR USE WITH REINFORCED CONCRETE STRUCTURES**

#### **2.4.1 Introduction**

Corrosion inhibitors are chemicals that cause changes at the steel/concrete interface which result in a reduction of the overall corrosion rate of steel in concrete. Since the 1970s, corrosion inhibitors have been used as admixtures for new structures as a



preventative measure. However, more recently, several commercially available proprietary repair systems have been developed which involve the inhibitors being applied as a coating on to the concrete surface, applied into drilled holes in the concrete cover or incorporated into concrete overlays. It is claimed that corrosion inhibitors for the rehabilitation of reinforced concrete lead to reduced costs, pollution and inconvenience to the owners and users of structures when compared to other techniques that can be employed. However, there is very little independent evidence to support this and there are several concerns relating to the application of corrosion inhibitors for restorative purposes. These include reservations about the effectiveness of such treatments, which include depths of inhibitor penetration, quantities required at the steel surface, side effects and longevity of protection afforded. There has been little independent research to address these issues.

Corrosion inhibitors as admixtures for use in new construction have been reviewed by Treadaway and Russell (1968), Craig and Wood (1970), Griffin (1975), Slater (1983), Berke (1989 and 1991) and Berke and Weil (1994). Page, Ngala and Page (2000) have reviewed corrosion inhibitors for use in repair systems for concrete structures with corrosion problems.

This section of the literature review defines the different types of corrosion inhibitors before reviewing the research that has been carried out on the use of corrosion inhibitors as preventative measures and then discussing the use of corrosion inhibitors for the rehabilitation of reinforced concrete.

#### **2.4.2 Types of Corrosion Inhibitor**

Corrosion inhibitors can be classified into three main categories; i.e. anodic, cathodic and mixed. Anodic inhibitors suppress the anodic reaction, i.e. by the formation of a protective film on the anode, resulting in a more positive shift of the corrosion potential of the inhibited metal. Cathodic inhibitors suppress the cathodic reaction, i.e. by

retarding oxygen reduction or hydrogen discharge, and induce a negative shift in the corrosion potential of the metal. Mixed inhibitors suppress, to a certain degree, both the anodic and the cathodic reactions.

#### **2.4.3 Corrosion Inhibitors as Preventative Measures**

Early studies looked at numerous inhibitors to be used as concrete admixtures with most attention focused on sodium nitrite, sodium benzoate, potassium chromate and stannous chloride. However, from the evidence gathered as a result of the early research it is not surprising that corrosion inhibitors were not in large-scale use up to the mid-seventies.

Sodium nitrite was identified as a good inhibitor, but it caused severe strength loss (Craig and Wood, 1970) and was believed to be a potential exacerbator of localised corrosion if used at concentrations below the level required for complete passivation of steel in chloride-containing media (Treadaway and Russell, 1968; Nurnberger, 1988; Short, Lambert and Page, 1989). The reduction in strength was associated with the presence of the sodium cation while the efficiency of inhibition was associated with the nitrite anion. Investigations by Lewis, Mason and Brereton (1956) and Treadaway and Russell (1968) found that sodium or potassium salts of benzoates and chromates were not very promising in their corrosion inhibition and Craig and Wood (1970) observed that they caused a reduction in strength.

Arber and Vivian (1961) indicated that stannous chloride acted as a corrosion inhibitor and appeared to be a non-corrosive accelerator whilst, more recently, Hope and Ip (1989) pointed out that stannous chloride did not appear to be a promising inhibitor. Sagoe-Crentsil, Glasser and Yilmaz (1994) reported a strong inhibiting effect of stannous tin on chloride induced corrosion of steel in Portland cement. However, the obvious problems associated with stannous chloride are that it contains chloride and it is relatively expensive.



During the 1970's calcium nitrite was introduced as a concrete admixture to inhibit the corrosion of steel in concrete. In the USA, since 1978, calcium nitrite has been used in over 300 parking, marine and highway structures, apparently with very successful results (Jeknevorian, Chin and Saidha, 1995) in the battle to inhibit chloride-induced corrosion. Gaidis and Rosenberg (1979) reported that calcium nitrite behaves as an anodic inhibitor and that there is no reaction between ferric ions and nitrite ions; however, ferrous ions react with nitrite ions according to equation 2.10;



This reaction reinforces the passive film, therefore, blocking further passage of ferrous ions from the steel into the pore solution.

Calcium nitrite, unlike sodium nitrite, in which the sodium cation is detrimental to concrete strength, was found to be non-detrimental to mechanical properties (Rosenberg, Gaidis and Kossivas, 1977). Recently, it has been confirmed (Tomosawa et al., 1990; Collins, Weyers and Al-Qadi, 1993) that calcium nitrite acts as a set accelerator. The authors, however, disagree on the effect of calcium nitrite on the compressive strength of mortar. Large scale investigations (Virmani, Clear and Pasko, 1983) revealed that calcium nitrite can provide more than an order of magnitude reduction in corrosion rates. However, the study recommended that calcium nitrite was effective at  $[\text{NO}_2^-]/[\text{Cl}^-]$  ratios above 1.0 based on admixed chlorides, while ratios lower than 1.0 might be tolerable for chlorides that have penetrated into initially chloride-free concrete. Several other researchers (Gaidis and Rosenberg, 1987; El-Jazairi and Berke, 1990; Tomosawa et al., 1992; Collins, Weyers and Al-Qadi, 1993) have estimated the critical  $[\text{NO}_2^-]/[\text{Cl}^-]$  ratio in concrete, with values ranging from 0.5 to greater than 1.0.



Within the last decade Andrade and co-workers (Alonso, Acha and Andrade, 1990; Alonso and Andrade, 1990; Andrade, Alonso and Gonzalez, 1986) have demonstrated that nitrite based corrosion inhibitor admixtures can also protect steel in carbonated concrete. The authors concluded that calcium nitrite did improve corrosion protection and did not appear to induce pitting corrosion when nitrites were not present at sufficient concentrations to inhibit corrosion fully. However, the authors also show that inhibition was not apparent when carbonation was combined with significant chloride contamination.

The major problem associated with nitrites is that they are toxic, and their addition to concrete in quantities required for protection of steel is thus prohibited in some countries, e.g. Switzerland and Germany (Maeder, 1994). This has led to the search for alternative corrosion inhibiting admixtures and several have been introduced as proprietary corrosion inhibiting systems (Maeder, 1994; Nmai, Farrington and Bobrowski, 1992). More recently, Calder (2000) reported that an amino alcohol-based inhibitor 'cast in' at a dose recommended by the supplier to laboratory specimens with a water to cement ratio of 0.5, increased the time to the onset of corrosion. The author also reported that no corrosion protection was given by the amino alcohol-based inhibitor when 'cast in' to laboratory specimens with a water to cement ratio of 0.65. In conclusion, the proven track record of calcium nitrite has yet to be realistically challenged by alternative inhibiting admixtures.

#### **2.4.4 Corrosion Inhibitors for Rehabilitative Purposes**

##### **2.4.4.1 Nitrite Ions**

As reported in section 2.4.3, nitrite ions have been used extensively as a concrete admixture to prevent the corrosion of steel in concrete. It was, therefore, only a matter of time before their inhibitive qualities were exploited as part of concrete repair systems. A proprietary repair system based on calcium nitrite was introduced in the USA (Berke et

al., 1992). The author claimed that a column could be impregnated using calcium nitrite in a mortar and a bridge was impregnated by a liquid solution of calcium nitrite.

Collins, Weyers and Al-Qadi (1993) identified calcium nitrite as a potential rehabilitative inhibitor by a method which involved the removal of chloride contaminated concrete, followed by ponding with an aqueous solution at the level of the bars and then providing a reservoir of nitrite ions in a cementitious mortar overlay. However, Gonzalez et al. (1996) reported that the effect of nitrite ions, whether included during mortar fabrication or supplied by immersion in an appropriate solution, is inadequate for passivating strongly pre-rusted reinforcement. Tomosawa et al. (1992) expressed concern over the effect of the nitrite concentration distribution on the corrosion of steel in concrete. The authors reported that in areas of insufficient nitrite concentration corrosion could be accelerated due to macrocell formation between areas of high and low nitrite concentration. Page, Ngala and Page (2000) reported reductions in corrosion rates for steel bars at a depth of 12mm in concretes containing relatively low amounts of chloride when a calcium nitrite-based solution was applied to the concrete surface and a mortar overlay containing calcium nitrite added. Page, Ngala and Page (2000) also reported that the same method of application reduced corrosion rates in chloride free carbonated concrete, although the inhibitive effect was completely lost when chlorides were present.

Lithium nitrite has been introduced in Japan (Sakaguchi et al., 1989) as a potential corrosion inhibitor. The nitrite ions provide the inhibiting effect on the corrosion process whilst lithium has proved to be a successful inhibitor of alkali-silica reaction.

In conclusion, nitrite ions can be successfully applied to structures where modest levels of chloride ions are apparent. However, their application is limited where chloride levels are relatively high; particularly where carbonation is present. The process of removing contaminated concrete and replacing with a mortar layer containing nitrite ions is not a



particularly convenient method of rehabilitation. In addition, long-term site trials are required to investigate concerns over the effects of varying nitrite ion concentration on a structure and the possibility of intensifying corrosion due to inadequate concentrations to significantly suppress corrosion.

#### 2.4.4.2 Sodium Monofluorophosphate

Monofluorophosphate-based inhibitors are relatively new to the European market and are not as well established as calcium nitrite. The most common form of monofluorophosphate-based inhibitor is sodium monofluorophosphate ( $\text{Na}_2\text{PO}_3\text{F}$ ), although, Duprat et al. (1985) states that zinc monofluorophosphate has good inhibiting properties over a wide concentration range.

Sodium monofluorophosphate (MFP) was first used in the harsh Canadian winters (Gassner and Malric, 1995) as an additive to road de-icing salts (sodium chloride) in order to protect reinforced concrete highway structures from the aggressive action of the chlorides. An aqueous solution of MFP is applied to structures suffering from reinforcement corrosion by repeated spraying, brushing or rolling on to the concrete surface. MFP tends not to be used in cementitious mortar overlays as it acts as a set retarder (Haynes, 1996).

The value of MFP as a curative corrosion inhibitor against chlorides in reinforced concrete has been studied in laboratories such as the Spanish Eduardo Torroja Institute (Andrade et al., 1992) and the French Laboratoire Central des Ponts et Chaussees (Raharinaivo, 1996). Furthermore, Dressman et al. (1991) studied the relative efficiencies of corrosion inhibitors to be used in reinforced concrete, which included studies on MFP. More recently, Calder (2000) investigated the efficiency of sodium monofluorophosphate in reducing the corrosion rates of steel in laboratory concretes with water to cement ratios of 0.5 and 0.65 containing 2% chloride ions by weight of cement cast-in. Once corrosion activity was established, MFP was ponded on to the



concrete surface twice daily for five days, using a solution of 5% MFP by weight for the first 5 applications and 15% MFP by weight for the remaining 5 applications. The author concluded that, under the conditions investigated, there was no evidence from electrochemical monitoring that treatment with MFP reduced the rate of corrosion in laboratory specimens. Calder (2000) also describes a site trial that involved applying MFP to a structure where the reinforcement was already corroding. The author concluded that the application of MFP did not significantly affect the measured corrosion rates.

The main reservation with respect to sodium monofluorophosphate is its ability to penetrate significant depths of cover. The exact mechanism of penetration is also a subject that needs clarification. It has been claimed that in the long term MFP penetrates into concrete by both diffusion and absorption. Gassner and Malric (1995) claim that the ingress of MFP is analogous to that of chloride ions, with the two compounds having the same parameters that determine their penetration. Haynes (1996) stated that solution penetration depths achieved to date exceed 40mm, while typical cover depths of 20-30mm can be achieved readily. Alonso et al. (1996) claimed that practical applications of MFP show that it can penetrate more than 30mm. The penetration depth seems to depend on the number of applications and the time between saturation of the concrete with MFP. There are no documented cases where young laboratory concretes have achieved these penetration depths. Page et al. (in preparation) analysed aqueous extracts of samples of MFP treated non-carbonated concrete by ion chromatography and they concluded that, under the conditions studied, penetration of MFP or  $\text{PO}_4^{3-}$  did not exceed 4mm. Kuznetsov (1996) and Elsener (1999) document field trials where inadequate penetration depths resulted.

Researchers have stated (Gassner and Malric, 1995; Andrade et al., 1992) that MFP is an inorganic anodic inhibitor of reinforcement corrosion, although some cathodic action should not be excluded. Gassner and Malric (1995) stated that, when MFP hydrolyses,

the fluoride ion reacts with the calcium in the lime forming insoluble minerals such as fluorite ( $\text{CaF}_2$ ) and apatite ( $\text{Ca}_5\text{F}(\text{PO}_4)_3$  or  $\text{Ca}_5\text{Cl}(\text{PO}_4)_3$  or  $\text{Ca}_5\text{OH}(\text{PO}_4)_3$ ), a process which they claim leads to the blocking of pores. It is also claimed that chloride binding is improved by the formation of fluoroapatite, which in turn reduces the amount of free chloride available to assist corrosion. Collins, Weyers and Al-Qadi (1993) claim that monofluorophosphate-based inhibitors work by the absorption of fluoride and/or phosphate ions onto the steel surface, leading to the enhancement of the oxide layer. Collins, Weyers and Al-Qadi (1993) also mentioned that the exact mechanism of this enhancement is unclear, an opinion which was also expressed by Andrade et al. (1992). Haynes (1996) states that the exact mechanism is complex but has been found to be beneficial for inhibiting reinforced concrete corrosion. Page, Ngala and Page (2000) detail a possible series of reactions that could attribute any inhibitive qualities associated with MFP to an increase in the concentration of hydroxyl ions in the pore solution.

Recently, Alonso et al. (1996) suggested that MFP may be used as a corrosion inhibitor to reduce the corrosion rate of corroding bars in carbonated concrete. This conclusion was reached on the basis of tests, which involved immersing steel bars in solutions that were supposed to simulate pore solutions in carbonated concrete. Haynes (1996) also claims that the presence of MFP in the concrete pores after the treatment also influences the rate of progression of carbonation. If the carbonated zone has not yet reached the reinforcement, and MFP treatment has been carried out, the slow-down of the carbonation rate provides important protection. He claims that, compared with untreated concrete, the rate of carbonation is reduced by 500% following MFP treatment. Page et al. (in preparation) found that MFP anions did not penetrate significantly into carbonated concrete. The authors have revealed that substantial hydrolysis of MFP takes place in carbonated concrete and that the hydrolysis products, i.e. water-soluble fluoride and phosphate, were readily detectable at depths beyond the cover zone. However, they also concluded that, under the conditions investigated, no significant reduction of the corrosion rate was detected.



In conclusion, the research to date has yet to provide convincing evidence that MFP can be used successfully as a corrosion inhibitor for the rehabilitation of reinforced concrete.

#### 2.4.4.3 Organic Inhibitors

Organic inhibitors have been used extensively in industries such as oil and gas production, transmission, refineries etc; however, they are a relatively new class of inhibitors for reinforcement corrosion in concrete structures. These inhibitors are generally a water-based organic blend of alkanolamines and/or amines, occasionally with surfactants and/or esters added. Various organic inhibitors have been promoted within the past few years in both the USA and Europe, some of which have been used as concrete admixtures (Nmai, Farrington and Bobrowski, 1992; SHRP-S-666, 1993). Some manufacturers of such substances call them 'Migrating Corrosion Inhibitors' because it is claimed, from the limited literature available on organic inhibitors, that these inhibitors can easily penetrate and diffuse through hardened concrete to the reinforcement in both the pore solution phase and, because of their relatively high vapour pressures, through the gaseous phase of the material when exposed to unsaturated atmospheres (Bjegovic et al., 1994; Miksic et al., 1995; Mackay, 1996).

Most of the small number of publications available on organic inhibitors for application to concrete have been contributed by companies who are actively promoting their products with little information about the potential limitations and minimal details about the inhibitor formulations. Dressman et al. (1991), Elsener (1999) and Buchler et al. (1999a and 1999b) tested specific organic inhibitor formulations, known to contain amine and/or alkanolamine in solutions intended to simulate the pore solution phase of various concretes, and found that against chlorides the results were promising. In the USA, a report backed by the Strategic Highway Research Program (SHRP-S-666, 1993) compared the effectiveness of two types of organic inhibitors in reducing chloride-induced reinforcement corrosion against a calcium nitrite-based system. The inhibitors



were ponded or sprayed on to concrete surfaces and admixed within a concrete overlay. The report concluded that only the organic inhibitors were able to reduce corrosion regardless of the initial corrosion of the specimen. However, it was reported that they had a detrimental effect on bond strength when applied as an overlay to the extent that sandblasting of the concrete surface was considered necessary. The report came to no conclusions as to the relative length of time of inhibition offered by the organic systems, or of their effectiveness against corrosion of steel in carbonated concrete. However, similar inhibitors were used at high dosages in tests by Buchler et al. (1999a and 1999b) and it was found that the corrosion rate, after inhibitor application as a rehabilitative measure to chloride containing and carbonated mortars, was not affected.

Page, Ngala and Page (2000) carried out investigations on a proprietary, alkanolamine-based inhibitor known to contain ethanolamine and potassium hydrogen phosphate applied by ponding concrete surfaces. The inhibitor appeared to cause a slight reduction in the corrosion rate of pre-corroding bars in 0.65 water to cement ratio non-carbonated concrete with low levels of chloride contamination. Under the conditions investigated, its ability to reduce corrosion rates in non-carbonated concrete with high levels of chloride contamination and carbonated concrete proved to be minimal. The authors also reported that, by using ion chromatography, the alkanolamine component penetrated beyond 20mm whilst the phosphate component was not detected beyond 4mm. More recently, Calder (2000) investigated the efficiency of the same alkanolamine-based inhibitor in reducing the corrosion rates of steel in laboratory concretes with water to cement ratios of 0.5 and 0.65 containing 2% chloride ions by weight of cement cast-in. Once corrosion activity was established, the alkanolamine-based inhibitor was repeatedly spray-applied on to the concrete surface. The author concluded that, under the conditions investigated, there was no evidence from electrochemical monitoring to show that treatment with the alkanolamine-based inhibitor reduced the rate of corrosion in laboratory specimens. Calder (2000) also describes a site trial that involved applying the same alkanolamine-based inhibitor to a structure where the reinforcement was

already corroding. The author concluded that the application of the alkanolamine-based inhibitor did not significantly affect the measured corrosion rates. However, Jones and Wood (2000) carried out investigations on a similar inhibitor and reported an average of 95% reduction in the corrosion rate of steel in pre-cast concrete cladding panels suffering from carbonation, fifteen months after inhibitor treatment. Marazzani (1999) suggests that alkanolamine-based inhibitors may attain better results when applied to carbonated concrete that is only subjected to a humid atmosphere, thus, where the corrosion rate of the embedded steel will be low.

In conclusion, owing to the secrecy that surrounds the inhibitor formulations of commercially available organic inhibitors, researchers have found it very hard to replicate performance and thus determine reasonable independent conclusions as to their respective efficiencies. Much research needs to be done to provide more information on the duration of the protective film on the surface of the steel and the effectiveness of inhibition in carbonated concrete. In addition, research to date suggests that the inhibitors are ineffective when dealing with steel bars that are already undergoing significant corrosion.

#### **2.4.4.4 Physical Realkalisation**

Realkalisation is used as a rehabilitation technique on structures that are suffering from carbonation induced reinforcement corrosion, i.e. corrosion inhibition by hydroxyl ions which are known to act as anodic inhibitors. Physical realkalisation involves coating the surface of a structure with an alkaline cement-based coating and has been introduced on the basis of laboratory research in Germany (Bier, Kropp and Hilsdorf, 1987).

Bier, Kropp and Hilsdorf (1987) concluded that an alkaline environment can be restored in carbonated zones by application of cement mortars on the concrete surfaces as long as sufficient moisture is available. Mattila and Pentti (1996) carried out research into physical realkalisation and evaluated, via laboratory experiments, the conditions



necessary for the process to work. They concluded that relatively thick coatings (10-20mm) are required to provide a sufficient reservoir of hydroxyl ions and a suitable barrier to future carbonation. They reported that the carbonated concrete was realkalised not only from the direction of the coating but also from the direction of the uncarbonated concrete. They also stated that a relative humidity of 90% was required for reasonably rapid realkalisation in the concrete. This corresponds to a level of moisture that would be likely to sustain corrosion. Overall, they concluded that it seems possible to use realkalisation at least as a beneficial side effect when large-scale corrosion damage is to be repaired.

In conclusion, therefore, it appears that physical realkalisation may be a viable option for the rehabilitation of reinforced concrete structures suffering from the effects of carbonation-induced corrosion alone, where the structural integrity will allow a reasonably thick coating to be applied and where the environmental conditions are suitable.

#### 2.4.4.5 Electrochemical Realkalisation

Electrochemical realkalisation is an alternative way of replenishing the alkalinity in the pore solution of carbonated concrete. It involves passing a temporary current through the concrete between the reinforcement, acting as the cathode, and an externally applied anode placed within an alkaline electrolyte on the concrete surface. Sodium carbonate at a concentration of 1.0 molar is generally used as the electrolyte covering the concrete surface, although on-going research into the use of lithium hydroxide shows promise. The applied current density is in the region of  $1 \text{ A/m}^2$  and is applied for several days before being stopped and the temporary anode and electrolyte removed (Odden, 1994). A high concentration of alkalis is established around the steel cathode due to hydroxyl ions being produced by the electrochemical discharge of hydrogen from water with the accompanying migration of sodium and potassium ions to the cathode. Electrochemical realkalisation also results in the penetration of alkaline material into the concrete via



adsorption and diffusion from the external electrolyte (Mietz and Isecke, 1994; Mietz, 1995; Mietz, 1998).

The magnitude of the current density and length of application clearly affect the production of hydroxyl ions at the cathode whilst the porosity and moisture condition of the cover concrete affect the penetration of the external electrolyte. Also, the length of protection afforded depends on factors such as surface leaching and further carbon dioxide adsorption.

One of the first realkalisation projects was the State Bank of Norway in Stavanger (Odden, 1994). A survey prior to rehabilitation revealed that approximately 70% of the vertical reinforcement was corroding due to carbonation. The project was performed in 1988 using 1.0 molar sodium carbonate solution as the electrolyte. Results obtained after 5 years have shown that apart from areas vulnerable to washing-out of the electrolyte there is no sign of significant reduction of the alkali content in the realkalised concrete. Phenolphthalein tests and sodium analyses of drilled cores 2 and 4 years after a realkalisation treatment on a church in Switzerland carried out in 1990 have shown that the alkali content adjacent to the reinforcement is sufficiently high to create a protective environment (Odden, 1994; Roti, 1994). Page and Yu (1995) and Page, Yu and Bertolini (1994) found that alkali-silica reaction could be triggered by redistribution of alkalis in concrete, induced by direct current. However, in terms of prevention, the authors report that the effect of lithium ions has been suggested as they form insoluble lithium silicate which has a very low propensity to expand although, they advise caution because inadequate concentrations of lithium ions can make the expansion of the alkali-silica reaction even worse.

In conclusion, electrochemical realkalisation appears a viable option for the rehabilitation of reinforced concrete structures suffering from carbonation induced corrosion. No side effects have been reported in laboratory specimens, however, caution

is advised when considering potential structures for its application as certain concrete structures are susceptible to alkali-silica reaction, particularly where non-uniform current distribution is likely or where prolonged application is necessary. In addition, long term monitoring of site trials using electrochemical methods are required to fully assess the durability of this method of rehabilitation.

#### 2.4.4.6 Other Inhibitors

In the SHRP-S-666 report (1993), 26 corrosion inhibitors were tested and sodium tetraborate was among five of the ones identified as having the potential of stopping the corrosion of steel of concrete. It is believed that the borate ion's application resulted in a reduction in the corrosion activity by acting as a barrier to increased metal dissolution. However, the borate compounds tended to act as cement retarders with zinc borate having a greater effect than sodium borate at similar concentrations. Although the compressive strength of the borate mortars were lower than the control at early stages, their 28 day strengths were comparable.

The injection of synergistic corrosion inhibitors into hardened concrete is another technique that has been examined by the Strategic Highway Research Program, (Asaro, Gaynor and Hettiarachchi, 1990; Hettiarachchi and Gaynor, 1992). The researchers developed an in-situ technique of electrically injecting quarternary ammonium and phosphonium compounds (molybdates and nitrites) as corrosion inhibitors into chloride contaminated hardened concrete. The results suggest that these inhibitors can provide 78-85% corrosion protection for the steel reinforcement. The technique is still new and extensive tests are required to address questions such as the length of the corrosion protection afforded and the effectiveness of the protection against chloride re-migration. The researchers claim that if the results of further research are positive then the technique's novelty, non-destructive nature and lack of permanent installation will make it a viable option for the future, although the costs of the technique make it economically comparable to electrochemical chloride extraction since it involves the

installation of a temporary anode. Broomfield (1999) describes an application in the field of an aminoalcohol inhibitor by surface application down holes drilled in concrete with over 1% chloride by weight of cement cast into the concrete as calcium chloride set accelerator. He reported only a slight reduction in the corrosion rate and the onset of cracking at approximately the same time as untreated controls.

This chapter has given a critical appreciation of the existing knowledge in the field. The following chapters in this thesis answer some of the questions that have arisen from this literature review by investigating the efficiency of some of the more promising inhibitor systems that have been discussed.



Equation	Parameters
$d = At^n$	d = carbonation depth t = time in years A = diffusion coefficient n = exponent (approximately 1/2)
$d = ABCt^{0.5}$	A = 1.0 for external exposure B = 0.07 to 1.0 depending on surface finish $C = R(w/c - 0.25) / (0.3(1.15 + 3w/c))^{1/2}$ $C = 0.37R(4.6w/c - 1.7)$ for $w/c < 0.6$ R = coefficient of neutralisation, a function of mix design and additives
$d = A(Bw/c - C)t^{0.5}$	A is a function of curing B and C are a function of fly ash used
$d = 0.43(w/c - 0.4)(12(t - 1))^{0.5} + 0.1$ $d = 0.53(w/c - 0.3)(12t)^{0.5} + 0.2$	28 day cured Uncured
$d = (2.6(w/c - 0.3)^2 + 0.16)t^{0.5}$ $d = ((w/c - 0.3)^2 + 0.07)t^{0.5}$	Sheltered Unsheltered
$d = 10.3e^{-0.123/f28}$ at 3 years	Unsheltered fX = strength at day X
$d = 3.4e^{-0.34/f28}$ at 3 years	Sheltered
$d = 680(f28 + 25)^{-1.5} - 0.6$ at 2 years	
$d = A + B / f28^{0.5} + c / (CaO - 46)^{0.5}$	CaO is the alkali content Expressed as CaO
$d = (0.508 / f35^{0.5} - 0.047)(365t)^{0.5}$	
$d = 0.846(10w/c / (10f7)^{0.5} - 0.193 - 0.076w/c)(12t)^{0.5} - 0.95$	
$d = A(T - t_i)t^{0.75} (C_1 / C_2)^{0.5}$	t <sub>i</sub> = induction time T = temperature in °K C <sub>1</sub> = CO <sub>2</sub> concentration C <sub>2</sub> = CO <sub>2</sub> bound by concrete

Table 2.1 – A selection of carbonation depth equations (Parrott, 1987b)

Total Chloride (%wt cem)	Free Chloride (M)	[Cl]:[OH]	Exposure	Sample	Reference
0.17 – 1.4	0.11	0.22	Outdoors	Structure	Stratful et al. (1975)
0.2 – 1.5			Outdoors	Structure	Vassie (1984)
0.5 – 0.7			Outdoors	Concrete	Thomas (1996)
0.25 – 0.5			Laboratory	Mortar	Elsener and Bohni (1986)
0.3 – 0.7			Outdoors	Structure	Henriksen (1993)
0.32 – 1.9			Outdoors	Concrete	Treadaway et al. (1989)
0.4			Outdoors	Concrete	Bamforth and Chapman-Andrews (1994)
0.4			Laboratory	Paste	Page et al. (1986)
0.4 – 1.6			Laboratory	Mortar	Hansson and Sorensen (1990)
0.5 – 2			Laboratory	Concrete	Schiessl and Raupach (1990)
0.5			Outdoors	Concrete	Thomas et al. (1990)
0.5 – 1.4			Laboratory	Concrete	Tuuti (1993)
0.6			Laboratory	Concrete	Locke and Siman (1980)
1.6 – 2.5			Laboratory	Concrete	Lambert et al. (1991)
1.8 – 2.2			Outdoors	Structure	Lukas (1985)
	0.14 – 1.8	2.5 – 6	Laboratory	Paste/ mortar	Pettersson (1993)
		0.26 – 0.8	Laboratory	Solution	Goni and Andrade (1990)
		0.3	Laboratory	Paste/ Solution	Diamond (1986)
		0.6	Laboratory	Solution	Hausmann (1967)
		1 – 40	Laboratory	Mortar/ solution	Yonezawa et al. (1988)

Table 2.2 – A summary of chloride threshold values (Glass and Buenfeld, 1997)



Aston University

Illustration removed for copyright restrictions

**Figure 2.1 – Principal hydration reactions of Portland cement materials (Double, 1983)**



Aston University

Illustration removed for copyright restrictions

**Figure 2.2 – Pore size classification for cement pastes (Young, 1988)**



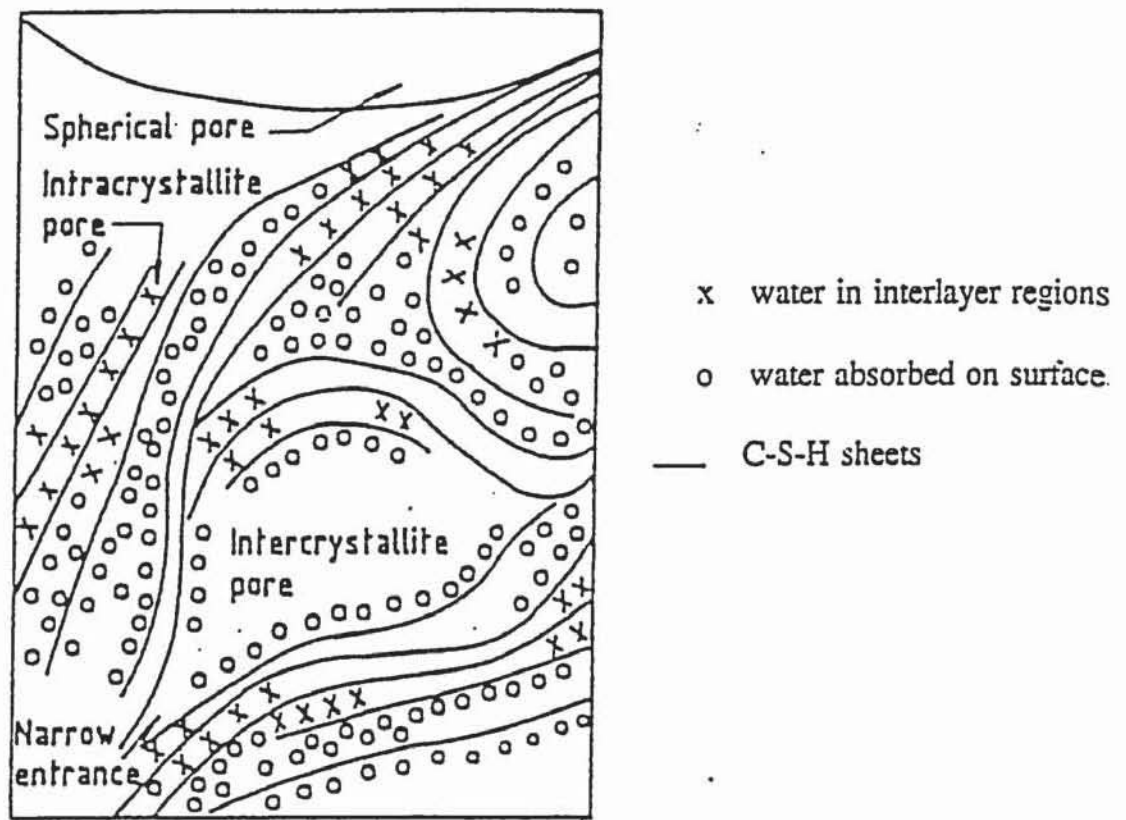


Figure 2.3 – Schematic representation of Feldman-Sereda pore structural model



Figure 2.4 – Hydroxyl ion concentrations of cement pastes of water/cement ratio 0.5  
Cured for 28 days unless otherwise stated (Nixon and Page, 1987)

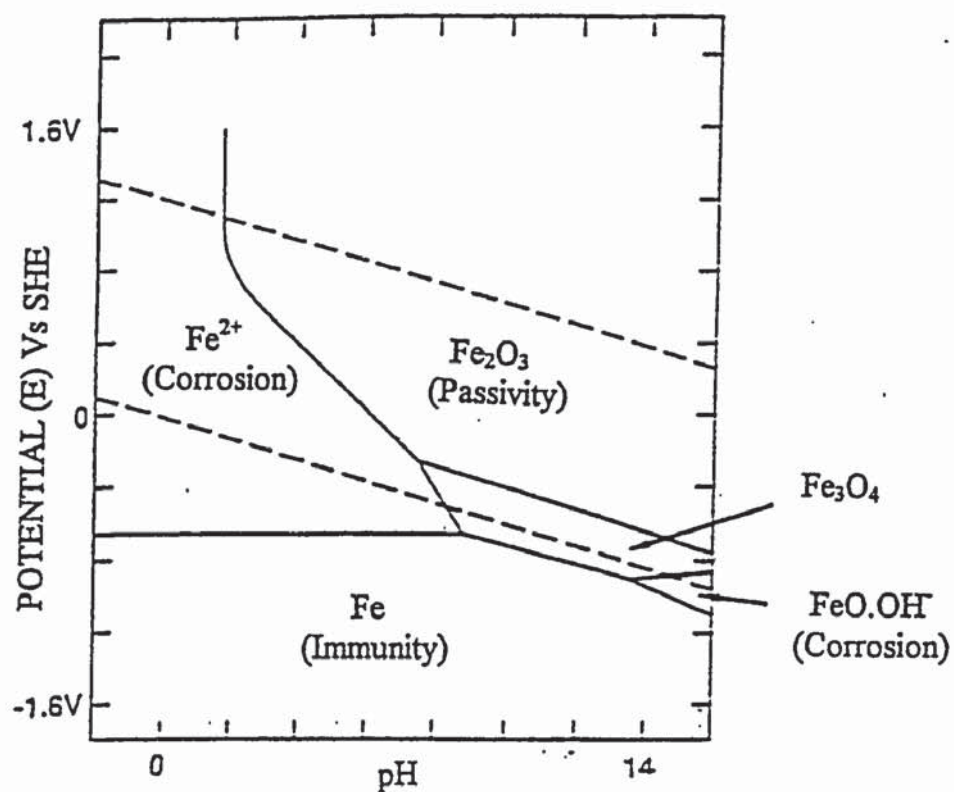


Figure 2.5 – Simplified Equilibrium Potential-pH diagram for iron in water  
(Pourbaix, 1966)

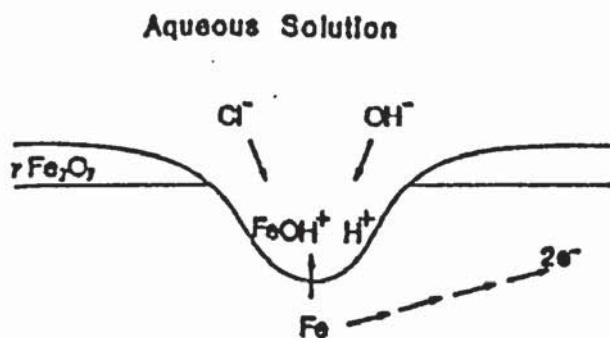


Figure 2.6 – Mechanism of pitting corrosion of iron in aqueous  
solutions containing chloride

## **CHAPTER THREE**

### **MATERIALS AND EXPERIMENTAL TECHNIQUES**

#### **3.1 INTRODUCTION**

This chapter describes the main materials used and the experimental techniques employed in this investigation.

#### **3.2 MATERIALS**

##### **3.2.1 Ordinary Portland Cement**

The cement used throughout this investigation was a standard Ordinary Portland Cement (OPC). The OPC was obtained from Blue Circle Cement Ltd and its chemical analysis and potential phase compositions are shown in Tables 3.1 and 3.2 respectively. The calculations for the potential phase compositions are detailed in Appendix A.

##### **3.2.2 Water**

De-ionised water was used throughout this research.

##### **3.2.3 Steel**

Bright drawn mild steel bars of 6mm diameter with a chemical composition as shown in Table 3.3 were used for the experimental investigations reported in Chapter Four.

##### **3.2.4 Counter Electrodes**

Mixed metal oxide coated activated titanium mesh was used for the counter electrodes required in the experimental investigations reported in Chapter Four.



### **3.2.5 Corrosion Inhibitors**

The corrosion inhibitors used for this investigation include sodium nitrite, sodium monofluorophosphate, sodium hydroxide and ethanolamine, which were all of analytical reagent grade (99.5% pure). Also, a proprietary alkanolamine-based inhibitor was used which was supplied as an aqueous solution of potassium hydrogen phosphate in addition to ethanolamine and possibly other substances of unidentified composition. Finally, a proprietary calcium nitrite-based inhibitor was used which was supplied as an aqueous solution of calcium nitrite and possibly other substances of unidentified composition.

### **3.2.6 Sodium Chloride**

Analytical reagent grade sodium chloride was used in this research to provide the required chloride ions for the experimental investigations presented in Chapter Four and Chapter Eight. A saturated solution of sodium chloride, again of analytical reagent grade, was used in order to provide a controlled relative humidity for the experimental investigations presented in Chapter Six.

### **3.2.7 Potassium Nitrate**

Analytical reagent grade Potassium Nitrate was used for the experimental investigations presented in Chapter Four.

### **3.2.8 Carbon Dioxide Absorber**

A proprietary carbon dioxide absorber by the name of Carbosorb was used for the experimental investigations reported in Chapter Four.

### **3.2.9 Pyroclean**

Pyroclean, which is a proprietary solution containing hydrochloric acid and inhibitive substances of unidentified composition, was used in order to remove the corrosion

products from the steel bars used in the experimental investigations reported in Chapter Four.

#### **3.2.10 Saturated Salt Solutions**

Sodium Dichromate, Magnesium Nitrate, Sodium Nitrite and Ammonium Nitrate were all used, along with Sodium Chloride as mentioned in section 3.2.6; in order to provide controlled relative humidity's for the experimental investigations presented in Chapter Six. All were of analytical reagent grade. A saturated salt solution of analytical reagent grade sodium nitrite was also used for the experimental investigations presented in Chapter Seven.

#### **3.2.11 Carbon Dioxide**

Carbon Dioxide was supplied, for the experimental investigations presented in Chapter Six, at three different concentrations. These concentrations included air, 5% carbon dioxide (with 21% oxygen and 74% nitrogen) and 100% carbon dioxide. 100% Carbon Dioxide was also used for the experimental investigations presented in Chapter Seven.

### **3.3 EXPERIMENTAL TECHNIQUES**

#### **3.3.1 Manufacture of Cement Paste Specimens**

All the Ordinary Portland Cement that was used for this project was sieved through a 150  $\mu\text{m}$  mesh in order to remove coarse particles. The required proportion of the OPC was then weighed and de-ionised water was added to the mix to produce a paste of the desired water to cement ratio (w/c). The mixture was blended thoroughly by hand for about 5 minutes with a spatula. The mixture was then poured into cylindrical PVC containers (49mm diameter by 75mm in height), which were vibrated for 2-4 minutes to get rid of any trapped air bubbles. On at least two occasions, the foamy layer that had accumulated on the surface was removed and replaced with fresh paste. A polythene sheet was placed on the surface of the paste in each of the cylinders to prevent the entrapment of air by the cap which was subsequently fitted on top. The cylinders were



rotated end over end at a speed of 8 rpm for at least 24 hours in order to minimise segregation and bleeding. This enables uniform as cast specimens to be formed. After seven days the specimens were de-moulded and placed in their respective curing environments.

### **3.3.2 Determination of Bulk Density**

Bulk density measurements were conducted on each batch of cement paste samples produced as a quality control procedure.

Each specimen was saturated for 24 hours by use of a vacuum pump. The specimen then had its weight immersed in water measured and recorded ( $W_1$ ). The specimen was then removed from the water, surface dried with a lens tissue, re-weighed in air and the saturated surface dry weight ( $W_2$ ) recorded. The bulk density was recorded according to Archimedes' principle as the ratio of weight in air to the loss of weight in water (see equation 3.1);

$$\text{Bulk Density (g/cm}^3\text{)} = W_2 / (W_2 - W_1) \quad (\text{equation 3.1})$$

### **3.3.3 Pore Solution Expression**

A method to express pore solutions from hardened cement paste, mortar and concrete samples was originally devised by Longuet, Burglen and Zelwer (1973) and this was refined by Barneyback and Diamond (1981).

The pore solution expression device consists of four main sections, i.e. support cylinder, platen, die body and piston assembly, as shown in Figures 3.1 and 3.2. PTFE spray is applied to the cylinder and piston to minimise friction. A PTFE disc is inserted between the piston and the hardened cement paste to seal the whole diameter of the die to prevent liquid from escaping upward. Pressure was then applied slowly at a rate of 0.3 kN/s. The solution was then drawn through the outlet tube and stored in sealed plastic vials in order to prevent it from being exposed to air. The pressure being applied to the



piston stopped automatically when a load of 600 kN was achieved. The parts of the pore expression device were then cleaned with water and acetone and sprayed with PTFE lubricant before re-use.

### **3.3.4 pH Meter**

A Pye Unicam pH electrode in conjunction with a Philips digital pH meter was used to determine the pH of the solutions used in the experimental investigations presented in Chapter Four and Chapter Six. It was necessary to calibrate the pH meter with buffers of pH 4, 7 and 10. This method of determination gives results accurate to within 0.01 of a pH unit.

### **3.3.5 Corrosion Potential Measurements**

Electrochemical measurements were required to assess the condition of the steel bars immersed in model electrolyte solutions. The corrosion potential is the electrical potential difference that exists at the steel/electrolyte interface compared with a standard reference half-cell of nominally fixed electrode potential. A saturated calomel electrode was used as the reference half-cell which was connected, along with the steel, to a high impedance digital voltmeter.

### **3.3.6 Linear Polarisation**

Linear polarisation is a non-destructive technique used to measure the instantaneous corrosion rate of steel in an electrolyte. The method was developed by Stern and Geary (1957) and Stern (1958) and it involves polarising the steel a few millivolts ( $\Delta E$ ) either side of its corrosion potential ( $E_{\text{corr}}$ ) and measuring the change in current ( $\Delta I$ ). The polarisation resistance can then be calculated using the Stern-Geary equation (see equation 3.2).

$$R_p = \Delta E / \Delta I = \beta_a \beta_c / [2.3 I_{\text{corr}} (\beta_a + \beta_c)] \quad (\text{equation 3.2})$$

Where:  $\beta_a$  and  $\beta_c$  are anodic and cathodic Tafel constants.

$$I_{\text{corr}} = \text{corrosion rate } (\mu\text{A}/\text{cm}^2)$$

The Tafel constants are assumed to be constant giving a simplified Stern-Geary equation (see equation 3.3).

$$I_{\text{corr}} = B / R_p \quad (\text{equation 3.3})$$

Where the value of B is assumed to be 26 mV.

An EC & G FieldCorr Portable Corrosion Analyser was used to carry out linear polarisation measurements (see Figure 3.3) on mild steel bars in model electrolytes as reported in Chapter Four. The preparation of the mild steel bars is described in Chapter Four.

### **3.3.7 Gravimetric Measurements**

Before the steel bars were placed in the model electrolytes their initial weights were recorded ( $W_{\text{init}}$ ) on a Sartorius Research R160 P Electronic Balance. Immediately after removing the steel bars from solutions they were photographed and then placed in a cleaning solution of 25% (by weight) Pyroclean. At five minute intervals the bars were removed from the cleaning solution, washed in tap water, then washed in de-ionised water before being dipped into methanol, dried and finally weighed. When all the corrosion products had been removed the final weight ( $W_{\text{final}}$ ) was recorded. The gravimetric weight loss is then determined according to equation 3.4.

$$\text{Weight Loss (mg/cm}^2\text{)} = (W_{\text{init}} - W_{\text{final}}) / A \quad (\text{equation 3.4})$$

Where A is the exposed surface area of steel ( $\text{cm}^2$ ).

### **3.3.8 Photography**

Many photographs were taken during this investigation. A 35mm camera mounted on a copy stand (see Figure 3.4) was used to photograph the steel bars before and after immersion in the model electrolytes. A JVC video camera with a macro zoom lens attached to a digital image capture program (see Figure 3.5) was used to obtain magnified digital photos of specific areas of interest on the steel bars.

### **3.3.9 Water and Acid Extraction**

For Chapter Five, cylindrical cores, 75mm in diameter, were obtained from site so that one end of each cylinder was derived from the inhibitor-treated face. The cores were profile ground a millimetre at a time from the inhibitor-treated face (see Figure 3.6) and the constituents of the concrete were then gathered in 2mm thick layers parallel to the treated surface. The powdered samples were then dried at 105°C for at least 24 hours. A sample weighing  $2.000 \pm 0.001\text{g}$  was taken from each layer and placed into a 100cm<sup>3</sup> beaker. In order to extract the water-soluble ions 80cm<sup>3</sup> of de-ionised water was added, and in order to extract the acid-soluble ions 20cm<sup>3</sup> of 2% nitric acid (HNO<sub>3</sub>) with 60cm<sup>3</sup> de-ionised water was added. The mixture was vigorously agitated and placed in an ultrasonic water-bath for at least 5 minutes, after which it was again agitated. After the concrete particles had settled, the extract was filtered through Whatman Number 3 filter paper into a 250cm<sup>3</sup> volumetric flask. The concrete particles were washed with 80cm<sup>3</sup> portions of de-ionised water, agitated thoroughly, allowed to settle and the washings poured through the filter paper into the flask. This was repeated until there was nearly 250cm<sup>3</sup> of filtrate in the flask, which was then made up to 250cm<sup>3</sup> with de-ionised water. The resulting solution was then analysed using ion chromatography.

### **3.3.10 Ion Chromatography**

A Dionex DX-500 ion chromatography system (see Figure 3.7) was used to analyse pore solutions for both anions and cations. Solutions were analysed for fluoride, chloride, nitrite, bromide, nitrate, monofluorophosphate, phosphate and sulphate anions; along with lithium, sodium, potassium, magnesium, calcium and ethanalamine cations.



Samples are diluted and passed through a column containing an ion exchange resin that strips out the ions. The column is then 'washed' with an eluent solution. The eluent will remove different ions from the column at different rates, dependent on the balance between that particular ion's affinities for the column and the eluent. Consequently, the eluent will become contaminated with particular ions at different times. If the conductivity of the eluent leaving the column is plotted against time, a number of peaks will be displayed, each at a time corresponding to a different ion. By comparison of the appearance time and areas of these peaks with plots derived from standard solutions, quantitative analysis of the ions in each solution was obtained.

Solutions of 1:100 dilution were used with a 2mM  $\text{Na}_2\text{CO}_3$  + 2.5mM  $\text{NaHCO}_3$  solution eluent to analyse for anions and a 7.5mM  $\text{H}_2\text{SO}_4$  solution eluent to analyse for cations.

A calculation is presented in Appendix B.

#### **3.3.11 Carbonation Depth**

In order to assess the depth of carbonation a freshly broken piece of concrete or hydrated cement paste was sprayed with phenolphthalein indicator solution which will show no colour change below pH 10 to a purple red above pH 10, thus giving an indication of carbonation depth (i.e. depth from the exposed face which undergoes no colour change). Phenolphthalein was chosen because of its convenience and reproducibility (RILEM CPC-18, 1984; Forrester, 1976; Verbeck, 1958).

#### **3.3.12 Hydroxyl Ions**

Hydroxyl ion concentrations within pore solutions were measured by titration. This was carried out by neutralising a 0.1ml sample of pore solution, made up to 1ml with de-ionised water, with 0.01M nitric acid or by neutralising a 1.0ml sample of pore solution with 0.001M nitric acid. Phenolphthalein was used as the pH indicator.

The pH of the solution was then calculated from the hydroxyl ion concentration (equation 3.5). A detailed calculation is presented in Appendix C.

$$\begin{aligned}
 \text{pH} &= -\text{Log}_{10}[\text{H}^+] \\
 \text{pOH} &= -\text{Log}_{10}[\text{OH}^-] \\
 \text{pH} + \text{pOH} &= 14 \\
 \text{pH} &= 14 + \text{Log}_{10}[\text{OH}^-] \quad (\text{equation 3.5})
 \end{aligned}$$

### **3.3.13 Bicarbonate and Carbonate Ions**

Pore solutions were analysed for bicarbonate and carbonate ions by the titration of a 1.0ml sample of pore solution with 0.001M nitric acid whilst monitoring the pH using the pH meter described in section 3.3.4. When titrating a carbonate solution with acid, two inflections are established at around pH 9 and pH 4, where the first coincides with the point of conversion to bicarbonate and the second with complete neutralisation (Vogel, 1978).

No such clear inflections were observed and many of the solutions had an initial pH of below 9. However, the amount of acid needed to neutralise the total amount of carbonate and bicarbonate down to pH 4 was recorded. From this, the amount of carbonate and/or bicarbonate present in the pore solution was estimated as detailed in Appendix D.

### **3.3.14 Evaporable Water Content**

The evaporable water content was calculated in order to express ionic species as free amounts present in the hydrated cement paste as a fraction of the unhydrated cement.

Small fragments totalling about 2g of hydrated cement paste were weighed in a platinum crucible immediately after crushing. The crucible and contents was then

heated in an oven at 105°C for 24 hours and the weight recorded. It was then transferred to a furnace at 950°C for 30 minutes after which the weight was again recorded.

The loss on ignition was determined according to the method given in BS 4550 (1970). This involved about 1g of unhydrated cement being weighed in a platinum crucible before and after heating at 950°C. The loss on ignition is reported as the loss of mass as a percentage of the weight at 950°C.

The evaporable water was then calculated in grams of water per gram of unhydrated cement after correction for ignition loss and for admixtures as shown in equation 3.6.

$$\text{E.W.(\%)} = [(W_0 - W_{105}) \times (100 - i - a)] / W_{950} \text{ (equation 3.6)}$$

Where:	E.W.	=	evaporable water (% by weight of cement)
	$W_0$	=	weight of hydrated cement paste (g)
	$W_{105}$	=	weight at 105°C (g)
	$W_{950}$	=	weight at 950°C (g)
	i	=	loss on ignition (% by weight of cement)
	a	=	total admixtures (% by weight of cement)

A detailed calculation is presented in Appendix E.

### **3.3.15 Water Desorption**

Thin disc specimens were used for water desorption experiments. Each specimen was saturated for 24 hours by use of a vacuum pump. Each specimen then had its weight immersed in water measured and recorded ( $W_1$ ). Each specimen was then removed from the water, surface dried with a lens tissue, re-weighed in air and the saturated surface dry weight ( $W_2$ ) recorded. Each specimen was then exposed to an environment of 90.7% relative humidity at a temperature of 22°C until a near constant weight ( $W_3$ ) was achieved and recorded. The environment of 90.7% relative humidity was achieved by



placing the specimens over a saturated solution of hydrated barium chloride ( $\text{BaCl}_2 \cdot 2\text{H}_2\text{O}$ ) within an air-tight container. Each specimen was then finally dried at  $105^\circ\text{C}$  for 24 hours and its weight ( $W_4$ ) recorded.

If a specimen is saturated with water and then dried, the loss in weight is a direct reflection of the void volume since water has a density of about  $1 \text{ g/cm}^3$ . Porosity is given by the ratio of the void volume to the total volume. The total volume as calculated during the bulk density measurement is the loss in weight of a sample when weighed in water to that still saturated in water but weighed in air. Therefore the capillary porosity is given equation 3.7.

$$\text{Capillary porosity (\%)} = [(W_2 - W_3) / (W_2 - W_1)] \times 100 \quad (\text{equation 3.7})$$

Where the capillary porosity, as measured, represents the pore sizes greater than approximately 30nm (Parrott, 1992), while the total porosity is given by equation 3.8.

$$\text{Total porosity (\%)} = [(W_2 - W_4) / (W_2 - W_1)] \times 100 \quad (\text{equation 3.8})$$

A detailed calculation is presented in Appendix F.

### **3.3.16 X-Ray Diffraction Analysis**

A Philips X-Ray Diffractometer (see Figures 3.8 and 3.9) with  $\text{CuK}\alpha$  radiation was used in this investigation. Most materials are crystalline and hence show some symmetry and regularity. When irradiating material by monochromatic X-rays, a pattern is obtained which is characteristic for the sample (i.e., like a fingerprint). In this way any crystalline compound can be identified.

Hydrated cement paste samples were ground to a fine powder, which basically consisted of thousands of small crystals (crystallites). The random orientation of these crystallites

in the specimen ensures that every possible reflection plane is presented parallel to the specimen surface by at least some crystallites. X-ray diffraction shows the typical lines of each compound separately.

An electronic counter tube was used to measure the intensity of the X-ray reflections. The counter tube was rotated at twice the speed of the specimens in order to receive the reflected rays. A trace intensity (I) is recorded against the Bragg angle ( $\theta$ ) from which the d spacing can be determined. The reflection of X-rays will only occur when Bragg's Law is satisfied (see equation 3.9). Thus for a given wavelength and angle of incidence where reflection occurs the atom spacing may be calculated.

$$n\lambda = 2d \sin \theta \quad \text{(equation 3.9)}$$

Where:      n is the order of reflection (1,2 etc)  
               $\lambda$  is the wavelength of the X-ray  
              d is the spacing of the crystal planes  
               $\theta$  is the angle of incidence or reflection of the X-ray beam

### **3.3.17 Differential Thermal Analysis / Thermo-Gravimetric Analysis**

A PL Thermal Sciences STA 1500 was used for the thermal analysis conducted during this investigation (see Figure 3.10). Thermal analysis involves measuring changes in property as a function of increasing temperature. When subjected to thermal treatment a substance can undergo physical and/or chemical changes. Differential thermal analysis (DTA) enables energy changes to be measured by monitoring the temperature difference between an inert reference material and the sample to be tested as they are subjected simultaneously to a defined temperature program. Thermo-gravimetric analysis (TGA) involves measuring weight changes as a function of temperature. The two types of analysis were run simultaneously on each specimen.



A small weight of specimen (35-40 mg) was taken as a crushed powder and it was subjected to a controlled program of temperature rise, alongside an inert reference sample of alumina powder. The resultant thermograph was used to determine the minerals present in each sample (using the DTA trace) and the quantity of each compound present (using the TGA trace).

### **3.3.18 Mercury Intrusion Porosimetry**

Mercury Intrusion Porosimetry (MIP) was carried out using a Micromeritics Pore Sizer 9310 (see Figure 3.11). About 2.5 to 3g of hydrated cement paste was broken into small pieces. A solvent replacement technique was considered the most effective way of removing the water from the cement paste without causing considerable damage to the pore structure (Feldman and Beaudoin, 1991). The alcohol used for this study was propan-2-ol (iso-propanol), because its effect on the pore structure is of a lesser degree than when other solvents are used, as recommended in previous investigations (Konecny and Naqvi, 1993; Feldman and Beaudoin, 1991). Each sample was immersed in propan-2-ol and placed in a jar which was vibrated in an ultrasonic waterbath for approximately 5 minutes with the cloudy alcohol being discarded. The process of vibration was repeated until the alcohol ceased to become cloudy. It was then assumed that most of the water in the sample had been removed, since water is miscible with alcohol producing the cloudy appearance. Following the last vibration, the sample was dried, using a cold air blower, and stored in a vacuum desiccator for approximately 3 days. MIP determines the pore size distribution of accessible pores in hydrated cement pastes. Pressure is increased stepwise and volumes intruding pores are measured. The total volume of mercury indicates the total porosity of the hydrated cement paste whilst the pressure at which the pores are penetrated is related to the pore diameter (d) by the Washburn equation (equation 3.10).

$$P = (4\gamma\cos\theta) / d \qquad \text{(equation 3.10)}$$



Where:         $P$  is the applied pressure  
                $\gamma$  is the surface tension  
                $\theta$  is the contact angle

The Micromeritics Pore Sizer 9310 applies a maximum pressure of 30,000 psi. A contact angle of  $117^\circ$  was adopted for this study based on earlier work by Winslow and Diamond (1970) where it was reported that the contact angle for cylindrical pores in hydrated cement pastes which have been oven-dried at  $105^\circ\text{C}$  was  $117^\circ$ . Although the assumed contact angle does not strictly apply to the method of drying adopted for these investigations, it was considered adequate since the investigations were looking at comparisons rather than exact pore size distributions.

#### **3.3.19 Relative Humidity and Temperature**

Relative humidity and temperature measurements were obtained using a hand held Vaisala HM 34 Humidity and Temperature Meter which could be placed into containers through pre-drilled holes (see Figure 3.12).

Material	% (by weight)
CaO	63.86
SiO <sub>2</sub>	19.07
Al <sub>2</sub> O <sub>3</sub>	5.13
Fe <sub>2</sub> O <sub>3</sub>	2.83
SO <sub>3</sub>	3.25
MgO	1.35
Na <sub>2</sub> O	0.11
K <sub>2</sub> O	0.74
Cl	0.015
F. CaO	1.49

Table 3.1 – Chemical analysis of Ordinary Portland Cement

C <sub>3</sub> S	C <sub>2</sub> S	C <sub>3</sub> A	C <sub>4</sub> AF
61.16	8.54	8.81	8.61

Table 3.2 – Potential Phase Compositions of Ordinary Portland Cement (% by weight)  
(Taylor, 1997)

Fe	C	Si	Mn	P	S	Cr	Mo	Ni	Al	Cu	Sn
98.5	0.08	0.13	0.58	0.02	0.03	0.11	0.02	0.10	0.01	0.30	0.02

Table 3.3 – Chemical composition of mild steel bars (% by weight)

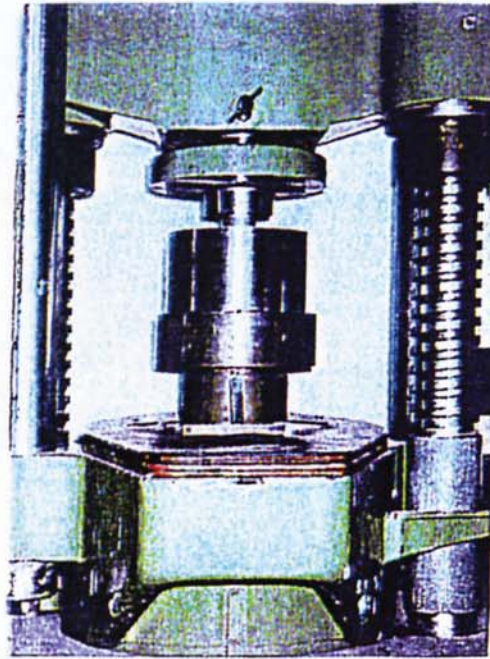


Figure 3.1 – Pore solution expression device

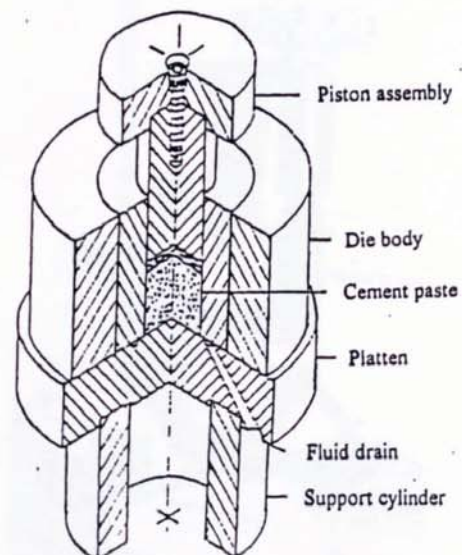


Figure 3.2 – Schematic representation of pore solution expression device





Figure 3.3 – EC & G FieldCorr Portable Corrosion Analyser

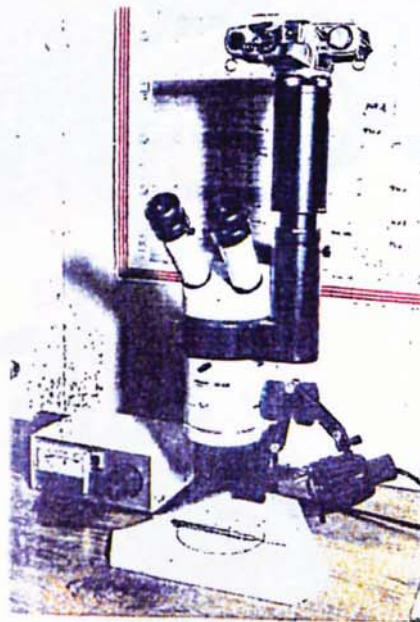


Figure 3.4 – 35mm camera mounted on a copy stand

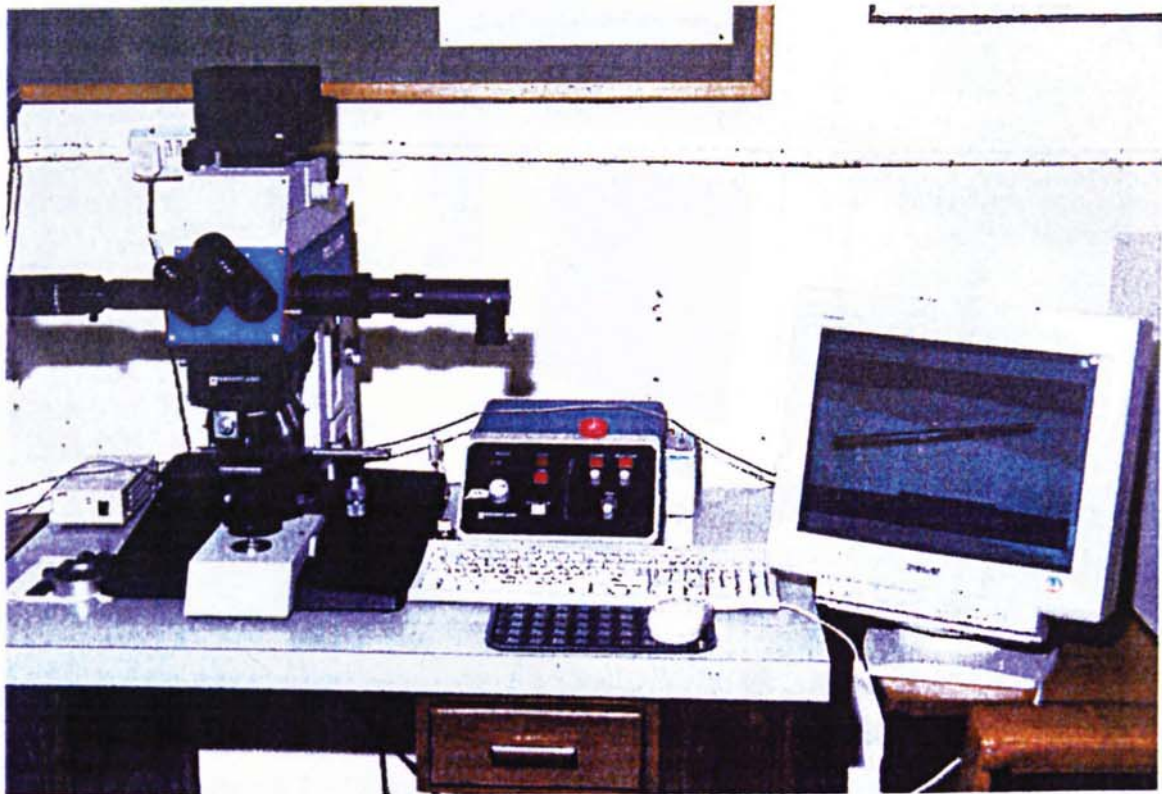


Figure 3.5 – JVC video camera with digital image capture facility

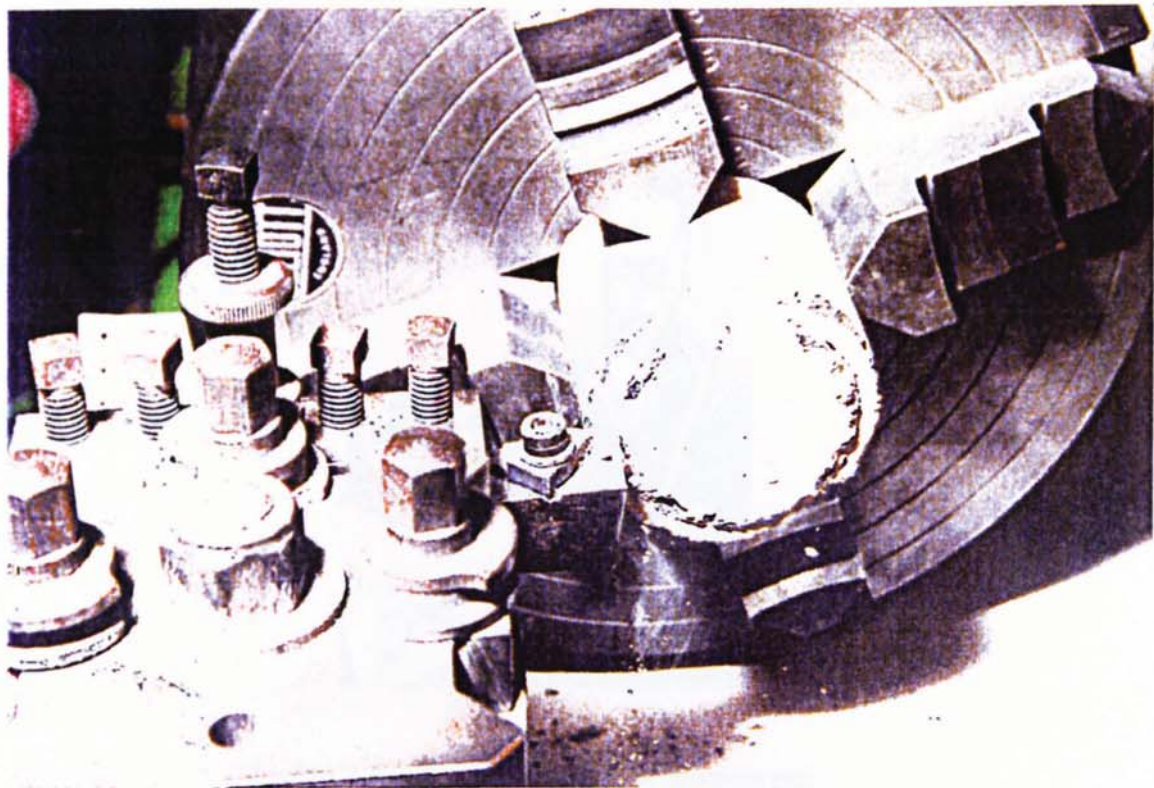


Figure 3.6 – Profile grinding of a cylindrical core





Figure 3.7 – Dionex DX-500 ion chromatography system



Figure 3.8 – Phillips X-Ray Diffractometer



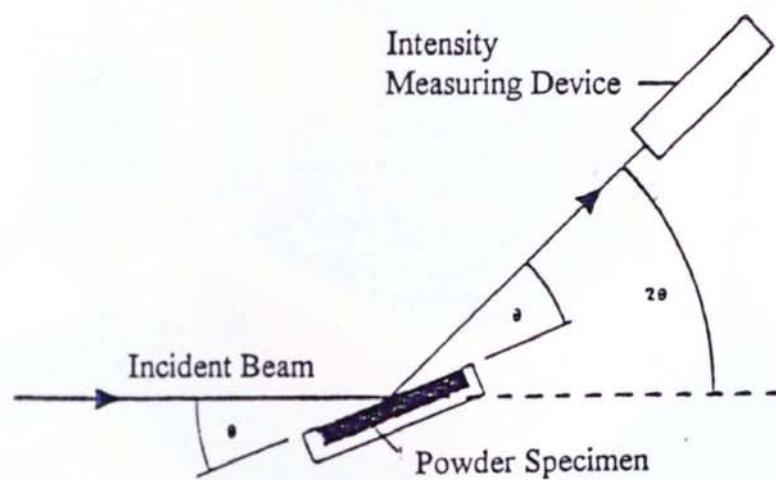


Figure 3.9 – Geometric arrangement of X-ray diffractometer

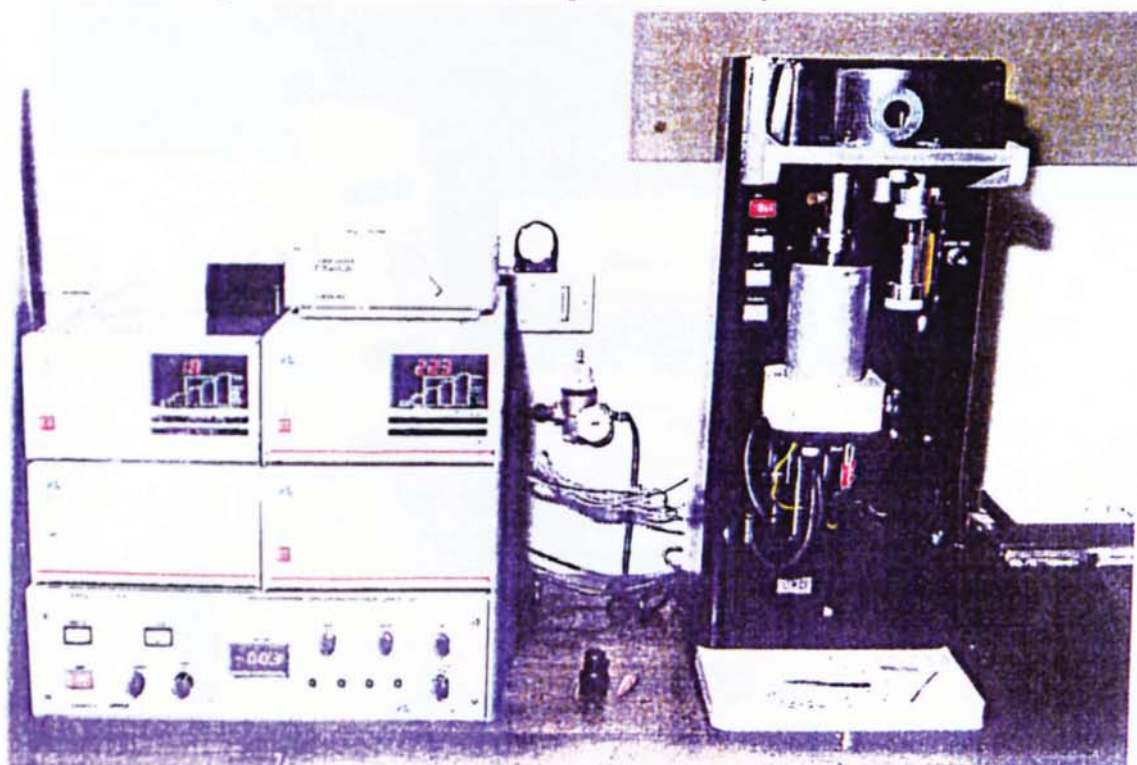


Figure 3.10 – PL Thermal Sciences STA 1500

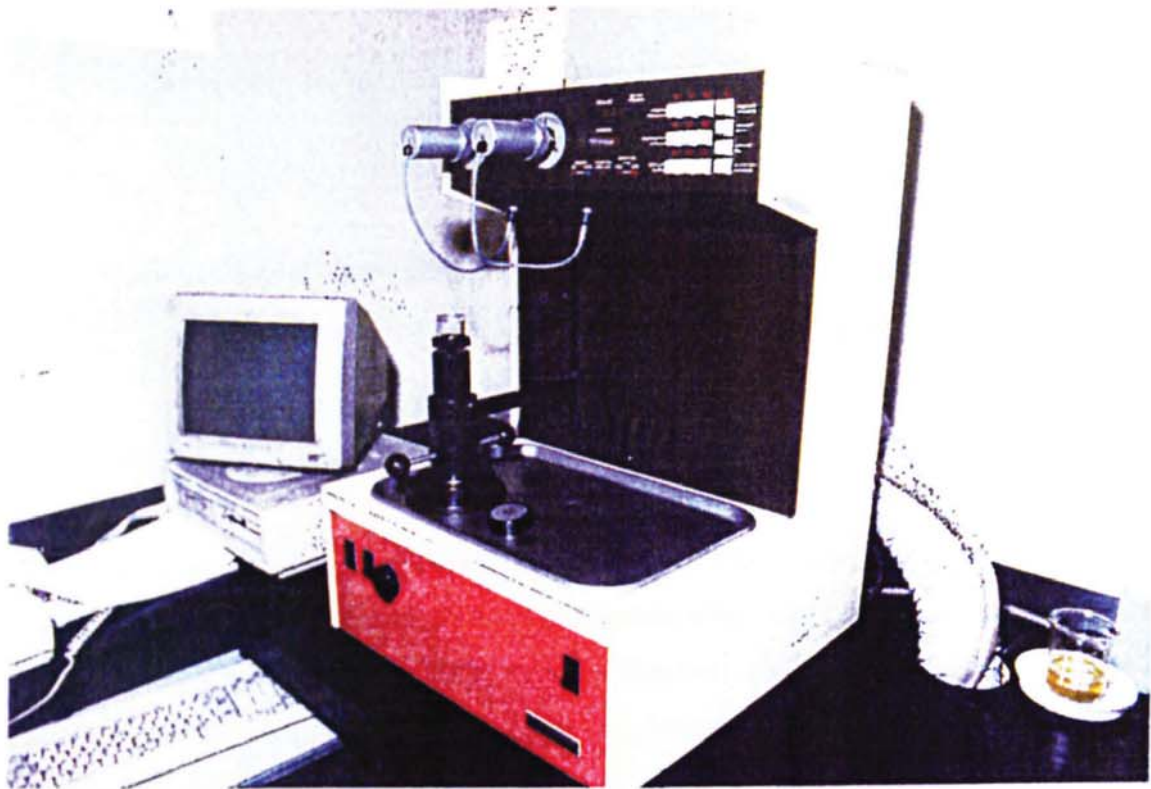


Figure 3.11 – Micromeritics Pore Sizer 9310



Figure 3.12 – Vaisala HM 34 Humidity and Temperature Meter



## CHAPTER FOUR

### MECHANISMS OF INHIBITOR ACTION IN MODEL ELECTROLYTE SYSTEMS

#### 4.1 INTRODUCTION

There are several novel proprietary repair systems that involve corrosion inhibitors being applied to the surfaces of reinforced concrete structures suffering from the effects of carbonation and/or chloride contamination. However, there are reservations about the effectiveness of such treatments because of uncertainty over depths of inhibitor penetration, quantities required at the steel surface, deleterious side effects and longevity of protection afforded. There has been little independent research to date on these issues.

Following a review of the available literature, three corrosion inhibitors were selected for investigation in this chapter, namely nitrite ions (in the form of  $\text{NaNO}_2$ ), sodium monofluorophosphate ( $\text{Na}_2\text{PO}_3\text{F}$ ) and a proprietary alkanolamine-based inhibitor. The alkanolamine-based inhibitor was found to contain ethanolamine as a major constituent and it was therefore decided to add analytical reagent grade ethanolamine ( $\text{NH}_2\text{CH}_2\text{CH}_2\text{OH}$ ) to the list of inhibitors to be investigated.

The aim of Chapter Four was to study the behaviour of the inhibitors in model electrolytes intended to simulate the pore solution phase present within carbonated and/or chloride contaminated concrete. This involved investigating the behaviour of the inhibitors in an ideal situation, i.e. penetration of the inhibitors was not required so their concentrations could be controlled and also, the steel was in a passive condition before immersion in the model electrolytes. With this overall aim in mind, the experimental investigations were carried out with two main objectives. The first objective was to



establish whether the inhibitors investigated behave as anodic, cathodic or mixed inhibitors in air-saturated neutral and alkaline aqueous solutions with varying additions of chloride ions. The second objective was to gain an insight into the concentrations of inhibitors required for the inhibition of corrosion of steel in air-saturated neutral and alkaline aqueous solutions with varying additions of chloride ions. These objectives were achieved by immersing mild steel bars in air-saturated model electrolytes for 42 days and carrying out corrosion potential and linear polarisation measurements at regular intervals. At the end of the immersion tests, weight loss determinations and photographic examinations of the specimens were carried out.

## **4.2 EXPERIMENTAL PROCEDURES**

### **4.2.1 Preparation of Model Electrolytes**

Aqueous solutions of varied pH and chloride concentration were made up to simulate the pore solution phase present within carbonated and/or chloride contaminated concrete. Six control conditions were considered, namely de-ionised water, de-ionised water with 0.01M sodium chloride, de-ionised water with 0.1M sodium chloride, 0.1M sodium hydroxide, 0.1M sodium hydroxide with 0.1M sodium chloride and, 0.1M sodium hydroxide with 1.0M sodium chloride.

Four corrosion inhibitors were used, namely sodium monofluorophosphate, sodium nitrite, ethanolamine and an alkanolamine-based inhibitor. These inhibitors were added to the above listed solutions at three different concentrations, namely 0.01M, 0.1M and 1.0M. Sodium monofluorophosphate was also added to some of the above controls at 0.2M and 0.5M concentrations. Sodium nitrite, rather than calcium nitrite, was used in this section of the present study for economic reasons and because calcium nitrite interacts within a cement matrix to form sodium nitrite in the pore solution. The alkanolamine-based inhibitor was supplied as an aqueous solution of ethanolamine with potassium di-hydrogen phosphate and possibly other substances of unidentified composition. Ion chromatography was carried out on the inhibitor solution, as described

in section 3.3.10, and its concentrations of ethanolamine, phosphate and potassium were found to be 2.3M, 1.2M and 1.2M respectively. The concentrations of the alkanolamine-based inhibitor to be used in the experiments described in this chapter were calculated by considering only the ethanolamine concentration, i.e. 1.0M alkanolamine-based inhibitor actually means 1.0M ethanolamine, 0.52M phosphate, 0.52M potassium and possibly other substances of unidentified composition. Differences in performance between solutions of pure ethanolamine and those of the alkanolamine-based inhibitor could therefore be attributed to substances other than ethanolamine present in the proprietary inhibitor.

#### **4.2.2 Preparation of Mild Steel Bars**

Bright drawn mild steel bars of 6mm diameter with a chemical composition as shown in Table 3.3 were used for the experimental investigations reported in this chapter. The bars were cut into 100mm lengths and each of the ends was squared off in a lathe. One end of each bar was drilled and tapped to take a 12mm long M4 stainless steel slotted pan head screw. The bars were cleaned in a drill chuck with P1200 (600 grit) silicon carbide (SiC) abrasive paper, then de-greased using methanol and acetone, before being placed in a desiccator for one week in order to allow an air oxide film to form. They were then weighed and identified. Finally, the bars were covered except for an area of  $8\text{cm}^2$  on the end opposite to that which had been tapped and drilled. The masking process involved applying Fortolac (a proprietary stopping-off lacquer) on the bottom end of the bars in a 5mm band and in a 20mm band from the proposed exposed steel/cover interface towards the tapped end of the bars. Shrink fit tubing was applied throughout the area between the exposed steel/cover interface and the drilled end (great care was taken to avoid excessive heat when shrink fitting). Fortolac was then applied once more around the steel/cover interface. Each Fortolac application was deemed satisfactory when no defects were visible after drying. The masking was carried out in order that a known surface area could be exposed to the model electrolytes. Once prepared, the mild steel bars were as shown in Figure 4.1.



#### **4.2.3 Gel Bridge Construction**

An aqueous solution containing 3.5% agar and 15% potassium nitrate by weight was prepared by heating gently until it reached a temperature of approximately 80°C upon which the agar goes into solution. The solution was maintained at 80°C until clear of air bubbles. It was then transferred into prepared glass U-tubes with the aid of a syringe and allowed to cool and form a gel. Once cooled, the gel bridges were kept in water until required further in order to prevent them from drying out.

#### **4.2.4 Cell Assembly**

A typical cell consisted of a 100ml tall form beaker with a loose fitting rigid PVC lid which had been drilled to allow the steel bar to be suspended centrally in the model electrolyte solution, so that the exposed steel area was fully submerged and not touching the sides or bottom of the beaker. Holes were also drilled in the lid to accommodate the counter electrode (Figure 4.2) and gel bridge. A schematic of the cell assembly is shown in Figure 4.3.

#### **4.2.5 Final Set-Up**

The final set-up is as shown in Figures 4.4 and 4.5. Clear perspex boxes, of internal dimensions 500mm by 500mm by 200mm high, were filled to a depth of approximately 20mm with de-ionised water. This maintained the relative humidity within the boxes at around 100%, which prevented the model electrolytes from evaporating. A tray was placed in the bottom of each box, which allowed the cells to stand clear of the water. Also, a pot of carbosorb was placed within each box in order to absorb any carbon dioxide and thus prevent the pH of the model electrolytes from undergoing significant changes. Twenty-four cells were placed within each box, in groups of six. In the middle of each group of six a pot containing an aqueous solution of 2M potassium nitrate was placed and this was connected, via six gel bridges, to each of the six surrounding model electrolytes. Also, each of the potassium nitrate solutions within the groups of six was connected, via gel bridges, to a central pot of 2M potassium nitrate that contained a saturated calomel reference electrode. The purpose of the gel bridges and the potassium



nitrate solutions was to allow all the experiments within a box to be conducted using the same saturated calomel reference electrode.

The reference electrode, mild steel bars and counter electrodes, within each box, were connected to wires that passed through the side of the box. All bare metal at the connections etc., was lacquered in order to prevent corrosion cells from being set up away from the test area. Once set up, the lids on the boxes were sealed and the electrochemical monitoring was carried out externally. This allowed the environment within each box to remain unchanged throughout the experiments. All tests were carried out in triplicate, i.e. three bars were exposed to each model electrolyte.

#### **4.2.6 pH Measurements**

The pH of each model electrolyte was obtained, before the cells were assembled, using the method described in 3.3.4.

#### **4.2.7 Electrochemical Monitoring**

The electrochemical monitoring was carried out with measurements being taken after 1, 2, 3, 7, 14, 21, 28, 35 and 42 days from the time of immersion of the steel bars in the model electrolytes. Corrosion potential measurements ( $E_{corr}$ ) were made as described in section 3.3.5. Corrosion rate determinations ( $I_{corr}$ ) were carried out using the linear polarisation technique as described in section 3.3.6.

#### **4.2.8 Gravimetric Measurements**

After 42 days the steel bars were carefully removed from the solutions and experimental weight loss determinations were carried out using the technique described in 3.3.7.

#### **4.2.9 Theoretical Weight Loss Determinations**

Theoretical weight loss determinations for the steel bars were achieved by integrating the linear polarisation results with respect to time, i.e.  $\int I dt$ , and relating this to

Faraday's laws of electrolysis. Integrating the linear polarisation results with respect to time gives the area under the corrosion rate versus time graph for a particular bar and therefore the total charge passed, i.e. current  $\times$  time. The total charge passed is proportional to the quantity of anodic and cathodic products produced as the passage of a given quantity of charge will yield amounts of anodic and cathodic products proportional to the equivalent weights of the substances concerned, i.e. molar weight/number of electrons transferred ( $56/2 = 28\text{g}$  for iron). Faraday's constant (96500 coulomb) is the quantity of charge required to yield the equivalent weight of a substance (in grams).

#### **4.2.10 Photography**

The steel bars were photographed as described in section 3.3.8.

### **4.3 DISCUSSION OF RESULTS**

#### **4.3.1 pH Determinations**

It can be seen in Table 4.1 that the pH of the control model electrolyte solutions, that contained 0.1M NaOH, generally remained unchanged when the inhibitors were added with the pH ranging between 12.7 – 13.0. The only exceptions to this were the model electrolytes which contained 1.0M alkanolamine-based inhibitor. These had pH values in the range 12.1 – 12.2. In the neutral solutions, the addition of sodium monofluorophosphate had very little effect on the pH. Addition of 1.0M sodium nitrite raised the pH from approximately 6.3 to 7.3. Addition of 1.0M of the alkanolamine-based inhibitor raised the pH to above 10.0, whilst the addition of 1.0M ethanolamine raised the pH to 11.8.

#### **4.3.2 Electrochemical Monitoring**

##### **4.3.2.1 Sodium Nitrite**

Figures 4.6 to 4.19 show the results of the electrochemical monitoring on the mild steel bars immersed in the model electrolytes with various additions of sodium nitrite.



Corrosion potential measurements ( $E_{\text{corr}}$ ) were carried out alongside the  $I_{\text{corr}}$  measurements. The  $E_{\text{corr}}$  values quoted in this discussion are  $E_{\text{corr}}$  versus a saturated calomel electrode (SCE scale).

Figures 4.6 and 4.7 show the variation of  $I_{\text{corr}}$  and  $E_{\text{corr}}$  respectively with time for mild steel bars immersed for 42 days in air-saturated aqueous solutions of de-ionised water with various additions of sodium nitrite. From these graphs it can be clearly seen that even 0.01M sodium nitrite is effective in maintaining the steel bars in a passive condition, i.e. maintaining the steel at values of  $I_{\text{corr}}$  below  $0.1\mu\text{A}/\text{cm}^2$  and  $E_{\text{corr}}$  above -200mV (SCE scale).

Figures 4.8 and 4.9 show the variation of  $I_{\text{corr}}$  and  $E_{\text{corr}}$  respectively with time for mild steel bars immersed for 42 days in air-saturated aqueous solutions of de-ionised water with 0.01M sodium chloride and various additions of sodium nitrite. It can be seen that sodium nitrite inhibits corrosion fully at all concentrations, although the  $E_{\text{corr}}$  values are significantly more negative with 0.01M sodium nitrite when compared to the higher inhibitor concentrations.

Figures 4.10 and 4.11 show the variation of  $I_{\text{corr}}$  and  $E_{\text{corr}}$  respectively with time for mild steel bars immersed for 42 days in air-saturated aqueous solutions of de-ionised water with 0.1M sodium chloride and various additions of sodium nitrite. Figure 4.10 shows that at least an order of magnitude inhibiting effect is seen, however, only 1.0M sodium nitrite is sufficient to maintain the steel bars in a passive condition.

Figures 4.12 and 4.13 show the variation of  $I_{\text{corr}}$  and  $E_{\text{corr}}$  respectively with time for mild steel bars immersed for 42 days in air-saturated aqueous solutions of 0.1M sodium hydroxide with various additions of sodium nitrite. As expected, all bars remained in a passive condition, even those without nitrite addition. This is because of the inhibitive effect of hydroxyl ions. In 0.1M sodium hydroxide (pH 13), without chloride addition,



the steel will behave as is shown in the simplified equilibrium potential-pH diagram for iron in water (Figure 2.5).

Figures 4.14 and 4.15 show the variation of  $I_{corr}$  and  $E_{corr}$  respectively with time for mild steel bars immersed for 42 days in air-saturated aqueous solutions of 0.1M sodium hydroxide with 0.1M sodium chloride and various additions of sodium nitrite. Figure 4.14 shows that at least an order of magnitude inhibiting effect is seen, however, only 1.0M sodium nitrite is sufficient to maintain the steel bars in a passive condition. However, 0.1M sodium nitrite did maintain passivity for 28 days, beyond which passivity appeared to be lost.

Figures 4.16 and 4.17 show the variation of  $I_{corr}$  and  $E_{corr}$  respectively with time for mild steel bars immersed for 42 days in air-saturated aqueous solutions of 0.1M sodium hydroxide with 1.0M sodium chloride and various additions of sodium nitrite. These figures show that even at 1.0M nitrite addition, passivity could not be maintained beyond 3 days, although an order of magnitude reduction in values of  $I_{corr}$  was seen throughout the duration of immersion. Figures 4.16 and 4.17 also show that sodium nitrite, when present at 0.01M and 0.1M concentrations, does not have a significant effect on  $I_{corr}$  and  $E_{corr}$ .

Figure 4.18 shows the variation of corrosion potential with log corrosion rate for mild steel bars immersed in air-saturated aqueous solutions of de-ionised water with various additions of sodium chloride and sodium nitrite. The best-fit lines shown throughout this chapter were obtained using the least-squares method (Stroud, 1995). It can be seen that as the corrosion rate is reduced, i.e. inhibited, the corrosion potential shifts in the more positive direction. Figure 4.19 shows the variation of corrosion potential with log corrosion rate for mild steel bars immersed in air-saturated aqueous solutions of 0.1M sodium hydroxide with various additions of sodium chloride and sodium nitrite. Once again, it can be seen that as the corrosion rate is reduced the corrosion potential shifts in the more positive direction. This demonstrates that the nitrite anion ( $\text{NO}_2^-$ ) behaves as a

passivating anodic inhibitor of steel corrosion in air-saturated aqueous solutions of varied pH and chloride concentration. This finding was as expected, because the mechanism of action of the nitrite ion is believed to depend on reinforcing the passive film on steel by oxidation of  $\text{Fe}^{2+}$  ions formed anodically at defects in the passive film (Gaidis and Rosenberg, 1979). This process of reinforcing the passive film retards the anodic process of metal dissolution and is characteristic of anodic inhibitors.

In summary it can be seen that in neutral solutions, with no chlorides, i.e. those intended to simulate the pore solution phase of carbonated concrete without chloride contamination, concentrations as low as 0.01M sodium nitrite will inhibit corrosion fully, however, in neutral solutions with chloride contamination, i.e. those intended to simulate the pore solution phase of carbonated concrete with chloride contamination, the critical  $[\text{NO}_2^-]/[\text{Cl}^-]$  ratio required to inhibit corrosion fully was between 1 and 10. Figures 4.12 to 4.17 show that in 0.1M sodium hydroxide with various additions of chloride contamination, intended to simulate the pore solution phase present within non-carbonated chloride contaminated concrete, the critical  $[\text{NO}_2^-]/[\text{Cl}^-]$  ratio required to inhibit corrosion fully was between 1 and 10. Further experiments with  $[\text{NO}_2^-]/[\text{Cl}^-]$  ratios between 1 and 10 could estimate this ratio more accurately. In alkaline solutions the  $[\text{NO}_2^-]/[\text{Cl}^-]$  ratio should, in theory, be lower than that required in neutral solutions owing to the added inhibiting effect of hydroxyl ions. Several researches (Virmani, Clear and Pasko, 1983; Gaidis and Rosenberg, 1987; El-Jazairi and Berke, 1990; Tomosawa et al., 1992; Collins, Weyers and Al-Qadi, 1993) have estimated the critical  $[\text{NO}_2^-]/[\text{Cl}^-]$  ratio in concrete, with values ranging from 0.5 to greater than 1.0.

#### **4.3.2.2 Sodium Monofluorophosphate**

Figures 4.20 to 4.33 show the results of the electrochemical monitoring of the mild steel bars immersed in the model electrolytes with various additions of sodium monofluorophosphate. Figures 4.20 and 4.21 show the variation of  $I_{\text{corr}}$  and  $E_{\text{corr}}$  respectively with time for mild steel bars immersed for 42 days in air-saturated aqueous solutions of de-ionised water with various additions of sodium monofluorophosphate. It



can be seen that the addition of sodium monofluorophosphate has no consistent effect on the  $I_{corr}$  and  $E_{corr}$  values. Even with 1.0M sodium monofluorophosphate addition,  $I_{corr}$  values remain above  $1\mu A/cm^2$  and  $E_{corr}$  values in the range of  $-600$  to  $-700mV$  (SCE scale). The results for 0.5M inhibitor addition seem anomalous.

Figures 4.22 and 4.23 show the variation of  $I_{corr}$  and  $E_{corr}$  respectively with time for mild steel bars immersed for 42 days in air-saturated aqueous solutions of de-ionised water with 0.01M sodium chloride and various additions of sodium monofluorophosphate. It can be seen that the addition of sodium monofluorophosphate significantly reduces the  $I_{corr}$  values. However, the  $I_{corr}$  values still remain above  $1\mu A/cm^2$  and the  $E_{corr}$  values below  $-600mV$  (SCE scale). Once again the results for 0.5M inhibitor addition seems anomalous.

Figures 4.24 and 4.25 show the variation of  $I_{corr}$  and  $E_{corr}$  respectively with time for mild steel bars immersed for 42 days in air-saturated aqueous solutions of de-ionised water with 0.1M sodium chloride and various additions of sodium monofluorophosphate. It can be seen that the  $I_{corr}$  values are reduced by an order of magnitude with monofluorophosphate addition, however,  $I_{corr}$  values still remained at approximately  $1\mu A/cm^2$  and  $E_{corr}$  values below  $-600mV$  (SCE scale), even at 1.0M inhibitor concentration.

Figures 4.26 and 4.27 show the variation of  $I_{corr}$  and  $E_{corr}$  respectively with time for mild steel bars immersed for 42 days in air-saturated aqueous solutions of 0.1M sodium hydroxide with various additions of sodium monofluorophosphate. As expected, all bars remained in a passive condition, even those without monofluorophosphate addition. This is because of the inhibitive effect of hydroxyl ions.

Figures 4.28 and 4.29 show the variation of  $I_{corr}$  and  $E_{corr}$  respectively with time for mild steel bars immersed for 42 days in air-saturated aqueous solutions of 0.1M sodium



hydroxide with 0.1M sodium chloride and various additions of sodium monofluorophosphate. It can be seen that sodium monofluorophosphate does reduce the corrosion rate although, it is only at 1.0M concentration that corrosion is inhibited fully. At 0.5M inhibitor concentration the steel remains passive for 7 days before depassivation occurs and  $I_{corr}$  values reach  $1\mu A/cm^2$  by 21 days.

Figures 4.30 and 4.31 show the variation of  $I_{corr}$  and  $E_{corr}$  respectively with time for mild steel bars immersed for 42 days in air-saturated aqueous solutions of 0.1M sodium hydroxide with 1.0M sodium chloride and various additions of sodium monofluorophosphate.  $I_{corr}$  values are reduced with all additions of monofluorophosphate. At 1.0M monofluorophosphate concentration, values of  $I_{corr}$  are reduced by an order of magnitude, although values still remain at approximately  $1\mu A/cm^2$ .

Figure 4.32 shows the variation of corrosion potential with log corrosion rate for mild steel bars immersed in air-saturated aqueous solutions of de-ionised water with various additions of sodium chloride and sodium monofluorophosphate. It can be seen that as the corrosion rate is reduced the corrosion potential shifts in the more positive direction. Figure 4.33 shows the variation of corrosion potential with log corrosion rate for mild steel bars immersed in air-saturated aqueous solutions of 0.1M sodium hydroxide with various additions of sodium chloride and sodium monofluorophosphate. Once again, it can be seen that as the corrosion rate is reduced the corrosion potential shifts in the more positive direction. This demonstrates that the monofluorophosphate anion ( $PO_3F^{2-}$ ) behaves as a passivating anodic inhibitor of steel corrosion in air-saturated aqueous solutions of varied pH and chloride concentration. The mechanism of inhibitor action is difficult to predict as there remains the possibility that any inhibition achieved may be due to the effect of phosphate anions ( $PO_4^{3-}$ ), which are produced as a result of the hydrolysis of monofluorophosphate anions. Phosphate is a known anodic inhibitor (Mayne and Menter, 1954).

In summary the present study showed that in neutral solutions, without chlorides, sodium monofluorophosphate had no consistent effect on reducing  $I_{corr}$  values, even at 1.0M inhibitor addition. In neutral solutions with chloride additions, sodium monofluorophosphate caused a significant reduction in  $I_{corr}$  values, although the values still remained high. In alkaline solutions, with chloride additions, sodium monofluorophosphate also caused significant reductions in  $I_{corr}$  values. The critical  $[PO_3F^{2-}]/[Cl^-]$  ratio to inhibit corrosion fully in alkaline solutions with chloride addition was found to be between 5 and 10. Further investigations are required to produce a more accurate figure. Andrade et al. (1992) reported that a  $[PO_3F^{2-}]/[Cl^-]$  ratio of 1.0 is required to inhibit corrosion fully in saturated calcium hydroxide solutions with 0.5M sodium chloride.

#### **4.3.2.3 Alkanolamine-based Inhibitor**

Figures 4.34 to 4.47 show the results of the electrochemical monitoring on the mild steel bars immersed in the model electrolytes with various additions of an alkanolamine-based inhibitor. Figures 4.34 and 4.35 show the variation of  $I_{corr}$  and  $E_{corr}$  respectively with time for mild steel bars immersed for 42 days in air-saturated aqueous solutions of de-ionised water with various additions of the alkanolamine-based inhibitor. It can be seen that corrosion is inhibited fully at 0.1M and 1.0M inhibitor concentrations. Even at the 0.01M inhibitor concentration,  $I_{corr}$  values are significantly inhibited to below  $0.2\mu A/cm^2$  for 28 days, after which values of  $I_{corr}$  increase to above  $1\mu A/cm^2$ . This increase in  $I_{corr}$  is mirrored by a subsequent decrease in  $E_{corr}$  from  $-200mV$  to below  $-700mV$  (SCE scale).

Figures 4.36 and 4.37 show the variation of  $I_{corr}$  and  $E_{corr}$  respectively with time for mild steel bars immersed for 42 days in air-saturated aqueous solutions of de-ionised water with 0.01M sodium chloride and various additions of the alkanolamine-based inhibitor. The inhibitor inhibits corrosion fully at inhibitor concentrations of 0.1M and



1.0M. At a concentration of 0.01M, the inhibitor significantly reduces corrosion by greater than an order of magnitude although corrosion still proceeds at a rate of approximately  $0.5\mu\text{A}/\text{cm}^2$ .

Figures 4.38 and 4.39 show the variation of  $I_{\text{corr}}$  and  $E_{\text{corr}}$  respectively with time for mild steel bars immersed for 42 days in air-saturated aqueous solutions of de-ionised water with 0.1M sodium chloride and various additions of the alkanolamine-based inhibitor. At inhibitor concentrations of 0.01M and 0.1M the corrosion rate is significantly reduced, however, high rates of corrosion are still apparent. At a concentration of 1.0M the alkanolamine-based inhibitor inhibits corrosion fully.

Figures 4.40 and 4.41 show the variation of  $I_{\text{corr}}$  and  $E_{\text{corr}}$  respectively with time for mild steel bars immersed for 42 days in air-saturated aqueous solutions of 0.1M sodium hydroxide with various additions of the alkanolamine-based inhibitor. As expected, all bars remained in a passive condition, even those without inhibitor addition. This is because of the inhibitive effect of hydroxyl ions.

Figures 4.42 and 4.43 show the variation of  $I_{\text{corr}}$  and  $E_{\text{corr}}$  respectively with time for mild steel bars immersed for 42 days in air-saturated aqueous solutions of 0.1M sodium hydroxide with 0.1M sodium chloride and various additions of the alkanolamine-based inhibitor. The inhibitor appears to be effective at maintaining passivity even at 0.01M concentration. However, at 0.01M inhibitor concentration, the  $E_{\text{corr}}$  values steadily decrease which suggests that depassivation could be imminent.

Figures 4.44 and 4.45 show the variation of  $I_{\text{corr}}$  and  $E_{\text{corr}}$  respectively with time for mild steel bars immersed for 42 days in air-saturated aqueous solutions of 0.1M sodium hydroxide with 1.0M sodium chloride and various additions of the alkanolamine-based inhibitor. A slight reduction in the corrosion rate is observed; however, values of  $I_{\text{corr}}$  still remain significantly above  $1\mu\text{A}/\text{cm}^2$ , even at 1.0M inhibitor concentration.



Figure 4.46 shows the variation of corrosion potential with log corrosion rate for mild steel bars immersed in air-saturated aqueous solutions of de-ionised water with various additions of sodium chloride and the alkanolamine-based inhibitor. It can be seen that as the corrosion rate is reduced the corrosion potential shifts in the more positive direction. Figure 4.47 shows the variation of corrosion potential with log corrosion rate for mild steel bars immersed in air-saturated aqueous solutions of 0.1M sodium hydroxide with various additions of sodium chloride and the alkanolamine-based inhibitor. Once again, it can be seen that as the corrosion rate is reduced the corrosion potential shifts in the more positive direction. This demonstrates that the alkanolamine-based inhibitor behaves as a passivating anodic inhibitor of steel corrosion in air-saturated aqueous solutions of varied pH and chloride concentration.

In summary it can be seen that in neutral solutions, with no chlorides, alkanolamine-based inhibitor concentrations of 0.1M have inhibited corrosion fully. However, in neutral solutions with chloride contamination, it can be seen that the critical inhibitor/chloride ratio required to inhibit corrosion fully was found to be between 1 and 10. In aqueous solutions of 0.1M sodium hydroxide with various additions of chloride the critical inhibitor/chloride ratio required to inhibit corrosion fully was found to be dependent upon the chloride level. For example, at 0.1M sodium hydroxide with 0.1M sodium chloride, the critical inhibitor/chloride ratio was found to be between 0.1 and 1.0, however, at 1.0M sodium chloride concentration, even a ratio of 1.0 is insufficient to maintain passivity.

#### 4.3.2.4 Ethanolamine

Figures 4.48 to 4.61 show the results of the electrochemical monitoring of the mild steel bars immersed in the model electrolytes with various additions of ethanolamine. Figures 4.48 and 4.49 show the variation of  $I_{corr}$  and  $E_{corr}$  respectively with time for mild steel bars immersed for 42 days in air-saturated aqueous solutions of de-ionised water with various additions of ethanolamine. It can be seen that ethanolamine inhibits corrosion

fully at 0.1M and 1.0M concentrations. However, at 0.01M concentration no significant inhibiting effect is observed.

Figures 4.50 and 4.51 show the variation of  $I_{corr}$  and  $E_{corr}$  respectively with time for mild steel bars immersed for 42 days in air-saturated aqueous solutions of de-ionised water with 0.01M sodium chloride and various additions of ethanolamine. At 1.0M concentration ethanolamine inhibits corrosion fully whilst at 0.1M concentration corrosion appears to be inhibited fully until 42 days, upon which passivity appears to be lost. At a concentration of 0.01M, ethanolamine causes a slight reduction in observed values of  $I_{corr}$ .

Figures 4.52 and 4.53 show the variation of  $I_{corr}$  and  $E_{corr}$  respectively with time for mild steel bars immersed for 42 days in air-saturated aqueous solutions of de-ionised water with 0.1M sodium chloride and various additions of ethanolamine. Corrosion reduction is observed with all concentrations of ethanolamine. At a concentration of 1.0M ethanolamine, values of  $I_{corr}$  are reduced by more than an order of magnitude, however, these values still remained above levels corresponding to passivity.

Figures 4.54 and 4.55 show the variation of  $I_{corr}$  and  $E_{corr}$  respectively with time for mild steel bars immersed for 42 days in air-saturated aqueous solutions of 0.1M sodium hydroxide with various additions of ethanolamine. As expected, all bars remained in a passive condition, even those without inhibitor addition. This is because of the inhibitive effect of hydroxyl ions.

Figures 4.56 and 4.57 show the variation of  $I_{corr}$  and  $E_{corr}$  respectively with time for mild steel bars immersed for 42 days in air-saturated aqueous solutions of 0.1M sodium hydroxide with 0.1M sodium chloride and various additions of ethanolamine. At inhibitor concentrations of 0.1M and 1.0M, corrosion is inhibited fully and even at 0.01M ethanolamine concentration  $I_{corr}$  values are suppressed to below  $0.2\mu A/cm^2$ .



Figures 4.58 and 4.59 show the variation of  $I_{corr}$  and  $E_{corr}$  respectively with time for mild steel bars immersed for 42 days in air-saturated aqueous solutions of 0.1M sodium hydroxide with 1.0M sodium chloride and various additions of ethanolamine. An order of magnitude reduction in the  $I_{corr}$  values was observed, however, rates still remained above levels corresponding to passivity, even at 1.0M ethanolamine concentration.

Figure 4.60 shows the variation of corrosion potential with log corrosion rate for mild steel bars immersed in air-saturated aqueous solutions of de-ionised water with various additions of sodium chloride and ethanolamine. It can be seen that as the corrosion rate is reduced the corrosion potential shifts in the more positive direction. Figure 4.61 shows the variation of corrosion potential with log corrosion rate for mild steel bars immersed in air-saturated aqueous solutions of 0.1M sodium hydroxide with various additions of sodium chloride and ethanolamine. Once again, it can be seen that as the corrosion rate is reduced the corrosion potential shifts in the more positive direction. This demonstrates that ethanolamine behaves as a passivating anodic inhibitor of steel corrosion in air-saturated aqueous solutions of varied pH and chloride concentration.

In summary it can be seen that in neutral solutions, with no chlorides, inhibitor concentrations of 0.1M have inhibited corrosion fully. However, in neutral solutions with chloride contamination, it can be seen that the critical inhibitor/chloride ratio required to inhibit corrosion fully varied with chloride concentration. In aqueous solutions of 0.1M sodium hydroxide with various additions of chloride contamination the critical inhibitor/chloride ratio required to inhibit corrosion fully was also found to be dependent upon the chloride level.

#### 4.3.2.5 Comparison of Inhibitor Efficiencies

Figures 4.62 to 4.67 compare the efficiencies of the various inhibitors in terms of the steel corrosion rates recorded after 42 days immersion. In neutral solutions, without chloride addition, it can be seen that sodium nitrite is the most effective inhibitor, as



even 0.01M has reduced the corrosion rate to below the level corresponding to passivity. The alkanolamine-based inhibitor and ethanolamine show similar results with corrosion being inhibited fully at 0.1M and 1.0M inhibitor concentrations, and very little or no corrosion inhibition at 0.01M inhibitor concentration. Sodium monofluorophosphate appears to be less effective than the other inhibitors, even when present at 1.0M concentration.

In neutral solutions with chloride addition, sodium nitrite is again the most effective inhibitor although high concentrations (1.0M nitrite) are required to inhibit corrosion fully. The alkanolamine-based inhibitor also managed to inhibit corrosion fully at 1.0M concentration. Ethanolamine, when present at 1.0M concentration, inhibited corrosion fully when only 0.01M chloride was present and had a significant effect on corrosion when 0.1M chloride was present. Sodium monofluorophosphate had a significant inhibiting effect although it failed to inhibit corrosion fully even when present at a monofluorophosphate/chloride concentration of one hundred.

In alkaline solutions, the performances of the inhibitors were very similar to one another. At 0.1M chloride addition the alkanolamine-based inhibitor and ethanolamine appeared to inhibit corrosion fully, even at 0.01M inhibitor concentrations. However, with 1.0M chloride addition, none of the inhibitors maintained passivity, even when present at 1.0M inhibitor concentrations.

#### **4.3.3 Weight Loss Determinations**

Figures 4.68 to 4.73 show the weight loss determinations for sodium nitrite. It can be seen from Figure 4.68 that, even at 0.01M concentration, no weight loss was measured in neutral solutions of sodium nitrite without chloride addition. This supports the electrochemical results which suggest that sodium nitrite has the potential to be a successful inhibitor of corrosion of steel in carbonated concrete without chloride contamination. Figure 4.69 shows that in neutral solutions with 0.01M chloride addition, corrosion is inhibited fully even at 0.01M sodium nitrite. Figure 4.70 shows

that some weight loss is observed and only 1.0M concentration appears to inhibit metal dissolution fully. In alkaline solutions, with chloride additions, the measured weight loss decreases with increasing inhibitor concentration. The 0.01M inhibitor concentration actually appears to have slightly more weight loss than those solutions without nitrite addition. This suggests that sodium nitrite could lead to increased severity of localised corrosion if used at concentrations below the level required for complete passivation of steel in chloride-containing media as reported in several researches (Short, Lambert and Page, 1989; Nurnberger, 1988; Treadaway and Russell, 1968). However, these results are in contradiction to the theoretical weight loss determinations (see section 4.2.9) which suggest that no increase in weight loss should be encountered with sodium nitrite addition.

Figures 4.74 to 4.79 show the weight loss determinations for sodium monofluorophosphate. It can be seen that an increase in monofluorophosphate concentration causes a resultant reduction in experimentally measured weight loss, for all conditions. However, it is apparent that sodium monofluorophosphate has only a moderate effect on weight loss. The correspondence between the theoretical and experimental weight loss determinations was not good for monofluorophosphate in neutral solutions as can be seen in Figures 4.74 and 4.75.

Figures 4.80 to 4.85 show that an increase in the alkanolamine-based inhibitor concentration causes a decrease in weight loss. In neutral solutions, without chloride addition, the inhibitor appears to be very effective with no weight loss observed, even at 0.01M inhibitor concentration. In neutral solutions, with chloride contamination, 1.0M inhibitor concentration appears effective even at 0.1M chloride addition. In alkaline solutions with chloride addition, the inhibitor appears effective at suppressing corrosion where 0.1M chloride was present. However, the inhibitor was unable to prevent metal dissolution when 1.0M chloride was present, even at 1.0M inhibitor concentration.



Figures 4.86 to 4.91 show the weight loss determinations for ethanolamine. In neutral solutions, ethanolamine appears ineffective at 0.01M concentration. At 0.1M and 1.0M concentration, ethanolamine performs very well in neutral solutions apart from where the chloride addition is 0.1M, at which the inhibitor failed to prevent significant weight losses. In alkaline solutions with chloride contamination, the inhibitor significantly reduced weight loss. However, at 1.0M chloride concentration, significant weight losses were still observed even with 1.0M inhibitor concentration.

Figures 4.92 to 4.97 compare the effectiveness of the inhibitors in reducing experimentally determined weight losses. It can be seen that sodium nitrite is the most effective inhibitor in suppressing weight loss in neutral solutions, with and without chlorides, at all inhibitor concentrations. In alkaline solutions, all the inhibitors effectively reduce metal dissolution with the lower amount of chloride, although high concentrations are required. When the chloride level is at 1.0M, none of the inhibitors perform effectively, although ethanolamine appears to cause the most significant reduction in weight loss.

It is important to note that the experimentally determined weight loss measurements are generally accurate to within a factor of two or three times the theoretical weight loss determinations. This shows that a fairly good correlation has been achieved between the weight loss measurements and the electrochemical monitoring.

#### **4.3.4 Photographic Observations**

Figures 4.98 to 4.115 show some of the more interesting photographic observations taken of the bars, after removal of corrosion products, following immersion in the model electrolytes. Figures 4.98 to 4.101 show the typical appearance of the control bars, i.e. those that were immersed in model electrolytes with no inhibitor addition. The difference can be clearly seen between general corrosion (Figure 4.98), general corrosion with some localised corrosion (Figure 4.99), and localised corrosion alone



(Figure 4.101). Figures 4.103 to 4.105 show evidence that, when compared to Figure 4.101, the severity of localised corrosion appears to have been increased where sodium nitrite is present at concentrations lower than those required to inhibit corrosion fully. This gives some support to the weight loss determinations. Figures 4.108 and 4.109 give similar evidence of intensified localised corrosion when using sodium monofluorophosphate. This effect was not apparent from the weight loss determinations involving sodium monofluorophosphate. The reason this effect did not become apparent is because the weight loss determinations in the present study considered the overall corrosion rate. Weight loss determinations using a method of analysis similar to that carried out by Page, Ngala and Page (2000) may have revealed this phenomenon of intensified localised corrosion. No intensification of localised corrosion was observed on the bars immersed in model electrolytes containing the alkanolamine-based inhibitor or ethanolamine.

#### **4.4 CONCLUSIONS**

Sodium nitrite behaves as a passivating anodic inhibitor of steel corrosion in air-saturated aqueous solutions of varied pH and chloride concentration. In neutral solutions, i.e. those intended to simulate the pore solution phase present in carbonated concrete, sodium nitrite appears to be very effective in maintaining passivity on bare steel. In both neutral and alkaline solutions with low levels of chloride contamination, this effect is maintained. However, high concentrations of sodium nitrite are required to significantly inhibit corrosion where high chloride levels are present. Some evidence has been found to suggest that sodium nitrite, when present at concentrations lower than that required to inhibit corrosion fully, may intensify the severity of localised corrosion.

Sodium monofluorophosphate behaves as a passivating anodic inhibitor of steel corrosion in air-saturated aqueous solutions of varied pH and chloride concentration. Sodium monofluorophosphate appears to be less effective than the other inhibitors investigated in neutral solutions without chloride addition. In the presence of chlorides,

sodium monofluorophosphate has a significant inhibiting effect, although high concentrations were required to achieve this. Evidence was also found to suggest that sodium monofluorophosphate, when present at concentrations lower than that required to inhibit corrosion fully, may intensify the severity of localised corrosion.

The alkanolamine-based inhibitor behaves as a passivating anodic inhibitor of steel corrosion in air-saturated aqueous solutions of varied pH and chloride concentration. In neutral solutions, high concentrations are required for the alkanolamine-based inhibitor to maintain passivity, especially in the presence of chlorides. In alkaline solutions with low levels of chloride contamination the alkanolamine-based inhibitor maintains passivity on bare steel, even at low inhibitor concentrations. In alkaline solutions with high levels of chloride contamination, the alkanolamine-based inhibitor has little effect on the corrosion rate, even when trying to protect initially passive steel. No evidence was found to suggest that the alkanolamine-based inhibitor, when present at concentrations lower than that required to inhibit corrosion fully, may intensify the severity of localised corrosion.

Ethanolamine behaves as a passivating anodic inhibitor of steel corrosion in air-saturated aqueous solutions of varied pH and chloride concentration. In neutral solutions, high concentrations are required for ethanolamine to significantly reduce corrosion, even with low levels of chloride contamination. In alkaline solutions, ethanolamine appears to be the most effective corrosion inhibitor investigated. No evidence was found to suggest that ethanolamine, when present at concentrations lower than that required to inhibit corrosion fully, may intensify the severity of localised corrosion.



Table 4.1 – Results of pH determinations of the model electrolytes

pH	C	N1	N2	N3	M1	M2	A1	A2	A3	E1	E2	E3
H <sub>2</sub> O	6.4	6.4	6.8	7.3	6.6	6.4	9.8	10.0	10.5	10.5	11.0	11.8
H <sub>2</sub> O + 0.01M NaCl	6.4	6.4	6.7	7.3	6.6	6.4	9.8	10.0	10.5	10.5	11.0	11.8
H <sub>2</sub> O + 0.1M NaCl	6.3	6.3	6.7	7.3	6.5	6.4	9.8	10.0	10.5	10.4	11.0	11.8
0.1M NaOH	13.0	13.0	13.0	12.8	13.0	13.0	13.0	12.9	12.2	13.0	12.8	12.7
0.1M NaOH + 0.1M NaCl	12.9	12.9	12.9	12.8	13.0	12.9	13.0	12.8	12.1	13.0	12.8	12.7
0.1M NaOH + 1.0M NaCl	12.7	12.7	12.7	12.7	12.7	12.7	13.0	12.8	12.1	13.0	12.7	12.7

Key

C = Control Solutions (no inhibitor addition)

N1 = 0.01M Sodium Nitrite

N2 = 0.1M Sodium Nitrite

N3 = 1.0M Sodium Nitrite

M1 = 0.1M Sodium Monofluorophosphate

M2 = 1.0M Sodium Monofluorophosphate

A1 = 0.01M Alkanolamine-based Inhibitor

A2 = 0.1M Alkanolamine-based Inhibitor

A3 = 1.0M Alkanolamine-based Inhibitor

E1 = 0.01M Ethanolamine

E2 = 0.1M Ethanolamine

E3 = 1.0M Ethanolamine



Figure 4.1 – Mild steel bar ready for immersion in model electrolyte

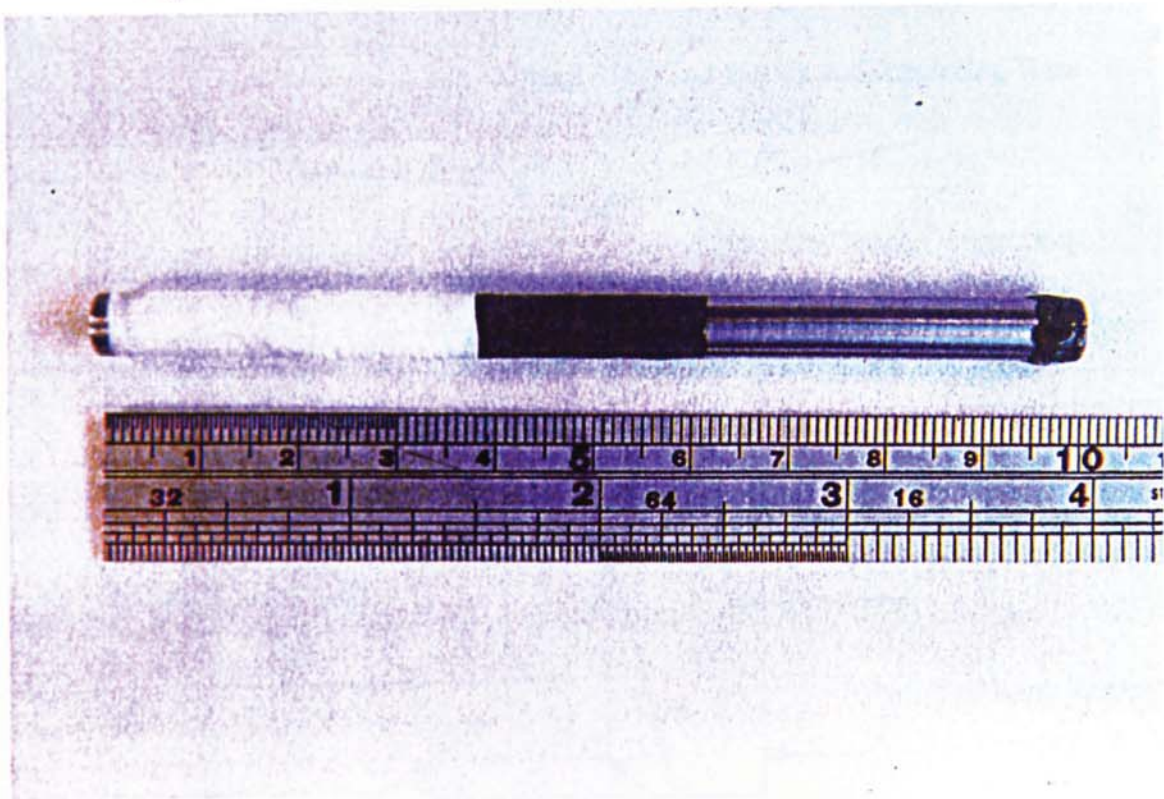


Figure 4.2 – Titanium mesh counter electrode

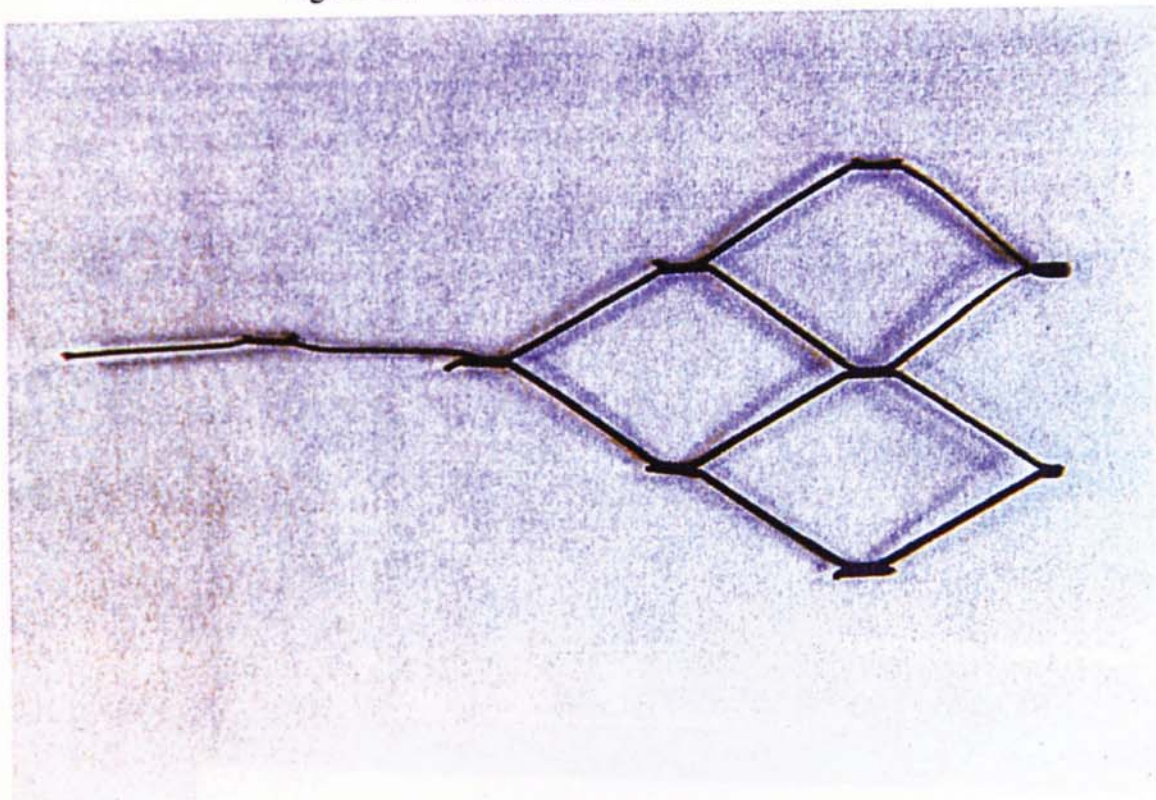




Figure 4.3 – Schematic diagram of the cell assembly (not to scale)

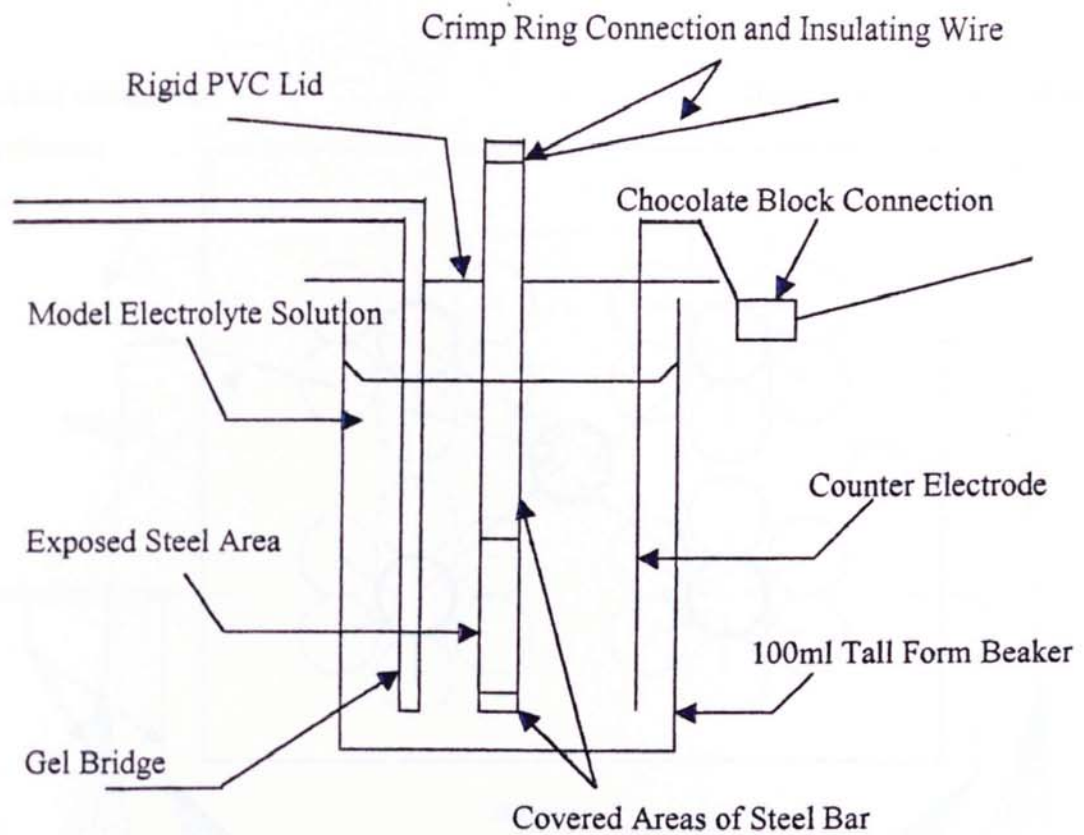


Figure 4.4 – Photograph showing experimental set-up for the immersion tests

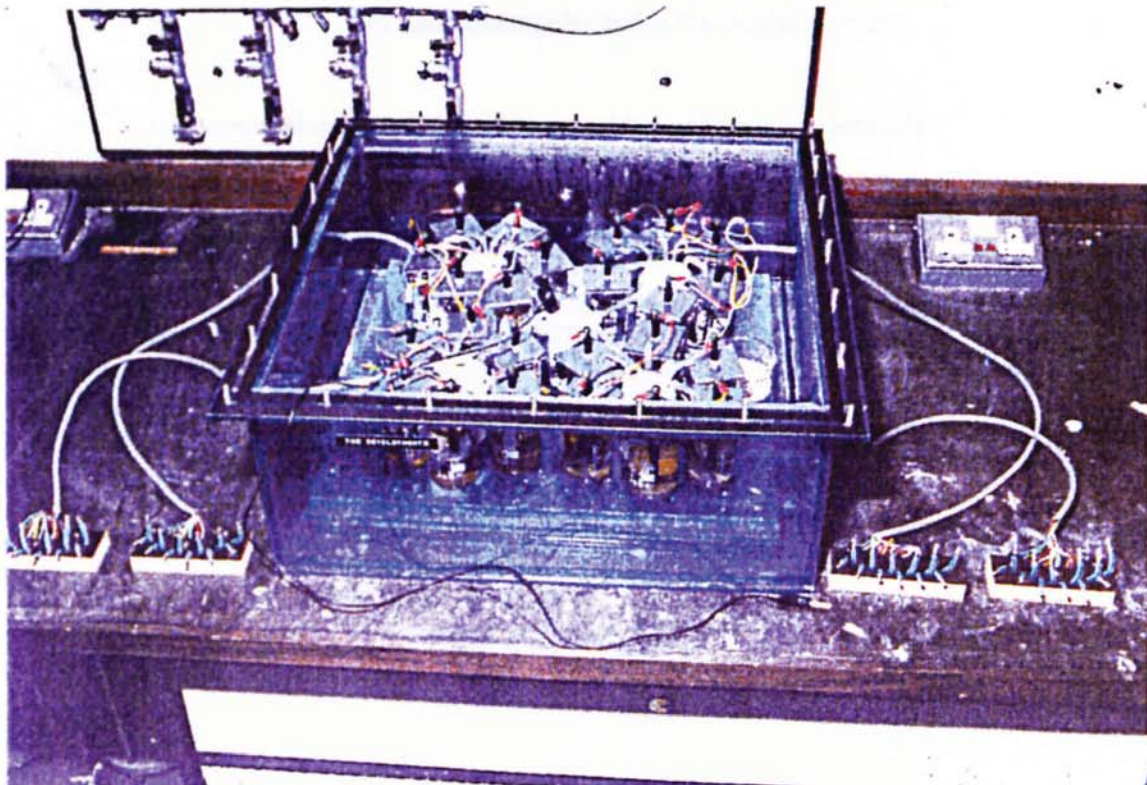
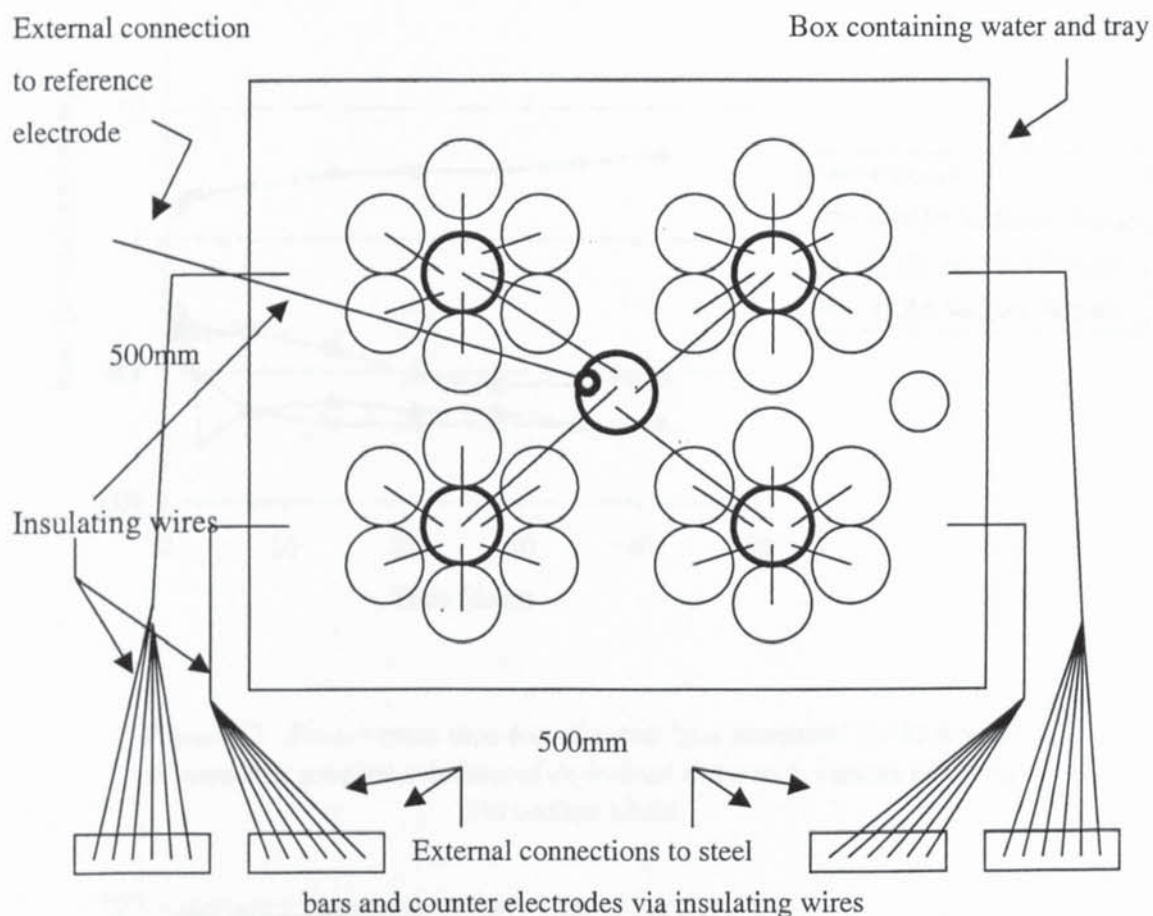


Figure 4.5 - Schematic plan of experimental set-up for the immersion tests (not to scale)



Key






-  Cell containing model electrolyte, steel bar and counter electrode
-  Pot containing 2M Potassium Nitrate
-  Saturated Calomel Reference Electrode
-  Pot of Carbosorb
-  Gel Bridge



Figure 4.6 -  $I_{corr}$  versus time for mild steel bars immersed for 42 days in air-saturated aqueous solutions of de-ionised water with various additions of sodium nitrite

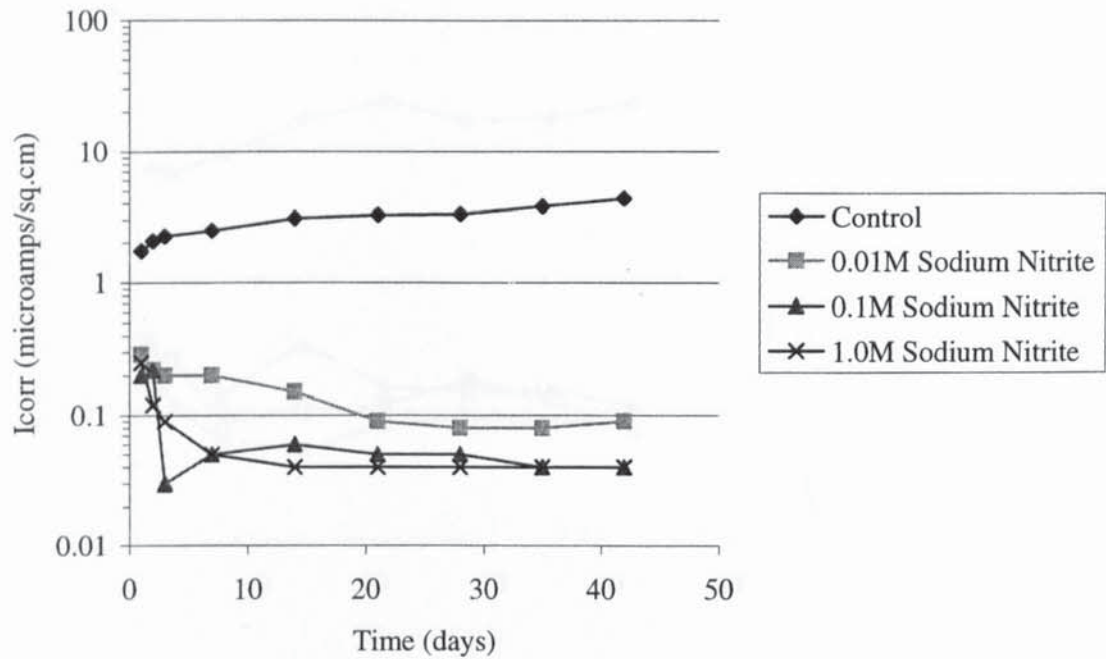


Figure 4.7 -  $E_{corr}$  versus time for mild steel bars immersed for 42 days in air-saturated aqueous solutions of de-ionised water with various additions of sodium nitrite

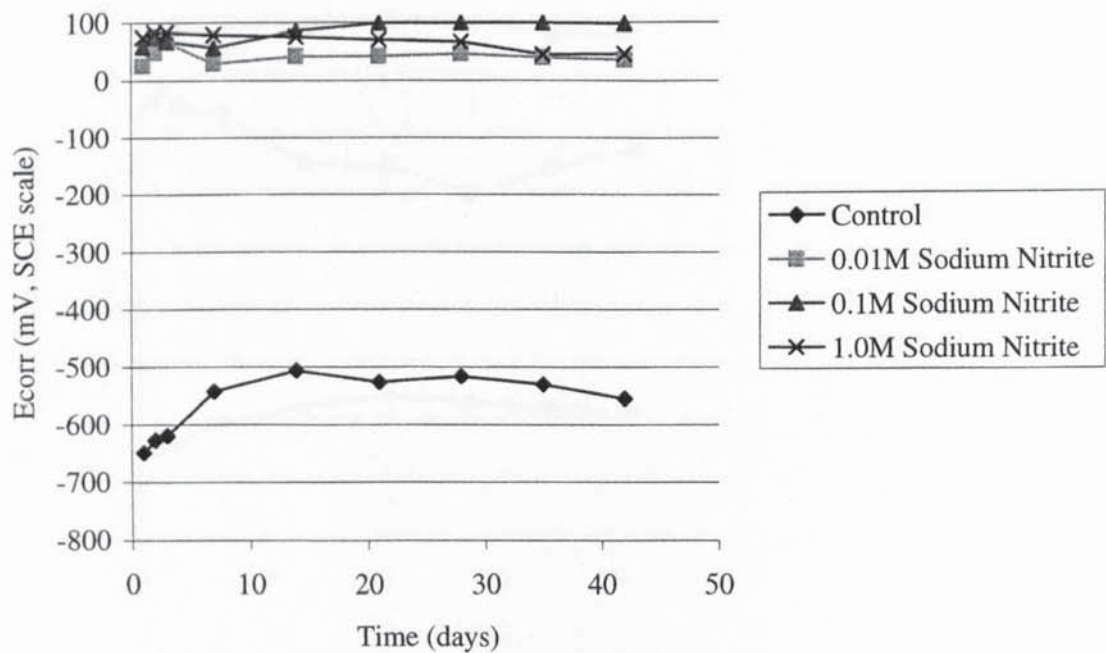


Figure 4.8 -  $I_{corr}$  versus time for mild steel bars immersed for 42 days in air-saturated aqueous solutions of de-ionised water with 0.01M sodium chloride and various additions of sodium nitrite

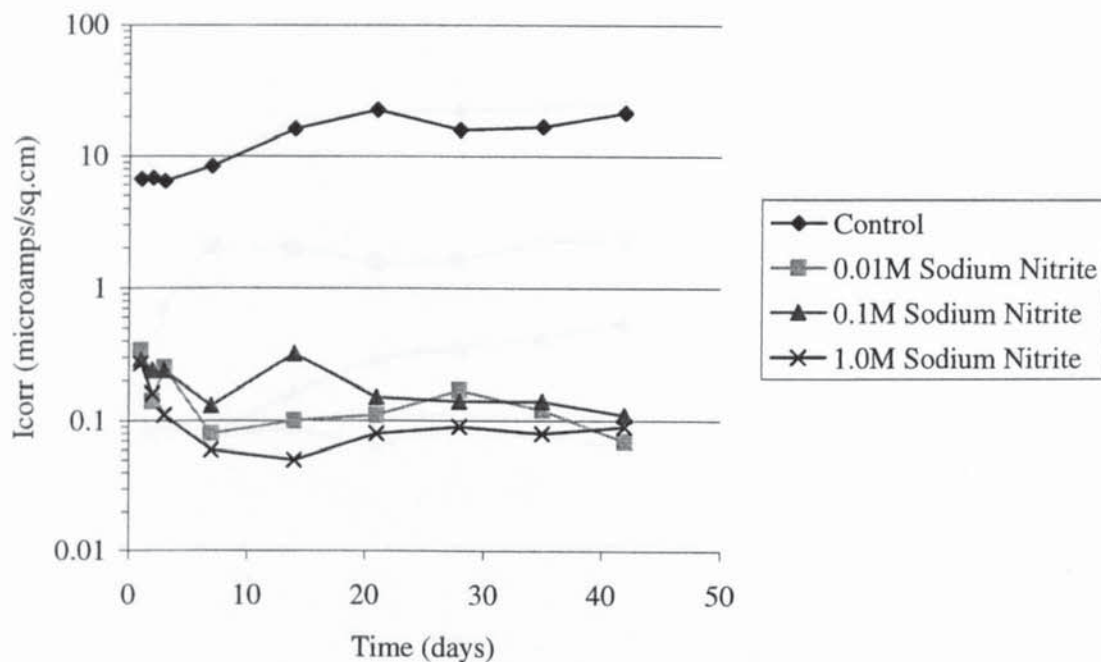


Figure 4.9 -  $E_{corr}$  versus time for mild steel bars immersed for 42 days in air-saturated aqueous solutions of de-ionised water with 0.01M sodium chloride and various additions of sodium nitrite

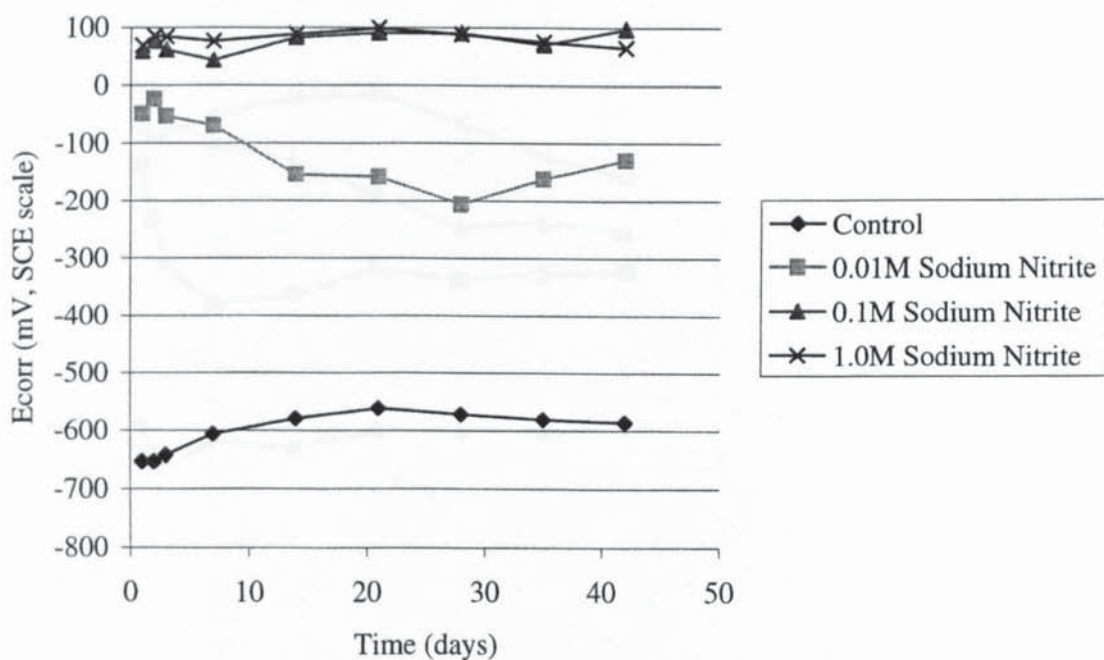




Figure 4.10 -  $I_{corr}$  versus time for mild steel bars immersed for 42 days in air-saturated aqueous solutions of de-ionised water with 0.1M sodium chloride and various additions of sodium nitrite

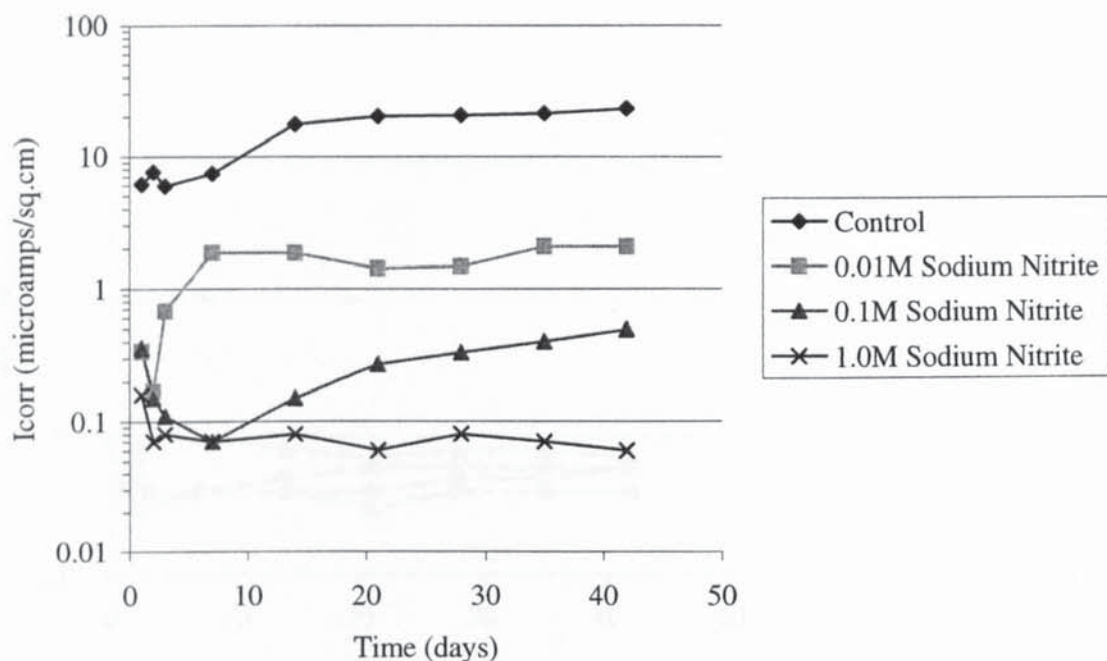


Figure 4.11 -  $E_{corr}$  versus time for mild steel bars immersed for 42 days in air-saturated aqueous solutions of de-ionised water with 0.1M sodium chloride and various additions of sodium nitrite

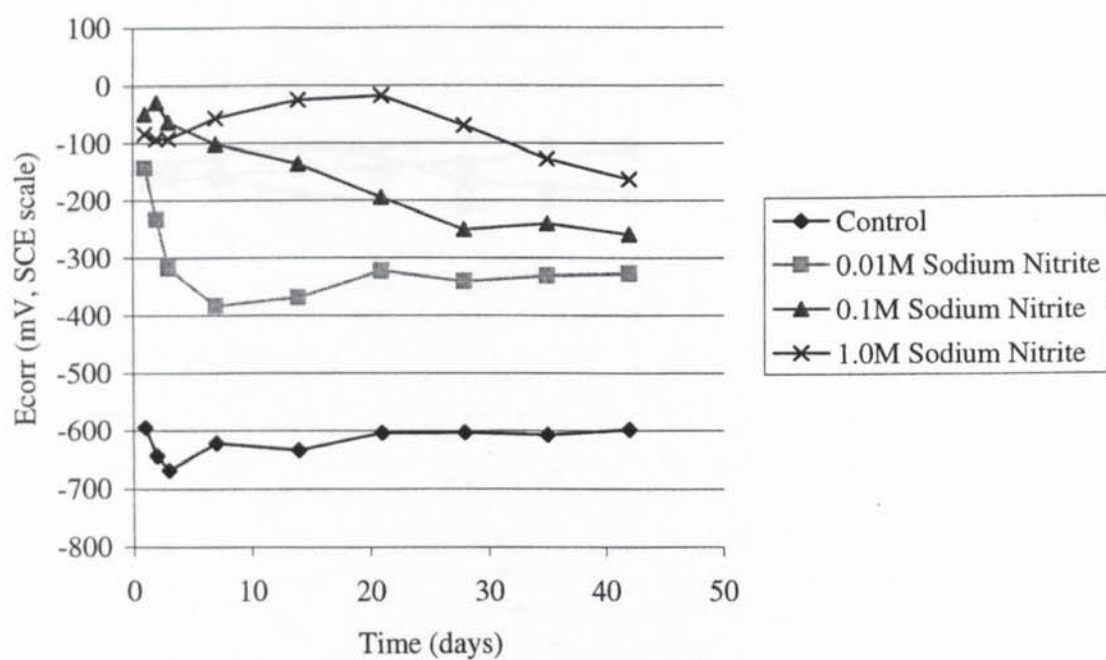


Figure 4.12 -  $I_{corr}$  versus time for mild steel bars immersed for 42 days in air-saturated aqueous solutions of 0.1M sodium hydroxide with various additions of sodium nitrite

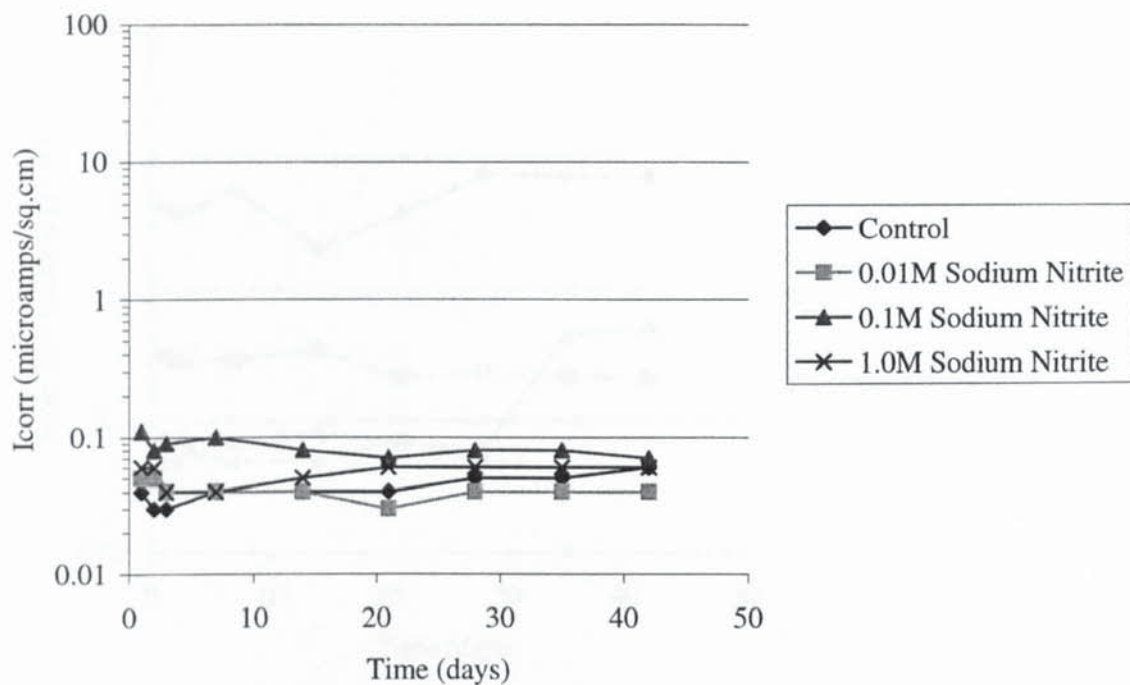


Figure 4.13 -  $E_{corr}$  versus time for mild steel bars immersed for 42 days in air-saturated aqueous solutions of 0.1M sodium hydroxide with various additions of sodium nitrite

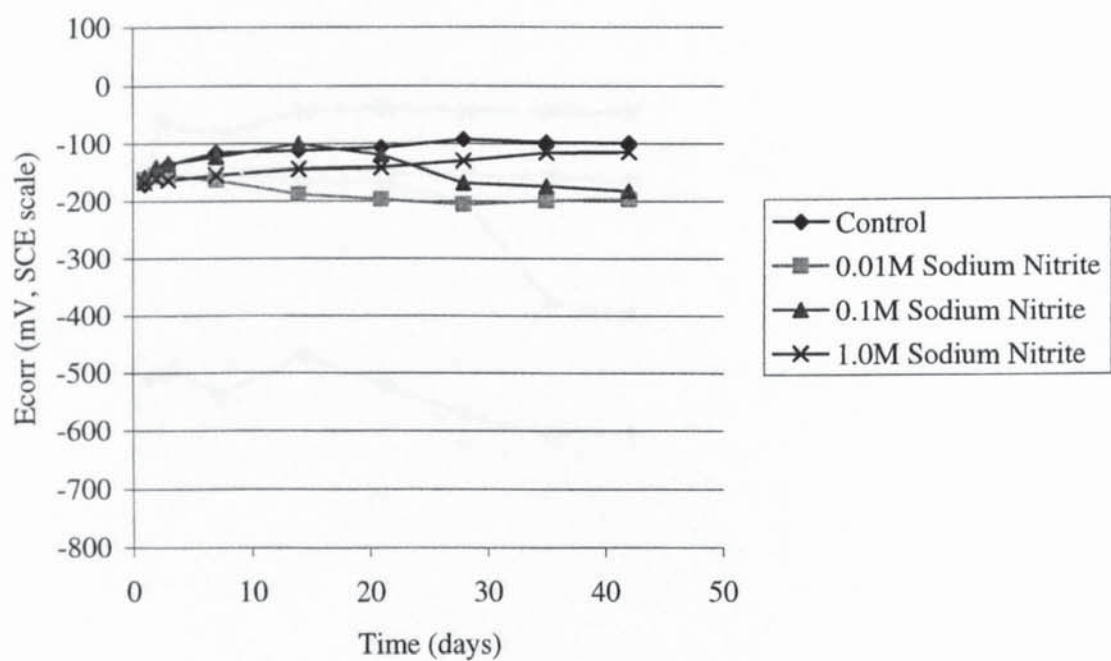


Figure 4.14 -  $I_{corr}$  versus time for mild steel bars immersed for 42 days in air-saturated aqueous solutions of 0.1M sodium hydroxide with 0.1M sodium chloride and various additions of sodium nitrite

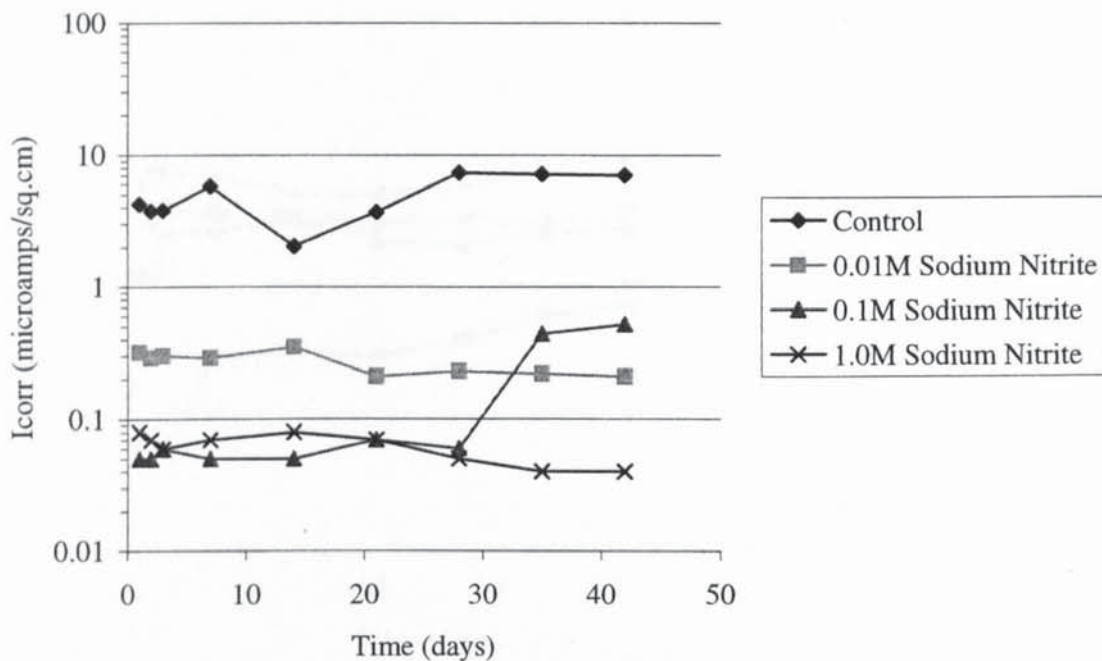


Figure 4.15 -  $E_{corr}$  versus time for mild steel bars immersed for 42 days in air-saturated aqueous solutions of 0.1M sodium hydroxide with 0.1M sodium chloride and various additions of sodium nitrite

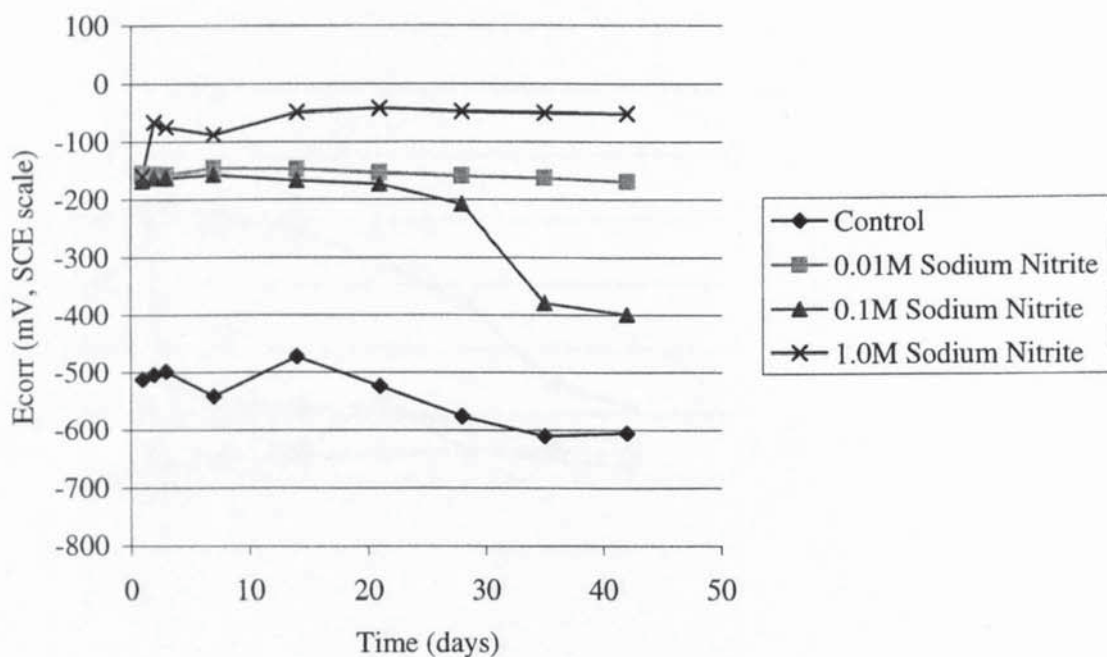




Figure 4.16 -  $I_{corr}$  versus time for mild steel bars immersed for 42 days in air-saturated aqueous solutions of 0.1M sodium hydroxide with 1.0M sodium chloride and various additions of sodium nitrite

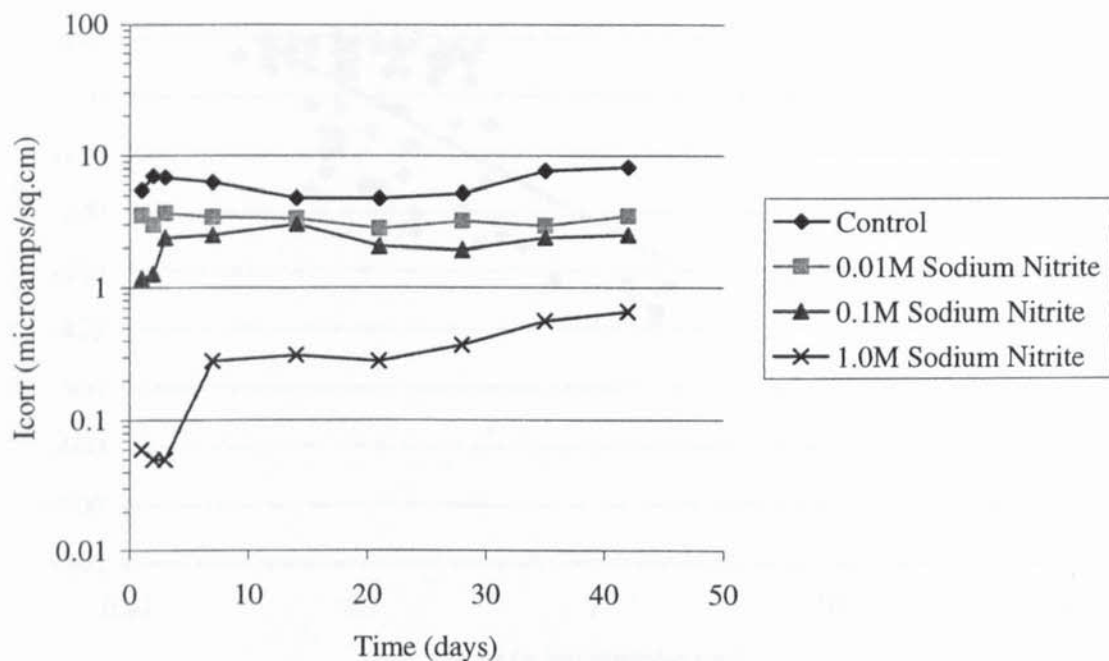


Figure 4.17 -  $E_{corr}$  versus time for mild steel bars immersed for 42 days in air-saturated aqueous solutions of 0.1M sodium hydroxide with 1.0M sodium chloride and various additions of sodium nitrite

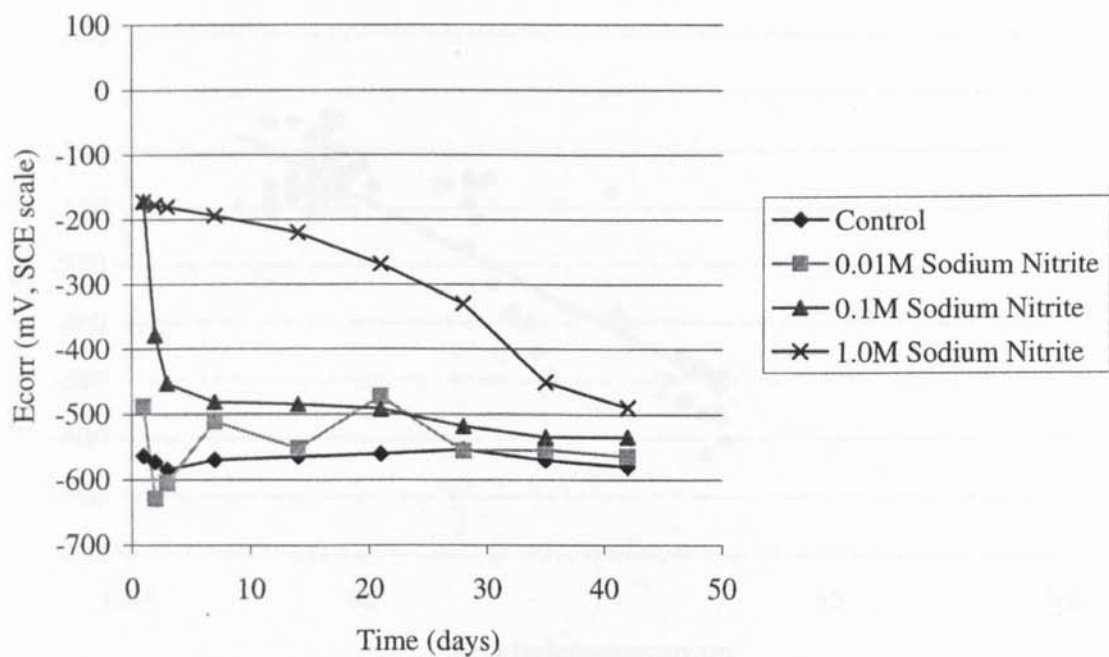


Figure 4.18 -  $E_{\text{corr}}$  versus  $I_{\text{corr}}$  for mild steel bars immersed in air-saturated aqueous solutions of de-ionised water with varying amounts of sodium chloride and sodium nitrite

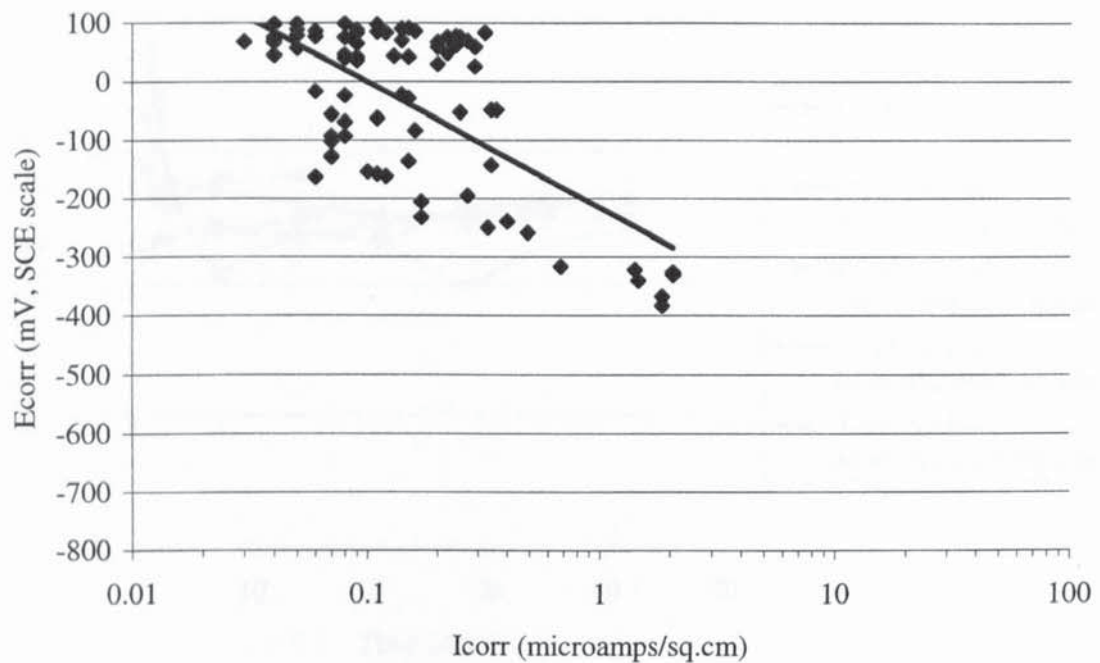


Figure 4.19 -  $E_{\text{corr}}$  versus  $I_{\text{corr}}$  for mild steel bars immersed in air-saturated aqueous solutions of 0.1M sodium hydroxide with varying amounts of sodium chloride and sodium nitrite

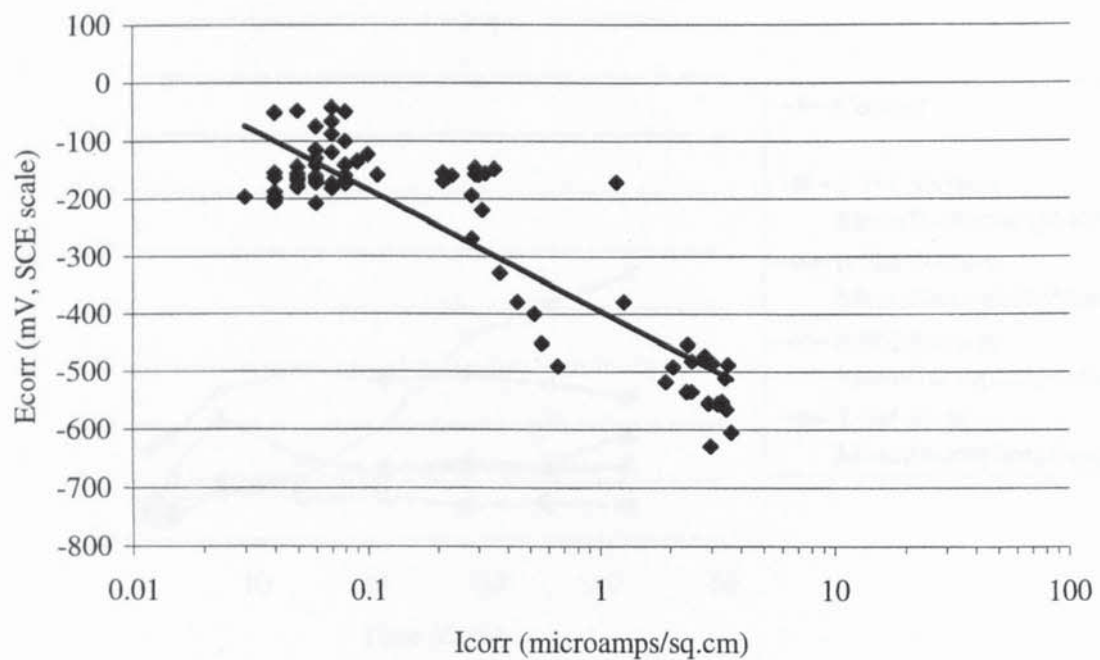


Figure 4.20 -  $I_{corr}$  versus time for mild steel bars immersed for 42 days in air-saturated aqueous solutions of de-ionised water with various additions of sodium monofluorophosphate

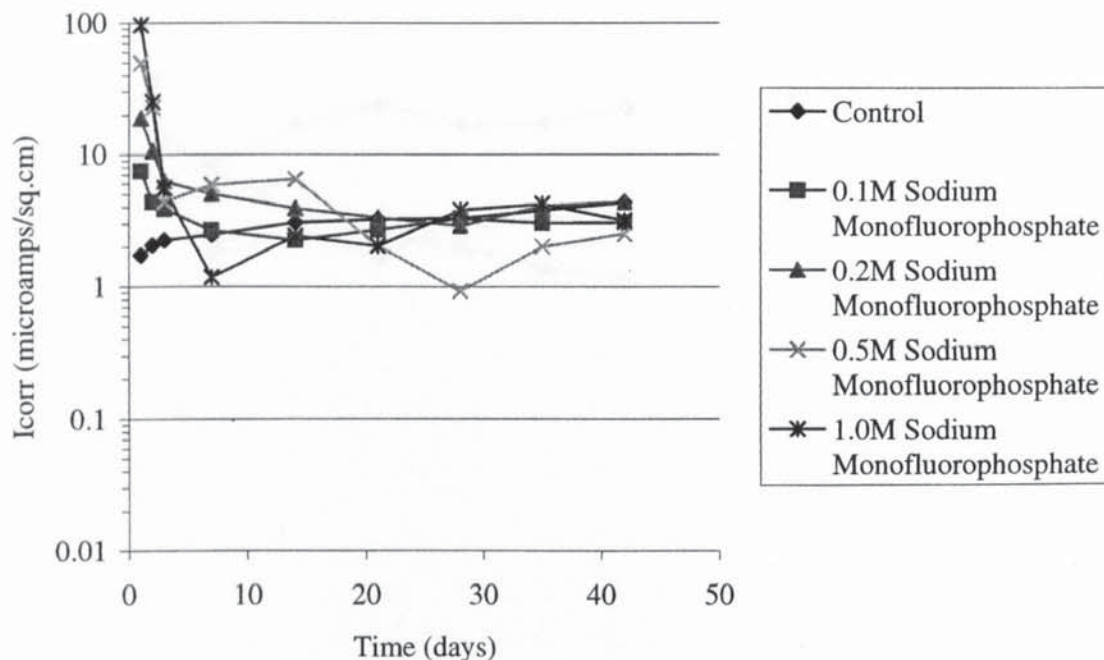


Figure 4.21 -  $E_{corr}$  versus time for mild steel bars immersed for 42 days in air-saturated aqueous solutions of de-ionised water with various additions of sodium monofluorophosphate

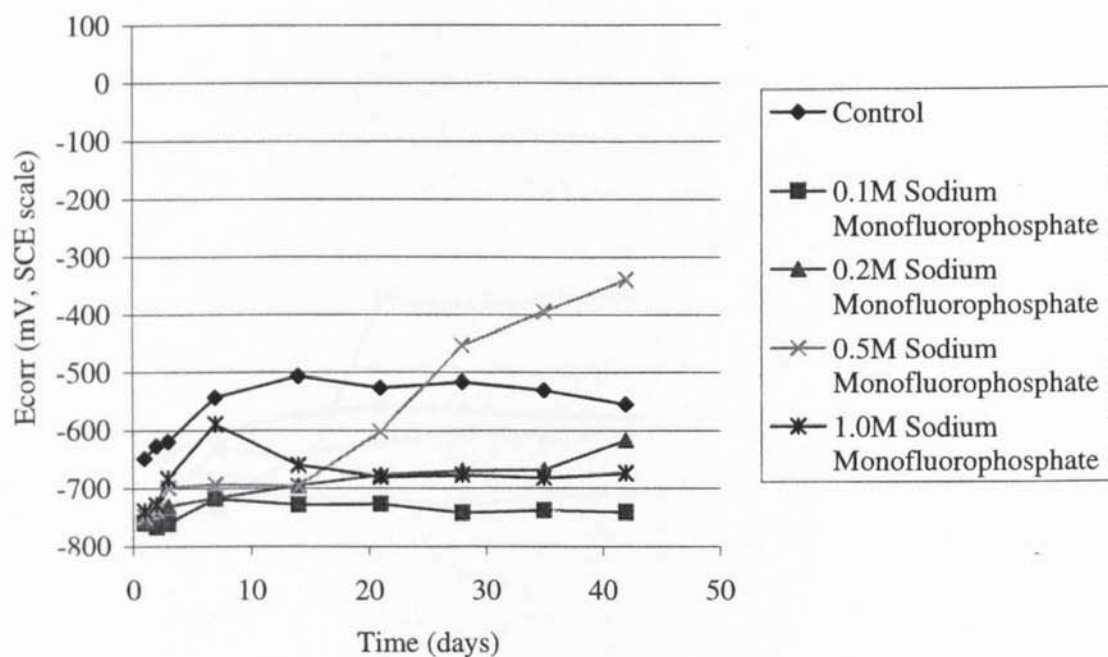




Figure 4.22 - Icorr versus time for mild steel bars immersed for 42 days in air-saturated aqueous solutions of de-ionised water with 0.01M sodium chloride and various additions of sodium monofluorophosphate

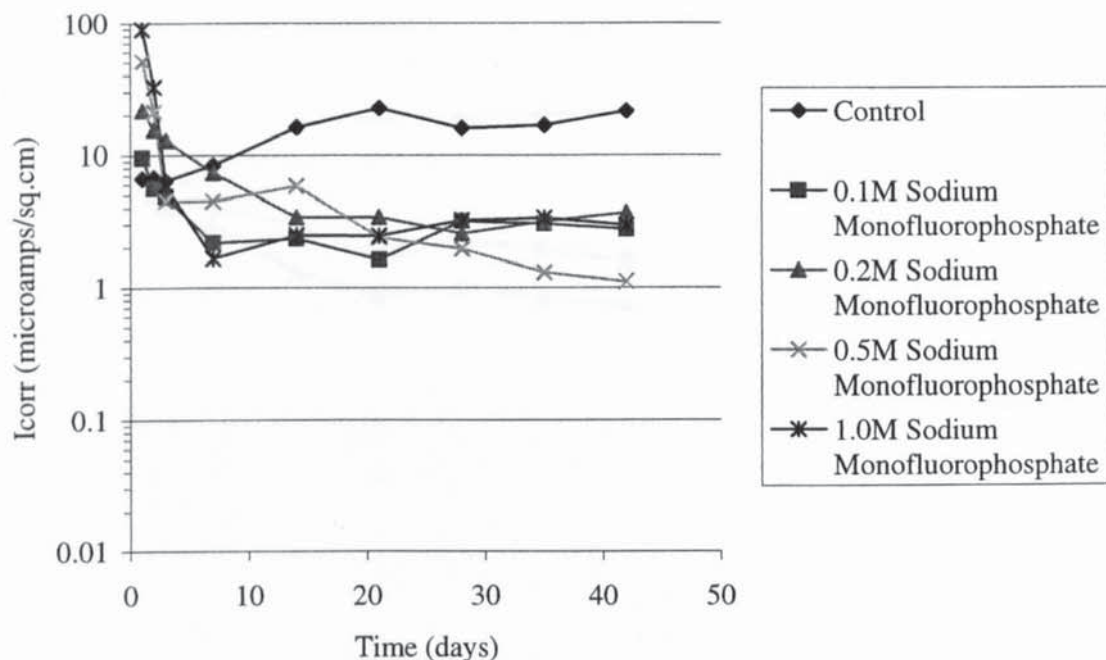


Figure 4.23 - Ecorr versus time for mild steel bars immersed for 42 days in air-saturated aqueous solutions of de-ionised water with 0.01M sodium chloride and various additions of sodium monofluorophosphate

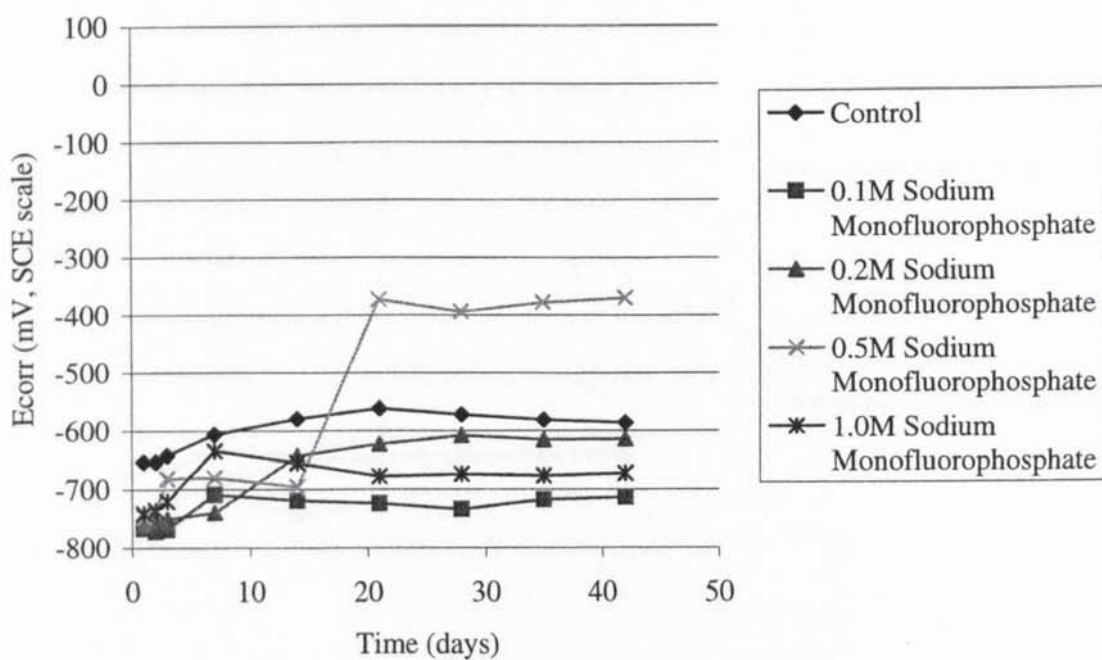


Figure 4.24 - Icorr versus time for mild steel bars immersed for 42 days in air-saturated aqueous solutions of de-ionised water with 0.1M sodium chloride and various additions of sodium monofluorophosphate

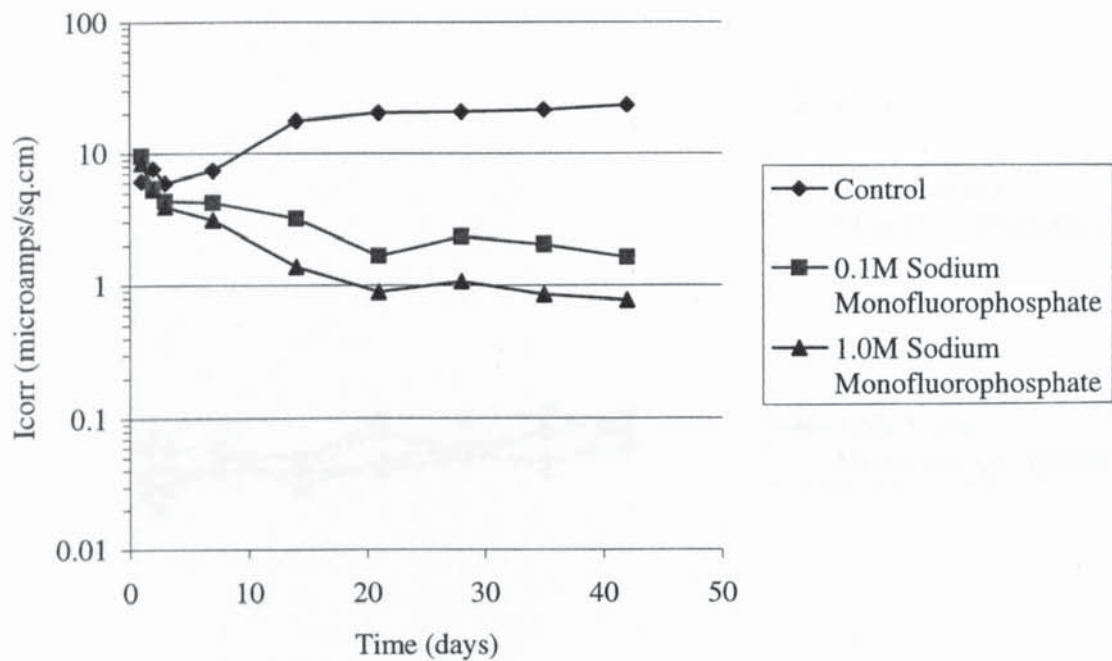


Figure 4.25 - Ecorr versus time for mild steel bars immersed for 42 days in air-saturated aqueous solutions of de-ionised water with 0.1M sodium chloride and various additions of sodium monofluorophosphate

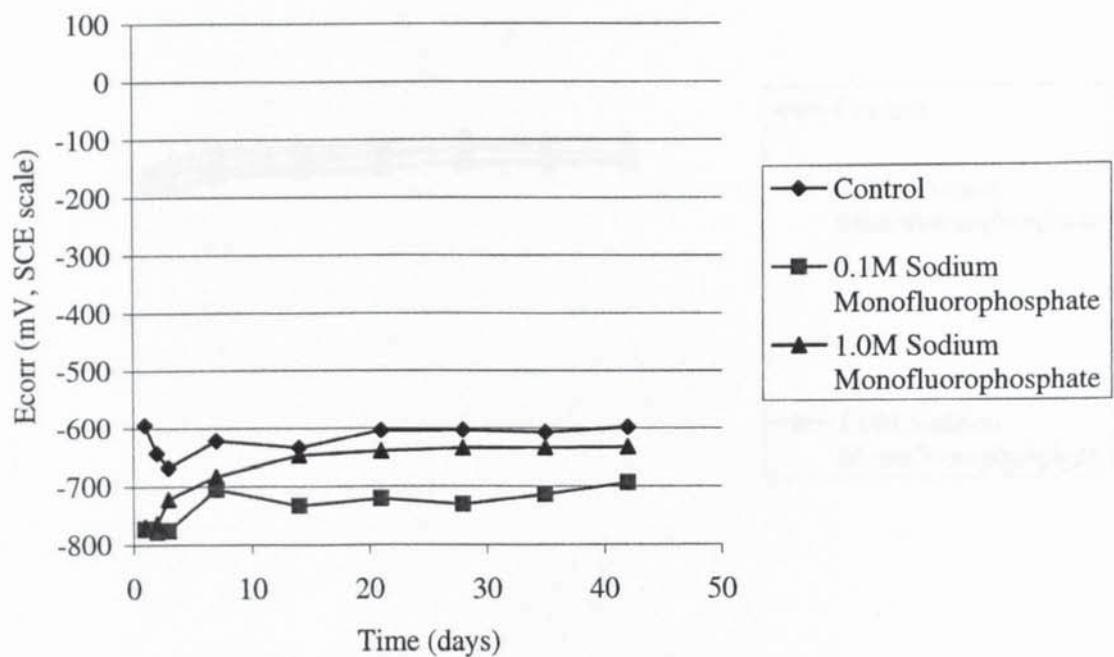


Figure 4.26 -  $I_{corr}$  versus time for mild steel bars immersed for 42 days in air-saturated aqueous solutions of 0.1M sodium hydroxide with various additions of sodium monofluorophosphate

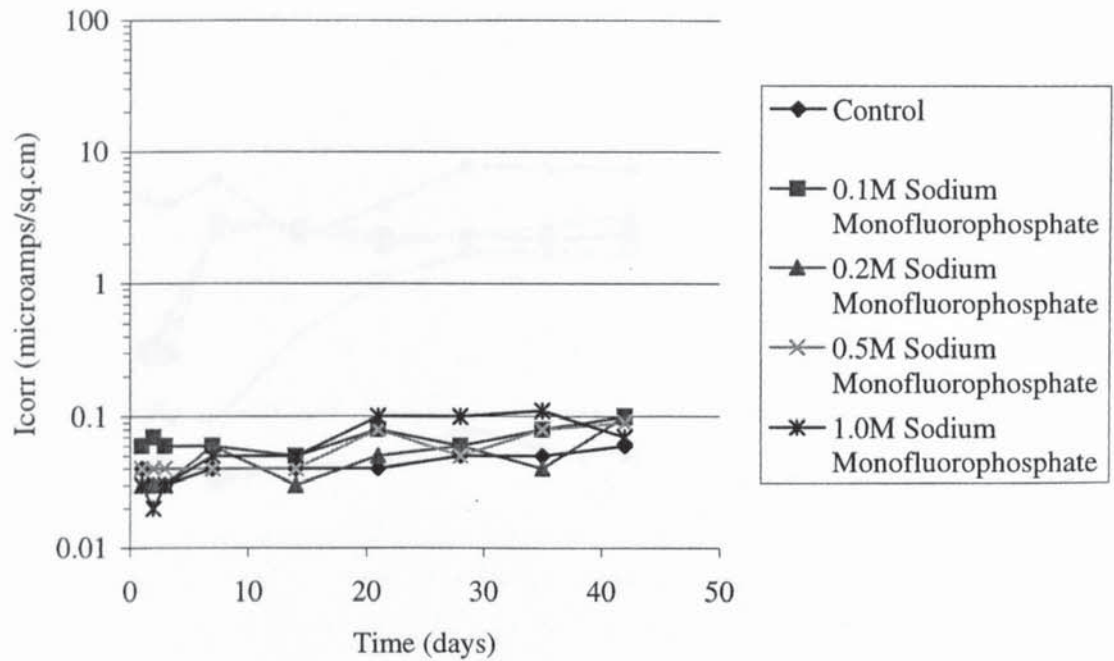


Figure 4.27 -  $E_{corr}$  versus time for mild steel bars immersed for 42 days in air-saturated aqueous solutions of 0.1M sodium hydroxide with various additions of sodium monofluorophosphate

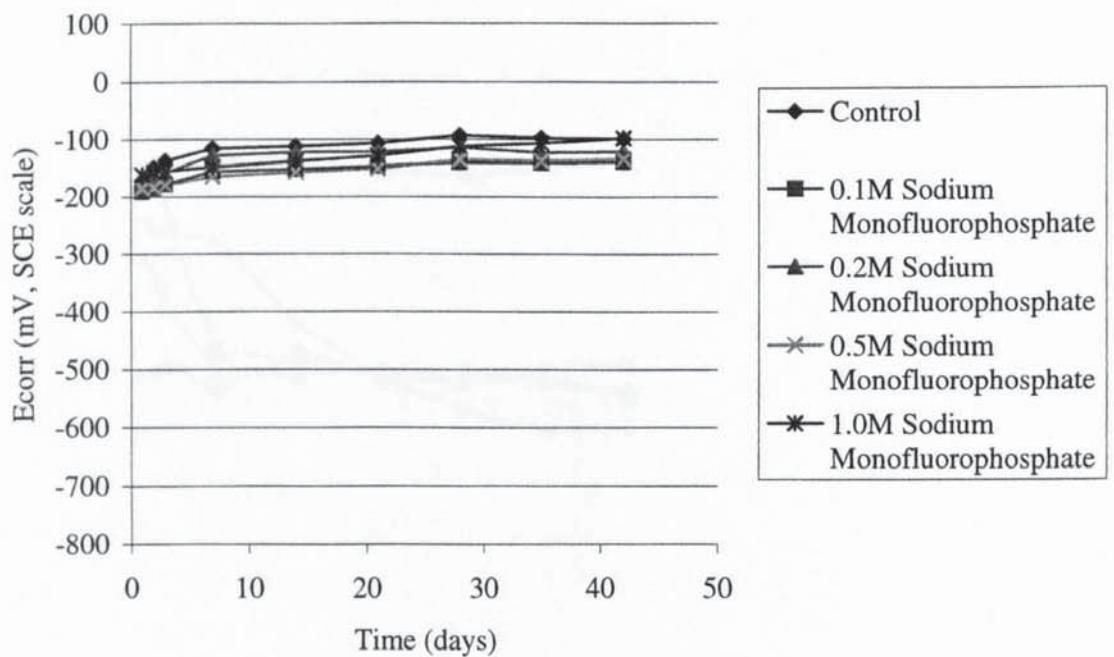




Figure 4.28 -  $I_{corr}$  versus time for mild steel bars immersed for 42 days in air-saturated aqueous solutions of 0.1M sodium hydroxide with 0.1M sodium chloride and various additions of sodium monofluorophosphate

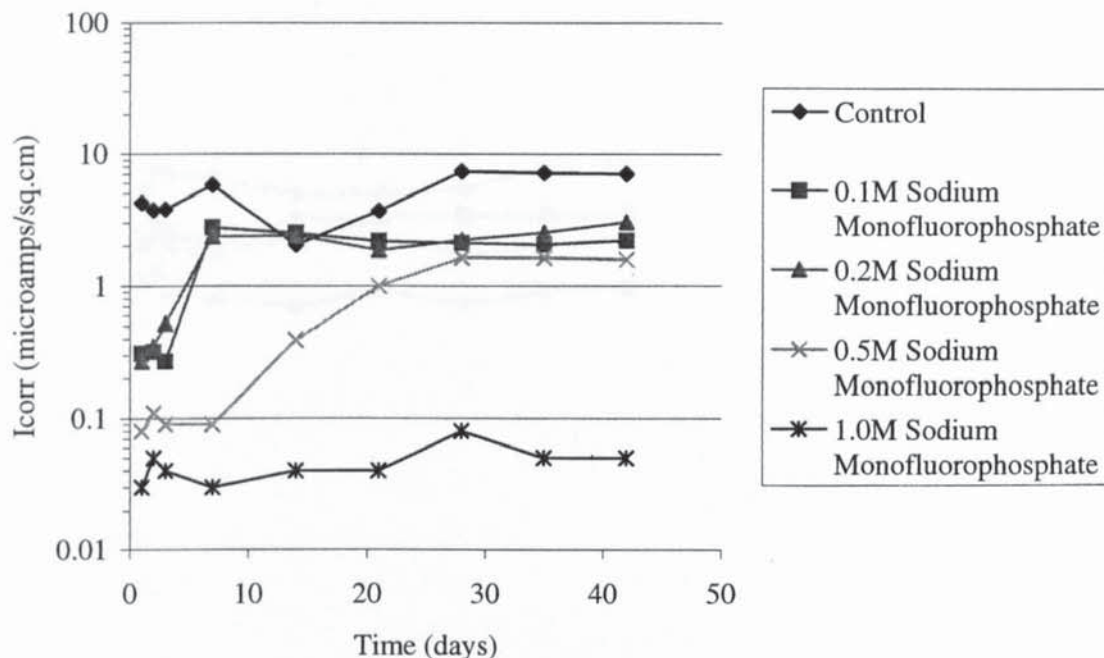


Figure 4.29 -  $E_{corr}$  versus time for mild steel bars immersed for 42 days in air-saturated aqueous solutions of 0.1M sodium hydroxide with 0.1M sodium chloride and various additions of sodium monofluorophosphate

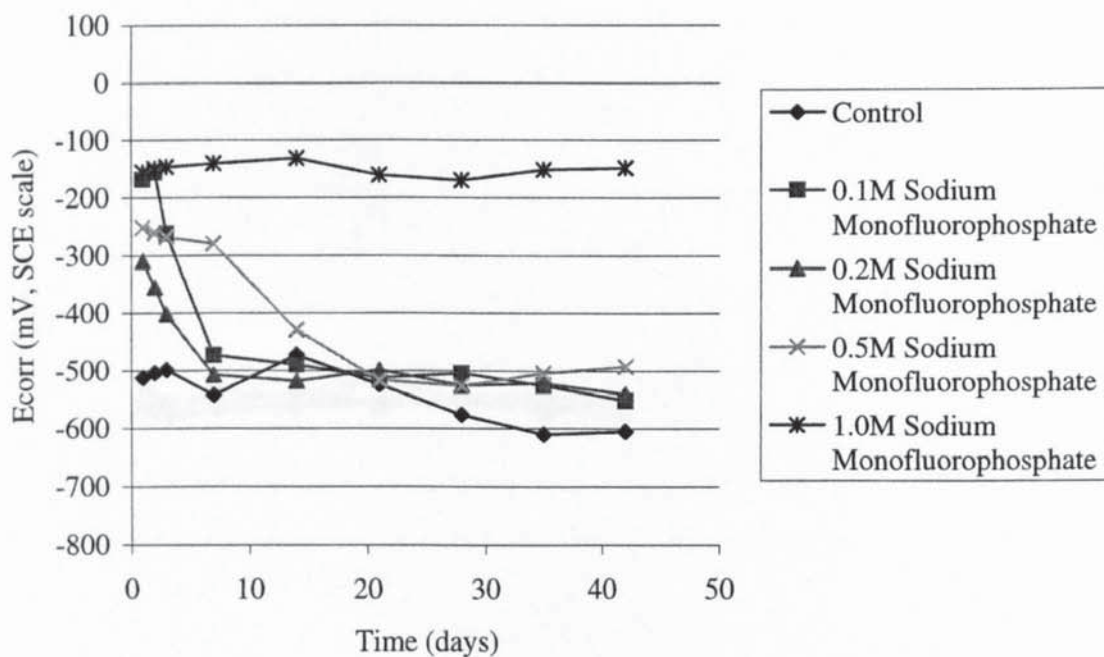


Figure 4.30 - Icorr versus time for mild steel bars immersed for 42 days in air-saturated aqueous solutions of 0.1M sodium hydroxide with 1.0M sodium chloride and various additions of sodium monofluorophosphate

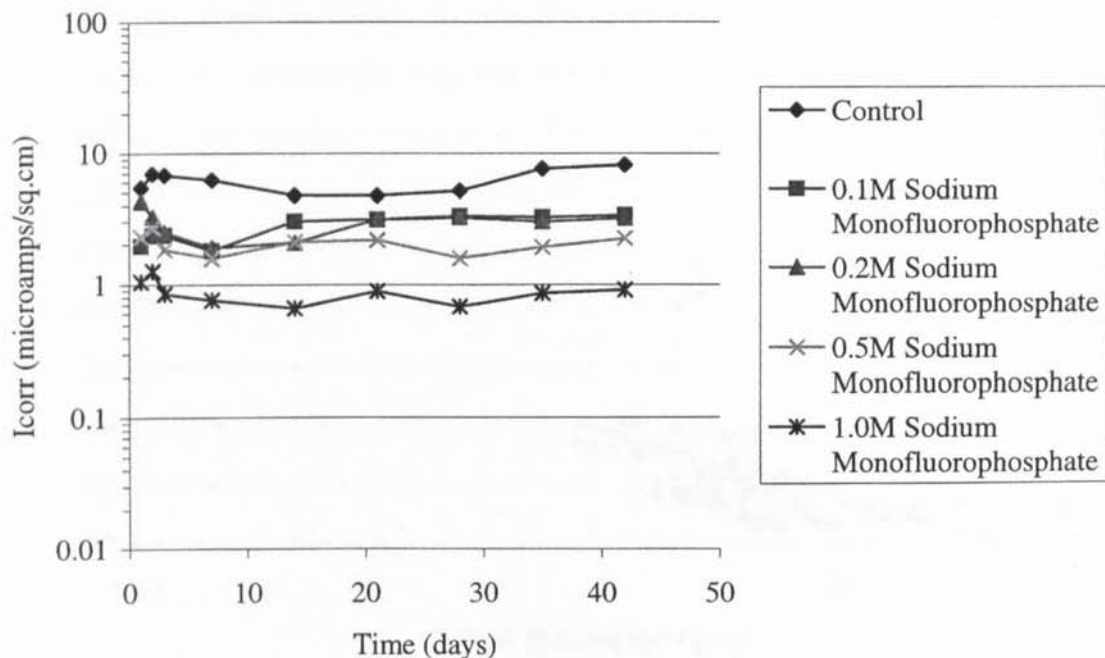


Figure 4.31 - Ecorr versus time for mild steel bars immersed for 42 days in air-saturated aqueous solutions of 0.1M sodium hydroxide with 1.0M sodium chloride and various additions of sodium monofluorophosphate

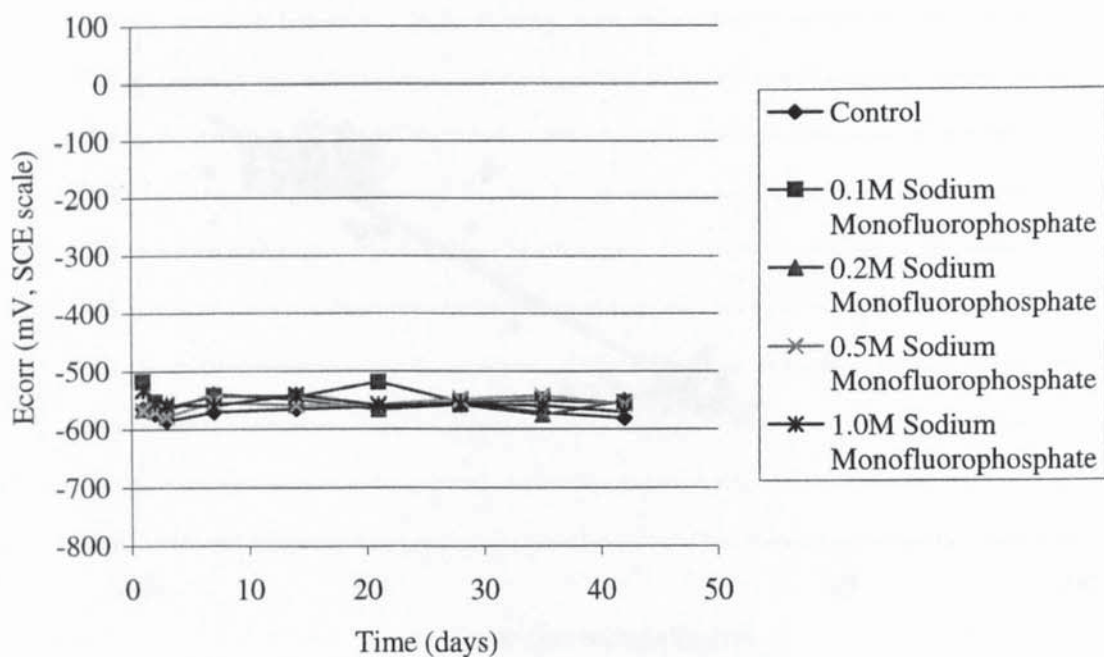


Figure 4.32 -  $E_{corr}$  versus  $I_{corr}$  for mild steel bars immersed in air-saturated aqueous solutions of de-ionised water with varying amounts of sodium chloride and sodium monofluorophosphate

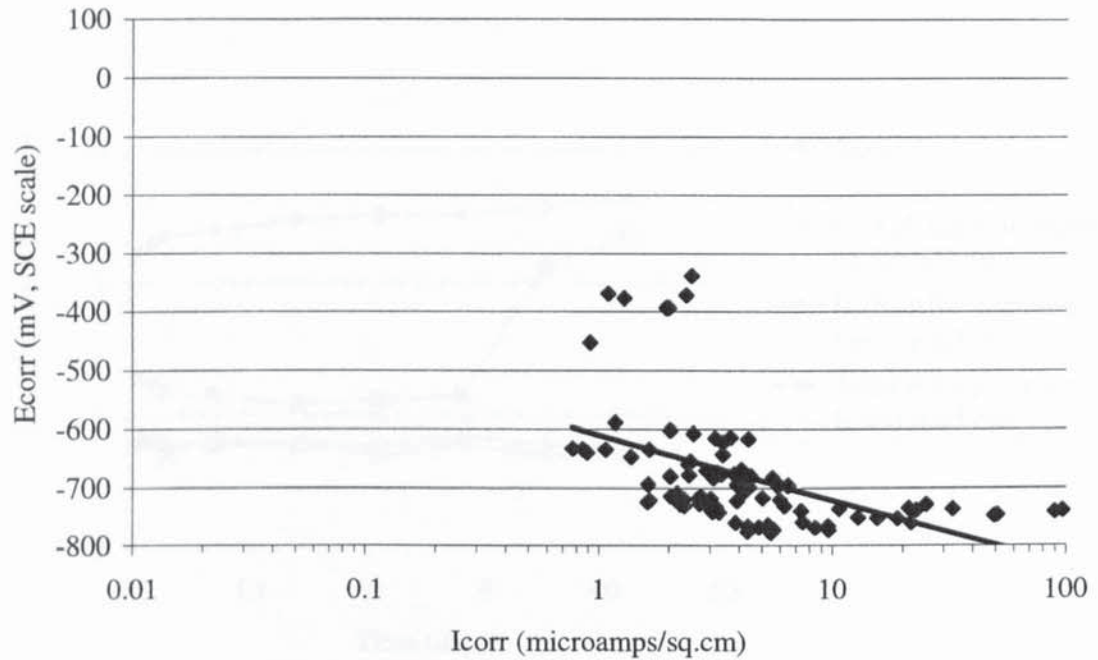


Figure 4.33 -  $E_{corr}$  versus  $I_{corr}$  for mild steel bars immersed in air-saturated aqueous solutions of 0.1M sodium hydroxide with varying amounts of sodium chloride and sodium monofluorophosphate

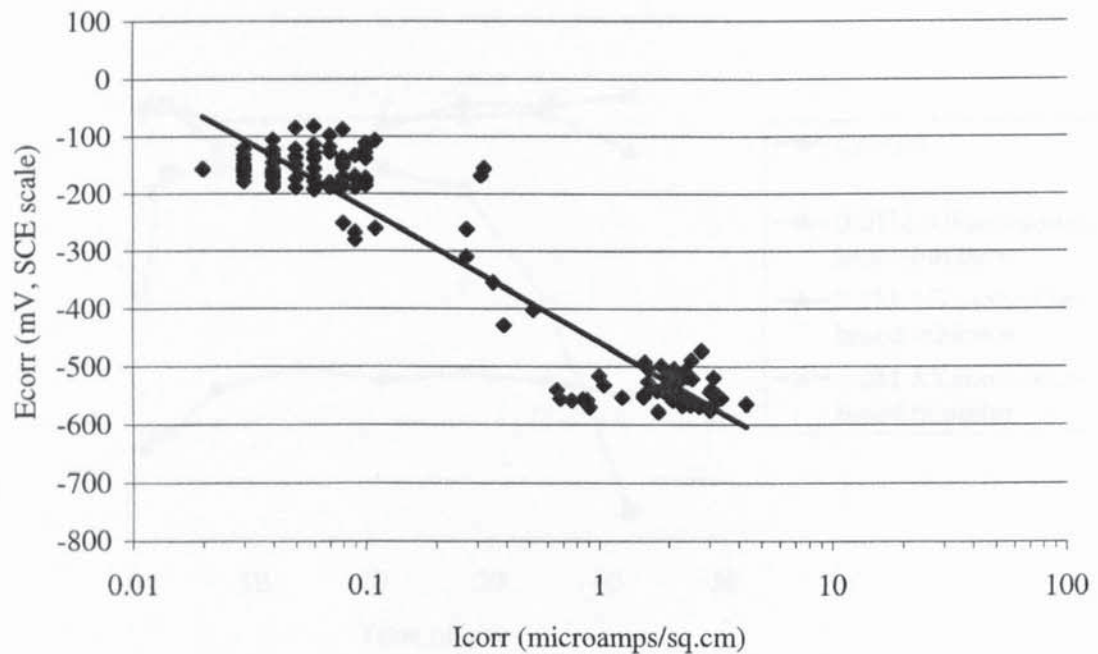




Figure 4.34 -  $I_{corr}$  versus time for mild steel bars immersed for 42 days in air-saturated aqueous solutions of de-ionised water with various additions of an alkanolamine-based inhibitor

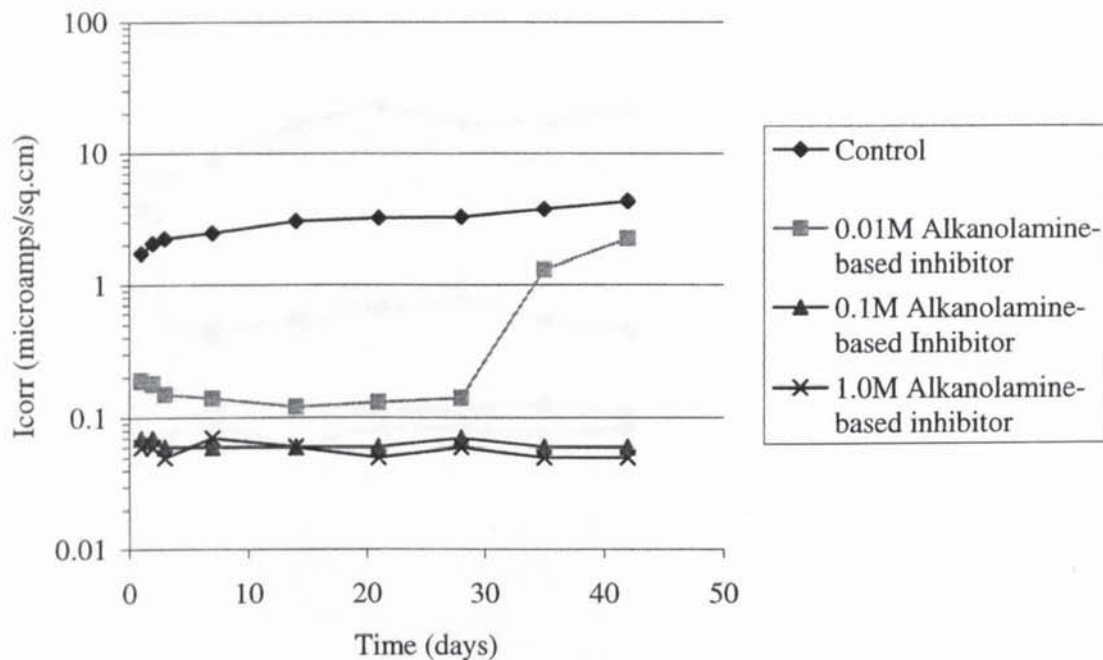


Figure 4.35 -  $E_{corr}$  versus time for mild steel bars immersed for 42 days in air-saturated aqueous solutions of de-ionised water with various additions of an alkanolamine based inhibitor

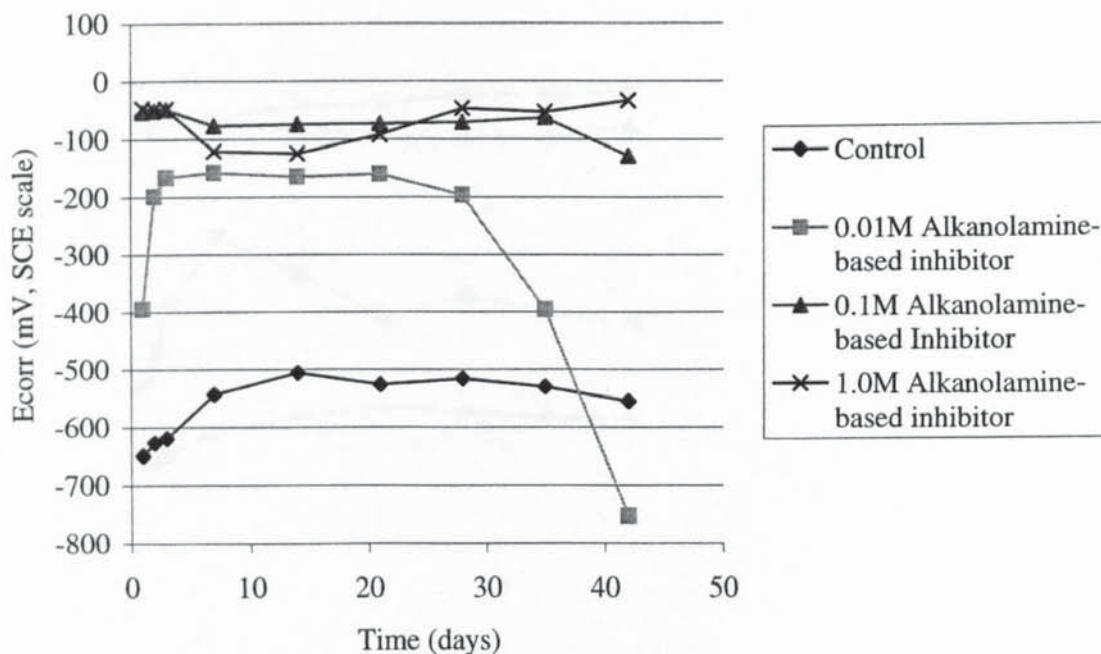


Figure 4.36 - Icorr versus time for mild steel bars immersed for 42 days in air-saturated aqueous solutions of de-ionised water with 0.01M sodium chloride and various additions of an alkanolamine-based inhibitor

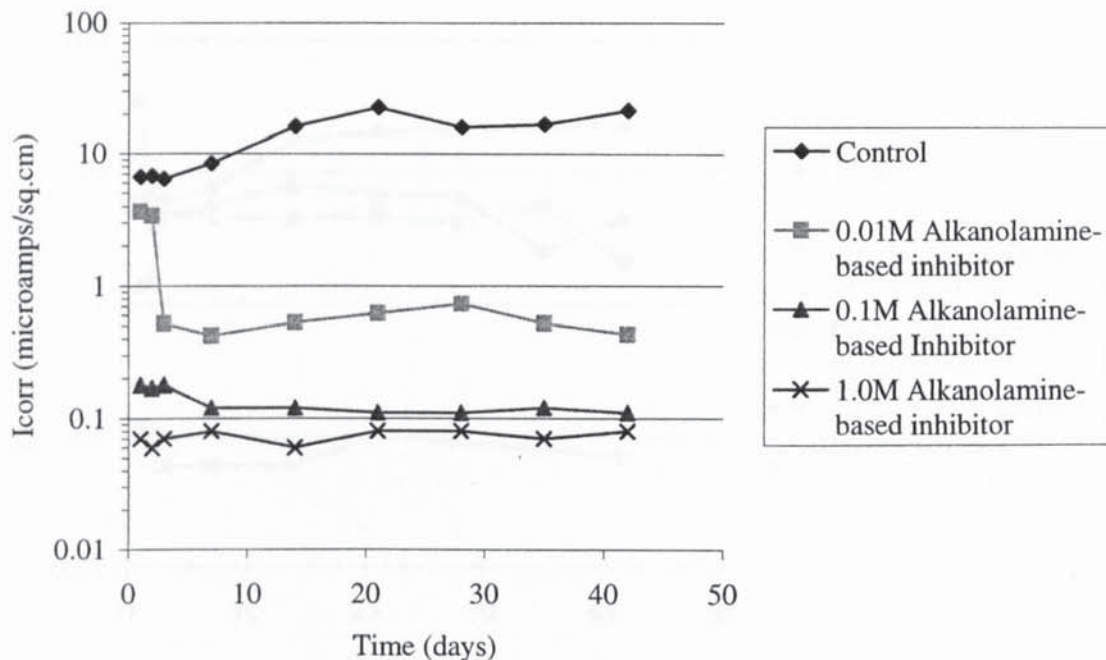


Figure 4.37 - Ecorr versus time for mild steel bars immersed for 42 days in air-saturated aqueous solutions of de-ionised water with 0.01M sodium chloride and various additions of an alkanolamine-based inhibitor

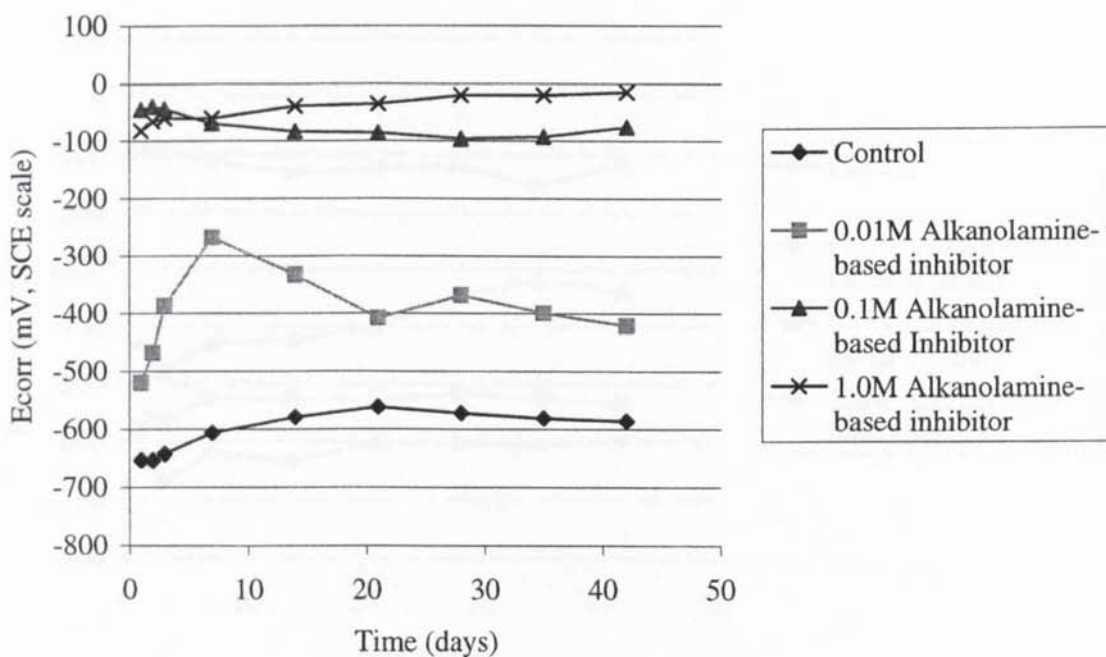


Figure 4.38 -  $I_{corr}$  versus time for mild steel bars immersed for 42 days in air-saturated aqueous solutions of de-ionised water with 0.1M sodium chloride and various additions of an alkanolamine-based inhibitor

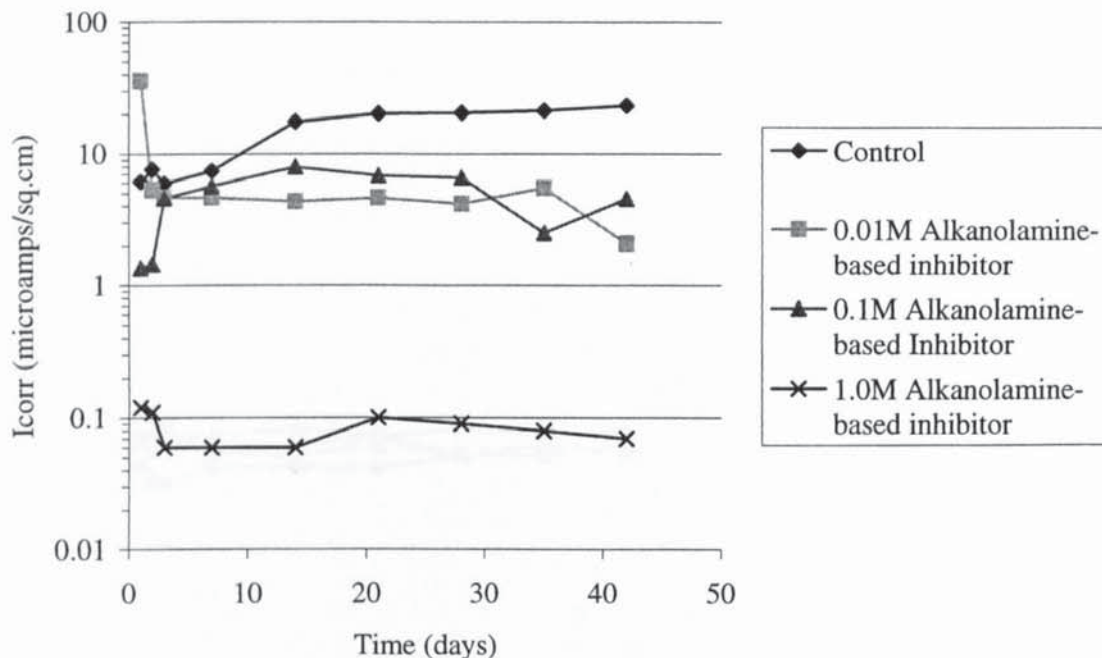


Figure 4.39 -  $E_{corr}$  versus time for mild steel bars immersed for 42 days in air-saturated aqueous solutions of de-ionised water with 0.1M sodium chloride and various additions of an alkanolamine-based inhibitor

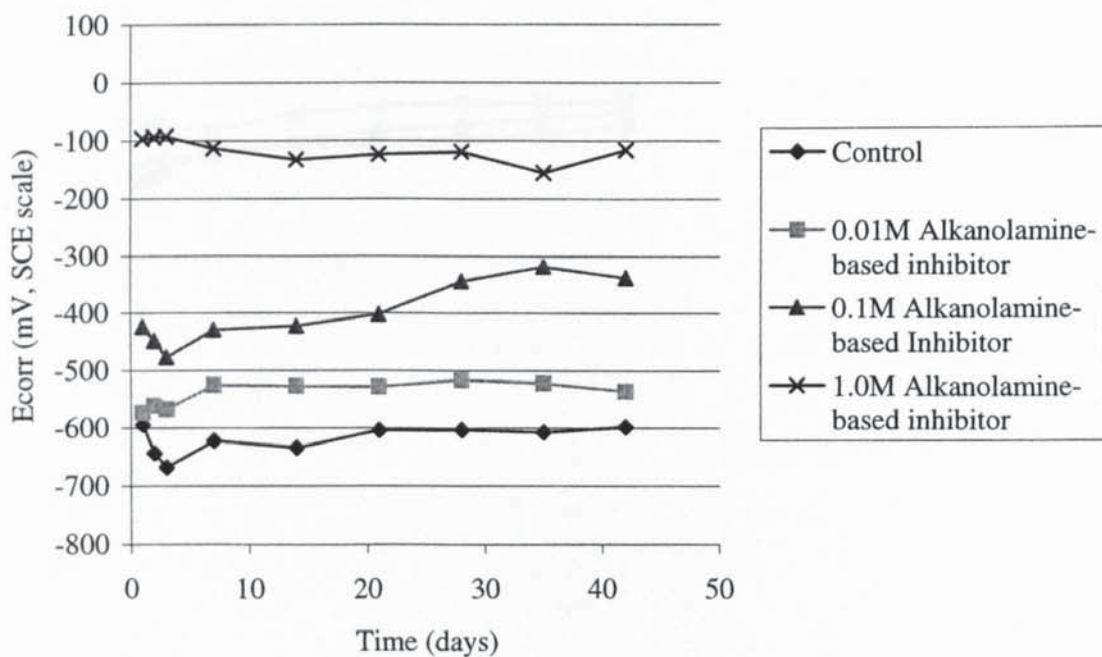




Figure 4.40 -  $I_{corr}$  versus time for mild steel bars immersed for 42 days in air-saturated aqueous solutions of 0.1M sodium hydroxide with various additions of an alkanolamine-based inhibitor

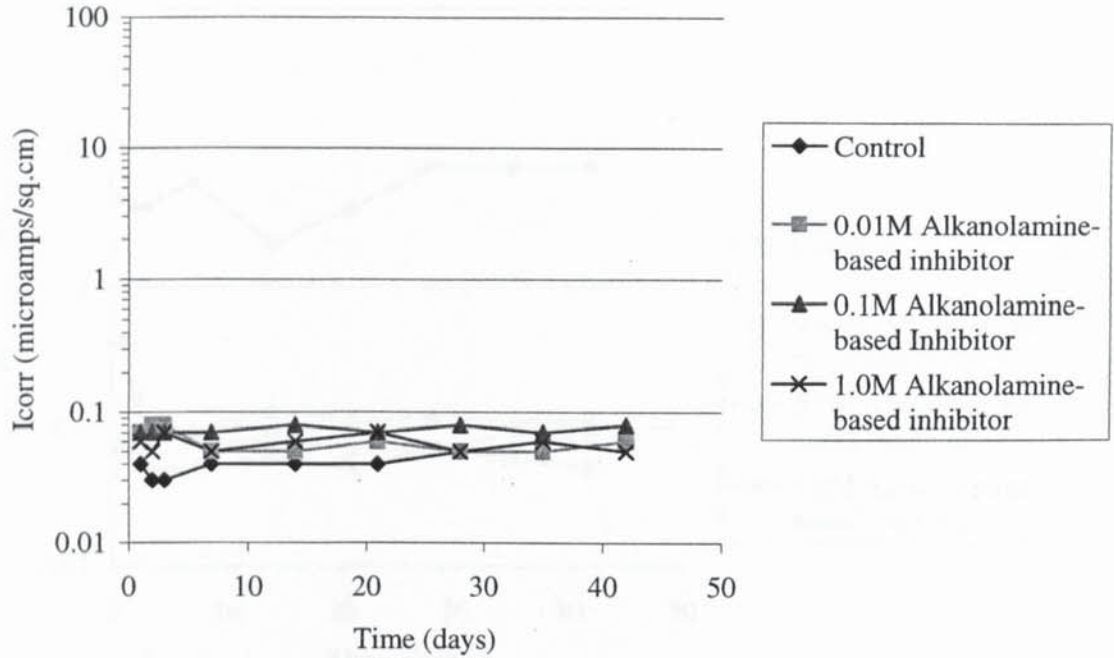


Figure 4.41 -  $E_{corr}$  versus time for mild steel bars immersed for 42 days in air-saturated aqueous solutions of 0.1M sodium hydroxide with various additions of an alkanolamine-based inhibitor

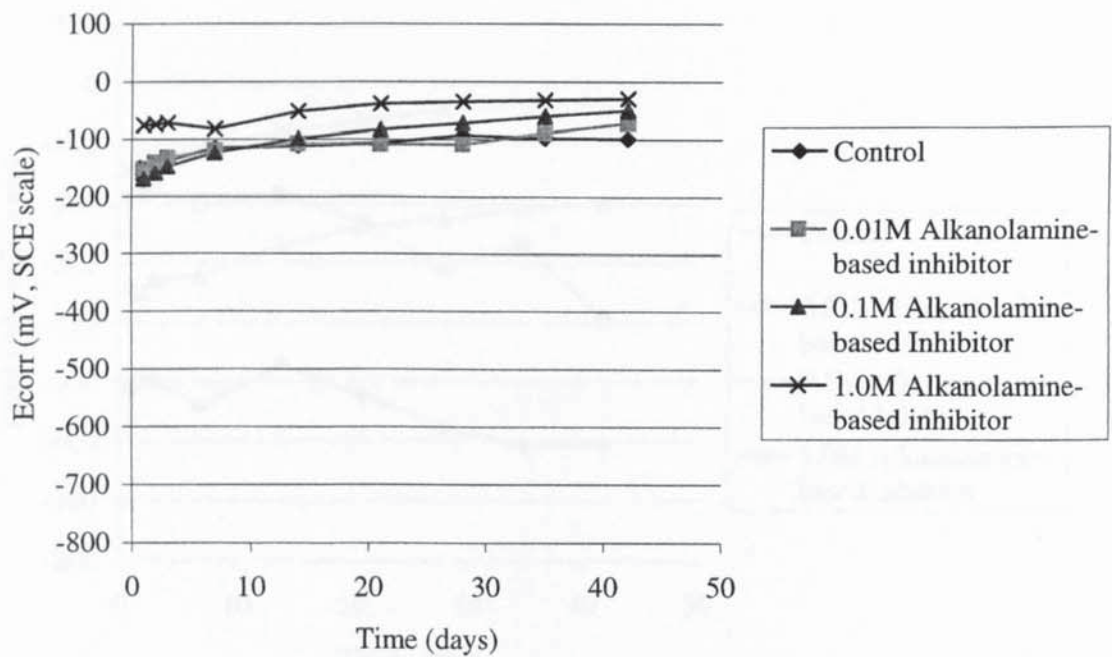


Figure 4.42 -  $I_{corr}$  versus time for mild steel bars immersed for 42 days in air-saturated aqueous solutions of 0.1M sodium hydroxide with 0.1M sodium chloride and various additions of an alkanolamine-based inhibitor

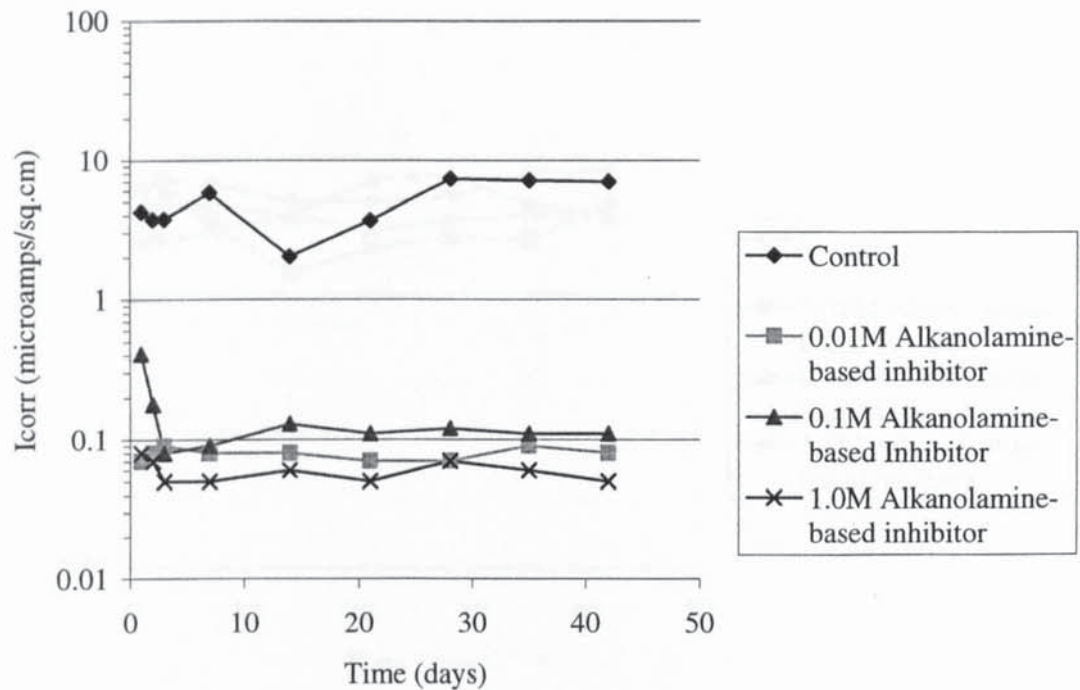


Figure 4.43 -  $E_{corr}$  versus time for mild steel bars immersed for 42 days in air-saturated aqueous solutions of 0.1M sodium hydroxide with 0.1M sodium chloride and various additions of an alkanolamine-based inhibitor

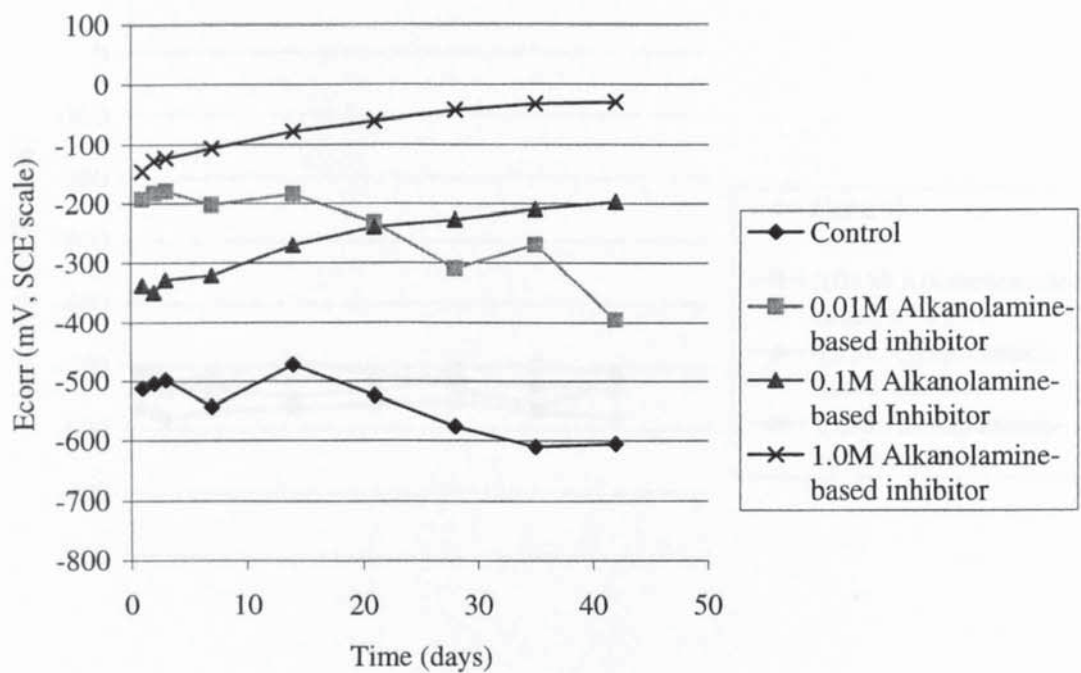


Figure 4.44 -  $I_{corr}$  versus time for mild steel bars immersed for 42 days in air-saturated aqueous solutions of 0.1M sodium hydroxide with 1.0M sodium chloride and various additions of an alkanolamine-based inhibitor

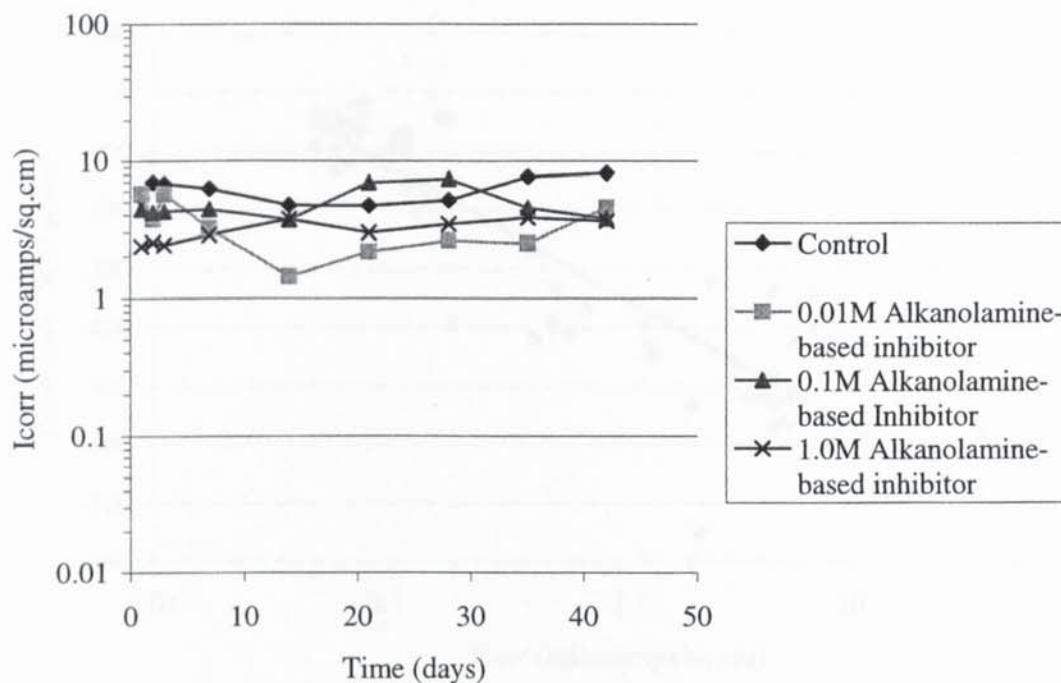


Figure 4.45 -  $E_{corr}$  versus time for mild steel bars immersed for 42 days in air-saturated aqueous solutions of 0.1M sodium hydroxide with 1.0M sodium chloride and various additions of an alkanolamine based inhibitor

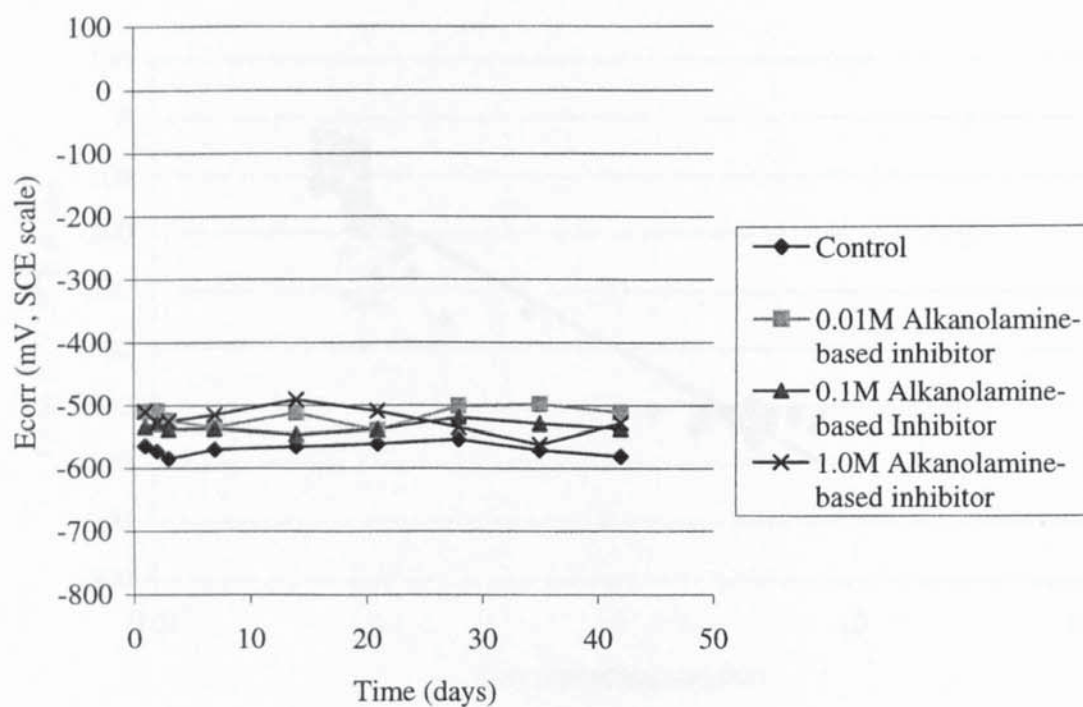




Figure 4.46 -  $E_{corr}$  versus  $I_{corr}$  for mild steel bars immersed in air-saturated aqueous solutions of de-ionised water with varying amounts of sodium chloride and an alkanolamine-based inhibitor

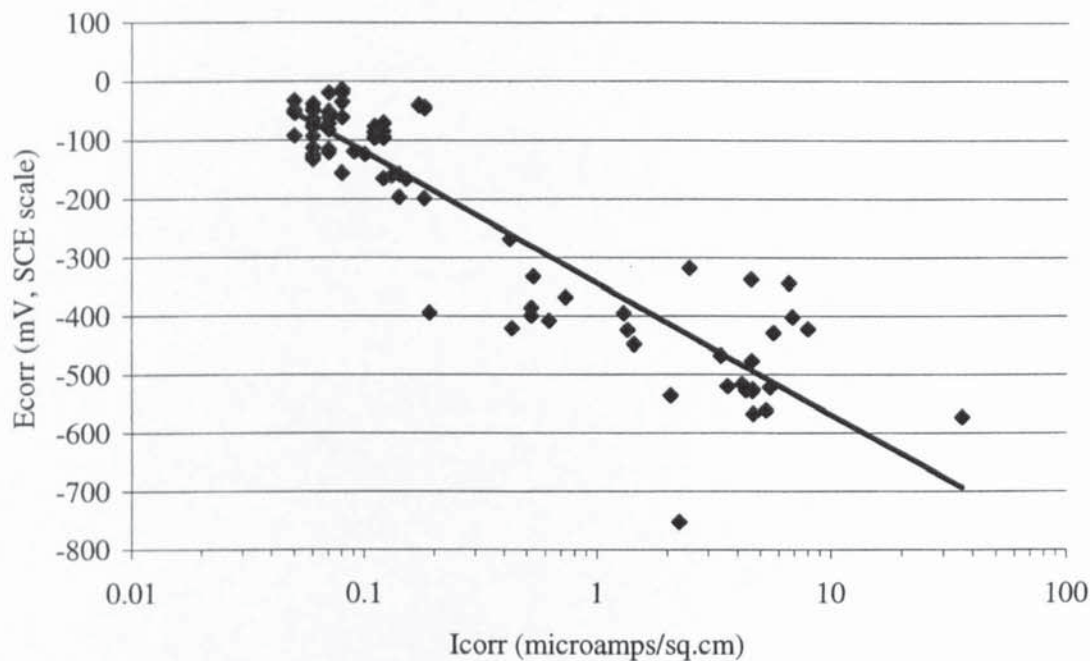


Figure 4.47 -  $E_{corr}$  versus  $I_{corr}$  for mild steel bars immersed in air-saturated aqueous solutions of 0.1M sodium hydroxide with varying amounts of sodium chloride and an alkanolamine-based inhibitor

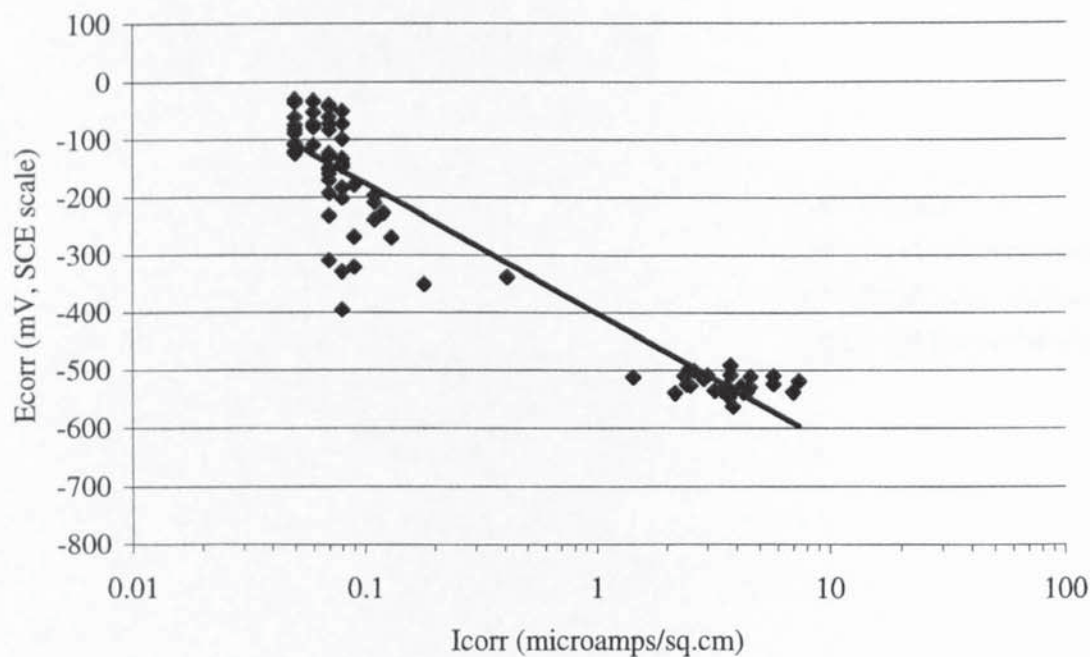


Figure 4.48 -  $I_{corr}$  versus time for mild steel bars immersed for 42 days in air-saturated aqueous solutions of de-ionised water with various additions of ethanolamine

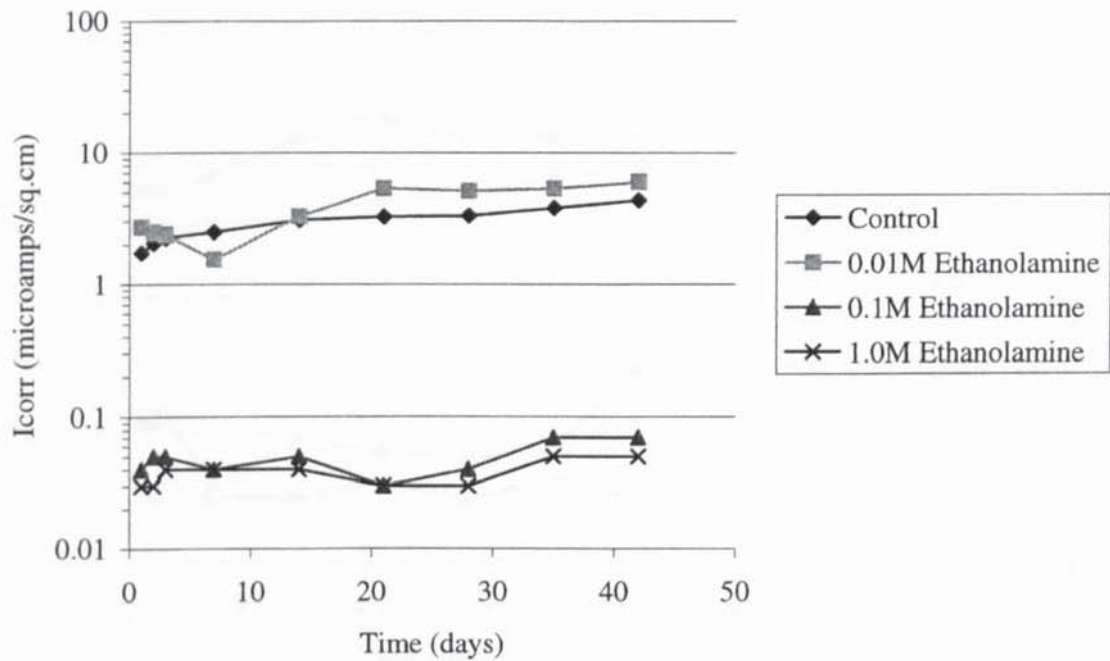


Figure 4.49 -  $E_{corr}$  versus time for mild steel bars immersed for 42 days in air-saturated aqueous solutions of de-ionised water with various additions of ethanolamine

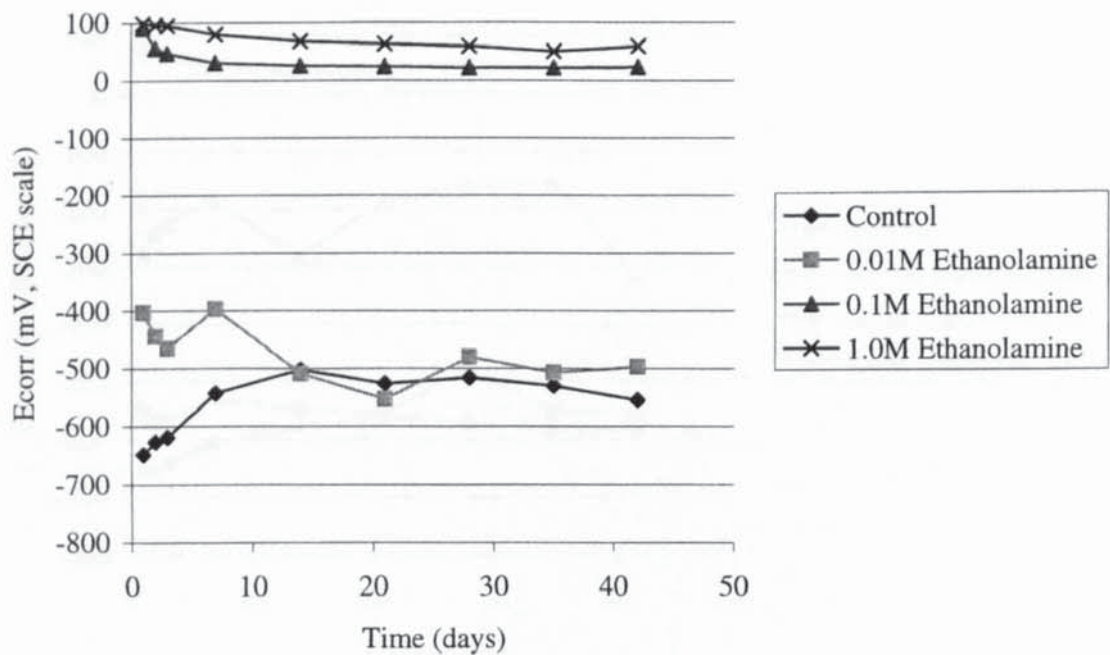


Figure 4.50 - Icorr versus time for mild steel bars immersed for 42 days in air-saturated aqueous solutions of de-ionised water with 0.01M sodium chloride and various additions of ethanolamine

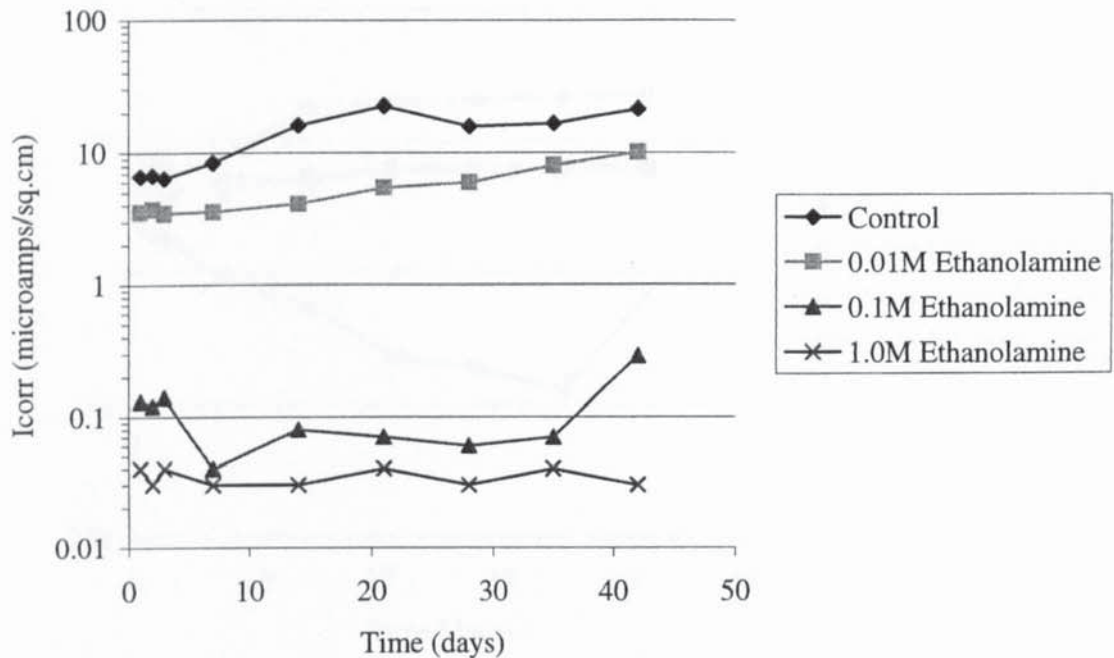


Figure 4.51 - Ecorr versus time for mild steel bars immersed for 42 days in air-saturated aqueous solutions of de-ionised water with 0.01M sodium chloride with various additions of ethanolamine

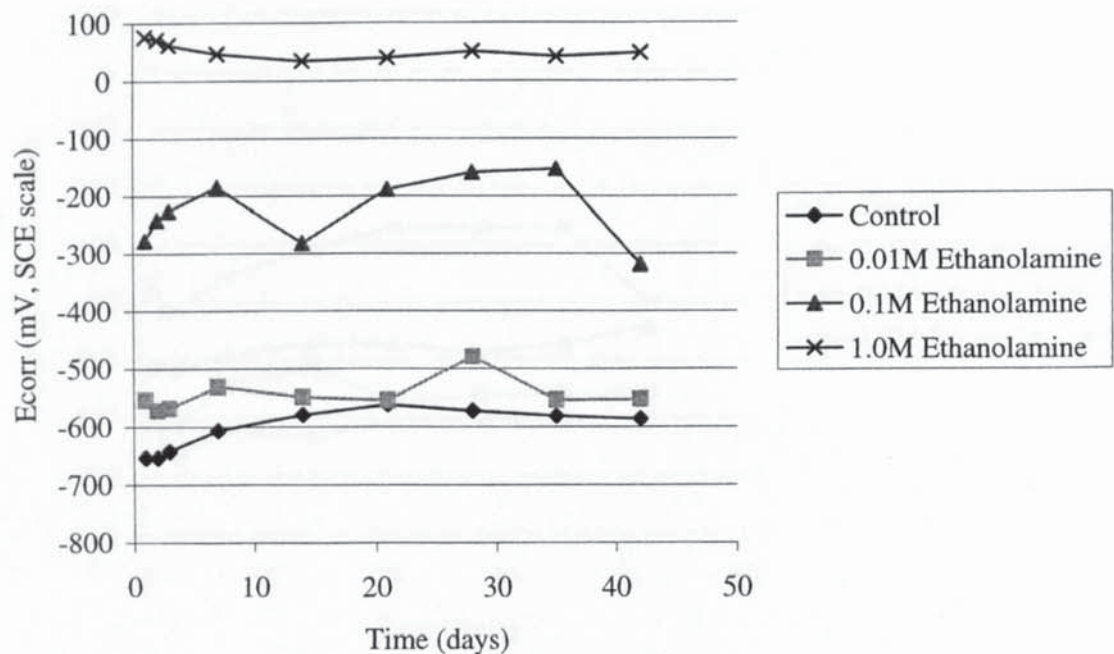




Figure 4.52 -  $I_{corr}$  versus time for mild steel bars immersed in air-saturated aqueous solutions of de-ionised water with 0.1M sodium chloride and various additions of ethanolamine

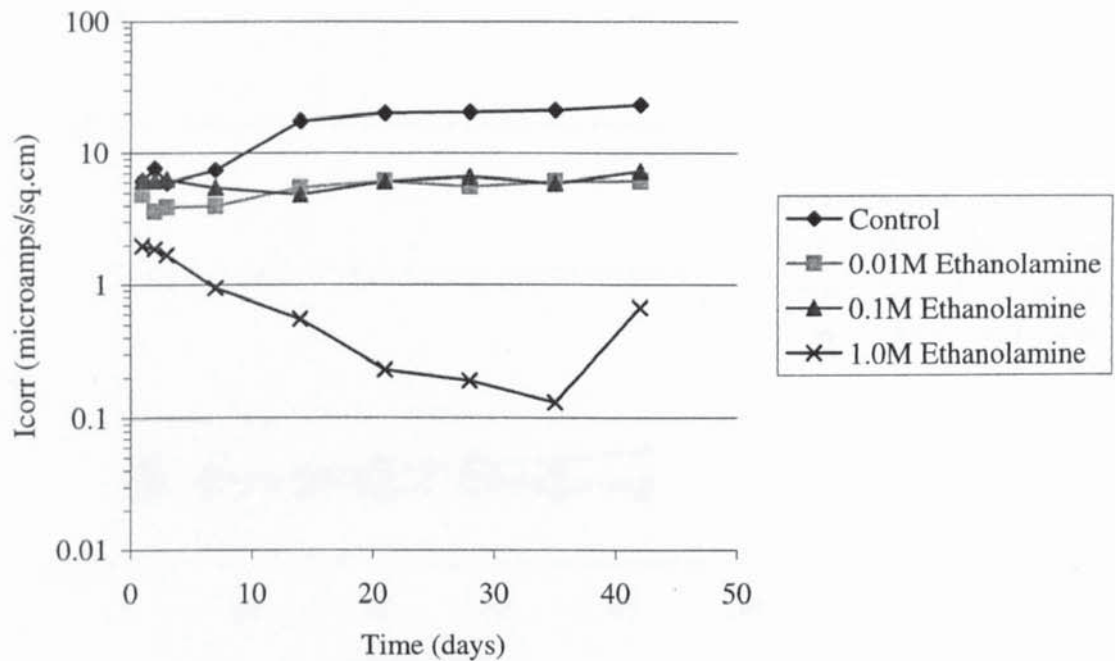


Figure 4.53 -  $E_{corr}$  versus time for mild steel bars immersed for 42 days in air-saturated aqueous solutions of de-ionised water with 0.1M sodium chloride and various additions of ethanolamine

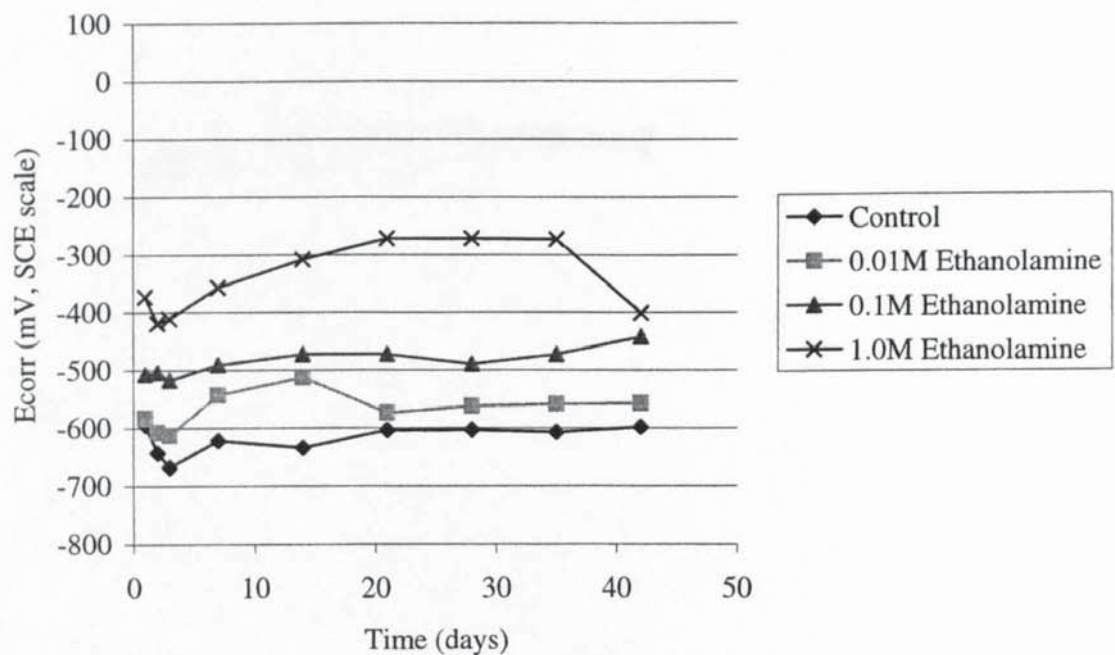


Figure 4.54 - Icorr versus time for mild steel bars immersed for 42 days in air-saturated aqueous solutions of 0.1M sodium hydroxide with various additions of ethanolamine

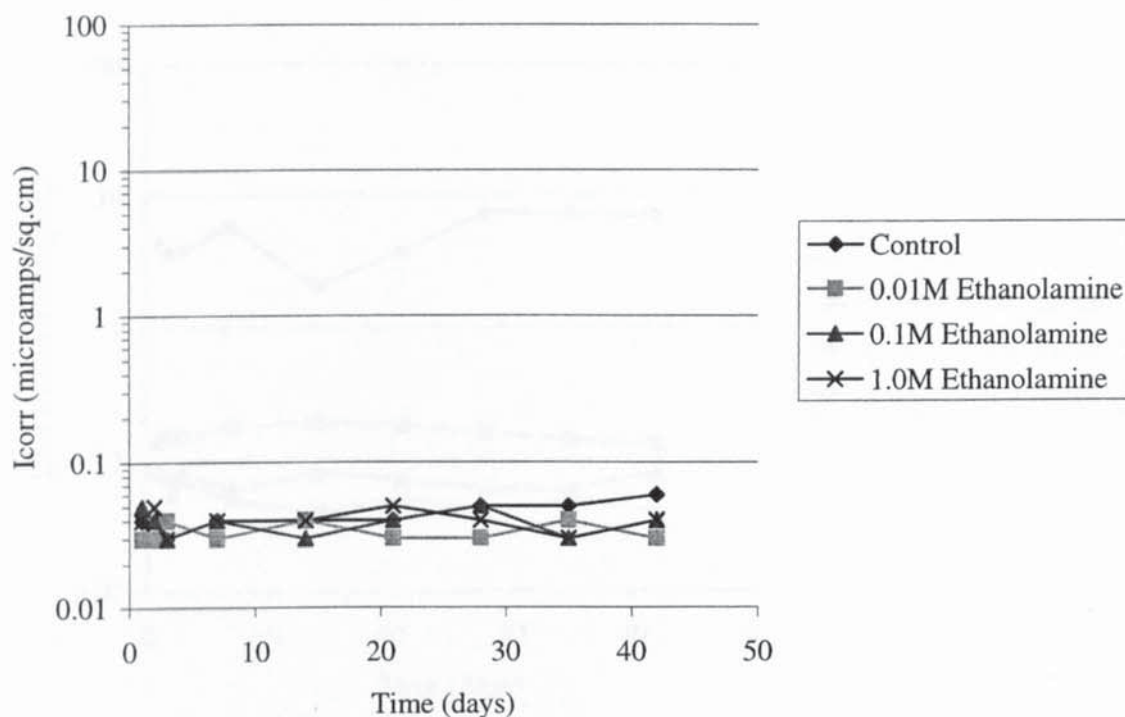


Figure 4.55 - Ecorr versus time for mild steel bars immersed for 42 days in air-saturated aqueous solutions of 0.1M sodium hydroxide with various additions of ethanolamine

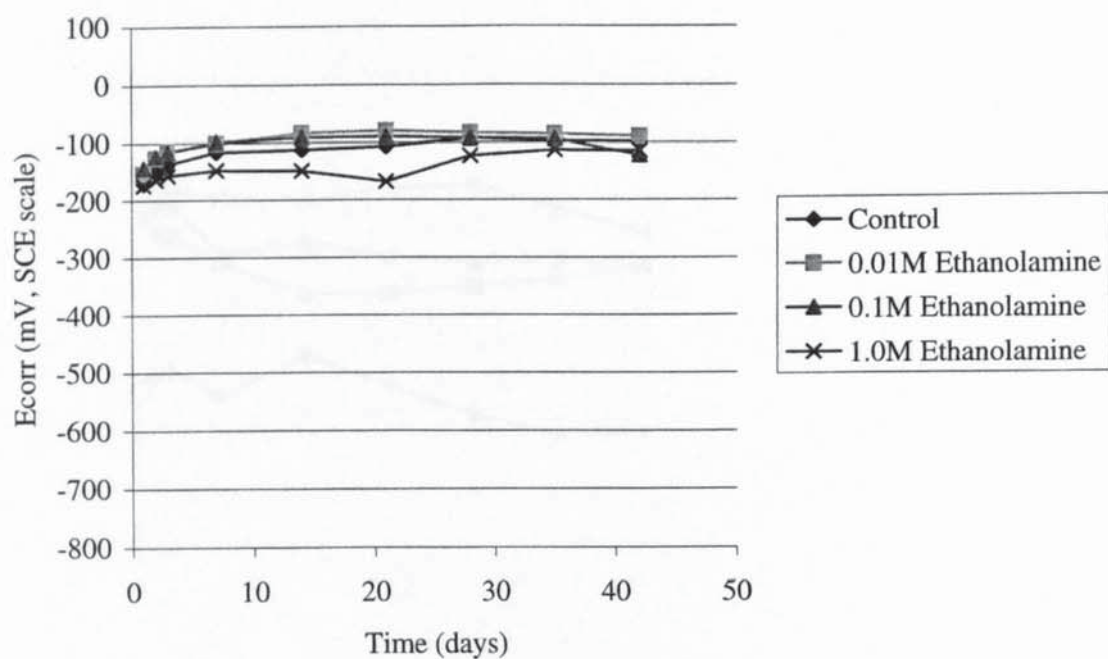


Figure 4.56 - Icorr versus time for mild steel bars immersed for 42 days in air-saturated aqueous solutions of 0.1M sodium hydroxide with 0.1M sodium chloride and various amounts of ethanolamine

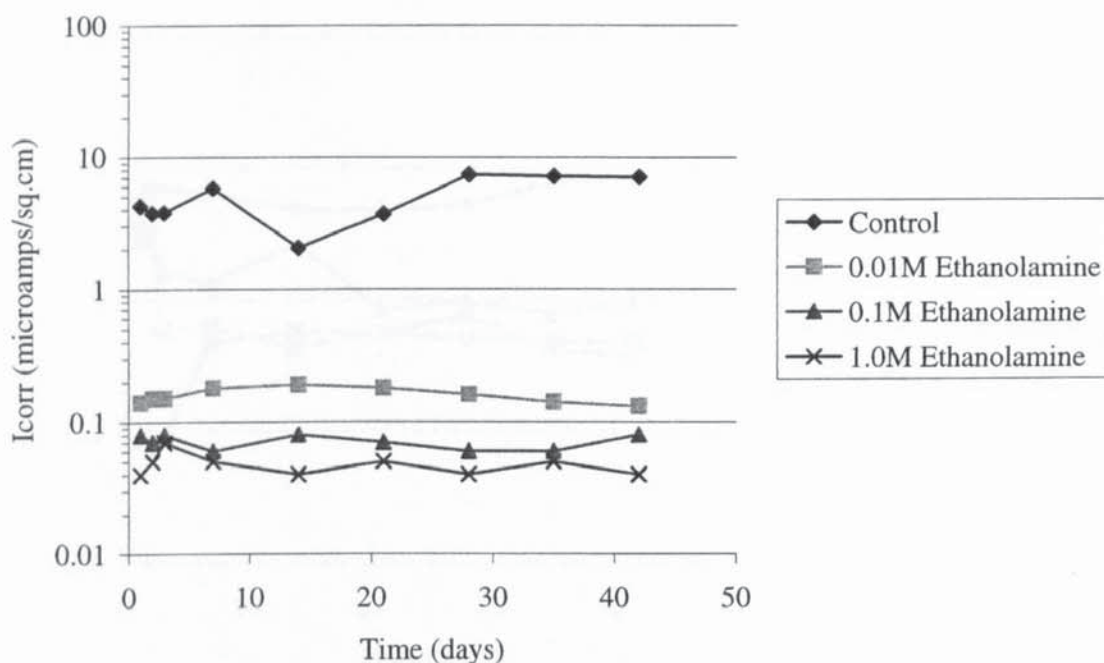


Figure 4.57 - Ecorr versus time for mild steel bars immersed for 42 days in air-saturated aqueous solutions of 0.1M sodium hydroxide with 0.1M sodium chloride and various additions of ethanolamine

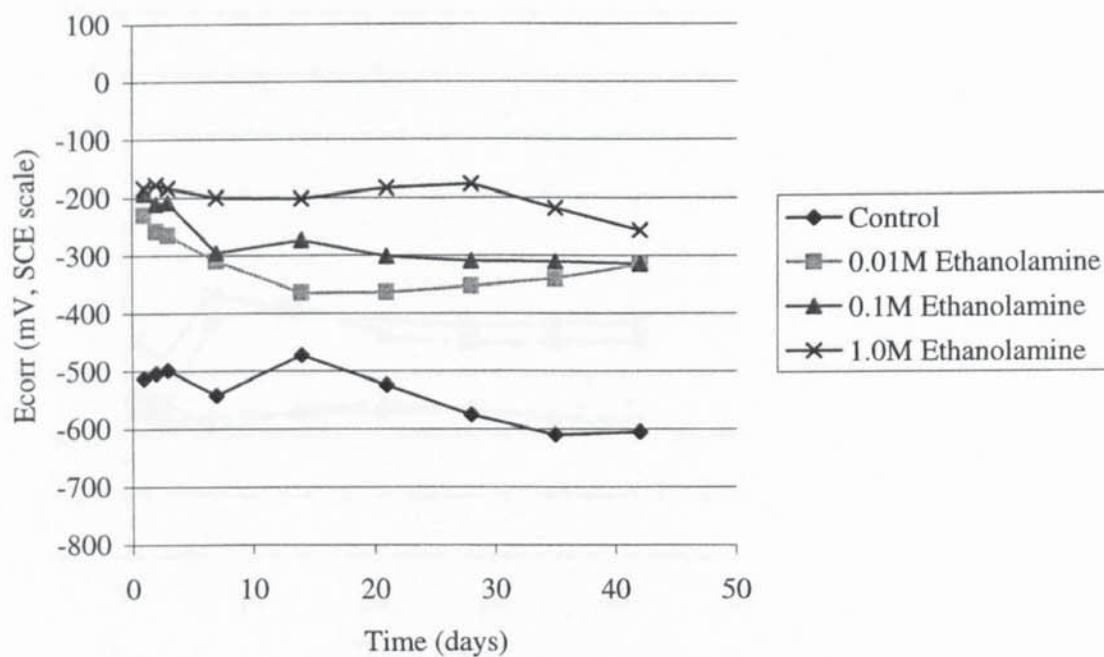




Figure 4.58 -  $I_{corr}$  versus time for mild steel bars immersed for 42 days in air-saturated aqueous solutions of 0.1M sodium hydroxide with 1.0M sodium chloride and various additions of ethanolamine

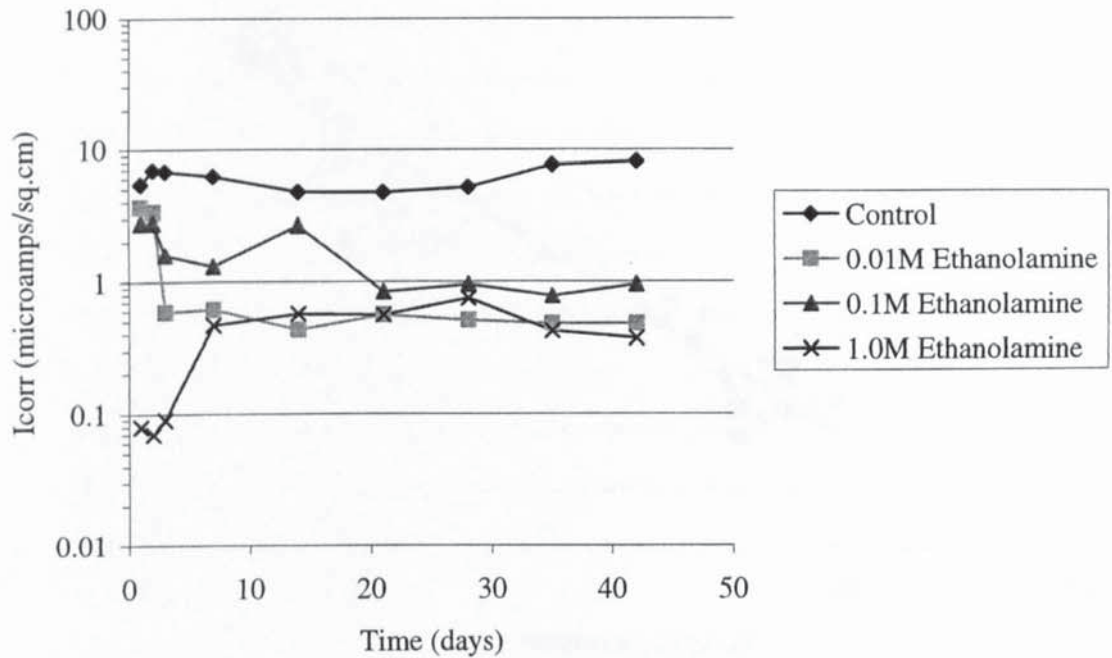


Figure 4.59 -  $E_{corr}$  versus time for mild steel bars immersed for 42 days in air-saturated aqueous solutions of 0.1M sodium hydroxide with 1.0M sodium chloride and various additions of ethanolamine

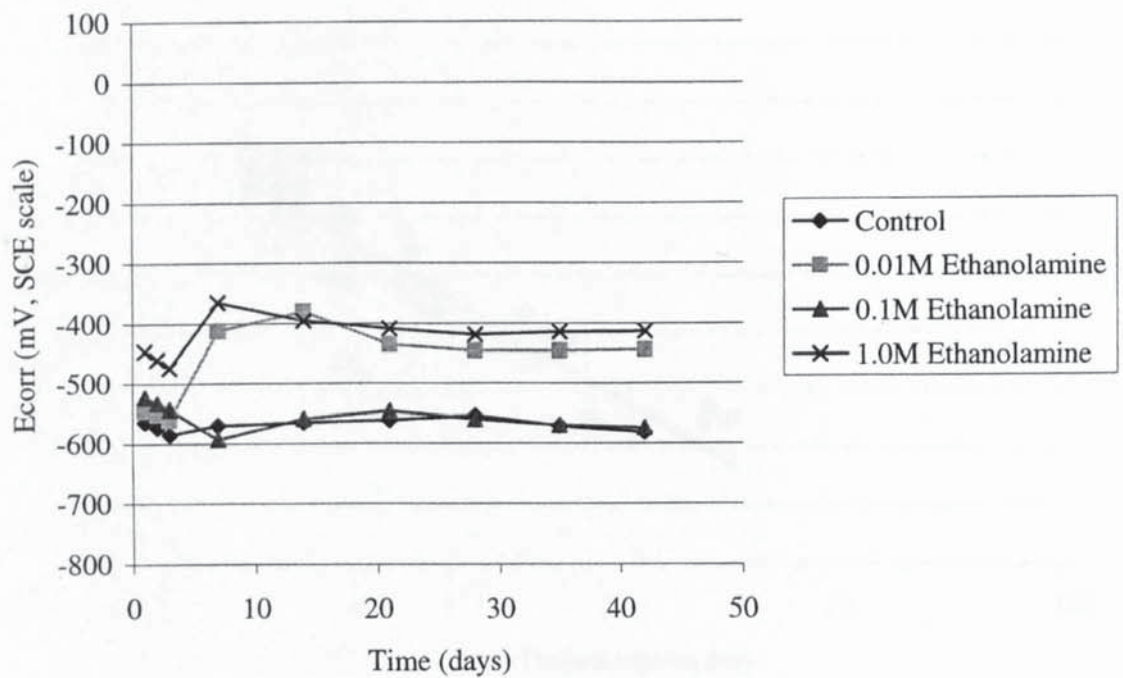


Figure 4.60 -  $E_{corr}$  versus  $I_{corr}$  for mild steel bars immersed in air-saturated aqueous solutions of de-ionised water with varying amounts of sodium chloride and ethanolamine

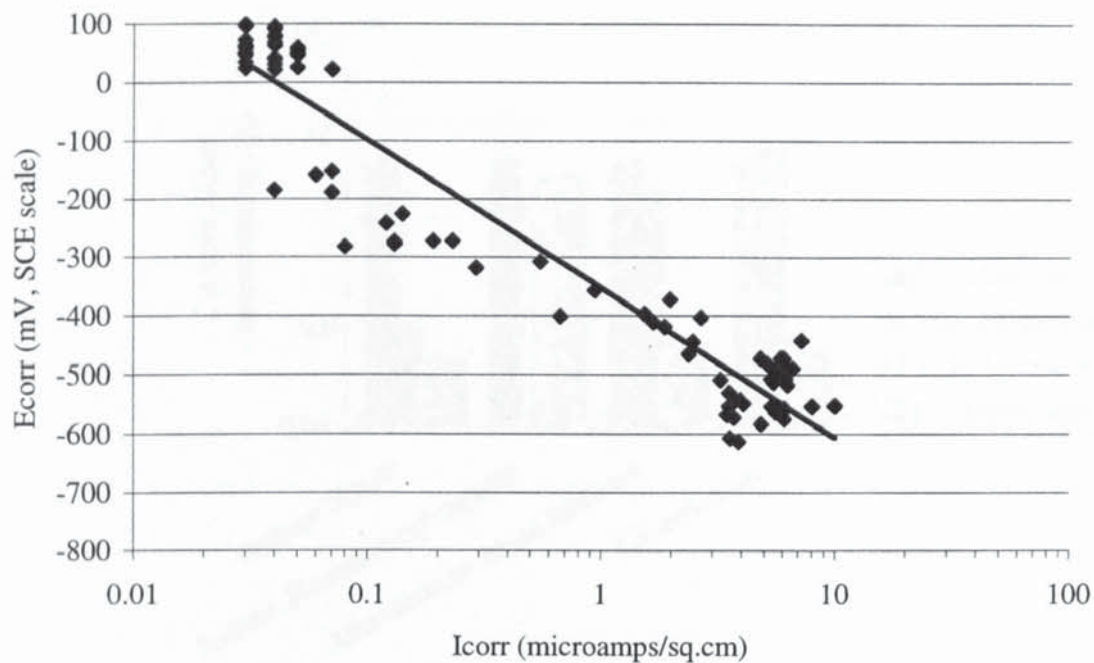


Figure 4.61 -  $E_{corr}$  versus  $I_{corr}$  for mild steel bars immersed in air-saturated aqueous solutions of 0.1M sodium hydroxide with varying amounts of sodium chloride and ethanolamine

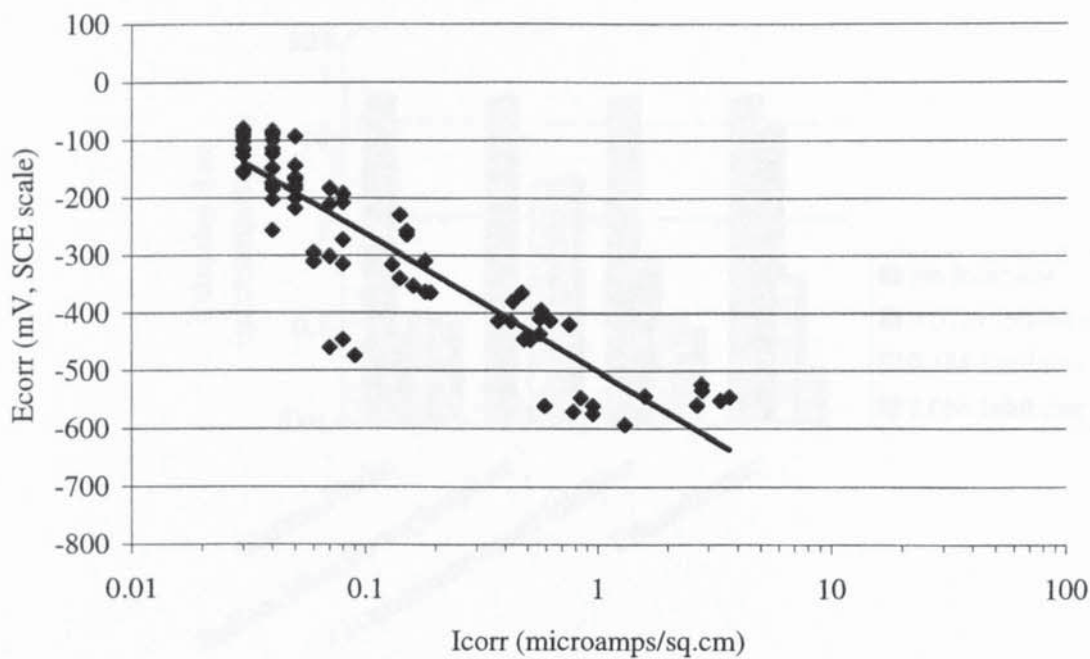


Figure 4.62 - Comparison of corrosion rates, after 42 days, for mild steel bars immersed in air-saturated aqueous solutions of de-ionised water with various additions of inhibitors

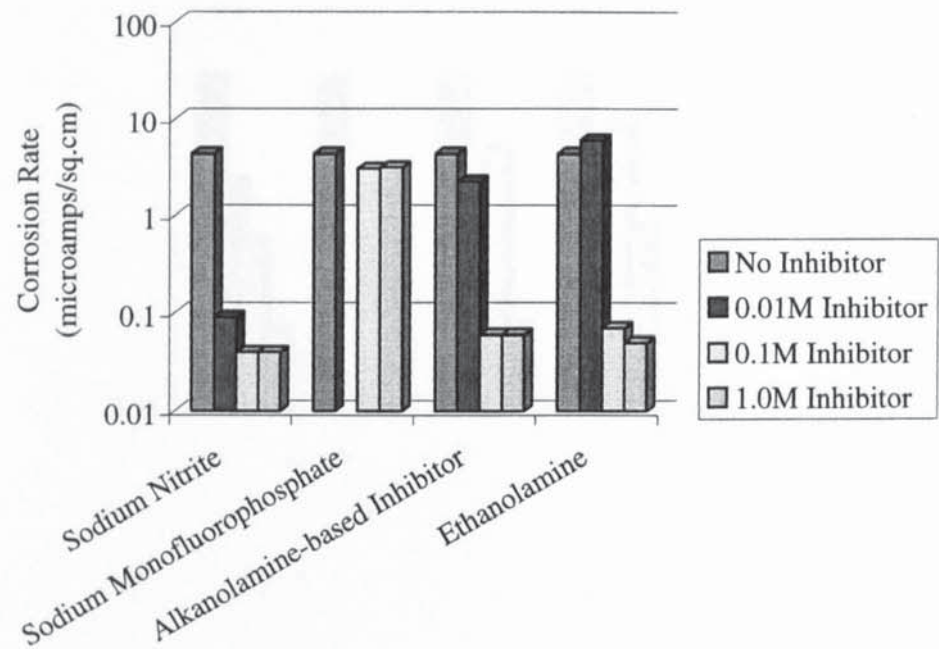


Figure 4.63 - Comparison of corrosion rates, after 42 days, for mild steel bars immersed in air-saturated aqueous solutions of 0.01M sodium chloride with various additions of inhibitors

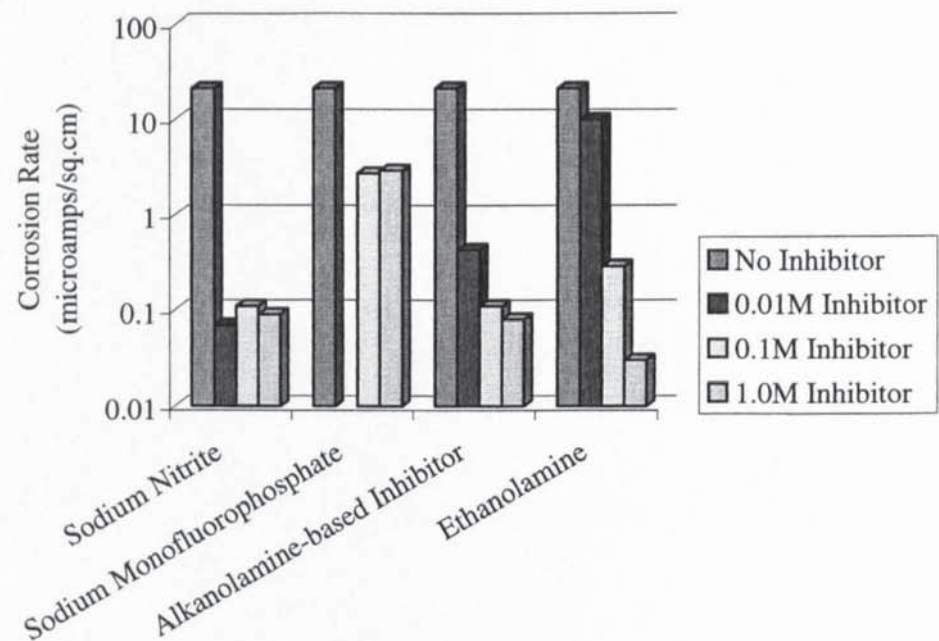




Figure 4.64 - Comparison of corrosion rates, after 42 days, for mild steel bars immersed in air-saturated aqueous solutions of 0.1M sodium chloride with various additions of inhibitors

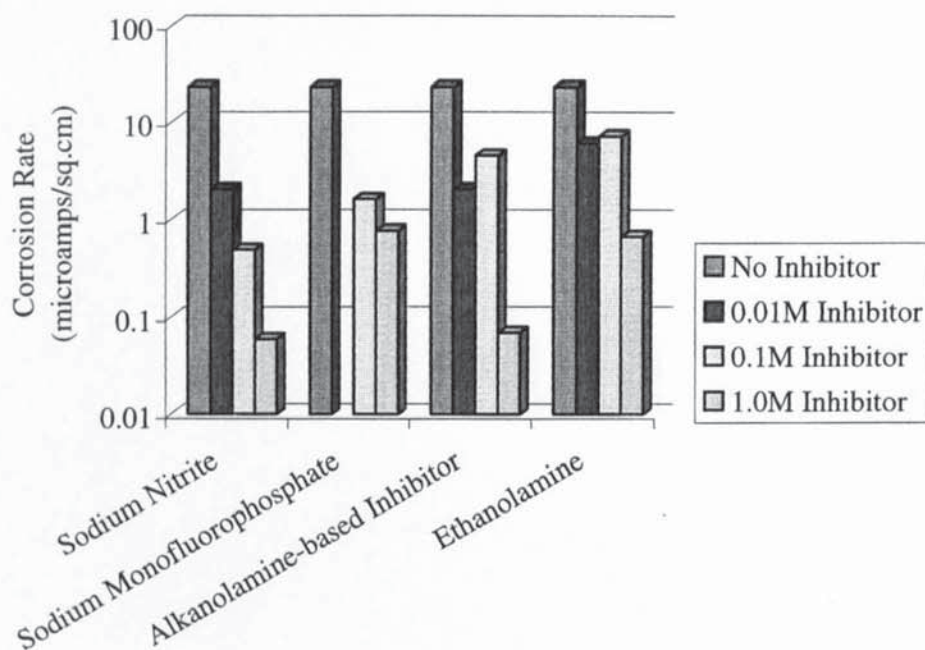


Figure 4.65 - Comparison of corrosion rates, after 42 days, of mild steel bars immersed in air-saturated aqueous solutions of 0.1M sodium hydroxide with various additions of inhibitors

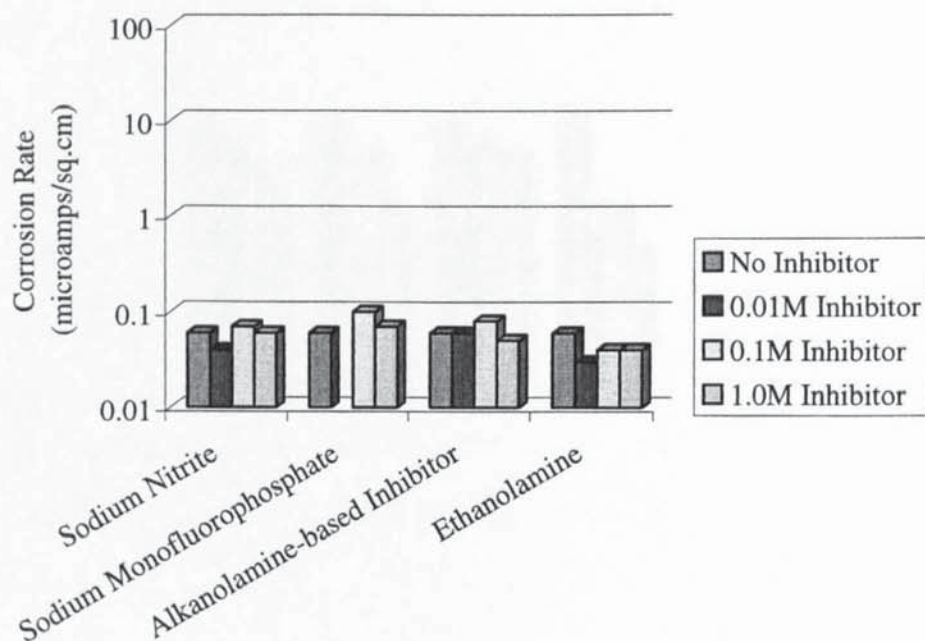


Figure 4.66 - Comparison of corrosion rates, after 42 days, of mild steel bars immersed in air-saturated aqueous solutions of 0.1M sodium hydroxide with 0.1M sodium chloride and various additions of inhibitors

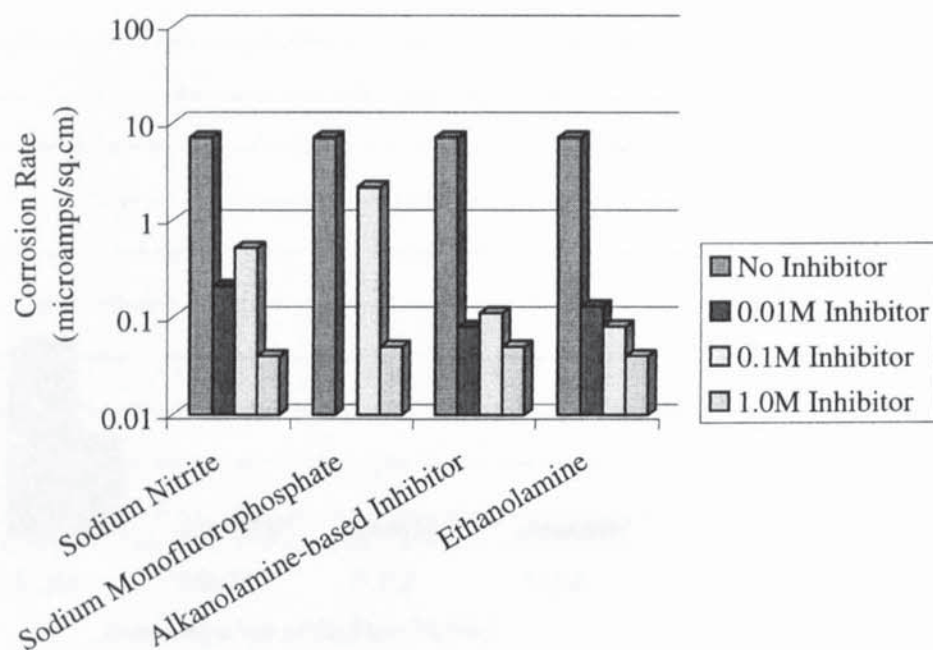


Figure 4.67 - Comparison of corrosion rates, after 42 days, for mild steel bars immersed in air-saturated aqueous solutions of 0.1M sodium hydroxide with 1.0M sodium chloride and various additions of inhibitors

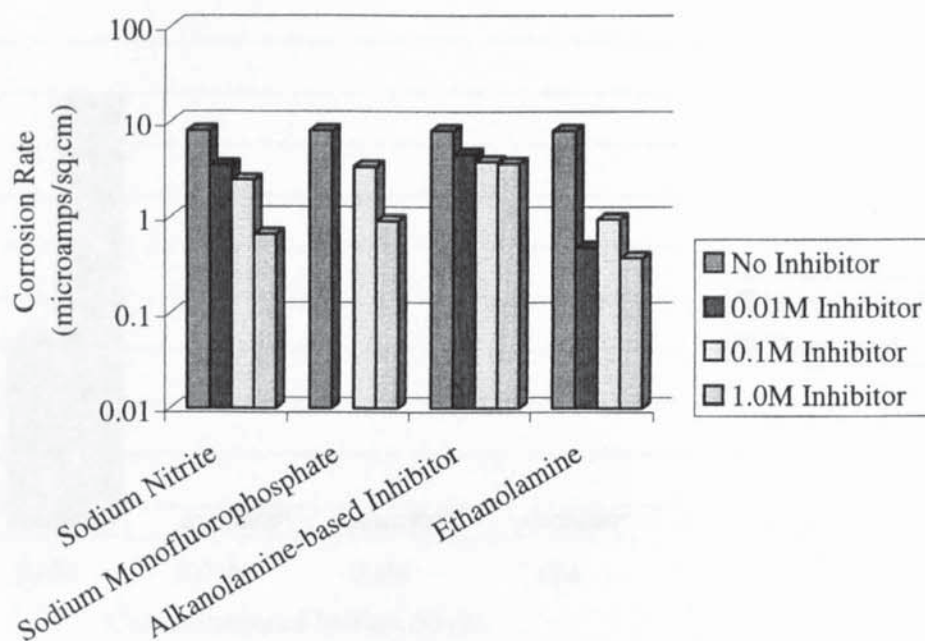


Figure 4.68 - Weight loss (experimental and theoretical) versus inhibitor concentration for mild steel bars immersed for 42 days in solutions of de-ionised water with various additions of sodium nitrite

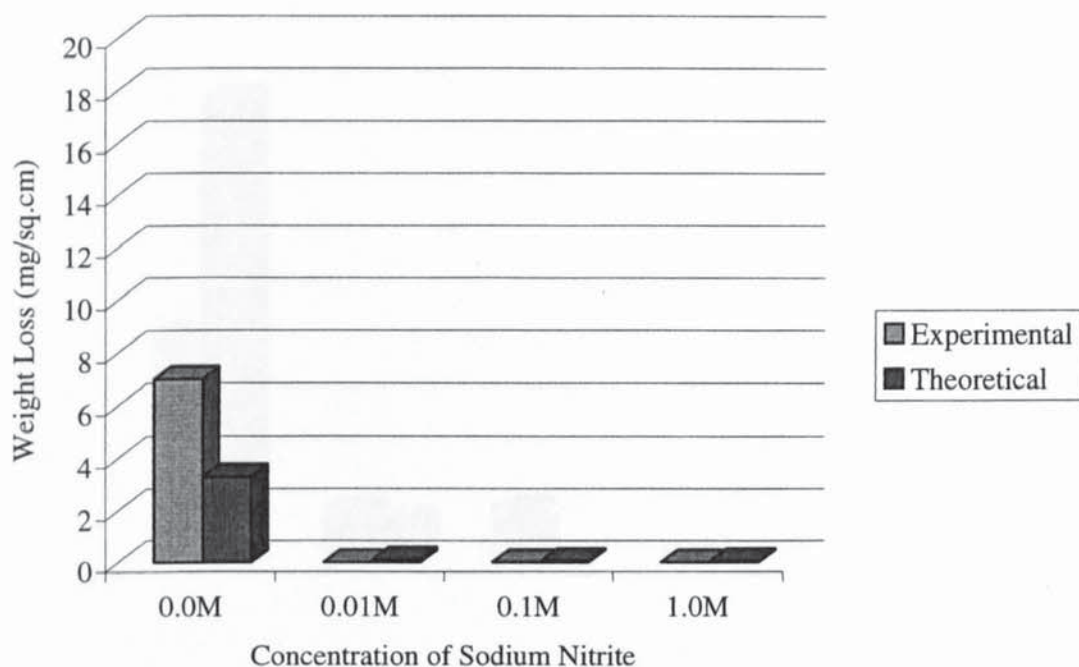


Figure 4.69 - Weight loss (experimental and theoretical) versus inhibitor concentration for mild steel bars immersed for 42 days in solutions of 0.01M sodium chloride with various additions of sodium nitrite

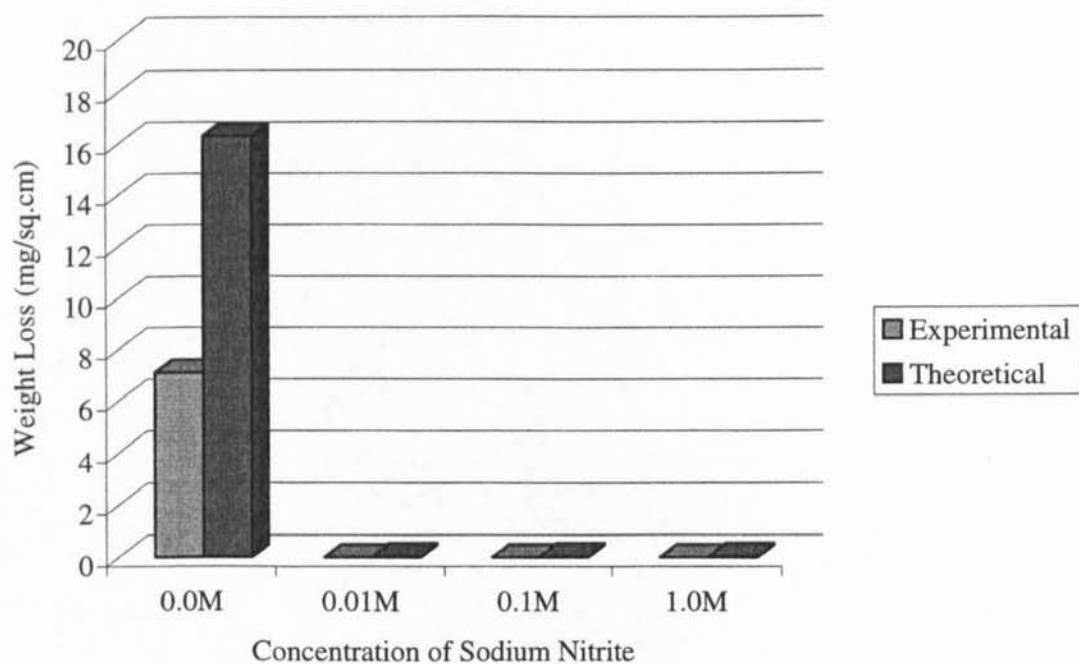




Figure 4.70 - Weight loss (experimental and theoretical) versus inhibitor concentration for mild steel bars immersed for 42 days in solutions of 0.1M sodium chloride with various additions of sodium nitrite

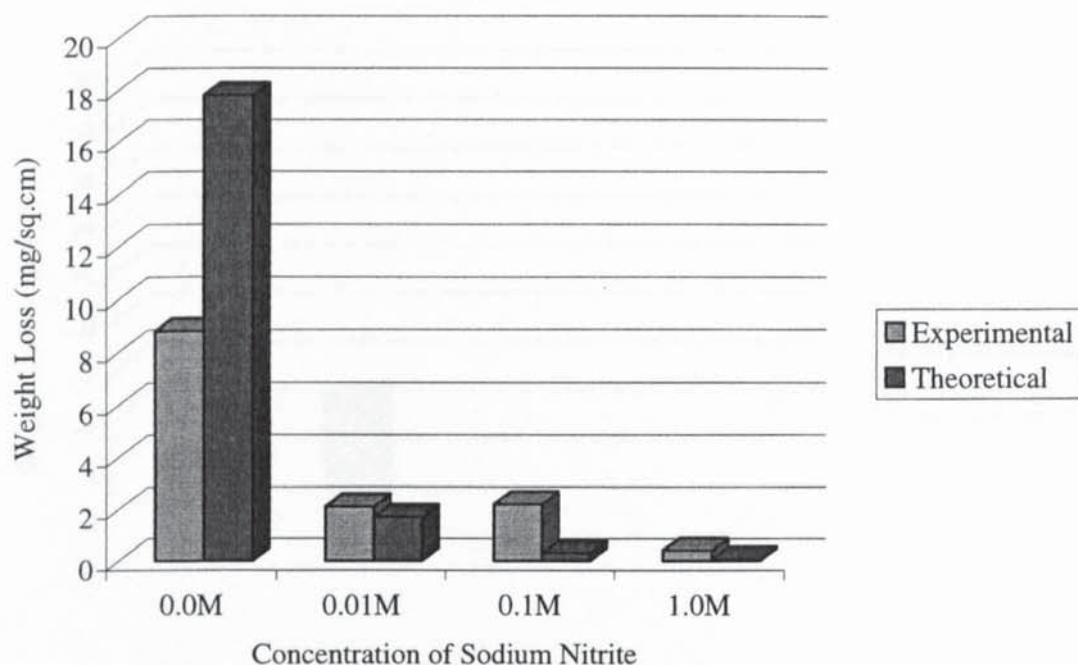


Figure 4.71 - Weight loss (experimental and theoretical) versus inhibitor concentration for mild steel bars immersed for 42 days in solutions of 0.1M sodium hydroxide with various additions of sodium nitrite

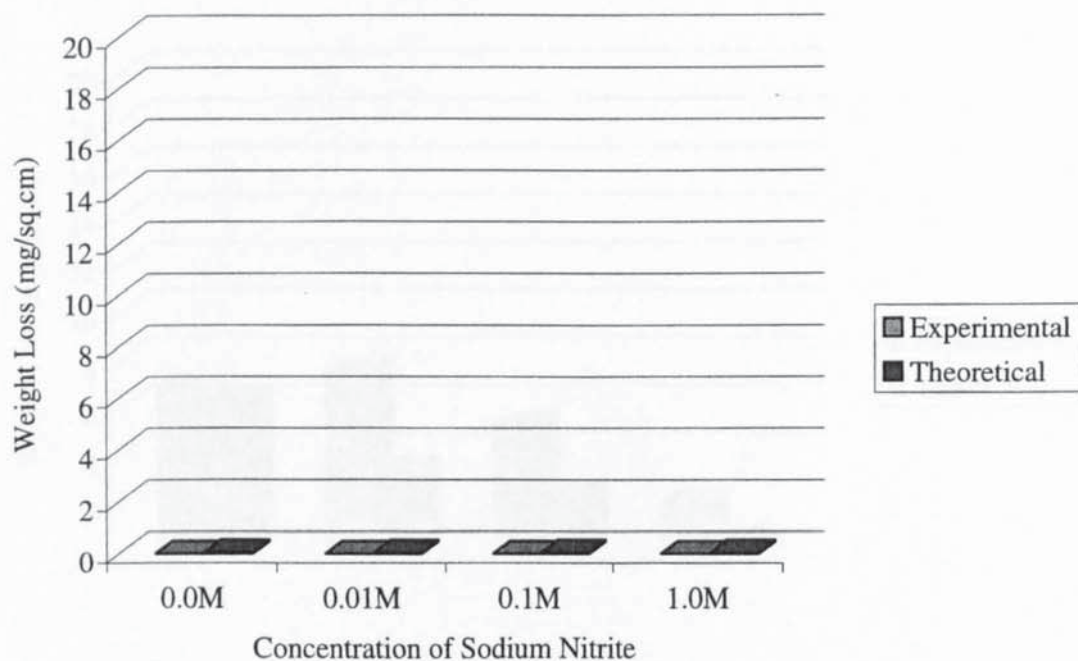


Figure 4.72 - Weight loss (experimental and theoretical) versus inhibitor concentration for mild steel bars immersed for 42 days in solutions of 0.1M sodium hydroxide with 0.1M sodium chloride and various additions of sodium nitrite

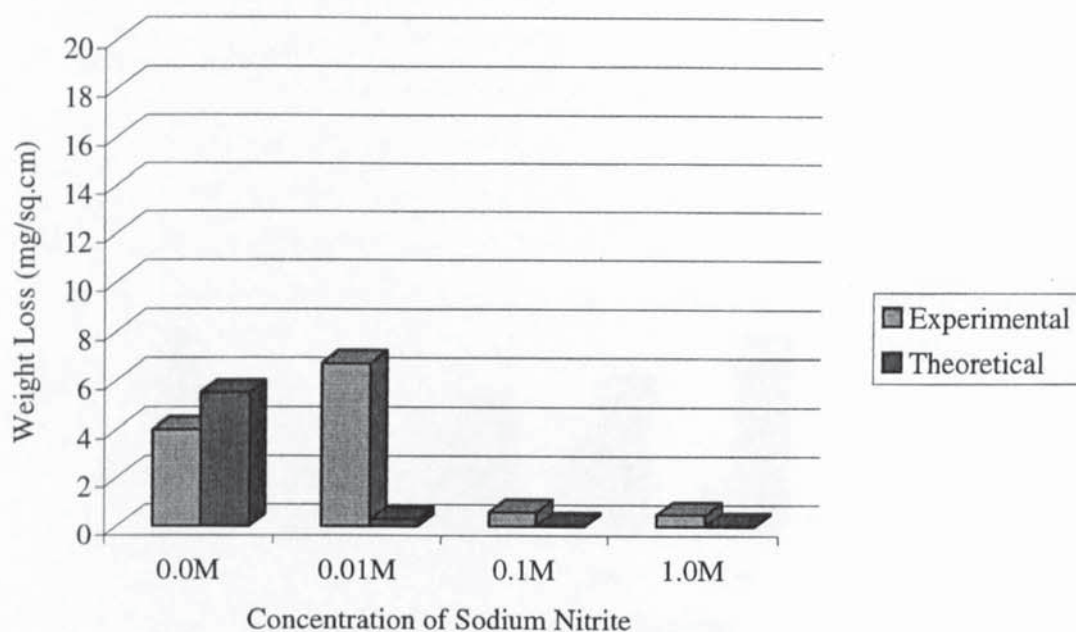


Figure 4.73 - Weight loss (experimental and theoretical) versus inhibitor concentration for mild steel bars immersed for 42 days in solutions of 0.1M sodium hydroxide with 1.0M sodium chloride and various additions of sodium nitrite

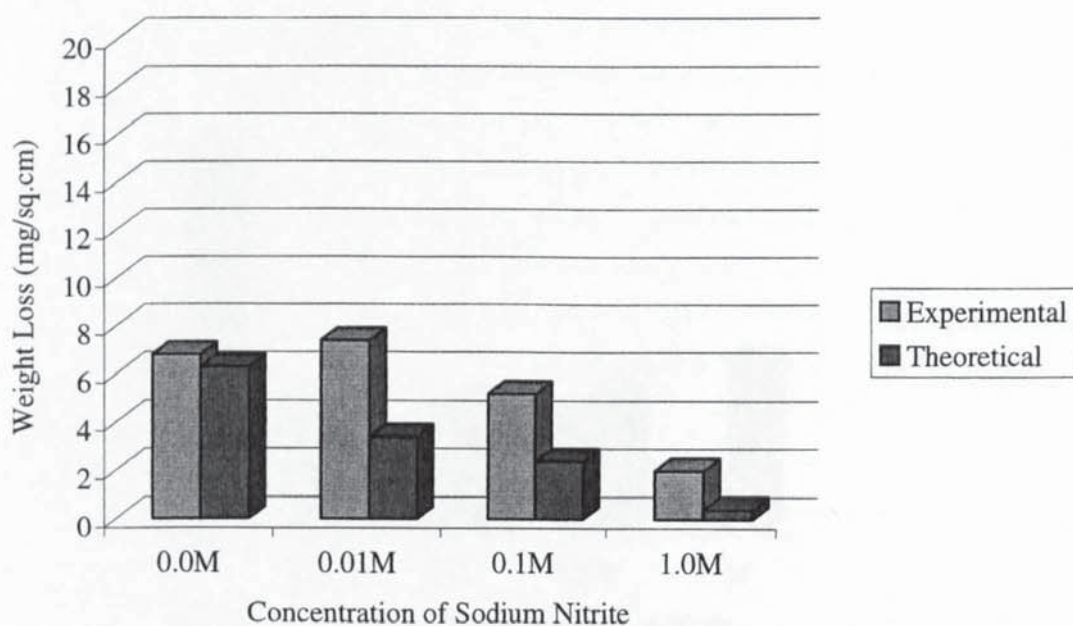


Figure 4.74 - Weight loss (experimental and theoretical) versus inhibitor concentration for mild steel bars immersed for 42 days in solutions of de-ionised water with various additions of sodium monofluorophosphate

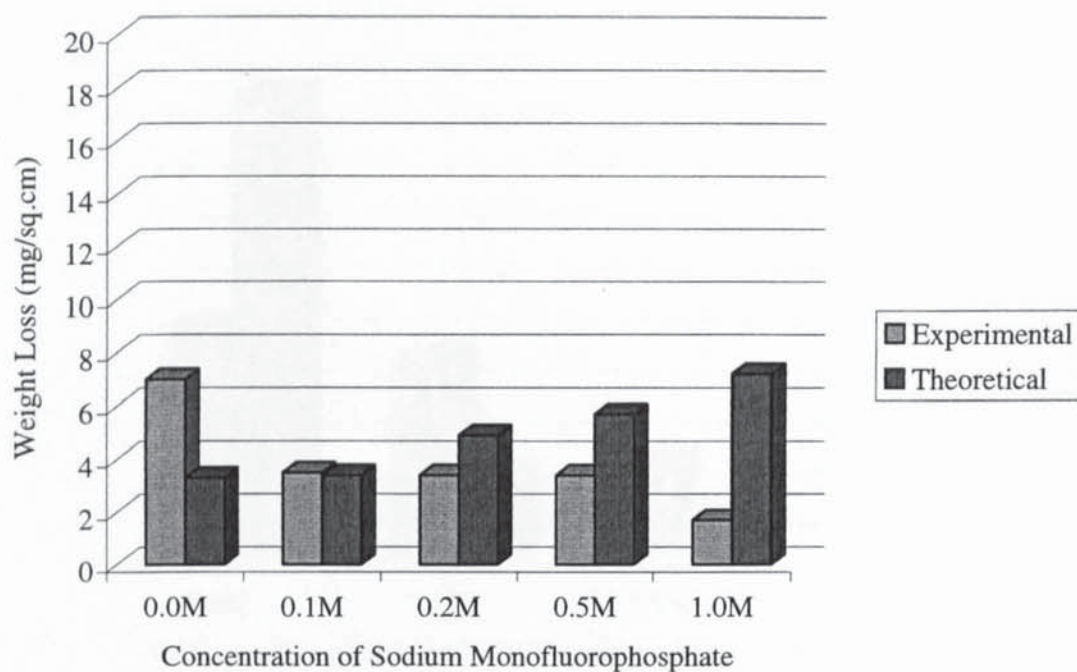


Figure 4.75 - Weight loss (experimental and theoretical) versus inhibitor concentration for mild steel bars immersed for 42 days in solutions of 0.01M sodium chloride and various additions of sodium monofluorophosphate

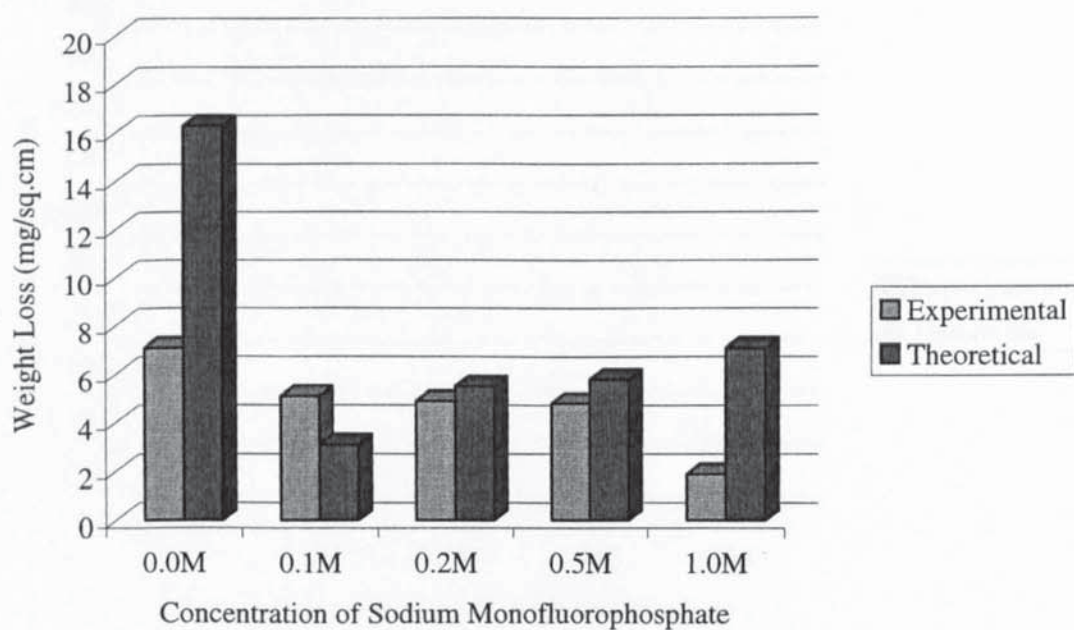




Figure 4.76 - Weight loss (experimental and theoretical) versus inhibitor concentration for mild steel bars immersed for 42 days in solutions of 0.1M sodium chloride with various additions of sodium monofluorophosphate

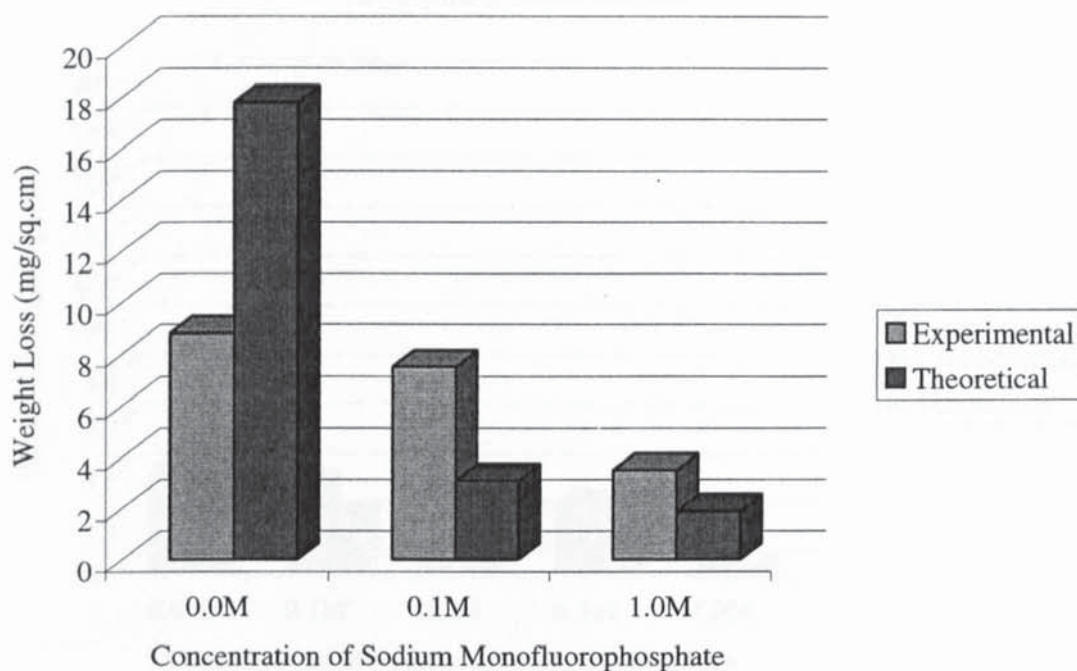


Figure 4.77 - Weight loss (experimental and theoretical) versus inhibitor concentration for mild steel bars immersed for 42 days in solutions of 0.1M sodium hydroxide with various additions of sodium monofluorophosphate

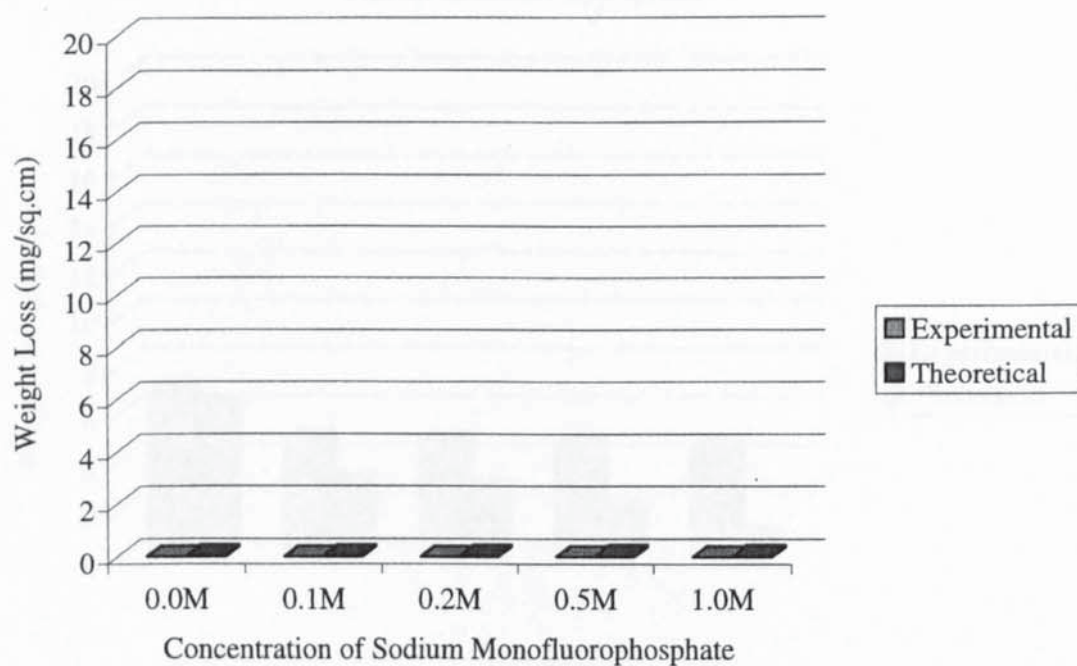


Figure 4.78 - Weight loss (experimental and theoretical) versus inhibitor concentration for mild steel bars immersed for 42 days in solutions of 0.1M sodium hydroxide with 0.1M sodium chloride and various additions of sodium monofluorophosphate

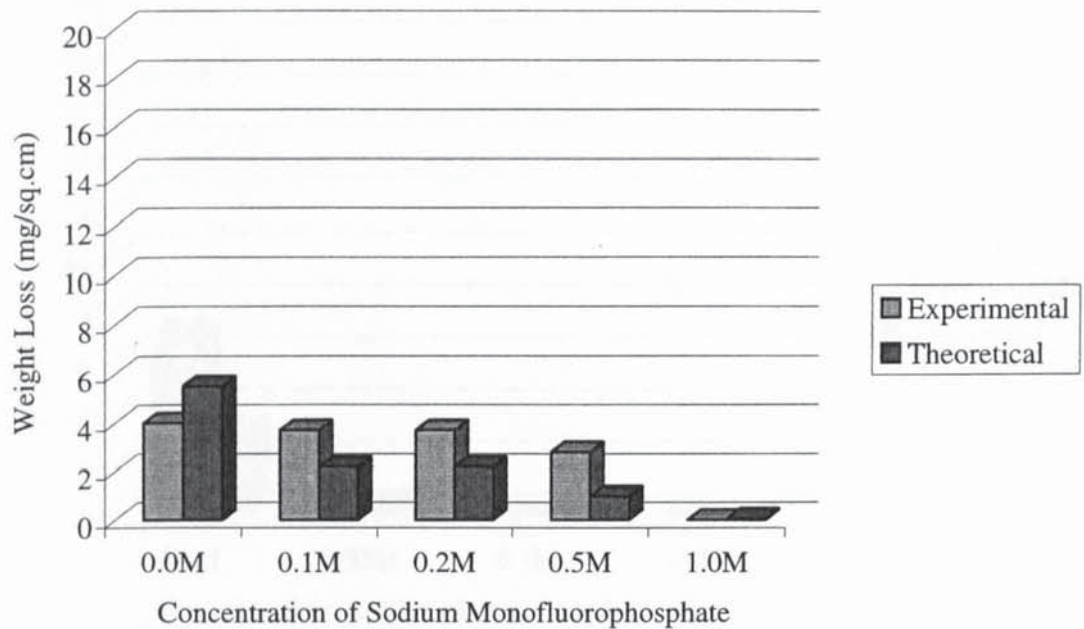


Figure 4.79 - Weight loss (experimental and theoretical) versus inhibitor concentration for mild steel bars immersed for 42 days in solutions of 0.1M sodium hydroxide with 1.0M sodium chloride and various additions of sodium monofluorophosphate

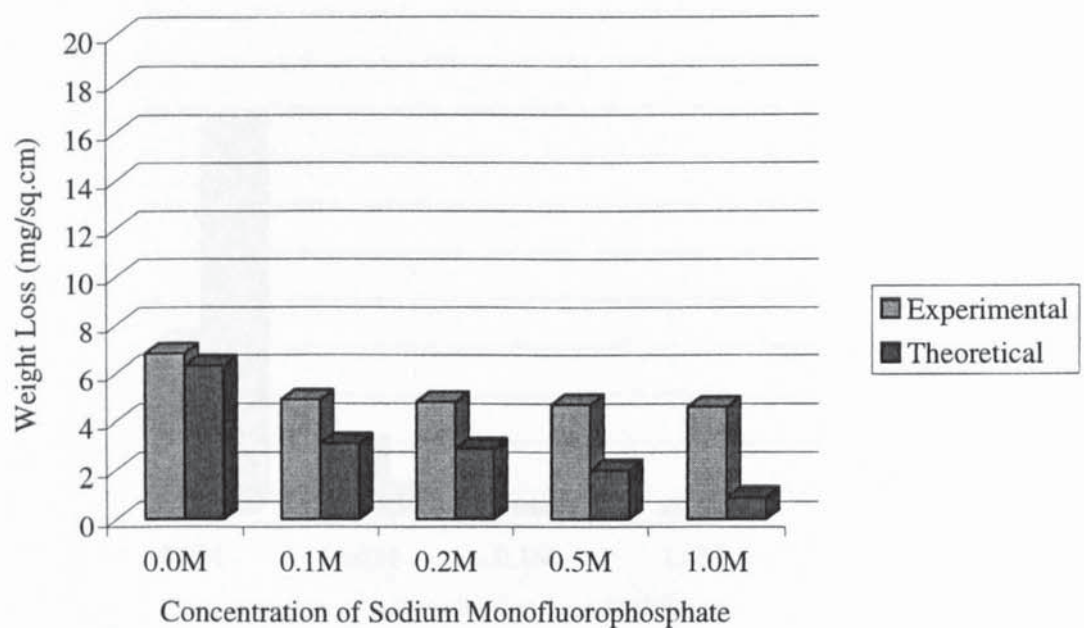


Figure 4.80 - Weight loss (experimental and theoretical) versus inhibitor concentration for mild steel bars immersed for 42 days in solutions of de-ionised water with various additions of an alkanolamine-based inhibitor

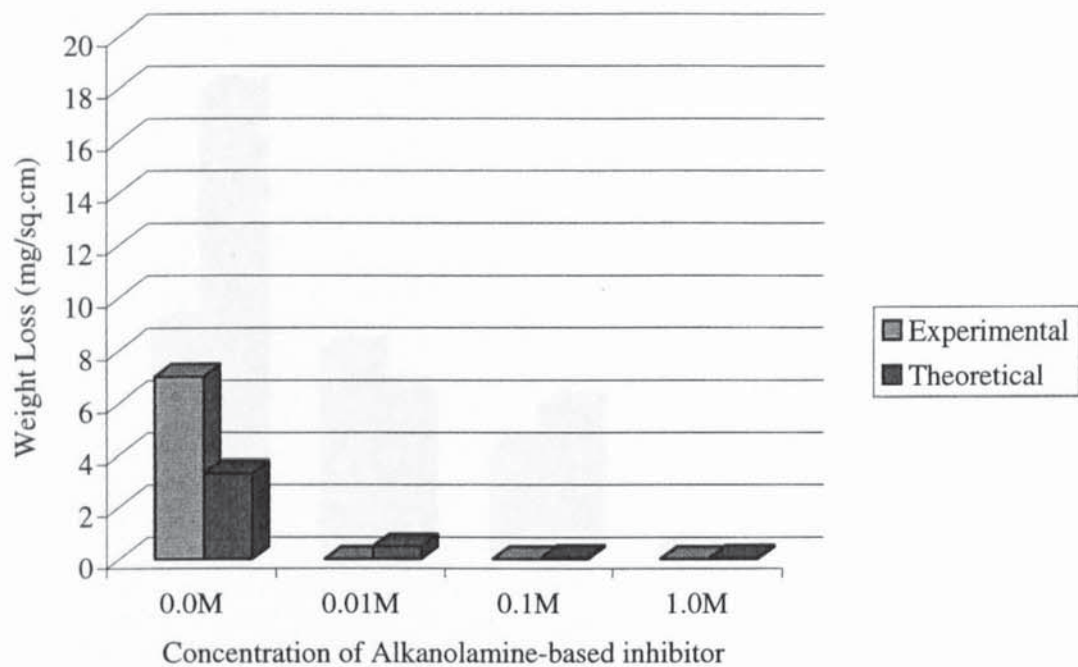


Figure 4.81 - Weight loss (experimental and theoretical) versus inhibitor concentration for mild steel bars immersed for 42 days in solutions of 0.01M sodium chloride with various additions of an alkanolamine-based inhibitor

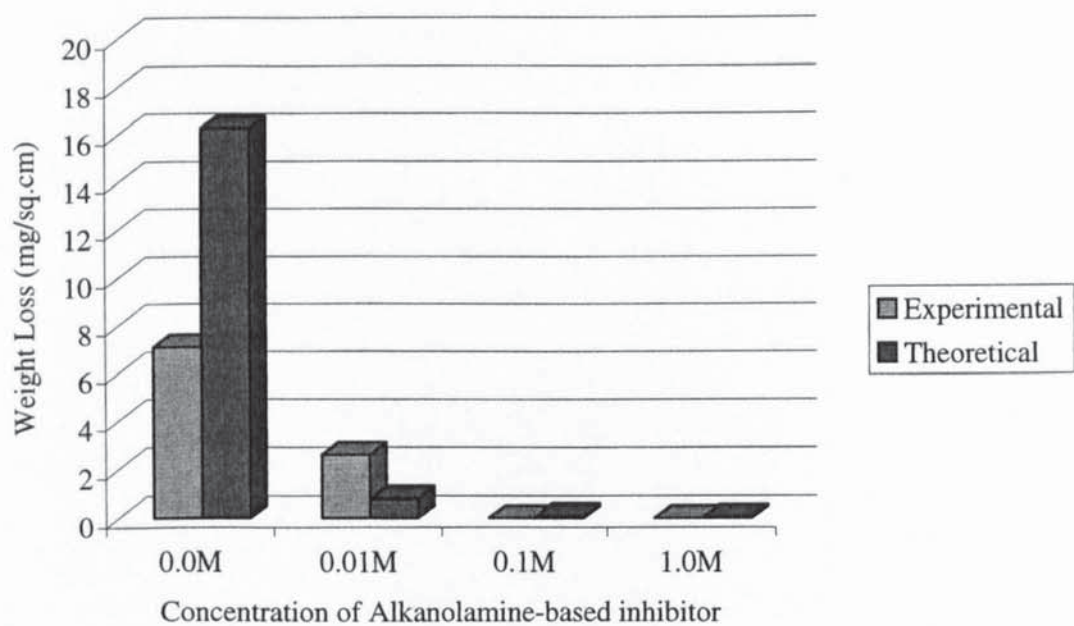




Figure 4.82 - Weight loss (experimental and theoretical) versus inhibitor concentration for mild steel bars immersed or 42 days in solutions of 0.1M sodium chloride with various additions of an alkanolamine-based inhibitor

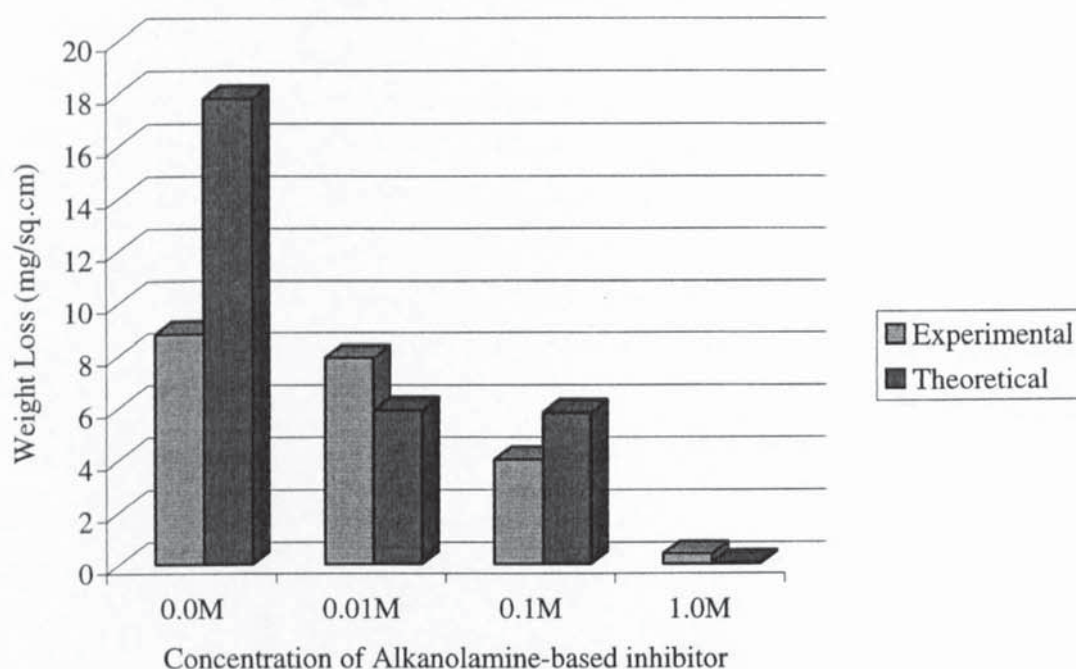


Figure 4.83 - Weight loss (experimental and theoretical) versus inhibitor concentration for mild steel bars immersed for 42 days in solutions of 0.1M sodium hydroxide with various additions of an alkanolamine-based inhibitor

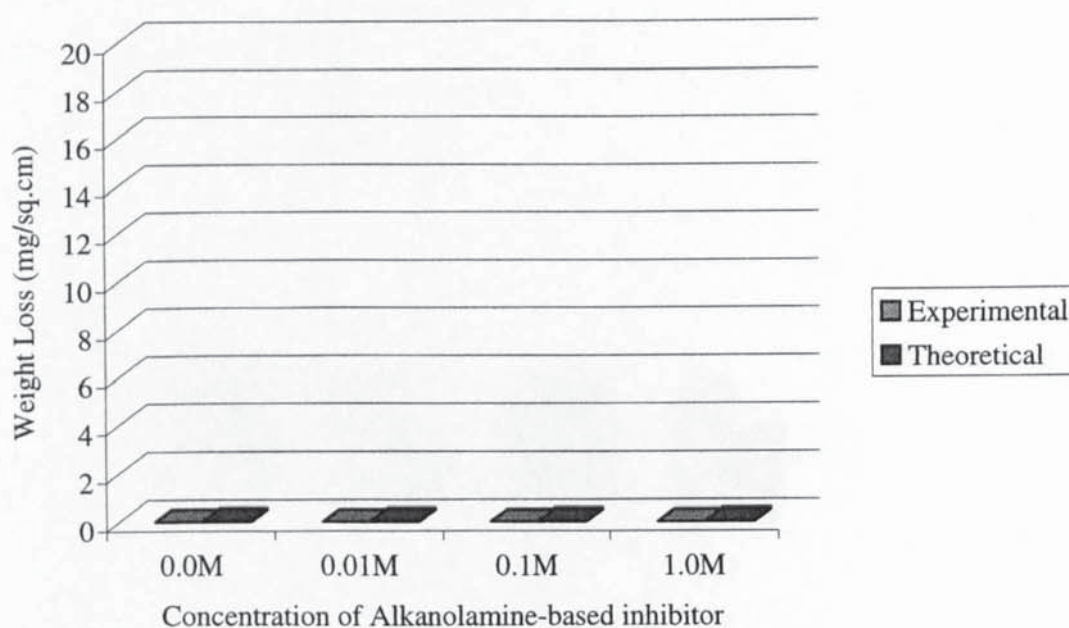


Figure 4.84 - Weight loss (experimental and theoretical) versus inhibitor concentration for mild steel bars immersed for 42 days in solutions of 0.1M sodium hydroxide with 0.1M sodium chloride and various additions of an alkanolamine-based inhibitor

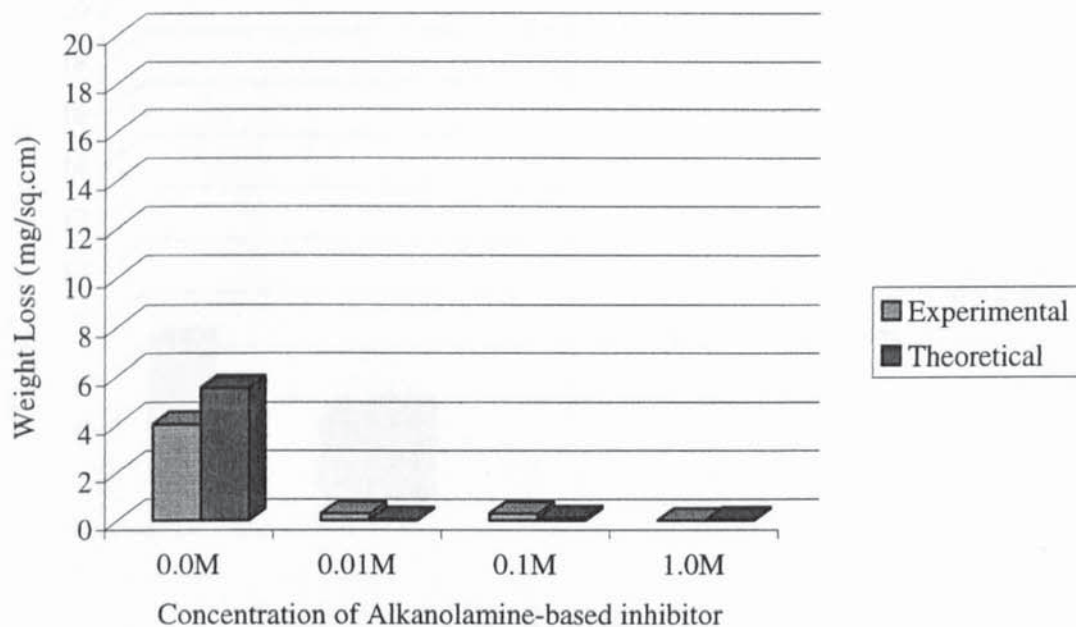


Figure 4.85 - Weight loss (experimental and theoretical) versus inhibitor concentration for mild steel bars immersed for 42 days in solutions of 0.1M sodium hydroxide with 1.0M sodium chloride and various additions of an alkanolamine-based inhibitor

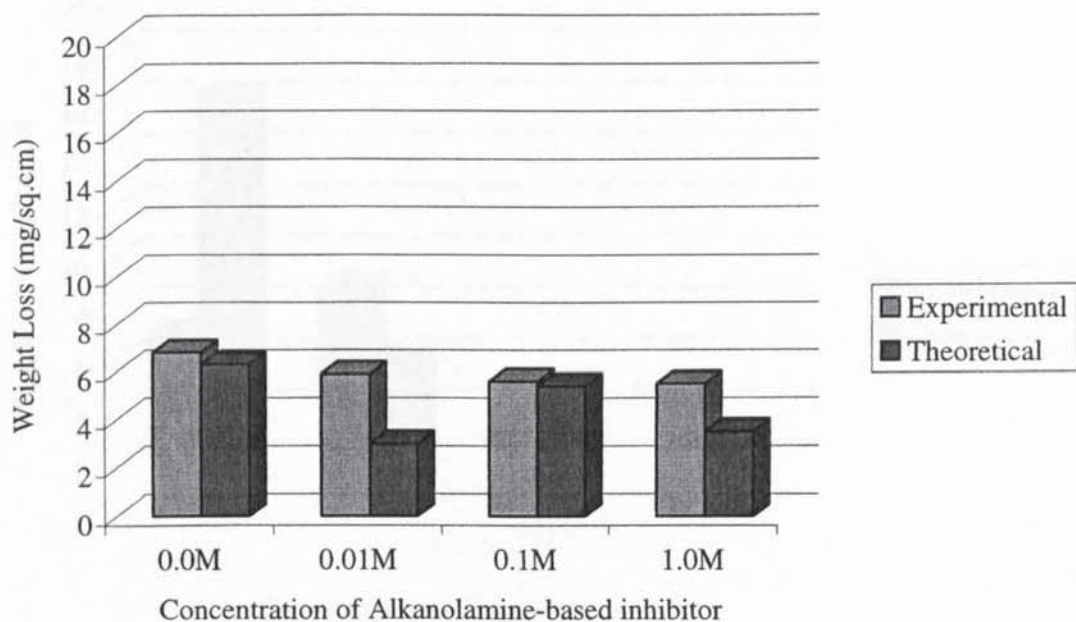


Figure 4.86 - Weight loss (experimental and theoretical) versus inhibitor concentration for mild steel bars immersed for 42 days in solutions of de-ionised water with various additions of ethanolamine

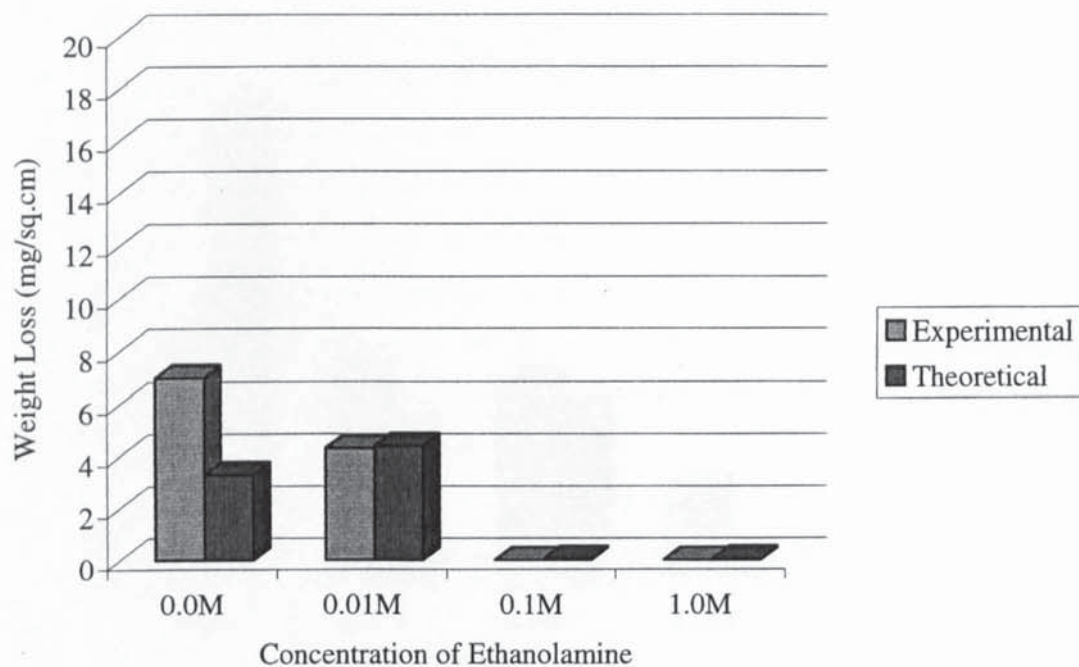


Figure 4.87 - Weight loss (experimental and theoretical) versus inhibitor concentration for mild steel bars immersed for 42 days in solutions of 0.01M sodium chloride with various additions of ethanolamine

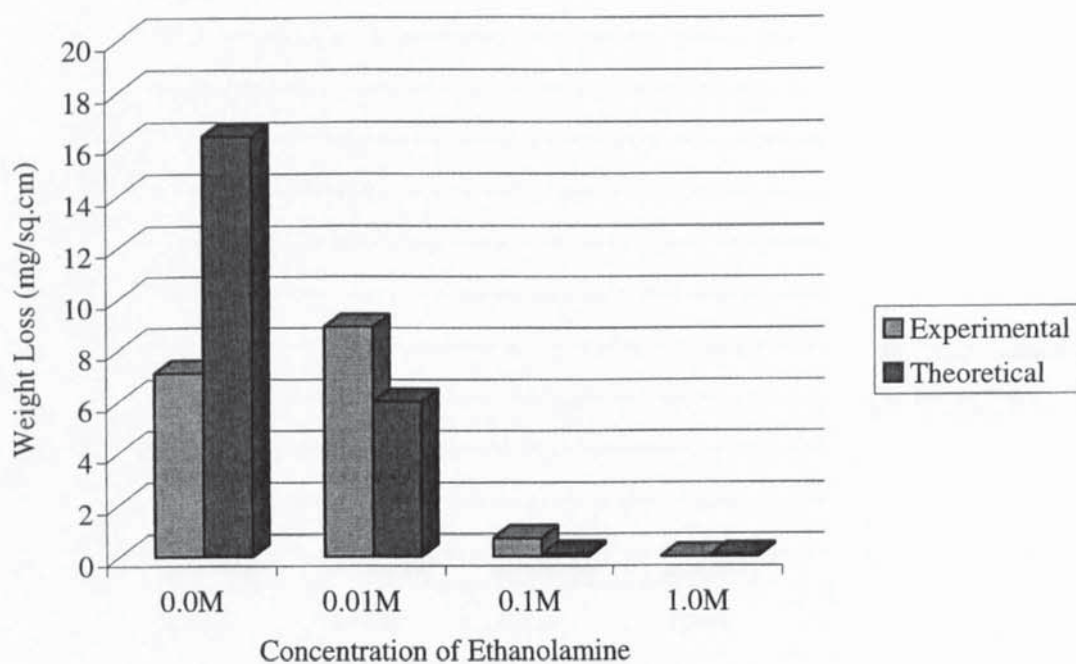




Figure 4.88 - Weight loss (experimental and theoretical) versus inhibitor concentration for mild steel bars immersed for 42 days in solutions of 0.1M sodium chloride with various additions of ethanolamine

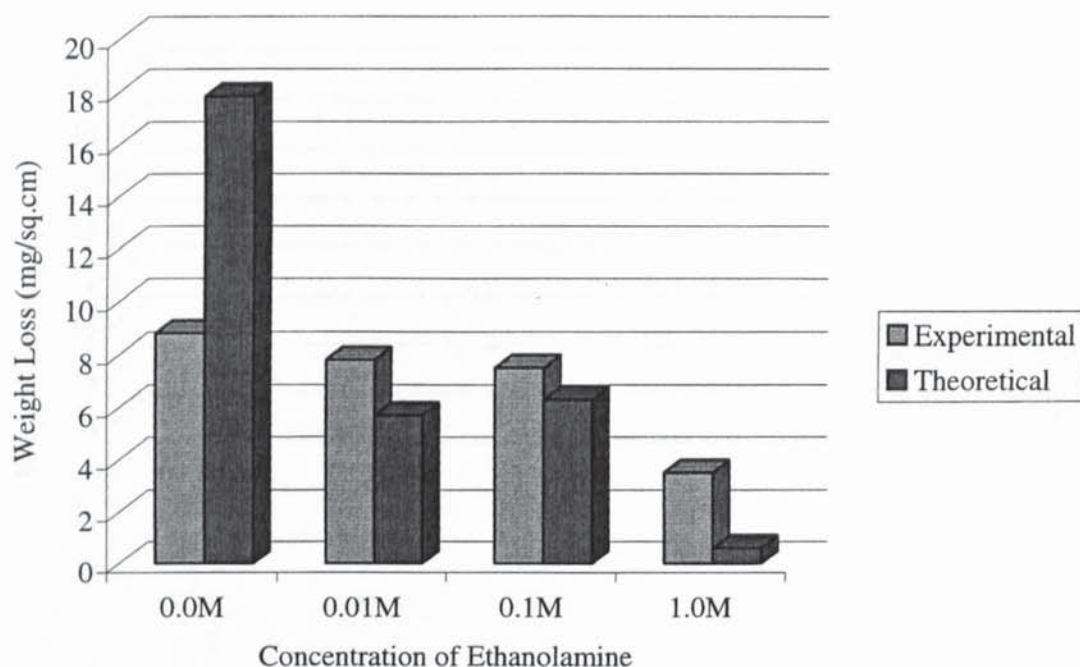


Figure 4.89 - Weight loss (experimental and theoretical) versus inhibitor concentrations for mild steel bars immersed for 42 days in solutions of 0.1M sodium hydroxide with various additions of ethanolamine

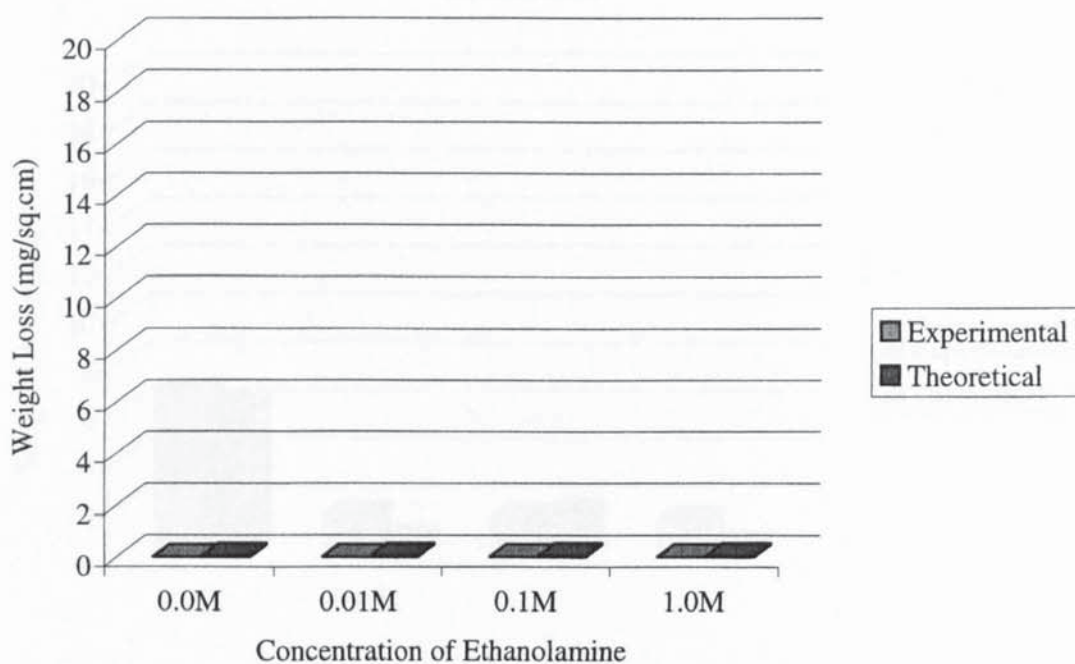


Figure 4.90 - Weight loss (experimental and theoretical) versus inhibitor concentration for mild steel bars immersed for 42 days in solutions of 0.1M sodium hydroxide with 0.1M sodium chloride and various additions of ethanolamine

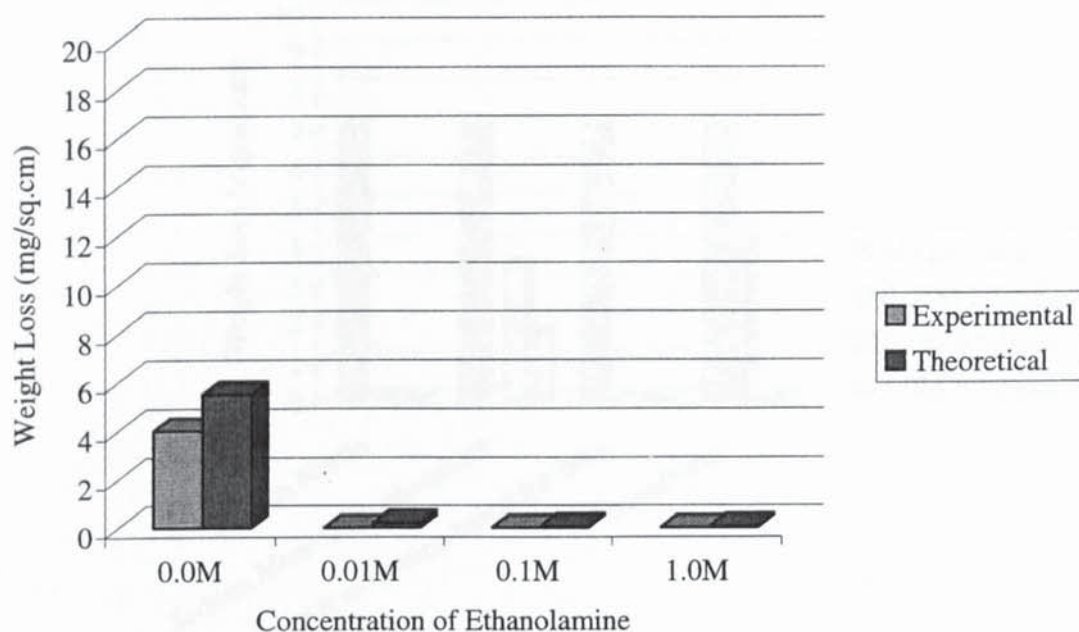


Figure 4.91 - Weight loss (experimental and theoretical) versus inhibitor concentration for mild steel bars immersed for 42 days in solutions of 0.1M sodium hydroxide with 1.0M sodium chloride and various additions of ethanolamine

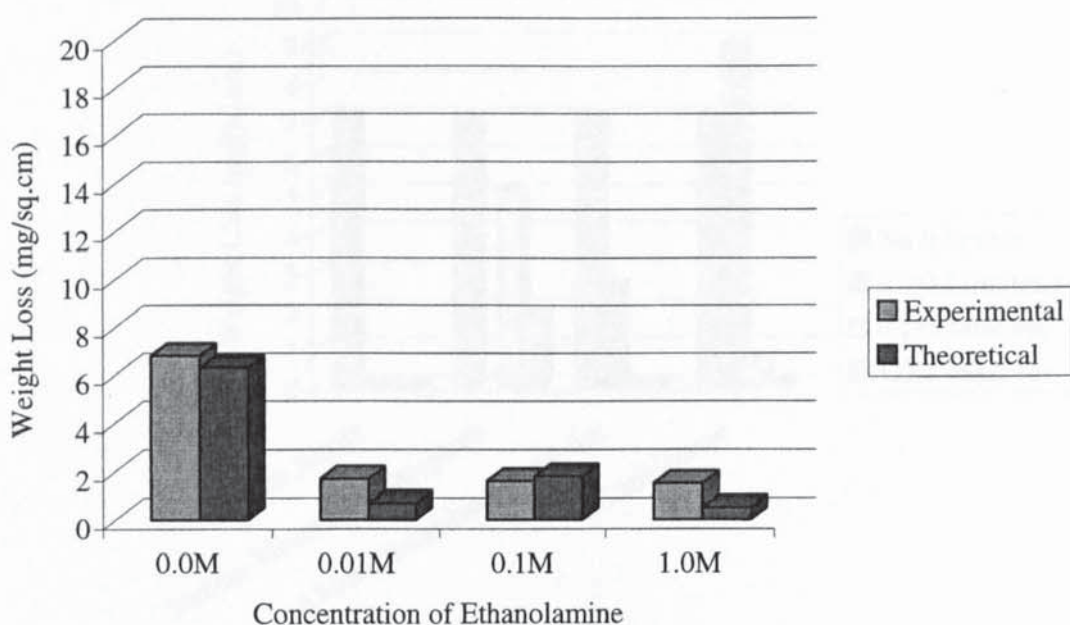


Figure 4.92 - Comparison of experimentally-determined weight loss measurements for mild steel bars immersed for 42 days in solutions of de-ionised water with various additions of inhibitors

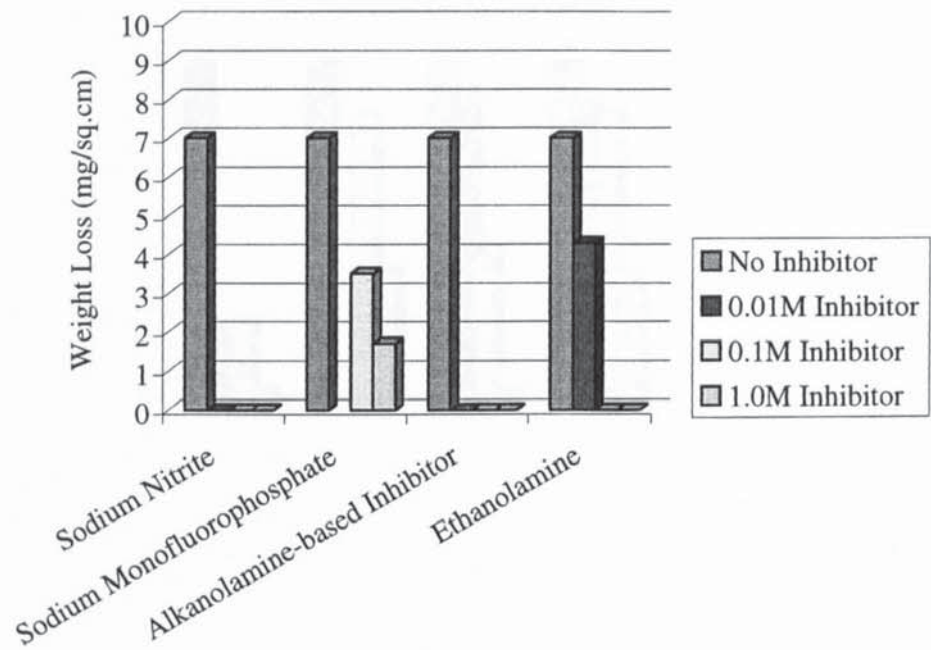


Figure 4.93 - Comparison of experimentally-determined weight loss measurements for mild steel bars immersed for 42 days in solutions of 0.01M sodium chloride with various additions of inhibitors

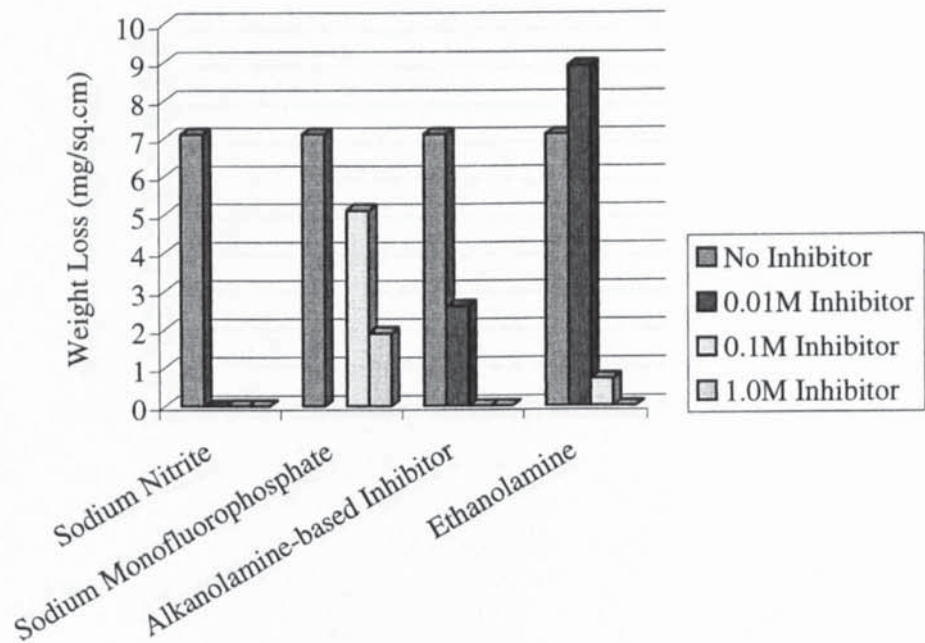




Figure 4.94 - Comparison of experimentally-determined weight loss measurements for mild steel bars immersed for 42 days in solutions of 0.1M sodium chloride with various additions of inhibitors

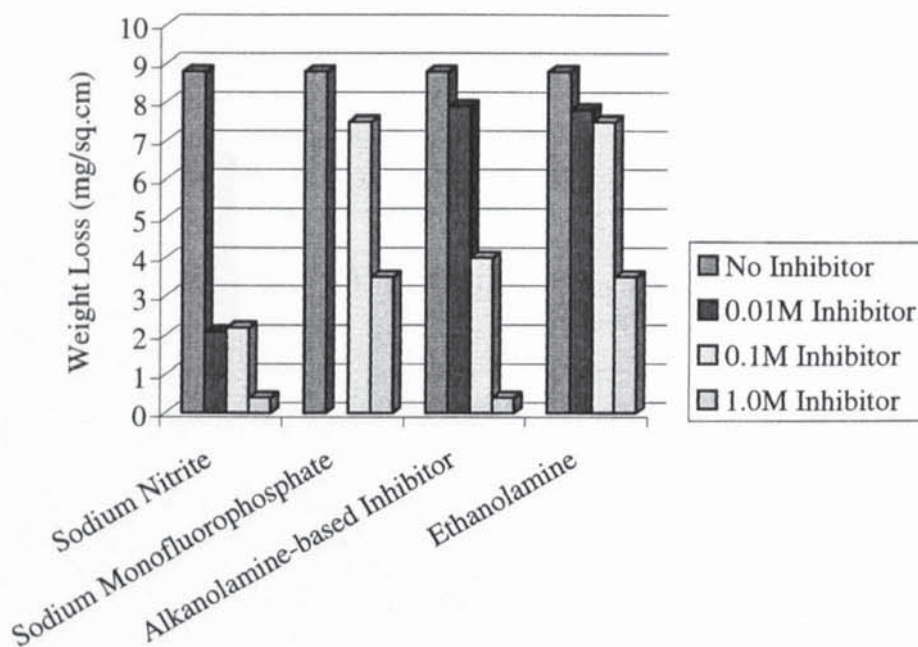


Figure 4.95 - Comparison of experimentally-determined weight loss measurements for mild steel bars immersed for 42 days in solutions of 0.1M sodium hydroxide with various additions of inhibitors

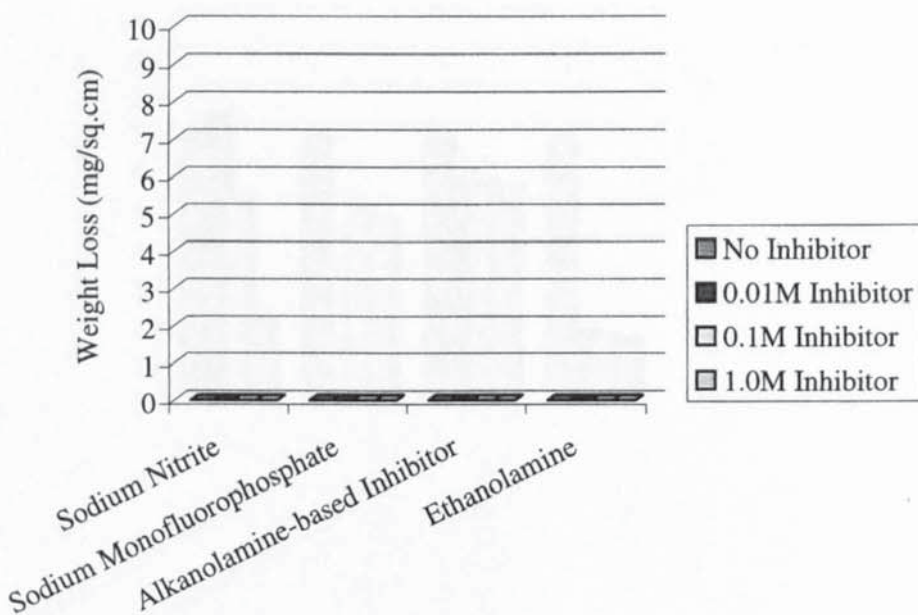


Figure 4.96 - Comparison of experimentally-determined weight loss measurements for mild steel bars immersed in solutions of 0.1M sodium hydroxide with 0.1M sodium chloride and various additions of inhibitors

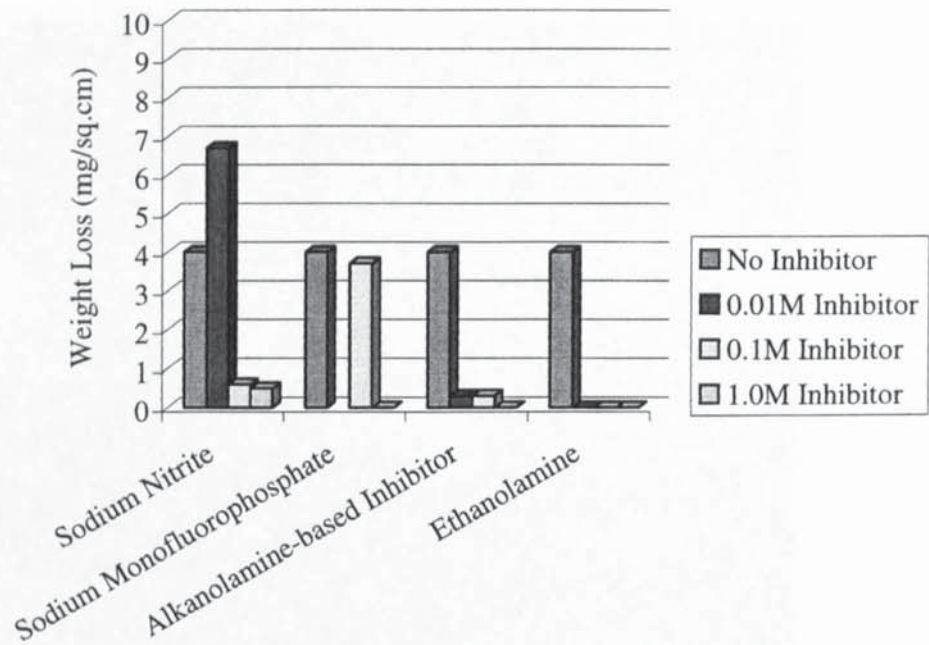


Figure 4.97 - Comparison of experimentally-determined weight loss measurements for mild steel bars immersed in solutions of 0.1M sodium hydroxide with 1.0M sodium chloride and various additions of inhibitors

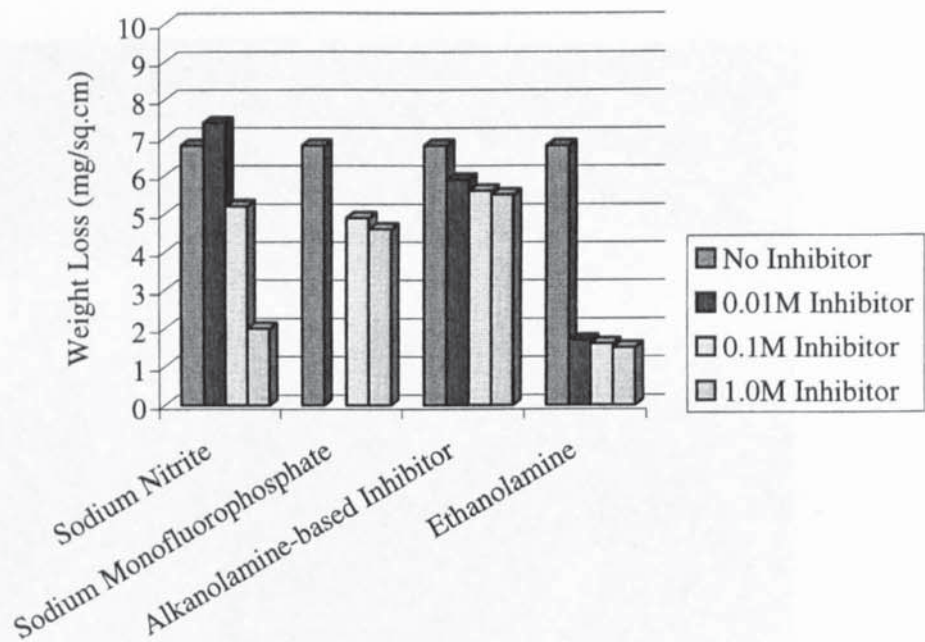




Figure 4.98 – Bar, after removal of corrosion products, following immersion in de-ionised water (scale: bar diameter = 6mm)

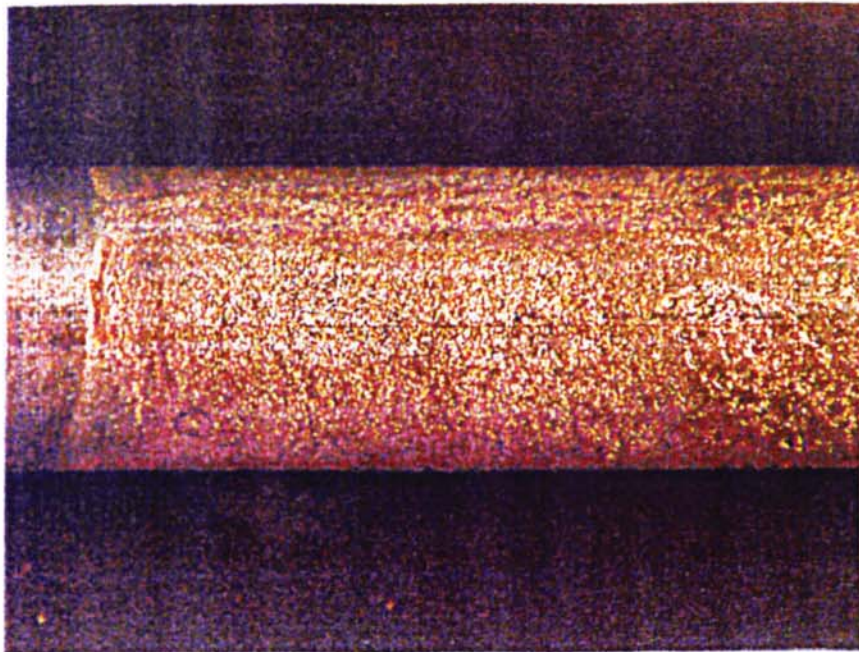


Figure 4.99 – Bar, after removal of corrosion products, following immersion in 0.01M sodium chloride (scale: bar diameter = 6mm)

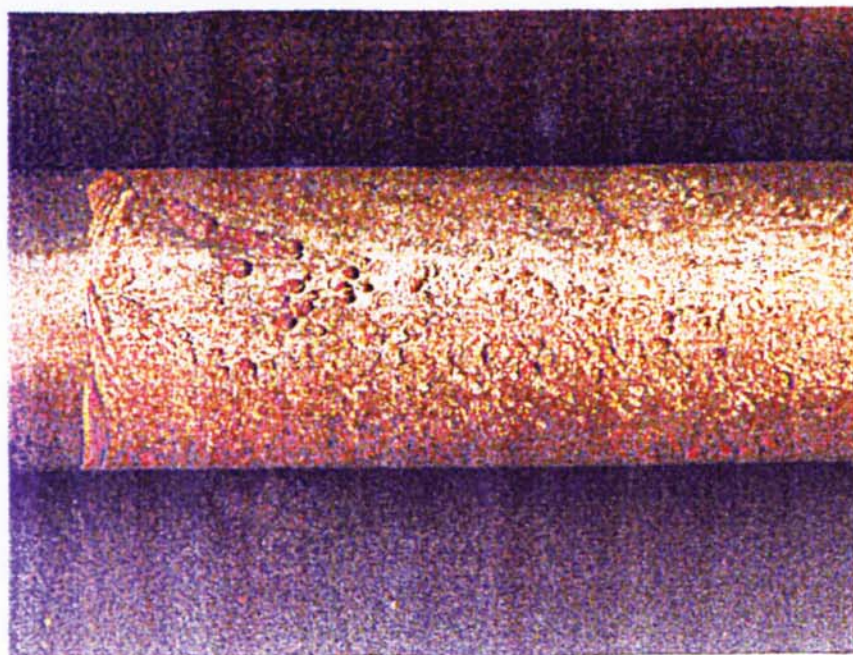




Figure 4.100 – Bar, after removal of corrosion products, following immersion in 0.1M sodium chloride (scale: bar diameter = 6mm)

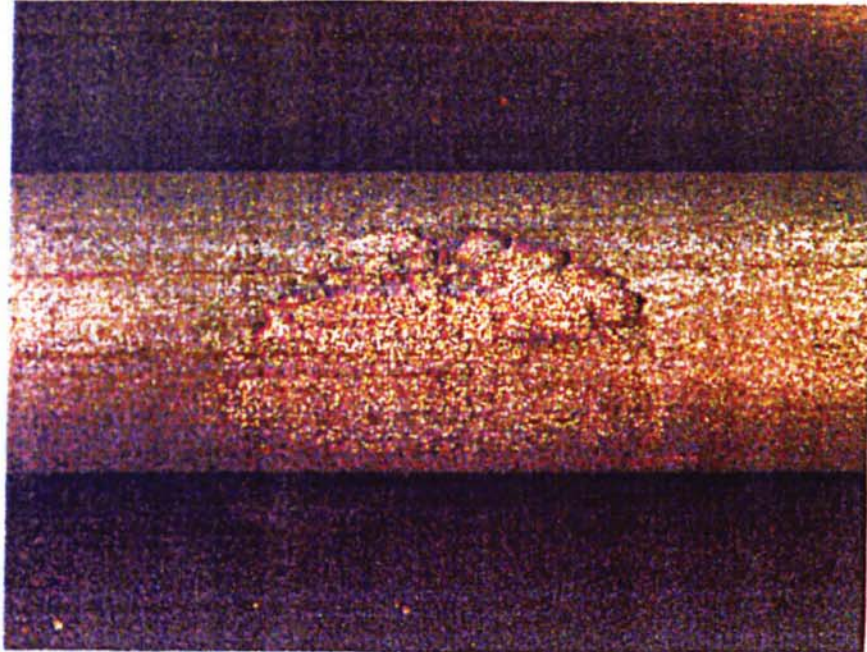


Figure 4.101 – Typical pit on bar, after removal of corrosion products, following immersion in 0.1M sodium hydroxide with 1.0M sodium chloride (scale: bar diameter = 6mm)

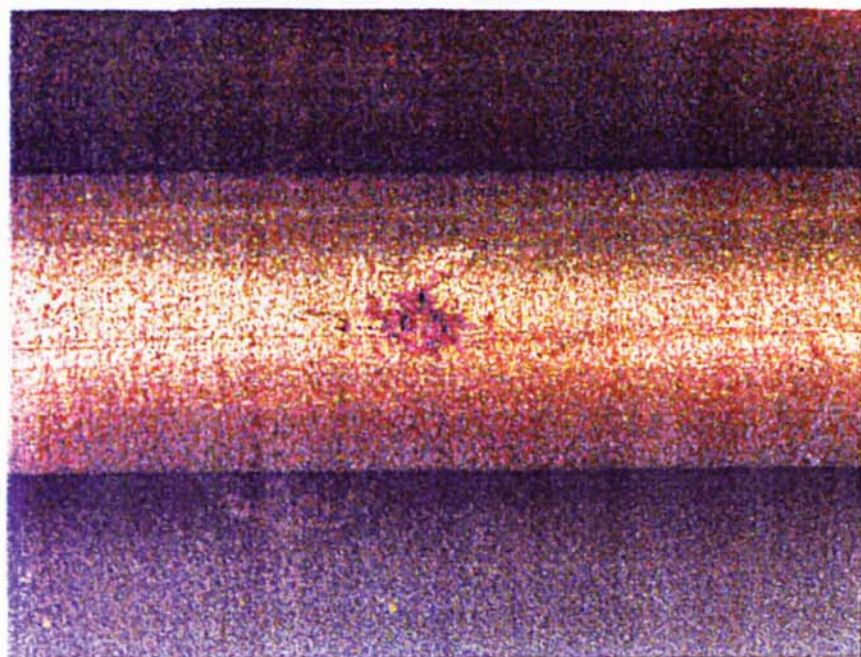




Figure 4.102 – Bar, after removal of corrosion products, following immersion in 0.1M sodium hydroxide with 0.1M sodium chloride and 0.01M sodium nitrite (scale: bar diameter = 6mm)

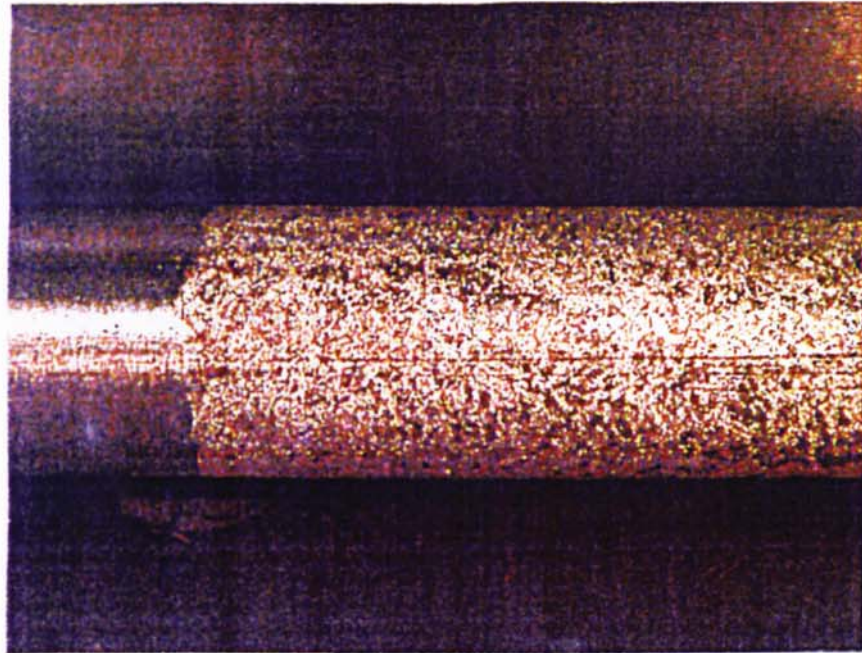


Figure 4.103 – Bar, after removal of corrosion products, following immersion in 0.1M sodium hydroxide with 0.1M sodium chloride and 0.1M sodium nitrite (scale: bar diameter = 6mm)

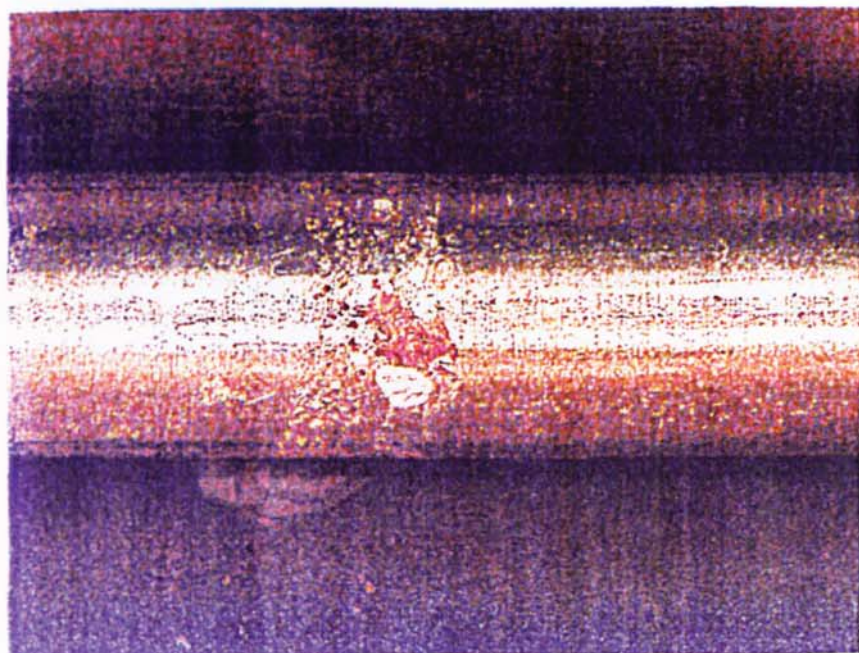




Figure 4.104 – Bar, after removal of corrosion products, following immersion in 0.1M sodium hydroxide with 1.0M sodium chloride and 0.01M sodium nitrite (scale: bar diameter = 6mm)

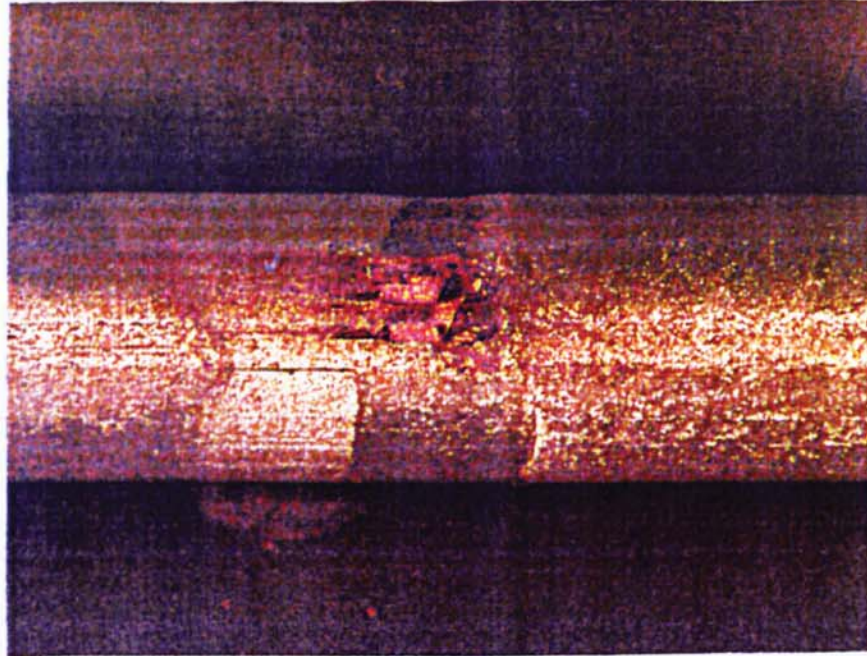


Figure 4.105 – Bar, after removal of corrosion products, following immersion in 0.1M sodium hydroxide with 1.0M sodium chloride and 0.1M sodium nitrite (scale: bar diameter = 6mm)

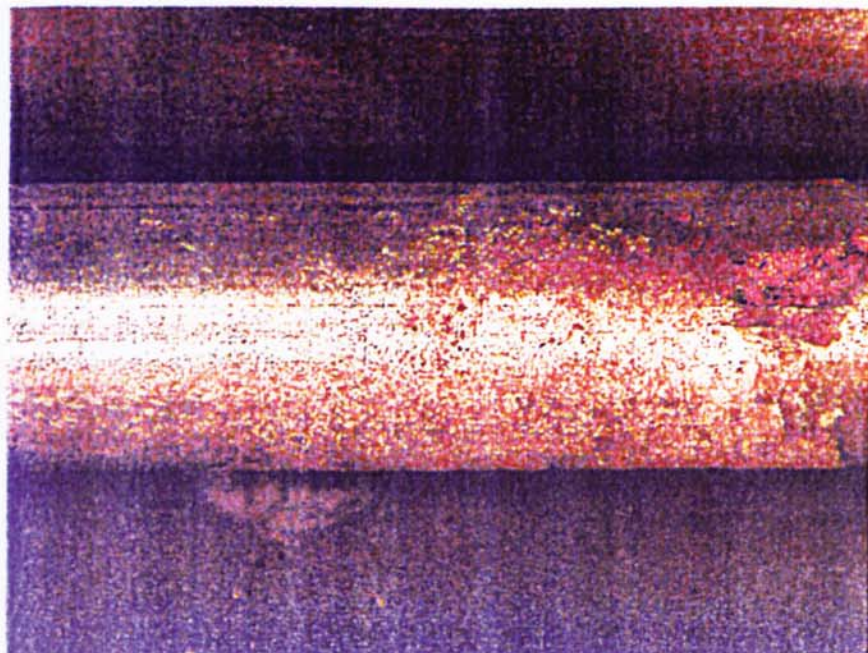




Figure 4.106 – Bar, after removal of corrosion products, following immersion in 0.01M sodium chloride with 0.1M sodium monofluorophosphate (scale: bar diameter = 6mm)

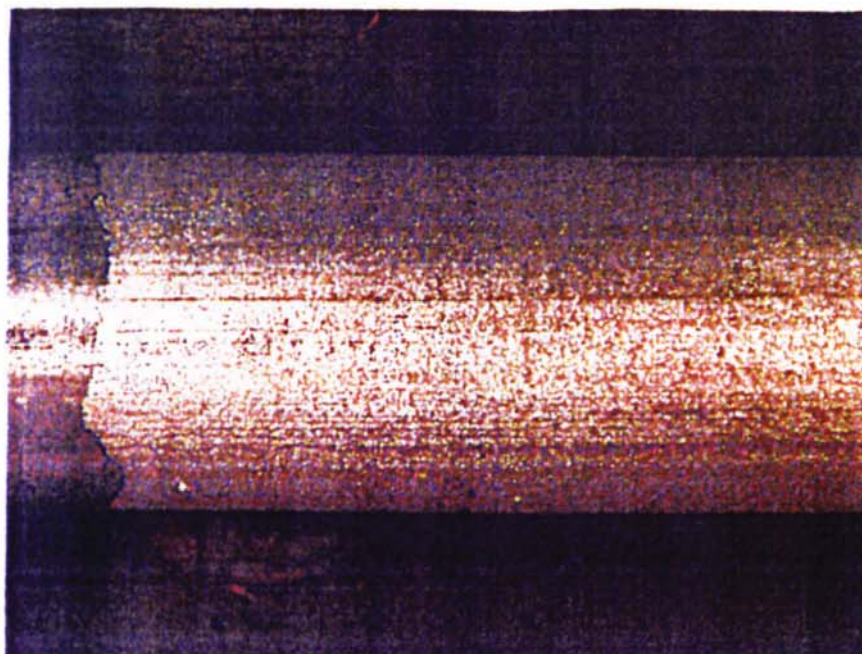


Figure 4.107 – Bar, after removal of corrosion products, following immersion in 0.1M sodium chloride with 1.0M sodium monofluorophosphate (scale: bar diameter = 6mm)

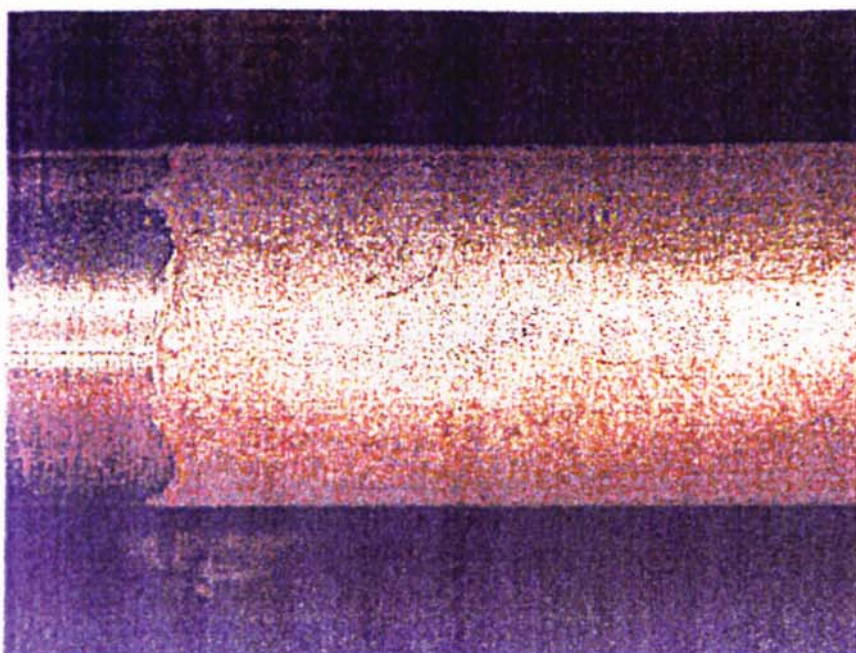




Figure 4.108 – Bar, after removal of corrosion products, following immersion in 0.1M sodium hydroxide with 0.1M sodium chloride and 0.1M sodium monofluorophosphate (scale: bar diameter = 6mm)

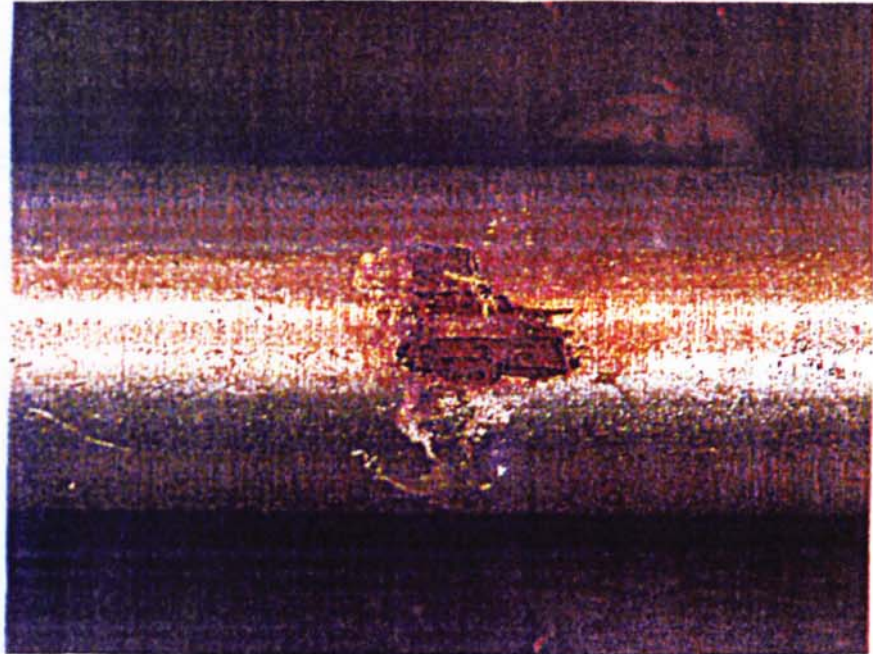


Figure 4.109 – Bar, after removal of corrosion products, following immersion in 0.1M sodium hydroxide with 1.0M sodium chloride and 0.1M sodium monofluorophosphate (scale: bar diameter = 6mm)

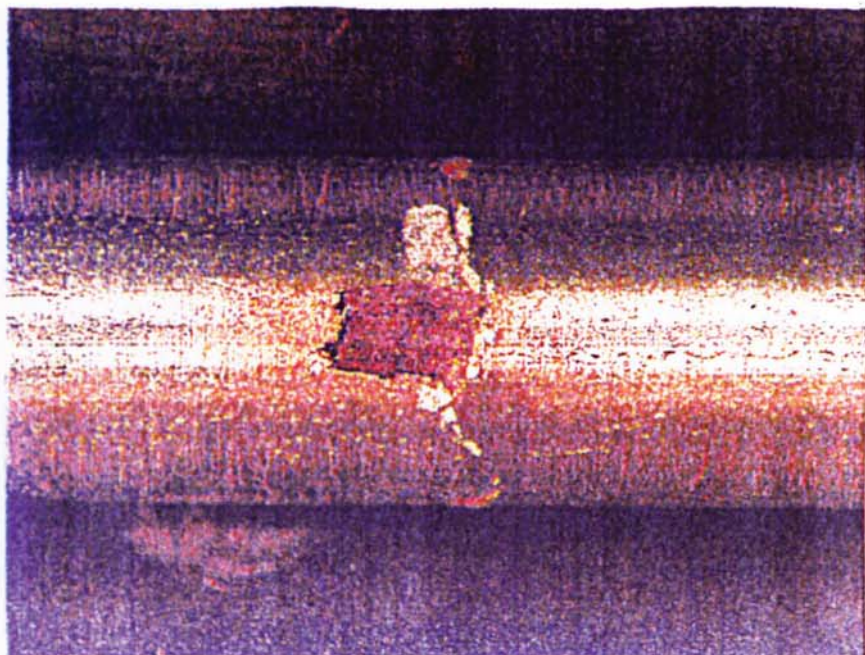




Figure 4.110 – Bar, after removal of corrosion products, following immersion in 0.01M sodium chloride with 0.01M alkanolamine-based inhibitor (scale: bar diameter = 6mm)

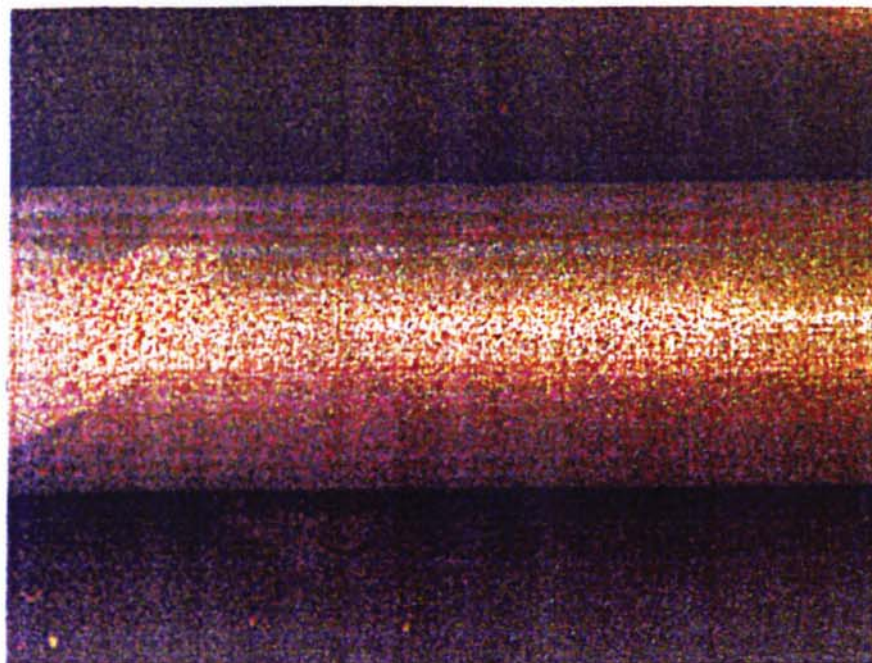


Figure 4.111 – Bar, after removal of corrosion products, following immersion in 0.1M sodium chloride with 0.01M alkanolamine-based inhibitor (scale: bar diameter = 6mm)

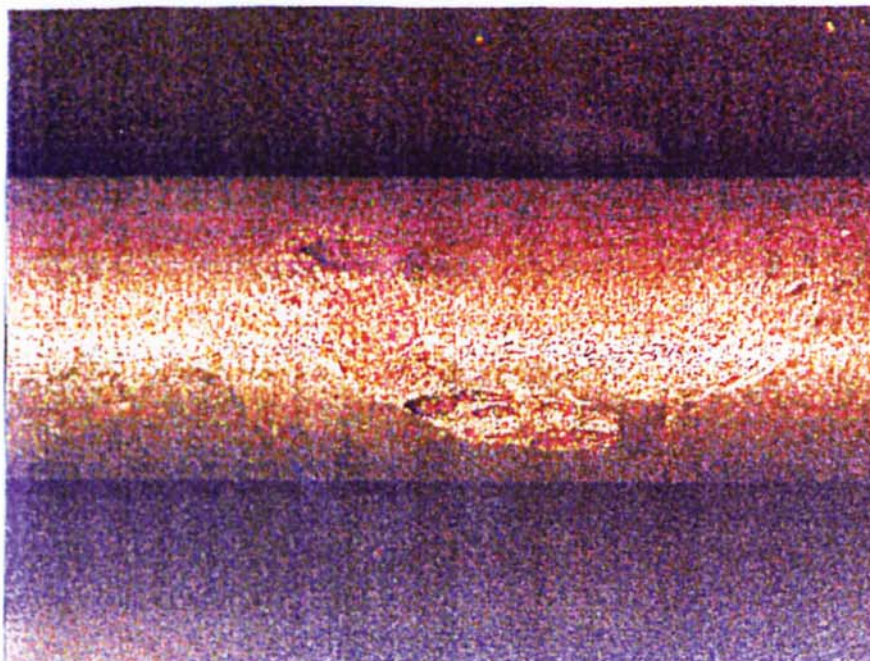




Figure 4.112 – Bar, after removal of corrosion products, following immersion in 0.1M sodium chloride with 0.1M alkanolamine-based inhibitor (scale: bar diameter = 6mm)

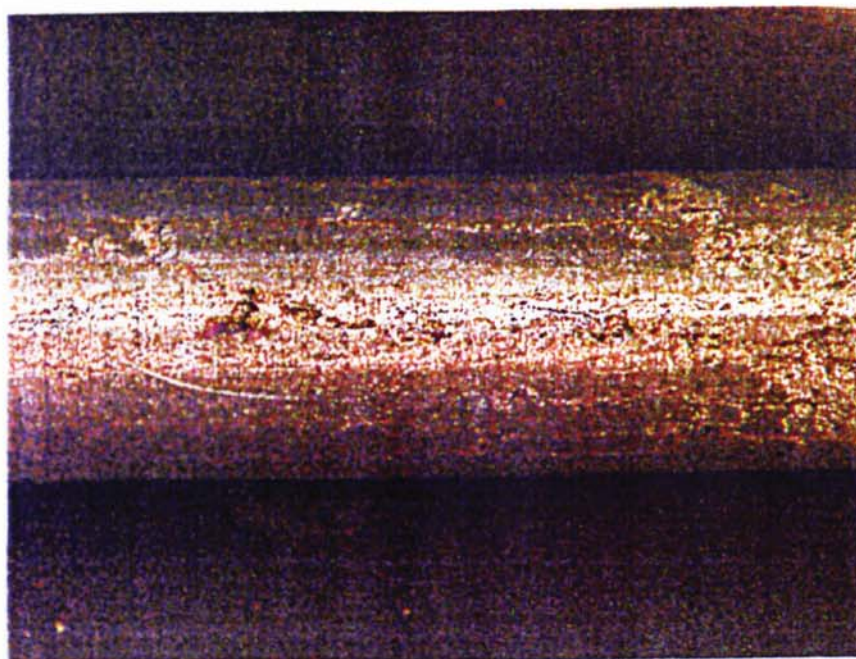


Figure 4.113 – Bar, after removal of corrosion products, following immersion in 0.1M sodium chloride with 1.0M alkanolamine-based inhibitor (scale: bar diameter = 6mm)

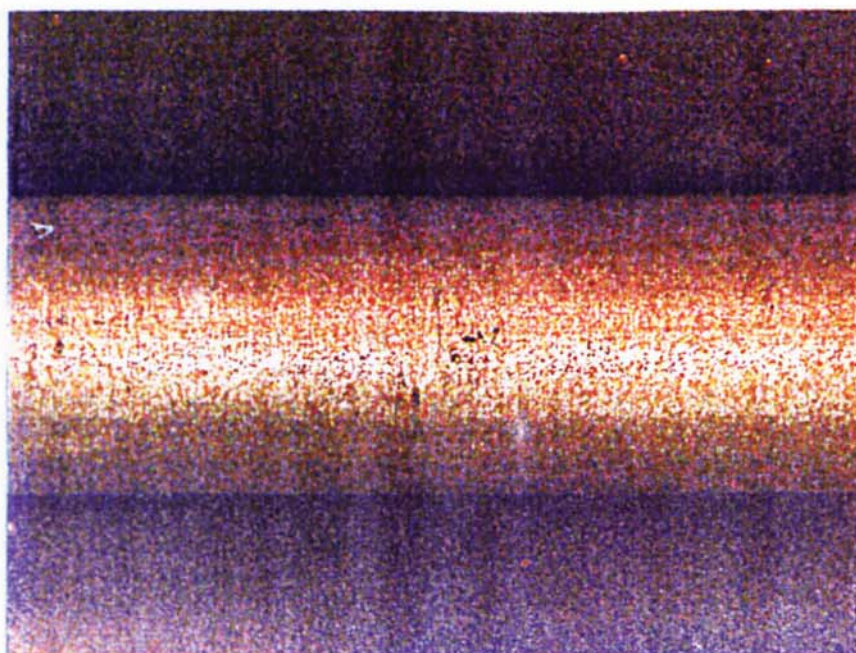




Figure 4.114 – Bar, after removal of corrosion products, following immersion in 0.1M sodium hydroxide with 1.0M sodium chloride and 0.01M alkanolamine-based inhibitor (scale: bar diameter = 6mm)

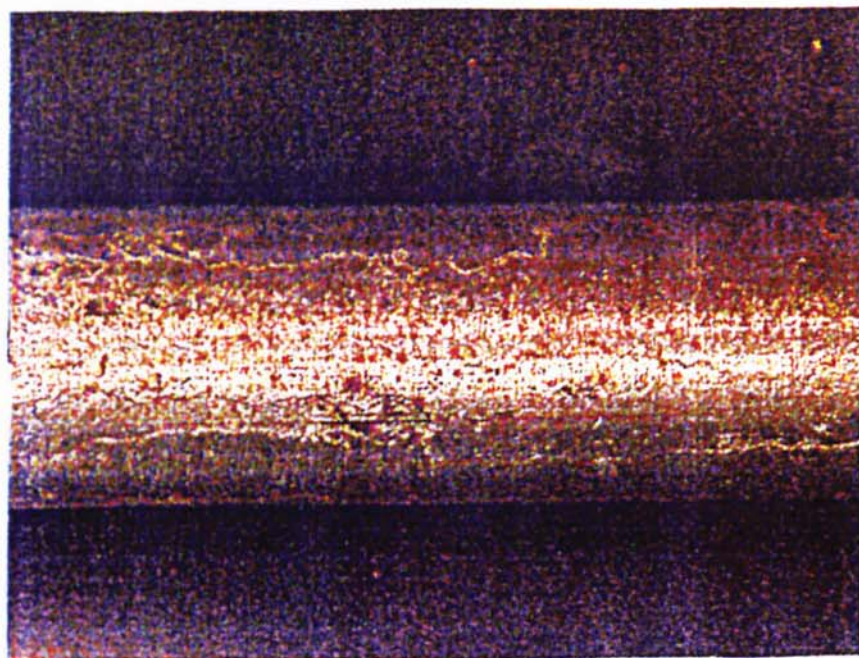
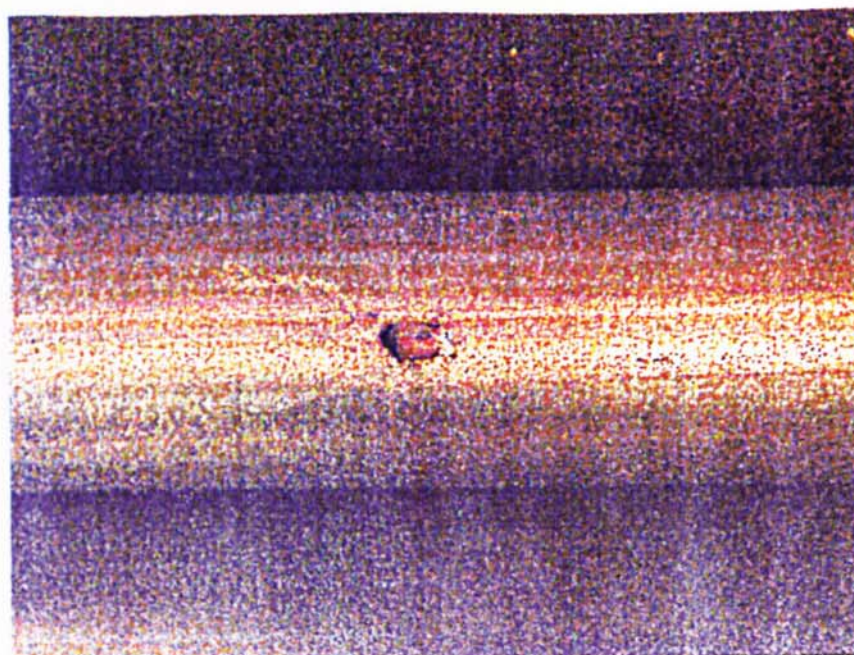


Figure 4.115 – Bar, after removal of corrosion products, following immersion in 0.1M sodium chloride with 1.0M ethanolamine (scale: bar diameter = 6mm)



## **CHAPTER FIVE**

### **SITE TRIALS TO DETERMINE THE DEPTH OF PENETRATION AND DISTRIBUTION OF INHIBITORS AND/OR THEIR DECOMPOSITION PRODUCTS**

#### **5.1 INTRODUCTION**

Chapter Four investigated the mechanisms of action and concentration dependence of four inhibitors in model electrolyte systems intended to simulate the pore solution phase present within carbonated and/or chloride contaminated concrete. The inhibitors chosen were nitrite ions, sodium monofluorophosphate, ethanolamine and a proprietary alkanolamine-based formulation. It was found that all of the inhibitors behaved as passivating anodic inhibitors to steel corrosion in air-saturated aqueous solutions of varied pH and chloride concentration. Generally however, high concentrations were required for the inhibitors to inhibit corrosion fully even when applied to initially passive steel. The exception was nitrite in neutral solutions with no chloride contamination, which appeared to inhibit corrosion fully even at very low concentrations.

Now that some idea of the concentration dependence has been obtained, this section of the present study addresses the question of inhibitor penetration into site concrete. Previous work at Aston University (Page et al., in preparation) has concentrated on depths of penetration of the inhibitors into laboratory specimens and these results will be discussed in section 5.3. Therefore, the objective of this chapter was to carry out medium term site trials to determine the depth of penetration and distribution of certain inhibitors and/or their decomposition products.



The inhibitors chosen for investigation in this chapter were sodium monofluorophosphate and an alkanolamine-based inhibitor. These were chosen as they are two of the most commonly used proprietary corrosion inhibitor systems for the rehabilitation of reinforced concrete. Both inhibitors are surface-applied to the concrete structure. A calcium nitrite-based system is another common repair method that shows some promise as a corrosion inhibitor, however, the system requires removal of the cover concrete and applying a thick mortar overlay and therefore it would have proved very costly to carry out site trials for the present study. However, the calcium nitrite-based system has been investigated, via laboratory studies and mathematical modelling, in the present study and the findings are reported in Chapter Eight.

British Energy collaborated in this research by providing two columns at a Power Station in North East England to be treated with the inhibitors. The two columns were nominally identical and a photograph is shown in Figure 5.1. The structure was 25 years old.

## **5.2 EXPERIMENTAL PROCEDURES**

### **5.2.1 Pre-inhibitor Application Investigations**

Cores were taken from each structure before application of the inhibitors so that carbonation depths and a chloride concentration profile could be obtained. Carbonation depths were obtained as described in section 3.3.11 and found to be between 10 and 15mm (see Figure 5.2). The chloride penetration profile was obtained using water extraction (see section 3.3.9) and ion chromatography (see section 3.3.10) and is shown in Figure 5.3. It can be seen from Figure 5.3 that chloride concentrations range from 0.1 to 0.6 mg/g of concrete and the variation of concentration with depth suggests that the structure was built with admixed chlorides that had subsequently begun to leach out of the columns.

### **5.2.2 Application of Sodium Monofluorophosphate**

Sodium monofluorophosphate was applied as recommended by the supplier. The structure was inspected for dirt etc., before undergoing ten applications of the inhibitor by hand spraying until the surface appeared saturated throughout the test area. Four applications were carried out with an aqueous solution of 5% (0.35M) sodium monofluorophosphate by weight and six were carried out with an aqueous solution of 10% (0.69M) sodium monofluorophosphate by weight. The ten applications were made over sixteen days, from 22<sup>nd</sup> July to 6<sup>th</sup> August 1998, and the structure was subjected to natural weathering in between, and after, the applications.

### **5.2.3 Application of the Alkanolamine-based Inhibitor**

The alkanolamine-based inhibitor was applied as recommended by the supplier. The structure was thoroughly cleaned with a wirebrush before undergoing five applications of an aqueous solution of the alkanolamine based-inhibitor (consisting of an aqueous solution of ethanolamine in addition to potassium hydrogen phosphate and possibly other substances of unidentified composition). Ion chromatography was performed on the inhibitor solution, as described in section 3.3.10, and its concentrations of ethanolamine, phosphate and potassium were found to be 2.3M, 1.2M and 1.2M respectively. The inhibitor was applied by hand spraying until the surface appeared saturated throughout the test area. The period of drying between applications varied in duration (minimum 3–4 hours) but as soon as the surface appeared dry it was deemed suitable for the next application. The five applications were carried out over the 30<sup>th</sup> September and 1<sup>st</sup> October 1998, and the structure was subjected to natural weathering in between, and after, the applications.

### **5.2.4 Determination of Penetration Profiles**

The column treated with sodium monofluorophosphate was cored 15 months after inhibitor treatment. Water extraction and ion chromatography was carried out in order to determine penetration profiles of monofluorophosphate and its decomposition products, namely phosphate and fluoride. The column treated with the alkanolamine-



based inhibitor was cored 12 months after inhibitor treatment. Water and acid extraction, along with ion chromatography, was carried out on these cores to determine penetration profiles for both ethanolamine and phosphate. The required profile grinding, water and acid extraction was carried out as described in section 3.3.9 and ion chromatography was performed on the aqueous extractions of the concrete as described in section 3.3.10.

## **5.3 DISCUSSION OF RESULTS**

### **5.3.1 Sodium Monofluorophosphate**

Ion chromatography is a very sensitive and quantitative method for determining monofluorophosphate concentrations. However, it was found in the present study that monofluorophosphate had failed to penetrate significantly into the concrete when applied as recommended by the supplier. It was, however, found that phosphate and fluoride did appear to penetrate to a depth of about 5mm as shown in Figures 5.4 and 5.5 respectively. Any fluoride detected beyond this depth was attributed to that which was already present in the concrete. These results support work by Page et al. (in preparation) who reported no detectable penetration of monofluorophosphate in carbonated laboratory concrete of 0.8 water to cement ratio subjected to cyclic wetting and drying for 18 months. The authors also reported that phosphate and fluoride were readily detectable at depths beyond the cover zone. This suggests that substantial hydrolysis of monofluorophosphate occurs in carbonated concrete and that any inhibition achieved on carbonated structures treated with sodium monofluorophosphate may be attributed to the known anodic inhibiting effects of phosphate (Mayne and Menter, 1954). Fluoride is not a corrosion inhibitor for steel in concrete. Alonso et al. (1996) suggested that the inhibition achieved on pre-corroded steel in neutral solutions, that were supposed to simulate the pore solution phase of carbonated concrete, resembled inhibition by phosphates and argued that these anions will be produced by hydrolysis of monofluorophosphate in neutral media. The difficulty in achieving significant monofluorophosphate penetration depths may help to explain the recent



findings in research conducted by Calder (2000). The author concluded that, under the conditions investigated, the application of MFP did not significantly affect the measured corrosion rates in either laboratory or site concrete.

### **5.3.2 Alkanolamine-based Inhibitor**

Figures 5.6 and 5.7 show that the ethanolamine component of the alkanolamine-based inhibitor appeared to penetrate significant depths into the concrete. The results show that the ethanolamine component penetrated beyond the carbonated zone and into the non-carbonated zone of the concrete. Whether the concentrations achieved at various depths are sufficient to inhibit corrosion fully is another question whose answer depends on many factors, such as the amount of corrosion already apparent on the steel and the longevity of protection afforded. This finding supports work by Page et al. (in preparation) who detected ethanolamine, using acid extraction, at depths beyond 20mm in laboratory specimens of high water to cement ratio that had undergone cyclic wetting and drying for 18 months after inhibitor treatment. However, Page, Ngala and Page (2000) found that, on pre-corroded bars in the specimens used for the investigations reported by Page et al. (in preparation), the penetrated inhibitor caused only modest reductions in corrosion rates in non-carbonated concrete with moderate levels of chloride, and no inhibiting effect in non-carbonated concrete with high chloride contamination or in carbonated concrete. In the present study, the phosphate component of the inhibitor did penetrate into the concrete to a depth of 9mm (Figure 5.8), but was only found using acid extraction (not found using water extraction). Page et al. (in preparation) found that, using acid extraction, the phosphate component did not penetrate beyond 4mm.

## **5.4 CONCLUSIONS**

Under the conditions employed, sodium monofluorophosphate failed to penetrate significantly into partially carbonated site concrete when applied as recommended by the supplier. Phosphate and fluoride were found, using a water-extraction method, to

penetrate 5mm into partially carbonated site concrete treated with sodium monofluorophosphate.

Under the conditions investigated, the ethanolamine component of the alkanolamine-based inhibitor did appear to penetrate significant depths and was found, using both water-extraction and acid-extraction, beyond the carbonation zone of partially carbonated site concrete. Under the conditions investigated, the phosphate component of the alkanolamine-based inhibitor did penetrate 9mm into the partially carbonated site concrete, but was only found using acid-extraction (not found using water extraction).

Figure 5.1 – Photograph of structure



Figure 5.2 – Typical section of core showing depth of carbonation

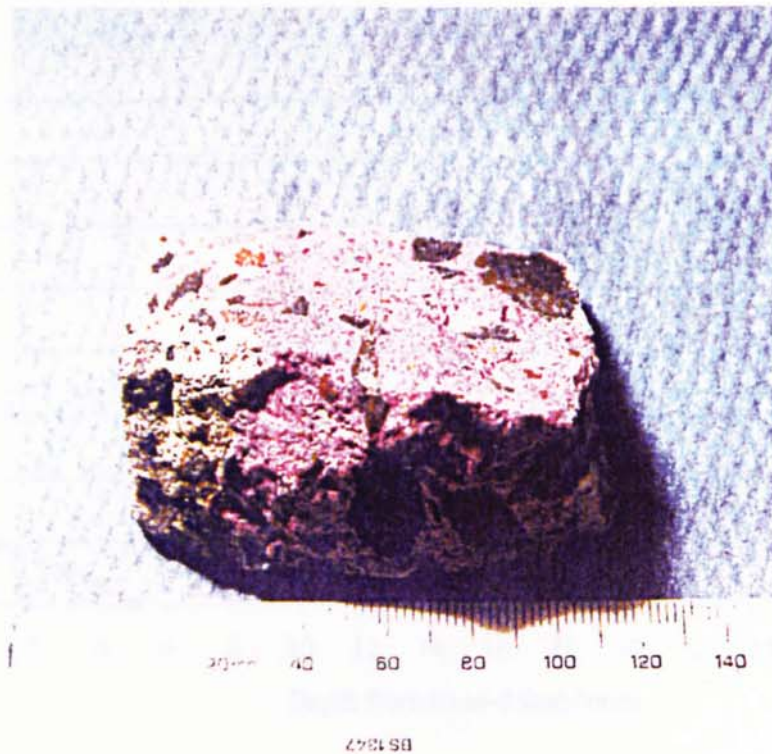




Figure 5.3 - Penetration profile for chloride in site concrete (water extraction method)

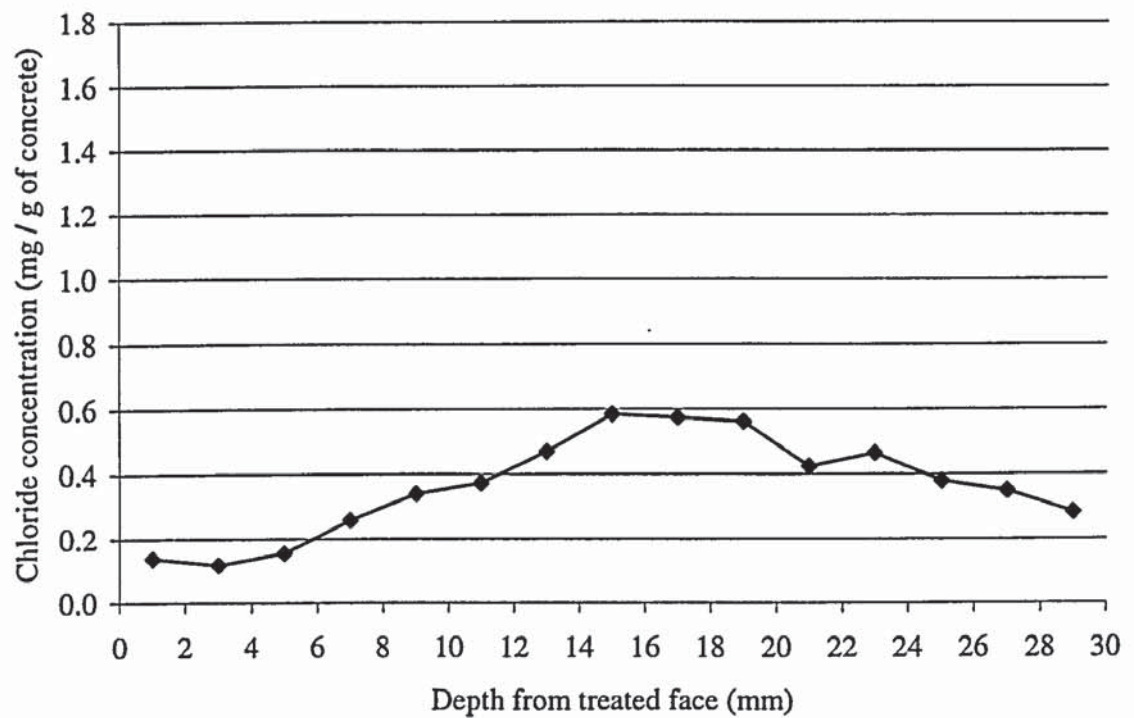


Figure 5.4 - Penetration profile for phosphate in site concrete treated with sodium monofluorophosphate corrosion inhibitor (water extraction)

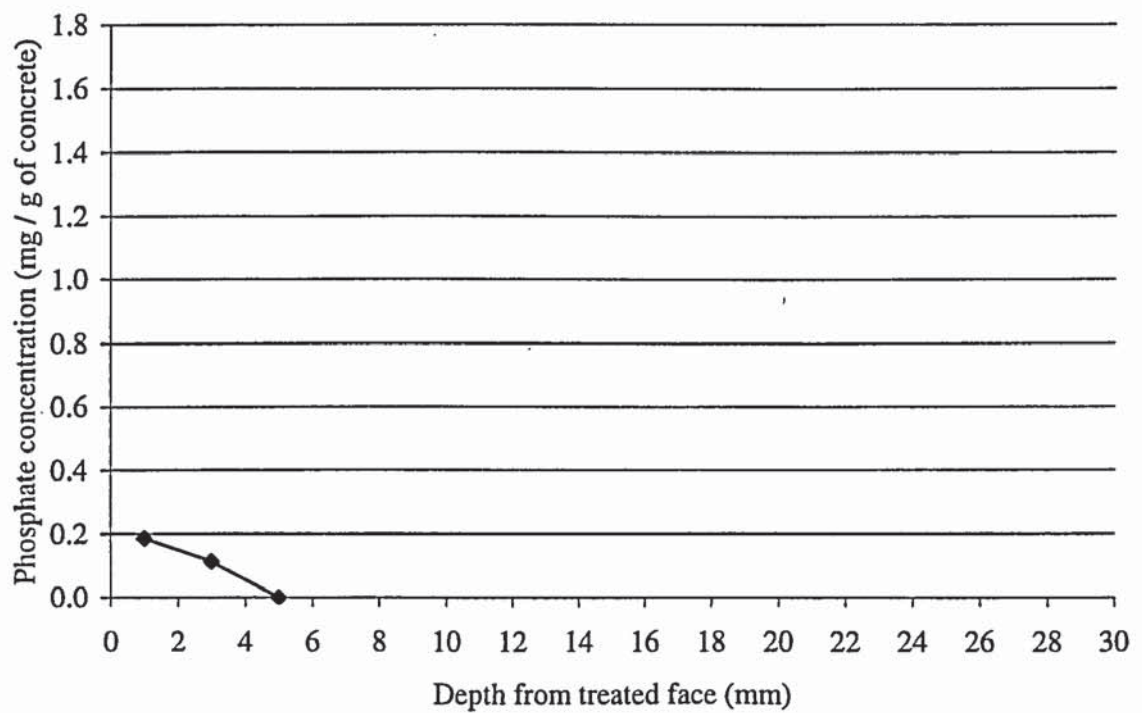


Figure 5.5 - Penetration profile for fluoride in site concrete treated with sodium monofluorophosphate corrosion inhibitor (water extraction method)

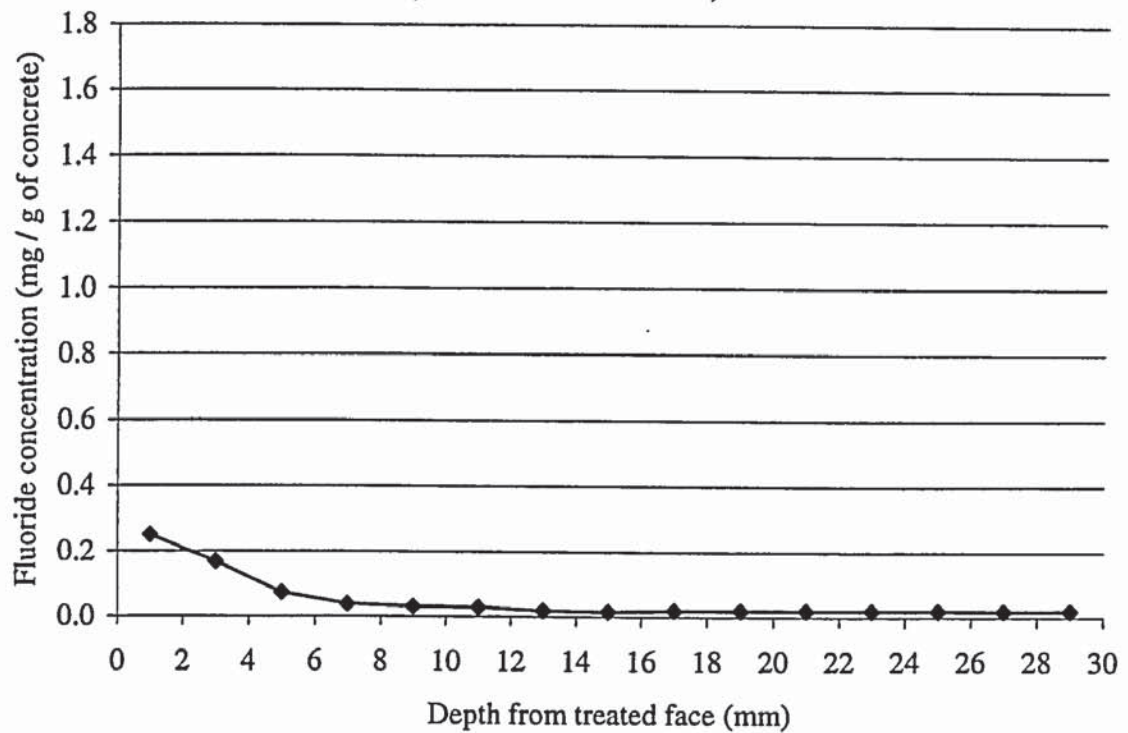


Figure 5.6 - Penetration profile for ethanolamine in site concrete treated with an alkanolamine-based corrosion inhibitor (water extraction method)

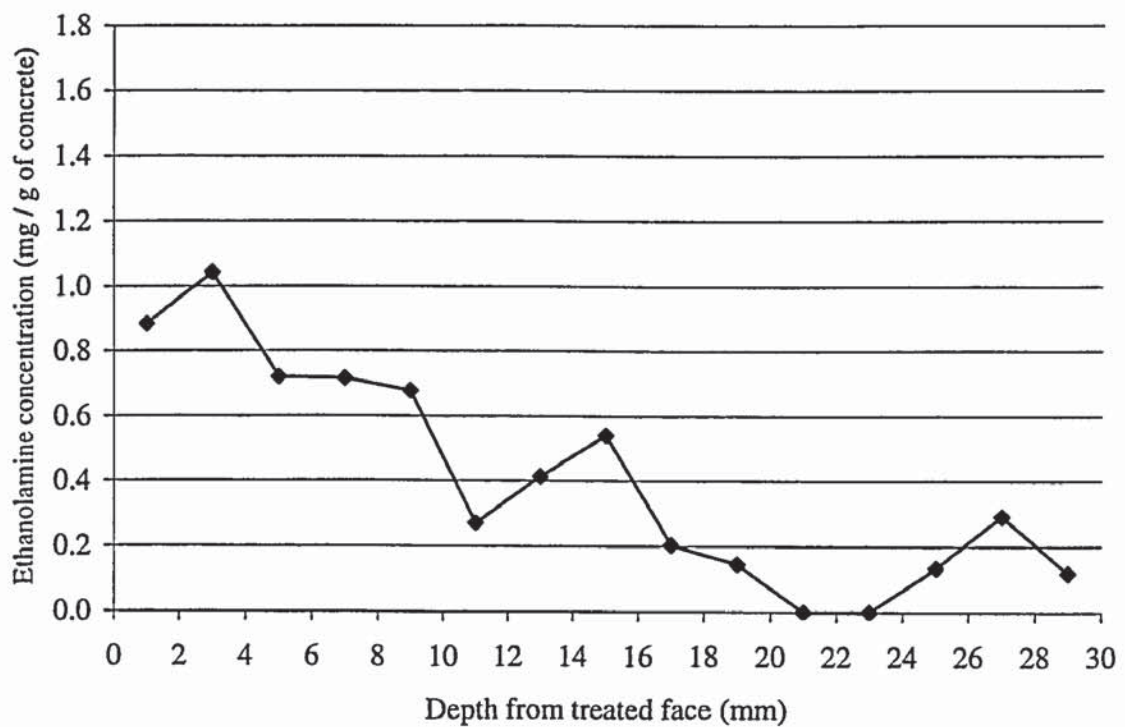


Figure 5.7 - Penetration profile for ethanolamine in site concrete treated with an alkanolamine-based corrosion inhibitor (acid extraction method)

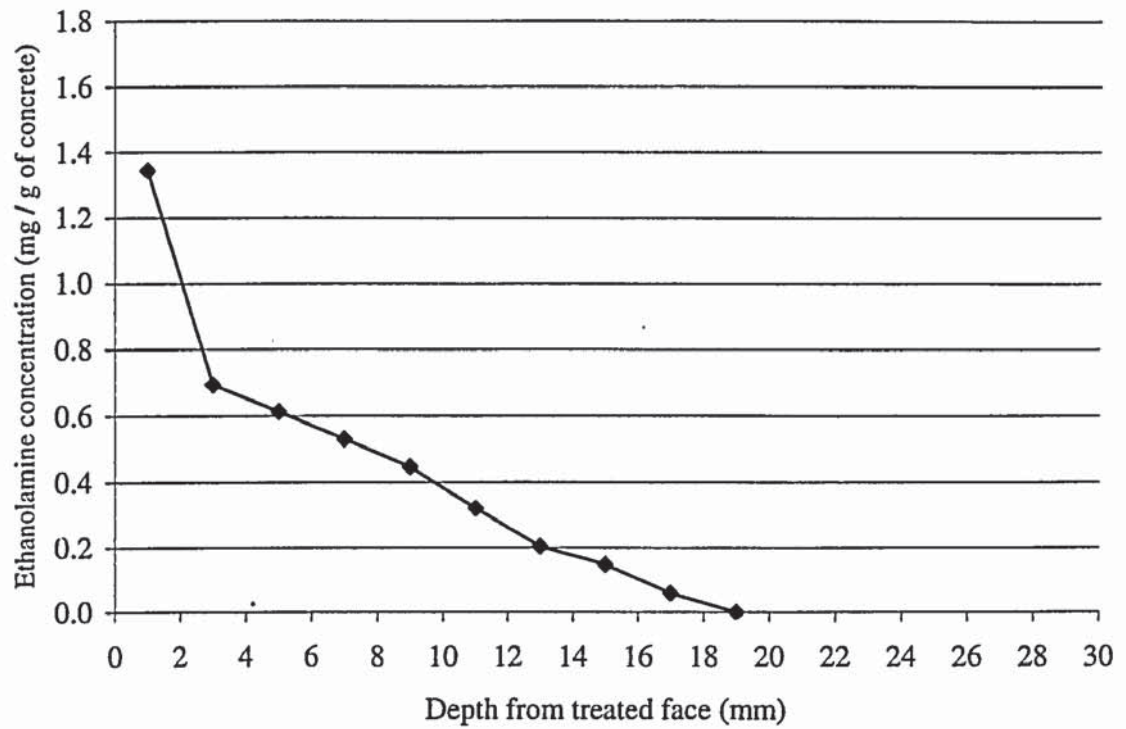
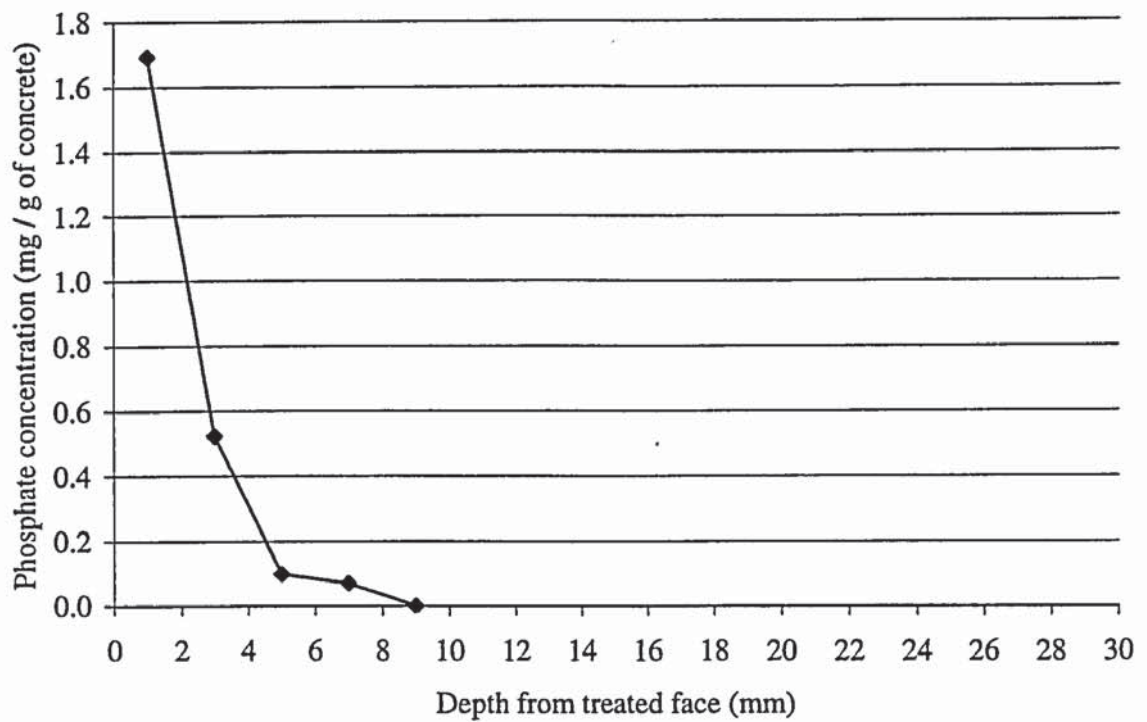


Figure 5.8 - Penetration profile for phosphate in site concrete treated with an alkanolamine-based corrosion inhibitor (acid extraction method)





## **CHAPTER SIX**

### **EFFECT OF CARBONATING ATMOSPHERE ON HYDRATED CEMENT PASTE**

#### **6.1 INTRODUCTION**

Chapter Seven of the present study discusses the results of laboratory investigations into the effectiveness of physical realkalisation as a curative method for the corrosion of steel in carbonated concrete. However, before carrying out these investigations, it was deemed important to manufacture reproducible carbonated hydrated cement paste specimens and to understand and quantify the influence of the carbonating atmosphere on these. It is important to clarify whether the accelerated carbonation regimes, required to produce carbonated cement paste for laboratory investigations over reasonable time-scales, may affect the corrosion-related properties of concretes.

The mechanisms of carbonation, mineralogical formations, rate of carbonation, factors influencing carbonation and the effect of carbonation on the pore structure of hydrated cement paste are discussed in section 2.3.5. The objective of this chapter is to address concerns over differences in the pore solution chemistry, porosity and solid phases of carbonated cement pastes produced in different atmospheres. This was achieved by exposing hydrated cement pastes to 100% carbon dioxide, 5% carbon dioxide (with 21% oxygen and 74% nitrogen) and air whilst being kept at relative humidities controlled by five different saturated salt solutions. The pore solutions of the resulting carbonated specimens were investigated using ion chromatography and a pH electrode. The porosities of the carbonated specimens were investigated by water desorption and mercury intrusion porosimetry. The solid phases of the carbonated cement paste specimens were investigated using X-ray diffraction analysis and differential thermal

analysis/thermo-gravimetric analysis. All experiments reported in this chapter were carried out in triplicate.

## **6.2 EXPERIMENTAL PROCEDURES**

### **6.2.1 Preparation of Hydrated Cement Paste Specimens**

The manufacture of Ordinary Portland Cement paste cylinders was carried out as described in section 3.3.1. All cement paste cylinders were constructed with a water to cement ratio of 0.6. After de-moulding, the cylinders were placed within sealed containers containing de-ionised water. The specimens were placed in an upright position on purpose-made platforms that supported them above the de-ionised water. The purpose of the de-ionised water was to create a curing environment of 100% relative humidity within the containers. The containers were then placed in a room, maintained at 20°C, for 14 days before being moved to another room, maintained at 38°C, for 84 days. The cylinders were finally cut, perpendicular to their longest axis, into 5mm thick discs using a mechanical hacksaw.

### **6.2.2 Carbonation of Cement Paste Discs**

The 5mm discs were placed in an upright position on specially constructed racks within sealed containers. Each set of discs was subjected to one of fifteen exposure environments. These exposure environments were achieved by placing one of five saturated salt solutions below the discs in the bottom of each container and pumping through, for 30 minutes per day, gas containing one of three carbon dioxide concentrations. The saturated salt solutions were sodium chloride (NaCl), sodium nitrite ( $\text{NaNO}_2$ ), ammonium nitrate ( $\text{NH}_4\text{NO}_3$ ), magnesium nitrate ( $\text{Mg}(\text{NO}_3)_2 \cdot 6\text{H}_2\text{O}$ ) and sodium dichromate ( $\text{Na}_2\text{Cr}_2\text{O}_7 \cdot 2\text{H}_2\text{O}$ ). The variation with temperature, of the relative humidity of the air over each saturated salt solution, is shown in Table 6.1. Relative humidity and temperature monitoring were carried out using a hand held Vaisala HM 34 Humidity and Temperature Meter as shown in Figure 3.12. The carbon dioxide concentrations were 100%, 5% (with 21% oxygen and 74% nitrogen) and



approximately 0.03% (air). The experimental set-up used to carbonate the discs is shown in Figure 6.1. The discs were monitored for depth of carbonation, using phenolphthalein as described in section 3.3.11, and all the discs in a particular environment were deemed to be carbonated when sample discs remained colourless after the phenolphthalein test.

### **6.2.3 Evaporable Water Determinations**

The evaporable water content, of fully carbonated sample discs from each carbonation environment, was calculated as described in section 3.3.14 in order to express ionic species as free amounts present in the hydrated cement paste as a fraction of the unhydrated cement. A detailed calculation is presented in Appendix E.

### **6.2.4 Pore Solution Analysis**

Once the discs appeared fully carbonated, as determined by the method described in section 3.3.11, the pore solution phase needed to be extracted for analysis. Each disc had been carbonated at a relative humidity between approximately 53% and 76% and at these humidities there is not a sufficient amount of pore solution available for extraction and subsequent analysis. Therefore, the fully carbonated discs were placed on purpose made platforms that supported them above de-ionised water. De-ionised water was added to each disc at a rate of 0.1ml per day, with the water that was not absorbed being carefully removed by lens tissue. The combination of water addition and 100% relative humidity was maintained until near constant weight was achieved. Each disc was weighed before and after the 'saturation' process. After 'saturation', five discs at a time from any particular carbonation atmosphere had their pore solution phases expressed as described in section 3.3.3. The 'saturation' process was essential to obtain sufficient pore solution for analysis and as the same procedure was followed for all discs, the results obtained for the different carbonation environments are comparable. The pore solutions were analysed using the pH meter and ion chromatography as described in sections 3.3.4 and 3.3.10 respectively. The pore solutions were also analysed for carbonate and bicarbonate ions using the procedure described in 3.3.13. The discs were



weighed before and after the 'saturation' process in order to calculate ionic species as free amounts present in the hydrated cement paste as a fraction of the unhydrated cement.

#### **6.2.5 Porosity Determinations**

The porosity and pore size distribution of the carbonated cement paste specimens were investigated using water desorption and mercury intrusion porosimetry respectively, as described in sections 3.3.15 and 3.3.18 respectively.

#### **6.2.6 Solid Phase Determinations**

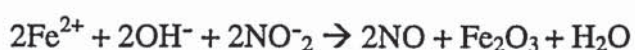
The solid phases of the carbonated cement paste specimens were investigated using X-ray diffraction analysis and differential thermal analysis/thermo-gravimetric analysis as described in sections 3.3.16 and 3.3.17 respectively.

### **6.3 DISCUSSION OF RESULTS**

#### **6.3.1 Pore Solution Composition**

Ionic concentrations and pH values of the extracted pore solution from each exposure atmosphere are presented in Tables 6.2 to 6.5. Tables 6.2 and 6.3 present ionic concentrations present within the pore solution in terms of millimoles per litre. Tables 6.4 and 6.5 present ionic concentrations within the pore solution in terms of millimoles per gram of unhydrated cement. The most interesting result is that the solutions extracted from the discs carbonated over sodium nitrite have actually been contaminated by significant levels of nitrite and nitrate. The amount of nitrite and nitrate increases with increasing carbon dioxide concentration and the levels present are actually greater than the levels present for any of the other anions. It appears that the nitrite is present in the form of calcium nitrite as the contaminated pore solutions also contain relatively high concentrations of calcium ions. Also, at 100% carbon dioxide concentration, the nitrite appears to be present as magnesium nitrite although the concentration is an order of magnitude less than that found for calcium nitrite. The nitrate is simply produced by

the oxidation of the nitrite. This result is significant as to regards whether the accelerated carbonation regimes affect the corrosion-related properties of concretes. Clearly, carbonating cement paste and therefore concrete over a saturated solution of sodium nitrite will result in a significant level of nitrite contamination. Chapter Four of the present study has demonstrated that nitrite is an effective anodic inhibitor of corrosion of steel in aerated neutral solutions even when present at 10mmol/l. This level of nitrite is exceeded even by carbonating samples over sodium nitrite in 0.03% carbon dioxide. The level of contamination achieved at 100% carbon dioxide has exceeded 100mmol/l which has been shown, in Chapter Four, to inhibit corrosion of steel significantly in air-saturated neutral solutions with 100mmol/l chloride contamination. Within the last decade Andrade and co-workers (Alonso, Acha and Andrade, 1990; Alonso and Andrade, 1990; Andrade, Alonso and Gonzalez, 1986) have demonstrated that nitrite based corrosion inhibitor admixtures can protect steel in carbonated concrete. In the USA, since 1978, calcium nitrite has been used in over 300 parking, marine and highway structures, apparently with very successful results (Jeknevorian, Chin and Saidha, 1995) in the battle to inhibit chloride-induced corrosion. Gaidis and Rosenberg (1979) reported that calcium nitrite behaves as an anodic inhibitor and that there is no reaction between ferric ions and nitrite ions; however, ferrous ions react with nitrite ions as shown below:



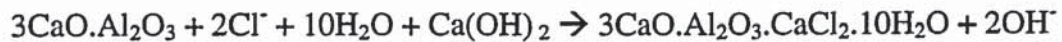
This reaction reinforces the passive film, therefore, blocking further passage of ferrous ions from the steel into the pore solution. Therefore, when investigating the effectiveness of rehabilitative methods of controlling the corrosion of steel in carbonated concrete it is important that any inhibitive effects attributable to the carbonating atmosphere are fully quantified.



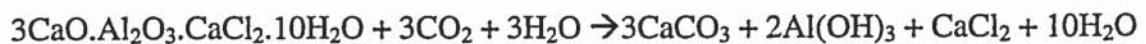
The results shown for carbonate and bicarbonate ions are the maximum possible that could have been present in the pore solutions. Although not totally representative, these results show that very little sodium or potassium carbonate can exist in the extracted pore solution and this is supported by the low concentrations found for sodium and potassium.

It is also evident from Table 6.2 that the pH of the pore solution decreases with increasing carbon dioxide concentration. This is clearly because higher carbon dioxide concentrations result in a more pronounced degree of carbonation, although in theory, even the samples carbonated in 0.03% carbon dioxide will eventually achieve complete carbonation if the conditions allow. It is important to note that although the phenolphthalein test can demonstrate the depth of carbonation it does not demonstrate the degree of carbonation and this is illustrated by the differences in measured pH values.

It may be seen that the concentration of chloride ions in the extracted pore solutions increase with increasing carbon dioxide concentration. This increase in chloride concentration is very significant due to the lack of hydroxyl ions in the pore solution of carbonated concrete and can therefore lead to an increase in the probability of corrosion. Chloride was present in the unhydrated cement and this was probably bound by the C<sub>3</sub>A phase following the possible reaction:



As this phase is a CaO phase it would be expected to carbonate as follows:



Therefore, the increased chloride concentrations observed in the pore solutions that underwent accelerated carbonation are probably due to the increased carbonation of the



calcium chloroaluminate phase present within the hydrated cement matrix. No other significant levels of contamination are observed in the pore solutions.

### **6.3.2 Porosity and Pore Size Distribution**

Table 6.6 and Figures 6.2 to 6.6 show the results of the water desorption experiments. It may be clearly seen that as the carbon dioxide concentration increases there is an associated increase in bulk density and capillary porosity and a decrease in total porosity. The increase in bulk density and decrease in total porosity are due to increased carbon dioxide concentration resulting in an increased amount of calcium carbonate being formed, which actually occupies a volume greater than that of the 'parent hydrates' from which it was formed as reported by Pihajavaara (1968) and Bier, Kropp and Hilsdorf (1987 and 1989). However, the capillary porosity (volume of pores greater than 30nm in diameter) is very important with respect to the corrosion related properties of concrete as these pores provide the major interconnected pathways along which aggressive substances most readily penetrate the cement matrix from the environment (Page, 1999a). With this in mind, it is apparent that cement pastes carbonated in accelerated carbonation atmospheres are more susceptible to chloride penetration than those carbonated in air.

The mercury intrusion porosimetry results presented in Table 6.7 and Figures 6.7 to 6.11 show a decrease in total intrusion volume and threshold diameter with increasing carbon dioxide concentration. The only exception is that the threshold diameter of samples carbonated over ammonium nitrate appear to increase with increasing carbon dioxide concentration. Generally, very little difference can be observed when comparing the effect of the saturated salt solutions in terms of porosity.

### **6.3.3 Solid Phases**

Table 6.8 and Figures 6.12 to 6.16 present the results obtained using X-ray diffraction. However, it must be noted that X-ray diffraction is a technique dependent on the

existence of crystal structures and, as such, it is very difficult to detect C-S-H gel owing to its poorly crystalline, gel-like structure. Therefore, it will not be discussed further in the X-ray diffraction results. It can be seen that calcite peak intensities increased with increased carbonation whereas the vaterite peaks remained more or less constant. Aragonite is present, at intensities between that observed for calcite and vaterite, in the samples carbonated in 0.03% carbon dioxide. Aragonite peaks also appear at significant intensities in those specimens carbonated over magnesium nitrate and sodium dichromate with 5% carbon dioxide. However, at higher levels of carbon dioxide concentration aragonite peaks are seldom seen. This suggests that aragonite transforms into the more stable calcite as the degree of carbonation is increased. Calcium hydroxide peaks are observed in all specimens carbonated in 0.03% carbon dioxide and to a lesser degree in samples carbonated over ammonium nitrate, magnesium nitrate and sodium dichromate with 5% carbon dioxide. This suggests that those samples carbonated in air and at the lower humidities in 5% carbon dioxide are not fully carbonated as calcium hydroxide is identified at significant intensities.

Table 6.9 and Figures 6.17 to 6.36 present the DTA/TG results. DTA is a qualitative technique that allows solid phases to be identified. The analysis of the DTA traces was performed with extensive reference to Ramachandran (1969) and Lea (1970). There are three primary endotherms typical of DTA on OPC, namely a low (<200°C) temperature effect, a sharp peak at about 500°C and a high (750 to 800°C) temperature effect. The corresponding perturbations in the TG traces can also be seen. The low temperature effect consists of three overlapping peaks, manifested by a strong central peak (130°C) with a shoulder on each side. It is generally accepted (Ramachandran, 1969; Lea, 1970) that this triple effect is caused by the evaporation of physically bound water, dehydration of C-S-H gel and dehydration of ettringite. Interpretation of the 495 to 505°C peak is far easier, being universally attributed to the dehydration of calcium hydroxide. The 800°C effect is attributed to the decomposition of calcium carbonate. The minor endotherm prior to the main effect may be attributable to the expulsion of carbon dioxide from poorly crystalline calcium carbonate.



In agreement with the results obtained by X-ray diffraction, calcium carbonate is observed in all samples. Calcium hydroxide endotherms can be clearly observed in all samples carbonated in 0.03% carbon dioxide and in the samples carbonated over ammonium nitrate, magnesium nitrate and sodium dichromate with 5% carbon dioxide. This is also in agreement with the results obtained by X-ray diffraction. Endotherms were observed for C-S-H/ettringite in all samples.

TG analysis allows quantitative results to be obtained. Table 6.9 and Figures 6.32 to 6.36 present these results. The quantitative results are obtained by determining weight loss during the three major reactions, i.e. the dehydration of C-S-H/ettringite between 50 and 250°C, the dehydration of calcium hydroxide between 450 and 550°C, and the decarbonation of calcium carbonate between 700 and 850°C. From the results it can be seen that the amount of calcium hydroxide present within the hydrated cement matrix generally decreased with increased carbon dioxide concentration. Generally, calcium carbonate is found at greater levels in those samples carbonated with 100% carbon dioxide when compared to those samples carbonated with other carbon dioxide concentrations. The opposite is true for C-S-H gel.

#### **6.4 CONCLUSIONS**

Carbonating hydrated cement paste over saturated solutions of sodium nitrite results in significant concentrations of nitrite in the pore solution of the carbonated paste. This has possible implications when considering the effects of accelerated carbonating regimes on the corrosion related properties of concrete, as nitrite has been shown to be an effective anodic inhibitor of steel corrosion. Saturated solutions of sodium chloride, ammonium nitrate, magnesium nitrate and sodium dichromate have been investigated and identified as alternatives for controlling the relative humidity of the carbonating environment.



The pH of the pore solution decreases with increase in the concentration of carbon dioxide in the carbonating atmosphere. The release of bound chloride ions is increased with increasing carbon dioxide concentration.

An increase in the carbon dioxide concentration of the carbonating atmosphere results in an associated increase in the bulk density and capillary porosity and a decrease in the total porosity of carbonated cement paste.

Calcium carbonate, formed by the carbonation of hydrated cement paste, was found to be mainly in the mineralogical formation of calcite, with substantial amounts of vaterite and a trace of aragonite. Aragonite appears to transform into the more stable calcite as the degree of carbonation is increased.

It is important to clarify whether the accelerated carbonation regimes, required to produce carbonated cement paste for laboratory investigations over reasonable time-scales, may affect the corrosion-related properties of concretes. This chapter has shown that accelerated carbonation regimes do affect the corrosion-related properties of concrete and this should be borne in mind when carrying out and quantifying research into the corrosion and control of corrosion of steel in concrete.

Saturated Salt Solution	Temperature (°C)		
	20	25	30
	Relative Humidity (%)		
Sodium Chloride	76	75	75
Sodium Nitrite	65	65	63
Ammonium Nitrate	65	62	59
Magnesium Nitrate	55	53	52
Sodium Dichromate	55	54	52

Table 6.1 - Relative Humidity of Air over Saturated Salt Solutions (B.S. 3718 : 1964)

Sat. Salt Sol <sup>n</sup>	CO <sub>2</sub> Conc <sup>n</sup> (%)	pH	OH <sup>-</sup>	Cl <sup>-</sup>	NO <sub>2</sub> <sup>-</sup>	NO <sub>3</sub> <sup>-</sup>	SO <sub>4</sub> <sup>2-</sup>	Σ <sup>-</sup>	Max Poss CO <sub>3</sub> <sup>2-</sup>	Max Poss HCO <sub>3</sub> <sup>-</sup>
NaCl	100	7.4	3×10 <sup>-4</sup>	20.5	-	-	16.7	53.9	-	5.4
NaNO <sub>2</sub>	100	7.2	2×10 <sup>-4</sup>	16.3	123.7	33.7	12.6	198.9	-	15.8
NH <sub>4</sub> NO <sub>3</sub>	100	9.6	4×10 <sup>-2</sup>	11.4	-	-	15.3	42.0	0.9	4.4
Mg(NO <sub>3</sub> ) <sub>2</sub> .6H <sub>2</sub> O	100	7.4	3×10 <sup>-4</sup>	23.4	-	-	18.0	59.7	-	5.8
Na <sub>2</sub> Cr <sub>2</sub> O <sub>7</sub> .2H <sub>2</sub> O	100	7.1	1×10 <sup>-4</sup>	23.4	-	-	20.3	64.3	-	6.9
NaCl	5	8.7	5×10 <sup>-3</sup>	13.1	-	-	19.7	52.5	-	2.8
NaNO <sub>2</sub>	5	10.4	0.3	10.8	22.3	0.4	19.3	72.4	1.5	0.8
NH <sub>4</sub> NO <sub>3</sub>	5	9.9	0.1	12.0	-	-	24.1	60.3	0.5	1.3
Mg(NO <sub>3</sub> ) <sub>2</sub> .6H <sub>2</sub> O	5	10.9	0.8	7.5	-	-	2.0	12.3	9.8	3.1
Na <sub>2</sub> Cr <sub>2</sub> O <sub>7</sub> .2H <sub>2</sub> O	5	10.8	0.6	11.2	-	-	6.9	25.6	8.2	2.1
NaCl	0.03	10.7	0.5	4.1	-	-	1.2	7.0	7.6	3.0
NaNO <sub>2</sub>	0.03	10.6	0.4	8.0	15.8	0.3	11.4	47.3	7.6	3.8
NH <sub>4</sub> NO <sub>3</sub>	0.03	10.6	0.4	7.5	-	-	10.9	29.7	6.5	3.3
Mg(NO <sub>3</sub> ) <sub>2</sub> .6H <sub>2</sub> O	0.03	10.9	0.8	8.4	-	-	1.9	13.0	8.0	2.0
Na <sub>2</sub> Cr <sub>2</sub> O <sub>7</sub> .2H <sub>2</sub> O	0.03	10.7	0.5	8.9	-	-	5.0	19.4	6.1	2.4

Table 6.2 – Concentration of anions (mmol/l) in the pore solution of hydrated cement paste after carbonation in various atmospheres

Sat. Salt Sol <sup>n</sup>	CO <sub>2</sub> Conc <sup>n</sup> (%)	Na <sup>+</sup>	K <sup>+</sup>	Mg <sup>2+</sup>	Ca <sup>2+</sup>	Σ <sup>+</sup>
NaCl	100	3.8	9.9	0.9	20.8	57.1
NaNO <sub>2</sub>	100	4.0	12.4	8.4	78.5	190.2
NH <sub>4</sub> NO <sub>3</sub>	100	1.7	5.5	-	20.3	47.8
Mg(NO <sub>3</sub> ) <sub>2</sub> .6H <sub>2</sub> O	100	5.2	11.4	1.0	22.1	62.8
Na <sub>2</sub> Cr <sub>2</sub> O <sub>7</sub> .2H <sub>2</sub> O	100	9.9	16.5	2.0	19.6	69.6
NaCl	5	3.9	8.9	-	22.3	57.4
NaNO <sub>2</sub>	5	6.8	19.2	-	26.9	75.8
NH <sub>4</sub> NO <sub>3</sub>	5	6.5	16.0	-	22.9	68.3
Mg(NO <sub>3</sub> ) <sub>2</sub> .6H <sub>2</sub> O	5	0.3	0.6	-	19.1	39.1
Na <sub>2</sub> Cr <sub>2</sub> O <sub>7</sub> .2H <sub>2</sub> O	5	0.5	1.2	-	25.0	51.7
NaCl	0.03	3.0	14.5	-	12.3	42.1
NaNO <sub>2</sub>	0.03	4.1	13.9	-	26.4	70.8
NH <sub>4</sub> NO <sub>3</sub>	0.03	3.5	13.2	-	18.2	53.1
Mg(NO <sub>3</sub> ) <sub>2</sub> .6H <sub>2</sub> O	0.03	3.1	26.4	-	7.1	43.7
Na <sub>2</sub> Cr <sub>2</sub> O <sub>7</sub> .2H <sub>2</sub> O	0.03	0.7	1.1	-	23.1	48.0

Table 6.3 – Concentration of cations (mmol/l) in the pore solution of hydrated cement paste after carbonation in various atmospheres

Sat. Salt Sol <sup>n</sup>	CO <sub>2</sub> Conc <sup>n</sup> (%)	OH <sup>-</sup>	Cl <sup>-</sup>	NO <sub>2</sub> <sup>-</sup>	NO <sub>3</sub> <sup>-</sup>	SO <sub>4</sub> <sup>2-</sup>	Σ <sup>-</sup>	Max Poss CO <sub>3</sub> <sup>2-</sup>	Max Poss HCO <sub>3</sub> <sup>-</sup>
NaCl	100	-	5	-	-	4	13	-	1
NaNO <sub>2</sub>	100	-	4	34	9	3	53	-	4
NH <sub>4</sub> NO <sub>3</sub>	100	-	3	-	-	5	13	-	1
Mg(NO <sub>3</sub> ) <sub>2</sub> ·6H <sub>2</sub> O	100	-	5	-	-	4	13	-	1
Na <sub>2</sub> Cr <sub>2</sub> O <sub>7</sub> ·2H <sub>2</sub> O	100	-	6	-	-	6	18	-	2
NaCl	5	-	4	-	-	7	18	-	1
NaNO <sub>2</sub>	5	-	4	8	-	7	26	1	-
NH <sub>4</sub> NO <sub>3</sub>	5	-	4	-	-	9	22	-	-
Mg(NO <sub>3</sub> ) <sub>2</sub> ·6H <sub>2</sub> O	5	-	3	-	-	1	5	4	1
Na <sub>2</sub> Cr <sub>2</sub> O <sub>7</sub> ·2H <sub>2</sub> O	5	-	4	-	-	3	10	3	1
NaCl	0.03	-	2	-	-	0	2	2	1
NaNO <sub>2</sub>	0.03	-	3	6	-	4	17	2	1
NH <sub>4</sub> NO <sub>3</sub>	0.03	-	3	-	-	4	11	2	1
Mg(NO <sub>3</sub> ) <sub>2</sub> ·6H <sub>2</sub> O	0.03	-	3	-	-	1	5	2	-
Na <sub>2</sub> Cr <sub>2</sub> O <sub>7</sub> ·2H <sub>2</sub> O	0.03	-	3	-	-	2	7	2	1

Table 6.4 – Free anionic concentrations (mmol / g of cement) × 10<sup>3</sup>

Sat. Salt Sol <sup>n</sup>	CO <sub>2</sub> Conc <sup>n</sup> (%)	Na <sup>+</sup>	K <sup>+</sup>	Mg <sup>2+</sup>	Ca <sup>2+</sup>	Σ <sup>+</sup>
NaCl	100	1	3	-	5	14
NaNO <sub>2</sub>	100	1	3	2	22	52
NH <sub>4</sub> NO <sub>3</sub>	100	1	2	-	6	15
Mg(NO <sub>3</sub> ) <sub>2</sub> ·6H <sub>2</sub> O	100	1	3	-	5	14
Na <sub>2</sub> Cr <sub>2</sub> O <sub>7</sub> ·2H <sub>2</sub> O	100	3	5	1	5	20
NaCl	5	1	3	-	8	20
NaNO <sub>2</sub>	5	2	7	-	10	29
NH <sub>4</sub> NO <sub>3</sub>	5	2	6	-	8	24
Mg(NO <sub>3</sub> ) <sub>2</sub> ·6H <sub>2</sub> O	5	-	-	-	7	14
Na <sub>2</sub> Cr <sub>2</sub> O <sub>7</sub> ·2H <sub>2</sub> O	5	-	-	-	9	18
NaCl	0.03	1	6	-	5	17
NaNO <sub>2</sub>	0.03	2	5	-	10	27
NH <sub>4</sub> NO <sub>3</sub>	0.03	1	5	-	7	20
Mg(NO <sub>3</sub> ) <sub>2</sub> ·6H <sub>2</sub> O	0.03	1	10	-	3	17
Na <sub>2</sub> Cr <sub>2</sub> O <sub>7</sub> ·2H <sub>2</sub> O	0.03	-	-	-	9	18

Table 6.5 – Free cationic concentrations (mmol / g of cement) × 10<sup>3</sup>



Sat. Salt Sol <sup>n</sup>	CO <sub>2</sub> Conc <sup>n</sup> (%)	Bulk Density (g/cm <sup>3</sup> )	Capillary Porosity (%)	Total Porosity (%)
NaCl	100	1.992	22.15	38.21
NaNO <sub>2</sub>	100	1.996	22.17	38.19
NH <sub>4</sub> NO <sub>3</sub>	100	1.993	22.87	38.67
Mg(NO <sub>3</sub> ) <sub>2</sub> .6H <sub>2</sub> O	100	1.992	23.07	39.17
Na <sub>2</sub> Cr <sub>2</sub> O <sub>7</sub> .2H <sub>2</sub> O	100	1.993	22.94	39.69
NaCl	5	1.984	15.58	39.62
NaNO <sub>2</sub>	5	1.982	16.02	41.54
NH <sub>4</sub> NO <sub>3</sub>	5	1.990	16.75	41.21
Mg(NO <sub>3</sub> ) <sub>2</sub> .6H <sub>2</sub> O	5	1.982	15.81	41.19
Na <sub>2</sub> Cr <sub>2</sub> O <sub>7</sub> .2H <sub>2</sub> O	5	1.985	16.29	41.05
NaCl	0.03	1.960	4.44	43.35
NaNO <sub>2</sub>	0.03	1.968	11.03	43.64
NH <sub>4</sub> NO <sub>3</sub>	0.03	1.960	16.15	45.31
Mg(NO <sub>3</sub> ) <sub>2</sub> .6H <sub>2</sub> O	0.03	1.960	3.54	44.16
Na <sub>2</sub> Cr <sub>2</sub> O <sub>7</sub> .2H <sub>2</sub> O	0.03	1.963	3.72	44.27

Table 6.6 – Water desorption results for hydrated cement paste after carbonation in various atmospheres

Sat. Salt Sol <sup>n</sup>	CO <sub>2</sub> Conc <sup>n</sup> (%)	Threshold Diameter (μm)	Total Intrusion Volume (cm <sup>3</sup> /g)
NaCl	100	0.318	0.170
NaNO <sub>2</sub>	100	0.182	0.141
NH <sub>4</sub> NO <sub>3</sub>	100	1.224	0.183
Mg(NO <sub>3</sub> ) <sub>2</sub> .6H <sub>2</sub> O	100	0.315	0.173
Na <sub>2</sub> Cr <sub>2</sub> O <sub>7</sub> .2H <sub>2</sub> O	100	0.254	0.150
NaCl	5	0.628	0.176
NaNO <sub>2</sub>	5	0.622	0.178
NH <sub>4</sub> NO <sub>3</sub>	5	0.823	0.195
Mg(NO <sub>3</sub> ) <sub>2</sub> .6H <sub>2</sub> O	5	0.622	0.203
Na <sub>2</sub> Cr <sub>2</sub> O <sub>7</sub> .2H <sub>2</sub> O	5	0.807	0.198
NaCl	0.03	1.214	0.202
NaNO <sub>2</sub>	0.03	0.823	0.202
NH <sub>4</sub> NO <sub>3</sub>	0.03	0.802	0.204
Mg(NO <sub>3</sub> ) <sub>2</sub> .6H <sub>2</sub> O	0.03	0.828	0.214
Na <sub>2</sub> Cr <sub>2</sub> O <sub>7</sub> .2H <sub>2</sub> O	0.03	1.592	0.209

Table 6.7 – Mercury intrusion porosimetry results for hydrated cement paste after carbonation in various atmospheres

Sat. Salt Sol <sup>n</sup>	CO <sub>2</sub> Conc <sup>n</sup> (%)	Largest Peak Intensity (arbitrary units)				
		Calcite	Vaterite	Aragonite	Calcium Hydroxide	Anhydrite
NaCl	100	196	23	9	10	-
NaNO <sub>2</sub>	100	189	25	-	-	-
NH <sub>4</sub> NO <sub>3</sub>	100	198	29	-	-	-
Mg(NO <sub>3</sub> ) <sub>2</sub> .6H <sub>2</sub> O	100	180	22	15	-	-
Na <sub>2</sub> Cr <sub>2</sub> O <sub>7</sub> .2H <sub>2</sub> O	100	205	24	-	-	-
NaCl	5	180	24	-	-	-
NaNO <sub>2</sub>	5	182	8	-	-	10
NH <sub>4</sub> NO <sub>3</sub>	5	182	12	-	10	-
Mg(NO <sub>3</sub> ) <sub>2</sub> .6H <sub>2</sub> O	5	118	23	19	49	-
Na <sub>2</sub> Cr <sub>2</sub> O <sub>7</sub> .2H <sub>2</sub> O	5	149	23	15	28	-
NaCl	0.03	65	23	34	75	11
NaNO <sub>2</sub>	0.03	104	24	32	37	12
NH <sub>4</sub> NO <sub>3</sub>	0.03	131	18	25	28	11
Mg(NO <sub>3</sub> ) <sub>2</sub> .6H <sub>2</sub> O	0.03	49	27	45	59	16
Na <sub>2</sub> Cr <sub>2</sub> O <sub>7</sub> .2H <sub>2</sub> O	0.03	68	28	36	40	-

Table 6.8 – XRD results for hydrated cement paste after carbonation in various atmospheres

Sat. Salt Sol <sup>n</sup>	CO <sub>2</sub> Conc <sup>n</sup> (%)	TG Mass Loss (%)		
		Ettringite/CSH (50-250°C)	Calcium Hydroxide (450-550°C)	Calcium Carbonate (700-850°C)
NaCl	100	5.2	1.7	12.3
NaNO <sub>2</sub>	100	5.6	2.0	12.0
NH <sub>4</sub> NO <sub>3</sub>	100	5.2	1.9	11.5
Mg(NO <sub>3</sub> ) <sub>2</sub> .6H <sub>2</sub> O	100	5.5	1.8	11.9
Na <sub>2</sub> Cr <sub>2</sub> O <sub>7</sub> .2H <sub>2</sub> O	100	6.0	1.9	12.2
NaCl	5	8.1	2.1	9.7
NaNO <sub>2</sub>	5	8.7	2.0	9.6
NH <sub>4</sub> NO <sub>3</sub>	5	7.3	2.0	9.2
Mg(NO <sub>3</sub> ) <sub>2</sub> .6H <sub>2</sub> O	5	6.7	3.0	9.7
Na <sub>2</sub> Cr <sub>2</sub> O <sub>7</sub> .2H <sub>2</sub> O	5	7.4	2.3	9.5
NaCl	0.03	6.7	2.9	11.4
NaNO <sub>2</sub>	0.03	6.8	2.7	10.4
NH <sub>4</sub> NO <sub>3</sub>	0.03	6.9	3.0	10.4
Mg(NO <sub>3</sub> ) <sub>2</sub> .6H <sub>2</sub> O	0.03	6.5	2.4	12.3
Na <sub>2</sub> Cr <sub>2</sub> O <sub>7</sub> .2H <sub>2</sub> O	0.03	6.5	2.4	12.3

Table 6.9 – TG mass loss results for hydrated cement paste after carbonation in various atmospheres

Figure 6.1 – Experimental set-up used for the carbonation of cement pastes

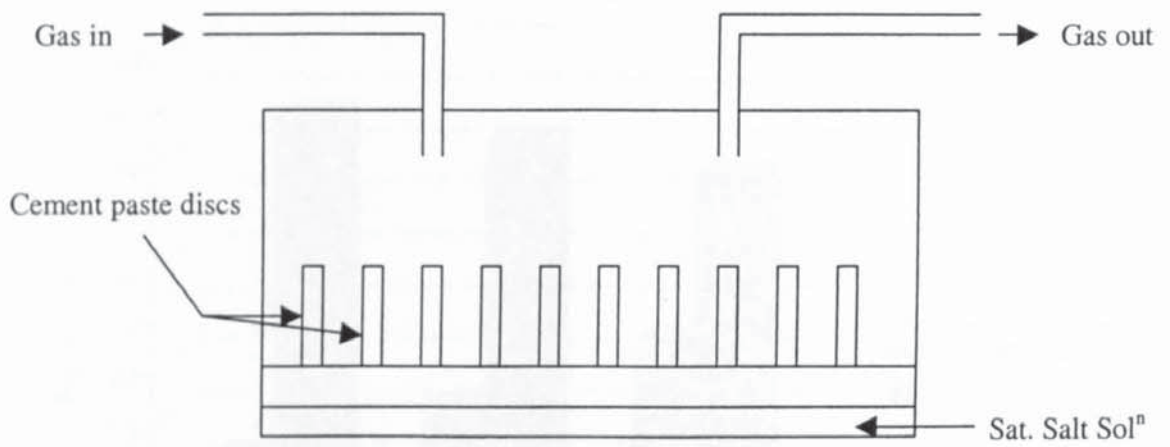


Figure 6.2 - Water desorption results for hydrated cement paste carbonated over saturated solutions of sodium chloride with various carbon dioxide concentrations

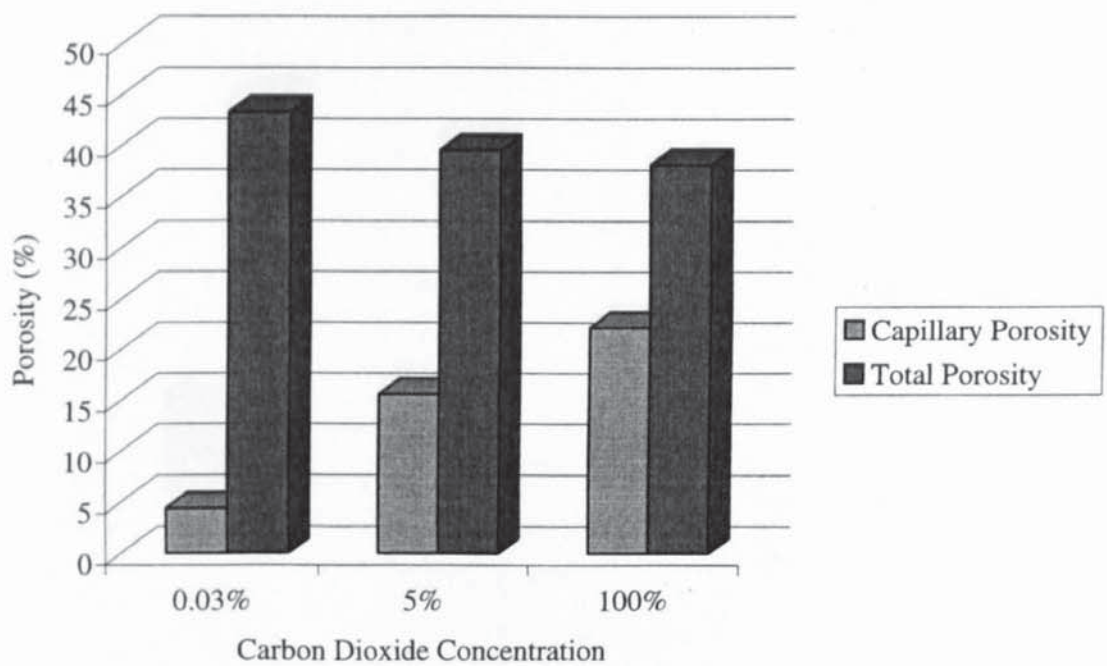




Figure 6.3 - Water desorption results for hydrated cement paste carbonated over saturated solutions of sodium nitrite with various carbon dioxide concentrations

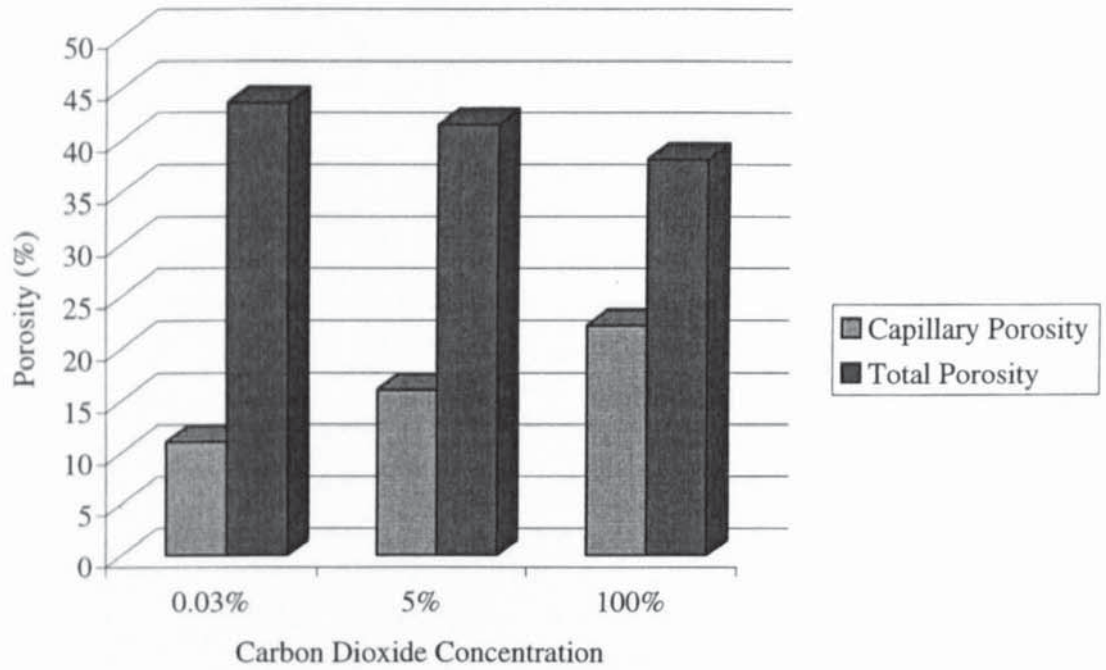


Figure 6.4 - Water desorption results for hydrated cement paste carbonated over saturated solutions of ammonium nitrate with various carbon dioxide concentrations

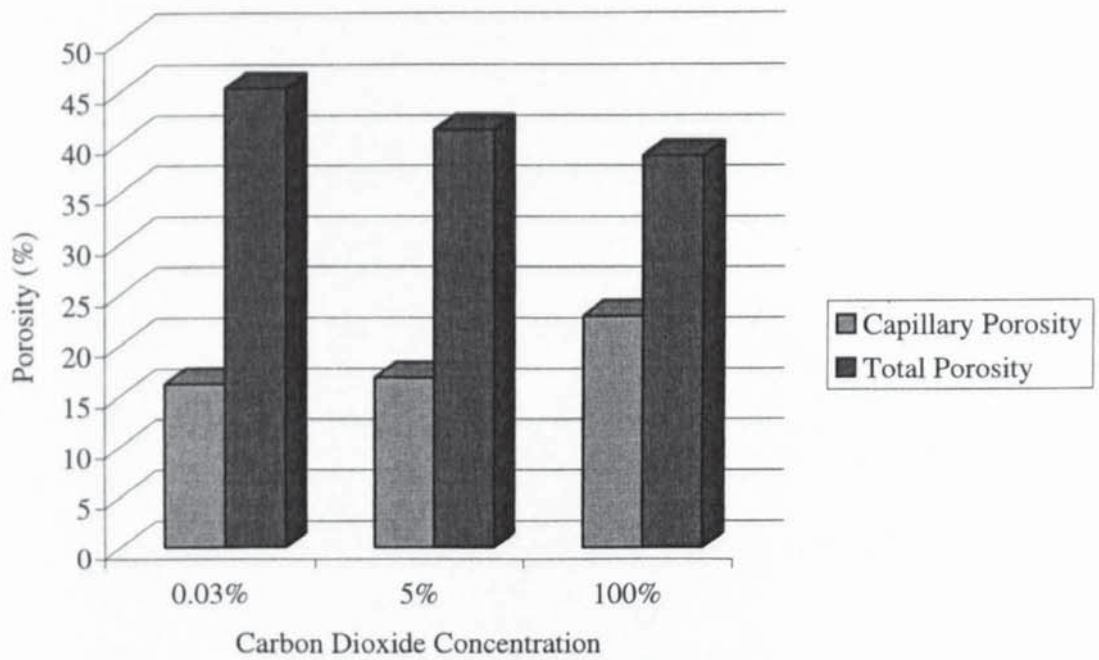


Figure 6.5 - Water desorption results for hydrated cement paste carbonated over saturated solutions of magnesium nitrate with various carbon dioxide concentrations

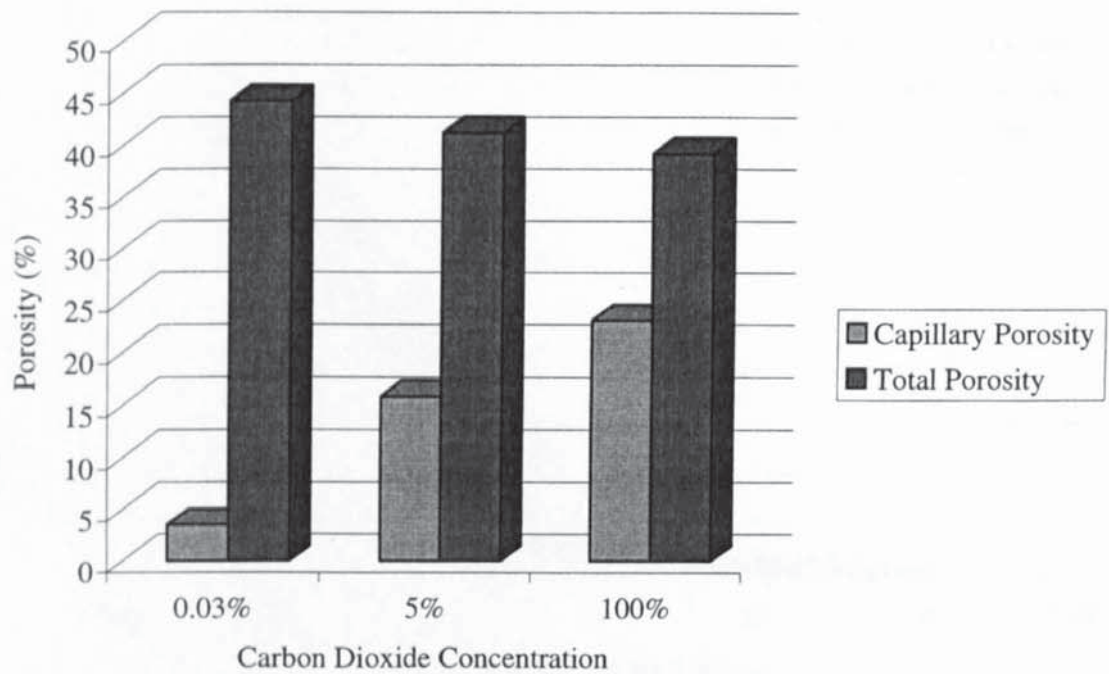


Figure 6.6 - Water desorption results for hydrated cement paste carbonated over saturated solutions of sodium dichromate with various carbon dioxide concentrations

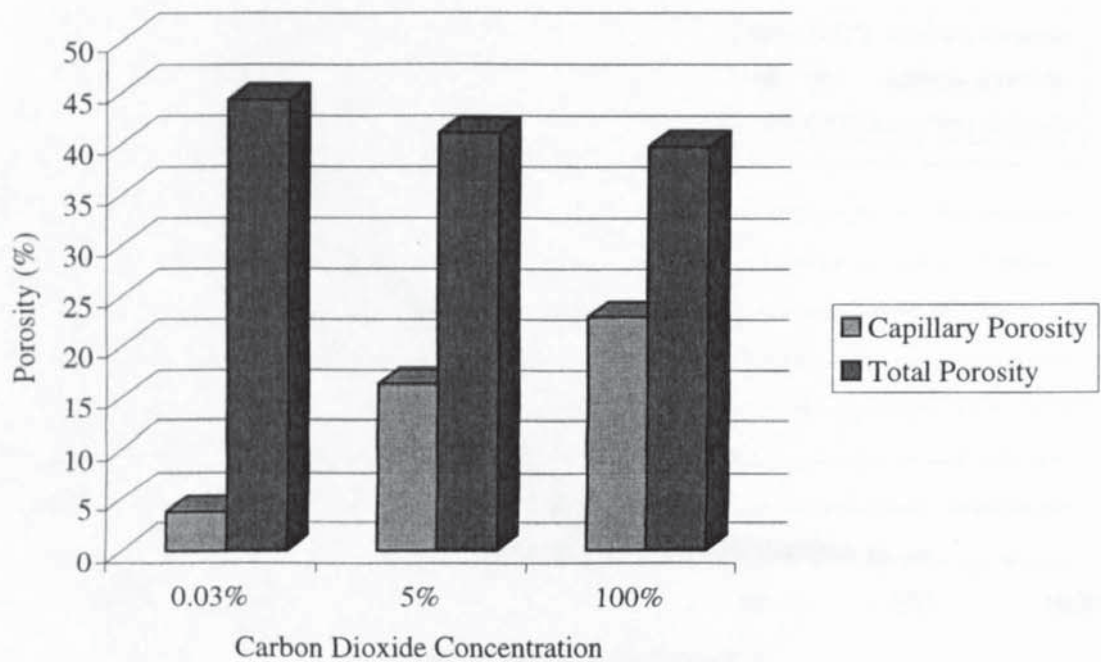


Figure 6.7 - Pore size distribution curves for hydrated cement pastes carbonated over saturated solutions of sodium chloride with various carbon dioxide concentrations

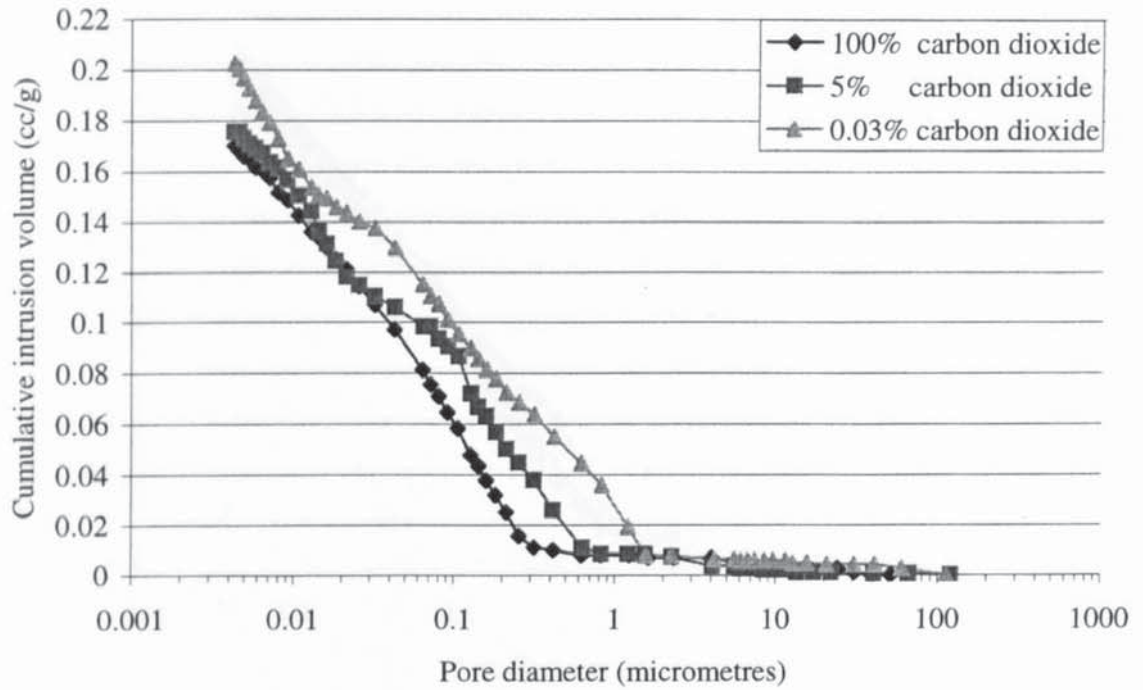


Figure 6.8 - Pore size distribution curves for hydrated cement pastes carbonated over saturated solutions of sodium nitrite with various carbon dioxide concentrations

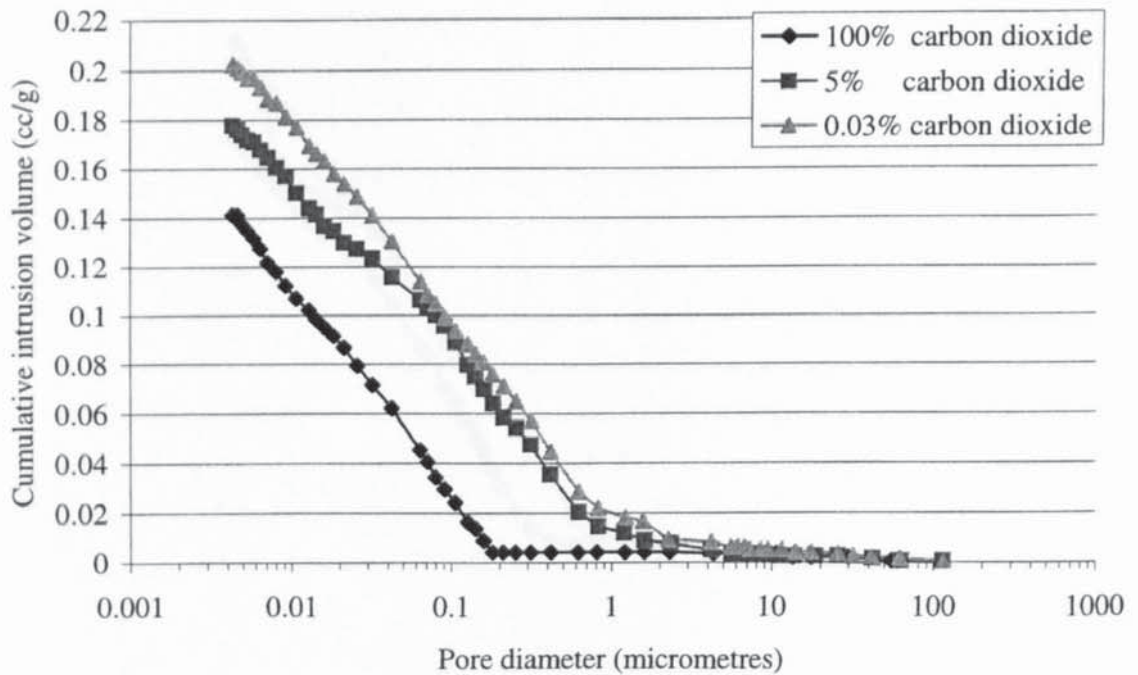




Figure 6.9 - Pore size distributions for hydrated cement pastes carbonated over saturated solutions of ammonium nitrate with various carbon dioxide concentrations

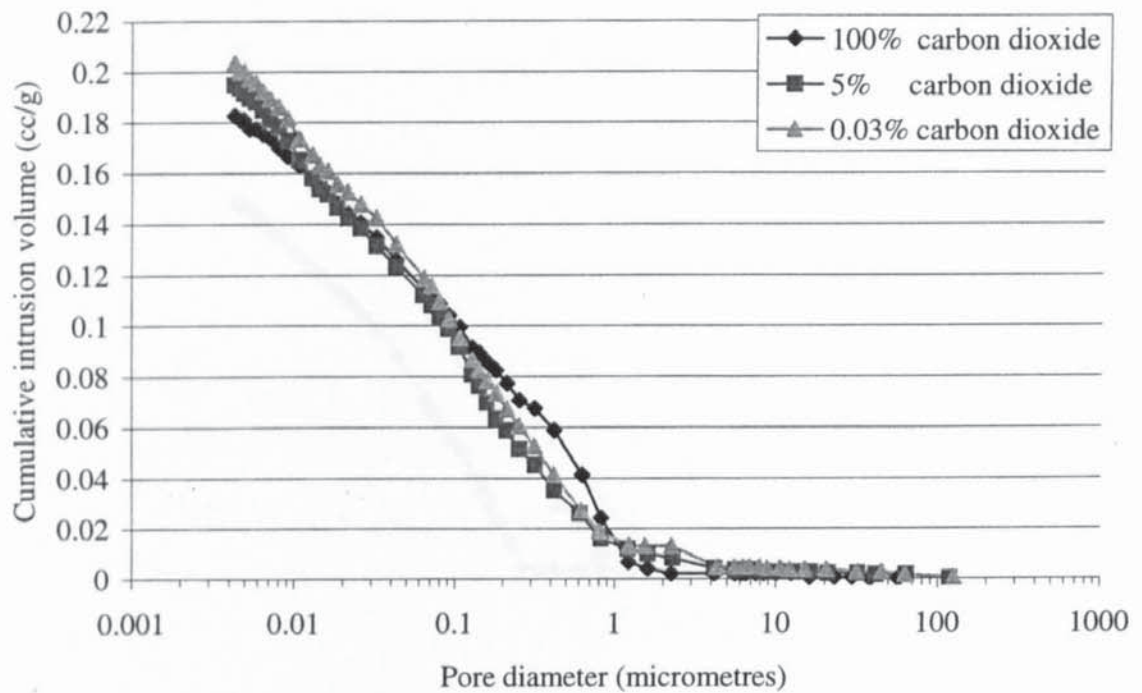


Figure 6.10 - Pore size distributions for hydrated cement pastes carbonated over saturated solutions of magnesium nitrate with various carbon dioxide concentrations

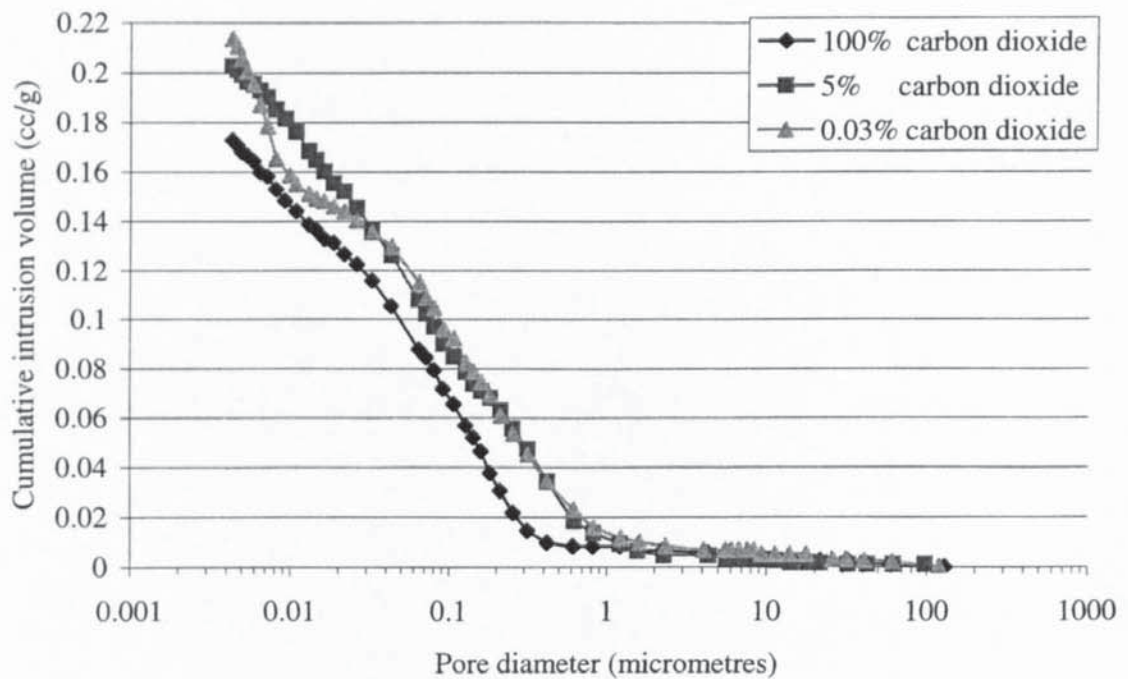


Figure 6.11 - Pore size distributions for hydrated cement pastes carbonated over saturated solutions of sodium dichromate with various carbon dioxide concentrations

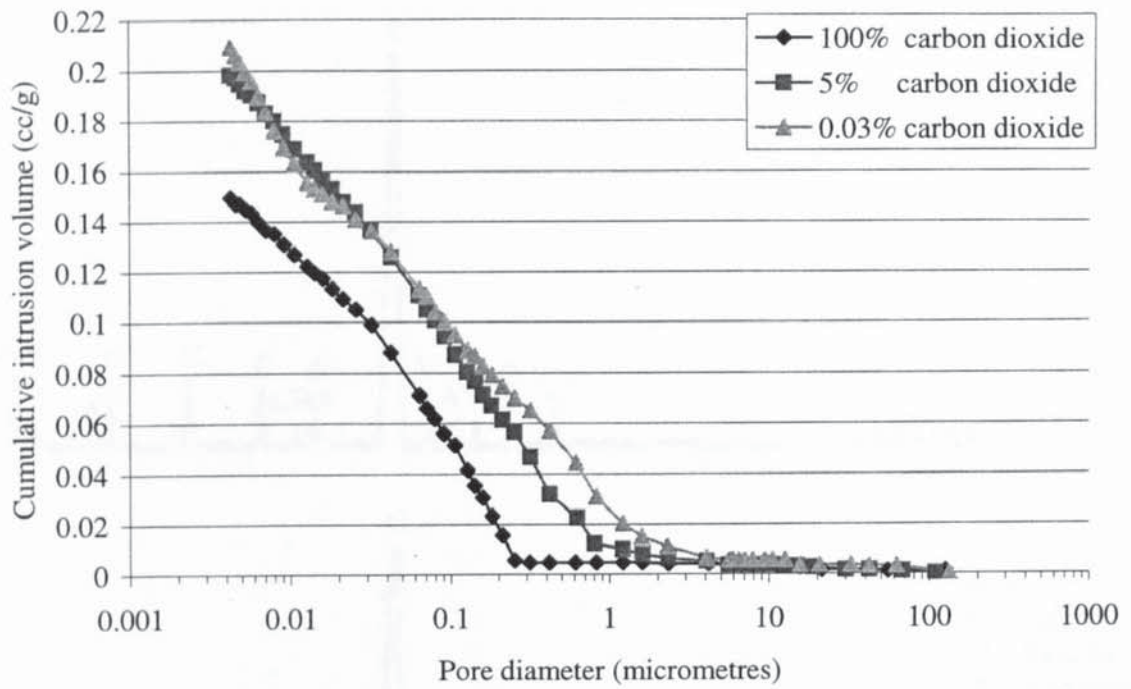


Figure 6.12 – XRD traces of hydrated cement paste carbonated over saturated solutions of sodium chloride with various concentrations of carbon dioxide

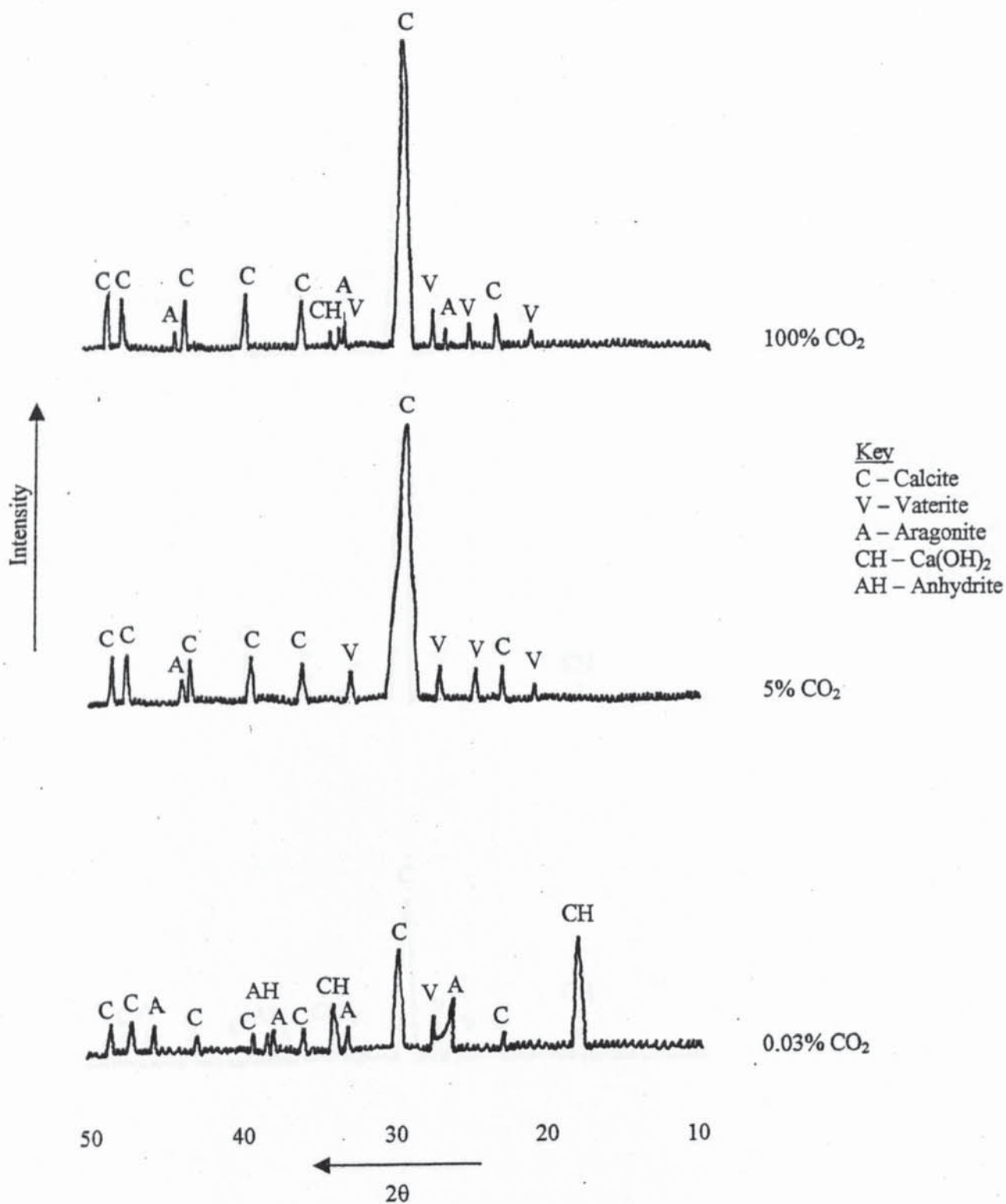




Figure 6.13 – XRD traces of hydrated cement paste carbonated over saturated solutions of sodium nitrite with various concentrations of carbon dioxide

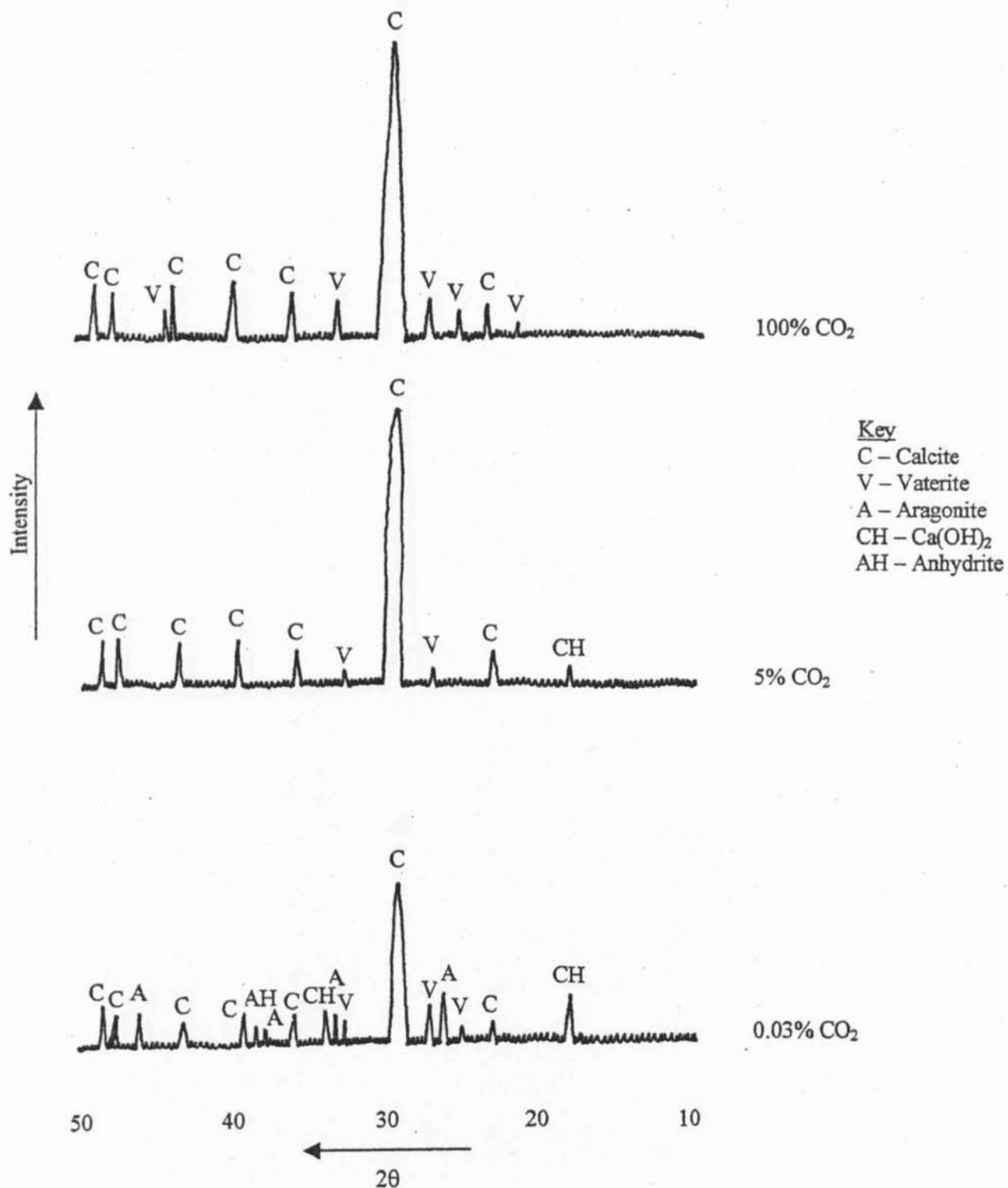


Figure 6.14 – XRD traces of hydrated cement paste carbonated over saturated solutions of ammonium nitrate with various concentrations of carbon dioxide

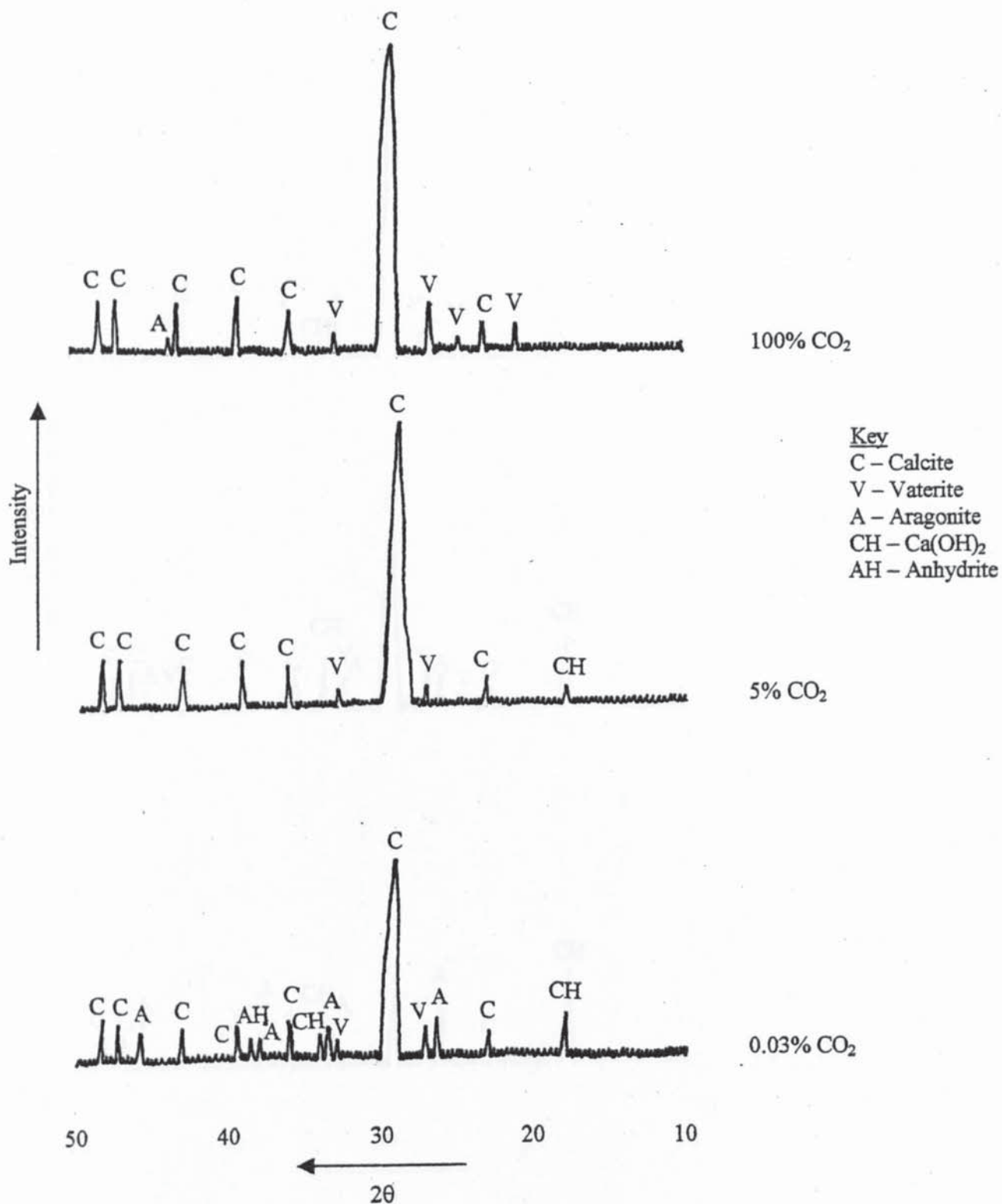


Figure 6.15 – XRD traces of hydrated cement paste carbonated over saturated solutions of magnesium nitrate with various concentrations of carbon dioxide

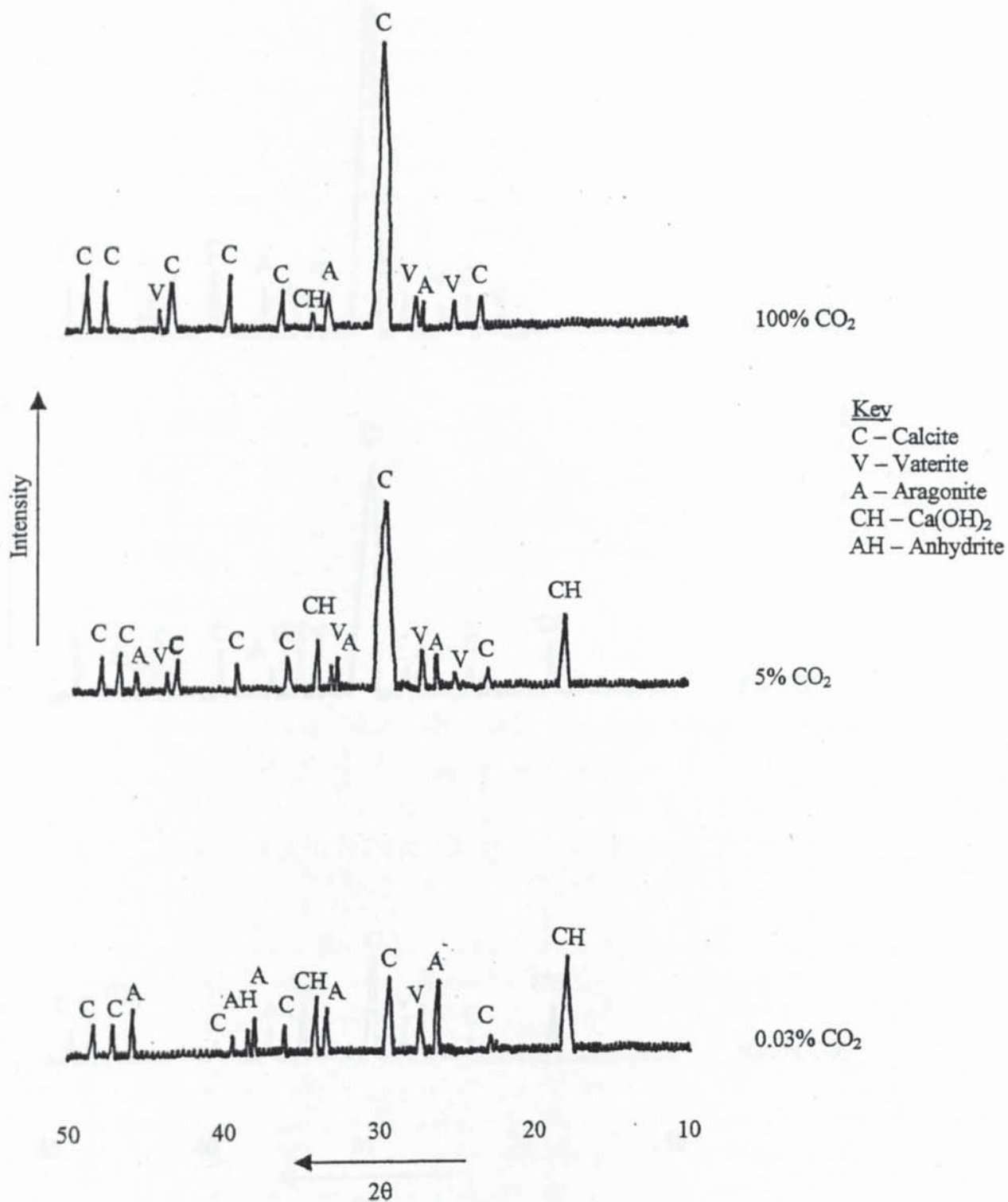




Figure 6.16 – XRD traces of hydrated cement paste carbonated over saturated solutions of sodium dichromate with various concentrations of carbon dioxide

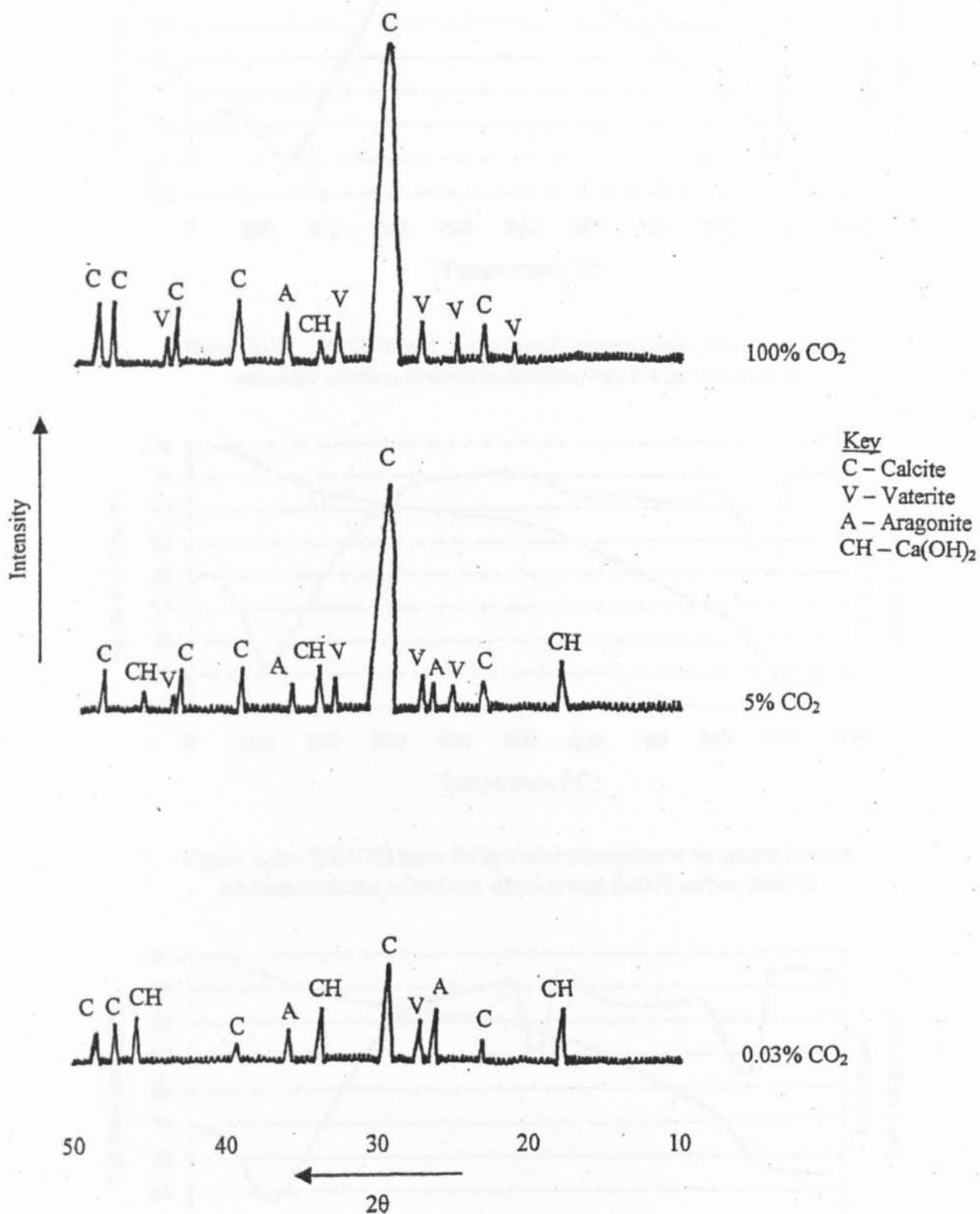


Figure 6.17 - DTA/TG trace for hydrated cement paste carbonated over a saturated solution of sodium chloride with 100% carbon dioxide

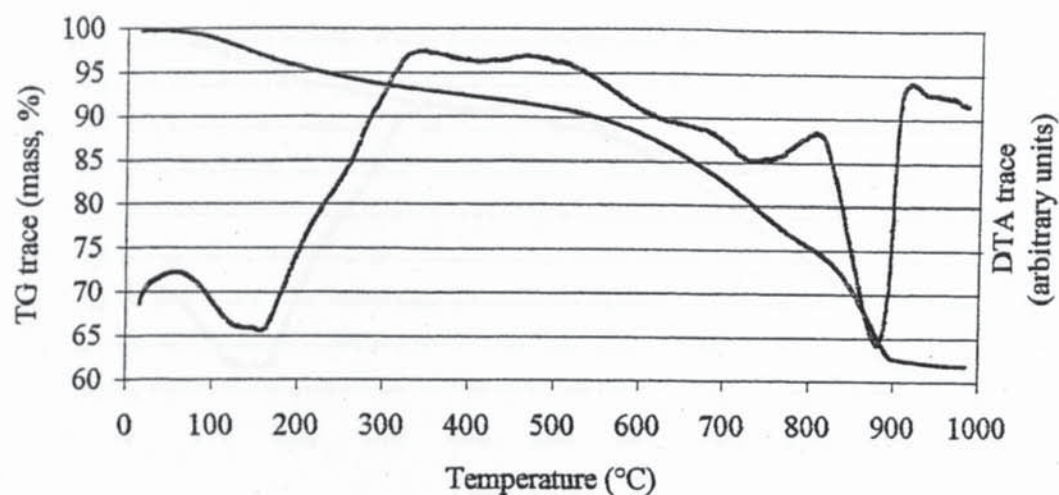


Figure 6.18 - DTA/TG trace for hydrated cement paste carbonated over a saturated solution of sodium chloride with 5% carbon dioxide

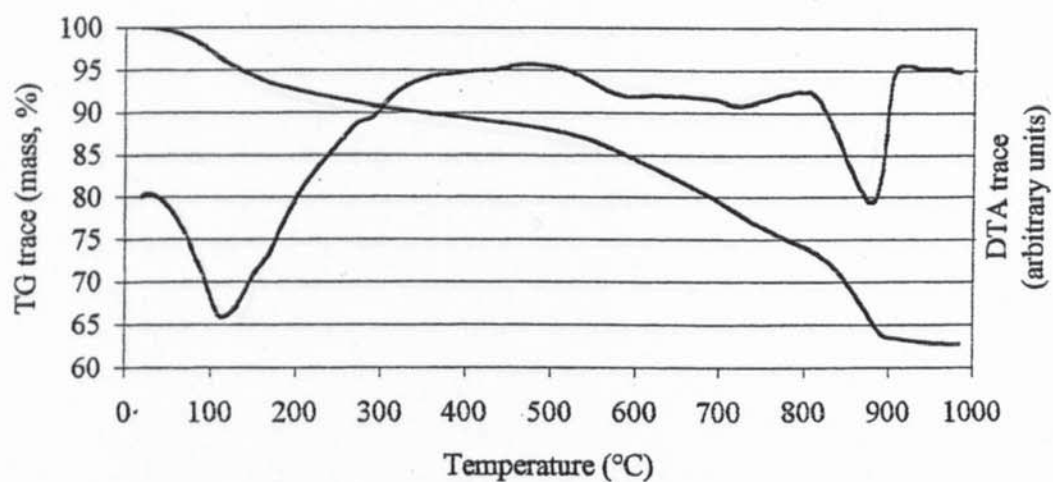


Figure 6.19 - DTA/TG trace for hydrated cement paste carbonated over a saturated solution of sodium chloride with 0.03% carbon dioxide

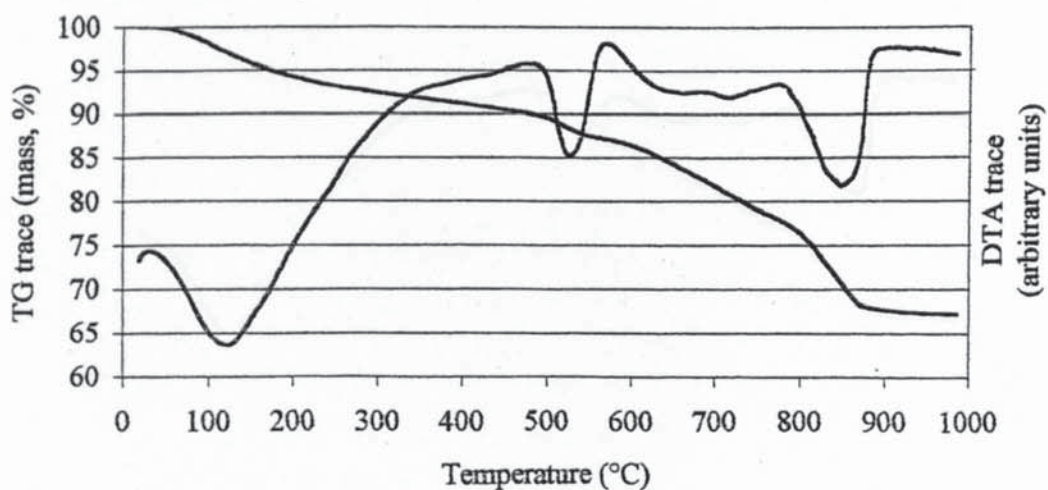


Figure 6.20 - DTA/TG trace for hydrated cement paste carbonated over a saturated solution of sodium nitrite with 100% carbon dioxide

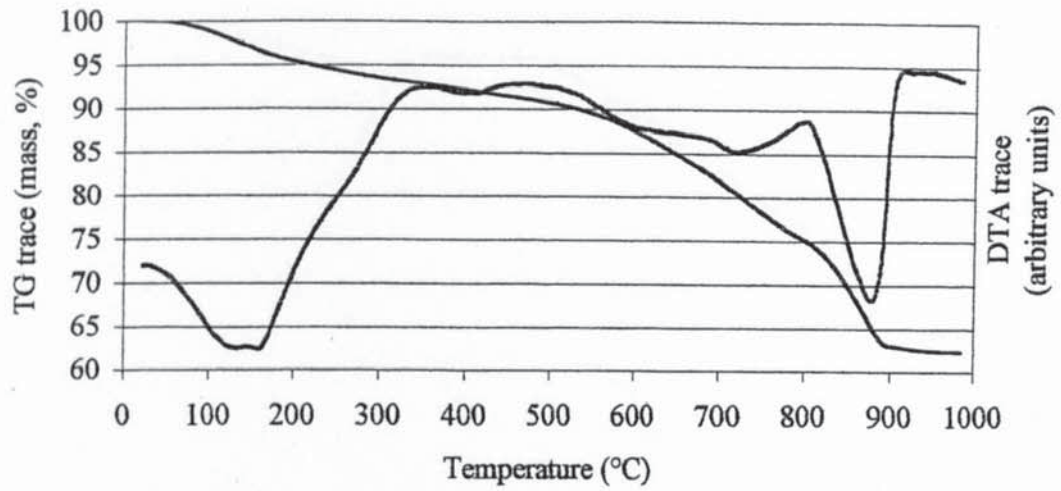


Figure 6.21 - DTA/TG trace for hydrated cement paste carbonated over a saturated solution of sodium nitrite with 5% carbon dioxide

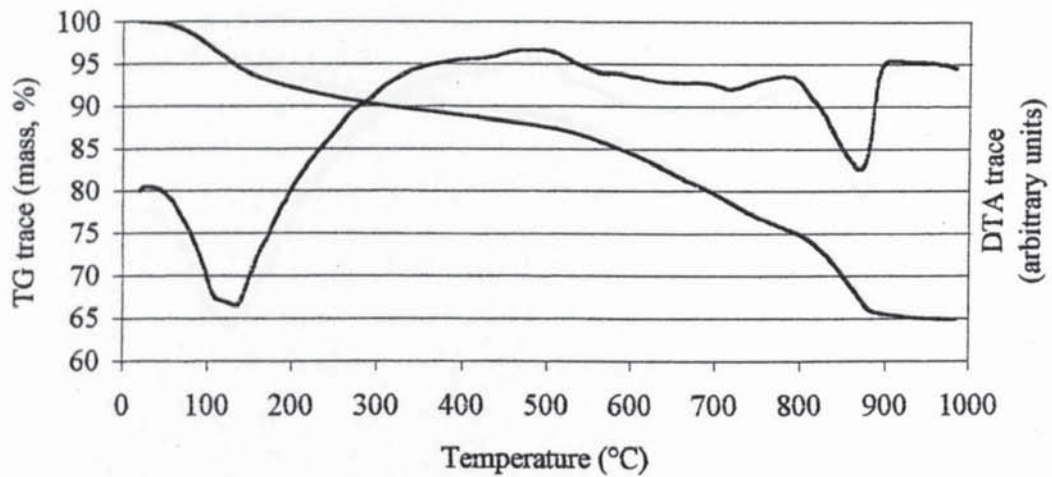


Figure 6.22 - DTA/TG trace for hydrated cement paste carbonated over a saturated solution of sodium nitrite with 0.03% carbon dioxide

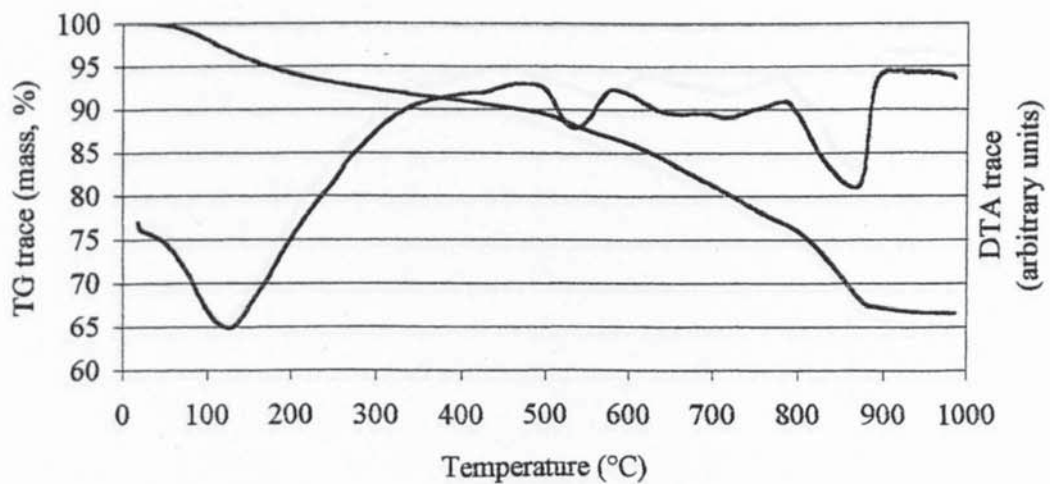




Figure 6.23 - DTA/TG trace for hydrated cement paste carbonated over a saturated solution of ammonium nitrate with 100% carbon dioxide

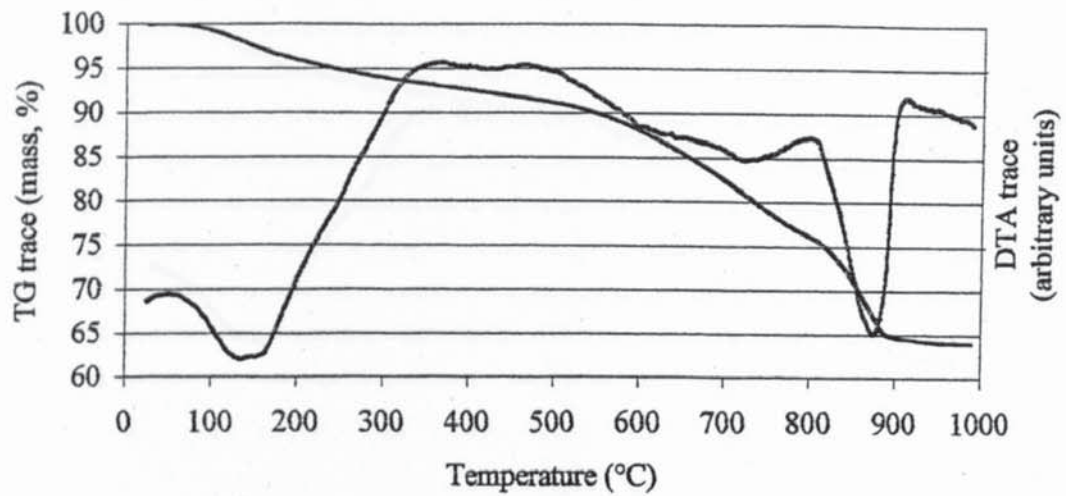


Figure 6.24 - DTA/TG trace for hydrated cement paste carbonated over a saturated solution of ammonium nitrate with 5% carbon dioxide

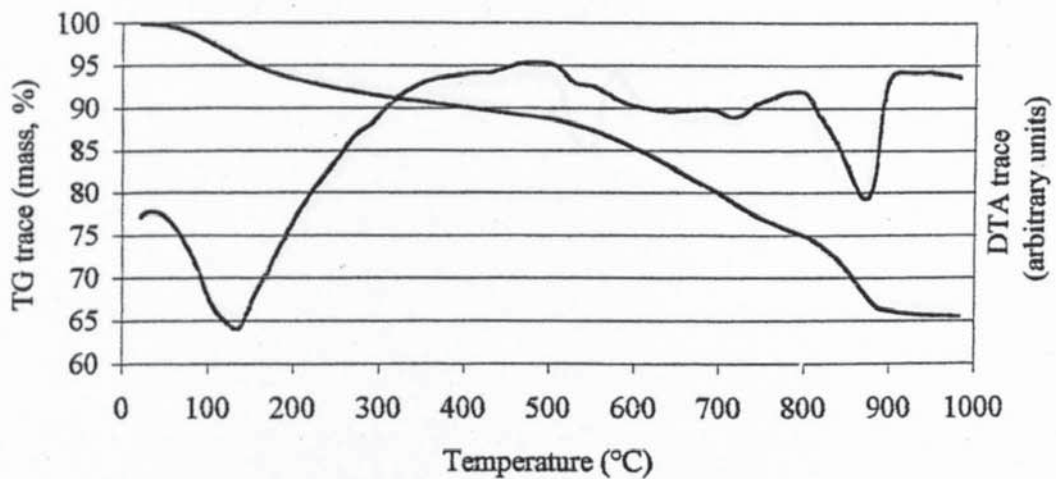


Figure 6.25 - DTA/TG trace for hydrated cement paste carbonated over a saturated solution of ammonium nitrate with 0.03% carbon dioxide

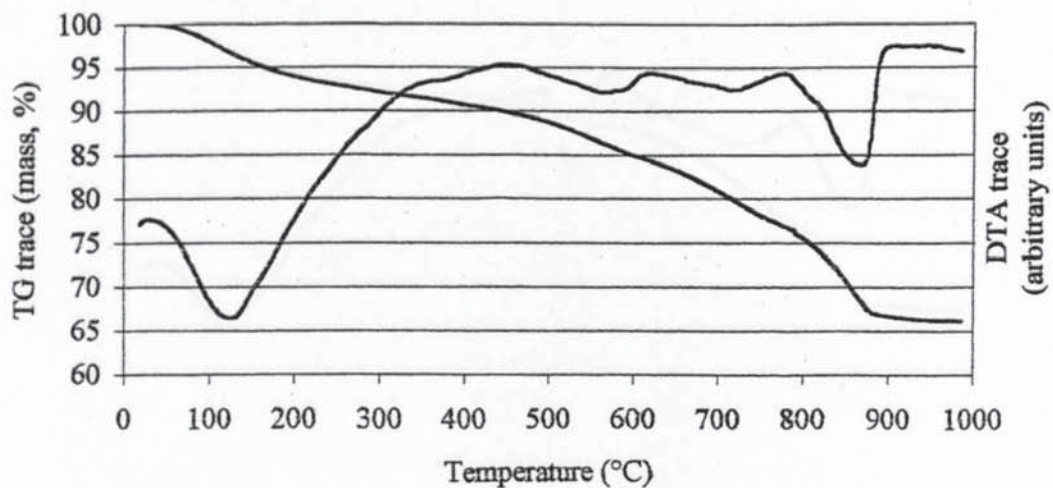


Figure 6.26 - DTA/TG trace for hydrated cement paste carbonated over a saturated solution of magnesium nitrate with 100% carbon dioxide

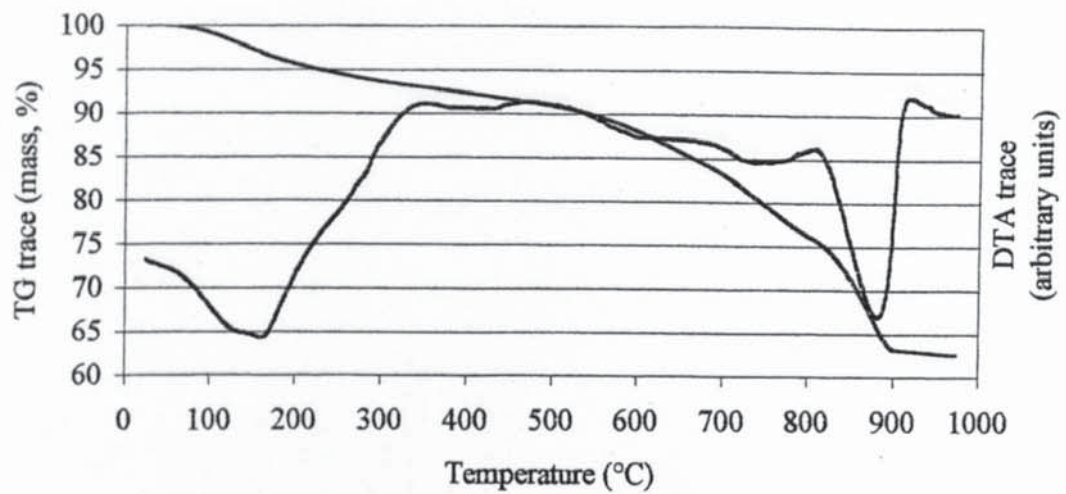


Figure 6.27 - DTA/TG trace for hydrated cement paste carbonated over a saturated solution of magnesium nitrate with 5% carbon dioxide

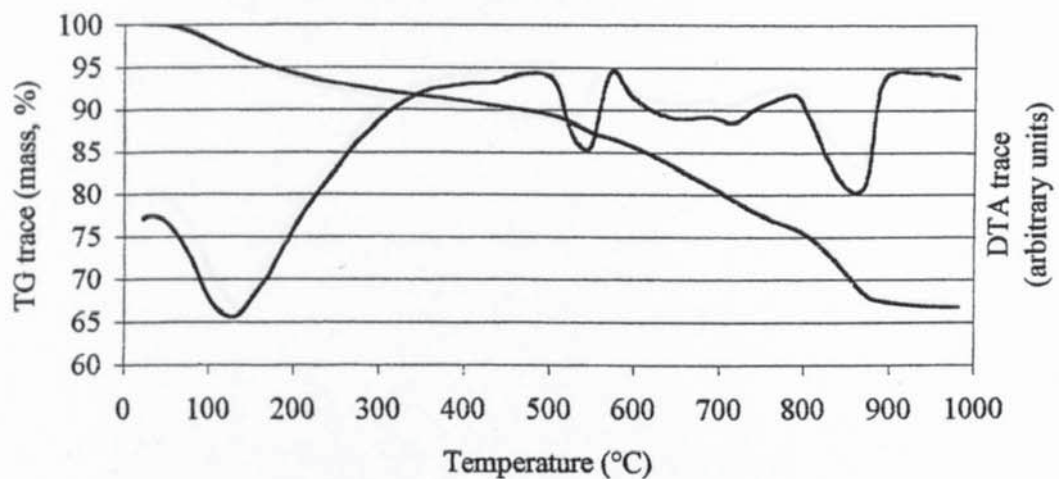


Figure 6.28 - DTA/TG trace for hydrated cement paste carbonated over a saturated solution of magnesium nitrate with 0.03% carbon dioxide

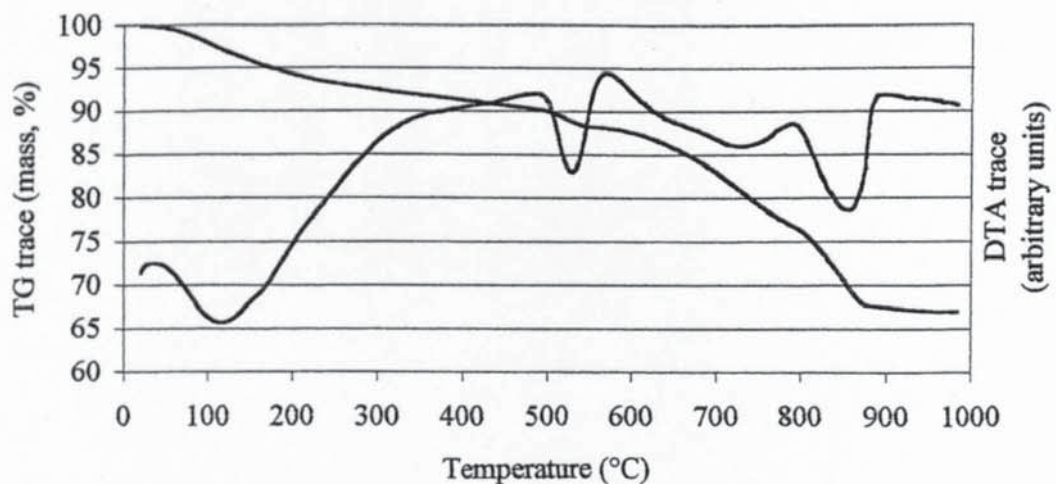




Figure 6.29 - DTA/TG trace for hydrated cement paste carbonated over a saturated solution of sodium dichromate with 100% carbon dioxide

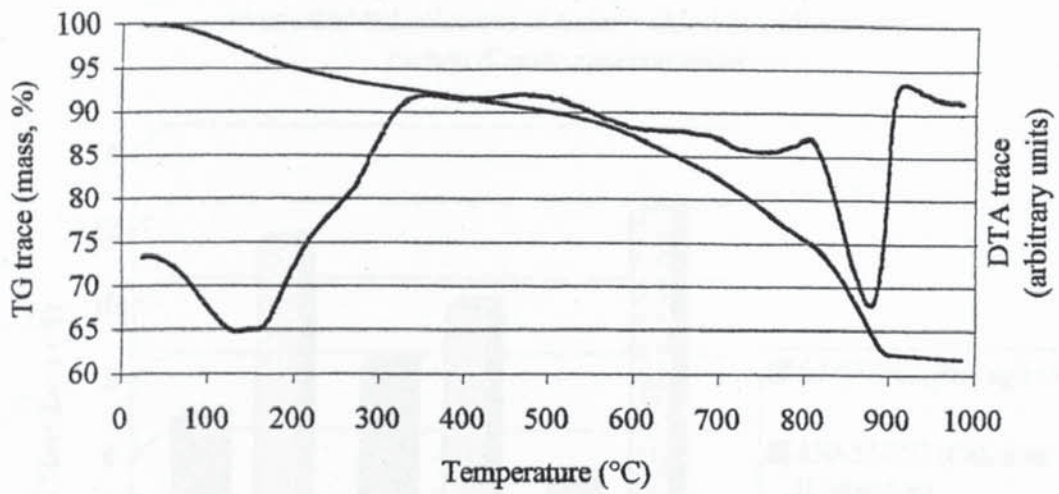


Figure 6.30 - DTA/TG trace for hydrated cement paste carbonated over a saturated solution of sodium dichromate with 5% carbon dioxide

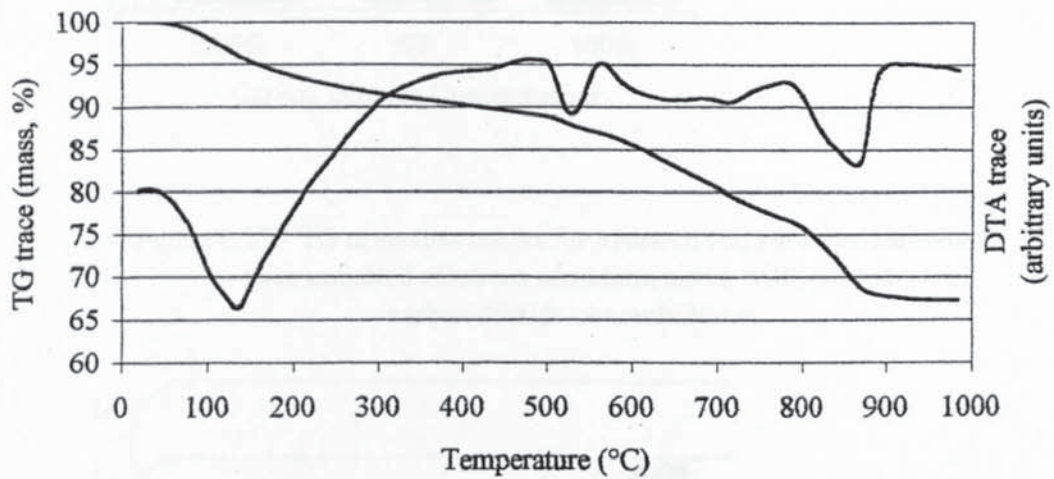


Figure 6.31 - DTA/TG trace for hydrated cement paste carbonated over a saturated solution of sodium dichromate with 0.03% carbon dioxide

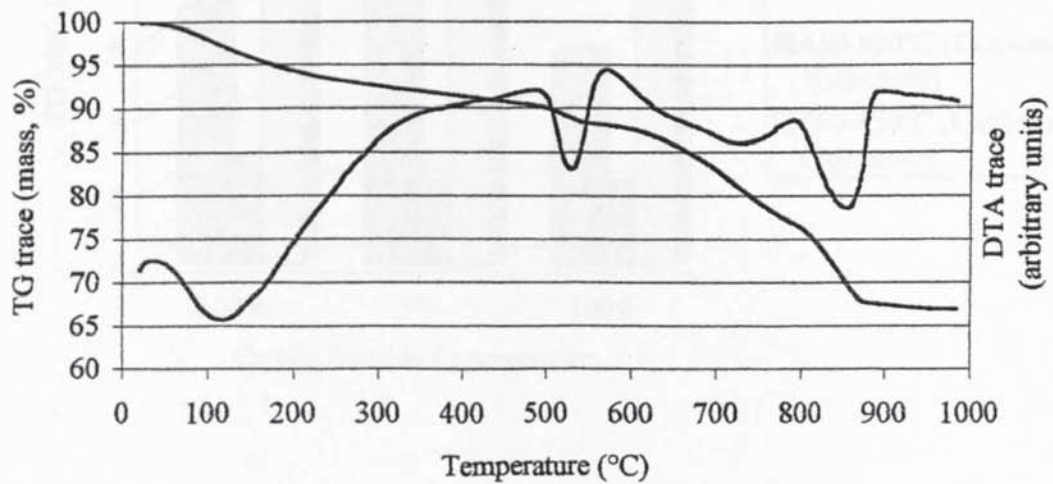




Figure 6.32 - TG mass loss results for hydrated cement paste carbonated over saturated solutions of sodium chloride with various carbon dioxide concentrations

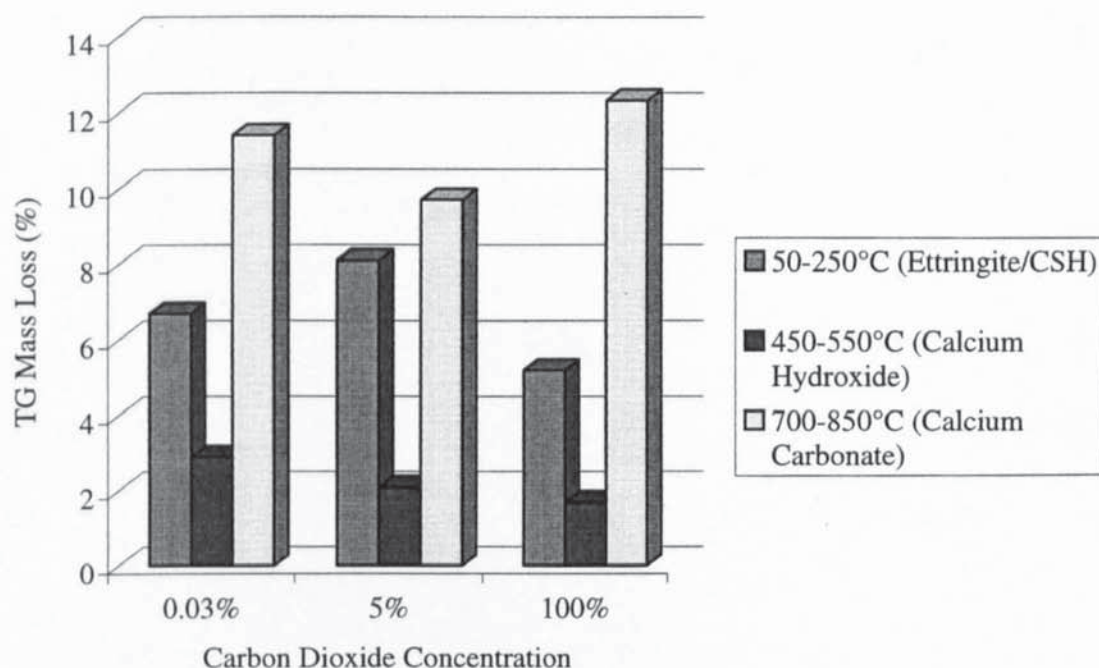


Figure 6.33 - TG mass loss results for hydrated cement paste carbonated over saturated solutions of sodium nitrite with various carbon dioxide concentrations

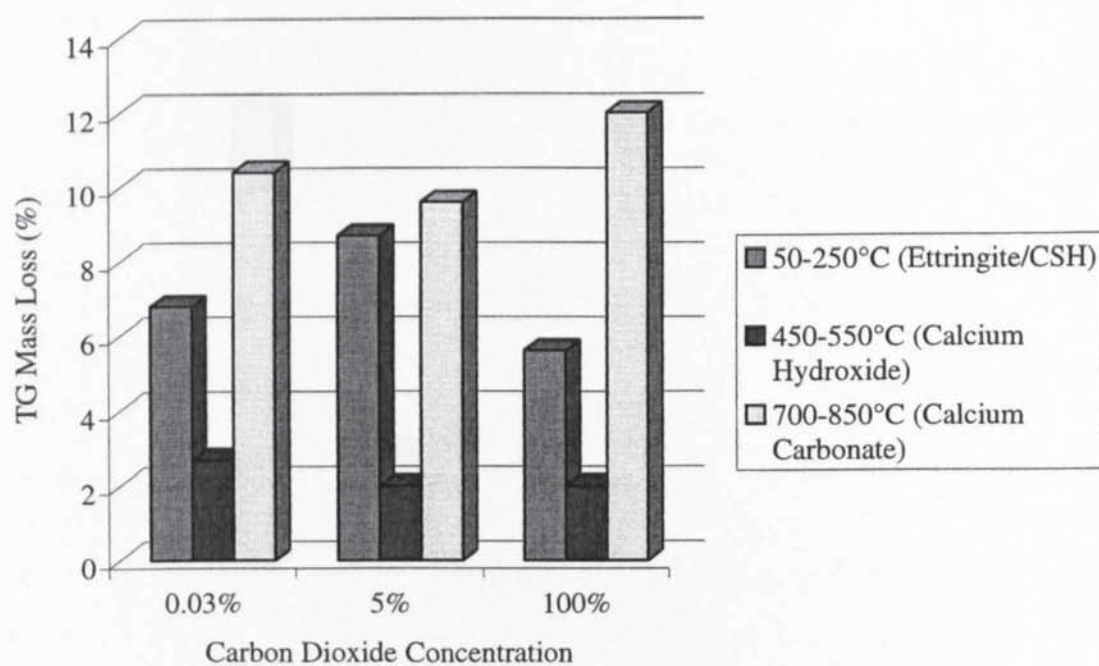


Figure 6.34 - TG mass loss results for hydrated cement paste carbonated over saturated solutions of ammonium nitrate with various carbon dioxide concentrations

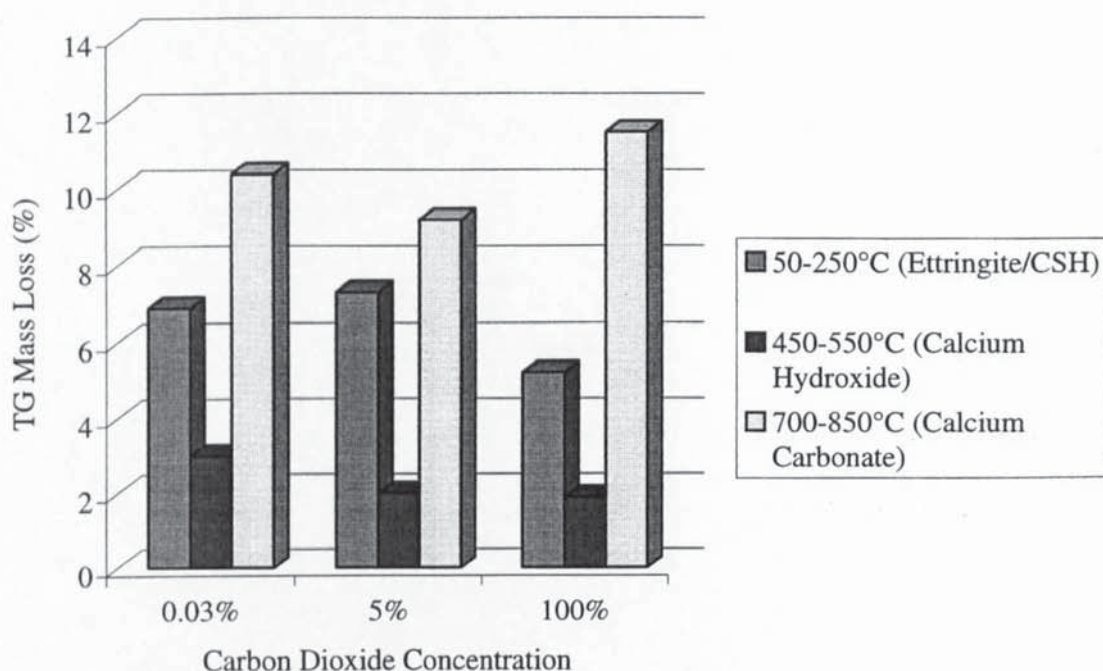


Figure 6.35 - TG mass loss results for hydrated cement paste carbonated over saturated solutions of magnesium nitrate with various carbon dioxide concentrations

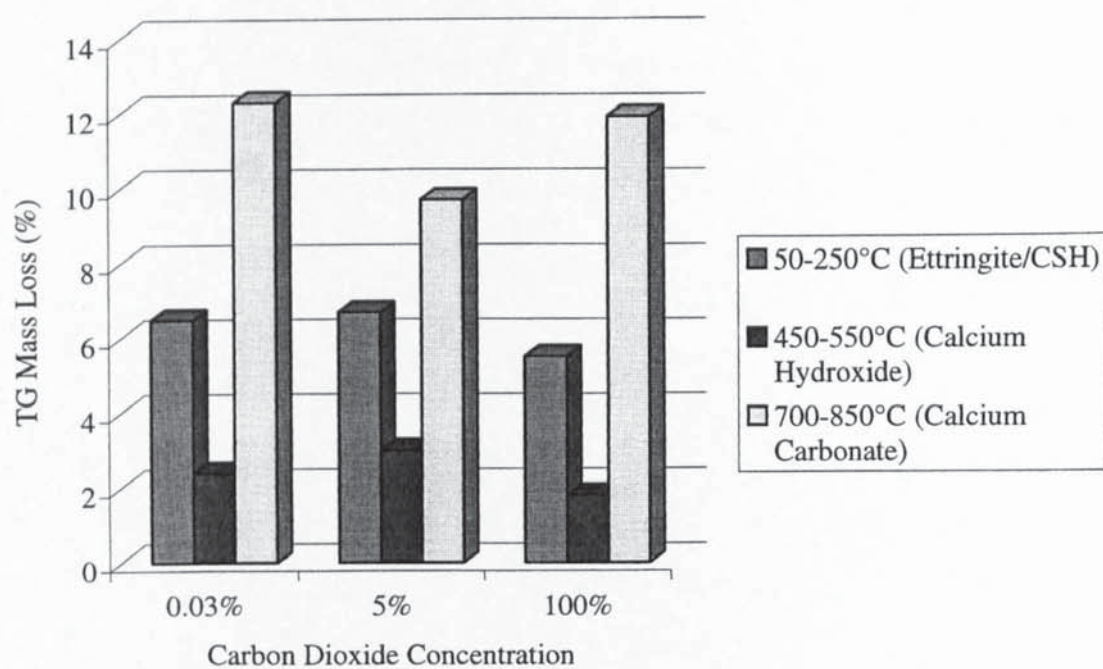
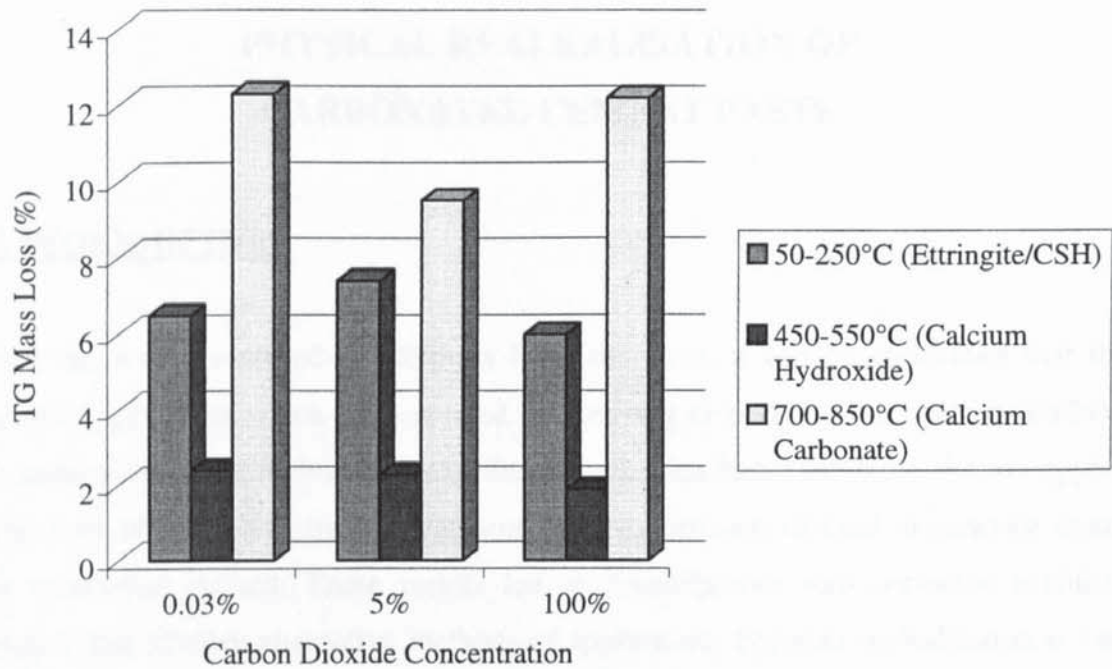


Figure 6.36 - TG mass loss results for hydrated cement paste carbonated over saturated solutions of sodium dichromate with various carbon dioxide concentrations





## **CHAPTER SEVEN**

### **PHYSICAL REALKALISATION OF CARBONATED CEMENT PASTE**

#### **7.1 INTRODUCTION**

From the work presented in Chapters Four and Five, it can be concluded that the corrosion inhibitors which were applied by spraying or ponding the concrete surface, i.e. sodium monofluorophosphate and the alkanolamine-based inhibitor, did not appear to be very effective as curative treatments for the corrosion of steel in concrete under the conditions studied. These results led to investigations into corrosion inhibitor systems that involve alternative methods of application. Physical realkalisation is one such system used for the rehabilitation of reinforcement corrosion in carbonated concrete. Physical realkalisation involves coating the surface of a structure with an alkaline cement-based coating, i.e. corrosion inhibition by hydroxyl ions. The inhibitor reservoir achieved by applying the cement-based overlay appears to offer a far more effective and durable rehabilitation option than simply spraying or ponding the inhibitor on to the surface of a structure. Physical realkalisation was introduced as a repair option on the basis of research by Bier, Kropp and Hilsdorf (1987) although, apart from work by Mattila and Pentti (1996), very little research has followed.

The objective of this chapter was to carry out laboratory investigations into physical realkalisation of saturated carbonated hydrated cement paste and to present a mathematical model to simulate the transport behaviour of hydroxyl ions in a saturated porous medium. This model was then applied to predict the increase in the pH of the pore solution of the cement pastes used in the laboratory investigations. The numerical results obtained from the model were then compared with the results obtained

experimentally. The effectiveness of physical realkalisation in relation to the rehabilitation of corrosion of steel in carbonated concrete was then discussed.

## **7.2 EXPERIMENTAL PROCEDURES**

### **7.2.1 Preparation of Cement Paste Specimens**

Three types of cement paste were required for this chapter, namely uncarbonated cement paste, carbonated cement paste and repair cement paste.

#### **7.2.1.1 Preparation of Uncarbonated Cement Paste Specimens**

The manufacture of the uncarbonated cement paste cylinders was carried out as described in section 3.3.1. All the uncarbonated cement paste cylinders were constructed with a water to cement ratio of 0.6. After de-moulding, the cylinders were placed within sealed containers containing de-ionised water. The specimens were placed in an upright position on purpose made platforms that supported them above the de-ionised water. The purpose of the de-ionised water was to create a curing environment of 100% relative humidity within the containers. The containers were then placed in a room, maintained at 20°C, for 14 days before being moved to another room, maintained at 38°C, for 28 days. Each cylinder was then finally cut at both ends, perpendicular to its longest axis using a mechanical hacksaw, to leave an uncarbonated cement paste cylinder of length 50mm and diameter 49mm. The cylinders were then placed above de-ionised water until sticking, as described in section 7.2.2.

#### **7.2.1.2 Preparation of Carbonated Cement Paste Specimens**

The initial manufacture of the carbonated cement paste cylinders was carried out as described in section 3.3.1. All the carbonated cement paste cylinders were constructed with a water to cement ratio of 0.6. After de-moulding, the cylinders were placed within sealed containers containing de-ionised water. The specimens were placed in an upright position on purpose made platforms that supported them above the de-ionised water. The purpose of the de-ionised water was to create a curing environment of 100%



relative humidity within the containers. The containers were placed in a room, maintained at 20°C, for 14 days before being moved to another room, maintained at 38°C, for 28 days. The cylinders were then placed within sealed containers containing a saturated solution of sodium nitrite. The specimens were placed in an upright position, on purpose made platforms that supported them above the sodium nitrite, and 100% carbon dioxide gas was pumped into the containers at a rate of 30 minutes per day. The purpose of the saturated solution of sodium nitrite was to create a carbonating atmosphere of 65% relative humidity within the containers, this being an optimum relative humidity for the carbonation reactions to occur. The nitrite contamination of the pore solution due to the carbonating environment, as discussed in Chapter Six, had no effect on the results obtained in this chapter as only the movements of hydroxyl ions were being investigated. The experimental set-up used to carbonate the cylinders is as shown in Figure 6.1. The cylinders were monitored for depth of carbonation, by using phenolphthalein as described in section 3.3.11, and all the cylinders were deemed to be carbonated when sample cylinders remained colourless after the phenolphthalein test. Following this, the cylinders remained at 65% relative humidity for two years to ensure full carbonation and to produce specimens of a reasonable age. Each cylinder was then cut at both ends, perpendicular to its longest axis using a mechanical hacksaw, to leave a cylinder of length 60mm and diameter 49mm which was, in turn, finally cut in half to leave two fully carbonated cylinders of length 30mm and diameter 49mm. The specimens were then vacuum saturated at a pressure below 0.1 bar with de-ionised water to constant weight. The specimens were then placed above de-ionised water until casting of the repair cement paste, as described in section 7.2.1.3.

#### 7.2.1.3 Preparation of Repair Cement Paste

As can be seen from Table 3.1, the sodium oxide equivalent ( $\text{Na}_2\text{O}_{\text{eq}}$ ) of the cement used throughout the present study is 0.6% by weight of cement according to equation 7.1.

$$\% \text{Na}_2\text{O}_{\text{eq}} = \% \text{Na}_2\text{O} + (0.659 \times \% \text{K}_2\text{O}) \quad (7.1)$$



Each repair cement paste was manufactured with one of two %Na<sub>2</sub>O<sub>eq</sub> concentrations, i.e. 0.6% and 1.2%. The additional 0.6% Na<sub>2</sub>O<sub>eq</sub> required for the repair cement pastes containing 1.2% Na<sub>2</sub>O<sub>eq</sub> by weight of cement was achieved by adding a calculated amount of sodium hydroxide (NaOH) to the mix water and allowing it to dissolve. Also two thicknesses of repair cement paste were chosen for investigation, i.e. 10mm and 20mm.

The cement was sieved through a 150µm mesh in order to remove coarse particles. The required proportion of the cement was weighed and de-ionised water (containing dissolved NaOH for the 1.2% Na<sub>2</sub>O<sub>eq</sub> pastes) was added to the mix to produce a paste of water to cement ratio equal to 0.4. The mixture was blended thoroughly by hand for about 5 minutes with a spatula. The mixture was then poured into formwork fitted on top of the carbonated cement paste. This was vibrated for 2-4 minutes to get rid of any trapped air bubbles. On at least two occasions, the foamy layer that had accumulated on the surface was removed and replaced with fresh paste. Following this, each specimen was left to cure in an upright position for 24 hours in air at 20°C and this was followed by removal of the formwork. All specimens were then set-up in their respective experimental exposure environments.

### **7.2.2 Final Set-Up**

Twelve different set-ups were investigated, as is shown in Figures 7.1 – 7.12, with three specimens per set-up. The uncarbonated cement paste was joined to the carbonated cement paste, where required, by producing a cement paste slurry of 0.6 w/c which was spread onto the surfaces requiring sticking. These surfaces were then joined, taking great care not to trap any air bubbles, thus ensuring electrical continuity. This sticking procedure was carried out within 24 hours of the casting of the repair cement paste. The specimens stored above the de-ionised water (set-ups 1, 2, 3, 5, 7, 8, 9 and 11) were intended to simulate physical realkalisation in an environment of 100% relative humidity where surface leaching would be kept to a minimum, i.e. in a situation on site

where a surface coating would be applied to the repair material. The 100% relative humidity environment was adopted in order that the pores within the specimens remained saturated. The specimens which were placed in an upright position with the repair paste 'cast face' immersed to a maximum depth of 2mm in de-ionised water (set-ups 4, 6, 10 and 12), were intended to simulate physical realkalisation in an environment of 100% relative humidity where surface leaching was apparent. It was decided to simulate surface leaching by actually placing the cast surfaces of the samples in de-ionised water as this was a situation that could be mathematically modelled, as described in section 7.3. The volume and surface area of the de-ionised water was large compared with the cast surface and it was replaced twice weekly in order to avoid excessive changes in its hydroxyl ion concentration during the experiments.

### **7.2.3 Pore Solution Analysis**

The specimens were removed from the exposure environments 120 days after casting of the repair pastes. Each specimen was cut into 10mm discs, starting from the cast face. The three 10mm discs (as all specimens were produced in triplicate) corresponding to each segment of each experimental set-up then had their pore solution expressed using the method described in section 3.3.3. The extracted pore solution was analysed for hydroxyl ions by acid titration, as described in section 3.3.12, with a 1.0ml sample of pore solution and 0.001M nitric acid. The hydroxyl ion concentration was then used to calculate the pH of the pore solution, as described in section 3.3.12. m

## **7.3 MATHEMATICAL MODELLING**

### **7.3.1 Governing Equations**

#### **7.3.1.1 Flux**

It was assumed in the present study that the flux was determined by Fick's first law of diffusion (Crank, 1975), therefore



$$J = - D \frac{\partial C}{\partial x} \quad (7.2)$$

where  $J$  is the flux of diffusing substance i.e. hydroxyl ions ( $\text{mmol}/\text{cm}^2/\text{s}$ ),  $D$  the diffusion coefficient ( $\text{cm}^2/\text{s}$ ),  $C$  the concentration of diffusing substance in the pore solution ( $\text{mmol}/\text{l}$ ), and  $x$  the space coordinate measured normal to the cast face. The negative sign arises because diffusion occurs in the direction opposite to that of increasing concentration.

#### 7.3.1.2 Differential Equation of Diffusion

It was assumed in the present study that diffusion is unidirectional, i.e. that there is a gradient of concentration only along the  $x$ -axis (normal to the cast face), and that  $D$  is different for each of the three types of hydrated cement paste. Therefore for an ion that does not bind or desorb from the cement matrix, the rate of change of concentration of diffusing substance, with respect to time, within the pore solution ( $\partial C/\partial t$ ) may be derived (Crank, 1975) from Fick's first law to become

$$\frac{\partial C}{\partial t} = \frac{\partial}{\partial x} \left( D \frac{\partial C}{\partial x} \right) \quad (7.3)$$

#### 7.3.1.3 Ionic Binding

It is assumed in the present study that hydroxyl ions can be bound on to the pore surfaces within the cement matrix and that this binding is not permanent. Therefore, hydroxyl ions will be released again if the concentration is lowered as there is a balance between bound and free concentrations. In the present study it was assumed that the relationship between the bound and free hydroxyl ion concentrations could be approximated by the Langmuir adsorption isotherm as expressed by

$$S = \frac{\alpha C}{1 + \beta C} \quad (7.4)$$

where  $S$  is the quantity of bound ions ( $\text{mmol}/\text{g}$  of cement), and  $\alpha$  and  $\beta$  ( $\text{mmol}/\text{l}$ )<sup>-1</sup> are constants. It is, of course, not suggested that the assumptions from which the Langmuir



adsorption isotherm is theoretically derived (Glasstone and Lewis, 1960) will apply in the present study.

Therefore, the rate of change of concentration of bound hydroxyl ions, with respect to time, in the cement matrix ( $\partial S/\partial t$ ) may be derived as follows

$$\frac{\partial S}{\partial t} = \frac{\partial S}{\partial C} \cdot \frac{\partial C}{\partial t} \quad (7.5)$$

$$\frac{\partial S}{\partial t} = \frac{\partial C}{\partial t} \left[ \frac{\alpha(1 + \beta C) - \beta \alpha C}{(1 + \beta C)^2} \right] \quad (7.6)$$

$$\frac{\partial S}{\partial t} = \frac{\partial C}{\partial t} \left[ \frac{\alpha + \alpha \beta C - \alpha \beta C}{(1 + \beta C)^2} \right] \quad (7.7)$$

$$\frac{\partial S}{\partial t} = \frac{\partial C}{\partial t} \left[ \frac{\alpha}{(1 + \beta C)^2} \right] \quad (7.8)$$

#### 7.3.1.4 Mass Conservation

For the present study, which considers unidirectional diffusion and a diffusion coefficient that varies with the type of cement paste, mass conservation may be expressed by

$$\frac{\partial C}{\partial t} + \frac{1}{w} \frac{\partial S}{\partial t} = \frac{\partial}{\partial x} \left( D \frac{\partial C}{\partial x} \right) \quad (7.9)$$

where  $w$  is the content of water in which diffusion occurs, expressed per unit weight of cement.

#### **7.3.1.5 Ionic Concentration Profile**

It therefore follows from the equations describing flux, ionic binding and mass conservation that the concentration profile of hydroxyl ions in the pore solution will be governed by

$$\frac{\partial C}{\partial t} \left[ 1 + \frac{\alpha}{w (1 + \beta C)^2} \right] = \frac{\partial}{\partial x} \left( D \frac{\partial C}{\partial x} \right) \quad (7.10)$$

#### **7.3.2 Assumptions**

Apart from the assumptions made in section 7.3.1, several other assumptions were made in order to carry out the mathematical modelling. First, it was assumed that the initial concentrations of hydroxyl ions within the pore solutions of the 1.2% Na<sub>2</sub>O<sub>eq</sub> repair paste, 0.6% Na<sub>2</sub>O<sub>eq</sub> repair paste, carbonated paste and uncarbonated paste were 850, 500, 0 and 300 mmol/l, respectively. It was also assumed that no hydroxyl ions had leached out of the specimens apart from those that did so through the cast face of the specimens that were set up to simulate surface leaching. The content of water in which diffusion occurs (*w*), expressed per unit weight of cement, was assumed to be 0.3. In reality, *w* would have varied between the different types of cement paste. It was also assumed that the pores remained saturated throughout the duration of the experiments. Surface leaching on a specimen was simulated by assuming that its cast face was in constant contact, over its entire surface area, with a solution whose hydroxyl ion concentration remained at 0.004mmol/l throughout the duration of the experiment.

#### **7.3.3 Computer Simulation**

Initial values of the hydroxyl ion concentrations within the pore solution and assumed diffusion coefficients for the 1.2% Na<sub>2</sub>O<sub>eq</sub> repair paste, 0.6% Na<sub>2</sub>O<sub>eq</sub> repair paste, carbonated paste and uncarbonated paste were substituted into equation (7.10) along with assumed values of  $\alpha$  and  $\beta$ . The numerically determined hydroxyl ion concentration profiles within the pore solution, after 120 days, were obtained using the Backward-Time Centred-Space finite difference method (Hoffman, 1997) to solve

equation 7.10. The combination of assumed diffusion coefficients and assumed values of  $\alpha$  and  $\beta$  that produced numerically obtained concentration profiles, within the pore solutions of the various set-ups, which best-fitted (using the least-squares criterion (Stroud, 1995)) the experimental profiles was then achieved. In order to carry out the enormous number of calculations, required to achieve the best-fit combination of assumed diffusion coefficients and assumed values of  $\alpha$  and  $\beta$ , a computer program was written in Matlab programming language and is provided in Appendix G.

## **7.4 DISCUSSION OF RESULTS**

### **7.4.1 Experimental Results**

The initial experimentally determined hydroxyl ion concentrations within the pore solutions of the various cement pastes are shown in Table 7.1. The experimentally determined hydroxyl ion concentration profiles within the pore solution after 120 days are shown in Tables 7.2 and 7.3. The graphs of pH versus depth from the cast face are shown in Figures 7.13 to 7.24 and these correspond to the set-ups shown in Figures 7.1 to 7.12. The 'depth from cast face' values shown in Tables 7.2 and 7.3 and Figures 7.13 to 7.24 represent the distance to the centre of each disc from the cast face.

For the present study it was assumed that a hydroxyl ion concentration of 1.0mmol/l (pH 11) indicates realkalisation. It can be seen from the results that hardened carbonated cement paste can be realkalised to a limited extent due to the diffusion of hydroxyl ions under saturated conditions. This is in agreement with previous work by Bier, Kropp and Hilsdorf (1987) and Mattila and Pentti (1996). It can be seen from the results for set-ups 1,3 and 4 that a 30mm thick hardened carbonated cement paste layer can be realkalised. However, hydroxyl ion concentrations remained below 5mmol/l within the pore solution of the realkalised cement paste in all the set-ups investigated. Whether the extent of realkalisation provided is sufficient to repassivate actively corroding steel



depends on many other factors such as chloride levels and the durability of physical realkalisation.

It can be clearly seen when comparing Table 7.1 with Tables 7.2 and 7.3 that the quantities of hydroxyl ions lost from the pore solution of the repair and uncarbonated cement paste are greater than those present within the pore solution of the initially carbonated cement paste. This indicates that a substantial proportion of the hydroxyl ions, which diffused into the carbonated cement paste, became bound into the cement matrix.

It can be seen from Tables 7.2 and 7.3 that the realkalisation process was more efficient in the set-ups that employed repair pastes with 1.2%  $\text{Na}_2\text{O}_{\text{eq}}$ . It is also evident that the cement paste is realkalised to a limited extent from both the direction of the repair cement paste and the direction of the uncarbonated cement paste. The realkalisation process appears to be slightly more efficient from the direction of the uncarbonated paste than from the direction of the repair paste, which is in agreement with Mattila and Pentti (1996). It can be seen from Table 7.2 that, even with a 10mm thick 1.2%  $\text{Na}_2\text{O}_{\text{eq}}$  repair coating, limited realkalisation is evident when uncarbonated cement paste is also present. However, the results also indicate that the repair coating alone is not adequate to realkalise, even to a limited extent, the entire carbonated zone within the timescale investigated.

Caution is advised when raising the % $\text{Na}_2\text{O}_{\text{eq}}$  levels within the repair cement paste as concrete can deteriorate as a result of the interaction between alkaline pore fluids and the reactive minerals in certain types of aggregates. The mechanism of deterioration is known as alkali-aggregate reaction. The most common form of alkali-aggregate reaction is alkali-silica reaction, which results in the formation of a calcium alkali silicate gel that imbibes water producing a volume expansion which can disrupt the concrete. Three conditions are necessary for alkali-silica reaction to occur; a sufficiently alkaline solution in the pore structure of the concrete, an aggregate or aggregate combination

susceptible to attack by this alkaline solution and a sufficient supply of water (Sibbeck, Blackwell and Nixon, 1999). With this in mind, Lithium Hydroxide could be investigated in future work as an alternative way of raising the levels of hydroxyl ions in the pore solution as lithium compounds have shown a low propensity to expand (Sakaguchi et al., 1989).

The results presented in Table 7.3 suggest that even with a repair thickness of 20mm, the 0.6%  $\text{Na}_2\text{O}_{\text{eq}}$  cement paste generally fails to provide any significant increase in the hydroxyl ion concentration within the pore solution.

It is also apparent from the experimental results that surface leaching significantly reduces the hydroxyl ion concentration within the pore solution of the repair cement pastes. Therefore, surface leaching will lead to a significant decrease in the durability of this type of repair.

#### **7.4.2 Mathematical Modelling**

It may be seen from Figures 7.13 to 7.24 that the numerical profiles, obtained using equation 7.10, show a very good fit to the experimentally determined profiles. Therefore, the mathematical model could be used in further work to investigate the long term effectiveness and durability of physical realkalisation.

The modelling process has enabled the present study to establish a better understanding of the mechanisms taking place during physical realkalisation. The assumed diffusion coefficients of the different types of cement paste and the assumed values of  $\alpha$  and  $\beta$  that, when combined, produced the best-fit profiles to the experimental data are shown in Tables 7.4 and 7.5, respectively. Table 7.4 shows that the assumed diffusion coefficient, required to obtain the best-fit profiles to the experimental data, for hydroxyl ions in the carbonated cement paste is significantly higher than the corresponding values for the uncarbonated and repair pastes. This may be due to several reasons such



as the associated increase in capillary porosity due to carbonation as reported by Page and Ngala (1995). Chapter Six of the present study showed that the increase in capillary porosity due to carbonation is more pronounced in pastes that have been carbonated in an atmosphere of 100% carbon dioxide, when compared to pastes that have been carbonated in air. The increased diffusivity of hydroxyl ions in carbonated cement paste could also be due to the actions of the co-diffusing cations such as sodium, calcium and potassium. It is possible that, in carbonated cement paste, the interactions that are believed to exist between diffusing ions and the pore walls of uncarbonated cement paste do not exist, thus enabling the co-diffusing cations to diffuse more quickly (Sergi, 1986). Table 7.4 shows that the assumed diffusion coefficient in the repair cement paste, required to obtain the best-fit profiles to the experimental data, was approximately three times lower than that assumed for the uncarbonated cement paste. This is due to the differences in porosity that are associated with a cement paste of water to cement ratio 0.4 when compared to a cement paste with a water to cement ratio of 0.6.

The assumed values of the constants  $\alpha$  and  $\beta$  that gave best-fit data to the experimental profiles, i.e.  $\alpha = 150$  and  $\beta = 0.04 \text{ (mmol/l)}^{-1}$ , are important parameters that give an insight into the mechanisms that are taking place during realkalisation. The value of  $\alpha$  suggests that for every 1mmol that is present within the pore solution there have been 150mmol bound into the cement matrix. This suggests that although realkalisation appears to be a limited process, when considering the pore solution only, it actually is a process by which the cement matrix is building its own reservoir of hydroxyl ions which may act as a buffer if the concentration within the pore solution was to be lowered once more. From the work presented in Chapter Six of the present study it can be seen that very little calcium, sodium or potassium exists in the pore solution of carbonated cement paste. Therefore, it appears that the co-diffusing cations will also build a reservoir within the cement matrix as the pH rises. It can therefore be suggested that the co-diffusing cations are adsorbed into the cement matrix at the same rate as the



hydroxyl ions. This would therefore satisfy the condition of electroneutrality within the pore solution and requires further investigation.

The value of  $\beta$  is very important as  $1/\beta$ , i.e. 25mmol/l, gives an indication of the concentration of hydroxyl ions within the pore solution which, when reached and surpassed, corresponds to  $\partial S/\partial t = 0$ . This implies that no hydroxyl ions entering the previously carbonated cement paste will be bound within the solid cement matrix when  $C > 25\text{mmol/l}$ . Therefore, although physical realkalisation appears to be a limited process, it is suggested that it is a durable process as the cement matrix will be able to buffer the pore solution as re-carbonation proceeds. This is in disagreement with Mattila and Pentti (1996) who suggested that realkalisation occurs through the pore solution of concrete and therefore reserves can not easily develop within the realkalised concrete. However, there is also a relatively thick repair cement paste of low water to cement ratio that the carbonation front must penetrate before it can reach the realkalised zone and thus cause re-carbonation. It is suggested that this repair cement paste layer is very important in terms of the durability of physical realkalisation. In agreement with the experimental results, it was found by numerical modelling that surface leaching significantly reduces the hydroxyl ion concentration within the pore solution of the repair cement pastes. In order to limit the effects of surface leaching a coating is recommended for the repair cement paste.

## **7.5 CONCLUSIONS**

Hardened carbonated cement paste can be realkalised to a limited extent due to the diffusion of hydroxyl ions under saturated conditions.

The quantities of hydroxyl ions lost from the pore solution of the repair and uncarbonated cement paste are greater than those present within the pore solution of the initially carbonated cement paste. This indicates that a substantial proportion of the

hydroxyl ions that diffused into the carbonated cement paste became bound into the cement matrix.

The realkalisation process is more efficient when repair pastes containing 1.2%  $\text{Na}_2\text{O}_{\text{eq}}$  are employed rather than those containing 0.6%  $\text{Na}_2\text{O}_{\text{eq}}$ . It is also evident that the cement paste is realkalised to a limited extent from both the direction of the repair cement paste and from the direction of the uncarbonated cement paste. The realkalisation process appears slightly more efficient from the direction of the uncarbonated paste than from the direction of the repair paste. However, hydroxyl ion concentrations remained below 5mmol/l in the pore solution of the realkalised cement paste in all the set-ups investigated.

The results also indicate that, within the timescale investigated, the repair coating alone is not adequate to realkalise the entire 30mm thick carbonated zone, even to a limited extent. This may have implications for the realkalisation process on fully carbonated cladding panels, which have no uncarbonated zone.

Surface leaching significantly reduces the hydroxyl ion concentration within the pore solution of the repair cement pastes. Therefore, surface leaching will lead to a significant decrease in the durability of this type of repair option.

The mathematical model described provides predictions of hydroxyl ion profiles in very good accord with experimental values for carbonated hardened cement paste subjected to physical realkalisation. Therefore, the model could be employed in further investigations.

Type of cement paste	Pore solution hydroxyl ion concentration (mmol/l)
1.2% Na <sub>2</sub> O <sub>eq</sub> repair cement paste	853
0.6% Na <sub>2</sub> O <sub>eq</sub> repair cement paste	514
Carbonated cement paste	0
Uncarbonated cement paste	307

Table 7.1 – Experimentally determined initial hydroxyl ion concentrations

Depth from cast face (mm)	Hydroxyl ion concentration within pore solution (mmol/l)					
	Set-up 1	Set-up 2	Set-up 3	Set-up 4	Set-up 5	Set-up 6
5	231	231	488	240	488	185
15	1.5	0.2	300	195	300	195
25	1.3	0.1	1.5	1.5	1.2	1.5
35	4.7	0.1	1.3	1.3	0.8	1.0
45	156		2.5	2.4	0.5	0.7
55	227		172	127		
65	252		245	190		
75	266		281	225		
85	270		287	246		
95			287	246		

Table 7.2 - Experimentally determined pore solution hydroxyl ion profiles for set-ups 1 to 6



Depth from cast face (mm)	Hydroxyl ion concentration within pore solution (mmol/l)					
	Set-up 7	Set-up 8	Set-up 9	Set-up 10	Set-up 11	Set-up 12
5	167	167	272	117	272	91
15	0.4	0.2	180	113	180	111
25	0.1	0.1	1.0	0.6	0.5	1.2
35	1.7	0.1	0.3	0.2	0.4	0.9
45	136		1.4	1.6	0.1	0.6
55	212		151	116		
65	248		225	172		
75	264		259	219		
85	264		269	237		
95			269	239		

Table 7.3 - Experimentally determined pore solution hydroxyl ion profiles for set-ups 7 to 12

Type of cement paste	Hydroxyl ion diffusion coefficient (cm <sup>2</sup> /s)
Repair cement paste	$1.3 \times 10^{-7}$
Carbonated cement paste	$1.4 \times 10^{-5}$
Uncarbonated cement paste	$4.5 \times 10^{-7}$

Table 7.4 - Assumed hydroxyl ion diffusion coefficients that gave best-fit data

Constant	
$\alpha$	150
$\beta$	$0.04 \text{ (mmol/l)}^{-1}$

Table 7.5 – Assumed constants for use in Langmuir adsorption isotherm that gave best-fit data

Figure 7.1 – Set-up number 1 (dimensions in mm)

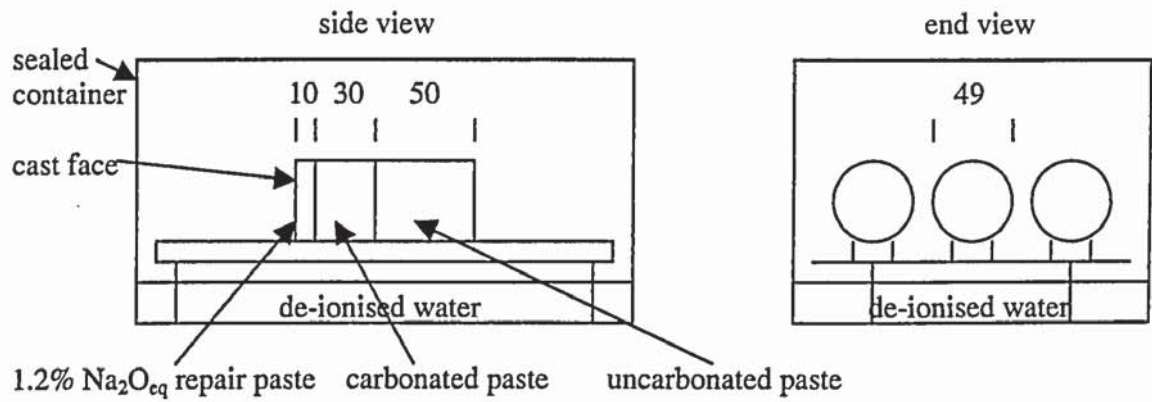


Figure 7.2 – Set-up number 2 (dimensions in mm)

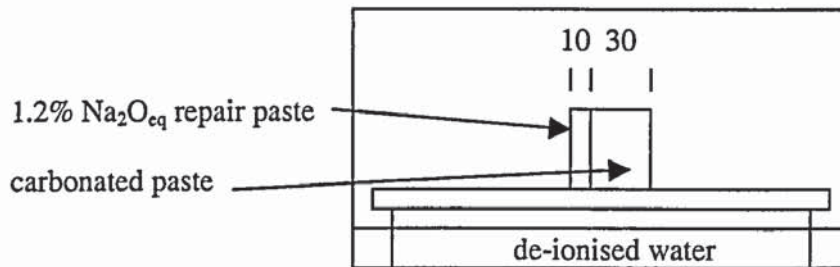


Figure 7.3 – Set-up number 3 (dimensions in mm)

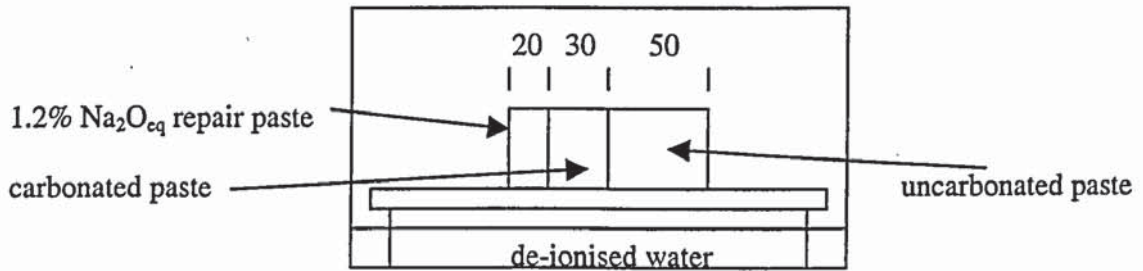


Figure 7.4 – Set-up number 4 (dimensions in mm)

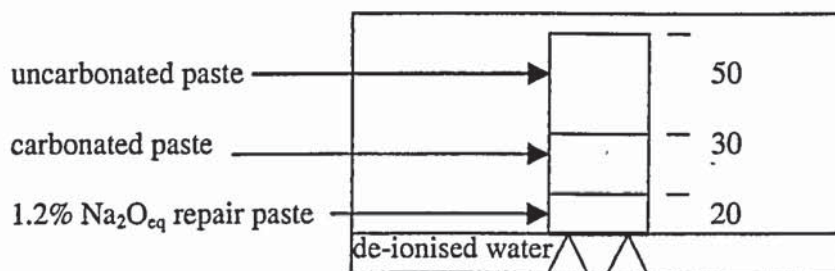


Figure 7.5 – Set-up number 5 (dimensions in mm)

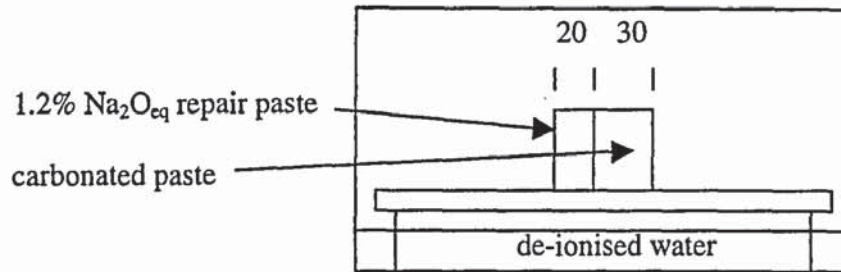


Figure 7.6 – Set-up number 6 (dimensions in mm)

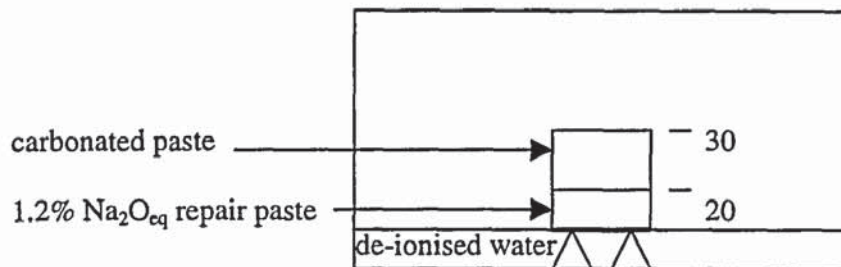


Figure 7.7 – Set-up number 7 (dimensions in mm)

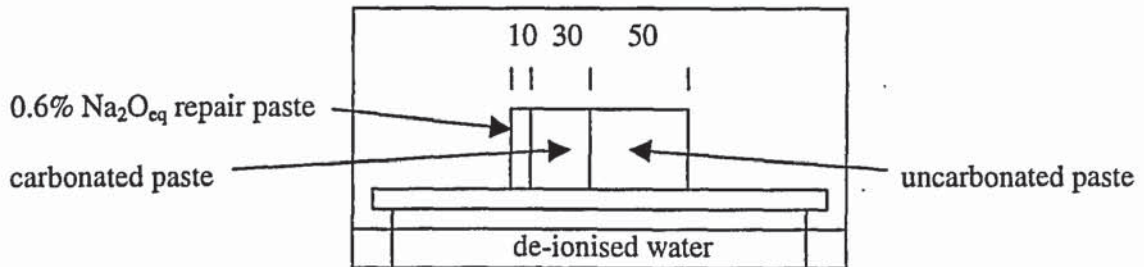


Figure 7.8 – Set-up number 8 (dimensions in mm)

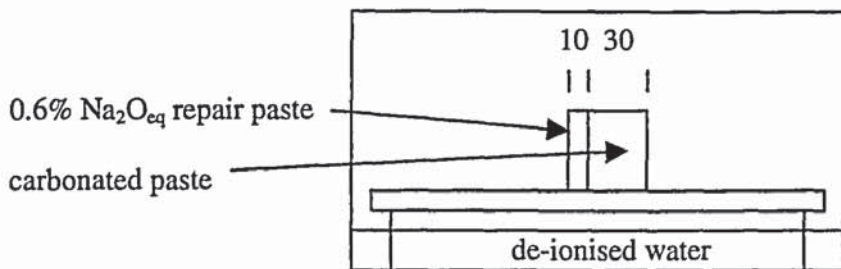




Figure 7.9 – Set-up number 9 (dimensions in mm)

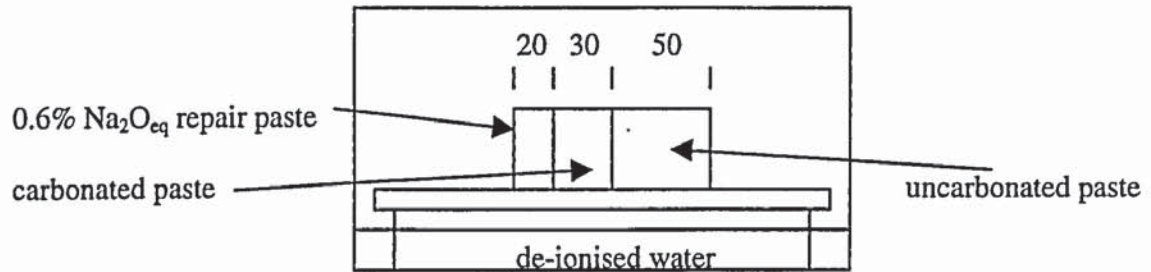


Figure 7.10 – Set-up number 10 (dimensions in mm)

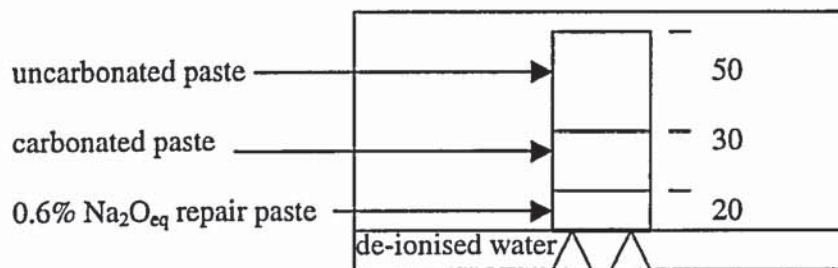


Figure 7.11 – Set-up number 11 (dimensions in mm)

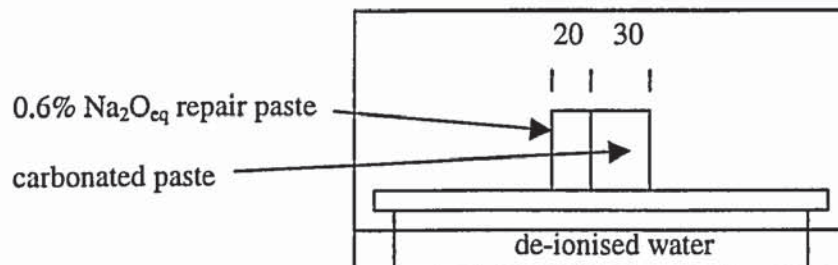


Figure 7.12 – Set-up number 12 (dimensions in mm)

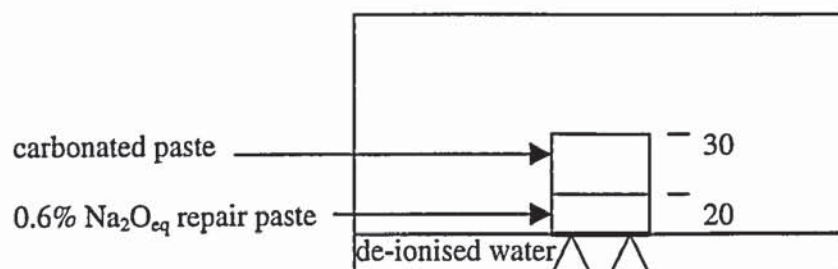


Figure 7.13 - Comparison of experimental and numerical results for set-up number 1

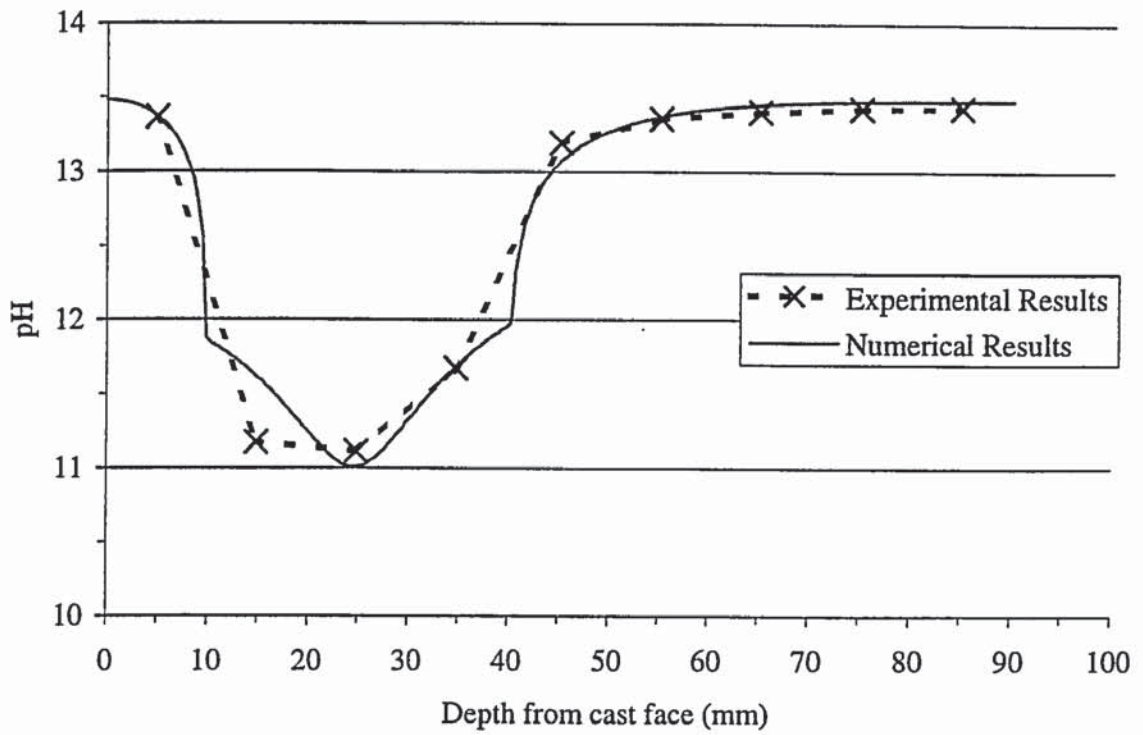


Figure 7.14 - Comparison of experimental and numerical results for set-up number 2

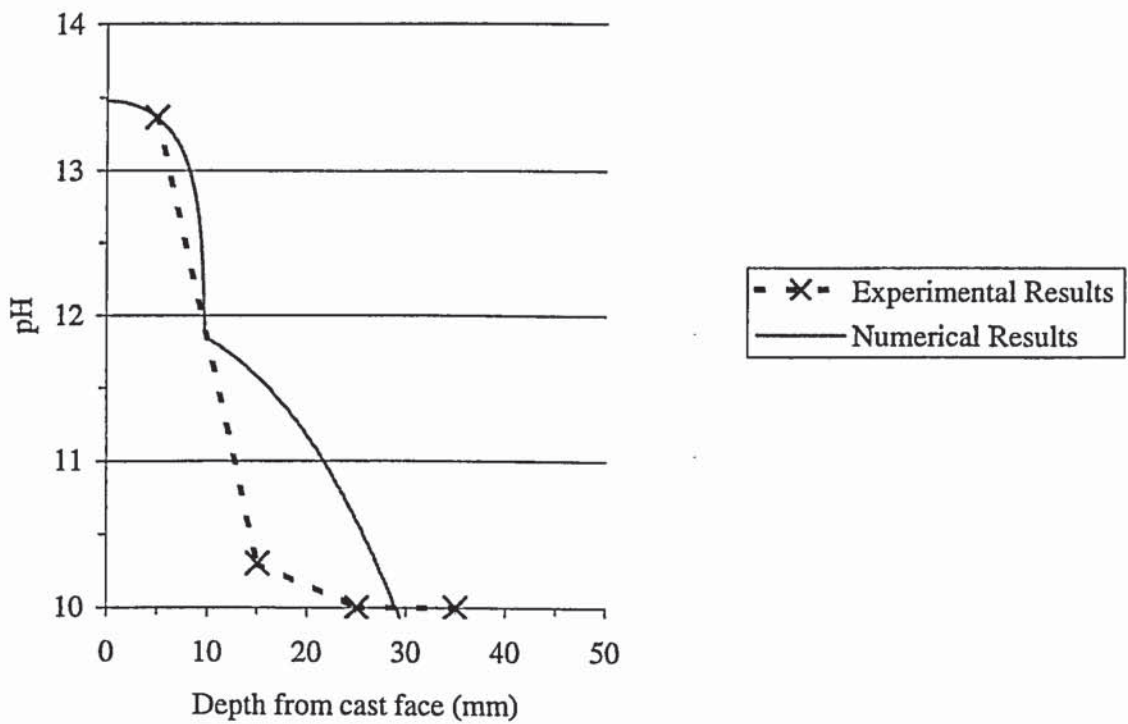


Figure 7.15 - Comparison of experimental and numerical results for set-up number 3

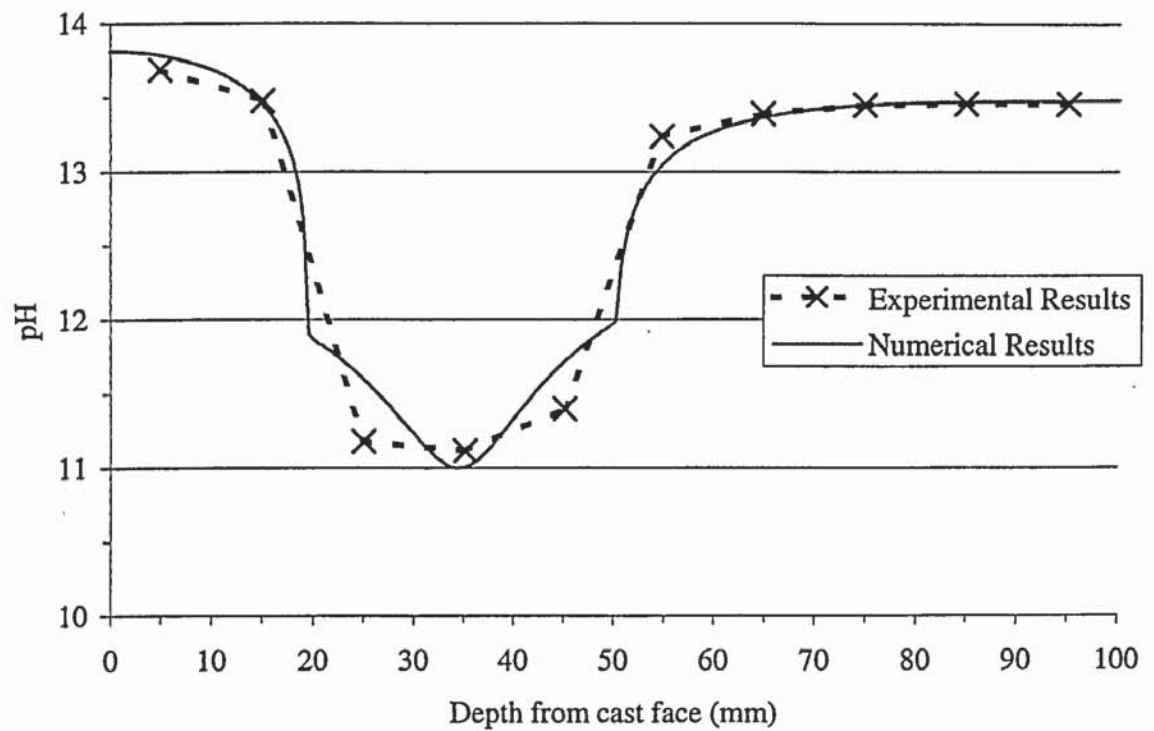


Figure 7.16 - Comparison of experimental and numerical results for set-up number 4

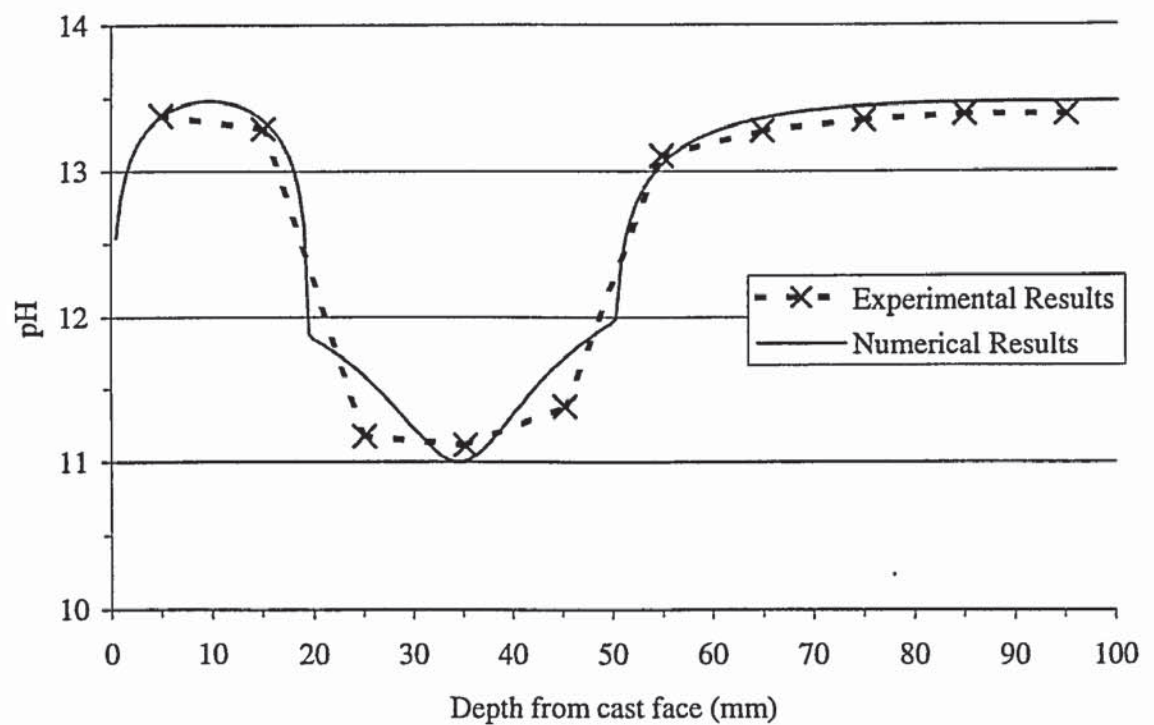




Figure 7.17 - Comparison of experimental and numerical results for set-up number 5

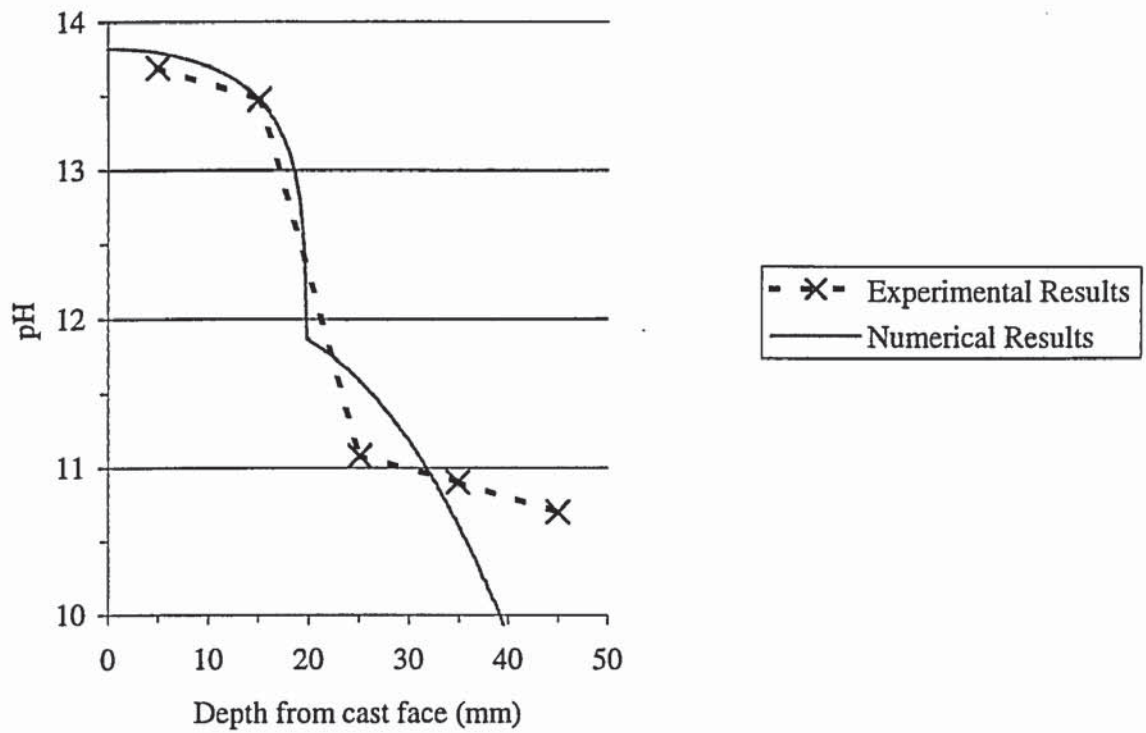


Figure 7.18 - Comparison of experimental and numerical results for set-up number 6

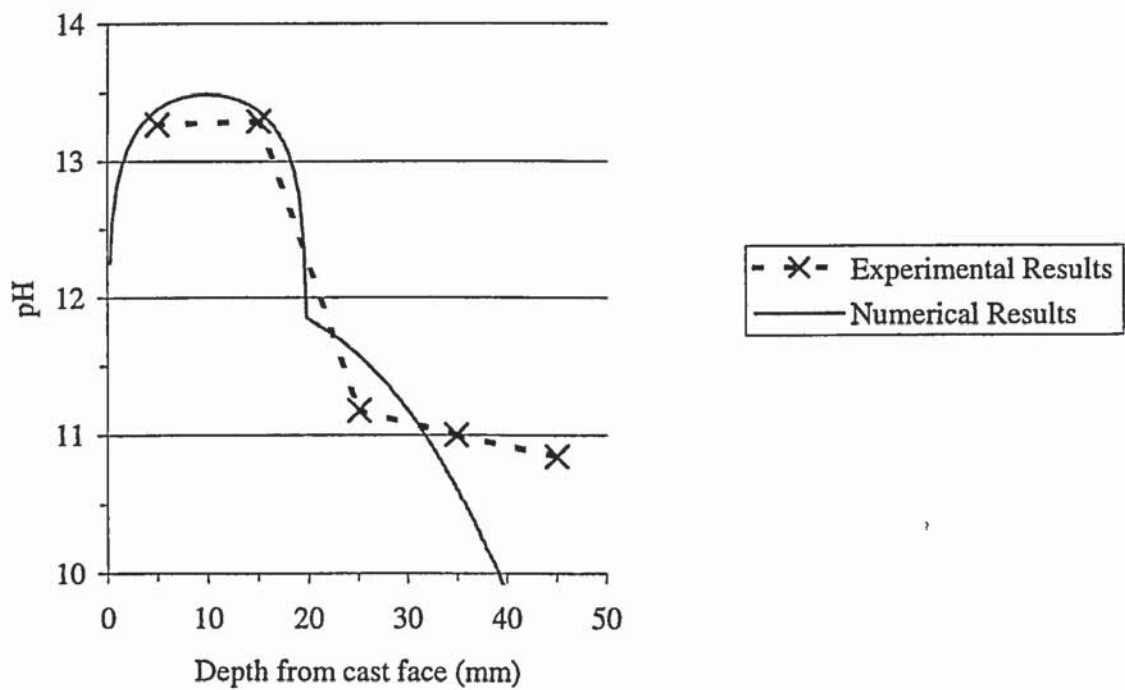


Figure 7.19 - Comparison of experimental and numerical results for set-up number 7

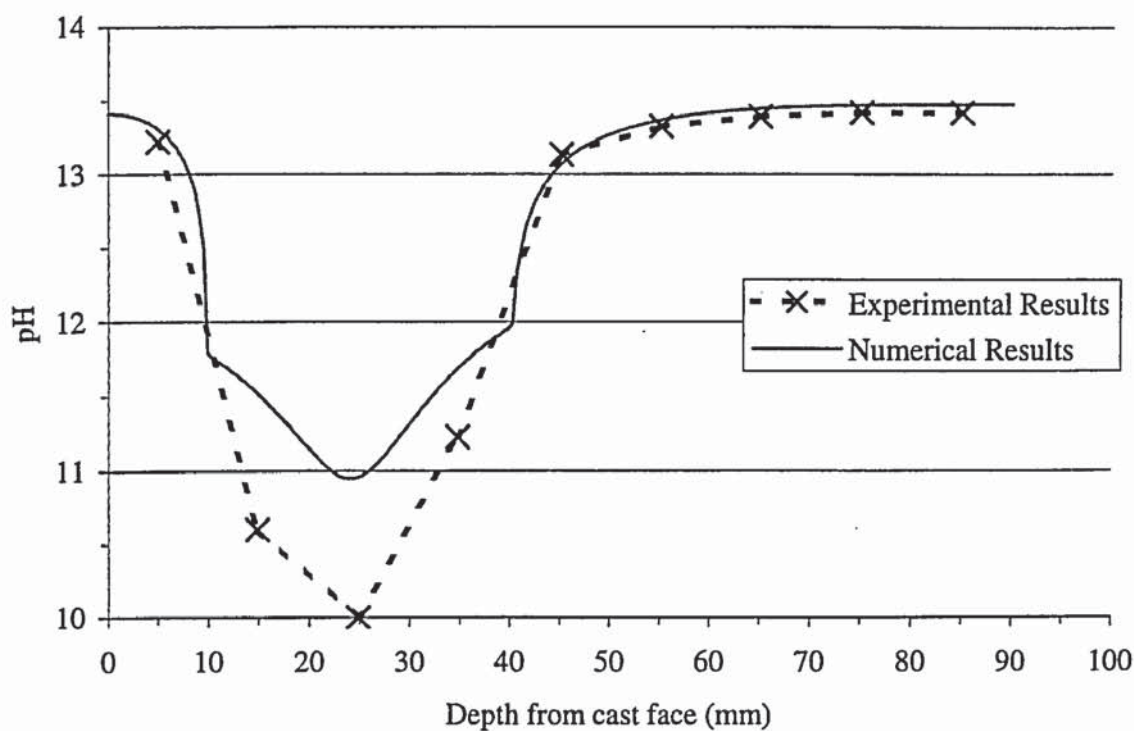


Figure 7.20 - Comparison of experimental and numerical results for set-up number 8

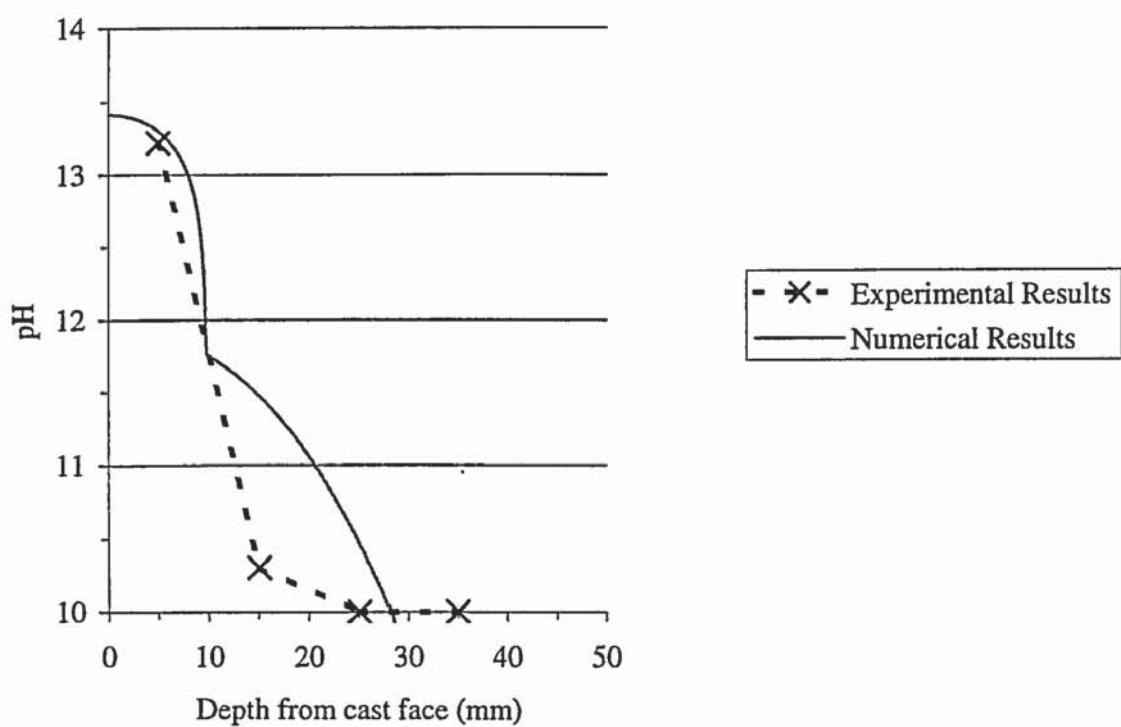


Figure 7.21 - Comparison of experimental and numerical results for set-up number 9

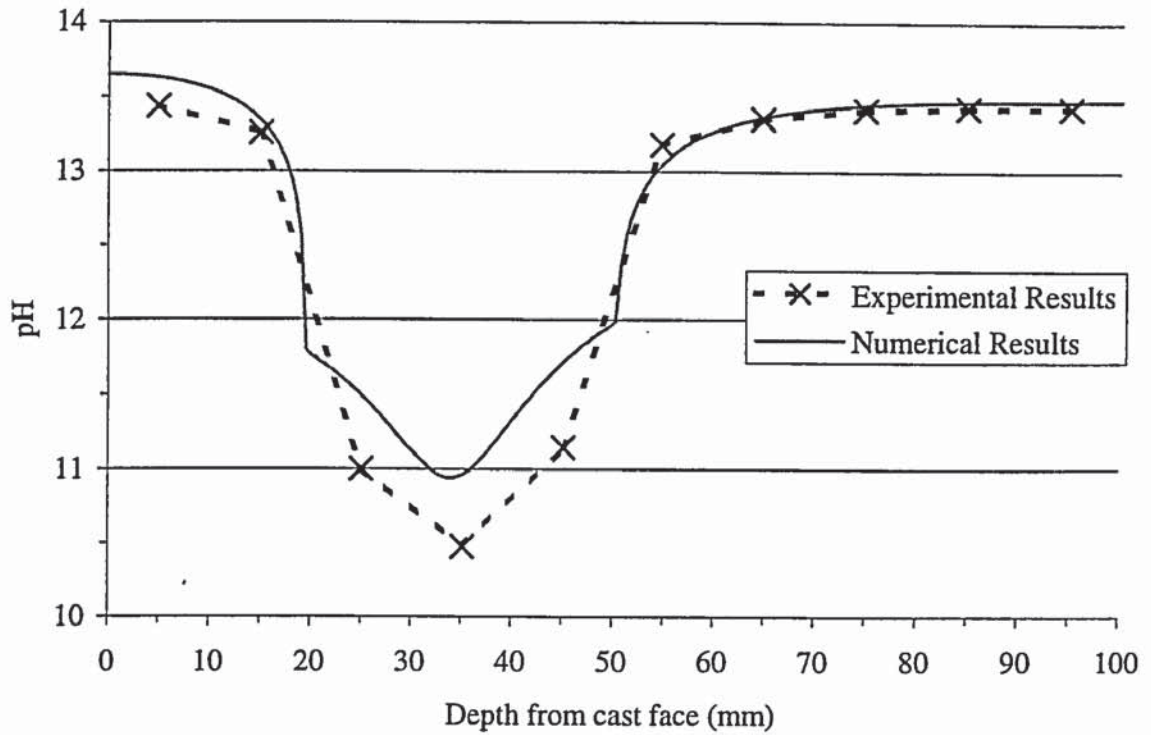


Figure 7.22 - Comparison of experimental and numerical results for set-up number 10

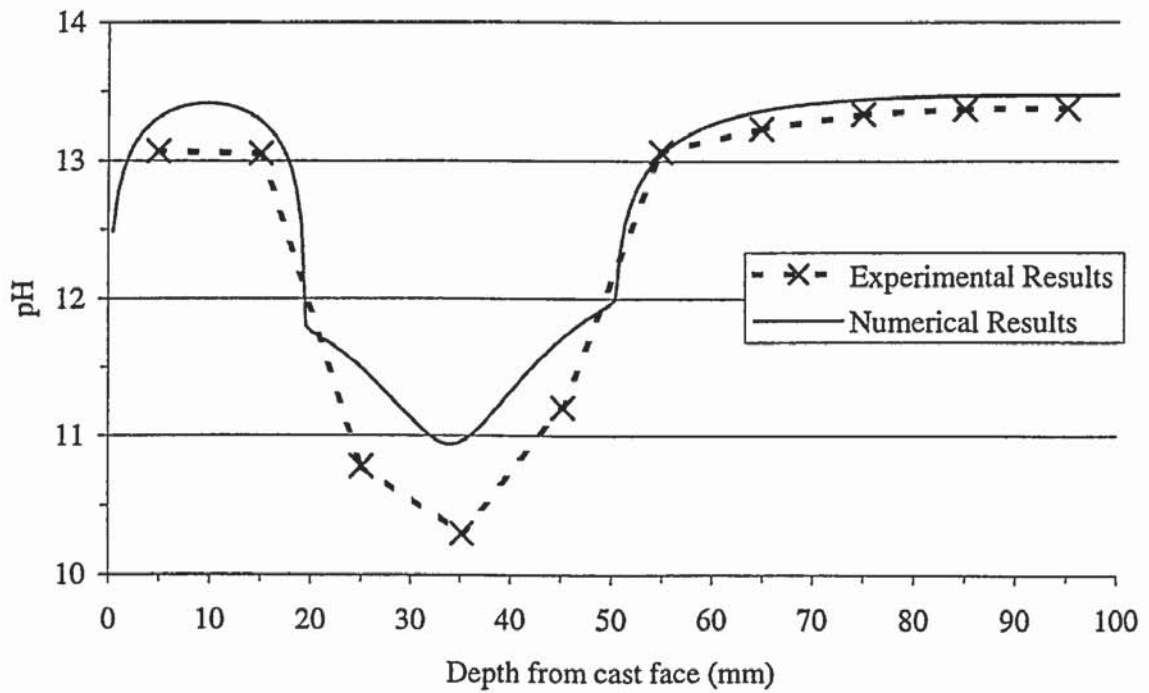




Figure 7.23 - Comparison of experimental and numerical results for set-up number 11

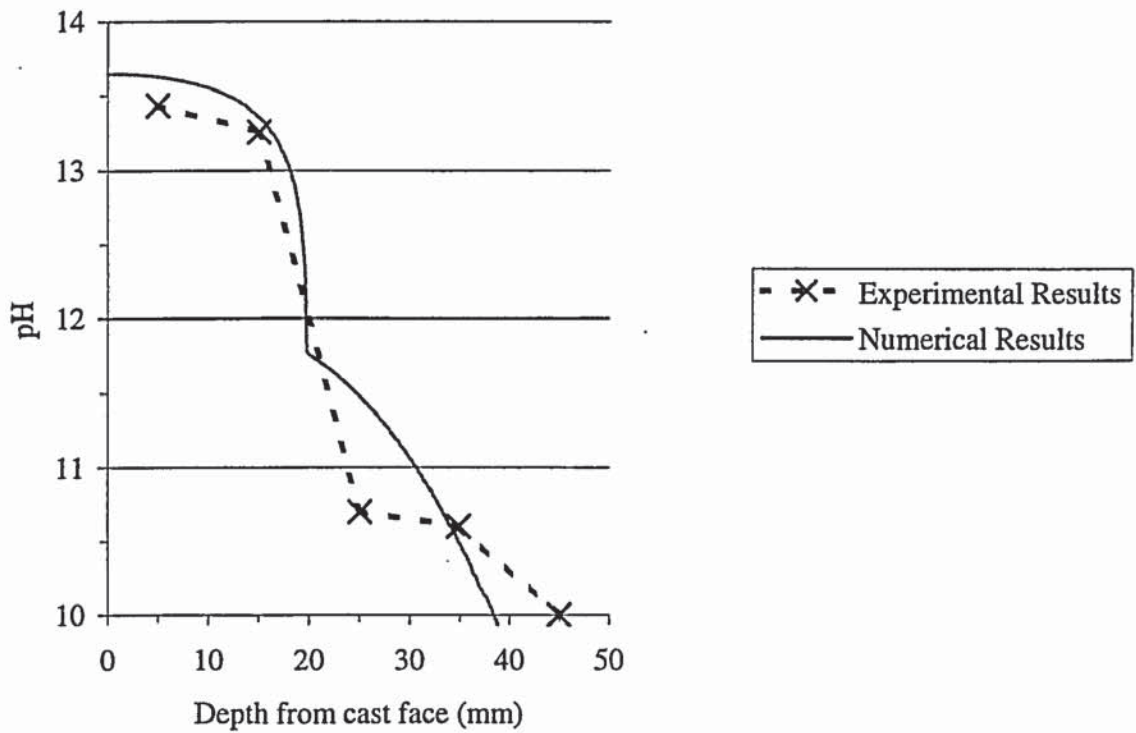
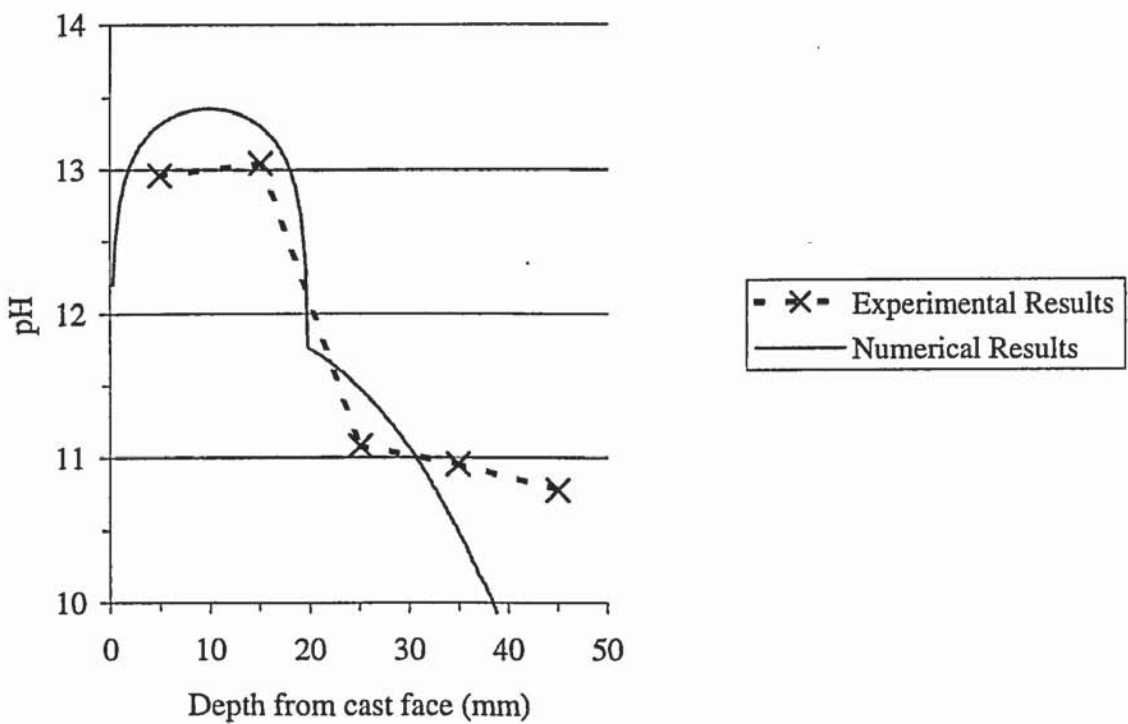


Figure 7.24 - Comparison of experimental and numerical results for set-up number 12



## **CHAPTER EIGHT**

### **CALCIUM NITRITE-BASED CORROSION REHABILITATION SYSTEM**

#### **8.1 INTRODUCTION**

During the 1970's calcium nitrite was introduced as a concrete admixture to inhibit the corrosion of steel in concrete. In the USA, since 1978, calcium nitrite has been used in over 300 parking, marine and highway structures, apparently with very successful results (Jeknevorian, Chin and Saidha, 1995) in the battle to inhibit chloride-induced corrosion. Within the last decade Andrade and co-workers (Alonso, Acha and Andrade, 1990; Alonso and Andrade, 1990; Andrade, Alonso and Gonzalez, 1986) have demonstrated that nitrite-based corrosion inhibitor admixtures can also protect steel in carbonated concrete. The proven track record of calcium nitrite has yet to be realistically challenged by alternative inhibiting admixtures. It was, therefore, only a matter of time before the inhibitive qualities of nitrites were exploited as part of concrete repair systems.

A proprietary repair system based on calcium nitrite was first introduced in the USA (Berke et al., 1992). The author claimed that a column could be impregnated using calcium nitrite in a mortar and a bridge was impregnated by a liquid solution of calcium nitrite. Collins, Weyers and Al-Qadi (1993) identified calcium nitrite as a potential rehabilitative inhibitor by a method which involved the removal of chloride-contaminated concrete, followed by ponding with an aqueous solution at the level of the bars and then providing a reservoir of nitrite ions in a cementitious mortar overlay.

The objective of this chapter is to investigate a calcium nitrite-based corrosion rehabilitation system for chloride-contaminated hydrated cement paste. In this chapter,

40mm thick repair cement pastes containing calcium nitrite are applied to chloride-contaminated cement pastes and the transport of several ions are monitored. A mathematical model is then developed to simulate the process. The numerical results obtained from the model are then compared with the results obtained experimentally and the efficiency of the repair system is discussed.

## **8.2 EXPERIMENTAL PROCEDURES**

### **8.2.1 Preparation of Hydrated Cement Paste**

Seven types of hydrated cement paste were required; i.e. six types of chloride-contaminated cement paste and the repair cement paste. The water to cement ratio, chloride levels by weight of cement, and experimentally determined initial pore solution compositions of the different types of cement paste are shown in Tables 8.1 and 8.2.

#### **8.2.1.1 Preparation of Chloride-Contaminated Cement Paste Specimens**

The manufacture of the chloride-contaminated cement paste cylinders was carried out as described in section 3.3.1. Two water to cement ratios were investigated, i.e. 0.4 and 0.6. Three different concentrations of chloride contamination were created for each of the water to cement ratios, i.e. 0.5, 1.0 and 1.5% chloride by weight of cement. The chloride contamination was achieved by dissolving the required concentration of sodium chloride into the mix water. After de-moulding, the cylinders were placed within sealed containers containing de-ionised water. The specimens were placed in an upright position on purpose-made platforms that supported them above the de-ionised water. The purpose of the de-ionised water was to create a curing environment of 100% relative humidity within the containers. The containers were then placed in a room, maintained at 38°C, for 28 days. Each cylinder was then finally cut at both ends, perpendicular to its longest axis using a mechanical hacksaw, to leave a chloride-contaminated cement paste cylinder of length 60mm and diameter 49mm ready for casting of the repair cement paste.



#### **8.2.1.2 Preparation of Repair Cement Paste Specimens**

The cement was sieved through a 150 $\mu$ m mesh in order to remove coarse particles. The required proportion of the cement was weighed and de-ionised water (mixed with the calcium nitrite-based inhibitor) was added to the mix to produce a paste of water to cement ratio 0.4. The proprietary calcium nitrite-based inhibitor solution was added to the mix water at a dosage of 50ml per kilogram of cement. The weight of the mix water was reduced, as recommended by the supplier, to compensate for the addition of the corrosion inhibitor. The adjustment factor was 0.84 kg of water for every litre of corrosion inhibitor added to the mix. Ion chromatography was carried out on the inhibitor solution, as described in section 3.3.10, and its concentration of nitrite ions was found to be 6.0M. The mixture was blended thoroughly by hand for about 5 minutes with a spatula. The mixture was then poured into formwork fitted on top of the chloride-contaminated cement paste. The repair cement paste was vibrated for 2-4 minutes to get rid of any trapped air bubbles. On at least two occasions, the foamy layer that had accumulated on the surface was removed and replaced with fresh paste. Following this, each specimen was left to cure in an upright position for 24 hours in air at 20°C and this was followed by removal of the formwork.

#### **8.2.2 Final Set-Up**

Six different set-ups (set-ups A to F) were investigated, as is shown in Figures 8.1 – 8.6, with three specimens per set-up. Following removal of the repair cement paste formwork, the specimens were stored above de-ionised water for the duration of the experiments in order to create an environment of 100% relative humidity. The 100% relative humidity environment was adopted in order that the pores within the specimens remained saturated.

#### **8.2.3 Pore Solution Analysis**

The specimens were removed from the exposure environments 90 days after casting of the repair pastes. Each specimen was cut into 10mm thick discs, starting from the cast

face. The three 10mm thick discs (as all specimens were produced in triplicate) corresponding to each segment of each experimental set-up then had their pore solution expressed using the method described in section 3.3.3. The extracted pore solution was analysed for nitrite, chloride, sulphate, nitrate, sodium, potassium and calcium ions using ion chromatography as described in section 3.3.10. The extracted pore solution was also analysed for hydroxyl ions using acid titration, as described in section 3.3.12, using a 0.1ml sample of pore solution and 0.01M nitric acid.

## **8.3 MATHEMATICAL MODELLING**

### **8.3.1 Introduction**

In this chapter, a mathematical model is presented which deals with the transport of several ions, as occurs with the calcium nitrite-based corrosion rehabilitation system for chloride-contaminated saturated hydrated cement paste. In order to simulate the transport of several ions within the pore electrolyte, the model deals with the electrostatic coupling of these ions. Mathematical models that consider the transport of only a single ionic species, such as the model presented in Chapter Seven, do not deal with this complex feature. It is assumed that the hydrated cement paste is fully saturated and that the pore solution within the hydrated cement paste is an ideal dilute solution.

### **8.3.2 Governing Equations**

#### **8.3.2.1 Mass Conservation**

For the present study, which considers unidirectional mass transport, mass conservation may be expressed by

$$\frac{\partial C_i}{\partial t} + \frac{1}{w} \frac{\partial S_i}{\partial t} = -\nabla J_i \quad (8.1)$$

where  $C_i$  is the concentration of diffusing substance in the pore solution (mmol/l),  $i$  is the species index,  $t$  is the diffusion time (s),  $w$  is the content of water in which diffusion

occurs (per unit weight of cement),  $S_i$  is the quantity of bound ions (mmol/g of cement), and  $J_i$  is the flux of diffusing substance (mmol/cm<sup>2</sup>/s).

As there is no externally applied current

$$\sum z_i J_i = 0 \quad (8.2)$$

where  $z_i$  is the charge number. The charge balance may also be expressed by

$$\sum z_i C_i = 0 \quad (8.3)$$

### 8.3.2.2 Flux

It was assumed in the present study that the flux was determined by the Nernst-Planck equation (Bard and Faulkner, 1980)

$$J_i = -D_i \nabla C_i - z_i D_i \left( \frac{F}{RT} \nabla \Phi \right) C_i + C_i v \quad (8.4)$$

where  $D_i$  is the diffusion coefficient (cm<sup>2</sup>/s),  $F$  is the Faraday constant (Coulombs),  $R$  is the gas constant (J/mol/K),  $T$  is the temperature (K),  $\Phi$  is the electrostatic potential (V) and  $v$  is the bulk velocity of the solution (cm/s). For the present study it was assumed that convection is minimal, i.e.  $C_i v = 0$ . Therefore it follows that the flux can be expressed by

$$J_i = -D_i \nabla C_i - z_i D_i \left( \frac{F}{RT} \nabla \Phi \right) C_i \quad (8.5)$$

### 8.3.2.3 Ionic Concentration Profile

Substituting equation (8.5) into equations (8.1) and (8.2), yields

$$\frac{\partial C_i}{\partial t} + \frac{1}{w} \frac{\partial S_i}{\partial t} = \nabla \left[ D_i \nabla C_i + z_i D_i C_i \left( \frac{F}{RT} \nabla \Phi \right) \right] \quad (8.6)$$

$$\frac{F}{RT} \nabla \Phi = - \frac{\sum z_i D_i \nabla C_i}{\sum z_i^2 D_i C_i} \quad (8.7)$$



The electroneutrality condition (8.3) is automatically satisfied. Therefore, the ionic transport behaviour in the pore solution will be governed by equations (8.6) and (8.7).

### **8.3.3 Assumptions**

Apart from the assumptions already mentioned, several other assumptions were made in order to carry out the mathematical modelling. Firstly, it was assumed that the initial concentrations of the ions within the pore solutions of the various types of cement pastes were as shown in Table 8.11. For the purpose of the mathematical modelling it was assumed that the only anions present within the pore solution were nitrite ions, hydroxyl ions and chloride ions. The cations were treated collectively for the purpose of mathematical modelling and thus are denoted by  $M^+$ . It was assumed that no ions leached out of the specimens and that the pores remained saturated throughout the duration of the experiments and that the content of water in which diffusion occurs ( $w$ ), expressed per unit weight of cement, was 0.3.

Chloride ions can be physically bound on to the pore surfaces within the cement matrix and they can also react chemically to form chloroaluminates. It was assumed in the present study that chloride binding occurs and that this binding is not permanent. Therefore, chloride ions will be released again if the concentration is lowered as there is a balance between the bound and free chloride concentrations. Sergi, Yu and Page (1992) showed that the relationship between the bound and free chloride ion concentrations could be approximated by the Langmuir adsorption isotherm as expressed by

$$S_{cl^-} = \frac{\alpha C_{cl^-}}{1 + \beta C_{cl^-}} \quad (8.8)$$

where  $S_{Cl^-}$  is the quantity of bound chloride ions (mmol/g of cement),  $C_{Cl^-}$  is the concentration of chloride ions in the pore solution (mmol/l),  $\alpha=1.67$  and  $\beta=4.08 \text{ (mol/l)}^{-1}$  for  $w=0.3$ . Therefore  $\partial S_{Cl^-}/\partial t$  can be expressed by

$$\frac{\partial S_{Cl^-}}{\partial t} = \frac{\partial C_{Cl^-}}{\partial t} \left[ \frac{\alpha}{(1 + \beta C_{Cl^-})^2} \right] \quad (8.9)$$

In order that the charge balance is retained it is assumed that the adsorption of chloride ions is balanced by the desorption of hydroxyl ions. Nitrite ions and the cations are assumed not to undergo any adsorption or desorption to or from the pore surfaces.

#### **8.3.4 Computer Simulation**

The assumed initial values of the ionic concentrations within the pore solution and assumed diffusion coefficients, for each of the ions within the 0.4 w/c chloride-contaminated paste, 0.6 w/c chloride-contaminated paste and repair paste, were substituted into equations (8.6) and (8.7). The numerically determined ionic concentration profiles within the pore solution, after 90 days, were obtained using the Crank-Nicolson finite difference method (Hoffman, 1997). The combination of assumed diffusion coefficients that produced numerically obtained ionic concentration profiles, within the pore solutions of the various set-ups, which best fitted (using the least-squares criterion (Stroud, 1995)) the experimental profiles was then achieved. In order to carry out the enormous number of calculations, required to achieve the best-fit combination of assumed diffusion coefficients, a computer program was written in Fortran programming language and is provided in Appendix H.

## **8.4 DISCUSSION OF RESULTS**

### **8.4.1 Experimental Results**

The experimentally determined initial anionic and cationic concentrations, within the pore solution, are shown in Tables 8.1 and 8.2 respectively. The experimentally determined ionic concentrations, within the pore solutions after 90 days, are shown in Tables 8.3 to 8.10 and Figures 8.7 to 8.34. The 'depth from cast face' values shown in Tables 8.3 to 8.10 and Figures 8.7 to 8.34 represent the distance to the centre of each disc from the cast face.

It can be seen from Table 8.3 that nitrite ions have penetrated 60mm in each of the set-ups. However, nitrite concentrations are very low beyond 15mm and 25mm penetration (55mm and 65mm from the cast face) in 0.4 and 0.6 water to cement ratio cement paste, respectively. Under the conditions investigated it is clear that all the anions and cations diffused to some extent. The repair paste had relatively low concentrations, within its pore solution, of hydroxyl, chloride, sulphate and sodium ions when compared to the chloride-contaminated paste. Thus diffusion of these ions took place from the chloride-contaminated paste into the repair paste. However, diffusion of nitrite, nitrate, potassium and calcium ions took place in the opposite direction as the experimentally determined initial concentrations were greater within the repair cement paste when compared to the chloride-contaminated paste.

### **8.4.2 Mathematical Modelling**

The assumed initial ionic concentrations, within the pore solution, are shown in Table 8.11. The assumed diffusion coefficients that, when combined, produced the best-fit profiles to the experimental data are shown in Table 8.12. It can be seen from Figures 8.7 to 8.24 that the mathematical model provides predictions of anionic concentration profiles that are in very good accord with experimental values for chloride-contaminated hardened cement paste subjected to the calcium nitrite-based corrosion rehabilitation system. Further development of the model would allow the cations to be



treated separately as well as incorporating other ions, such as sulphate and nitrate, into the model in order to provide a more realistic picture of the mass transport occurring within the pore solution.

It can be seen from Table 8.12 that the assumed diffusion coefficients, required to produce the best-fit profiles to the experimental data, for nitrite ions are lower than the corresponding values for chloride ions. However, it is also noted that the assumed diffusion coefficient for the cations, required to obtain the best-fit profiles to the experimental data, does appear to be somewhat higher than expected in the case of the 0.6 water to cement ratio chloride-contaminated paste. This may require further investigation.

Several researches (Virmani, Clear and Pasko, 1983; Gaidis and Rosenberg, 1987; El-Jazairi and Berke, 1990; Tomosawa et al., 1992; Collins, Weyers and Al-Qadi, 1993) have estimated the critical  $[\text{NO}_2^-]/[\text{Cl}^-]$  ratio required in concrete to effectively inhibit corrosion, with values ranging from 0.5 to greater than 1.0. On the basis of this research, it was simply assumed for the purpose of the present study that a  $[\text{NO}_2^-]/[\text{Cl}^-]$  ratio of 1 could be used as a measure of the effectiveness of the calcium nitrite-based rehabilitation system being investigated. Table 8.13 shows the depth from the cast face to which the critical  $[\text{NO}_2^-]/[\text{Cl}^-]$  ratio of 1 is achieved for each of the set-ups, using the mathematical model with the assumed diffusion coefficients from Table 8.12. It can be seen from Table 8.13 that the depth to which the critical ratio is achieved decreases with increased chloride concentration for each of the water to cement ratios investigated. When one considers that the repair cement paste is 40mm thick, it can be seen from Table 8.13 that, after 90 days, the only set-up that achieved the critical ratio beyond 10mm into the chloride-contaminated paste is set-up D. The other set-ups failed to achieve the critical ratio beyond 6mm into the chloride-contaminated paste. These results suggest that the calcium nitrite-based rehabilitation system investigated may be effective as a rehabilitation option for corroding steel bars within a 13mm zone of hydrated cement paste with a water to cement ratio of 0.6 and up to 0.5% chlorides by

weight of cement. However, the mathematical model can be used to demonstrate that if the diffusion time is extended, so that the nitrite and chloride levels could become constant throughout the test specimens, the rehabilitation system would create a  $[\text{NO}_2^-]/[\text{Cl}^-]$  ratio of greater than 1 throughout the contaminated cement paste in set-ups A, D and E. This of course would be dependent, in reality, on minimising surface leaching and maintaining a near saturated pore structure.

## **8.5 CONCLUSIONS**

Nitrite ions penetrate significant distances by diffusion within the pore solution of saturated uncarbonated hydrated cement paste. However, it was assumed for the purpose of the present study that a critical  $[\text{NO}_2^-]/[\text{Cl}^-]$  ratio of 1 could be used as a measure of the effectiveness of the calcium nitrite-based rehabilitation system. The mathematical model presented in this chapter demonstrated that the assumed critical  $[\text{NO}_2^-]/[\text{Cl}^-]$  ratio was achieved to a depth of 13mm within the 0.6 water to cement ratio cement paste with 0.5% chlorides by weight of cement. This suggests that the calcium nitrite-based corrosion rehabilitation system may be effective at suppressing corrosion on steel bars located within this zone.

The mathematical model provides predictions of nitrite, hydroxyl and chloride ion concentration profiles, within the pore solution, that are in very good accord with experimental values for chloride-contaminated hardened cement paste subjected to the calcium nitrite-based corrosion rehabilitation system.

Cement paste type	w/c ratio	Chloride conc <sup>n</sup> (% by wt of cement)	Pore solution conc <sup>n</sup> (mmol/l)				
			NO <sub>2</sub> <sup>-</sup>	OH <sup>-</sup>	Cl <sup>-</sup>	SO <sub>4</sub> <sup>2-</sup>	NO <sub>3</sub> <sup>-</sup>
Repair cement paste	0.4	-	724	124	1	2	6
Cl <sup>-</sup> contaminated paste	0.4	0.5	-	577	228	38	-
Cl <sup>-</sup> contaminated paste	0.4	1.0	-	525	900	67	-
Cl <sup>-</sup> contaminated paste	0.4	1.5	-	466	1513	78	-
Cl <sup>-</sup> contaminated paste	0.6	0.5	-	436	89	8	-
Cl <sup>-</sup> contaminated paste	0.6	1.0	-	411	432	13	-
Cl <sup>-</sup> contaminated paste	0.6	1.5	-	378	763	21	-

Table 8.1 – Experimentally determined initial anionic pore solution concentrations

Cement paste type	w/c ratio	Chloride conc <sup>n</sup> (% by wt of cement)	Pore solution conc <sup>n</sup> (mmol/l)		
			Na <sup>+</sup>	K <sup>+</sup>	Ca <sup>2+</sup>
Repair cement paste	0.4	-	94	656	4
Cl <sup>-</sup> contaminated paste	0.4	0.5	355	409	1
Cl <sup>-</sup> contaminated paste	0.4	1.0	727	446	1
Cl <sup>-</sup> contaminated paste	0.4	1.5	1055	439	2
Cl <sup>-</sup> contaminated paste	0.6	0.5	205	225	1
Cl <sup>-</sup> contaminated paste	0.6	1.0	442	250	2
Cl <sup>-</sup> contaminated paste	0.6	1.5	625	244	2

Table 8.2 – Experimentally determined initial cationic pore solution concentrations



Depth from cast face (mm)	Nitrite ion concentration within pore solution (mmol/l)					
	Set-up A	Set-up B	Set-up C	Set-up D	Set-up E	Set-up F
5	632	680	709	489	510	609
15	668	662	720	540	559	631
25	632	654	683	517	556	603
35	520	537	589	385	417	439
45	183	201	213	171	170	167
55	7.8	16	25	42	61	48
65	0.5	1.7	2.0	4	9	8
75	0.5	1.5	1.3	0.5	1.9	1.6
85	0.8	2.7	2.7	0.9	2.2	1.6
95	1.0	0.5	1.0	1.7	2.2	1.6

Table 8.3 – Experimentally determined nitrite ion profiles

Depth from cast face (mm)	Hydroxyl ion concentration within pore solution (mmol/l)					
	Set-up A	Set-up B	Set-up C	Set-up D	Set-up E	Set-up F
5	150	202	194	126	124	146
15	193	176	206	146	154	166
25	197	209	208	175	206	187
35	270	318	286	220	261	231
45	454	412	387	341	343	326
55	517	445	402	402	373	345
65	535	440	415	427	384	357
75	513	442	403	413	388	356
85	530	421	403	397	382	345
95	502	410	370	393	367	345

Table 8.4 – Experimentally determined hydroxyl ion profiles

Depth from cast face (mm)	Chloride ion concentration within pore solution (mmol/l)					
	Set-up A	Set-up B	Set-up C	Set-up D	Set-up E	Set-up F
5	0.1	2	1	0.1	0.1	1
15	0.2	3	7	0.1	0.2	6
25	0.6	5	31	0.2	2	34
35	20	116	227	13	54	205
45	153	518	818	58	254	512
55	243	731	1175	86	391	662
65	250	761	1331	94	432	738
75	242	780	1302	90	439	716
85	242	754	1239	86	425	694
95	214	677	1060	84	407	652

Table 8.5 – Experimentally determined chloride ion profiles

Depth from cast face (mm)	Sulphate ion concentration within pore solution (mmol/l)					
	Set-up A	Set-up B	Set-up C	Set-up D	Set-up E	Set-up F
5	1.4	2.3	2	0.8	0.8	1.5
15	1.8	2.0	3	1.1	1.1	1.8
25	1.9	2.5	3	1.3	1.7	2.4
35	4	6	7	2.4	3	4
45	20	32	37	5	8	11
55	32	40	49	7	11	14
65	33	42	59	8	13	15
75	32	40	55	7	13	14
85	35	41	54	7	13	15
95	35	42	42	9	13	16

Table 8.6 – Experimentally determined sulphate ion profiles

Depth from cast face (mm)	Nitrate ion concentration within pore solution (mmol/l)					
	Set-up A	Set-up B	Set-up C	Set-up D	Set-up E	Set-up F
5	10	10	11	7	7	9
15	10	10	11	8	8	9
25	9	10	10	7	8	9
35	8	7	7	5	5	6
45	1	0.5	0.9	1	1	1
55	-	-	-	-	-	-
65	-	-	-	-	-	-
75	-	-	-	-	-	-
85	-	-	-	-	-	-
95	-	-	-	-	-	-

Table 8.7 – Experimentally determined nitrate ion profiles

Depth from cast face (mm)	Sodium ion concentration within pore solution (mmol/l)					
	Set-up A	Set-up B	Set-up C	Set-up D	Set-up E	Set-up F
5	96	105	119	86	98	111
15	98	125	134	92	105	131
25	107	134	178	104	139	180
35	172	300	406	146	238	327
45	308	532	769	215	386	509
55	339	595	877	248	414	557
65	349	609	954	246	436	586
75	308	606	936	236	436	592
85	339	579	911	226	425	578
95	333	568	817	235	424	575

Table 8.8 – Experimentally determined sodium ion profiles



Depth from cast face (mm)	Potassium ion concentration within pore solution (mmol/l)					
	Set-up A	Set-up B	Set-up C	Set-up D	Set-up E	Set-up F
5	551	621	667	451	497	553
15	602	629	690	499	534	570
25	583	579	645	503	563	535
35	542	514	541	409	450	420
45	428	400	417	323	317	302
55	387	370	370	295	278	270
65	401	372	398	277	270	249
75	356	370	389	263	267	245
85	392	356	371	255	262	244
95	378	346	338	265	262	245

Table 8.9 – Experimentally determined potassium ion profiles

Depth from cast face (mm)	Calcium ion concentration within pore solution (mmol/l)					
	Set-up A	Set-up B	Set-up C	Set-up D	Set-up E	Set-up F
5	5.8	3.4	2.2	8.2	7.0	4.9
15	3.8	2.2	1.9	6.3	4.3	3.7
25	3.9	2.8	3.5	3.8	2.7	3.9
35	1.1	1.4	4.3	2.7	4.2	2.9
45	1.1	2.5	2.2	2.3	2.1	2.2
55	1.3	1.1	1.5	1.0	1.4	1.5
65	1.0	1.6	1.8	1.5	1.6	2.2
75	1.2	1.5	1.6	1.7	1.9	2.0
85	1.3	1.3	1.5	1.1	1.4	2.1
95	0.6	0.7	0.7	1.8	1.5	1.8

Table 8.10 – Experimentally determined calcium ion profiles

Cement paste type	w/c ratio	Chloride conc <sup>n</sup> (% by wt of cement)	Pore solution conc <sup>n</sup> (mmol/l)			
			NO <sub>2</sub> <sup>-</sup>	OH <sup>-</sup>	Cl <sup>-</sup>	M <sup>+</sup>
Repair cement paste	0.4	-	720	120	-	840
Cl <sup>-</sup> contaminated paste	0.4	0.5	-	580	230	810
Cl <sup>-</sup> contaminated paste	0.4	1.0	-	530	900	1430
Cl <sup>-</sup> contaminated paste	0.4	1.5	-	470	1510	1980
Cl <sup>-</sup> contaminated paste	0.6	0.5	-	440	90	530
Cl <sup>-</sup> contaminated paste	0.6	1.0	-	410	430	840
Cl <sup>-</sup> contaminated paste	0.6	1.5	-	380	760	1140

Table 8.11 – Assumed initial pore solution concentrations for modelling

Cement paste type	W/c ratio	Assumed diffusion coefficient (cm <sup>2</sup> /s)			
		NO <sub>2</sub> <sup>-</sup>	OH <sup>-</sup>	Cl <sup>-</sup>	M <sup>+</sup>
Repair cement paste	0.4	4×10 <sup>-8</sup>	5×10 <sup>-7</sup>	4×10 <sup>-7</sup>	3×10 <sup>-7</sup>
Cl <sup>-</sup> contaminated paste	0.4	5×10 <sup>-8</sup>	5×10 <sup>-7</sup>	6×10 <sup>-8</sup>	3×10 <sup>-7</sup>
Cl <sup>-</sup> contaminated paste	0.6	8×10 <sup>-8</sup>	6×10 <sup>-7</sup>	2×10 <sup>-7</sup>	8×10 <sup>-7</sup>

Table 8.12 - Assumed diffusion coefficients that gave best-fit data

Set-up	Depth from cast face to which critical [NO <sub>2</sub> <sup>-</sup> ]/[Cl <sup>-</sup> ] ratio of 1 is achieved
A	46mm
B	43mm
C	41mm
D	53mm
E	44mm
F	41mm

Table 8.13 – Numerically determined depth to which critical [NO<sub>2</sub><sup>-</sup>]/[Cl<sup>-</sup>] ratio is achieved

Figure 8.1 – Set-up A (dimensions in mm)

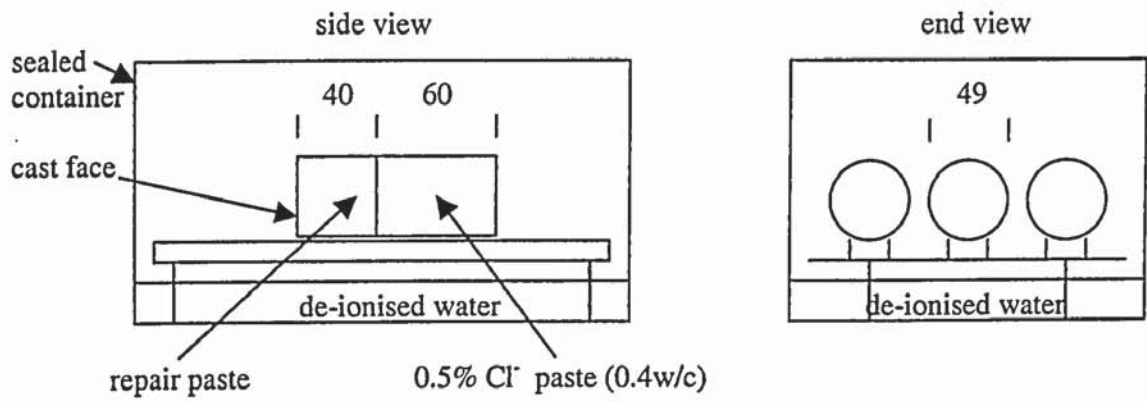


Figure 8.2 – Set-up B (dimensions in mm)

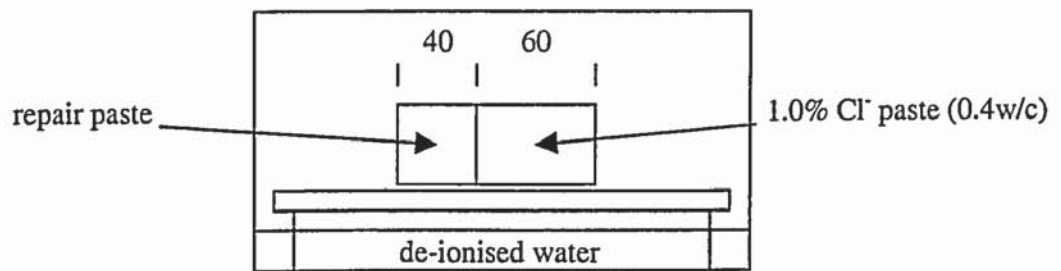


Figure 8.3 – Set-up C (dimensions in mm)

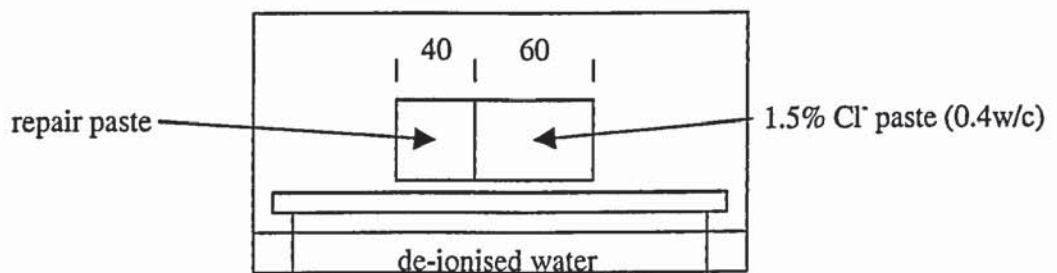




Figure 8.4 – Set-up D (dimensions in mm)

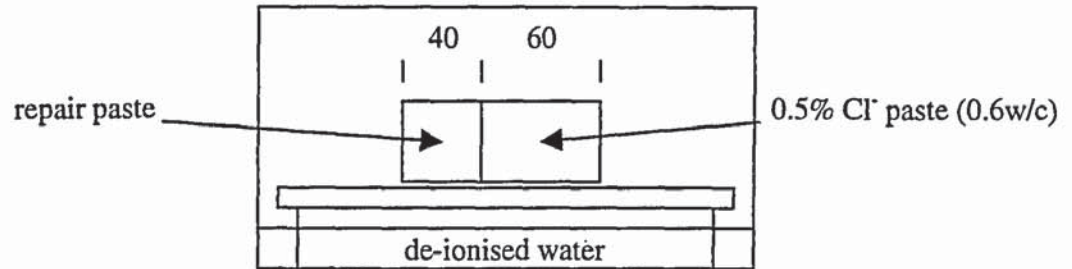


Figure 8.5 – Set-up E (dimensions in mm)

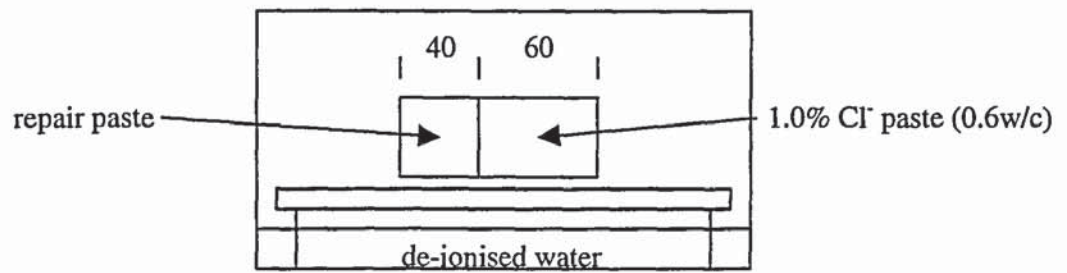


Figure 8.6 – Set-up F (dimensions in mm)

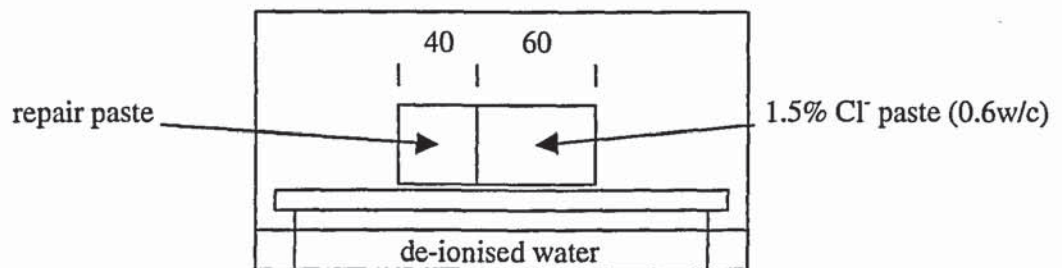


Figure 8.7 - Comparison of numerical and experimental nitrite ion profiles for set-up A

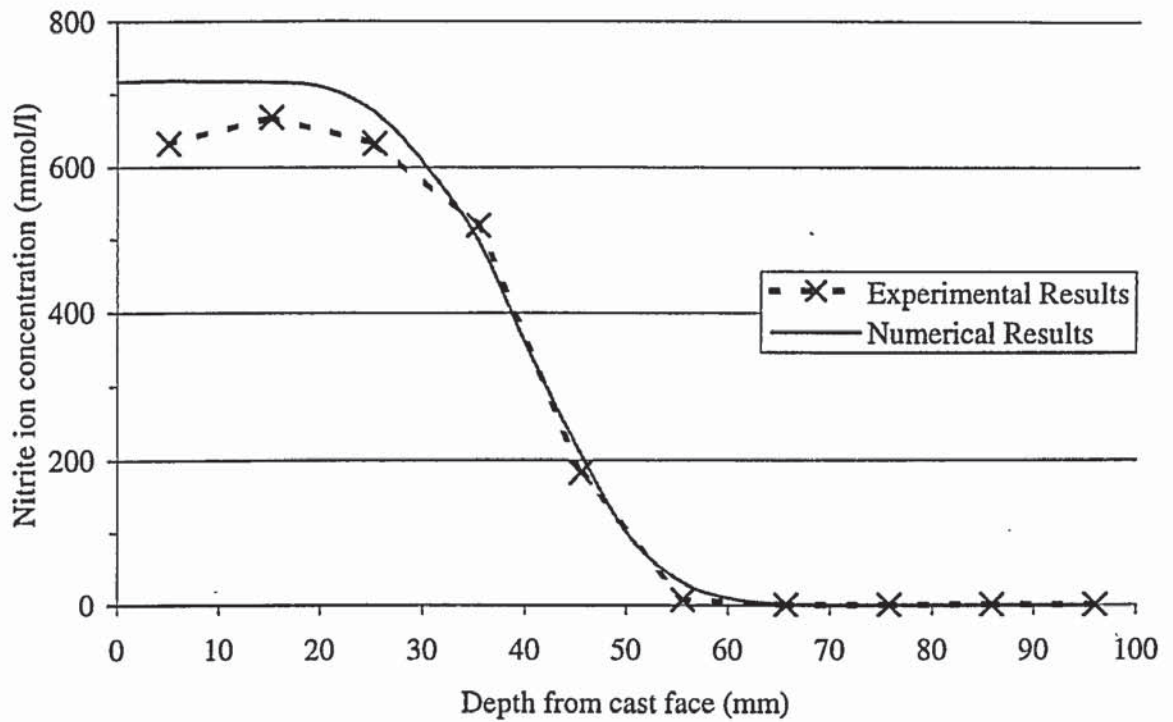


Figure 8.8 - Comparison of numerical and experimental nitrite ion profiles for set-up B

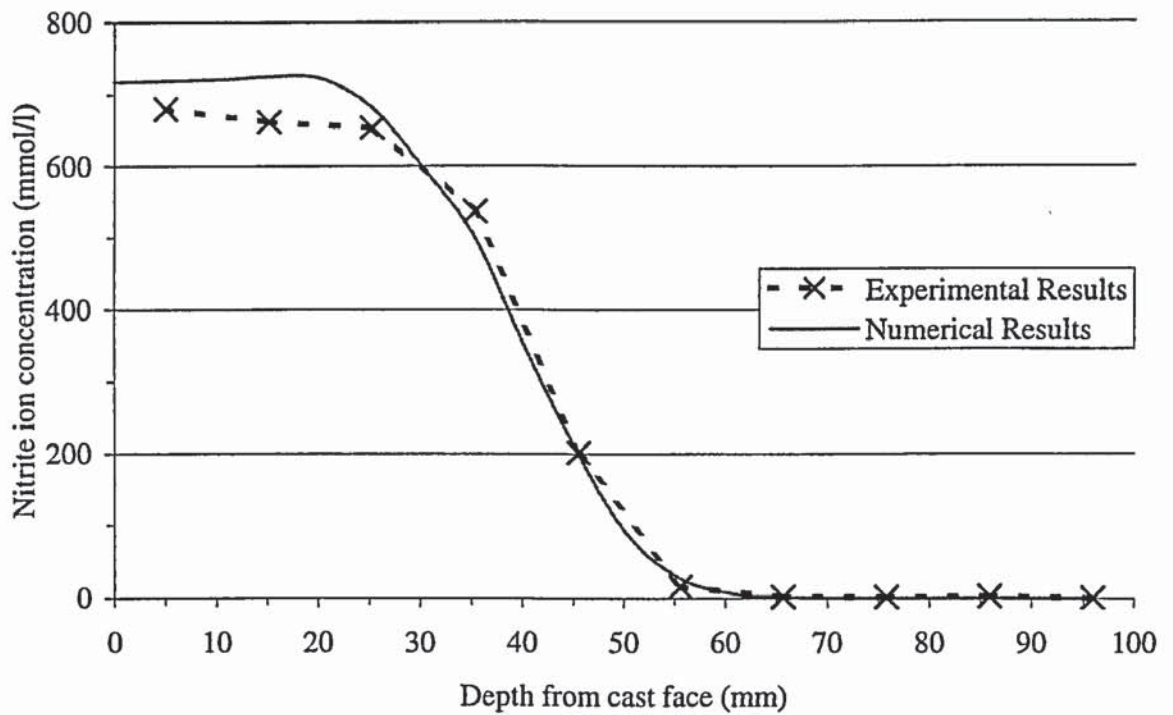


Figure 8.9 - Comparison of numerical and experimental nitrite ion profiles for set-up C

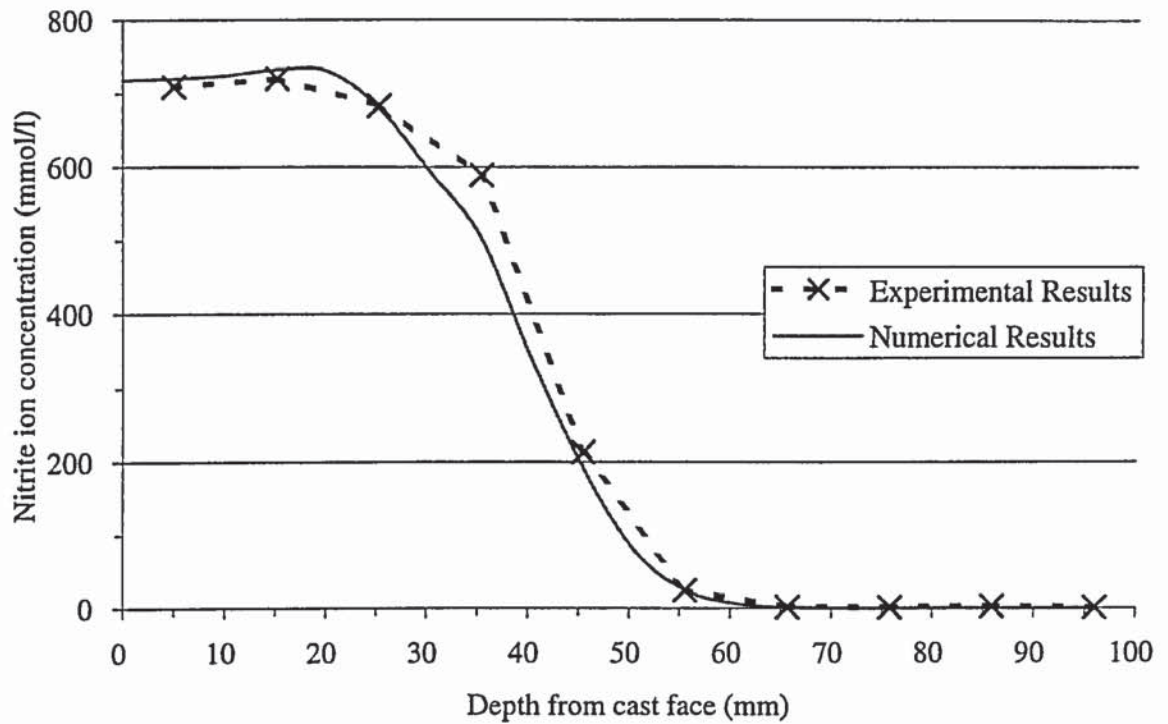


Figure 8.10 - Comparison of numerical and experimental nitrite ion profiles for set-up D

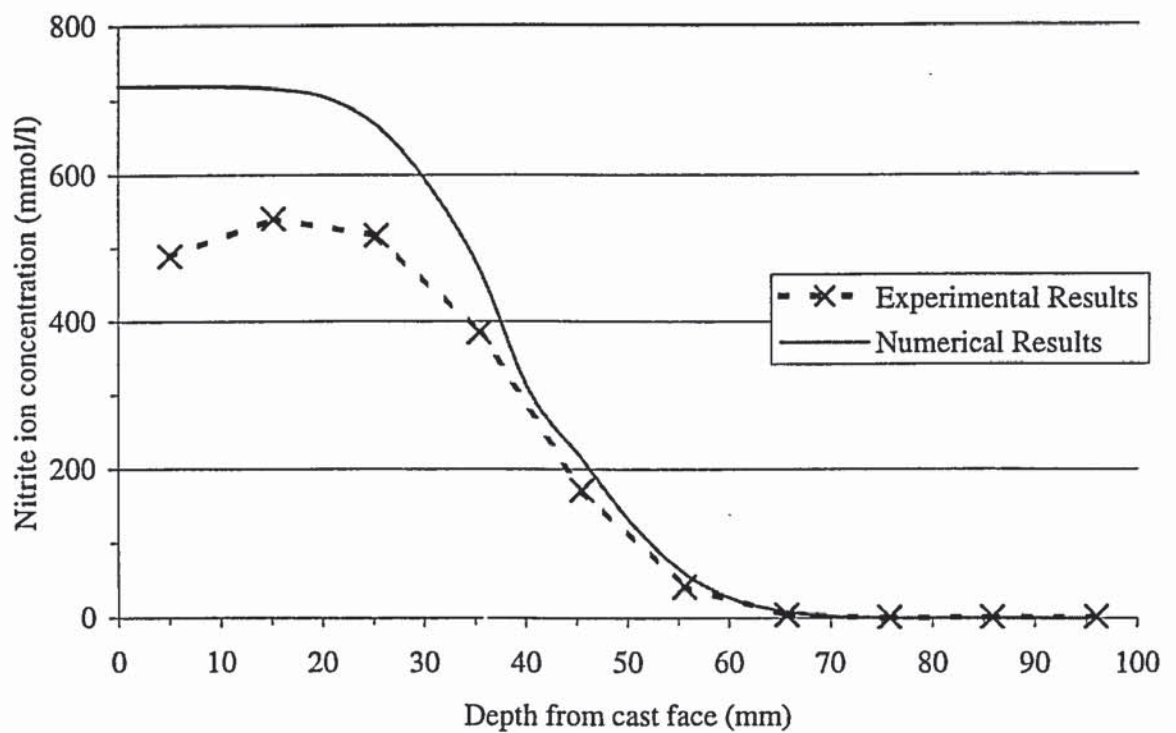




Figure 8.11 - Comparison of numerical and experimental nitrite ion profiles for set-up E

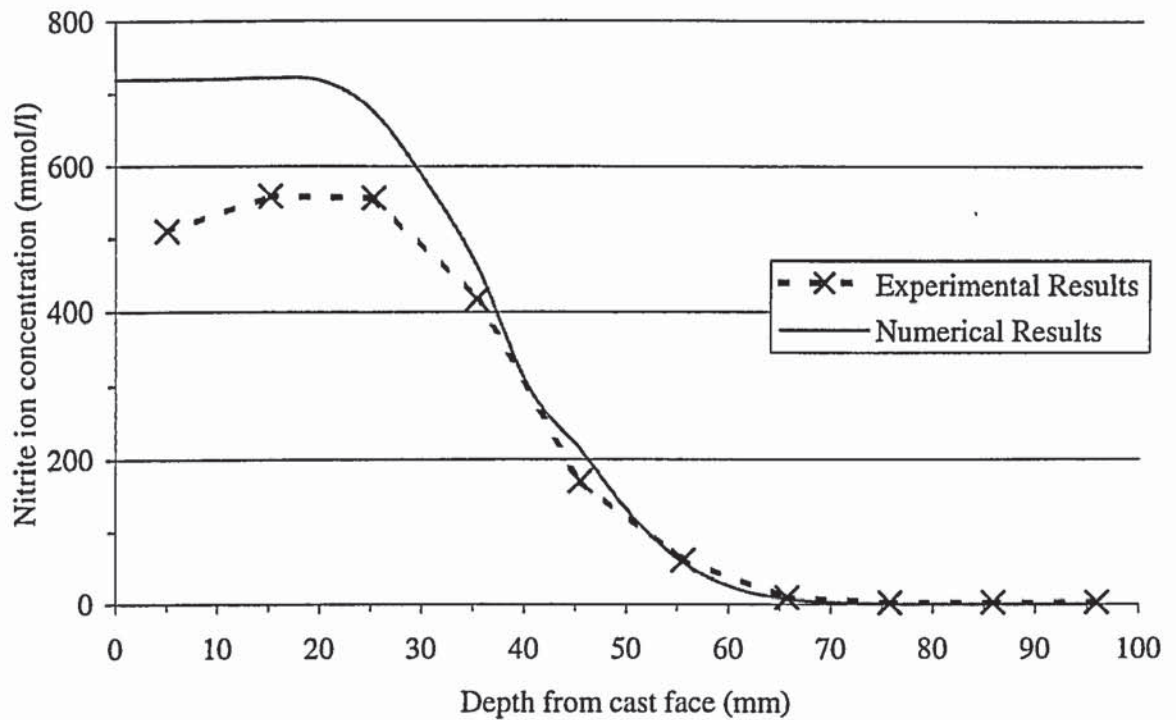


Figure 8.12 - Comparison of numerical and experimental nitrite ion profiles for set-up F

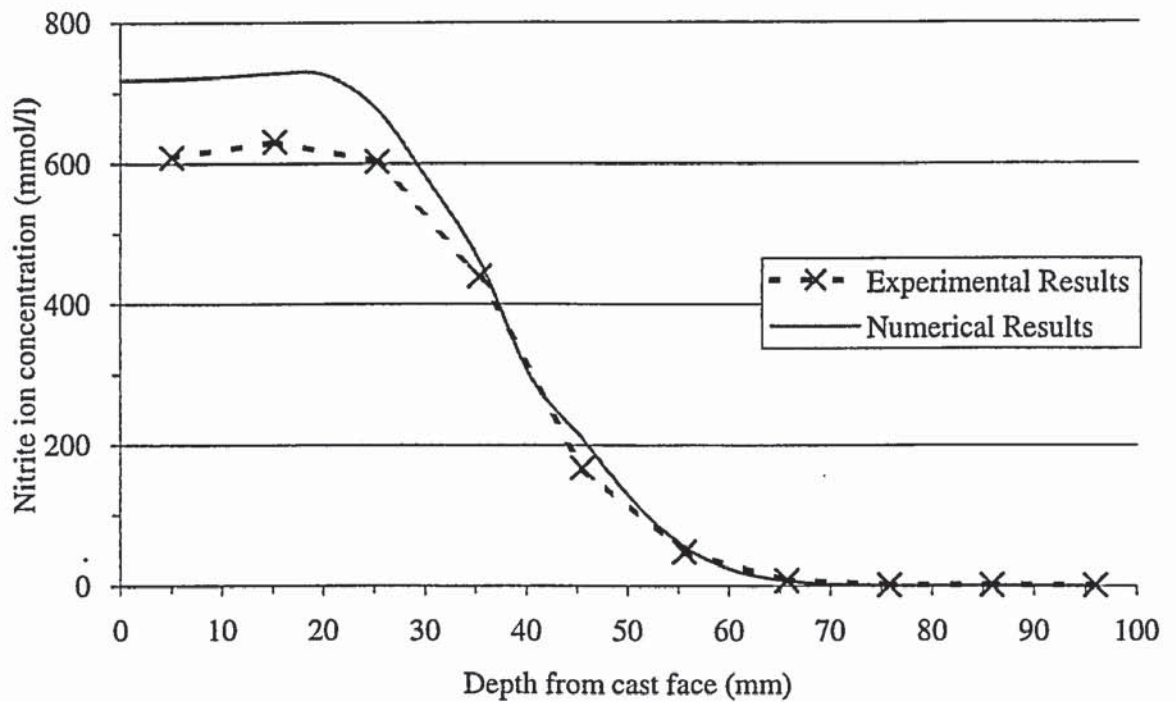


Figure 8.13 - Comparison of numerical and experimental hydroxyl ion profiles for set-up A

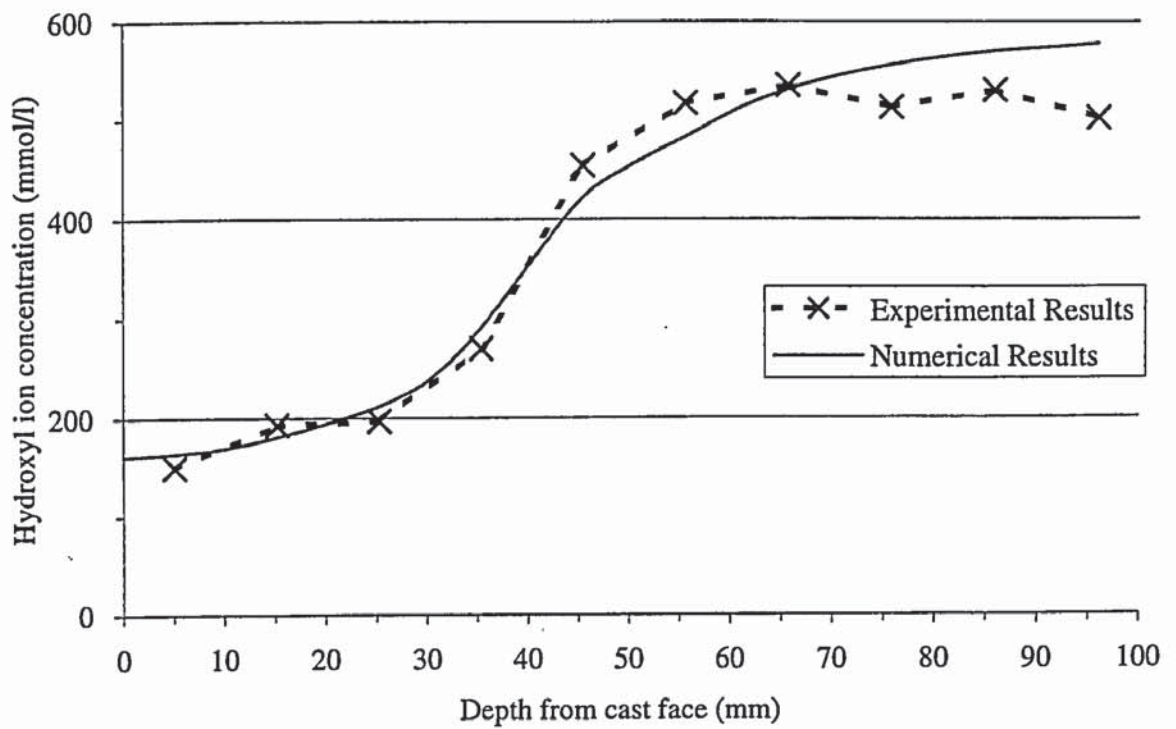


Figure 8.14 - Comparison of numerical and experimental hydroxyl ion profiles for set-up B

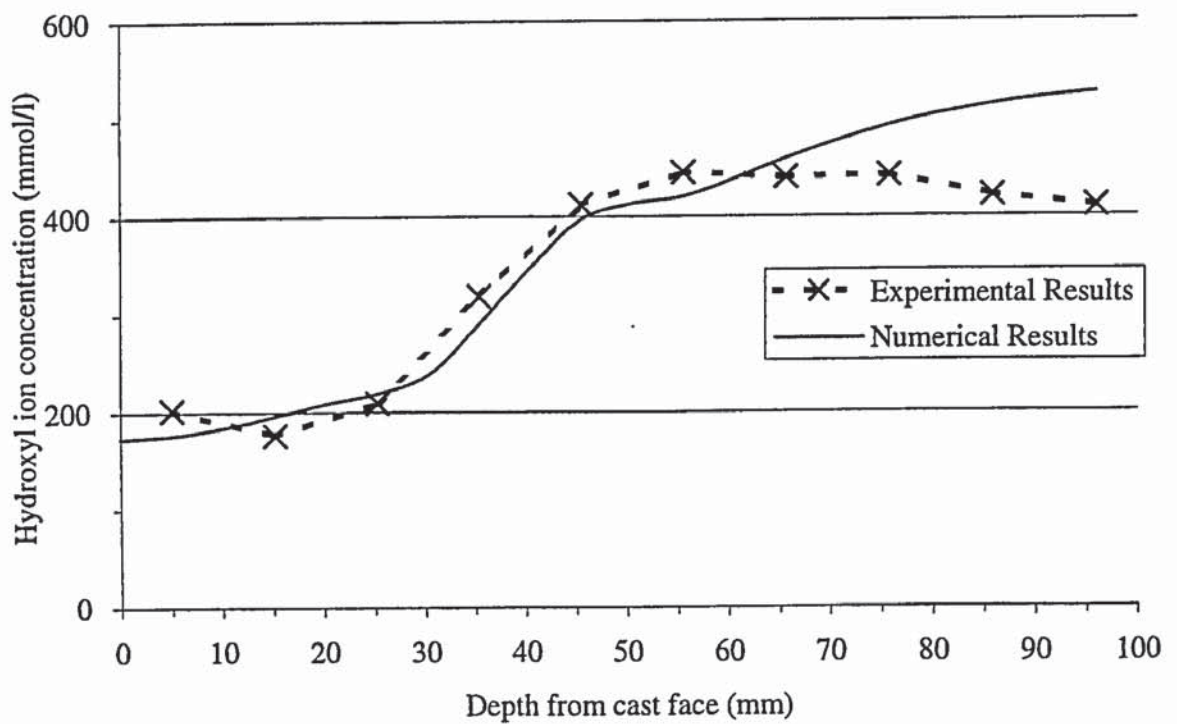


Figure 8.15 - Comparison of numerical and experimental hydroxyl ion profiles for set-up C

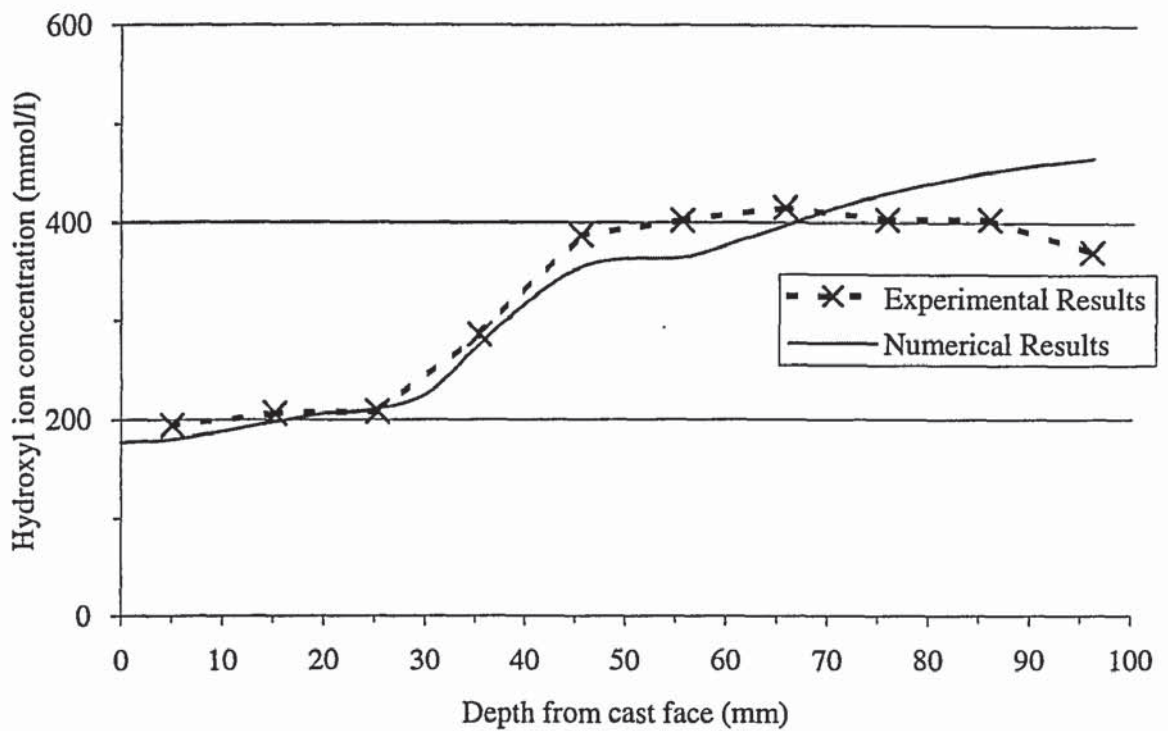


Figure 8.16 - Comparison of numerical and experimental hydroxyl ion profiles for set-up D

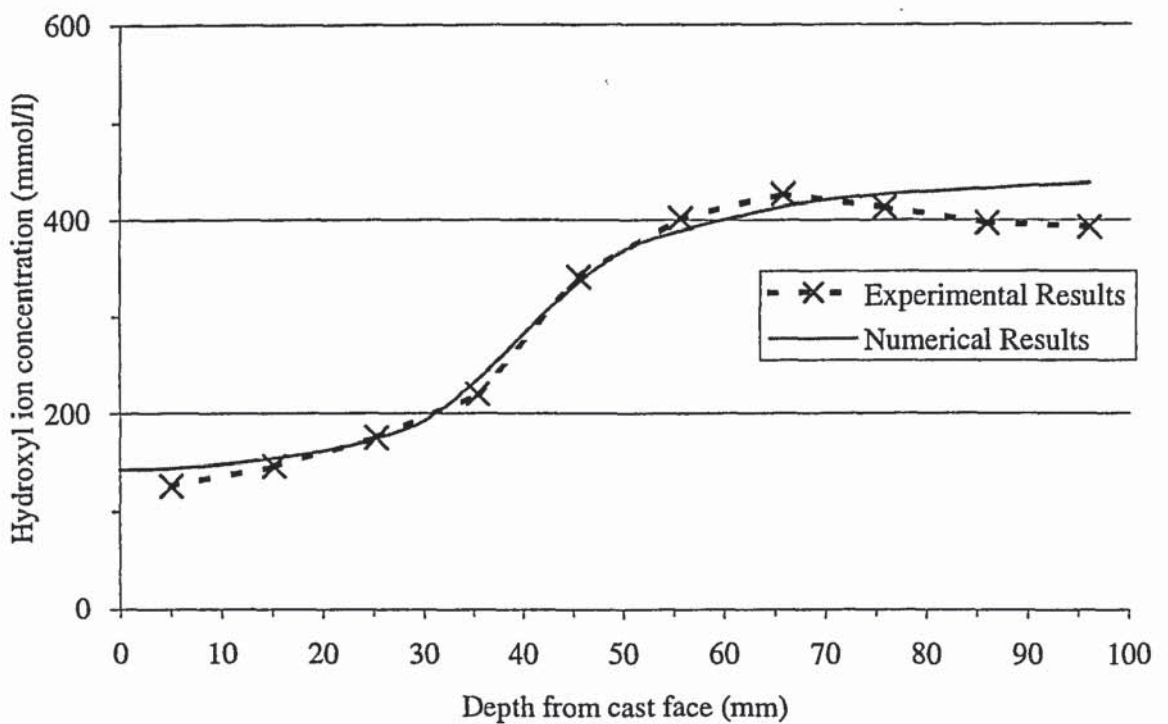




Figure 8.17 - Comparison of numerical and experimental hydroxyl ion profiles for set-up E

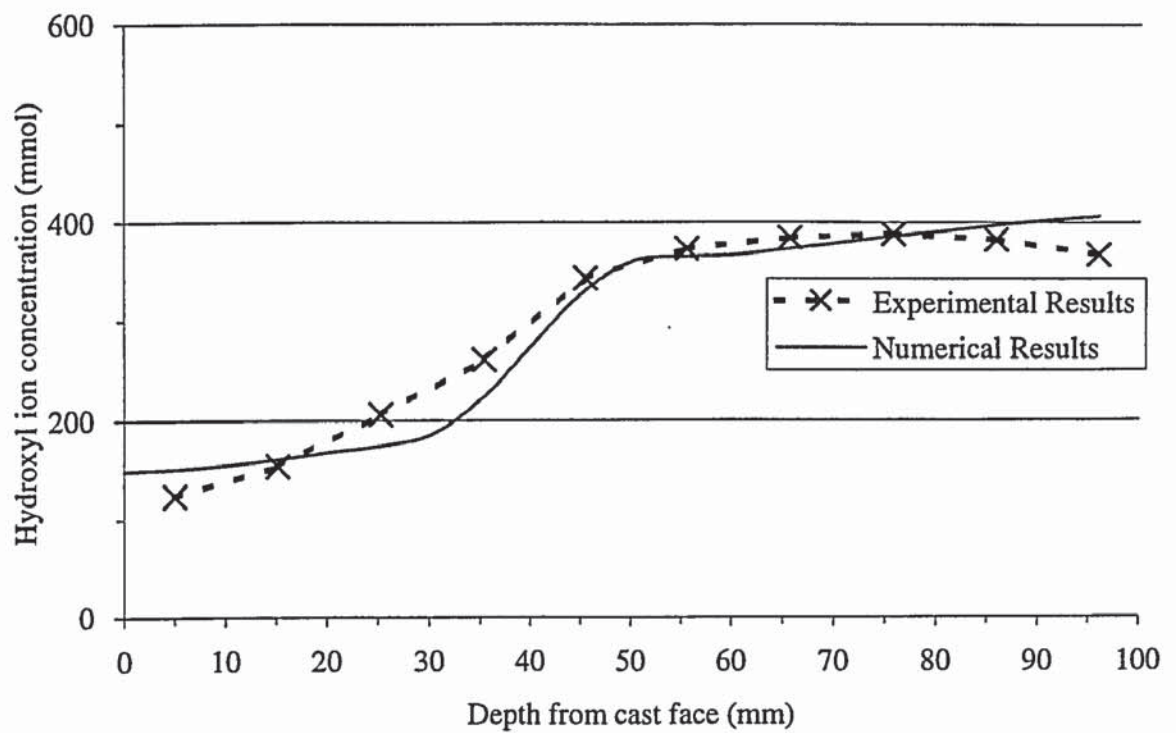


Figure 8.18 - Comparison of numerical and experimental hydroxyl ion profiles for set-up F

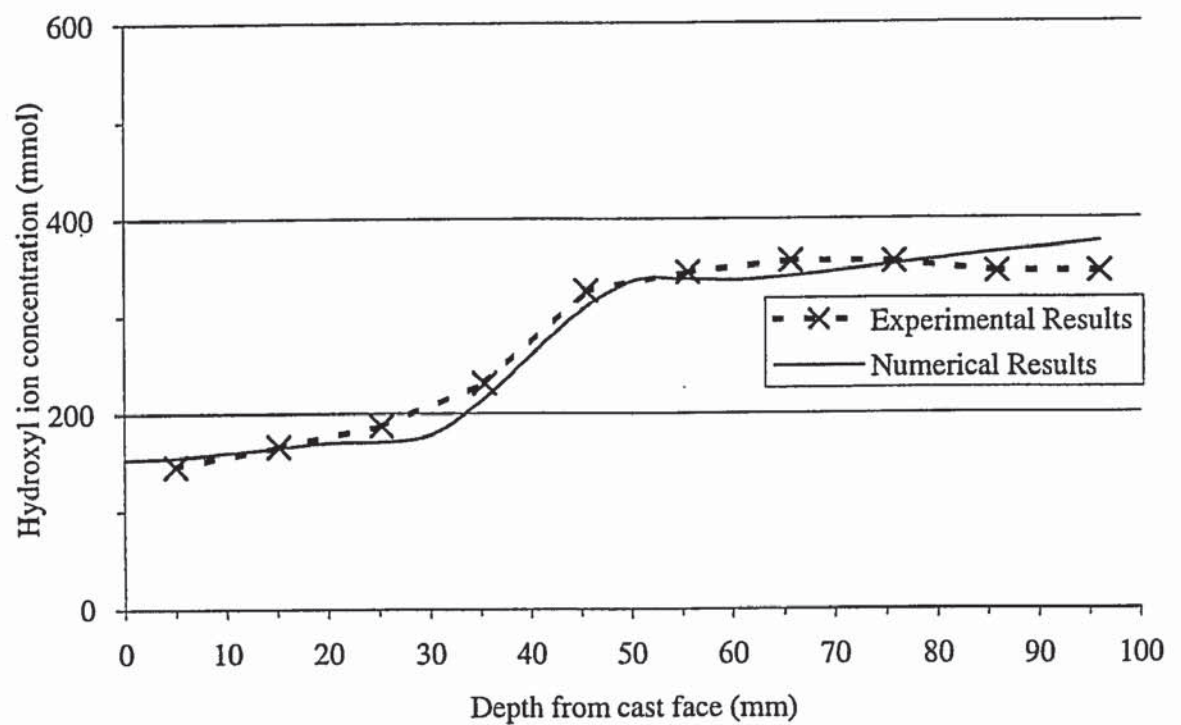


Figure 8.19 - Comparison of numerical and experimental chloride ion profiles for set-up A

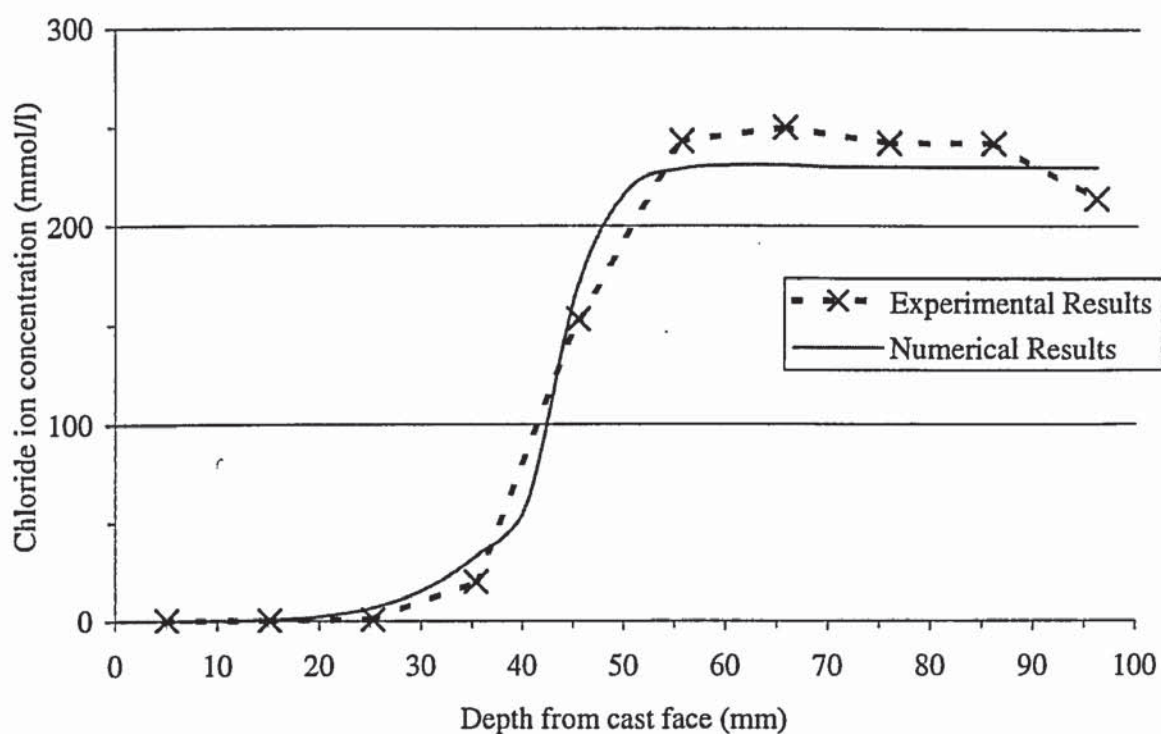


Figure 8.20 - Comparison of numerical and experimental chloride ion profiles for set-up B

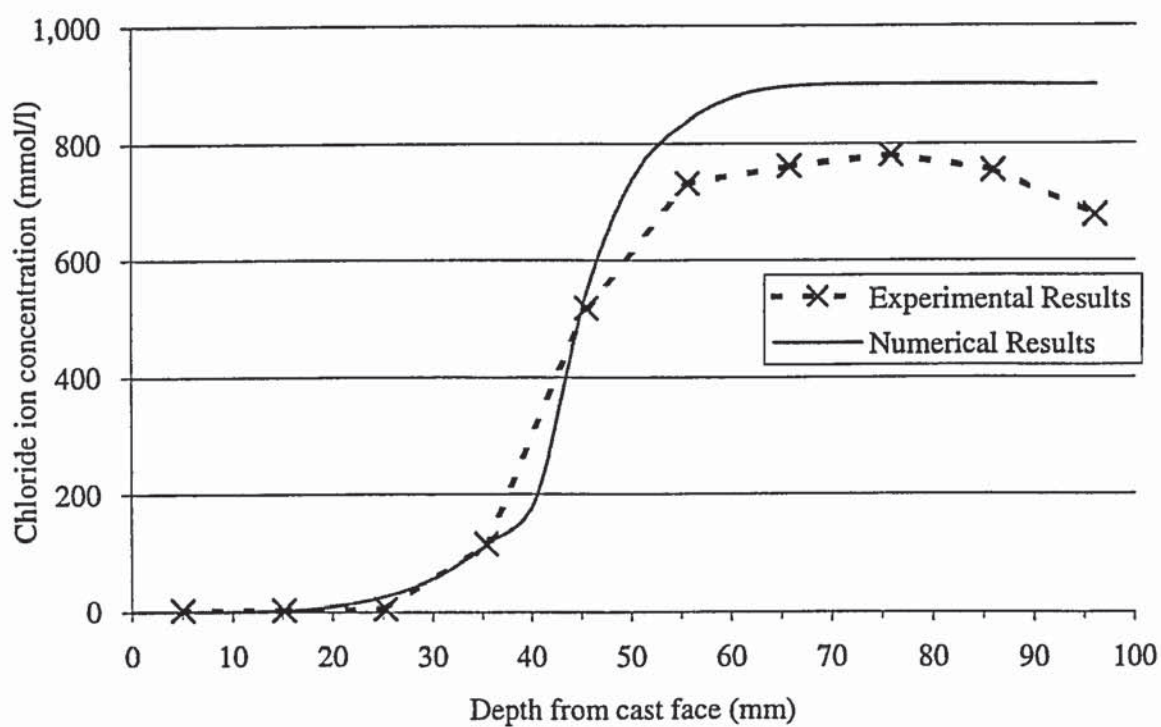


Figure 8.21 - Comparison of numerical and experimental chloride ion profiles for set-up C

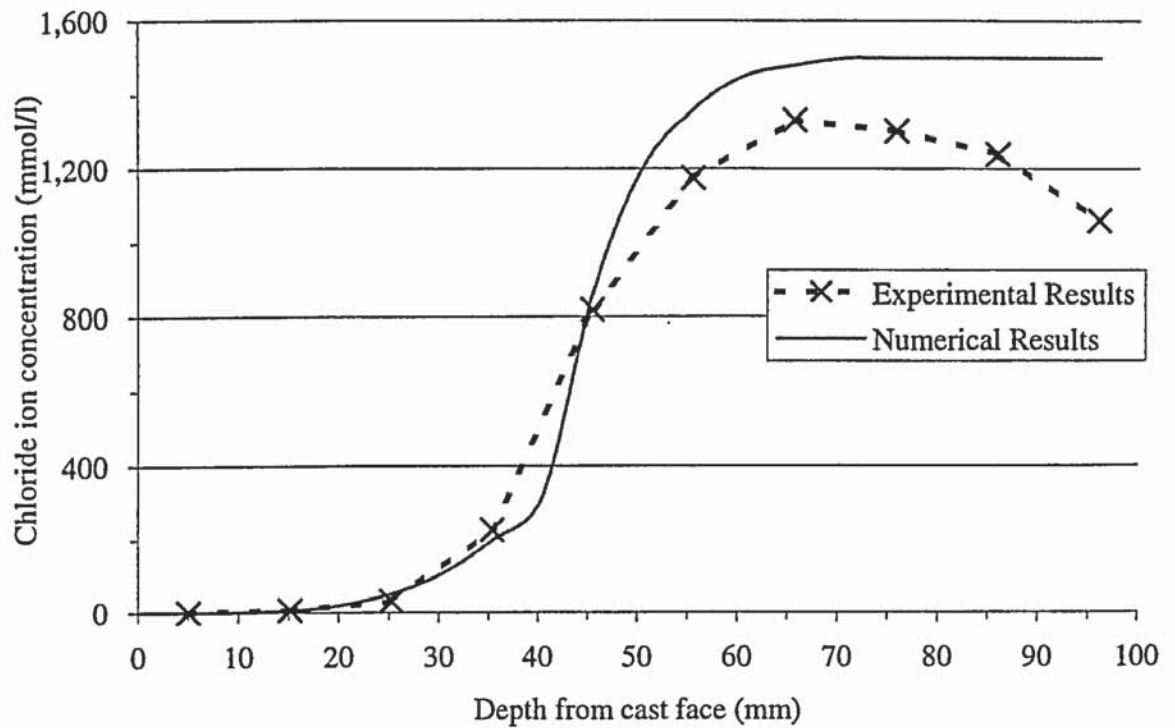


Figure 8.22 - Comparison of numerical and experimental chloride ion profiles for set-up D

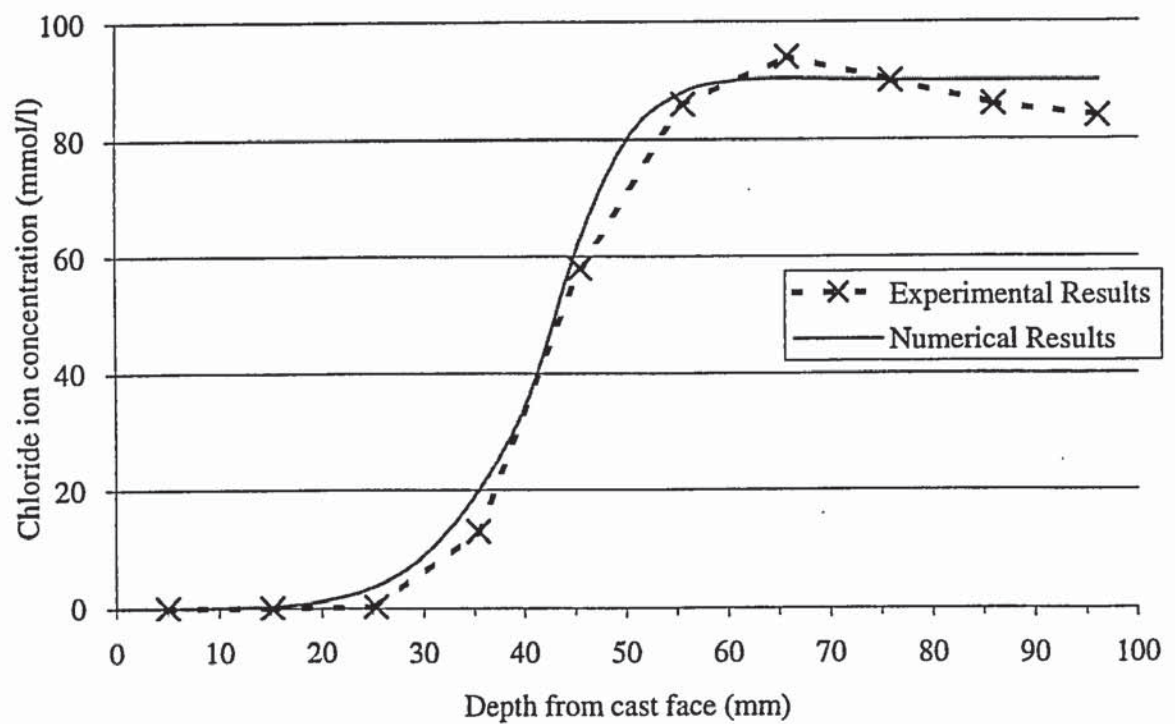




Figure 8.23 - Comparison of numerical and experimental chloride ion profiles for set-up E

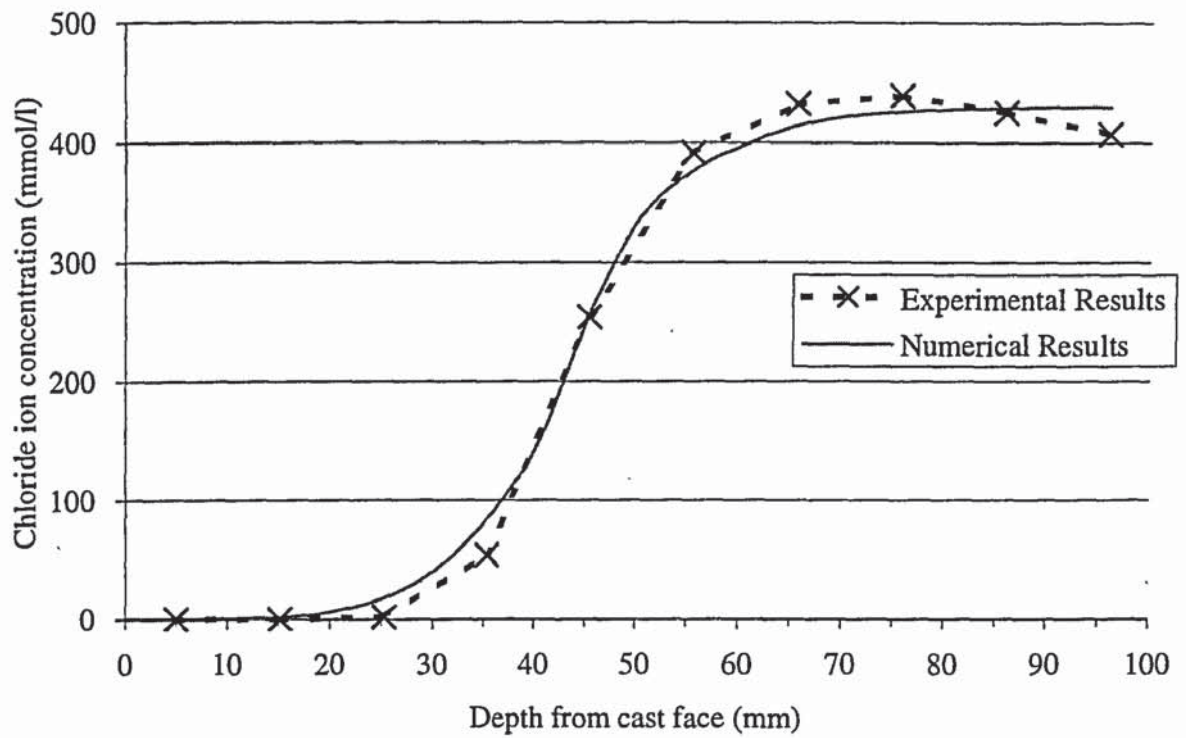


Figure 8.24 - Comparison of numerical and experimental chloride ion profiles for set-up F

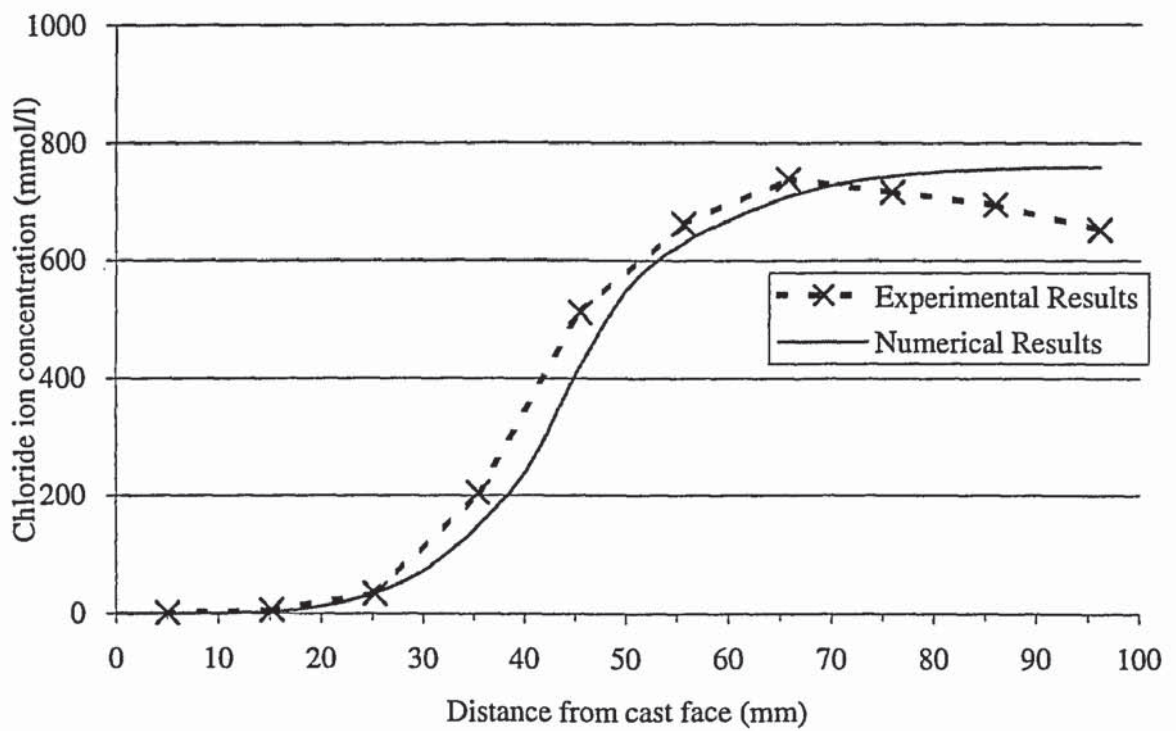


Figure 8.25 - Comparison of experimentally determined sulphate ion profiles for set-ups A, B and C

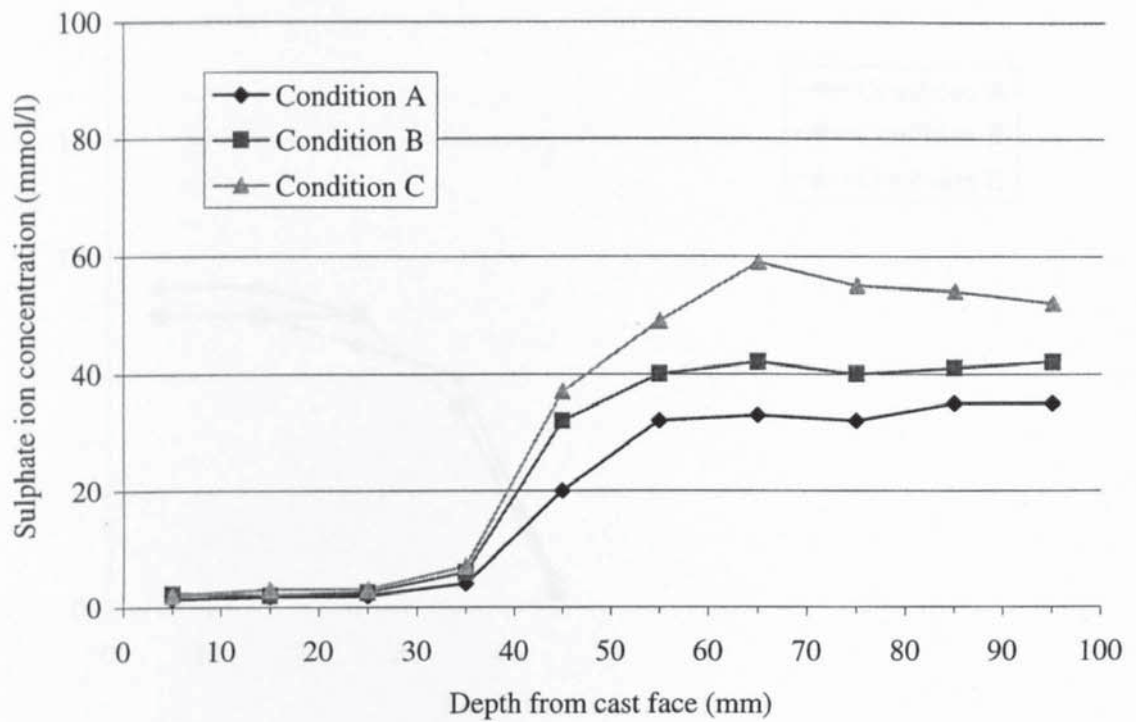


Figure 8.26 - Comparison of experimentally determined sulphate ion profiles for set-ups D, E and F

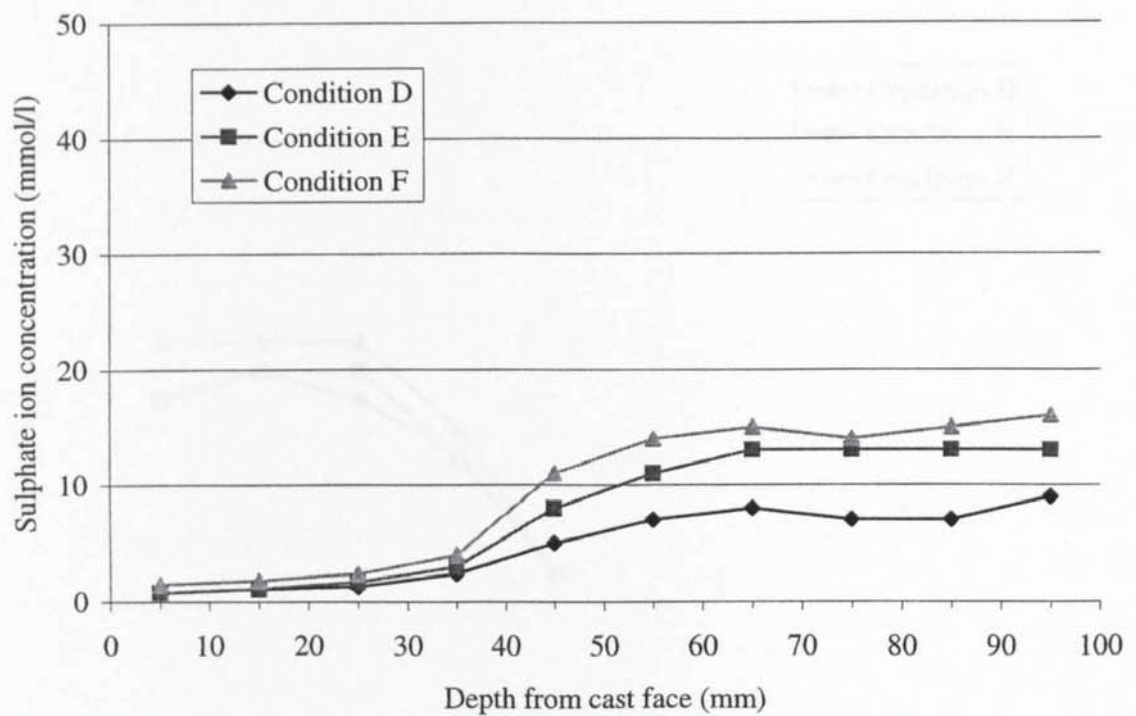


Figure 8.27 - Comparison of experimentally determined nitrate ion profiles for set-ups A, B and C

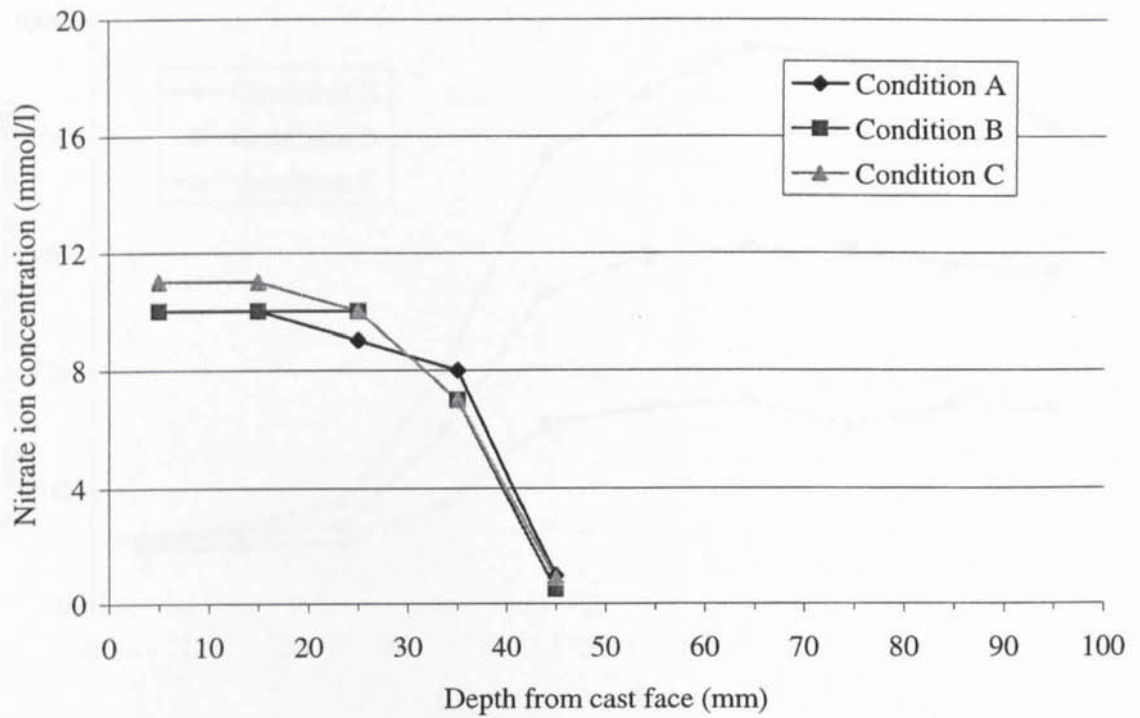


Figure 8.28 - Comparison of experimentally determined nitrate ion profiles for set-ups D, E and F

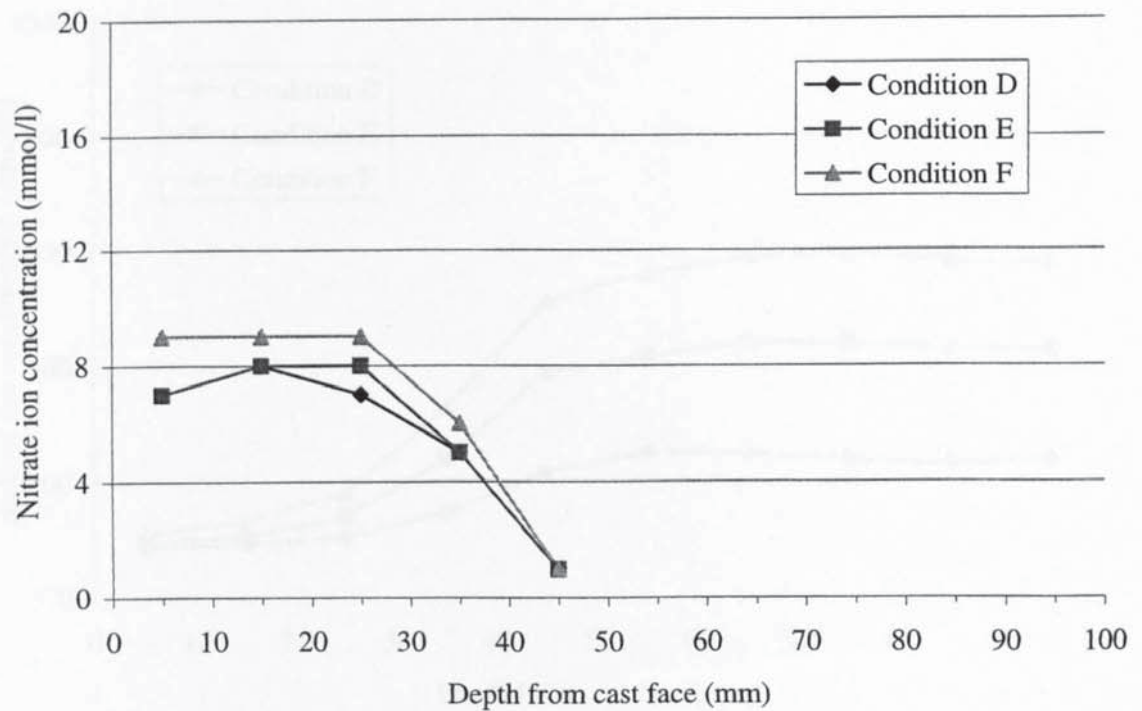




Figure 8.29 - Comparison of experimentally determined sodium ion profiles for set-ups A, B and C

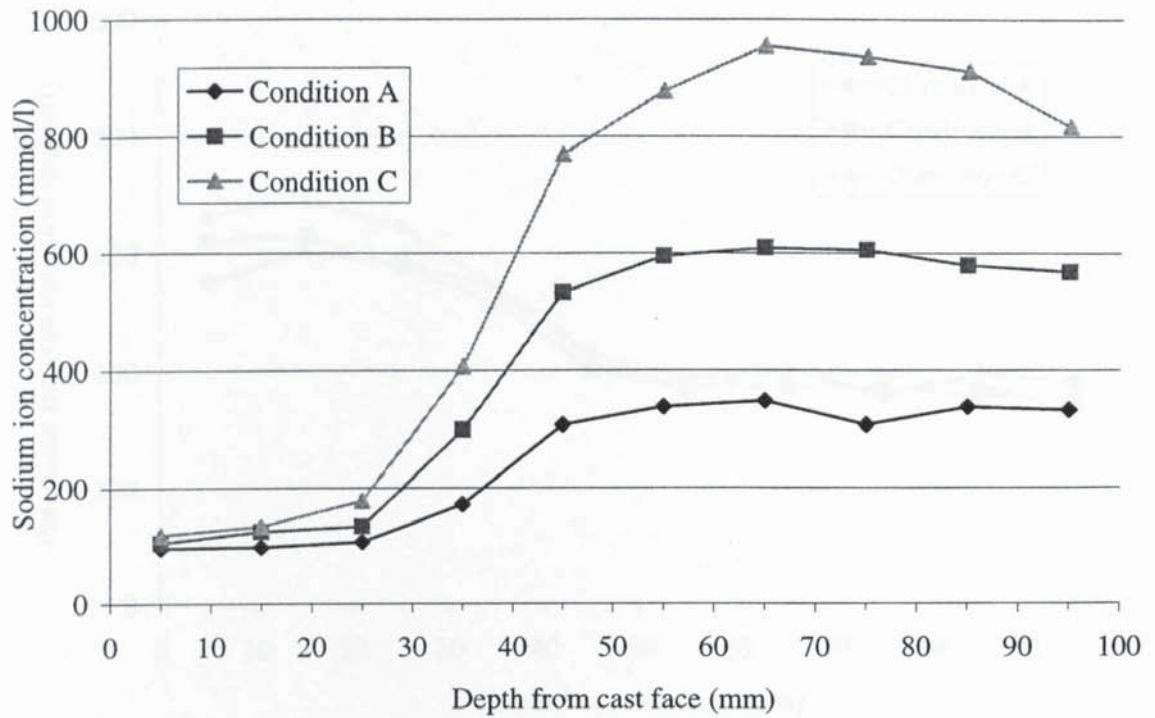


Figure 8.30 - Comparison of experimentally determined sodium ion profiles for set-ups D, E and F

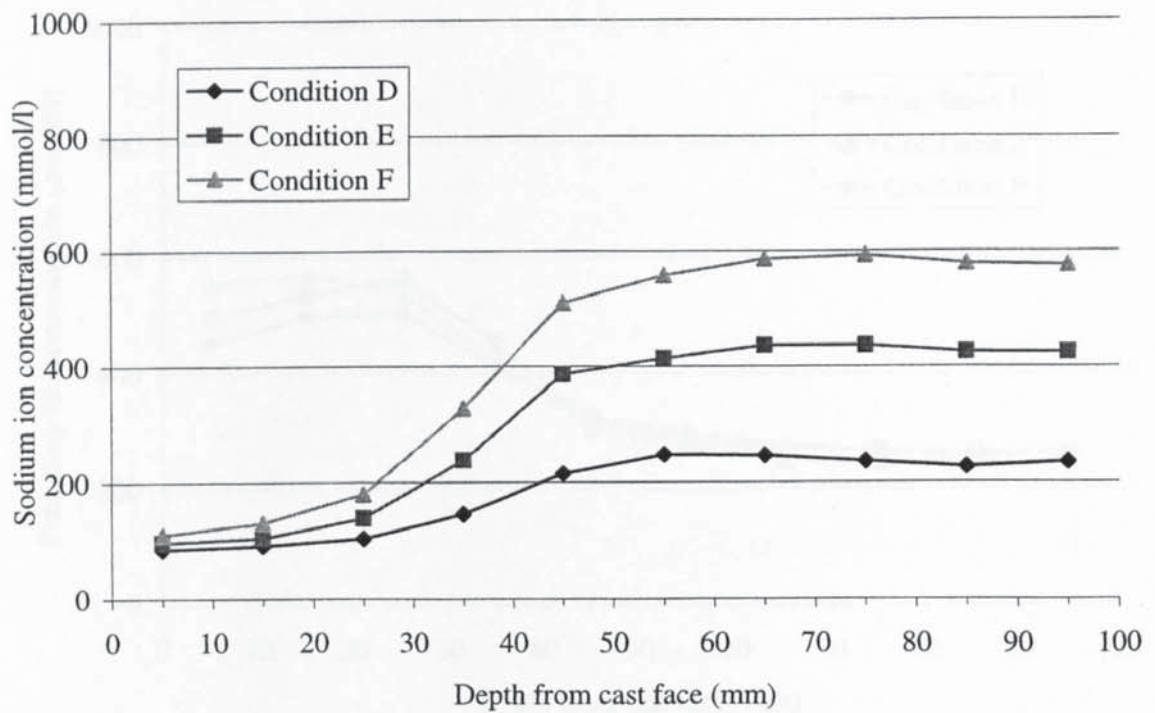


Figure 8.31 - Comparison of experimentally determined potassium ion profiles for set-ups A, B and C

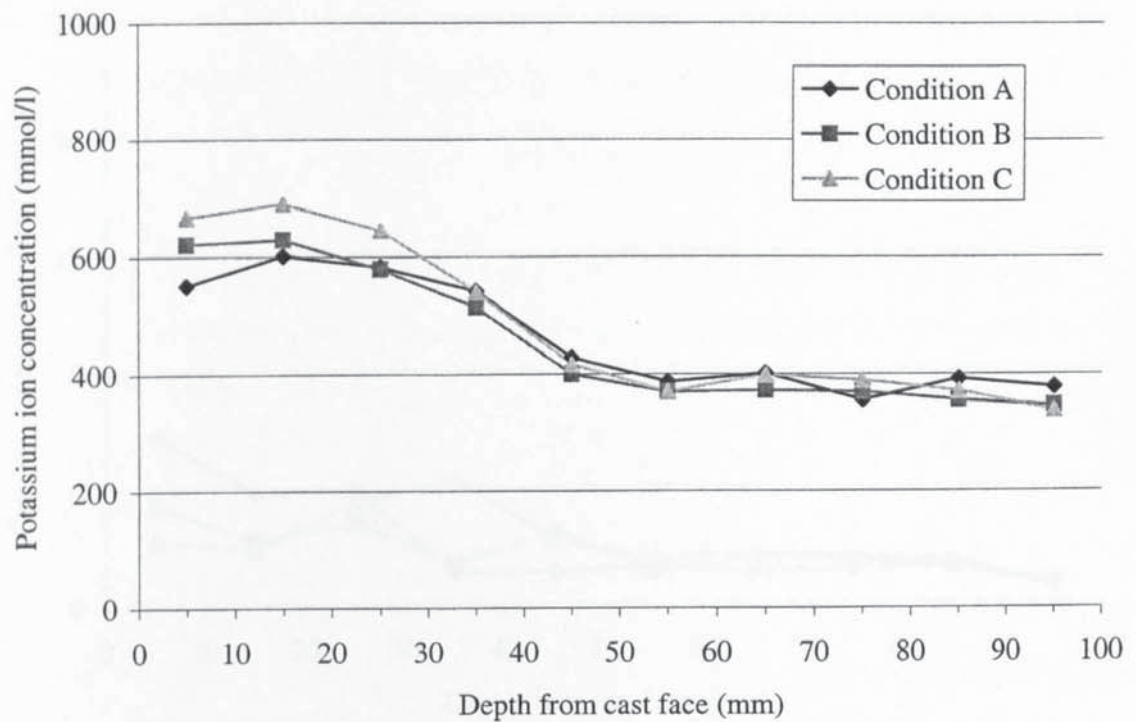


Figure 8.32 - Comparison of experimentally determined potassium ion profiles for set-ups D, E and F

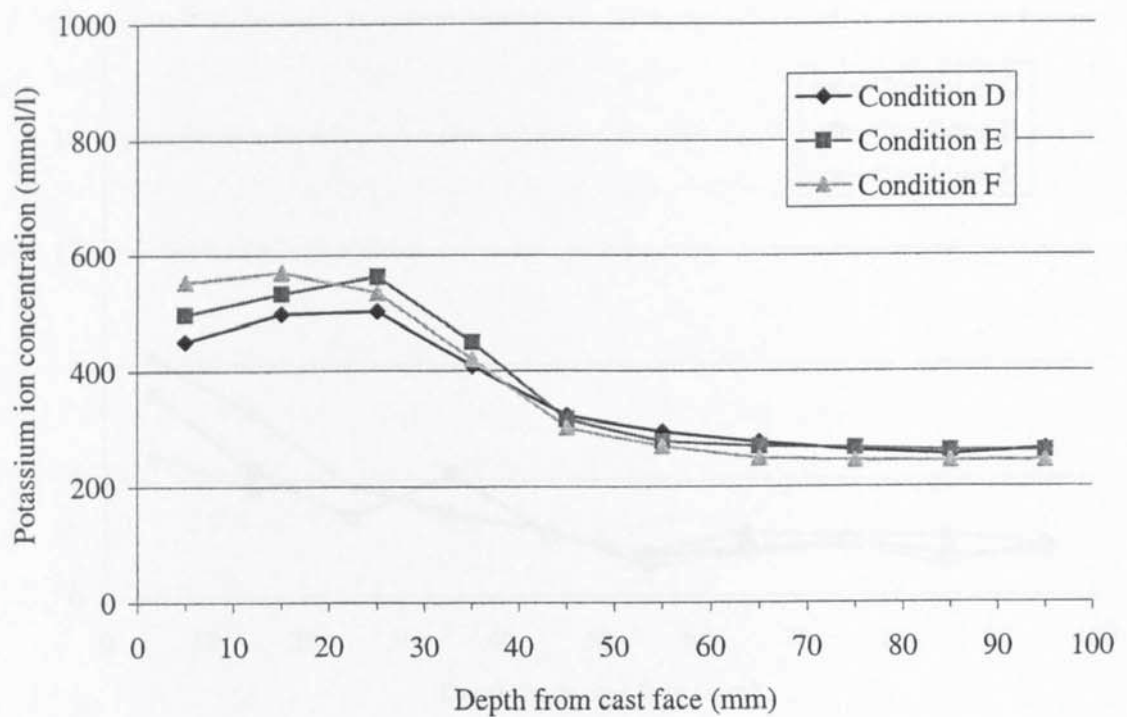


Figure 8.33 - Comparison of experimentally determined calcium ion profiles for set-ups A, B and C

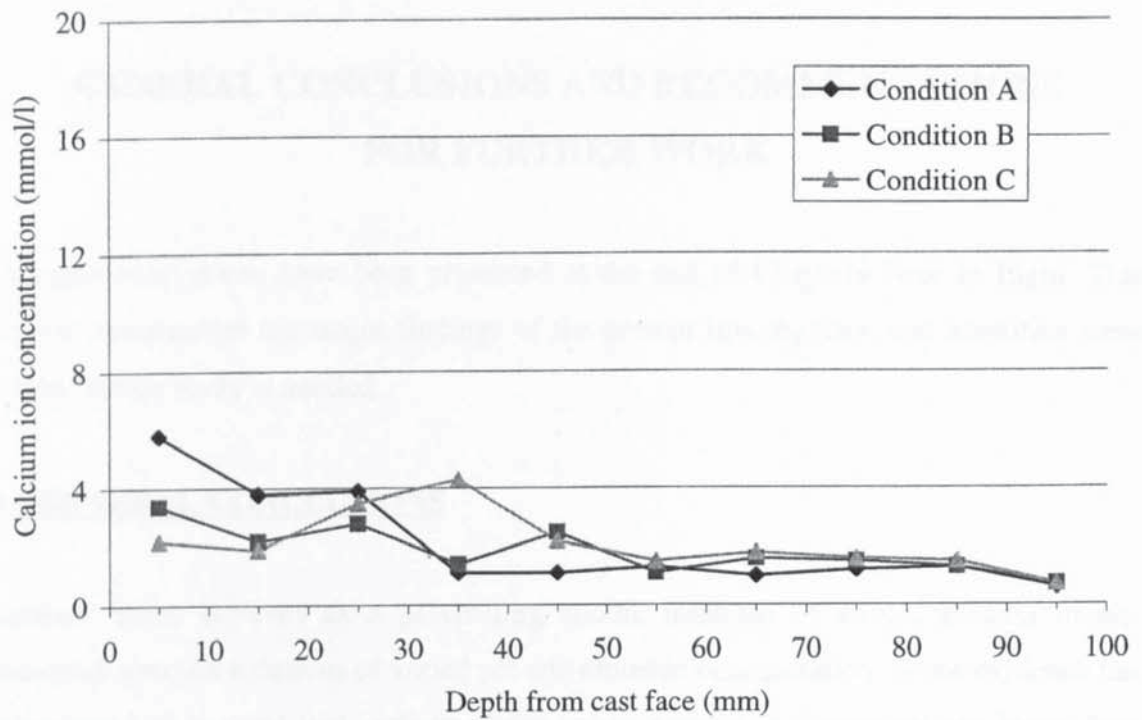
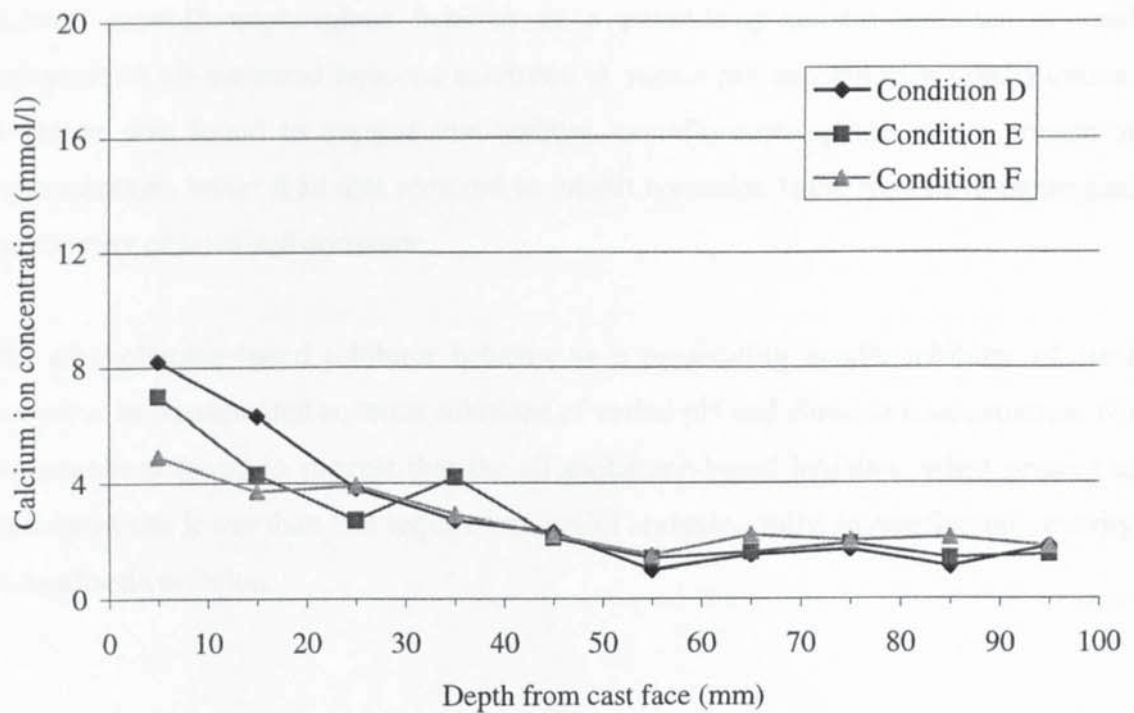


Figure 8.34 - Comparison of experimentally determined calcium ion profiles for set-ups D, E and F





## **CHAPTER NINE**

### **GENERAL CONCLUSIONS AND RECOMMENDATIONS FOR FURTHER WORK**

Detailed conclusions have been presented at the end of Chapters Four to Eight. This chapter summarises the major findings of the present investigation and identifies areas where further study is needed.

#### **9.1 GENERAL CONCLUSIONS**

Sodium nitrite behaves as a passivating anodic inhibitor of steel corrosion in air-saturated aqueous solutions of varied pH and chloride concentration. Some evidence has been found to suggest that sodium nitrite, when present at concentrations lower than that required to inhibit corrosion fully, may have intensified the severity of localised corrosion.

Sodium monofluorophosphate behaves as a passivating anodic inhibitor of steel corrosion in air-saturated aqueous solutions of varied pH and chloride concentration. Evidence was found to suggest that sodium monofluorophosphate, when present at concentrations lower than that required to inhibit corrosion fully, may have intensified the severity of localised corrosion.

The alkanolamine-based inhibitor behaves as a passivating anodic inhibitor of steel corrosion in air-saturated aqueous solutions of varied pH and chloride concentration. No evidence was found to suggest that the alkanolamine-based inhibitor, when present at concentrations lower than that required to inhibit corrosion fully, intensified the severity of localised corrosion.

Ethanolamine behaves as a passivating anodic inhibitor of steel corrosion in air-saturated aqueous solutions of varied pH and chloride concentration. No evidence was found to suggest that ethanolamine, when present at concentrations lower than that required to inhibit corrosion fully, intensified the severity of localised corrosion.

Under the conditions employed, sodium monofluorophosphate failed to penetrate significantly into partially carbonated site concrete when applied as recommended by the supplier. Phosphate and fluoride were found, using a water-extraction method, to penetrate 5mm into partially carbonated site concrete treated with sodium monofluorophosphate.

Under the conditions investigated, the ethanolamine component of the alkanolamine-based inhibitor did appear to penetrate significant depths and was found, using both water-extraction and acid-extraction, beyond the carbonation zone of partially carbonated site concrete. Under the conditions investigated, the phosphate component of the alkanolamine-based inhibitor did penetrate 9mm into the partially carbonated site concrete, but was only found using acid-extraction (not found using water extraction).

Carbonating hydrated cement paste over saturated solutions of sodium nitrite results in significant concentrations of nitrite in the pore solution of the carbonated paste. This has possible implications when considering the effects of accelerated carbonating regimes on the corrosion related properties of concrete, as nitrite has been shown to be an anodic inhibitor of steel corrosion. Saturated solutions of sodium chloride, ammonium nitrate, magnesium nitrate and sodium dichromate have been investigated and identified as alternatives for controlling the relative humidity of the carbonating environment.

An increase in the carbon dioxide concentration of the carbonating atmosphere results in an associated increase in the release of bound chloride ions, bulk density and capillary porosity and a decrease in the pH of the pore solution and total porosity of the resultant carbonated cement paste.



Calcium carbonate, formed by the carbonation of hydrated cement paste, was found in the present study to be mainly in the mineralogical form of calcite, with substantial amounts of vaterite and a trace of aragonite.

From the investigations into physical realkalisation it appeared that hardened carbonated cement paste can be realkalised to a limited extent due to the diffusion of hydroxyl ions under saturated conditions. A substantial proportion of the hydroxyl ions that diffused into the carbonated cement paste however, became bound into the cement matrix and hydroxyl ion concentrations remained below 5mmol/l within the pore solution of the realkalised cement paste. It is also evident from the results presented in this study that the carbonated cement paste is realkalised to a limited extent from both the direction of the repair cement paste and from the direction of the uncarbonated cement paste, when present beyond the carbonated zone.

From the investigations into the calcium nitrite-based rehabilitation system it is apparent that nitrite ions penetrate significant distances by diffusion within the pore solution of saturated uncarbonated hydrated cement paste. However, on the basis of previous researches (Virmani, Clear and Pasko, 1983; Gaidis and Rosenberg, 1987; El-Jazairi and Berke, 1990; Tomosawa et al., 1992; Collins, Weyers and Al-Qadi, 1993), it was assumed for the purpose of the present study that a critical  $[\text{NO}_2^-]/[\text{Cl}^-]$  ratio of 1 could be used as a measure of the effectiveness of the calcium nitrite-based rehabilitation system. The mathematical model presented in Chapter Eight demonstrated that the assumed critical  $[\text{NO}_2^-]/[\text{Cl}^-]$  ratio was achieved to a depth of 13mm within the 0.6 water to cement ratio cement paste with 0.5% chlorides by weight of cement. This suggests that the calcium nitrite-based corrosion rehabilitation system may be effective at suppressing corrosion on steel bars located within this zone.



## **9.2 RECOMMENDATIONS FOR FURTHER WORK**

Further immersion tests could be carried out in order to establish the critical inhibitor to chloride ratios required to inhibit corrosion fully in model electrolytes of varied pH and chloride concentrations. Further immersion tests using mild steel bars that are already undergoing significant corrosion would provide a more realistic assessment on the effectiveness of the inhibitors as a rehabilitation option.

Steel bars could be placed within specimens such as those presented in Chapter Seven and the effect of physical realkalisation on the anodic or cathodic polarisation response of such bars could be monitored. The use of lithium hydroxide within the repair cement paste used for physical realkalisation could be evaluated in terms of reducing the risk of inducing alkali aggregate reaction. The mathematical model could be modified to take into account the transport of the other ions that are associated with the physical realkalisation process, such as sodium. Further experimental investigations could be carried out to determine the bound sodium concentrations within the cement pastes in order to verify the conclusion that substantial amounts of hydroxyl ions become bound into the hydrated cement matrix.

The calcium nitrite-based corrosion rehabilitation system investigated in Chapter Eight could be assessed as to regards its effectiveness for the rehabilitation of steel in carbonated concrete. The investigations presented in Chapter Four showed that nitrite ions were promising as regards to their ability to inhibit corrosion fully in air-saturated solutions intended to simulate the pore solution phase within carbonated concrete. Steel bars could be placed within carbonated cement paste specimens and also chloride-contaminated cement paste specimens such as those presented in Chapter Eight, and the effect of the rehabilitation system on the anodic or cathodic polarisation response of such bars could be monitored.

Further work is needed to define the nature and the stability of the passive film formed around steel reinforcement after treatment with particular inhibitors. It would be useful to know the thickness and quality of the passive film so that a better understanding of the mechanisms of inhibitor action could be achieved. Investigations of this nature could be carried out using techniques such as scanning electron microscopy or X-ray photoelectron spectroscopy.

Long-term site trials on the durability of concrete structures after treatment by corrosion inhibitors are needed. Monitoring the structures for corrosion potential and corrosion rate of embedded reinforcement would give a better understanding of the effectiveness and longevity of protection afforded by such inhibitor treatments. However, there are several problems that may arise with such trials which need to be addressed. For example, isolating the effectiveness of the inhibitors alone may be difficult in structures that have been treated with other methods of rehabilitation, such as surface coatings, in addition to the inhibitor treatment. Also, monitoring techniques that involve the use of embedded electrodes have added difficulties in that the monitoring relies heavily on the long term performance and calibration of such electrodes.



## LIST OF REFERENCES

- Ahmed, H.E.H., (1990)**, "Transportation and occurrence of chlorides in PFA concrete", PhD Thesis, University of Dundee, 219 pp.
- Alonso, C. and Andrade, C. (1990)**, "Effect of nitrite in contaminated and chloride-free carbonated mortars", *ACI Materials Journal*, Vol. 87(2), pp. 130-137.
- Alonso, C., Acha, M. and Andrade, C. (1990)**, "Inhibiting effect of nitrite on the corrosion of rebars embedded in carbonated concrete", *Proc. RILEM Int. Symp. On Admixtures for Concrete – Improvement of Materials*, ed. E. Vazquez, Barcelona, May 1990, pp. 219-228.
- Alonso, C., Andrade, C., Argiz, C. and Malric, B. (1996)**, " $\text{Na}_2\text{PO}_3\text{F}$  as Inhibitor of Corroding Reinforcement in Carbonated Concrete", *Cement and Concrete Research*, 26(3), pp. 405-415.
- Andrade, C., Alonso, C. and Gonzalez, J.A. (1986)**, "Some laboratory experiments on the inhibitor effect of sodium nitrite on reinforcement corrosion", *Cement, Concrete and Aggregates*, Vol. 8(2), pp. 110-116.
- Andrade, C., Alonso, C., Acha, M. and Malric, B. (1992)**, "Preliminary Testing of  $\text{Na}_2\text{PO}_3\text{F}$  as a Curative Corrosion Inhibitor for Steel Reinforcements in Concrete", *Cement and Concrete Research*, 22, pp. 869-881.
- Arber, M.G. and Vivian, H.E. (1961)**, *Australian Journal of Applied Science*, 12, pp. 339 & 436.
- Asano, S., Ozu, M., Inoue, Y. and Hashizume, G. (1962)**, "The Hydration and Carbonation of Various Kinds of Cement Compounds", *Review of the 16<sup>th</sup> General Meeting, Cement Association of Japan, Tokyo*, Vol. 16, pp. 68-69.
- Asaro, M.F., Gaynor, A.T. and Hettiarachchi, S. (1990)**, "Electrochemical Chloride Removal and Protection of Concrete Bridge Components (Injection of Synergistic Corrosion Inhibitors)", *Strategic Highway Research Program, Report SHRP-S/FR-90-002*, National Research Council, Washington DC.
- Bager, D.H. and Sellevold, E.J. (1986)**, *Cement and Concrete Research*, Vol. 16(709).
- Bard, A.J. and Faulkner, L.R. (1980)**, "Electrochemical Methods", Wiley, New York, p. 120. (ISBN 0 471 08753 X).



**Barneyback, R.S. and Diamond, S. (1981)**, "Expression and analysis of pore fluid from hardened cement pastes and mortars", *Cement and Concrete Research*, Vol. 11, pp. 279-285.

**Bensted, J. (1997)**, "Cements: Past, Present and Future", An Inaugural Lecture at the University of Greenwich, 23<sup>rd</sup> January 1997, pp.16.

**Bentz, D.P., (1994)**, "Evolution of porosity and calcium hydroxide in laboratory concretes containing silica fume", *Cement and Concrete Research*, Vol. 24(6), pp. 1044-1050.

**Berke, N.S. (1989)**, "A Review of Corrosion Inhibitors in Concrete", *Materials Performance*, 28(10), pp. 41-44.

**Berke, N.S. (1991)**, "Corrosion Inhibitors in Concrete", *Concrete International*, 13(7), PP. 24-27.

**Berke, N.S. and Weil, T.G. (1994)**, "World wide review of corrosion inhibitors in concrete", *Advances in Concrete Technology*, ed. V.M. Malhotra, CANMET, Ottawa, 1994, pp. 899-1022.

**Berke, N.S., Dallaire, M.P., Weyers, R.E., Henry, M.B., Peterson, J.E. and Prowell, B.D. (1992)**, "Impregnation of concrete with corrosion inhibitors", *Corrosion Forms and Control for Infrastructure*, ASTM STP-1137, ed. V. Chaker, Philadelphia, pp. 300-327.

**Bertolini, L., Yu, S.W. and Page, C.L. (1996)**, "Effect of Electrochemical Chloride Extraction on Chemical and Mechanical Properties of Hydrated Cement Paste", *Advanced Cement Research*, Vol. 8, pp. 93 – 100.

**Bier, T.A., Kropp, J., Hilsdorf, H.K., (1987)**, "Carbonation and realkalisation of concrete and hydrated cement paste", 1st Int. Rilem Congress from Materials Science to construction, *Materials Engineering*, 3, Versailles, France, pp. 927-934.

**Bier, T.A., Kropp, J., Hilsdorf, H.K., (1989)**, "The formation of silica gel during carbonation of cementitious systems containing slag cement", *Fly Ash, Silica Fume, Slag and Natural Pozzalans in Concrete*, ACI SP-114, Trondheim, 2, pp. 1413-1428.

**Bijen, J.M. (1985)**, "On the durability of Portland Furnace Slag Cement Concrete in Hot Marine Environment", *Proc. First Int. Conf. on Deterioration and Repair of Reinforced Concrete in the Arabian Gulf, Bahrein*, October 26-29, Vol. 1, pp. 215-232.

**Bjegovic, D, Sipos, L., Ukrainczyk, V. and Miksic, B. (1994), "Diffusion of the MCI 2020 and 2000 corrosion inhibitors into concrete", Proc. Corrosion and Corrosion Protection of Steel in Concrete, ed. R.N. Swamy, Sheffield, pp. 865-877.**

**British Cement Association (1999), "Concrete through the ages", BCA Publication, Crowthorne, U.K..**

**British Standard 4550 (1970), "Loss on Ignition", Part 2, Section 13.2.**

**Brooks, R., Clark, L.M. and Thurston, E.F. (1951), "Calcium Carbonate and its Hydrates", Phil. Trans. Roy. Soc., Vol. 243(A861), pp. 145-167.**

**Broomfield, J. (1997), "Corrosion of Steel in Concrete: Understanding, Investigation and Repair", E & FN Spon, An Imprint of Chapman & Hall.**

**Broomfield, J. (1999), "Field Experience and Evaluation", Inhibitors for the prevention and cure of reinforcement corrosion in concrete, SCI Conference, London, 30<sup>th</sup> September 1999.**

**Browne, R.D. (1982), "Design Prediction of the life for Reinforced Concrete in Marine and other Chloride Environments", Durability of Building Materials, July, Vol. 1(2), pp. 113-125.**

**Brunauer, S. (1962), American Scientist, Vol. 50(210).**

**Brunauer, S. and Greenberg, S.A. (1962), in 4<sup>th</sup> ISCC, Vol. 1, p. 135.**

**Buchler, M., Elsener, B., Stalder, F. and Bohni, H. (1999a), "A migrating corrosion inhibitor blend for reinforced concrete, Part 1: Prevention of Corrosion", Corrosion – in press**

**Buchler, M., Elsener, B., Stalder, F. and Bohni, H. (1999b), "A migrating corrosion inhibitor blend for reinforced concrete, Part 2: Inhibition and Repair Strategy", Corrosion – in press**

**Buenfeld, N. (1986), "Chloride in Concrete", Concrete Repair, Vol. 2, A selection of articles reprinted from the journals Construction Repair and Maintenance/Concrete, Palladian Publication Limited ISBN 0 86310 027 9.**

**Calder, A.J.J. (2000), "Experiments to assess the Performance of Corrosion Inhibitors in Concrete", Corrosion Inhibitors – Do they work?, One-day conference, Aston University, Birmingham, England, 26<sup>th</sup> January 2000, 12pp..**



**Cole, W.F. and Kroone, B. (1960)**, "Carbon Dioxide in Hydrated Portland Cement", American Concrete Institute Journal, Vol. 31(12), pp. 1275-1295.

**Collins, W.D., Weyers, R.E. and Al-Qadi, I.L. (1993)**, "Chemical treatment of corroding steel reinforcement after removal of chloride-contaminated concrete", Corrosion, 49(1), pp.74-87.

**Constantier, D. and Diamond, S. (1997)**, "Pore solution analysis: are there pressure effects?", in Mechanisms of chemical degradation of cement-based systems, eds. Scrivener, K.L. and Young, J.F., Spon, London, pp. 22-29.

**Craig, R.J. and Wood, L.E. (1970)**, "Effectiveness of Corrosion Inhibitors and their Influence on the Physical Properties of Portland Cement Mortars", Highway Research Record, No. 328, pp.77.

**Crank, J. (1975)**, "The Mathematics of Diffusion", 2<sup>nd</sup> Edition, pp. 21, Clarendon Press, Oxford, 347pp..

**Day, R.L. and Marsh, B.K., (1988)**, "Measurement of porosity in blended cement paste", Cement and Concrete Research, 18, pp. 63-73.

**Dhir, R.K., (1989)**, "Near-surface characteristics of concrete: prediction of carbonation resistance", Magazine of Concrete Research, 41(148), pp. 137-143.

**Dhir, R.K. (1993)**, "PFA concrete: chloride diffusion rate", Magazine of Concrete Research, Vol. 45(162), pp. 1-9.

**Diamon, M., Abo-El-Enein, A., Hosaka, G., Goto, S. and Kondo, R. (1977)**, "Pore structure of calcium silicate hydrate in hydrated tricalcium silicate", Jour. Amer. Ceram. Soc., Vol. 60(3-4), pp. 110-114.

**Diamond, S. (1976)**, "Cement paste microstructure", Conf. on Hydraulic Cement Pastes: Their Structure and Properties, Sheffield, Cement and Concrete Association, pp. 2-30.

**Double, D.D. (1983)**, "New developments and understanding the chemistry of cement hydration", Phil. Trans. R. Soc. A310, pp. 53-66.

**Draffin, J. (1976)**, "A Brief History of Lime, Cement, Concrete and Reinforced Concrete", in A Selection of Historic American Papers on Concrete, 1876-1926, ACI Publication SP-52, ed. H. Newlon Jr, American Concrete Institute, pp. 3-40.



**Dressman, S., Osiroff, T., Dillard, J., Glanville, J. & Weyers, J. (1991), "A Screening Test for Rebar Corrosion Inhibitors", Transportation Research Board 70<sup>th</sup> Annual Meeting, Washington DC.**

**Duchesne, J. and Berube, M.A. (1994), "Evaluation of the validity of the pore solution expression method from hardened cement paste and mortar", Cement and Concrete Research, Vol. 24, pp. 456-462.**

**Dullien, F., (1979), "Transport phenomena in porous media and pore structure", Academic Press 1979.**

**Duprat, M., Lafont, M.C., Moran, F. & Rocher, S. (1985), "Inhibition de la corrosion d'un acier au carbone en milieux neutres aeres par les monofluorophosphates", Revue Francais des SCIENCES DE L'EAU, 4, PP.1-15, (In French).**

**El-Jazairi, B. and Berke, N.S. (1990), "The use of calcium nitrite as a corrosion inhibiting admixture to steel reinforcement in concrete", in Corrosion of Reinforcement in Concrete, eds. C.L. Page, K.W.J. Treadaway and P.B. Bamforth, Elsevier, London, pp. 571-585.**

**Elsener, B. (1999), "Corrosion inhibitors for steel in concrete – state of the art report", The Institute of Materials, London, European Federation of Corrosion Publications – in press**

**Feldman, R.F. (1969), in 5<sup>th</sup> ISCC, Vol. 3, p. 53.**

**Feldman, R.F. and Sereda, P.J. (1970), "A new model for hydrated Portland cement and its practical implications", J. Amer. Ceram. Soc., Vol. 53(8-8), pp. 53-59.**

**Feldman, R.F. and Beaudoin, J.J., (1991), "Pretreatment of hardened cement pastes for mercury intrusion measurements", Cement and Concrete Research, 21, pp. 297-308.**

**Fookes, P.G., Pollock, D.J. and Kay, E.A. (1981), "Middle East Concretes – Rates of Deterioration", Concrete, Vol. 15(9), pp. 12-19.**

**Forrester, J.A. (1976), "Measurement of Carbonation", Proc. RILEM Int. Symposium on Carbonation of Concrete, C&CA, Fulmer Grange, April 5-6, 6pp..**

**Gaidis, J.M. and Rosenberg, A.M. (1979), "The mechanism of nitrite inhibition of chloride attack on reinforcing steel in alkaline aqueous environments", Materials Performance, Vol. 18(11), pp. 45-48.**

**Gaidis, J.M., and Rosenberg, A.M. (1987), "The Inhibition of Chloride-Induced Corrosion in Reinforced Concrete by Calcium Nitrite", Cement, Concrete and Aggregates, 9(1), pp.30-33.**

**Garboczi, E.J. and Bentz, D.P. (1991), in Advances in Cementitious Materials, Ceramic Trans., Vol. 16, ed. S. Mindess, American Ceramic Society, p. 365.**

**Gassner, P. and Malric, B. (1995), "Concrete Restoration with MFP", Locher & Cie AG, Zurich, Germany, 30pp..**

**Glass, G.K. and Buenfeld, N.R. (1997), "The Presentation of the Chloride Threshold Level for Corrosion of Steel in Concrete", Corrosion Science, Vol. 39(5), pp. 1001-1013.**

**Glasstone, S. and Lewis, D. (1960), "Elements of Physical Chemistry", MacMillan, London, 1960, 2<sup>nd</sup> Edition, 758pp..**

**Gonzalez, J.A., Ramirez, E., Bautista, A. and Feliu, S. (1996), "The behaviour of pre-rusted steel in concrete", Cement and Concrete Research, Vol. 26, pp. 501-511.**

**Gregg, S. and Sing, K., (1982), "Adsorption, surface area and porosity", 2<sup>nd</sup> Edition, Academic Press 1985.**

**Griffin, D.F. (1975), "Corrosion Inhibitors for Reinforced Concrete", Corrosion of Metals in Concrete, SP-49, ACI, Detroit, pp.95-102.**

**Grube, H. and Lawrence, C.D. (1984), "Permeability of Concretes to Oxygen", Proc. RILEM Int. Seminar on the Durability of Concrete under normal outdoor exposure, 26-29 March 1984, Hannover, pp. 68-79.**

**Hancock, P. and Mayne, J.E.O. (1958), "The effect of inhibitors on the corrosion of iron on the air-formed film", Jour. Chem. Soc., pp. 4172-4175.**

**Hausmann, D.A. (1967), "Steel Corrosion in Concrete. How does it occur?", Material Protection, Vol. 6(11), pp. 19-23.**

**Haynes, M.D. (1996), "MFP Technical Information Package", Balvac Whitley Moran, Alfreton, UK.**

**Hettiarachichi, S. and Gaynor, A.T. (1992), "Corrosion Inhibitors for Rebar Corrosion Control", Materials Performance, 31(3), pp. 62-66.**



**Hilsdorf, H., Kropp, J. and Gunter, M., (1984), "Carbonation, pore structure and durability", Proc. RILEM Seminar, Hanover, pp. 182-196.**

**Hime, W.G. (1994), "Chloride-Caused Corrosion of Steel in Concrete: A new Historical Perspective", Concrete International, May 1994, pp. 56-61.**

**Hoffman, J.D. (1997), "Numerical Methods for Engineers and Scientists", McGraw-Hill Inc.**

**Hope, B.B. and Ip, A.K.C. (1989), "Corrosion Inhibitors for Use in Concrete", ACI Materials Journal, 86(6), pp. 602-608.**

**Idorn, G.M. and Thaulow, N. (1983), "Examination of 136 years old Portland cement concrete", Cement and Concrete Research, Vol. 13(5), pp. 739-743.**

**Jeknevorian, A.A., Chin, D. & Saidha, L. (1995), "Determination of a Nitrite-Based Corrosion Inhibitor in Plastic and Hardened Concrete", Cement, Concrete and Aggregates, CCAGDP, 17(1), pp.48-54.**

**Jones, G. and Wood, I. (2000), "Performance of Corrosion Inhibitors in Practice", Corrosion Inhibitors – Do they work?, One-day conference, Aston University, Birmingham, England, 26<sup>th</sup> January 2000, 9pp..**

**Keer, J.G., Chadwick, J.R. and Thompson, D.M. (1990), "Protection of Reinforcement by Concrete Repair Materials against Chloride Induced Corrosion", Corrosion of Reinforcement in Concrete, ed. C.L. Page, K.W.J. Treadaway and P.B. Bamforth, Society of Chemical Industry, pp. 420-433.**

**Kondo, R., Daimon, M. and Akiba, T. (1969), "Mechanisms and Kinetics on Carbonation of Hardened Cement", Proc. Fifth International Symposium on the Chemistry of Cement, Tokyo 1968, Vol. 3, pp. 402-409.**

**Konecny, L. and Naqvi, S.J., (1993), "The effects of different techniques on the pore size distribution of blended cement mortars", Cement and Concrete Research, Vol. 23(3), pp. 1223-1228.**

**Kromer, R. (1993), "Concrete – Fragments of its History", Concrete Precasting Plant and Technology, Issue 1, pp. 40-51.**

**Kuznetsov, Y.I. (1996), "Organic Inhibitors of Corrosion of Metals", Plenum, New York.**



**Lambert, P., Page, C.L. and Vassie, P.R.W. (1991), "Investigation of Reinforcement Corrosion 2. Electrochemical Monitoring of Steel in Chloride Contaminated Concrete", Materials and Structures, Vol. 24, pp. 351-358.**

**Larbi, J.A., (1991), "The cement paste-aggregate interfacial zone in concrete", PhD Thesis, University of Delft, Netherlands, 127 pp..**

**Lea, F.M. (1970), The Chemistry of Cement and Concrete", 3<sup>rd</sup> Edition, London, Arnold 1970, 727pp..**

**Leek, D.S. and Poole, A.B. (1990), "The breakdown of the passive film on high yield steel by chloride ions" in Corrosion of Reinforcement in Concrete, ed. C.L. Page , Treadaway, K.W.J. and P.B. Bamforth, Elsevier Applied Science, London, pp. 65-73.**

**Lewis, J.M., Mason, C.E. & Brereton, D. (1956), Civil Engineering and Public Works Review, 51(602), pp. 881.**

**Li, S. and Roy, D.M., (1986), "Investigation of the relationship between porosity, pore structure and chloride diffusion of fly ash and blended cement pastes", Cement and Concrete Research, Vol. 16, pp. 749-759.**

**Litvan, G., (1976), "Variability of the nitrogen surface area of hydrated cement paste", Cement and Concrete Research, Vol. 6(1), pp. 139-144.**

**Longuet, P., Burglen, L. and Zelwer, A. (1973), "The liquid phase of hydrated cement", Revue des Matériaux de Construction, 676, pp. 35-41.**

**Loo, Y.H., Chin, M.S., Tam, C.T. and Ong, C.G. (1994), "A carbonation prediction model for accelerated carbonation testing of concrete", Magazine of Concrete Research, 46(168), pp. 191-200.**

**Mackay, D. (1996), "Development of Repair Systems to Satisfy Maintenance Requirements", Advances in Maintenance Strategies for Highway Structures, Aston University in Birmingham, UK, Sept. 24, 17pp.**

**Maeder, U. (1994), "A New Class of Corrosion Inhibitors", Proceedings of Corrosion and Corrosion of Steel in Concrete, Swamy (ed), Sheffield, UK, pp. 851-864.**

**Malami, C. and Kaloidas, V., (1994), "Carbonation and porosity of mortar specimens with pozzolanic and hydraulic cement admixtures", Cement and Concrete Research, 8, pp. 1444-1454.**

**Marazzani, B. (1999)**, "Testing of the corrosion-inhibiting impregnation Sika Ferrogard 903 on carbonated slabs containing slightly to moderately corroded rebars", Proc. Int. Workshop MESINA, Instituto Eduardo Torroja, Madrid, February 1999, pp. 18.1 – 18.10.

**Marsh, B.K. and Day, R.L., (1985)**, "Some difficulties in the assessment of pore structure of high performance blended cement pastes", Material Research Symposium Proceedings, 42, pp. 113-121.

**Marsh, B.K., Day, R.L., Bonner, D.G., (1985)**, "Pore structure characteristics affecting the permeability of cement paste containing fly ash", Cement and Concrete Research, 15, pp. 1027-1038.

**Mattila, J.S. and Pentti, M.J., (1996)**, "Realkalisation of carbonated concrete by cement-based coatings", Corrosion of Reinforcement in Concrete Construction, eds. C.L. Page, P.B. Bamforth & J.W. Figg, Royal Society of Chemistry, Cambridge, pp. 512-521.

**Mayne, J.E.O. and Menter, J.W., (1954)**, "The mechanism of inhibition of the corrosion of iron by solutions of sodium phosphate, borate and carbonate", J. Chem. Soc., pp. 103-107.

**McBeth, D.G. (1998)**, "Francois Hennebique (1842-1921), reinforced concrete pioneer", Proceedings of the Institute of Civil Engineers, 126, May 1998, pp. 86-95.

**McCarter, W.J., (1993)**, "Influence of surface finish on sorptivity on concrete", Journal of materials in civil engineering, 5(1), pp. 130-136.

**Meyer, A., (1968)**, "Investigation on the carbonation of concrete", Proc. Chem. Cement, Tokyo, 3, pp. 394-401.

**Mietz, J. (1995)**, "Electrochemical realkalisation for the rehabilitation of reinforced concrete surfaces", Mater. Corros. , Vol. 46, pp. 527-533.

**Mietz, J. (1998)**, "Electrochemical Rehabilitation Methods for Reinforced Concrete Structures – a State of the Art Report", The Institute of Materials, London, European Federation of Corrosion Publications, No. 24.

**Mietz, J. and Isecke, B. (1994)**, "Mechanisms of realkalisation of concrete", Proc. UK Corrosion and Eurocorr 94, The Institute of Materials, London, Vol. 3, pp. 216-227.



**Miksic, B., Gelner, L., Bjegovic, D. & Sipos, L. (1995)**, "Migrating Corrosion Inhibitors for Reinforced Concrete", Proc. 8<sup>th</sup> European Symposium on Corrosion Inhibitors, Ann. Univ. Ferrara, N.S., Sez.V, Suppl. No.10, pp.569-588.

**Moukwa, M. and Aitcin, P.C., (1988)**, "The effect of drying on cement paste pore structure as determined by mercury intrusion porosimetry", Cement and Concrete Research, 18(5), pp. 745-752.

**Nagayama, M. and Cohen, M. (1962)**, "The anodic oxidation of iron in a neutral solution. Part 1: The nature and composition of the passive film". Jour. Electrochem. Society, Vol. 109, pp. 781-790.

**Neville, A.M. and Brooks, J.J. (1987)**, "Concrete Technology", 1<sup>st</sup> Edition, Longman Group, UK.

**Neville, A.M. (1995)**, Properties of Concrete, 4<sup>th</sup> Edition, Longman, Harlow, pp. 844.

**Ngala, V.T., (1995)**, "Pore structure and diffusional properties of hardened cement pastes", PhD Thesis, Aston University, England, UK.

**Nixon, P. and Page, C.L. (1987)**, "Pore solution chemistry and alkali aggregate reaction", ACI SP-100 – Concrete Durability, ed. J.M. Scanlon, Amer. Conc. Inst., Detroit, pp. 1833-1862.

**Nmai, C.K., Farrington, S.A. & Bobrowski, G.S. (1992)**, "Organic-Based Corrosion-Inhibiting Admixture for Reinforced Concrete", Concrete International, 14(4), pp.45-51.

**Nurnberger, U. (1988)**, Series of Otto-Graf-Institute No.79, Ch.6, Stuttgart, U. Nurnberger and W. Beul, "Influence of galvanizing and PVC coating of reinforcing steels and of inhibitors on steel corrosion in cracked concrete", Werkstoffe and Korrosion, 1991, Vol. 42, pp. 537 – 546.

**Nyame, B.K. and Illston, J.M. (1981)**, "Relationships between Permeability and Pore Structure of Hardened Cement Paste", Magazine of Concrete Research, Vol. 33(116), pp. 139-146.

**Odden, L. (1994)**, "The repassivating effect of electrochemical realkalisation and chloride extraction", Proc. Int. Conf. on Corrosion and Corrosion Protection of Steel in Concrete, Sheffield, pp. 1473-1488.

**O'Grady, W.E. (1980)**, "Mossbauer study of the passive oxide film on iron", J. Electrochem. Society, Vol. 127, 555.



**Page, C.L. (1998)**, "Corrosion and its control in reinforced concrete – The Sixth Sir Frederick Lea Memorial Lecture", ICT Yearbook: 1998-1999, Institute of Concrete Technology, Crowthorne, pp. 37-51.

**Page, C.L. (1999a)**, "Concrete Materials", Degradation of Reinforced Concrete: Processes, Investigation and Control, 5 day Post Experience Course Master's Level Module, Aston University, May 1999, 12 pp..

**Page, C.L. (1999b)**, "Corrosion principles and their application to steel in concrete", Degradation of Reinforced Concrete: Processes, Investigation and Control, 5 day Post Experience Course Master's Level Module, Aston University, May 1999, 19 pp..

**Page, C.L. and Ngala, V.T. (1995)**, "Steady-State Diffusion Characteristics of Cementitious Materials", RILEM International Workshop on Chloride Penetration into Concrete, St Remy les Chevreuse, France, October 1995.

**Page, C.L. and Treadaway, K.W.J. (1982)**, "Aspects of the Electrochemistry of Steel in Concrete", Nature, 297, May 13 1982.

**Page, C.L. and Yu, S.W., (1995)**, "Potential Effects of Electrochemical Desalination of Concrete on Alkali Silica Reaction", Magazine of Concrete Research, 47, No. 170, pp23-31.

**Page, C.L., V.T. Ngala and Page, M.M. (2000)**, "Corrosion inhibitors in Concrete Repair Systems", Magazine of Concrete Research, Vol. 52(1), pp. 25-37.

**Page, C.L., Yu, S.W. and Bertolini, L. (1994)**, "Some potential side-effects of electrochemical chloride removal from reinforced concrete", Sheffield Conference, pp. 228-238.

**Page, M.M., Ngala, V.T., Anstice, D.J. and Page, C.L. (in preparation)**, "Ion chromatographic analysis of corrosion inhibitors in concrete".

**Parrott, L.J., (1981)**, "Effect of drying history upon the exchange of pore water with methanol and subsequent methanol sorption behaviour in hydrated alite paste", Cement and Concrete Research, 11(5), pp. 651-658.

**Parrott, L.J. (1987a)**, "Measurement and Modelling of Porosity in Drying Cement Paste", Proc. Mat. Res. Symp., Vol. 85, pp. 91-104, Mat. Res. Soc..

**Parrott, L.J. (1987b)**, "A Review of Carbonation in Reinforced Concrete", British Cement Association Report C/1-0987.

**Parrott, L.J. (1990)**, "Assessing carbonation in concrete structures", *Durability of Building Materials and Components*, pp. 575-585.

**Parrott, L.J. (1992)**, "Variations of water adsorption rate and porosity with depth from an exposed concrete surface: Effect of exposure conditions and cement type", *Cement and Concrete Research*, 22, pp. 1077-1088.

**Parrott, L.J., Hansen, W. and Berger, R. (1980)**, "Effect of first drying upon pore structure of hydrated alite", *Cement and Concrete Research*, 10(5), pp. 647-655.

**Parrott, L.J., Patel, R.G., Killoh, D.C. and Jennings, H.M. (1984)**, *J. Amer. Ceramic Society*, Vol. 67(233).

**Patel, R.G., Parrott, L.J., Martin, J.A. and Killoh, D.C. (1985)**, "Gradients of microstructure and diffusion properties in cement paste caused by drying", *Cement and Concrete Research*, Vol. 15, pp. 343-356.

**Phihlajavaara, S.E. (1968)**, "Some results of the effect of carbonation on the porosity and pore size distribution of cement paste", *Materials and Structures*, 6, pp. 521-526.

**Pourbaix, M. (1966)**, "Atlas of electrochemical equilibria in aqueous solutions", Pergamon, Oxford.

**Powers, T.C. (1958)**, "Structural and Physical Properties of Hydrated Cement Paste", *Jour. Am. Ceramic Soc.*, Vol. 41(1), pp. 1-6.

**Powers, T.C. and Brownyard, T.L. (1948)**, "Studies of physical properties of hardened Portland cement paste", *Bull. 22, Portland Cement Assoc.*, pp. 276-287.

**Raharinaivo, A. (1996)**, "Action des monofluorophosphates sur la corrosion des armatures dans la beton", *Laboratoire Central des Ponts et Chaussees, rapport DT/OAM/AR81-96*, (In French).

**Rahman, A.A. and Glassner, F.P. (1989)**, "Comparative studies of the carbonation of hydrated cements", *Advances in Cement Research*, 2(6), pp. 49-54.

**Ramachandran, V.S. (1969)**, "Applications of Differential Thermal Thermal Analysis in Cement Chemistry", New York, Chemical Publishing Co. Inc., 308pp..

**Rasheeduzzafar, Dakhil, F.H., Bader, M.A. and Khan, M.N. (1992)**, "Performance of corrosion resisting steel in chloride-bearing concrete", *ACI Materials Journal*, Vol. 89(5), pp. 439-448.



**Richardson, I.G. (1999)**, "The nature of C-S-H in hardened cements", *Cement and Concrete Research*, Vol. 29, pp. 1131 – 1147.

**RILEM Draft Recommendation CPC-18 (1984)**, "Measurement of hardened concrete carbonation depth", *Materiaux et Construction*, Vol. 17(102), pp. 434-440.

**RILEM Report 12 (1995)**, "Performance Criteria for Concrete Durability", eds. J. Kropp and H.K. Hilsdorf, Spon, London, 327 pp. (ISBN 0 419 19880 6).

**Rosenberg, A.M., Gaidis, J.M. and Kossivas, T.G. (1977)**, "Corrosion Inhibitor Formulated with Calcium Nitrite for Use in Reinforced Concrete", STP 629, ASTM, Philadelphia, pp. 89-99.

**Roti, J.A., (1994)**, "Betoninstandsetzung mittels elektrochemischer Realkalisierung und Chloridentfernung", 2. Int. Knogreb zur Bauwerkserhaltung, Berlin, pp. 9-11.

**Sagoe-Crentsil, K.K., Glasser, .P. and Yilmaz, V.T. (1994)**, "Corrosion inhibitors for mild steel: Stannous Tinn (SnII) in ordinary Portland cement", *Cement and Concrete Research*, Vol. 24, pp. 313-318.

**Sakaguchi, Y., Takakura, M., Kitigawa, A., Hori, T., Tomosawa, F. and Abe, M (1989)**, "The inhibiting effect of lithium compounds on alkali-silica reaction", Proc. 8<sup>th</sup> Int. Conf. On Alkali-Aggregate Reaction, Kyoto, July 1989, eds. K. Okada et al., Elsevier, London, pp. 229-234.

**Sauman, Z. (1971)**, "Carbonization of porous concrete and its main binding components", *Cement and Concrete Research*, Vol. 1(6), pp. 645-662.

**Scrivener, K.L. (1989)**, in *Advances in Cement Manufacture and Use*, ed. E. Gartner, Engineering Foundation, New York, p. 3.

**Scrivener, K.L. and Pratt, P.L. (1987)**, "The characterisation and quantification of cement paste and concrete microstructures", *Material Science to Construction Materials Engineering*, Vol. 3(1), pp. 61-68.

**Sellevold, E.J. and Bager, D.H. (1981)**, in 7<sup>th</sup> ICCI, Vol. 4., p. 394.

**Sereda, S., (1968)**, "Mechanism of the carbonation shrinkage of lime and hydrated cement", *Jour. Applied Chemistry*, 18, pp. 111-117.

**Sereda, P., Feldman, R. and Ramachandran, V. (1980)**, Proc. 7<sup>th</sup> Int. Congress on the Chemistry of Cement, VI-1/3-44 Paris.



**Sergi, G., (1986), "Corrosion of steel in concrete: Cement matrix variables", PhD Thesis, 395 pp..**

**Sergi, G., Yu, S.W. and Page, C.L. (1992), "Diffusion of chloride and hydroxyl ions in cementitious materials exposed to a saline environment", Magazine of Concrete Research, Vol. 44(158), pp. 63-69.**

**Short, N.R., Lambert, P. and Page, C.L. (1989), "Effect of corrosion inhibitors on pore solution chemistry of hardened cement pastes", Durability of Concrete: Aspects of Admixtures and Industrial By-Products, Proc. 2<sup>nd</sup> Int. Seminar, Gothenberg, June 1989, eds. L. Berntsson, S. Chandra & L.O. Nilsson, Swedish Council for Building Research, Stockholm, Document D9-1989, pp. 218-228.**

**SHRP-S-666 (1993), Strategic Highway Research Program, National Research Council, United States.**

**Sibbick, R.G., Blackwell, B.Q. and Nixon, P.J. (1999), "Damage to concrete from alkali aggregate reaction", Degradation of Reinforced Concrete: Processes, Investigation and Control, 5 day Post Experience Course Master's Level Module, Aston University, May 1999, 10 pp..**

**Sigalov, E. and Strongin, S. (1962), Reinforced Concrete, Foreign Languages Publishing House, Moscow, 1962, pp. 393.**

**Skjolsvold, O. (1986), Report SP-91, American Concrete Institute, pp. 1445-1462.**

**Slater, J.E. (1983), "Corrosion of metals in association with concrete", American Society for Testing and Materials Special Technical Publication 818, Philadelphia, pp.53.**

**Stern, M. and Geary, A.L. (1957), "A Theoretical Analysis of the Shape of Polarisation Curves", Journal of the Electrochemical Society, 104, pp. 56-63.**

**Stern, M. (1958), "A Method for Determining Corrosion Rates from Linear Polarisation Data", Corrosion NACE, Vol. 14(9), pp. 60-64.**

**Stroud, K.A. (1995), "Engineering Mathematics", 4<sup>th</sup> Edition, Macmillan Press Ltd, Houndmills, Basingstoke, Hampshire, RG21 2XS, pp. 526-532.**

**Taplin, J.H. (1959), "A method for following the hydration reaction in Portland cement paste", Australian Journal of Applied Sc. 10, pp. 329 – 345.**

**Taylor, H.F.W. (1997), "Cement Chemistry", 2<sup>nd</sup> Edition, Thomas Telford Publishing, 437 pp..**

**Thomas, M.D.A. and Matthews, J.D. (1992), "Carbonation of fly ash concrete", Magazine of Concrete Research, Vol. 44(160), pp. 217-228.**

**Tomozawa, F., Nogushi, T., Liao, N.C., Hori, T. and Hara, K. (1992), "Effect of nitrite and its concentration distribution on corrosion prevention of reinforcement in concrete containing chloride", Rehabilitation of Concrete Structures, eds. D.W.S. Ho and F. Collins, RILEM, Melbourne, Australia, pp. 319-328.**

**Tomozawa, F., Masuda, Y., Tanaka, H., Fukushi, I., Takakura, M., Hori, T. and Higashi, S. (1990), "Experimental Study on Effectiveness of Corrosion Inhibitor in Reinforced Concrete", RILEM Symposium on Concrete Durability, Barcelona, Spain, May, pp. 382-391.**

**Transportation Research Board (1991), "Highway Deicing: Comparing Salt and Calcium Magnesium Acetate", Special Report 235, National Research Council, Washington, DC.**

**Treadaway, K.W.J. and Russell, A.D. (1968), "Inhibition of the Corrosion of Steel in Concrete", Highway and Public Works, 36, pp. 40-45.**

**Tuutti, K. (1982), "Corrosion of steel in concrete", Swedish Cement and Concrete Institute, Stockholm, Report Fo 482, 469pp..**

**Vassie, P. (1984), "Reinforcement Corrosion and the Durability of Concrete Bridges", Proceedings of the Institute of Civil Engineers, Vol. 76(1), pp. 713-723.**

**Vaysburd, A.M., Sabnis, G.M. and Emmons, P.H. (1993), "Concrete carbonation - A fresh look", The Indian Concrete Journal, pp. 215-221.**

**Verbeck, G.J. (1958), "Carbonation of hydrated Portland cement", ASTM SP-205, pp. 17-36.**

**Virmani, Y.P., Clear, K.C. & Pasko, T.J. (1983), "Time to Corrosion of Reinforcing Steel in Concrete Slabs", v1.5, "Calcium Nitrite Admixture and Epoxy-Coated Reinforcing Bars as Corrosion Protection Systems", Reports No. FHWA RD-83 012, Washington DC, 17pp..**

**Vogel, A.I. (1978), Textbook of quantitative inorganic analysis, 4<sup>th</sup> Edition, Longmans, pp. 310-311.**



Wallbank, E.J. (1989), "The Performance of Concrete in Bridges: A Survey of 200 Highway Bridges", Her Majesty's Stationary Office, London.

Wittmann, F.H. (1976), in Hydraulic Cement Pastes: Their Structure and Properties, Cement and Concrete Association, Slough, UK, p. 96.

Wittmann, F.H. (1980), in 7<sup>th</sup> ICCI, Vol. 1, p. VI-2/1.

Winslow, D.N. and Diamond, S. (1970), "A mercury porosimetry study of the evaluation of porosity in Portland cement", Journal of Materials, Vol. 5(3), pp. 564-585.

Wood, J.G.M. (1990), "Predicting future decay in concrete structures" in Somerville, G. (ed), The Design Life of Structures, British Group of the International Association for Bridge and Structural Engineering Colloquium, Blackie A & P.

Young, J.F. (1988), "A review of the pore structure of cement paste and concrete and its influence on permeability", ACI, SP 108-1, pp. 1-18.



## **APPENDICES**

## APPENDIX A

### POTENTIAL PHASE COMPOSITION CALCULATIONS

The potential phase compositions for the Ordinary Portland Cement used throughout the present study are presented in Table 3.2. These values were calculated using the method described by Taylor (1997).

The chemical analysis of the cement is presented in Table 3.1. However, only the materials shown in the table below were required for the purpose of calculating the potential phase compositions of the cement.

Material	% (by weight)
CaO	63.86
SiO <sub>2</sub>	19.07
Al <sub>2</sub> O <sub>3</sub>	5.13
Fe <sub>2</sub> O <sub>3</sub>	2.83
SO <sub>3</sub>	3.25
F. CaO	1.49

First, correct the CaO for F.CaO and SO<sub>3</sub> as shown below

$$\begin{aligned} (\text{CaO} - \text{F.CaO}) - (0.7 \text{ SO}_3) &= (63.86 - 1.49) - (0.7 \times 3.25) \\ \text{corrected CaO} &= 60.095 \%(\text{by weight}) \end{aligned}$$

The following equations therefore apply, in which the corrected CaO value is used

$$\begin{aligned} \text{C}_3\text{S} &= 4.0710 \text{ CaO} - 7.6024 \text{ SiO}_2 - 6.7187 \text{ Al}_2\text{O}_3 - 1.4297 \text{ Fe}_2\text{O}_3 \\ \text{C}_2\text{S} &= -3.0710 \text{ CaO} + 8.6024 \text{ SiO}_2 + 5.0683 \text{ Al}_2\text{O}_3 + 1.0785 \text{ Fe}_2\text{O}_3 \\ &= 2.8675 \text{ SiO}_2 - 0.7544 \text{ C}_3\text{S} \\ \text{C}_3\text{A} &= 2.6504 \text{ Al}_2\text{O}_3 - 1.6920 \text{ Fe}_2\text{O}_3 \\ \text{C}_4\text{AF} &= 3.0432 \text{ Fe}_2\text{O}_3 \end{aligned}$$

Therefore

$$\begin{aligned} \text{C}_3\text{S} &= (4.0710 \times 60.095) - (7.6024 \times 19.07) - (6.7187 \times 5.13) - (1.4297 \times 2.83) = 61.16\% \\ \text{C}_2\text{S} &= (2.8675 \times 19.07) - (0.7544 \times 61.16) = 8.54 \% \\ \text{C}_3\text{A} &= (2.6504 \times 5.13) - (1.6920 \times 2.83) = 8.81 \% \\ \text{C}_4\text{AF} &= (3.0432 \times 2.83) = 8.61 \% \end{aligned}$$

## APPENDIX B

### CALCULATION OF FREE IONIC CONCENTRATIONS

Ion chromatography was used in the present study to quantitatively analyse solutions for both anions and cations. The anions that were analysed for included fluoride, chloride, nitrite, bromide, nitrate, phosphate and sulphate. The cations included lithium, sodium, potassium, magnesium, calcium and ethanolamine. The calculation below is an example of how to convert the output from the ion chromatographic analysis (ppm) to millimoles per litre (mmol/l). The example shown below is the calculation for nitrite ions within the pore solution of cement paste that was carbonated over a saturated solution of sodium nitrite in an atmosphere of 100% carbon dioxide (Table 6.2).

Concentration from the ion chromatographic analysis	= 56.92 ppm
Dilution factor	= 100
Atomic mass of nitrite anions ( $\text{NO}_2^-$ )	= 46
Concentration of nitrite anions	= $(56.92 \times 100)/46$ = 123.7 mmol/l



## APPENDIX C

### CALCULATION OF HYDROXYL ION CONCENTRATIONS AND pH BY ACID TITRATION

The example shown below shows the calculation for the initial hydroxyl ion concentration and pH of the pore solution of the calcium nitrite-based repair cement paste in Chapter Eight (Table 8.1).

Volume of pore solution	= 0.1ml
Molarity of acid ( $\text{HNO}_3$ )	= 0.01M
Volume of acid added	= 1.24ml

Concentration of hydroxyl ions	= (Vol. of acid $\times$ Molarity of acid)/Vol. of pore sol
	= $(1.24 \times 0.01)/0.1$
	= 0.124M
	= 124mmol/l

pH	= $14 + \text{Log}_{10}[\text{OH}^-]$
	= $14 + \text{Log}_{10}[0.124]$
	= 13.09

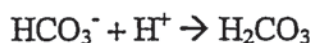
## APPENDIX D

### CALCULATION OF BICARBONATE AND CARBONATE CONCENTRATIONS WITHIN THE PORE SOLUTIONS

The example shown below shows the calculation for the maximum possible bicarbonate and carbonate ions within the pore solution of cement paste that was carbonated over a saturated solution of sodium nitrite in an atmosphere of 0.03% carbon dioxide (Table 6.2).

To titrate 1ml of pore solution from pH 10.6 to pH 4 it required 19.0ml of 0.001M  $\text{HNO}_3$ .

For bicarbonates we have:



$$M = (m \times v)/V$$

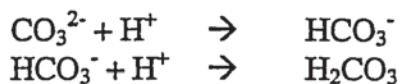
Where,

$$\begin{aligned} M &= \text{molarity of pore solution } (\text{HCO}_3^-) \\ V &= \text{volume of pore solution} = 1\text{ml} \\ m &= \text{molarity of acid } (\text{HNO}_3) = 0.001\text{M} \\ v &= \text{volume of acid} = 19.0\text{ml} \end{aligned}$$

Therefore,

$$M = (0.001 \times 19.0)/1 = 0.019\text{M} = 19\text{mmol/l } \text{HCO}_3^-$$

For carbonates we have:



i.e. two lots of acid are required to titrate  $\text{CO}_3^{2-}$

From ionization constants:

$$\text{Primary ionization constant} = ([\text{H}^+][\text{CO}_3^{2-}])/[\text{HCO}_3^-] = 5 \times 10^{-11}$$

At pH 10.6,

$$[\text{H}^+] = 2.51 \times 10^{-11} \quad (\text{pH} = -\text{Log}_{10}[\text{H}^+])$$

$$[\text{CO}_3^{2-}]/[\text{HCO}_3^-] = 5 \times 10^{-11}/2.51 \times 10^{-11} = 1.992$$

If  $y = \text{CO}_3^{2-}$  and  $x = \text{HCO}_3^-$ ,

$$\text{then } y = 1.992x \quad (1)$$

As twice as much acid is required for  $\text{CO}_3^{2-}$  we also have

$$x + 2y = 19.0 \text{ (mmol/l)} \quad (2)$$

Substituting (1) into (2)

$$x + 3.984x = 19.0 \quad \text{i.e. } 4.984x = 19.0$$

Therefore  $x = 3.81$

From (1)  $y = 1.992 \times 3.81 = 7.59$

Therefore  $\text{HCO}_3^- = 3.8 \text{ mmol/l}$  and  $\text{CO}_3^{2-} = 7.6 \text{ mmol/l}$



## APPENDIX E

### CALCULATION OF EVAPORABLE WATER CONTENT

The example shown below is the calculation for evaporable water content within cement paste that was carbonated over a saturated solution of sodium nitrite in an atmosphere of 100% carbon dioxide.

$$\text{E.W.}(\%) = [(W_0 - W_{105}) \times (100 - i - a)] / W_{950}$$

Where:

$$\begin{aligned} W_0 &= 2.1151 \text{ g} \\ W_{105} &= 1.9845 \text{ g} \\ W_{950} &= 1.3430 \text{ g} \\ i &= 3.7900 \% \text{ by weight of cement} \\ a &= 0.0000 \% \text{ by weight of cement} \end{aligned}$$

Therefore

$$\begin{aligned} \text{E.W.}(\%) &= [(2.1151 - 1.9845) \times (100 - 3.790 - 0.000)] / 1.343 \\ &= 9.36 \% \end{aligned}$$

The evaporable water content was calculated in order to express ionic species as free amounts present in the hydrated cement paste as a fraction of the unhydrated cement. The calculation for free nitrite ions in the cement paste that was carbonated over a saturated solution of sodium nitrite in an atmosphere of 100% carbon dioxide (Table 6.4) is shown below.

$$\begin{aligned} \text{Conc. of nitrite ions} \\ \text{in pore solution} &= 123.7 \text{ mmol/l (Table 6.2)} \end{aligned}$$

$$\text{E.W.} = 9.36 \%$$

$$\begin{aligned} \text{Water added during} \\ \text{'saturation' process} &= 18.24 \% \end{aligned}$$

Therefore

$$\begin{aligned} \text{Free conc. per g of cement} &= [123.7 \times (9.36 + 18.24)] / (100 \times 1000) \\ &= 0.034 \text{ mmol / g of cement} \\ &= 34 \times 10^{-3} \text{ mmol / g of cement} \end{aligned}$$

## APPENDIX F

### CALCULATION OF CAPILLARY AND TOTAL POROSITY

The example shown below is the calculation of capillary and total porosity for cement paste that was carbonated over a saturated solution of sodium nitrite in an atmosphere of 100% carbon dioxide (Figure 6.6).

$$\text{Saturated weight in water (W}_1\text{)} = 7.8860 \text{ g}$$

$$\text{Saturated surface dry weight (W}_2\text{)} = 15.7220 \text{ g}$$

$$\text{Weight at 90.7\% RH (W}_3\text{)} = 13.9848 \text{ g}$$

$$\text{Weight at 105}^\circ\text{C (W}_4\text{)} = 12.7297 \text{ g}$$

$$\begin{aligned}\text{Capillary porosity (\%)} &= [(W_2 - W_3) / (W_2 - W_1)] \times 100 \\ &= [(15.7220 - 13.9848) / (15.7220 - 7.8860)] \times 100 \\ &= 22.17 \%\end{aligned}$$

$$\begin{aligned}\text{Total porosity (\%)} &= [(W_2 - W_4) / (W_2 - W_1)] \times 100 \\ &= [(15.7220 - 12.7297) / (15.7220 - 7.8860)] \times 100 \\ &= 38.19 \%\end{aligned}$$

## APPENDIX G

### COMPUTER PROGRAM TO SIMULATE PHYSICAL REALKALISATION OF CARBONATED CEMENT PASTE

```
% COMPUTER PROGRAM, WRITTEN IN MATLAB, TO SIMULATE THE
% TRANSPORT BEHAVIOUR OF HYDROXYL IONS IN A SATURATED
% POROUS MEDIUM
clf; clear;
%
% x1 = repair cement paste thickness, cm
% x2 = carbonated cement paste thickness + x1, cm
% x3 = uncarbonated cement paste thickness + x2, cm
%
x1=1.0; x2=3.0+x1; x3=5.0+x2;
%
% alpha = ( $\alpha/w$ )
%  $\alpha$  = constant used in the Langmuir adsorption isotherm; (mmol/l)-1
% w = content of water in which diffusion occurs, expressed per unit weight of cement
% beta = constant ( $\beta$ ) used in the Langmuir adsorption isotherm; (mmol/l)-1
% nodes = total number of nodes
% dx = space increment used
% d1, d2, d3 = diffusion coefficients in the repair, carbonated and
% uncarbonated pastes, respectively; cm2/day
% c1, c2, c3 = initial hydroxyl ion concentrations in the pore solutions of the
% repair, carbonated and uncarbonated pastes respectively; mmol/l
% cb0, cbl = boundary concentrations at x=0 (cast face) and x=x3 (end face); mmol/l
% csmin = the minimum hydroxyl ion concentration required, in the pore solution of
% the carbonated paste, for realkalisation; mmol/l
% index1=1 for d(cold)/dx=0, i.e. no surface leaching of hydroxyl ions
% index1=-1 for cold(1)=cb0, i.e. surface leaching of hydroxyl ions
% index2=-1 for realkalisation of the carbonated paste
% index2=1 for re-carbonation due to surface leaching of hydroxyl ions
%
alpha=500; beta=0.04;
nodes=200; dx=x3/(nodes-1);
d1=0.011232; d2=1.2096; d3=0.03888;
c1=500; c2=0.0; c3=300;
cb0=0.004; cbl=300;
csmin=1; index1=1; index2=-1;
if index2 > 0; index1=-1; end;
%
```



```

% x(j) = coordinate at node j
% cold(j) = concentration at node j
% d(j) = diffusion coefficient at node j
%
for j=1: 1: nodes
    x(j)=dx*(j-1);
    if x(j) <= x1; d(j)=d1; cold(j)=c1; end;
    if x(j) > x1; d(j)=d2; cold(j)=c2; end;
    if x(j) > x2; d(j)=d3; cold(j)=c3; end;
end;
if index1 < 0 cold(1)=cb0; end; cold(nodes)=cbl;
semilogy(x,cold,'g-.'); hold on; %plot initial concentration profile
%
% maxtime = period of diffusion
% dt = time increment used
%
maxtime=120; dt=0.2; time=0.0; steps=maxtime/dt;
%
%
*****
***
%
for step=1: 1: steps
    time=time+dt
    %
    % form tridiagonal matrix: aa(j,3) and bb(j) to equations
    % aa(j,1)*cnew(j-1)+aa(j,2)*cnew(j)+aa(j,3)*cnew(j+1)=bb(j)
    %
    for j=2: 1: nodes-1
        %
        lambda=alpha/(1+beta*cold(j))^2;
        a1=dt/(dx*dx)/(1+lambda);
        aa(j,1)=-a1*(d(j-1)+d(j))/2.0;
        aa(j,2)=1+a1*(d(j-1)+2.0*d(j)+d(j+1))/2.0;
        aa(j,3)=-a1*(d(j)+d(j+1))/2.0;
        bb(j)=cold(j);
    %
    % Applying boundary condition at x=x3, cnew(j)=cold(j)
    %
    if j == nodes-1
        bb(j)=bb(j)-aa(j,3)*cold(j);
    end;
    %

```

```

end;
%
% transfer aa(j,3) to a lower triangular matrix aa(j,2)
% aa(j,1)*cnew(j-1)+aa(j,2)*cnew(j)=bb(j)
%
for j=nodes-2:-1:2
aa(j,2)=aa(j,2)-aa(j+1,1)*aa(j,3)/aa(j+1,2);
bb(j)=bb(j)-bb(j+1)*aa(j,3)/aa(j+1,2);
aa(j,3)=0.0;
end;
%
% Applying boundary condition at x=0
%
if index1 > 0; cnew(1)=bb(2)/(aa(2,1)+aa(2,2)); end;
if index1 < 0; cnew(1)=cold(1); end;
%
% forwards to solve cnew(j)
%
for j=2:nodes-1
cnew(j)=(bb(j)-aa(j,1)*cnew(j-1))/aa(j,2);
end;
cnew(nodes)=cold(nodes); cold=cnew;
%
if index2 < 0
%
% for realkalisation
% find lowest hydroxyl ion concentration (in the carbonated paste), ymin=min(cnew(j))
%
ymin=c3;
for j=1:nodes
if x(j) < x1; y(j)=c3; end;
if x(j) >= x1; y(j)=cnew(j); end;
if x(j) > x2; y(j)=c3; end;
if y(j) < ymin; ymin=y(j); result(2)=x(j); end;
end;
%
% if ymin>csmin then stop and print time (days) and distance
%
if ymin >= csmin
result(1)=time; semilogy(x,cnew,'r-'); hold on;
disp('critical level has reached at days and distance');
disp(result)
break

```

```

end;
%
end;
if index2 > 0
%
% for re-carbonation
% find highest hydroxyl ion concentration (in carbonated paste), ymax=max(cnew(j))
%
ymax=0.0;
for j=1:nodes
    if x(j) < x1; y(j)=0.0; end;
    if x(j) >= x1; y(j)=cnew(j); end;
    if x(j) > x2-(x2-x1)/2.0; y(j)=0.0; end;
    if y(j) > ymax; ymax=y(j); result(2)=x(j); end;
end;
%
% if ymax < csmin then stop and print time (days) and distance
%
if ymax < csmin
    result(1)=time; semilogy(x,cnew,'r-'); hold on;
    disp('critical level has reached at days and distance');
    disp(result)
    break
end;
%
end;
end;
%
%
*****
***
%
%print graph
%
xlabel('Depth from cast face, cm'); ylabel('Hydroxyl ion concentration, mmol/l');
print -deps model.ps
%
%place results into text file for ftp to excel
%
l=1:1:200; z=[x(l);cnew(l)];
fid = fopen('plot12.txt','w');
fprintf(fid,'%6.2f %6.2f\n',z);
fclose(fid);

```



## APPENDIX H

### COMPUTER PROGRAM TO SIMULATE A CALCIUM NITRITE-BASED CORROSION REHABILITATION SYSTEM

#### DATA FILE

13, 120, 0.006, 0.0, 3  
100, 0.04, 0.06, 0.0  
720, 840, 120, 0  
0, 1140, 380, 760  
4e-12, 3e-11, 5e-11, 4e-11  
8e-12, 8e-11, 6e-11, 2e-11  
1.67, 4.08

C COMPUTER PROGRAM, WRITTEN IN FORTRAN, TO SIMULATE THE  
C TRANSPORT BEHAVIOUR OF SEVERAL IONS IN A SATURATED POROUS  
C MEDIUM

C

C I = Chemical species, MI = Total species  
C J = Nodal number, MJ = Total nodal number  
C XJ(J) = coordinates  
C ZI(I) = valence number  
C DI(I,J) = diffusion coefficients  
C C(I,J), CI(I,J) = concentrations  
C AI = Externally applied current density  
C PHI(J) = Electrostatic potential  
C LAMBDA(J) = Conductivity  
C AIS(J) = Ionic strength

C

INTEGER MI,MJ,MMJ,MWEEKS,KWEEKS,KDAYS,KHS,KSECS,I,J,NN,  
+ STEP,MII,MMJJ, INDEX  
PARAMETER (MII=4, MMJ=400)  
DOUBLE PRECISION  
C,CI,XJ,ZI,AI1,PHI,PHINEW,DX,DIJ,ALPHA1,BETA1,  
+ ALPHA,X1,X2,X3,CO1,CO2,DO1,AIJ,GAMA1,DO2,  
+ TIME,WEEK,TAU,D0,RSTEP,RATIO,AR1  
DIMENSION C(MII,MMJ),CI(MII,MMJ),XJ(MMJ),ZI(MII),DO2(MII),  
+ PHI(MMJ),PHINEW(MMJ),ALPHA(5),DIJ(MII,MMJ),  
+ CO1(MII),CO2(MII),DO1(MII),AIJ(MMJ)

C

OPEN(5,FILE='nige.dat',STATUS='OLD')  
OPEN(9,FILE='nige.out',STATUS='UNKNOWN')

```

MI=MII
READ(5,*) MWEEKS,STEP,AR1,GAMA1,MMJJ
READ(5,*) MJ, X1, X2, X3
READ(5,*) (CO1(I),I=1,MI)
READ(5,*) (CO2(I),I=1,MI)
READ(5,*) (DO1(I),I=1,MI)
READ(5,*) (DO2(I),I=1,MI)
READ(*,*) ALPHA1, BETA1
AI1=0.0
TAU=1.0
DATA ZI/-1,1,-1,-1/
DATA ALPHA/0.0, 4.08, 0.3, 4.06e-02, 0.0/, GAMA1/0.0/
C
ALPHA(1)=ALPHA1
ALPHA(2)=BETA1
D0=10.06E-11
DX=(X1+X2+X3)/(MJ-1)
NN=X1/DX
C
C set x coordinate, concentrations, diffusion coeffs, current density
C
DO 100 J=1,MJ
XJ(J)=(J-1)*DX
AIJ(J)=(AI1*TAU)/(96500*D0)
DO 100 I=1,MI
IF(XJ(J).LE.X1) THEN
CI(I,J)=CO1(I)
DIJ(I,J)=DO1(I)/D0
ENDIF
IF(XJ(J).GT.X1) THEN
CI(I,J)=CO2(I)
DIJ(I,J)=DO2(I)/D0
ENDIF
100 CONTINUE
C
TIME=0.0
DO 2000 KWEEKS=1,MWEEKS
DO 1500 KDAY=1,7
DO 1300 KHS=1,24
DO 1000 KSECS=1, 60*60/STEP
C TIME INCREMENT = STEP IN SECONDS
RSTEP=(STEP*D0)/(TAU*TAU)
CALL DPHI(MI,MJ,MMJ,CI,XJ,ZI,DIJ,AIJ,PHI,ALPHA,NN)

```

```

DO 888 J=1,MJ
888 PHNEW(J)=PHI(J)
IF(TIME.LT.STEP) CALL PRINT(0,MI,MJ,MMJ,CI,PHI,XJ)
CALL SOLVER(MI,MJ,MMJ,CI,C,ZI,DIJ,PHI,PHNEW,RSTEP,AIJ,
+ XJ,ALPHA,X2)

```

C

```

INDEX=1
DO 999 J=1,MJ
DO 889 I=1,MI
889 CI(I,J)=C(I,J)
RATIO=DABS(CI(4,J)/(CI(3,J)+GAMA1*CI(1,J)))
IF(XJ(J).GT.(X1+X2).AND.RATIO.LE.AR1) INDEX=-1
999 CONTINUE
IF(INDEX.EQ.-1) THEN
RATIO=TIME/60.0/60.0/24.0
WRITE(*,733) RATIO
WRITE(9,733) RATIO
733 FORMAT(/,10X,TERMINATE TIME =, F12.5, 'DAYS')
CALL PRINT(RATIO,MI,MJ,MMJ,CI,PHI,XJ)
STOP
ENDIF
TIME=TIME+STEP
IF(MMJJ.EQ.0) CALL PRINT(0,MI,MJ,MMJ,CI,PHI,XJ)
1000 CONTINUE
IF(MMJJ.EQ.1) CALL PRINT(KHS,MI,MJ,MMJ,CI,PHI,XJ)
1300 CONTINUE
IF(MMJJ.EQ.2) CALL PRINT(KDAYS,MI,MJ,MMJ,CI,PHI,XJ)
1500 CONTINUE
WEEK=TIME/60.0/60.0/24.0/7.0
WRITE(*,533) WEEK, KWEEKS
IF(MMJJ.EQ.3) CALL PRINT(KWEEKS,MI,MJ,MMJ,CI,PHI,XJ)
2000 CONTINUE
533 FORMAT('weeks',2X,F5.2,3X,I5)
STOP
END

```

C

C

```

SUBROUTINE DPHI(MI,MJ,MMJ,CI,XJ,ZI,DIJ,AIJ,PHI,ALPHA,NN)
INTEGER MI,MJ,MMJ,I,J,NN
DOUBLE PRECISION CI,XJ,ZI,DIJ,AIJ,PHI,ALPHA,CONC
DIMENSION CI(MI,MMJ),XJ(MMJ),ZI(MI),DIJ(MI,MMJ),
+ AIJ(MMJ),PHI(MMJ),ALPHA(5),AIS(400)
DOUBLE PRECISION SUM1,SUM2,SUM3,DCX,AIS

```



```

C Calculate electrostatic potential, PHI(J), ionic strength, AIS(J)
  DO 200 J=1,MJ
    SUM1=0.0
    SUM2=0.0
    SUM3=0.0
    DO 100 I=1,MI
      IF(J.EQ.1) THEN
        DCX=(CI(I,J+1)-CI(I,J))/(XJ(J+1)-XJ(J))
        CONC=(CI(I,J)+CI(I,J+1))/2.0
      ENDIF
      IF(J.NE.1.AND.J.NE.MJ) THEN
        DCX=(CI(I,J+1)-CI(I,J-1))/(XJ(J+1)-XJ(J-1))
        CONC=CI(I,J)
      ENDIF
      IF(J.EQ.MJ) THEN
        DCX=(CI(I,J)-CI(I,J-1))/(XJ(J)-XJ(J-1))
        CONC=(CI(I,J)+CI(I,J-1))/2.0
      ENDIF
      SUM1=SUM1+ZI(I)*DIJ(I,J)*DCX
      SUM2=SUM2+ZI(I)**2*DIJ(I,J)*CONC
      100 SUM3=SUM3+ZI(I)**2*CI(I,J)
      PHI(J)=-(AIJ(J)+SUM1)/SUM2
C IF(PHI(J).LT.0.0) PHI(J)=0.0
      200 AIS(J)=SUM3/2.0
C
  PHI(NN)=0.5*(PHI(NN+2)+PHI(NN-2))
  PHI(NN+1)=0.75*PHI(NN+2)+0.25*PHI(NN-2)
  PHI(NN-1)=0.25*PHI(NN+2)+0.75*PHI(NN-2)
C
  RETURN
END
C
SUBROUTINE SOLVER(MI,MJ,MMJ,CI,C,ZI,DIJ,PHI,PHINEW,
+               RSTEP1,AIJ,XJ,ALPHA,X2)
  INTEGER MI,MJ,MMJ,I,J
  DOUBLE PRECISION CI,C,ZI,DIJ,PHI,PHINEW,AIJ,RSTEP1,ALPHA,XJ
  DIMENSION CI(MI,MMJ),C(MI,MMJ),ZI(MI),DIJ(MI,MMJ),PHI(MMJ),
+  PHINEW(MMJ),AIJ(MMJ),XJ(MMJ),AA(400,3),BB(400),ALPHA(5)
  DOUBLE PRECISION C1,C2,D1,FLUXI,FLUXO,AA,BB,DX,X2,
+  KS,RSTEP1,D2,D3,S1,S2,S3,S4
C
  DO 1000 I=1,MI
    DO 400 J=2,MJ-1

```

```

KS=ALPHA(3)*(1.0+ALPHA(5)*(2.0/J)**2)
C2=ALPHA(1)/KS/(1.0+ALPHA(2)/1000.0*CI(4,J))**2
IF(I.EQ.4) RSTEP=RSTEP1/(1.0+C2)
IF(I.NE.4) RSTEP=RSTEP1
DX=(XJ(J+1)-XJ(J-1))/2.0
C C1=-ZI(I)*DIJ(I,J-1)*PHI(J-1)*RSTEP/DX
C C2=-ZI(I)*DIJ(I,J+1)*PHI(J+1)*RSTEP/DX
C D2=DIJ(I,J)*RSTEP/(DX*DX)
C D3=(DIJ(I,J+1)/4.0+DIJ(I,J)-DIJ(I,J-1)/4.0)*RSTEP/(DX*DX)
C D1=(-DIJ(I,J+1)/4.0+DIJ(I,J)+DIJ(I,J-1)/4.0)*RSTEP/(DX*DX)
C
S1=0.5*(DIJ(I,J+1)+DIJ(I,J))*(CI(I,J+1)-CI(I,J))
S2=0.5*(DIJ(I,J)+DIJ(I,J-1))*(CI(I,J)-CI(I,J-1))
S3=DIJ(I,J+1)*ZI(I)*PHI(J+1)*CI(I,J+1)
S4=DIJ(I,J-1)*ZI(I)*PHI(J-1)*CI(I,J-1)
BB(J)=CI(I,J)+0.5*((S1-S2)*RSTEP/(DX*DX)+(S3-S4)*RSTEP/(2*DX))
S1=0.5*0.5*(DIJ(I,J+1)+DIJ(I,J))*RSTEP/(DX*DX)
S2=0.5*0.5*(DIJ(I,J)+DIJ(I,J-1))*RSTEP/(DX*DX)
S3=0.5*DIJ(I,J+1)*ZI(I)*PHI(J+1)*RSTEP/(2*DX)
S4=0.5*DIJ(I,J-1)*ZI(I)*PHI(J-1)*RSTEP/(2*DX)
AA(J,1)=-S2+S4
AA(J,3)=-S1-S3
AA(J,2)=1.0+S1+S2
C
C CRACK-NICOLSON METHOD & BACKWARD CENTERED SPACE
C
C AA(J,1)=- (0.5*C1+D1)
C AA(J,2)=2.0*(1+D2)
C AA(J,3)=(0.5*C2-D3)
C BB(J)=(0.5*C1+D1)*CI(I,J-1)+2.0*(1-D2)*CI(I,J)
C + -(0.5*C2-D3)*CI(I,J+1)
C
400 CONTINUE
C
C At the steel cathode
C
RSTEP=RSTEP1
IF(I.EQ.3) FLUXI=AIJ(1)/ZI(I)
IF(I.NE.3) FLUXI=0.0
DX=XJ(2)-XJ(1)
FLUXO=-DIJ(I,2)*(ZI(I)*PHI(2)*CI(I,2)+(CI(I,2)-CI(I,1))/DX)
BB(1)=2.0*RSTEP/DX*(FLUXI-0.5*FLUXO)+(CI(I,1)+CI(I,2))
AA(1,1)=0.0

```

```

      AA(1,2)=1.0+RSTEP/DX/DX*DIJ(I,2)
      AA(1,3)=1.0-RSTEP/DX*DIJ(I,2)*(ZI(I)*PHINNEW(2)+1.0/DX)
C
C Boundary condition at anode
C
C *****
      BB(MJ)=CI(I,MJ)
      AA(MJ,1)=0.0
      AA(MJ,2)=1.0
      AA(MJ,3)=0.0
C
      CALL SOLEQS(MJ,AA,BB,I,MI,CI,MJ,MMJ)
      DO 500 J=1,MJ
      500 C(I,J)=BB(J)
      1000 CONTINUE
      RETURN
      END
C
C
      SUBROUTINE SOLEQS(N,A,B,I,MI,C,MJ,MMJ)
      INTEGER K,N,I,MI,MJ,MMJ
      DOUBLE PRECISION A,B,C
      DIMENSION A(400,3),B(400),C(MI,MMJ)
C
      DO 500 K=1,N-1
      B(K)=B(K)/A(K,2)
      A(K,3)=A(K,3)/A(K,2)
      A(K,2)=1.0
      A(K+1,2)=A(K+1,2)-A(K,3)*A(K+1,1)
      B(K+1)=B(K+1)-B(K)*A(K+1,1)
      A(K+1,1)=0.0
      500 CONTINUE
      B(N)=B(N)/A(N,2)
C
      IF(B(N).LE.0) B(N)=0.0
C
      DO 800 K=1,N-1
      B(N-K)=(B(N-K)-A(N-K,3)*B(N-K+1))/A(N-K,2)
      800 IF(B(N-K).LT.0) B(N-K)=0.0
C
      RETURN
      END
C

```



```

C
  SUBROUTINE PRINT(KWEEKS,MI,MJ,MMJ,CI,PHI,XJ)
  INTEGER MI,MJ,MMJ,J,KWEEKS,JJ,INDEX,I,NN
  DOUBLE PRECISION CI,PHI,XJ,C15
  DIMENSION CI(MI,MMJ),PHI(MMJ),XJ(MMJ),C15(7)
  INDEX=-1
  WRITE(9,222) KWEEKS
  222 FORMAT(/,1X,'Weeks =',I5)
  NN=MJ/20
  IF(NN.LT.1) NN=1
  DO 100 JJ=1,MJ,NN
C J=4*(JJ-1)+1
    J=JJ
C IF(J.LT.MJ) THEN
    C15(1)=XJ(J)*100.0
    DO 50 I=1,MI
    50 C15(I+1)=CI(I,J)/1000.0
    C15(MI+2)=PHI(J)/100.0
    WRITE(9,444) (C15(I), I=1,MI+2)
C ENDIF
C IF(J.GE.MJ.AND.INDEX.LT.0) THEN
C J=MJ
C INDEX=1
C C15(1)=XJ(J)*100.0
C DO 70 I=1,MI
C 70 C15(I+1)=CI(I,J)/1000.0
C C15(MI+2)=PHI(J)/100.0
C WRITE(9,444) (C15(I), I=1,MI+2)
C ENDIF
    444 FORMAT(1X,7(E10.3,1X))
    100 CONTINUE
    RETURN
  END

```